AJSTR
of Scientific and Technological Reports

Vol.28 No.6
November - December 2025

ASEAN Journal

of Scientific and Technological Report (AJSTR)

Trace Metal Contamination and Biomarker Responses in Fish from a Mining-Impacted River Basin in Cebu, Philippines

John Jarold C. Leyson et at.

ISSN 2773-8752 (online)

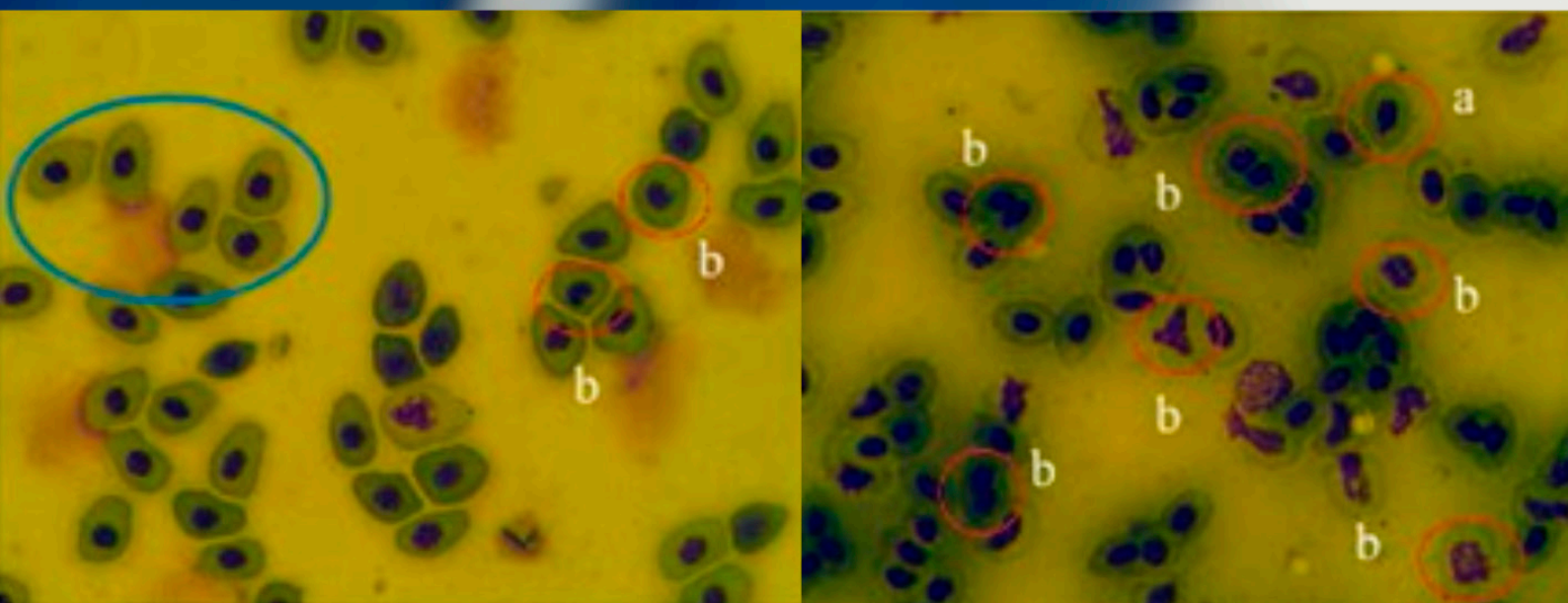

ASEAN
Journal of Scientific and Technological Reports
Online ISSN:2773-8752

ASEAN Journal of Scientific and Technological Reports (AJSTR)

Contact Us Institute of Research and Innovation, Thaksin University
222 M. 2 Ban-Prao sub-district, Pa-Pra-Yom district, Phatthalung province, Thailand
Tel. 0 7460 9600 # 7242 , E-mail: aseanjstr@tsu.ac.th

List of Contents

List of Contents

ASEAN
Journal of Scientific and Technological Reports
Online ISSN:2773-8752

ASEAN
Journal of Scientific and Technological Reports
Online ISSN:2773-8752

Research article

W UMa-type Light-Curve Analysis V700 Cyg Binary Star

Supat Sairattanain[1], Torik Hengpiya[2], and Wiraporn Maithong[3*]

[1] Faculty of Education and Human Development, Sisaket Rajabhat University, Sisaket, 33000, Thailand
[2] National Astronomical Research Institute of Thailand (Public Organization), Songkhla, 90000, Thailand
[3] Faculty of Science and Technology, Chiang Mai Rajabhat University, Chiang Mai, 50300, Thailand
* Correspondence: wiraporn_mai@cmru.ac.th

Citation:
Sairattanain, S.; Hengpiya, T.; Maithong, W. W UMa-type light-curve analysis V700 Cyg binary star. *ASEAN J. Sci. Tech. Report.* **2025**, *28*(6), e259261. https://doi.org/10.55164/ajstr.v28i5.259261.

Article history:
Received: May 10, 2025
Revised: August 25, 2025
Accepted: September 1, 2025
Available online: October 14, 2025

Abstract: V700 Cyg is a W Ursae Majoris (W UMa)-type contact binary star located in the constellation Cygnus. Photometric observations were conducted using a 0.7-meter reflecting telescope equipped with a CCD photometric system and *B* and *V* filters at the Regional Observatory for the Public, Songkhla, operated by the National Astronomical Research Institute of Thailand (Public Organization), during the night of August 6–7, 2021. The observational data were analyzed using the Wilson-Devinney method to generate a synthetic light curve that best represents the physical properties of the system. The results indicate that the effective temperatures of the primary and secondary components are 7692 K and 6078 K, respectively, with a mass ratio (q) of 2.98 and a degree of contact of 3.48%.

Keywords: V700 Cyg; W UMa-type star; Wilson-Devinney technique

1. Introduction

W Ursae Majoris-type (W UMa-type) contact binaries are close binary systems in which both stars share a common envelope, allowing continuous mass and energy exchange. These systems exhibit smooth, characteristic light curves, making them excellent subjects for studying stellar evolution and interactions in tight orbits [1-3]. We can learn about the physical characteristics of distant stars that are impossible to study directly by employing physically motivated light-curve modeling, such as the Wilson–Devinney models, that can infer otherwise inaccessible stellar parameters [4-6]. The V700 Cyg is a W-subtype contact binary star system. It was analyzed by using CCD imaging and the Wilson–Devinney model, and concluded that the system might be a triple system [7]. The Spot-induced asymmetry, similar to that seen in V700 Cyg [8], has been modeled in other W UMa systems, such as V523 Cas [9], which motivates our adoption of a spot hypothesis in the present analysis.

We selected V700 Cyg because existing solutions were obtained at earlier epochs, which leaves open the question of whether its spot configuration and contact degree persist. Additionally, its relatively large mass ratio and shallow contact make it a valuable test-bed for energy transfer in W-subtype systems. The target is also accessible from our site, enabling a dense phase coverage for an independent BV solution. According to the SIMBAD Astronomical Database [10], V700 Cyg, located in the constellation Cygnus, is a W-subtype W UMa contact binary. Its equatorial coordinates are Right Ascension (R.A.) = 20h 31m 05.247 s and Declination (Dec.) = +38° 47′ 00.461 ″ (J2000). In such systems, the less massive star is paradoxically hotter than its

more massive companion. Studying these binaries provides key insights into mass transfer mechanisms and the internal dynamics of short-period binary stars.

To analyze the observed light curves of contact binaries, we employed the Wilson–Devinney (WD) model, which remains the standard tool for light-curve synthesis. The WD code numerically solves the geometry of close binary systems under a Roche potential, allowing for the simultaneous adjustment of orbital inclination, temperature ratio, mass ratio, surface potentials, and luminosities of the components, as well as spot parameters if required. It incorporates physical effects such as limb darkening, gravity darkening, and reflection, thereby enabling realistic modeling of distorted stellar shapes and mutual irradiation. Since its original formulation [4], the WD code has undergone significant updates and refinements [5, 11-14], making it widely applicable to detached, semi-detached, and contact binaries. By citing and utilizing this framework, our analysis of V700 Cyg builds upon a robust and well-established foundation.

In this study, photometric data of V700 Cyg aims to determine the physical parameters using the Wilson-Devinney (WD) code, a widely used tool for modeling eclipsing binary systems.

2. Materials and Methods

Photometric observations of V700 Cyg were conducted on the night of August 6–7, 2021, using a 0.7-meter reflecting telescope equipped with an Apogee Altra U42 CCD camera and *B* and *V* filters of the standard *UBV* Johnson system. The observations were carried out at the Regional Observatory for the Public, Songkhla, operated by the National Astronomical Research Institute of Thailand (Public Organization). The V700 Cyg photograph and its information [10], as shown in Figure 1 and Table 1, respectively.

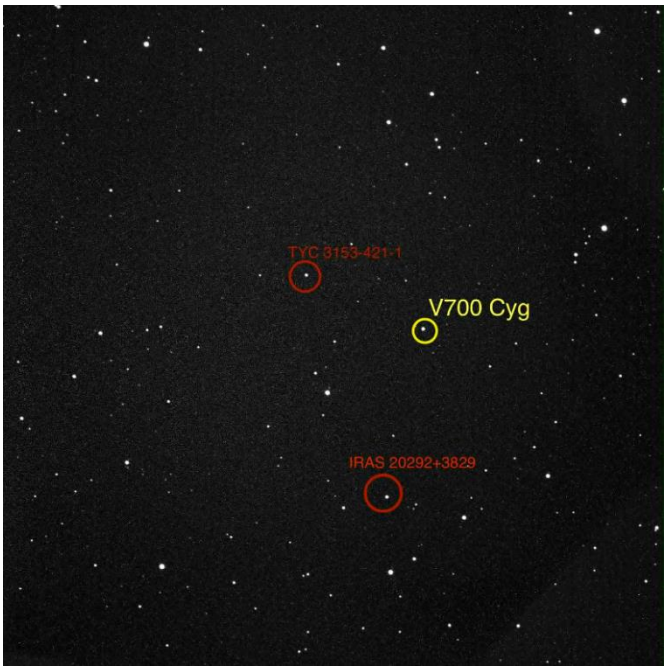

Figure 1. Photograph of the V700 Cyg

Table 1. Information of the V700 Cyg

Star	R.A. (h m s)	Dec (° ′ ″)	Magnitude *V*
V700 Cyg	20 31 05.247	+38 47 00.461	11.14
IRAS 20292+3829 (comparison)	20 31 10.959	+38 40 12.966	10.54
TYC 3153-421-1 (check)	20 31 29.629	+38 48 52.992	12.17

The image processing and photometric analysis were performed using MaxIm DL software. This observation was made in a partly cloudy and nearly clear sky. However, the V700 Cyg was observed in *the B*

filter with an exposure time of 60 seconds and the V filter with an exposure time of 50 seconds each. The data were collected, consisting of 176 pictures in the B filter and 181 pictures in the *V* filter. Furthermore, the noise reduction must use the dark, bias, and flat at the same time of observation too. The analysis began with the determination of the mass ratio ($q = m_2/m_1$) between the secondary and primary components. A range of trial mass ratios from 0.1 to 3.0 was systematically tested to identify the value that minimized the residuals between the observed and synthetic light curves.

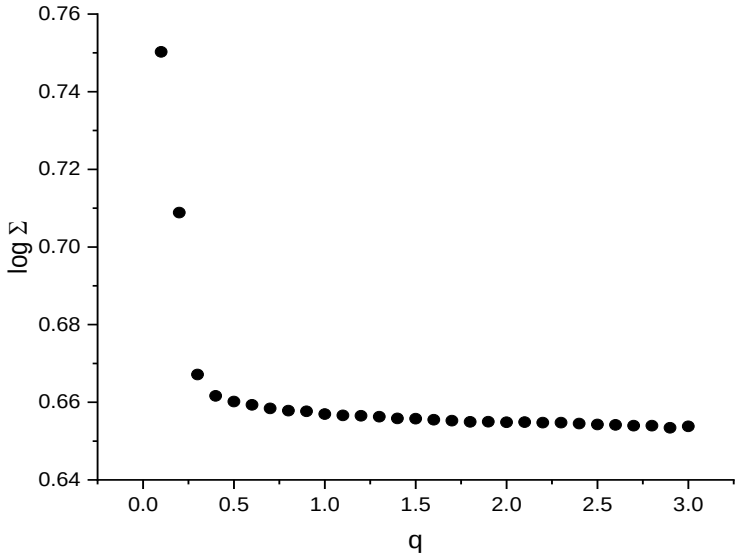

Figure 2. Variance of the mass ratio q of the V700 Cyg

Figure 2 illustrates that the optimal solution was obtained at q = 2.9, as shown in Figure 1, which presents the relationship between the mass ratio and the corresponding sum of squared residuals (Σ). This value served as a reference point for further modeling of the system's physical parameters.

3. Results and Discussion

The photometric data of V700 Cyg were analyzed using the Wilson-Devinney (WD) code to generate synthetic light curves, which were compared with observational data. The resulting light curve is presented in Figure 2, where the red line represents the theoretical model and the black dots denote observed data points. The overall shape and depth of the eclipses confirm that V700 Cyg is an eclipsing binary system of the W UMa type. According to Kim & Jeong (2012) [15], the optimal solution obtained from the light curve modeling is summarized; the orbital inclination of the system is approximately 79.9°. In the present study, the effective temperature of the primary component (T_1) was found to be 7692 K, and that of the secondary component (T_2) was 6078 K. The system's mass ratio was determined to be q = 2.984. These results are similar to the q 2.54028 from Liao, Qian, and Liu (2012) [8], but differ from those of Ostadnezhad, Forozani, and Ghanaatian (2019) [16], who reported a mass ratio of 0.544, indicating potential evolutionary processes such as mass transfer. The gravity darkening coefficients for both the primary and secondary components ($g_1 = g_2 = 0.32$) and the bolometric albedos ($A_1 = A_2 = 0.5$) suggest that both stars possess convective envelopes. The degree of contact was found to be 3.48%, indicating a shallow contact configuration. The best solution and the synthetic light curve of V700 Cyg are shown in Table 2 and Figure 3, respectively.

Table 2. Parameter for simulate the V700 Cyg

Parameter	The Best Solution
i	74.30 ± 1.79
g_1	0.32
g_2	0.32
$\Omega_1 = \Omega_2$	6.446986 ± 0.073870
Ωin	6.595188
Ωout	2.334606
T_1 (K)	7692 ± 239
T_2 (K)	6078
A_1	0.50
A_2	0.50
q	2.984122 ± 0.064080
$L_1/(L_1+L_2)_B$	0.54235 ± 0.02918
$L_1/(L_1+L_2)_V$	0.48928 ± 0.02026
Degree of Contact (%)	3.48
Lat (spot)$_2$ (degree)	62
Long (spot)$_2$ (degree)	90
R (spot)$_2$ (degree)	18
T.E. (spot)$_2$ (percent)	0.75

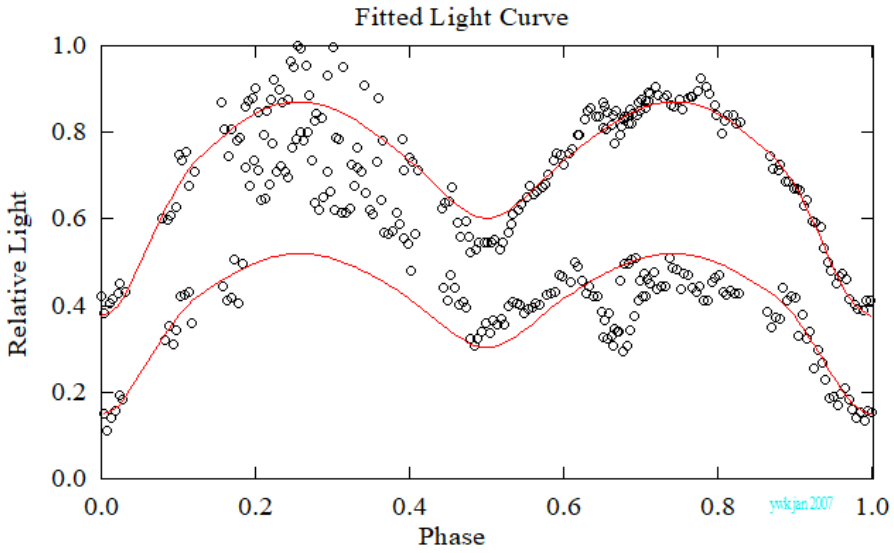

Figure 3. Synthetic light curve of the V700 Cyg.

Figure 3 shows an asymmetry between the two maxima of the light curve; maximum I (at phase ~0.25) is brighter than maximum II (at phase ~0.75). This phenomenon is known as the O'Connell effect. The phenomenon occurs exclusively in interacting close binary star systems, which may result from starspots on one or both components, hotspots caused by mass transfer, or the collision of circumstellar material with the stars during orbit [17]. Alternatively, the O'Connell effect is not a result of a static structure but rather a transient thermal variation on the stellar surface. This variation is correlated with the binary's orbit, causing an asymmetry in the system's brightness [18]. This interpretation is consistent with the findings of Ostadnezhad, Forozani, and Ghanaatian [16], who modeled a similar asymmetry in the *BVR* light curves of V700 Cyg by introducing a cold spot on the secondary component. The best parameters from Table 2 present the derived physical parameters used for simulation, such as the orbital inclination, effective temperature,

mass ratio, and spot characteristics. These parameters were utilized to construct the three-dimensional configuration of the binary system, as depicted in Figure 4.

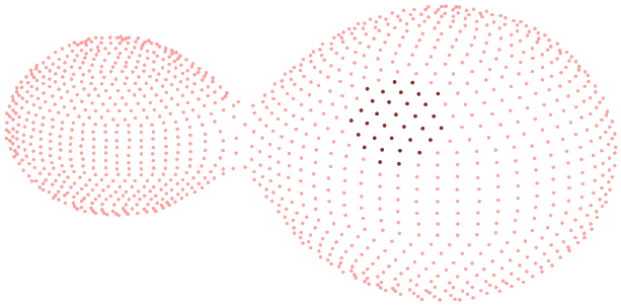

Figure 4. The V700 Cyg model at the orbital phase 0.2.

4. Conclusions

The physical and orbital parameters of the W UMa-type contact binary system V700 Cyg were determined using photometric data obtained on August 6–7, 2021, from the Regional Observatory for the Public in Songkhla, operated by the National Astronomical Research Institute of Thailand (Public Organization). The analysis, carried out using the Wilson-Devinney method, revealed that the system has a mass ratio of 2.984 and a contact degree of 3.48%, indicating a shallow-contact configuration. The primary and secondary components exhibit effective temperatures of 7692 K and 6078 K, respectively. Additionally, the presence of a cool spot with a radius of approximately 18 degrees on the surface of the secondary star was inferred to account for the observed O'Connell effect.

5. Acknowledgements

The authors would like to express their sincere gratitude to the National Astronomical Research Institute of Thailand (Public Organization) for providing access to observational facilities and support during this study.

Author Contributions: Conceptualization, methodology, investigation, formal analysis, S.S. and W.M., writing—original draft preparation, S.S.; Observation, T.H., writing—review and editing, and project administration, W.M.

Funding: This research received no external funding.

Conflicts of Interest: The authors declare no conflict of interest.

References

[1] Hilditch, R. W. *An Introduction to Close Binary Stars*; Cambridge University Press, **2001**. https://doi.org/10.1017/CBO9781139163576

[2] Lucy, L. B. The structure of contact binaries. *Astrophys. J.* **1968**, *151*, 1123–1131. https://doi.org/10.1086/149510

[3] Rucinski, S. M. W UMa-type binaries. *Mon. Not. R. Astron. Soc.* **2001**, *326*, 1279–1284.

[4] Wilson, R. E.; Devinney, E. J. Realization of accurate close-binary light curves: application to MR Cygni. *Astrophys. J.* **1971**, *166*, 605–619. https://doi.org/10.1086/150986

[5] Wilson, R. E. Eccentric orbit generalization and simultaneous solution of binary star light and velocity curves. *Astrophys. J.* **1979**, *234*, 1054–1066. https://doi.org/10.1086/157588

[6] Prša, A.; Zwitter, T. A computational guide to physics of eclipsing binaries. I. Demonstrations and perspectives. *Astrophys. J.* **2005**, *628*, 426–438. https://doi.org/10.1086/430591

[7] Yang, Y. G.; Dai, H. F. A new photometric study for the weak-contact binary V700 Cygni. *Publ. Astron. Soc. Jpn.* **2009**, *61*(3), 577–584. https://doi.org/10.1093/pasj/61.3.577

[8] Liao, W. P.; Qian, S. B.; Liu, N. P. A CCD photometric study of the contact binary star GSC 03526-01995. *Astron. J.* **2012**, *144* (6), 178. https://doi.org/10.1088/0004-6256/144/6/178
[9] Maithong, W. Physical Properties of an Eclipsing Binary System V523 Cas. *Sci. Technol. Nakhon Sawan Rajabhat Univ. J.* **2019**, *14* (11), 87–93. (In Thai)
[10] SIMBAD Astronomical Database - CDS (Strasbourg). (Accessed 2021-09-14). http://simbad.u-strasbg.fr/simbad/.
[11] Wilson, R. E. Accuracy and efficiency in the binary star reflection effect. *Astrophys. J.* **1990**, *356*, 613–622. https://doi.org/10.1086/168867
[12] Wilson, R. E. The modeling of eclipsing binary stars: outstanding problems and new directions. *New Astron. Rev.* **2004**, *48* (9), 695–701. https://doi.org/10.1016/j.newar.2004.03.015
[13] Wilson, R. E. The effect of spots on light curves of eclipsing binary stars. *Astrophys. J.* **2008**, *672* (1), 575–583. https://doi.org/10.1086/523634
[14] Wilson, R. E. Eclipsing binary solutions with apsidal motion. *Astron. J.* **2012**, *144* (3), 73.
[15] Kim, C. H.; Jeong, J. H. V700 Cygni: a dynamically active W UMa-type binary star II. *J. Astron. Space Sci.* **2012**, *29*(2), 151–161. https://doi.org/10.5140/JASS.2012.29.2.151
[16] Ostadnezhad, S.; Forozani, G.; Ghanaatian, M. New BVR photometric observations and light curve analysis of eclipsing binary V700 Cyg. *New Astron.* **2019**, *71*, 25–32. https://doi.org/10.1016/j.newast.2019.03.003
[17] Knote, M.; Caballero-Nieves, S.; Gokhale, V.; Johnston, K.; Perlman, E. Characteristics of Kepler Eclipsing Binaries Displaying a Significant O'Connell Effect. *Astrophys. J. Suppl. Ser.* **2022**, *262*(1), 1–32. https://doi.org/10.3847/1538-4365/ac770f
[18] Liu, Q.; Yang, Y. A Possible Explanation of the O'Connell Effect in Close Binary Stars. *Chin. J. Astron. Astrophys.* **2003**, *3*(2), 142–150. https://doi.org/10.1088/1009-9271/3/2/142

ASEAN
Journal of Scientific and Technological Reports
Online ISSN:2773-8752

Research article

Impact of Organic Fertilizer from Philippine Tree Fern (*Cyathea contaminans*) Leaves on Tuber Performance of Sweetpotato (*Ipomoea batatas)*

Marife Mustacisa-Lacaba[1*]

[1] Samar State University, Center for Lifelong Learning, Arteche Boulevard, Catbalogan City, Samar, 6700, Philippines
* Correspondence: marife.mustacisa@ssu.edu.ph

Citation:
Mustacisa-Lacaba, M. Impact of organic fertilizer from philippine tree fern (*Cyathea contaminans*) leaves on tuber performance of sweetpotato (*Ipomoea batatas*) Title. *ASEAN J. Sci. Tech. Report.* **2025**, *28*(6), e258761. https://doi.org/10.55164/ajstr.v28i6.258761.

Article history:
Received: April 12, 2025
Revised: August 18, 2025
Accepted: September 1, 2025
Available online: October 14, 2025

Abstract: Sweetpotato *(Ipomoea batatas)* is a staple crop in the Philippines, yet declining soil fertility poses a challenge to its sustainable production. This study investigates the impact of organic fertilizer from Philippine Tree Fern *(Cyathea contaminans*) leaves as a viable alternative to synthetic fertilizers. Conducted in Basey, Samar—where demonstration farms have been operating since 2019—the study employed a randomized complete block design (RCBD) to compare three treatments: (A) organic fertilizer from *C. contaminans*, (B) no fertilizer (control), and (C) commercial fertilizer (muriate of potash + urea). Results revealed that C. contaminans fertilizer significantly improved sweetpotato tuber survival rates, with the highest number of ridges with survived tubers (11 ridges) and the lowest number of ridges with diseased tubers (2 ridges), compared to the control (5 survived, 7 diseased) and synthetic fertilizer (6 survived, 13 diseased) ($\chi^2 = 9.143$, $p = 0.010$). Despite these benefits, no statistically significant differences were observed in tuber weight ($p = 0.698$) or circumference ($p = 0.671$) across treatments. However, treatment A produced slightly heavier (median weight of 0.240 kg) and larger (mean circumference of 133.41 cm) tubers on average. These findings suggest that *C. contaminans*-based fertilizer enhances plant resilience and disease resistance, making it a sustainable and eco-friendly alternative. Further research should explore its long-term impact on soil microbial composition, nutrient availability, and economic feasibility for large-scale adoption.

Keywords: Cultivation; disease resistance; surviving tuber

1. Introduction

Sweetpotato (*Ipomoea batatas*) is one of the most important root crops in the Philippines, serving as a staple food and a primary source of carbohydrates for many Filipinos [1]. It plays a significant role in food security, particularly in climate-vulnerable regions, due to its ability to adapt to extreme weather conditions [2]. The crop's ability to withstand typhoons, droughts, and floods makes it a dependable food source during pandemics and calamities, earning it the moniker "food and calamity." [3-4]. Additionally, sweet potatoes contribute to the economy by serving as a versatile raw material for various food products, including flour, fries, muffins, cookies, chips, and noodles [5], which cater to both local consumption and export markets. Sweetpotato production faces significant challenges due to decreased soil fertility, despite the crop's nutritional and economic benefits. The overuse of chemical fertilizers, inadequate land management, and the impact of climate change on soil nutrients

have all contributed to the gradual deterioration of soil quality. As a result, sustainable and efficient fertilizer management has become crucial for maintaining optimal sweetpotato production [6-7]. Traditionally, sweet potato farmers rely on synthetic fertilizers, particularly complete fertilizers (14-14-14) containing Nitrogen (N), Phosphorus (P), and Potassium (K) [8]. According to PhilRootcrops as cited from the work of Asio & Dela Cruz (2020) [9] and Mustacisa-Lacaba et al. (2023)[10], fertilizer application is divided into different stages: complete fertilizer is applied two weeks after planting to promote vegetative growth and a combination of nitrogen and potassium is added during the tuber bulking stage to enhance carbohydrate accumulation and sweetness.

However, concerns about soil degradation, environmental sustainability, and the rising cost of chemical fertilizers have led to increased interest in organic alternatives [6]. Studies suggest that organic fertilizers, such as animal manure and compost, can improve soil fertility, enhance microbial activity, and promote better root development, ultimately leading to higher sweetpotato yields [11]. However, a significant obstacle to broader adoption is still the scarcity of high-quality organic fertilizers. To address this issue, this study investigates the potential of *C. contaminans* (Philippine Tree Fern) leaves as a novel organic fertilizer for sweet potato farming. *C. contaminans*, locally known as "punit," is endemic to Samar and is rich in key macronutrients, particularly nitrogen (N), phosphorus (P), and potassium (K), which are essential for plant growth and tuber formation [12-13]. This fern has been historically underutilized in agriculture, despite its biodegradable nature and potential benefits as a soil conditioner [14]. A previous study on sweetpotato cultivation in the Philippines [15] highlighted the need for improved fertilizer strategies that balance yield enhancement with environmental sustainability. Findings from this prior research emphasized that soil amendments with organic components contribute to tuber quality, disease resistance, and soil nutrient retention, which aligns with the current study's goal of developing an alternative fertilizer that competes with commercially available synthetic fertilizers while remaining cost-effective and eco-friendly.

From a chemical perspective, the organic composition of *C. contaminans* is of particular interest due to its high polyphenol content, enzymatic antioxidants, and bioavailable forms of nitrogen and potassium. These substances have been shown to promote water retention, boost plant immunity against soil-borne diseases, and improve the development of plant root systems [16]. Unlike synthetic fertilizers, which deliver nutrients in an immediate but short-lived burst, organic fertilizers release nutrients gradually, thereby improving long-term soil structure and fertility. This study aims to formulate an organic fertilizer derived from *C. contaminans* leaves and evaluate its effectiveness compared to standard synthetic fertilizers. The research explicitly investigates its impact on sweet potato (Ipomoea batatas) tuber survival rate and disease resistance, addressing the challenges commonly encountered in disease-prone farming areas. By analyzing variations in tuber weight and circumference across different fertilizer treatments, this study aims to determine whether organic amendments contribute to enhanced tuber size and overall marketability. Additionally, the findings are expected to support sustainable agriculture initiatives by introducing a cost-effective and environmentally friendly alternative to conventional fertilizers. Such an innovation could offer significant benefits to small-scale farmers in the Philippines, promoting long-term soil health and reducing reliance on chemical fertilizers.

The results of this study will provide key insights into the viability of *C. contaminans* as an agricultural input, potentially offering a scalable solution to the declining soil fertility problem in sweetpotato farms. Furthermore, the findings from this research could inform future policy recommendations on the development of organic fertilizers and climate-resilient farming techniques. This study aims to formulate and evaluate the effectiveness of organic fertilizer derived from Philippine Tree Fern (*Cyathea contaminans*) leaves in improving the growth, yield, and disease resistance of sweetpotato (Ipomoea batatas) in a demonstration farm setting. Specifically, the study aimed to attain several objectives. First, it sought to develop and formulate an organic fertilizer using Cyathea contaminans leaves (Treatment A). Second, it aimed to assess the survival rate and disease resistance of sweetpotato tubers treated with *C. contaminans* fertilizer (Treatment A) in comparison with those without fertilizer application (Treatment B) and those applied with commercial fertilizer (Treatment C: muriate of potash + urea). Finally, the study intended to compare the effects of C. contaminans fertilizer (Treatment A), no fertilizer application (Treatment B), and commercial fertilizer (Treatment C: muriate of potash + urea) on sweetpotato tuber survival rate, disease incidence, weight, and circumference, and to determine the statistical significance of these differences. It tested the null hypothesis (Ho), there is no

significant difference in sweetpotato tuber survival rate, disease incidence, weight, and circumference among Treatment A (*C. contaminans* fertilizer), Treatment B (no fertilizer application), and Treatment C (commercial fertilizer: muriate of potash + urea)..

2. Materials and Methods

2.1 Development of C. contaminans-Based Fertilizer

Fresh *C. contaminans* leaves were collected from Brgy. Sto. Niño, Paranas, Samar, about 1 km from the nearest households, to minimize human disturbance. Mature leaves were selected for their higher nutrient content and better decomposition efficiency. Processing was conducted at Samar State University - Basey Campus using a standardized method. Leaves were washed to remove impurities, dried at 180°C for 10–15 minutes, flipped to ensure uniform drying, and then dried for an additional 10 minutes. They were then ground into a fine powder to enhance decomposition and nutrient availability, ensuring quality for experimental application (Refer to Figure 1 for the process flowchart).

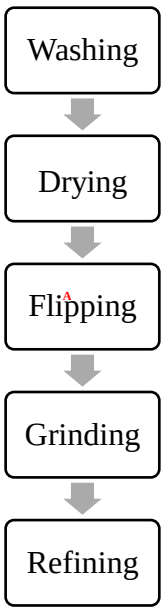

Figure 1. Process of *C. contaminans*-Based Fertilizer

2.2 Study Site and Experimental Design

The study was conducted in Brgy. Balante, Basey, Samar, a site with a semi-loam soil type that has been used for sweetpotato farming since 2019. The area experiences a tropical climate, characterized by warm temperatures ranging from 24°C to 32°C (75°F to 89°F) throughout the year. It receives significant annual rainfall, with the wettest months typically occurring between October and January, aligning with the Northeast Monsoon. The region is predominantly composed of rolling hills and upland terrain, with elevations ranging from 200 to 800 meters above sea level, making it suitable for root crop cultivation, particularly sweetpotato. The experiment employed a randomized complete block design (RCBD) with three fertilizer treatments and 15 replications. Each experimental unit consisted of a ridge measuring 60 cm in width at the top and 30 cm in height. Along each ridge, fifteen (15) sweetpotato cuttings were planted at 25 cm intervals, with each cutting set at an approximate planting depth of 30 cm (one standard ruler length) to ensure proper anchorage and root establishment. This configuration was maintained across all treatments to provide uniform plant density and allow accurate assessment of treatment effects on tuber growth.

2.3 Planting Material and Cultivation Practices

The VSP-6 sweet potato variety, sourced from the Tarlac Agricultural University, was chosen for its high yield potential (14+ tons per hectare), 32% dry matter content, and disease resistance. Its light yellow to white flesh makes it ideal for flour production without altering the final product's color. Known for its adaptability to various soils and climates, VSP-6 thrives in Samar's semi-loam soil and resists common sweetpotato viral infections, ensuring stable yields. To maintain genetic consistency, 25 cm cuttings with five nodes were taken from the mother plant, promoting strong root establishment and uniform growth.

2.4 Treatment Formulation and Application

The study evaluated the effects of three fertilizer treatments on sweetpotato growth, yield, and disease resistance. Treatment A used an organic fertilizer derived from Cyathea contaminans leaves, applied at 0.5 grams per ridge seven days before planting to enhance soil fertility and root establishment. Treatment B served as the control group, with no fertilizer application, to assess the natural growth potential of sweetpotato tubers. Treatment C involved a synthetic fertilizer mixture of muriate of potash and urea, applied at 0.5 grams per ridge 45 days after planting to support tuber bulking. Throughout the experiment, irrigation was provided as needed, and manual weeding was performed regularly to minimize nutrient competition and ensure optimal growth conditions. These management practices allowed for an accurate assessment of the effects of each fertilizer treatment.

2.5 Data Collection and Parameters Measured

Observations and data collection were conducted 90 days after planting to evaluate the effects of fertilizer treatments on sweetpotato growth and yield. The study measured survival rate, disease incidence, tuber weight, and circumference. Survival and disease incidence were assessed by recording the number of ridges with survived and insect-damaged tubers, with infected tubers referred to as "bukbok" in Waray-Waray. A Chi-square test ($p < 0.05$) determined statistical differences in survival and disease occurrence. Tuber weight was measured with a digital balance (0.01g precision), and circumference was measured at the widest point using a caliper for accuracy. Data normality was assessed using the Shapiro-Wilk test, while the Kruskal-Wallis test and ANOVA were employed to compare weight and circumference, ensuring a comprehensive statistical analysis.

2.6 Statistical Analysis

All data were analyzed using Statistics Kingdom, an online statistical tool that provided detailed results for various analyses. Nominal data, such as the incidence of survived and diseased sweetpotato tubers, were presented using frequency counts and analyzed using the Chi-square test to determine significant differences in survival and disease incidence among treatments. The Kruskal-Wallis test was applied to compare tuber weights, as the data exhibited a non-normal distribution, whereas ANOVA was used to analyze tuber circumference measurements, which followed a normal distribution. A significance level of $p < 0.05$ was set for all statistical tests to determine meaningful differences among treatments. Additionally, confidence intervals and boxplots were generated to visualize data distributions, providing a clear representation of the variability and trends across different fertilizer applications.

2.7 Experimental Limitations and Considerations

Environmental conditions, such as weather events that could have influenced the results, were not fully monitored. However, measures like irrigation and other interventions were implemented to minimize confounding variables and maintain uniform growth conditions across treatments.

3. Results and Discussion

3.1 Incidence of Survived and Diseased Sweetpotato Tubers Across Treatments

Table 1 presents the incidence of survival, insect damage, and mortality of sweetpotato tubers across the three treatments. To ensure comparability, each treatment was standardized to a total of 15 ridges. Both raw counts and percentages are reported, addressing potential bias that might arise if treatments had unequal numbers of ridges. This dual reporting allows for a more accurate comparison of treatment performance. Treatment A, which involved the application of Cyathea contaminans fertilizer seven days before planting,

achieved the highest survival rate (73.33%) and the lowest incidence of insect-damaged tubers (13.33%). In contrast, Treatment C, which received a commercial fertilizer mixture (muriate of potash and urea) applied 45 days after planting, recorded the highest incidence of insect damage (53.33%) and a relatively low survival rate (40.00%). Treatment B (control, no fertilizer) showed moderate survival (33.33%) and moderate insect damage (46.67%).

Table 1. Incidence of Survived and Insect-Damaged Sweetpotato Tubers (no. of ridges)

Treatment	Survived Tubers	% Survived	Insect-damaged tubers	% of insect-damaged tubers	Mortality	% Mortality	Total Ridges
Treatment A[1]	11	73.33%	2	13.33%	2	13.33%	15
Treatment B[2]	5	33.33%	7	46.67%	3	20.00%	15
Treatment C[3]	6	40.00%	8	53.33%	1	6.67%	15

[1]/ with *C. contaminans* fertilizer application 7 days before planting;
[2]/ no fertilizer application (control);
[3]/ with a mixture of muriate of potash and urea, applied 45 days after planting.

The findings suggest that *C. contaminans* fertilizer improved tuber survival while reducing insect damage, compared to both the control and the synthetic fertilizer treatment. The higher insect damage in Treatment C may indicate that synthetic fertilizer applications alter soil conditions in a way that increases tuber susceptibility.

3.2 Comparison of Sweetpotato Tuber Survival and Disease Incidence Across Treatments

To determine whether the differences in survival and disease incidence were statistically significant, a Chi-square test was conducted (*Table 2*). The overall Chi-square result ($\chi^2 = 9.143$, $p = 0.010$) indicated a significant difference among treatments, justifying the need for pairwise comparisons. The statistical analysis revealed significant differences in the survival and disease incidence of sweetpotato tubers among the different fertilizer treatments. The comparison between Treatment A (*C. contaminans* fertilizer) and Treatment B (no fertilizer application) showed a significant difference ($p = 0.025$), indicating that the application of *C. contaminans* fertilizer enhanced tuber survival and reduced disease incidence compared to no fertilizer at all. This suggests that *C. contaminans* could contribute to improved plant health and growth conditions.

Table 2. Statistical Comparison of Sweetpotato Tuber Survival and Disease Incidence Across Treatments

Test	df	Value	p-value	Interpretation
Overall Chi-square (X^2) across all treatments	2	9.143	0.010	Significant
Pairwise Chi-Square Tests				
Treatment A vs. Treatment B	1	4.996	0.025	Significant
Treatment A vs. Treatment C	1	8.719	0.003	Significant
Treatment B vs. Treatment C	1	0.327	0.567	Not Significant

decision rule: significant if $p < 0.05$; not significant if $p > 0.05$

Furthermore, the comparison between Treatment A (*C. contaminans*) and Treatment C (muriate of potash + urea) also showed a highly significant difference ($p = 0.003$). This result strongly suggests that *C. contaminans* fertilizer was more effective than the commercial fertilizer in promoting tuber survival and disease resistance. The enhanced growth observed in Treatment A implies that the organic fertilizer derived from *C. contaminans* may provide superior soil conditioning and nutrient availability compared to synthetic alternatives. On the other hand, the comparison between Treatment B (no fertilizer) and Treatment C (muriate of potash + urea) yielded a non-significant result ($p = 0.567$), suggesting that the application of the commercial fertilizer did not significantly improve tuber survival or disease resistance when compared to the control group. This finding suggests that the synthetic fertilizer mixture may not have significantly contributed to the growth performance of sweet potatoes under the given conditions, highlighting the potential limitations of relying solely on chemical fertilizers. The findings of this study demonstrate that the organic fertilizer derived

from *C. contaminans* had a positive impact on sweetpotato tuber survival and a protective effect against disease, making it a promising alternative to commercial fertilizers. The significant differences observed in tuber survival and disease rates underscore the potential of C. contaminans as an effective, sustainable, and eco-friendly fertilizer for sweet potato farming. These results support the broader application of *C. contaminans* fertilizer in promoting soil health and improving crop productivity in an environmentally sustainable manner.

3.3 Comparison of Sweetpotato Tuber Weight Across Three Treatments

Since the normality assumption was violated for Treatments A and C ($p = 0.000$ and $p = 0.003$, respectively), the Kruskal-Wallis test was used to compare tuber weights across the treatments. The median weights were highest in Treatment A (0.240 kg), followed by Treatment B (0.220 kg) and Treatment C (0.210 kg). However, despite these numerical differences, the Kruskal-Wallis test statistic ($H = 0.719$) and p-value (0.698) indicated that the differences were not statistically significant ($p > 0.05$). This suggests that the type of fertilizer did not have a significant impact on tuber weight (*Refer to Table 3)*.

Table 3. Comparison of Sweetpotato Tuber Weight

Descriptive Statistics and Normality Test			
Test	**Treatment A**	**Treatment B**	**Treatment C**
Excess Kurtosis	12.881	-1.171	3.795
Skewness	3.500	0.550	1.949
Normality (p-value)	0.000 (Non-normal)	0.137 (Normal)	0.003 (Non-normal)
Median	0.240	0.220	0.210
Sample Size (n)	15	15	15
Rank Sum (R)	335.500	242.000	242.500
R^2/n	7504.017	4,880.333	4,523.558
Kruskal-Wallis Test Results			
Test Statistic (H)		0.719	
p-value		0.698 (Not Significant)	

decision rule: for normality - normal if $p > 0.05$; non-normal if $p < 0.05$
for significance - significant if $p < 0.05$; not significant if $p > 0.05$;

The distribution of tuber weights varied across treatments. Treatment A (*C. contaminans* fertilizer) had the widest range of tuber weights, as shown in the boxplot (Figure 1), with some tubers achieving significantly higher weights than others. This was supported by its high positive skewness (3.500) and extreme kurtosis (12.881), indicating that while most tubers were smaller, a few had significantly higher weights. Treatment B (no fertilizer application) had a more balanced distribution (skewness = 0.550, kurtosis = -1.171), while Treatment C (muriate of potash + urea) displayed moderate skewness (1.949) and a sharper peak (kurtosis = 3.795). The histogram (*Figure 2*) further illustrates that most tubers, regardless of treatment, had lower weight values. Treatment A exhibited a more dispersed distribution, indicating greater variability in tuber weight. The findings suggest that applying *C. contaminans* fertilizer (Treatment A) did not significantly increase tuber weight compared to no fertilizer (Treatment B) or commercial fertilizer (Treatment C). While some tubers in Treatment A reached higher weights, the variability in weight distribution suggests inconsistent effects, possibly due to soil properties, environmental conditions, or genetic factors.

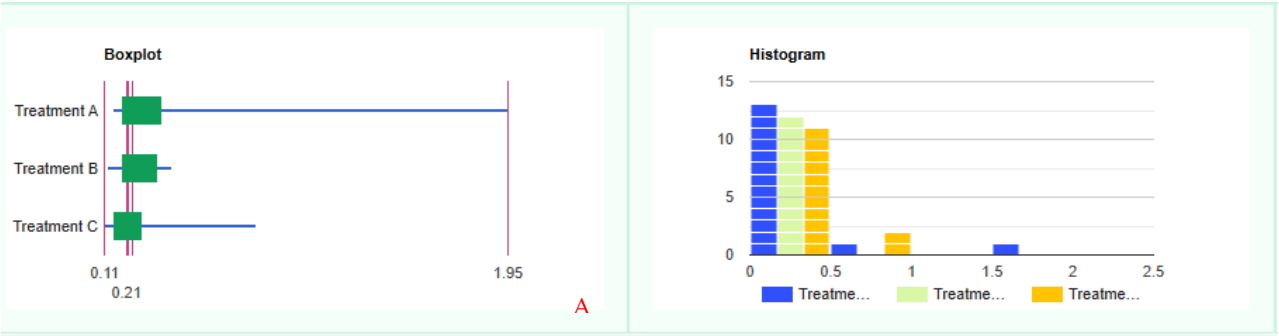

Figure 2. Boxplot and Histogram of Sweetpotato Tuber Weight Distribution Across Different Treatments

3.4 Comparison of Sweetpotato Tuber Circumference Across Three Treatments

The results in Table 4 show that not all treatments followed a normal distribution. Treatment A ($p = 0.382$) and Treatment C ($p = 0.211$) were normally distributed ($p > 0.05$), while Treatment B ($p = 0.006$) was non-normal. Because at least one group violated the assumption of normality, the non-parametric Kruskal-Wallis test was used instead of ANOVA.

Table 4. Comparison of Sweetpotato Tuber Circumference

Descriptive Statistics and Normality Test			
Test	**Treatment A**	**Treatment B**	**Treatment C**
Excess Kurtosis	0.826	-0.017	-0.951
Skewness	0.880	-1.115	-0.079
Normality (p-value)	0.382 (normal)	0.0006 (Non-Normal)	0.211 (Normal)
Median	128.81	119.38	94.25
Sample Size (n)	15	15	15
Rank Sum (R)	335.500	242.000	242.500
R^2/n	7504.017	4,880.333	4,523.558
Kruskal-Wallis Test Results			
Test Statistic (H)		3.231	
p-value		0.199 (p>0.05)	

decision rule: for normality - normal if $p > 0.05$; non-normal if $p < 0.05$
for significance - significant if $p < 0.05$; not significant if $p > 0.05$;

The descriptive statistics reveal differences in the central tendency and distribution of tuber circumferences. Treatment A exhibited slight positive skewness (0.880) and moderate kurtosis (0.826), suggesting that while most tubers were near the median (128.81 cm), a few larger values extended the distribution. Treatment B showed strong negative skewness (-1.115) and near-zero kurtosis (-0.017), indicating a more compressed distribution with smaller tubers pulling it leftward. Treatment C had near-symmetry (skewness = -0.079) with slightly platykurtic values (-0.951), showing a relatively even spread of tuber sizes around the median (94.25 cm). The Kruskal-Wallis test statistic ($H = 3.231$, $p = 0.199$) indicated no significant differences among the three treatments ($p > 0.05$). This means that the type of fertilizer or treatment applied did not have a significant effect on tuber circumference. The overlapping medians and distribution patterns across treatments reinforce this conclusion. The confidence interval plot (*Figure 3*) confirmed that the mean circumferences of all treatments overlapped, reinforcing the ANOVA results that no significant differences exist among treatments. The F-distribution curve in Figure 3 visually demonstrates the acceptance and rejection regions, with the computed F-statistic (0.403) falling within the acceptance region, meaning that the null hypothesis (no significant difference) was retained.

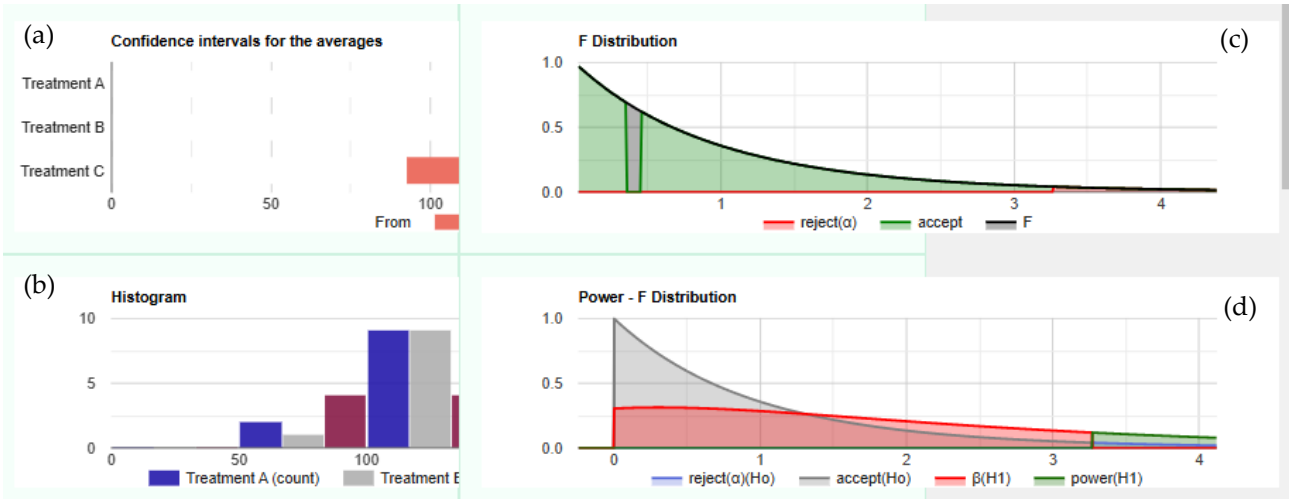

Figure 3. Statistical Distribution and Confidence Intervals for the ANOVA Test on Sweetpotato Tuber Circumference

The histogram illustrates the frequency of circumference measurements, displaying a relatively consistent distribution across treatments, with no extreme variations. The power analysis graph (Figure 1) illustrates the probability of detecting a real difference if one exists. The statistical power appears to be low, suggesting that a larger sample size may be needed for more precise differentiation among treatments. The results indicate that fertilizer type did not significantly affect tuber circumference. While Treatment A (*C. contaminans* fertilizer) produced slightly larger tubers on average, the differences were not substantial enough to be statistically significant. This suggests that environmental conditions, genetic factors, or nutrient absorption rates may have played a larger role in tuber growth than fertilizer application alone. The findings provide strong evidence that organic fertilizer derived from *Cyathea contaminans* leaves significantly enhanced sweetpotato tuber survival and reduced disease incidence compared to both the control (no fertilizer) and commercial fertilizer treatments. Chi-square test results confirmed significant differences in tuber survival and disease resistance among treatments, with Treatment A (C. contaminans fertilizer) showing the highest survival rate (11 ridges) and the lowest disease incidence (2 ridges). This aligns with previous research indicating that organic fertilizers rich in nitrogen, phosphorus, and potassium contribute to improved plant health and reduced disease susceptibility [17-18].

In contrast, the high disease incidence in Treatment C (muriate of potash + urea: 13 diseased ridges, 6 survived ridges) suggests that synthetic fertilizers may alter soil microbial activity, increasing plant vulnerability to diseases [19]. Studies indicate that while chemical fertilizers provide immediate nutrient availability, they may degrade soil quality over time, making crops more susceptible to pathogens. This could explain why tubers treated with C. contaminans fertilizer exhibited superior disease resistance, as organic fertilizers are associated with enhanced microbial diversity and improved nutrient cycling [19-24]. Despite these benefits, no statistically significant differences were observed in tuber weight and circumference across treatments. The Kruskal-Wallis test for weight and ANOVA for circumference confirmed that while Treatment A produced slightly heavier (0.240 kg) and larger (133.41 cm) tubers on average, the differences were not statistically significant ($p > 0.05$). This suggests that soil structure, environmental factors, and genetic variability may have had a greater influence on tuber growth than the type of fertilizer alone [25]. Further analysis of histogram and boxplot distributions revealed high variability in tuber weight within Treatment A, with skewness (3.500) and kurtosis (12.881) indicating that while some tubers were significantly larger, most were clustered around lower weight values. This aligns with Tadesco et al. [26], who suggested that organic fertilizers may not always increase yield but can enhance crop resilience and sustainability.

4. Conclusions

The findings provide strong evidence that organic fertilizer derived from *Cyathea contaminans* leaves significantly enhanced sweetpotato tuber survival and reduced disease incidence compared to both the control (no fertilizer) and commercial fertilizer treatments. Chi-square test results confirmed significant differences in tuber survival and disease resistance among treatments, with Treatment A *(C. contaminans fertilizer)* showing the highest survival rate (11 ridges) and the lowest disease incidence (2 ridges). This aligns with previous research indicating that organic fertilizers rich in nitrogen, phosphorus, and potassium contribute to improved plant health and reduced disease susceptibility [17-18]. In contrast, the high disease incidence in Treatment C (muriate of potash + urea: 13 diseased ridges, 6 survived ridges) suggests that synthetic fertilizers may alter soil microbial activity, increasing plant vulnerability to diseases [19]. According to studies, the use of chemical fertilizers may increase crop susceptibility to infections by degrading soil quality over time, even when they provide immediate nutrient availability. This could explain why tubers treated with *C. contaminans* fertilizer exhibited superior disease resistance, as organic fertilizers are linked to improved microbial diversity and nutrient cycling [19-24]. Despite these benefits, no statistically significant differences were observed in tuber weight and circumference across treatments. The Kruskal-Wallis test for weight and ANOVA for circumference confirmed that while Treatment A produced slightly heavier (0.240 kg) and larger (133.41 cm) tubers on average, the differences were not statistically significant ($p > 0.05$). This suggests that soil structure, environmental factors, and genetic variability may have had a greater influence on tuber growth than the type of fertilizer alone [25]. Further analysis of histogram and boxplot distributions revealed high variability in tuber weight within Treatment A, with skewness (3.500) and kurtosis (12.881) indicating that while some tubers were significantly larger, most were clustered around lower weight values. This aligns with Tadesco et al. [26], who suggested that organic fertilizers may not always increase yield but can enhance crop resilience and sustainability.

5. Acknowledgements

The author acknowledges the Center for Lifelong Learning (CeLL) of Samar State University for its support, particularly in data gathering through Mr. Mark Glyvan C. Albos, Mr. Louie D. Velardo, and Mr. Mar June J. Gabon, along with the CeLL staff. Gratitude is also extended to CeLL for funding this research.

Special appreciation is given to the farmers and processors of Balante, Basey, Samar, Philippines, for their valuable participation and contributions.

Author Contributions: All the contributions were made by the sole author

Funding: This research was funded by the Department of Science and Technology - Philippine Council for Agriculture, Aquatic and Natural Resources Research and Development (DOST-PCAARRD) through its Technology Transfer and Promotion Division (TTPD).

Conflicts of Interest: The author declares no conflict of interest.

References

[1] Macabudbud, S. S., Jr. Enhancing sustainability and flavor of waste coconut (Cocos nucifera) kernel and sweet potato peels creamy roll: Extension program guide. *J. Appl. Nat. Sci.* **2024**, *16*(1). https://doi.org/10.31018/jans.v16i1.5396

[2] Laranang, L. B.; Galo, E. D.; Locading, O. H. Climate-resilient agri-fisheries (CRA) assessment, targeting & prioritization for the adaptation and mitigation initiative for Tarlac Province. *AIP Conf. Proc.* **2022**, *2472* (1). https://doi.org/10.1063/5.0094762

[3] Maria, F. P. S. Fitting food to circumstances: Potential contributions of Philippine culinary heritage to disaster risk reduction. *Budhi* **2020**, *24*(2), 3–28.

[4] Siaciti, N. G.; Idris, K. Z.; Samiullah, M.; Khanum, R.; Nkrumah, E.; Althea, A. *Resource Management and Environmental Challenges*; IPR Journals and Book Publishers, **2024**.

[5] Laryea, D.; Akyereko, Y. G.; Wireko-Manu, F. D.; Oduro, I. Glycemic index of root and tuber crops: Increasing relevance in diet. In *Sustainable and Functional Foods from Plants: Health Impact, Bioactive Compounds, and Production Technologies*; **2024**; p 195. https://doi.org/10.1201/9781003415763-10

[6] Low, J. W.; Ortiz, R.; Vandamme, E.; Andrade, M.; Biazin, B.; Grüneberg, W. J. Nutrient-dense orange-fleshed sweetpotato: Advances in drought-tolerance breeding and understanding of management practices for sustainable next-generation cropping systems in Sub-Saharan Africa. *Front. Sustain. Food Syst.* **2020**, *4*, 50. https://doi.org/10.3389/fsufs.2020.00050

[7] George, J.; Reddy, G. V.; Wadl, P. A.; Rutter, W.; Culbreath, J.; Lau, P. W.; et al. Sustainable sweetpotato production in the United States: Current status, challenges, and opportunities. *Agron. J.* **2024**, *116*(2), 630–660. https://doi.org/10.1002/agj2.21539

[8] Nengparmoi, T. H. *Response of Sweet Potato [Ipomoea batatas (L.) Lam.] to Secondary Nutrients*; Doctoral Dissertation, Department of Agronomy, College of Horticulture, Vellanikkara, **2020**.

[9] Asio, L. G. E.-S.; Dela Cruz, N. E. Application of Mitscherlich-Bray equation to formulate fertilizer recommendations for sweetpotato in Leyte, Philippines. *Ann. Trop. Res.* **2020**, *42*(2), 30–40. https://doi.org/10.32945/atr4223.2020

[10] Mustacisa-Lacaba, M.; Tan, N.; Villanueva, R. The effect of eliminating the application of phosphorus-containing fertilizer for the bulking period of sweet potato production. *ASEAN J. Sci. Technol. Rep.* **2023**, *26* (3), 1–10. https://doi.org/10.55164/ajstr.v26i2.248752

[11] El-Sheshtawy, A. A.; Ghanem, K. M. How do biostimulants support sweet potato production in an organic and sustainable farming system? *J. Agric. Chem. Biotechnol.* **2023**, *14*(5), 51–56. https://doi.org/10.21608/jacb.2023.206216.1051

[12] Arenas, R. J. B.; Villanueva, R. M. D.; Simbahan, J. F.; Obusan, M. C. M. Antimicrobial activity of endophytic and rhizospheric fungi associated with soft fern (Christella sp.) and Cinderella weed (Synedrella nodiflora) inhabiting a hot spring in Los Baños, Laguna, Philippines. *Acta Med. Philipp.* **2022**, *56*(10).

[13] Dechimo, A. A., Jr.; Buot, I. E., Jr. Biophysical assessment of the plant biodiversity of Northern Negros Natural Park, Negros Island, Philippines. *Biodiversitas* **2023**, *24*(1). https://doi.org/10.13057/biodiv/d240167

[14] Mustacisa, M. M. Diversity, uses and economic value of ferns: An instrument for epistemological perception. *Int. J. Environ. Sci. Educ.* **2016**, *11*(18), 13111–13146.

[15] Adam, M. C.; Usop, M. S.; Salibo, A. U.; Dicolano, M. M.; Ebrahim, J. M. K. Fertility map of agricultural production areas in Barangay Sibuto and Tenonggos, Datu Odin Sinsuat, Maguindanao Del Norte. **2024**.

[16] Faizal, A.; Taufik, I.; Rachmani, A. F.; Azar, A. W. P. Antioxidant and antibacterial properties of tree fern Cyathea contaminans. *Biodiversitas* **2020**, *21*(5), 2201–2205. https://doi.org/10.13057/biodiv/d210548

[17] Pahalvi, H. N.; Rafiya, L.; Rashid, S.; Nisar, B.; Kamili, A. N. Chemical fertilizers and their impact on soil health. In *Microbiota and Biofertilizers, Vol. 2: Ecofriendly Tools for Reclamation of Degraded Soil Environs*; **2021**; pp 1–20. https://doi.org/10.1007/978-3-030-61010-4_1

[18] Tripathi, R.; Tewari, R.; Singh, K. P.; Keswani, C.; Minkina, T.; Srivastava, A. K.; et al. Plant mineral nutrition and disease resistance: A significant linkage for sustainable crop protection. *Front. Plant Sci.* **2022**, *13*, 883970. https://doi.org/10.3389/fpls.2022.883970

[19] Akanmu, A. O.; Babalola, O. O.; Venturi, V.; Ayilara, M. S.; Adeleke, B. S.; Amoo, A. E.; et al. Plant disease management: Leveraging on the plant-microbe-soil interface in the biorational use of organic amendments. *Front. Plant Sci.* **2021**, *12*, 700507. https://doi.org/10.3389/fpls.2021.700507

[20] Briones, R. M.; Pastolero, H. L. C.; Galang, I. M. R. Prospects for widespread adoption of organic-based fertilizers in the Philippines: A rapid appraisal. *PIDS Discuss. Pap. Ser.* **2024**, No. 2024-30. https://doi.org/10.62986/dp2024.30

[21] Lim, J. A.; Yaacob, J. S.; Mohd Rasli, S. R. A.; Eyahmalay, J. E.; El Enshasy, H. A.; Zakaria, M. R. S. Mitigating the repercussions of climate change on diseases affecting important crop commodities in Southeast Asia, for food security and environmental sustainability—A review. *Front. Sustain. Food Syst.* **2023**, *6*, 1030540. https://doi.org/10.3389/fsufs.2022.1030540

[22] Hossain, M. E.; Shahrukh, S.; Hossain, S. A. Chemical fertilizers and pesticides: Impacts on soil degradation, groundwater, and human health in Bangladesh. In *Environmental Degradation: Challenges*

and Strategies for Mitigation; Springer International Publishing: Cham, **2022**; pp 63–92. https://doi.org/10.1007/978-3-030-95542-7_4

[23] Bhunia, S.; Bhowmik, A.; Mallick, R.; Mukherjee, J. Agronomic efficiency of animal-derived organic fertilizers and their effects on biology and fertility of soil: A review. *Agronomy* **2021**, *11*(5), 823. https://doi.org/10.3390/agronomy11050823

[24] Rashmi, I.; Roy, T.; Kartika, K. S.; Pal, R.; Coumar, V.; Kala, S.; Shinoji, K. C. Organic and inorganic fertilizer contaminants in agriculture: Impact on soil and water resources. In *Contaminants in Agriculture: Sources, Impacts and Management*; **2020**; pp 3–41. https://doi.org/10.1007/978-3-030-41552-5_1

[25] Peter, T. M.; Michael, P. S. Sweet potato is a strategic root crop in Oceania: A synthesis of the past research and future direction. **2023**. https://doi.org/10.20961/stjssa.v20i1.66319

[26] Tedesco, D.; de Almeida Moreira, B. R.; Júnior, M. R. B.; Maeda, M.; da Silva, R. P. Sustainable management of sweet potatoes: A review on practices, strategies, and opportunities in nutrition-sensitive agriculture, energy security, and quality of life. *Agric. Syst.* **2023**, *210*, 103693. https://doi.org/10.1016/j.agsy.2023.103693.

ASEAN
Journal of Scientific and Technological Reports
Online ISSN:2773-8752

Research article

Trace Metal Contamination and Biomarker Responses in Fish from a Mining-Impacted River Basin in Cebu, Philippines

John Jarold C. Leyson[1], Lora Mae G. Villegas[2*], Lemuel M. Velasco[3], Hemres M. Alburo[4], and Rosalyn P. Alburo[5]

[1] Procter and Gamble, Philippines, Cabuyao City, 4025, Laguna, Philippines
[2] Department of Chemistry, University of San Carlos, Cebu City, 6000, Philippines; lgvillegas@usc.edu.ph
[3] Biodiversity, Environmental, and Natural Resources Research Center (BENRC), Cebu Technological University Argao Campus, 6021, Cebu, Philippines
[4] Biodiversity, Environmental, and Natural Resources Research Center (BENRC), Cebu Technological University Argao Campus, 6021, Cebu, Philippines
[5] Biodiversity, Environmental, and Natural Resources Research Center (BENRC), Cebu Technological University Argao Campus, 6021, Cebu, Philippines
* Correspondence: lgvillegas@usc.edu.ph

Citation:
Leyson, J.J.C.; Villegas, L.M.G; Veloso, L.M.; Alburo, H.M.; Alburo, R.P. Trace metal contamination and molecular biomarker responses in fish from the toledo river basin, ebu, Philippines. *ASEAN J. Sci. Tech. Report.* **2025**, *28*(6), e257772. https://doi.org/10.55164/ajstr.v28i6.257772.

Article history:
Received: February 6, 2025
Revised: August 27, 2025
Accepted: September 1, 2025
Available online: October 14, 2025

Abstract: Mining activities in Toledo City, Cebu, have created extensive mined-out lands and left a legacy of metal contamination in surrounding aquatic systems. This study assessed trace metal concentrations and molecular biomarker responses in fish from the downstream section of the Sapangdaku River and adjacent Tañon Strait coastline. Pore water and sediments were analyzed for Cd, Cr, Cu, Pb, and Zn using FAAS and ICP-MS, while biomarker assays measured metallothionein (MT) induction in liver tissues and genotoxicity through the assessment of micronuclei (MN) and nuclear abnormalities (NA) in erythrocytes. Results revealed that Cu was the dominant pollutant in pore water (mean 173 μg/L; peak 831 μg/L at Station 3), exceeding the U.S. EPA and Philippine DENR criteria by more than tenfold. Sediment indices (Igeo, CF, PLI) confirmed very high contamination from Cu, with Pb and Zn contributing moderately, while Cd and Cr remained near background levels. Fish analyses showed substantial bioaccumulation of Cu and Zn, particularly in benthic feeders (*Mugil cephalus*, *Eubleekeria jonesi*), which also exhibited the strongest biomarker responses. MT levels reached 299 μg/g in *M. cephalus*, while MN and NA frequencies were strongly correlated with Cu concentrations ($R > 0.98$, $p < 0.05$). NA were consistently more frequent than MN, suggesting their greater sensitivity as early markers of genotoxic stress. These results demonstrate that legacy mining continues to exert significant ecological stress on the Sapangdaku River system. The combined use of chemical analyses and biomarkers provides valuable baseline data, with MT, MN, and NA emerging as sensitive indicators of metal contamination and ecological risk.

Keywords: Porewater toxicity; metallothionein induction; risk assessment; mining; biomarker responses

1. Introduction

Mining is among the most significant anthropogenic activities contributing to environmental contamination worldwide. While mining operations provide economic benefits, they often result in long-term ecological disturbances, including acid mine drainage, soil enrichment with trace metals, and contamination of freshwater systems. These impacts are particularly severe in river basins where heavy metals accumulate in sediments and aquatic organisms, threatening ecosystem integrity and human health through the food

chain. Toledo City in Cebu, Philippines, is a major mining hub, encompassing approximately 35,000 hectares of mined-out land primarily from extensive copper extraction [1]. The legacy of mining has left a persistent ecological footprint, with copper and associated trace metals contaminating soils and river systems. Elevated concentrations of heavy metals in stream ecosystems near mining sites pose considerable ecological risks, particularly for aquatic organisms and higher trophic levels. Despite this, rehabilitation and monitoring initiatives in the Toledo River basin remain limited.

Several studies have already documented the extent of contamination in the region. Lo and Sakamoto [2] reported high levels of copper (>700 ppm) and zinc (>100 ppm) in sediments from the Sapangdaku River and the tailings outfall in Barangay Ibo. Aggangan et al. [1] described extremely acidic soils (pH ~2.5) with copper concentrations (154–638 mg/kg) far exceeding the permissible limit of 36 mg/kg. More recently, Sanchez et al. [3] confirmed that copper levels in the midstream and upstream sections of the Sapangdaku River remain above acceptable limits, primarily due to copper mining and the erosion of copper-rich landmasses. In addition, metal accumulation has been reported in plants, mollusks, and bivalves inhabiting the Toledo coastal area, but relatively few studies have examined fish populations that integrate contamination across habitats. Fish are considered effective sentinels of aquatic ecosystem health because they integrate exposure to contaminants over time and space, allowing for a comprehensive assessment of environmental health. Downstream fish, in particular, provide an important measure of cumulative pollution, as contaminants transported by river currents tend to accumulate in these areas with minimal dilution [4–6]. Studies from Alberta, Japan, and Vietnam have demonstrated that downstream sites reflect the highest contamination risks, making them reliable locations for biomonitoring.

Traditional monitoring has focused on quantifying metal concentrations in water, sediments, and biota. However, such measurements provide only part of the picture, as they cannot always reveal early biological stress. Molecular and cellular biomarkers—including metallothionein induction and genotoxicity assays (micronucleus and nuclear abnormalities)—offer sensitive indicators of sub-lethal toxic effects. They detect physiological stress responses in organisms before population-level declines occur, thereby serving as valuable tools for ecotoxicological monitoring and environmental risk assessment. Despite the ecological and human health significance of the Toledo River basin, recent work investigating biomarker responses in fish remains scarce. The absence of updated biomonitoring data poses challenges for environmental management, particularly in assessing rehabilitation needs and guiding local policy. This study, therefore, aimed to assess trace metal contamination and associated biomarker responses in fish from the downstream section of the Toledo River basin. Specifically, we quantified the levels of copper, zinc, lead, cadmium, and chromium in fish tissues and evaluated biomarker responses, including metallothionein induction and genotoxicity. By establishing baseline data, this study aims to contribute to the development of local environmental policies and provide a scientific foundation for future rehabilitation and monitoring programs.

2. Materials and Methods

2.1 Sampling sites.

The Sapangdaku River, also known as the Hinulawan River, is situated at an estimated terrain elevation of 5 meters above sea level, spanning a long stretch of 9 kilometers across 10 barangays in Toledo City. The three sampling sites, including the mouth of the Sapangdaku River and one from each side of the river mouth in the Tañon Strait, were used in the study, as shown in Figure 1. Sampling Site 1 was in the coastline of Barangay Dumlog near the Balamban Coast, Station 2 was located at the mouth of Sapangdaku River, and Station 3 was in the coastline of Daanglungsod near Atlas Fertilizer Plant (AFC) and Toledo City Port. Both coastlines are part of the Tañon Strait.

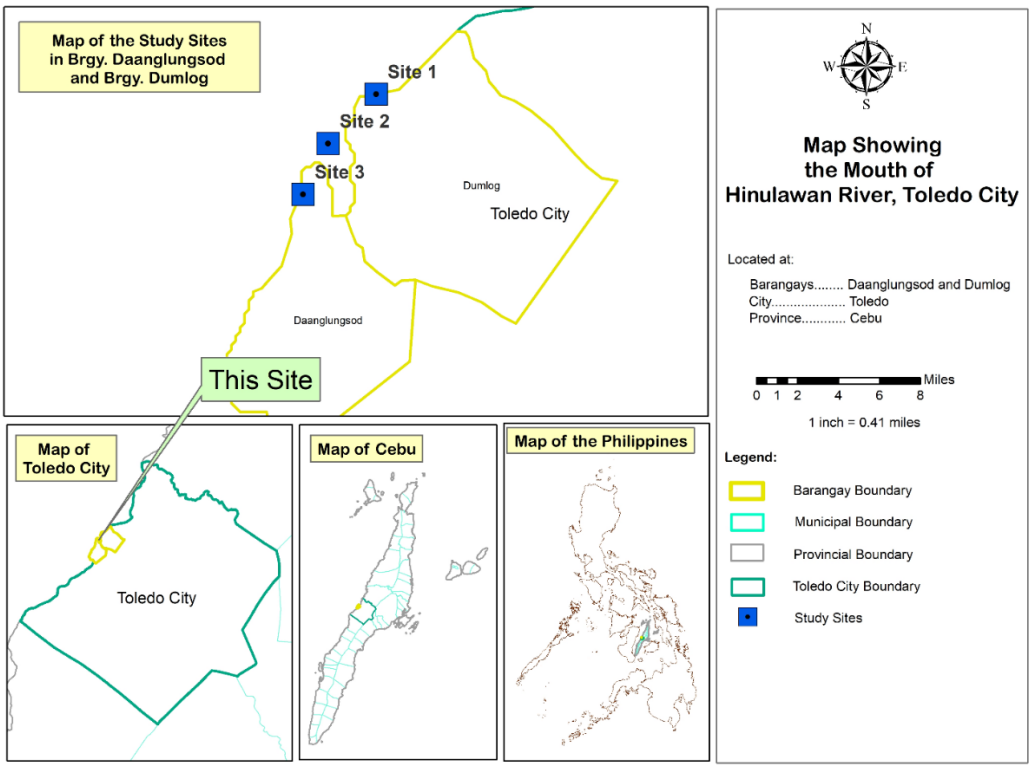

Figure 1. Location map of the sampling stations in the Hinulawan river.

The GPS coordinates of the sampling sites, along with a technical description of each site, are tabulated in Table 1. Station 1 in Barangay Dumlog is located near a ship-building facility, while Station 3 is situated near the Atlas Fertilizer Corporation (AFC). The color of the water in the sampling sites ranged from dark brown to black. All three sampling sites are abundant with Mangrove trees.

Table 1. Technical and Qualitative Description of Stations 1, 2, and 3 at Sapangdaku River, Toledo City, Cebu, Philippines.

Stations	GPS Coordinates	Description of Site
Station 1 Barangay Dumlog		
	N 10º 24.191′	Observable suspended solids
	E 123º 38.745′	Abundant Mangrove trees
		Coastline is black and brown
		Ship-building facility a few kilometers north
Station 2 Sapangdaku Estuary	N 10º 24.093′	The mouth of the river is covered with suspended solids
	E 123º 38.665′	Abundant Mangrove trees
		Coastline is dark brown
		The bed of the mouth of the river is soft
Station 3 Barangay DaangLunsod	N 10º 23.952′	Observable suspended solids
		Abundant Mangrove trees
	E 123º 38.552′	Coastline is dark brown
		AFC is a few kilometers south

2.2 Sampling Protocol and Design.

Sampling was conducted every other month from May to September 2017 at the mouth of the Sapangdaku River, as well as on both the left and right sides of the river's mouth along the coastline of the Tañon Strait. A 20-meter stretch of the site was designated as the study area for each sampling station. Within the study area, random samples of pore water and sediments were collected. Fifteen core samplers, each containing pore water and sediments, were collected per river to achieve a highly reliable composite sample.

2.3 Pore Water and Sediment Sample Collection and Analyses.

Pore water was collected using the method of Azcue et al. [8] and Kalnejais et al. [9]. Fifteen cores of undisturbed sediment were collected in each river using a previously acid-washed hand-held polyvinyl chloride corer with a diameter of 5 cm and a length of 20 cm, as shown in Figure 2. The cores were collected with at least 20 cm of sediment columns. The cores were securely covered with plastic and tightened with a rubber band, then placed in labeled ziplock plastic bags. These were then stored in a standing position in ice boxes and brought back to the laboratory.

Figure 2. Core samplers used in pore water collection.

In the laboratory, the sediments in core samplers were slowly removed and centrifuged at 4000 rpm for 30 min to separate the pore water. The pore water samples from each river were combined and filtered through a cellulose membrane with 0.45-µm pores, then preserved by adding 10% (v/v) reagent-grade nitric acid. The samples were placed in an ice bath and transported to TechnoLab, Labangon, Cebu, for analysis of heavy metals and total hardness. The samples were digested using the USEPA Method 3050B for sediments and the APHA-AWWA method for porewater. The metal concentrations were determined using a Flame Atomic Absorption Spectrophotometer (FAAS) via an external calibration method. Recovery tests were performed in triplicate per station per sampling month.

2.4 Pore Water Toxicity Analysis.

2.4.1. *Interstitial water criteria toxicity unit (IWCTU)*. The pore water quality can be evaluated for each metal using IWCTU as a water quality index, defined as:

$$IWCTU_{Me} = \frac{[Me]_{i.w.}}{FCV_{Me}} \quad (1)$$

Where $[Me]_{i.w.}$ is the dissolved metal (Me) concentration and FCV_{Me} is the hardness-dependent final chronic value for the metal [10, 11]. While the $IWCTU_{Me}$ exceeds 1, it implies a risk of toxicity to aquatic organisms. The method for calculating FCV_{Me} is presented in Table 1.

2.4.2 *Nemeraw Index (NI).* The Nemerow index was also used to estimate the pore water quality, and it was calculated as shown in Equation 2:

$$(NI) = \sqrt{\frac{(IWCTU)_{max}{}^2 + (IWCTU)_{mean}{}^2}{2}} \quad (2)$$

Five grades of toxic impact were used: no impact, slight impact, moderate impact, strong impact, and serious impact, with NI values of 5, respectively (Liu et al. [12]). These two indices, the total IWCTU and the NI, which combine the results for multiple metals, can be used to estimate pore water quality (Zhu et al. [13]).

2.5 Sediment Toxicity Risk Assessment.

The degree of contamination of heavy metals in the sediments was assessed by determining the geoaccumulation index (Igeo), contamination factor (CF), and pollution load index (PLI) (Islam et al. [14]).

2.5.1 Geo-accumulation index (Igeo). Geoaccumulation index (Igeo) values were calculated using equation 3:

$$I_{geo} = log_2 \frac{C_n}{1.5\ B_n} \quad (3)$$

Where Cn is the measured concentration of metal n in the sediment, and Bn is the geochemical background value of element n in the background sample.

2.5.2 Contamination Factor (CF). CF was calculated using equation 4 or by dividing the content of each metal by the background values in the sediment.

$$CF_{metal} = \frac{C_{metal}}{C_{background}} \quad (4)$$

2.5.3 Pollution load index (PLI). The PLI is defined as the nth root of the multiplication of the contamination factor of metals (CF), as shown in Equation 5. The greater its value, the more polluted is the river system (Islam et al. [16]).

$$PLI = (CF_1\ x\ CF_2\ \ldots .\ CF_n)^{1/n} \quad (5)$$

2.6 Fish Sample collection and blood extraction.

The sampling method and sample handling procedures prior to analysis in this study were approved by the University of San Carlos Institutional Animal Care and Use Committee. A total of four or more different fish species, available in all stations, were randomly collected from each sampling station using nets or fishhooks. Blood of each fish was extracted and smeared on a slide before the extraction of the liver. The fish samples were washed with distilled water and were then packed in plastic bags, labeled, and transported in ice boxes to the laboratory. The fish samples were rewashed with distilled water, placed in aluminum foil, and then in a ziplock bag, and will be frozen at -10°C until further treatment.

2.6.1 Sample Preparation and Heavy Metal Analysis in Fish.

Fish samples were oven-dried at 110°C until a constant weight was reached to remove water. Fish samples were pooled to obtain approximately 0.25-0.35 g of dry weight for microwave digestion, based on the AOAC Method 999.10, using 1 mL of 30% H_2O_2 and 7 mL of concentrated HNO_3. The microwave-digested samples were filtered using Whatman 42 filter paper and diluted to the mark in 25-mL volumetric flasks. The samples were analyzed with FAAS coupled with an external calibration method. A recovery test was also conducted.

2.6.2 Genotoxicity.

A blood smear was prepared according to the procedures described by Bacolod et al. [15]. A blood smear was air-dried for 24 hours and then fixed in absolute methanol for 30 seconds. It was washed with distilled water and air-dried for an additional 24 hours before staining. The dried smear was added with Gemsa stain in phosphate buffer solution and counterstained with May-Grunwald solution. Micronuclei (MN) and nuclear abnormalities were identified based on Al-Sabti and Metcalf [16] and Fenech et al. [17] using a microscope at 1000x magnification, with a total of 1000 erythrocytes observed at each slide. The final frequency was obtained after getting the average MN and NA of the three replicates per fish.

2.6.3 Metallothionein Assay.

To quantify metallothionein (MT) concentration in cells, the method was adapted from Linde and Garcia-Vazquez [18]. Briefly, the fish liver was homogenized in a 3-mL buffer (0.5 M sucrose, 20 mM Tris-HCl, pH 8.6, 0.01% β-mercaptoethanol), then centrifuged at 30,000 rpm for 10 minutes to obtain the supernatant. Cold ethanol (1.05 mL) and chloroform (80 µL) were added per mL of supernatant, followed by centrifugation at 6,000 rpm for 10 minutes at 0-4°C. The pellets were washed with a mixture of ethanol, chloroform, and buffer, then centrifuged again. The dried pellet was resuspended in 150 µL of 0.25 M NaCl, and 150 µL of 1N HCl with 4 mM EDTA was added. Next, 4.2 mL of 2 M NaCl containing 0.43 mM DTNB buffered with 0.2 M Na-phosphate (pH 8) was added, followed by centrifugation at 3,000 x g for 5 minutes. The supernatant absorbance at 412 nm was measured using a UV-Vis spectrophotometer. MT concentration was calculated using a standard curve of reduced glutathione (GSH) and assuming 1 mole of MT contained 20 moles of cysteine. The final MT content was determined by dividing the concentration by 20.

2.7 Statistical Treatment of Data.

Differences in the mean values of metal concentrations in pore water, sediments, fish tissues, genotoxicity, and metallothionein (MT) levels between stations and fish species were analyzed using two-way ANOVA with GraphPad Prism 7.04. The Pearson correlation coefficient was employed to assess the relationship between metal concentrations in fish, genotoxicity, and MT. Spearman's rank correlation coefficient (Spearman's rho) was used to evaluate the monotonic relationships between genotoxicity and metal accumulation, as well as between MT levels and metal accumulation.

3. Results and Discussion

3.1 Metal in Pore Water of Sapangdaku River and Tañon Strait Coastline

The pore water analysis revealed copper as the dominant contaminant across all stations and sampling months, with mean concentrations of 173 ± 9.23 µg/L and peaks reaching 831 ± 50.55 µg/L at Station 3. Zinc followed, while chromium, lead, arsenic, and cadmium occurred at comparatively lower levels. A two-way ANOVA revealed significant differences in metal concentrations among stations ($p < 0.001$) and among metals ($p < 0.001$), confirming both spatial variability and metal-specific patterns. Post-hoc tests indicated that Cu concentrations at Station 3 were significantly higher ($p < 0.05$) than at Stations 1 and 2. These differences reflect site-specific conditions: Station 2 (estuary) receives riverine discharges and tailings, Station 1 (Dumlog) experiences seawater dilution, while localized industrial discharges influence Station 3 (near the Atlas Fertilizer Corporation and port).

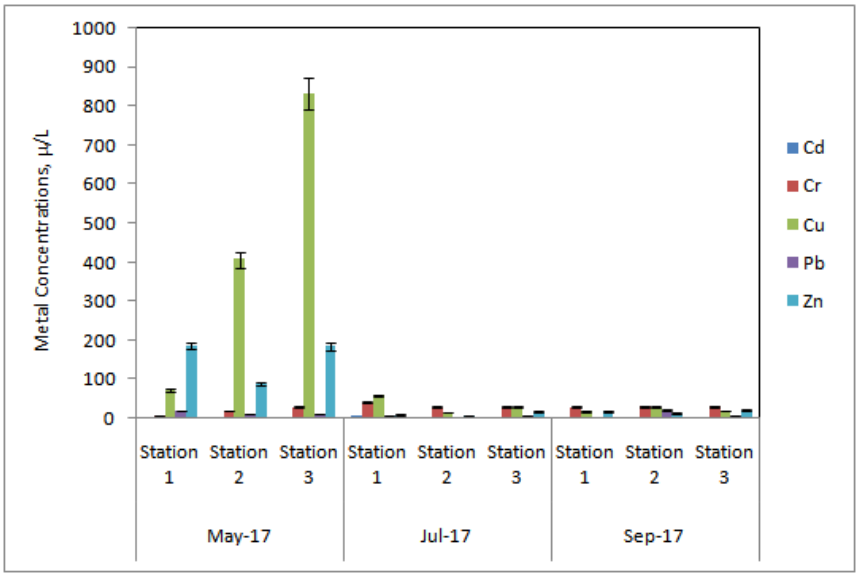

Figure 3. Trace metal concentrations in pore waters of Sapangdaku River and Tañon Strait Coastline

The dominance of copper is consistent with the geological and mining legacy of Toledo, which has resulted in extensive mined-out lands and soils enriched in copper with acidic properties. The relatively low pH and reducing conditions of sediments in this basin enhance copper solubility, allowing greater partitioning into pore water compared to other metals. Previous reports of highly acidic soils (pH ~2.5) with Cu concentrations ranging from 154 to 638 mg/kg [1] and sediments with Cu levels exceeding 700 ppm [2] support this enrichment. Compared with other regions, the severity in Toledo is striking: Deriner Dam Lake, Turkey, recorded only 9.0 µg/L Cu [22], while Shaocun River, China (123 µg/L) [13], and Cipeles River, Indonesia (322 µg/L) [23], still fall well below the values observed here. From a toxicological standpoint, the observed Cu levels are ecologically alarming. The U.S. EPA chronic water quality criterion for Cu is 16 µg/L, which was exceeded by more than an order of magnitude at all sites. IWCTU values also confirmed Cu toxicity risks across stations, while Cd exceeded thresholds at Station 1. Such exceedances suggest adverse impacts on aquatic organisms, including gill damage, reduced growth, and impaired reproduction in fish and invertebrates. Because pore water represents the most bioavailable fraction of metals, these concentrations indicate direct exposure risks to benthic fauna. Collectively, the statistical evidence highlights the strong influence of mining-derived Cu contamination in the Sapangdaku River and highlights its potential ecological consequences for the adjacent Tañon Strait.

3.2 Metal Concentrations in Sediments of Sapangdaku River and Tañon Strait Coastline

The sediment analysis revealed that Cu was the most abundant metal at all stations, except in July 2017, when the concentrations of Cu and Zn were nearly equal. Across sampling periods, the general trend was Cu > Zn > Pb > Cr > Cd, which is consistent with previous findings from the Balamban coastline [20]. Statistical testing indicated that metal concentrations were marginally significantly different between sampling sites (p = 0.0837). However, differences in metal concentrations were highly significant ($p < 0.001$), confirming that variation in overall sediment contamination is primarily driven by the type of metal rather than the location of collection.

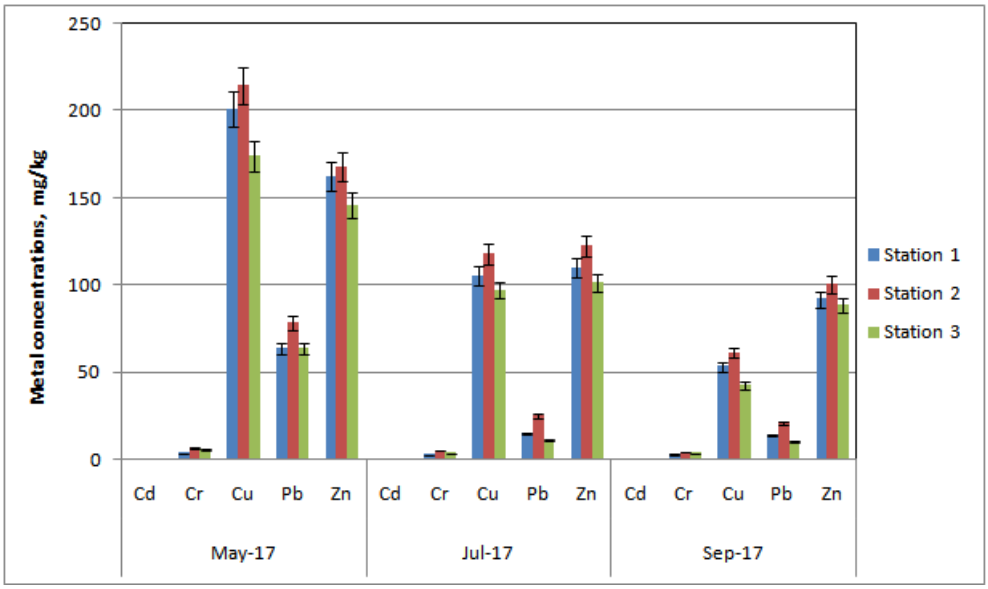

Figure 4. Heavy metal concentrations in sediments.

Copper and zinc were the dominant contributors to this variation, with Cu showing consistently higher concentrations across most stations and months, while Zn occasionally approached similar levels. Lead, chromium, and cadmium were present at much lower concentrations, contributing minimally to the observed differences. The predominance of Cu in sediments reflects the legacy of mining inputs, while elevated Zn may be linked to both natural sources and agricultural/industrial activities in the coastal zone.

Generally, higher concentrations of each metal were recorded in May 2017, which is attributed to the low water flow in May, resulting in the precipitation of the metals in the sediment and thereby increasing their

concentration [14]. This is supported by Duman and Kar [24], who reported that the combined effects of increased evaporation and decreased rainfall may indeed lead to higher metal concentrations in sediments. Considering the toxicity reference values (TRVs) proposed by the USEPA [25], Cu, Pb, and Zn in all stations exceeded the limits (16, 31, and 110 μg/L, respectively), while both Cd and Cr are below the limits. This means that the levels of the former metals in the rivers can harm the aquatic ecosystems associated with these rivers, especially after they receive urban water and wastewater, as seen in the downstream of the Tsurumi River in Japan [6].

3.3 Pore Water Toxicity Analysis

The Final chronic values (FCV) of the selected metals (Cd, Cu, Pb, and Zn) were determined in Table 2, and the IWCTU index was calculated from Eq. (1) for each metal at each river. The FCV for all metals in this study was higher compared to the values reported by Mehdizadeh et al. [26] in the pore water of Anzali wetland located in the southwestern part of the Caspian Sea.

Table 2. Hardness-dependent final chronic value (FCVMe) determined for Cd, Cu, Pb, and Zn in pore water.

Sites	$CaCO_3$, mg/L			FCV_{Cd}			FCV_{Cu}			FCV_{Pb}			FCV_{Zn}		
	May	Jul	Sep	Ma	Jul	Sep	Ma	Jul	Sep	Ma	Jul	Sep	Ma	Jul	Sep
1	4256	12775	11011	16.2	36.1	32.4	290	716	630	298	1208	1000	2508	6366	5612
2	7310	5676	15512	24.1	20.0	45.6	444	358	845	298	430	1547	3966	3205	7504
3	12987	14540	11559	36.5	39.7	33.6	726	799	657	1234	1424	1063	6455	7103	5848

Table 3 shows that the IWCTU values for Cd, Cu, Pb, and Zn in the porewater of the Sapangdaku River and Tañon Strait coastline exceeded the recommended water quality criteria set by the US Environmental Protection Agency. The IWCTU for Cu at all stations was>1, as was the IWCTU value of Cd at Station 1.

Table 3. Toxic unit analysis results for the pore water metals in Sapangdaku River and Tañon Strait Coastline

Site	Mean Interstitial Water Criteria Toxicity Unit (IWCTU)				ΣIWCTU	NI	Impact grade
	Cd	Cu	Pb	Zn			
1	**2.24**	**1.13**	0.049	0.32	3.53	1.58	Slight
2	0.39	**2.43**	0.77	0.17	2.42	1.72	Slight
3	0.27	**1.51**	0.32	0.41	1.58	1.08	slight

Data in bold exceeded the corresponding water quality criteria recommended by EPA (2002)

The IWCTU values indicated that copper posed potential toxicity risks across all stations, while cadmium exceeded thresholds at Station 1. Notably, the mean Cu concentrations in pore water (173 μg/L, peaking at 831 μg/L) were more than ten times higher than the U.S. EPA chronic water quality criterion of 16 μg/L for aquatic life [25]. Even the lowest Cu values observed in this study exceeded the EPA guideline by several orders of magnitude, highlighting the severity of Cu enrichment in the system. By contrast, Zn and Pb generally remained below their respective thresholds, and Cd exceedances were limited to Station 1. When compared to other international benchmarks, the ecological risk remains evident. The Canadian Council of Ministers of the Environment (CCME) sets a chronic guideline for Cu at 2–4 μg/L (depending on hardness), meaning that the observed values in the Sapangdaku River were up to two orders of magnitude higher. Similarly, the Australian and New Zealand Guidelines for Fresh and Marine Water Quality (ANZG, 2018) recommend Cu concentrations not exceeding 1.4 μg/L in freshwater, far below the levels measured in this study. Philippine national standards (DENR DAO 2016-08) set a Class C freshwater guideline for Cu at 50

µg/L, which was also consistently exceeded at all stations. Mehdizadeh et al. [26] reported Nemeraw Index values below 1 for the Anzali wetland, indicating no adverse impacts. While the release of heavy metals from sediment into the water column appears to be limited, transformation and migration processes require further investigation. The potential toxicity near surface sediments is likely due to the release of metals from biogenic material during aerobic degradation of organic matter [27]. These comparisons highlight the toxicological significance of the findings: pore water Cu concentrations not only surpass U.S. EPA thresholds but also significantly exceed those of Canadian, Australian/New Zealand, and Philippine water quality criteria. Given that pore water represents the most bioavailable fraction of metals, these exceedances suggest substantial risks to benthic organisms and higher trophic levels, with likely consequences for ecological health and fisheries in the Sapangdaku River and adjacent Tañon Strait.

3.4 Sediment Toxicity Risk Assessment of Metal Contamination

3.4.1 Geo-accumulation Index, Igeo.

The Igeo values revealed clear differences among metals and sampling months. Copper showed the highest contamination, with Igeo values ranging from 2.1 to 3.4 in May and 1.5 to 2.8 in July, indicating *moderate to high contamination* according to Müller's [28] classification. Lead also exhibited contamination during these months, with Igeo values ranging from 1.0 to 1.6 in May and from 0.7 to 1.2 in July, corresponding to *moderate contamination*. By September, Igeo values for both Cu and Pb had declined (<1.0), indicating dilution effects from increased rainfall and seasonal sediment flushing. In contrast, cadmium and chromium recorded Igeo values consistently below zero throughout all sampling periods, indicating that they are *uncontaminated*. Both source and geochemical behavior can explain this pattern. Cd inputs are likely minimal in the Toledo basin compared to Cu and Zn, as there are no major anthropogenic Cd sources reported in the area. For Cr, its strong affinity for sediment particles and tendency to form stable mineral phases reduce its mobility and bioavailability, keeping concentrations near natural background levels. These findings suggest that Cu and Pb are the primary contaminants of concern, driven by mining-derived inputs and industrial activities, while Cd and Cr remain at or near geochemical background levels. The dominance of Cu is consistent with the area's mining legacy and acidic sediment conditions, which enhance its solubility and accumulation. This emphasizes the need to prioritize ecological risk assessments for Cu and Pb, while acknowledging that not all trace metals contribute equally to sediment contamination in the Sapangdaku River and Tañon Strait.

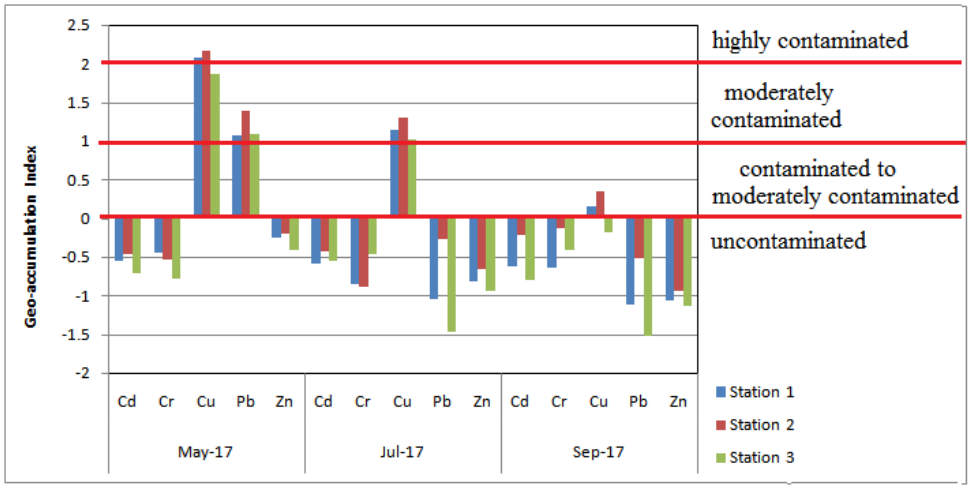

Figure 5. Geoaccumulation index (Igeo) values of heavy metals in the Tañon Strait.

3.4.2 Contamination factor, CF.

The CF values for all metals followed the order Cu > Pb > Zn > Cd > Cr, as shown in Figure 6. According to Hakanson's classification, CF < 1 indicates *low contamination*, 1–3 *moderate*, 3–6 *considerable*, and >6 *very high contamination*. In this study, copper consistently showed the highest CF values, reaching 6.2 at Station 2 in May, which falls into the *very high contamination* category. Pb also exhibited *considerable contamination* in May, with CF values between 3.1 and 4.8 across stations. By contrast, Zn recorded CF values of 1.8–2.4 in May,

corresponding to *moderate contamination*, while Cd and Cr remained below 1 throughout, indicating *low contamination*. The CF results confirm Cu and Pb as the dominant pollutants of concern, with Zn contributing moderately, particularly in May. The temporal variation reflects both local mining and industrial activities, as well as seasonal hydrological conditions. Meanwhile, Cd and Cr levels remain near background values, indicating that their ecological risks are minimal compared to those of the other metals in the Sapangdaku River and Tañon Strait.

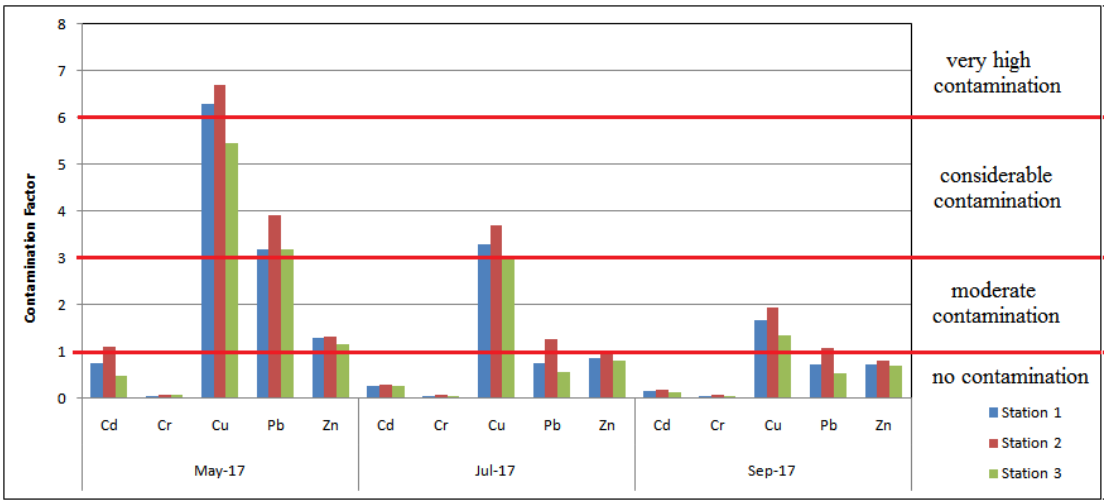

Figure 6. Contamination factor (CF) values of heavy metals in Tañon strait sediments.

3.4.3 Pollution Load Index.

Figure 7 shows the PLI values, which provide a composite measure of sediment quality by integrating CF values across metals; a PLI value greater than 1 indicates progressive site deterioration. In this study, only Station 2 in May recorded a PLI above 1 (1.23), signifying overall pollution pressure. This elevated value was primarily driven by copper, which showed very high contamination (CF > 6), and was further reinforced by *considerable contamination* from Pb (CF > 3). Zinc, while only *moderate* (CF ~2), also contributed to the cumulative index, whereas Cd and Cr remained negligible. Thus, the exceedance of PLI > 1 at Station 2 reflects the combined effects of multiple metals, with Cu as the dominant contributor. When compared to other regional and global studies, the severity at Station 2 is noteworthy but not unprecedented. For example, Mohiuddin et al. [5] reported PLI values ranging from 1.1 to 2.8 in downstream sections of urban rivers in Japan, while Islam et al. [14] documented values between 1.2 and 3.5 in contaminated river sediments in Bangladesh. In contrast, relatively unpolluted river systems typically exhibit PLI < 1, as observed in French riverine sediments by Louriño-Cabana et al. [11]. Locally, in Alburo and Villegas [29], a PLI of 41 was reported for Station 3 of the Lahug River in Cebu, attributed to intense urban activities, underscoring the potential for extreme contamination in urbanized catchments. By comparison, Villacarlos et al. [30] reported PLI values of ~2.3 in April and ~2.45 in November 2018 for the Balamban Coast, Cebu, Philippines, indicating moderate but persistent metal pollution in a coastal environment adjacent to industrial activities. Taken together, the PLI analysis highlights Station 2 in May as the site of the most significant ecological concern. The combined effect of elevated Cu, Pb, and Zn emphasizes the need for targeted monitoring at this estuarine location, which serves as both a sink for upstream contamination and a conduit for pollutant transport into the Tañon Strait.

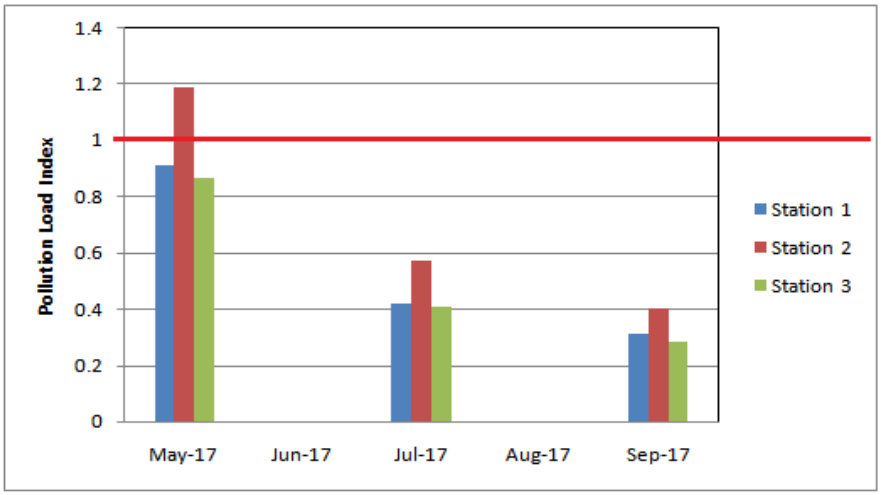

Figure 7. Pollution load index value of heavy metals in Tañon strait sediments.

3.5 Fish Analysis

Several different fish species were collected, with a maximum of four species available in situ in all three sampling sites in July 2017. The four fish species were identified by the curator of the Marine Biological Collection, Department of Biology, University of San Carlos, based on their visible external characteristics, as Mugil cephalus Linnaeus, Trichiurus lepturus Linnaeus, Strong*ylura leiura*, and *Eubleekeria jonesi*.

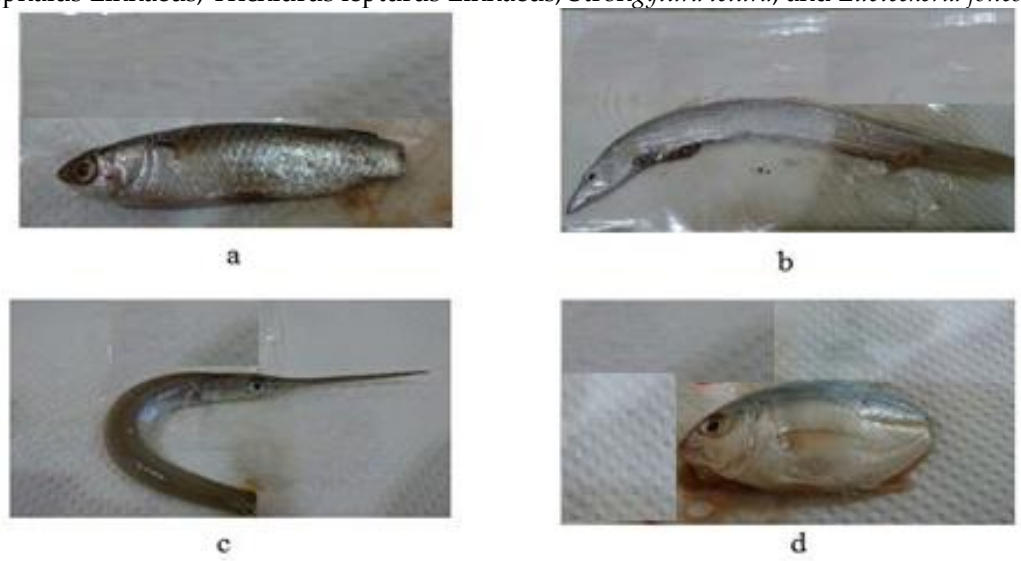

Figure 8. Identification of fish species: (a) Mugil cephalus Linneaus, (b) Trichiurus lepturus Linneaus, (c) Stronggylura leiura, and (d) Eubleekeria jonesi.

3.5.1 Heavy Metal Concentration in Fishes.

The metal content analysis of fish samples, presented in Figure 9, revealed significantly high accumulation levels of Cu and Zn across all species. The mean metal concentrations followed a descending order: Zn > Cu > Cd > Cr = Pb, with Pb and Cr below the detection limit of 0.01 mg/kg. Minor variations in metal concentrations were observed between sites, likely due to the mobility of fish between locations. As highlighted by Kalay and Canli [31], non-essential metals such as Pb, Cr, and Cd generally occur at very low levels.

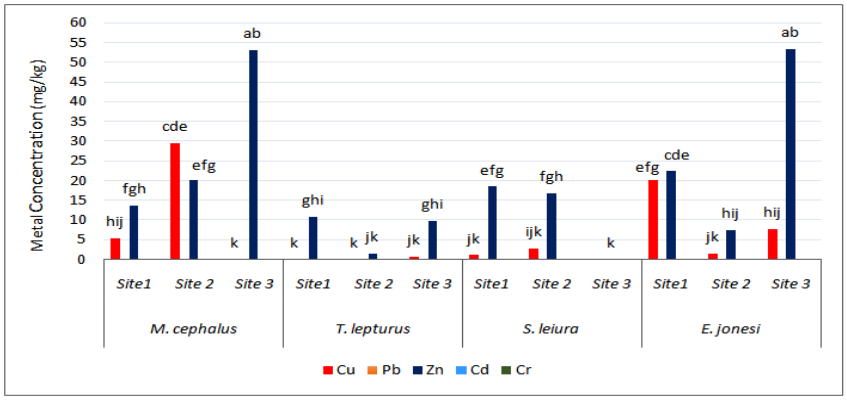

Figure 9. Heavy metal accumulation of the four fish species. Data are expressed in mg/kg. Different letters show significant differences in the concentration of Cu and Zn among species and sites.

3.5.1.1 Zinc

Zn levels in fish species were highest in *M. cephalus* (13.6–53.1 mg/kg) and *E. jonesi* (7.5–53.4 mg/kg), with lower levels detected in *T. lepturus* and *S. leiura* (below detection to 18.5 mg/kg). The elevated Zn levels in *M. cephalus* and *E. jonesi* can be explained by their feeding modes and habitat use. *M. cephalus* is a benthic detritivore, ingesting sediments and organic detritus where Zn accumulates, while *E. jonesi*, with its relatively larger muscle mass and benthic feeding habits, tends to store more trace metals. Both species are frequently found in sediment-rich estuarine zones, increasing their exposure to Zn-laden particulates compared to more pelagic feeders such as *T. lepturus*. Statistical analysis revealed significant differences in Zn concentrations between sites and species ($P < 0.05$), except for the comparison between *T. lepturus* and *S. leiura*. Although Zn levels were below the permissible limits set by Canadian (100 mg/kg), Hungarian (80 mg/kg), and Australian (150 mg/kg) standards, they exceeded the FAO limit of 40 mg/kg for potable fish, which could restrict their export potential and raise concerns about long-term consumption risks for local communities. Chronic dietary exposure to elevated zinc, while less acutely toxic than copper or lead, may still contribute to gastrointestinal distress, immune dysfunction, and metabolic imbalances in humans. Compared with other studies, Zn accumulation in the Sapangdaku basin was lower than that reported for *E. suratensis* in Indian reservoirs (98–303 mg/kg) but higher than values observed in some Philippine freshwater systems (e.g., *P. reticulata* from Butuanon River, 16.4–140 mg/kg) [32]. Thus, while not the highest globally, the Zn levels detected here are ecologically and commercially significant, particularly for species closely linked to benthic habitats.

3.5.1.2 Copper

River basin. As shown in earlier sections, pore water Cu concentrations reached up to 831 μg/L at Station 3 and sediments exceeded 700 ppm near the tailings outfall [2], both far above background levels and indicative of long-term mining discharges. The high Cu accumulation in fish, therefore, aligns with the extreme enrichment of surrounding sediments and pore water, confirming that benthic and detritivorous feeders, such as M. cephalus, are particularly vulnerable to exposure. The mean Cu concentrations in fish exceeded international food safety limits by approximately 12 times (mean, not maximum) relative to the WHO (3 mg/kg) [33], FAO (4 mg/kg) [34], EU (1 mg/kg) [35], and FEPA (1.3 mg/kg) [36] permissible thresholds. This consistent exceedance underscores a clear risk to food safety, with potential implications for both local consumption and compliance with export standards. While copper (Cu) is an essential trace element, excessive intake can disrupt gastrointestinal and hepatic functions in humans, and the concentrations measured in this study exceed tolerable dietary levels. From an ecological perspective, the Cu levels detected are high enough to elicit sub-lethal physiological stress in fish. Previous studies have demonstrated that chronic Cu exposure causes gill damage, impaired ion regulation, oxidative stress, and reduced growth rates in freshwater and estuarine fish [46, 44]. Similar Cu accumulation patterns were reported in *C. anguillari* and *O. niloticus* from the Nile River (22.87 and 18.37 mg/kg, respectively) and in Esox lucius and Abramis brama in Polish lakes (0.14–7.76 mg/kg) [38]. However, the concentrations in the present study were markedly higher. These effects

are consistent with the elevated metallothionein induction and genotoxic responses observed here, supporting the conclusion that Cu contamination in the Sapangdaku River is both bioaccumulative and biologically active at the molecular level.

Table 4. Permissible limit of metals set by different health organizations and toxicology values.

Standards	Cu (mg/kg)	Cd (mg/kg)	Cr (mg/kg)	Pb (mg/kg)	Zn (mg/kg)
FAO (2000)	4.00	0.50	1.00	6.00	40.0
WHO (2006)	3.00	0.50	0.15	2.00	-
EU (2001)	1.00	-	1.00	-	-
FEPA (2003)	1.30	-	0.15	2.00	-

3.5.1.3 Cadmium

Cadmium (Cd) concentrations in the sampled fish ranged from below the detection limit (<0.01 mg/kg) to 0.111 mg/kg in M. cephalus, 0.099 mg/kg in E. jonesi, 0.056 mg/kg in T. lepturus, and 0.052 mg/kg in S. leiura. Statistical analysis indicated no significant differences in Cd levels between fish species or sampling sites. Importantly, all values remained within the acceptable limits established by WHO and FAO (0.5 mg/kg) [32,33], suggesting no immediate food safety risks from Cd exposure in fish harvested from the Sapangdaku River basin. Both source and geochemical factors can explain the consistently low Cd levels. Unlike Cu and Zn, which are heavily influenced by mining discharges in Toledo, there are no major anthropogenic Cd inputs documented in the catchment. Cd also exhibits a strong affinity for sulfide phases under reducing conditions, which immobilizes it in sediments and reduces its bioavailability to aquatic organisms. This explains why Cd remained below toxic thresholds despite its well-recognized status as a highly toxic, non-essential metal. When compared globally, the Cd levels in this study are relatively low. Fish from contaminated freshwater systems often show much higher concentrations, such as Oreochromis niloticus from Egyptian rivers (0.2–1.2 mg/kg) or commercial species from Indian reservoirs (0.3–0.9 mg/kg) [37]. In contrast, the values reported here (<0.12 mg/kg) are closer to background levels typical of less polluted systems. Thus, while Cu and Zn clearly drive contamination risk in the Sapangdaku basin, Cd appears to pose minimal ecological or human health risk at present.

3.6 Metallothionein Assay.

Metallothionein (MT), a key metal-detoxifying protein in fish, was quantified to assess species-specific responses to heavy metal exposure. The highest MT levels were observed in *M. cephalus* (299.16 μg/g at Site 2), followed by *E. jonesi* (200.02 μg/g at Site 1), while *T. lepturus* and *S. leiura* exhibited comparatively lower responses, as shown in Figure 10. Statistical analysis confirmed significant variation in MT levels among species and sites ($p < 0.0001$), consistent with differences in both exposure pathways and physiological stress responses. These results align with findings in *O. niloticus* from the metal-contaminated Barra Mansa River, Brazil, where Linde and Garcia-Vazquez [18] reported MT values of 212.63 μg/g, suggesting that benthic-associated species generally show higher induction under polluted conditions.

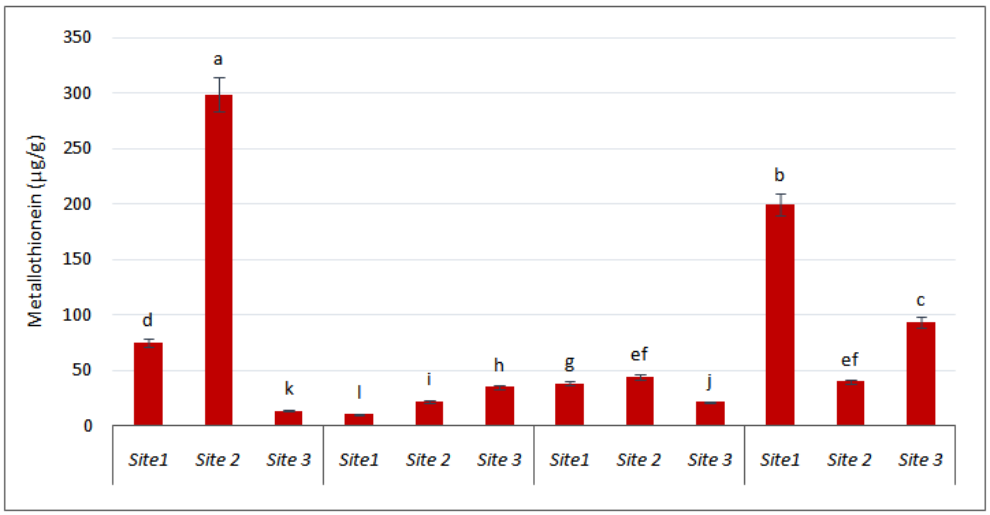

Figure 10. MT levels in the four fish species. Data are expressed in µg/g. Different letters show significant differences in the concentration of Cu and Zn among species and sites.

In addition to intrinsic metabolic differences, feeding ecology and habitat use strongly influence MT induction. Benthic detritivores such as *M. cephalus* ingest sediments and organic detritus that contain bioavailable metals, directly increasing their internal metal burden and stimulating MT production. Similarly, *E. jonesi*, which forages in benthic habitats and has larger muscle mass for storage, also exhibited elevated MT levels. In contrast, more pelagic feeders, such as T. lepturus, are less exposed to contaminated sediments, which explains their comparatively lower MT responses. These species-specific differences are consistent with earlier reports that benthic and detritivorous fish accumulate metals more efficiently due to direct interaction with sediment [30]. The pronounced MT induction in *M. cephalus*, therefore, reflects both its ecological niche and dietary habits. By resuspending and ingesting fine sediments at the estuary, this species is exposed to the elevated Cu and Zn concentrations documented in pore water and sediments (Sections 3.1 and 3.2). This sediment-associated exposure pathway likely explains why *M. cephalus* consistently showed the strongest biomarker response, reinforcing its role as a reliable sentinel species for monitoring heavy metal contamination in estuarine environments. Similar conclusions have been drawn in previous biomonitoring studies where high MT induction corresponded to Cu enrichment and sediment contact [20, 18].

3.7 Genotoxicity

Figure 11 illustrates genotoxicity parameters affected by excessive heavy metal uptake in fish. The micronucleus assay, widely used to measure genotoxicity in both laboratory and field conditions (Carrasco et al. [40]), reveals the formation of nuclear abnormalities such as lobed, blebbed, and notched nuclei in fish erythrocytes. These abnormalities result from exposure to environmental and chemical contaminants with cytotoxic, genotoxic, mutagenic, or carcinogenic activity. Micronuclei, shown in Figure 11a, form during cellular division and reflect cytogenetic effects, including the loss of chromosomal fragments or whole chromosomes that are excluded from the main nucleus during anaphase. The MN test in fish can detect clastogenic and aneugenic effects of environmental agents in aquatic media. Since teleost erythrocytes are nucleated, MN are counted in fish erythrocytes to assess clastogenic activity (Al-Sabti and Metcalfe [41]). Additionally, NA, including blebbed, lobed, and notched nuclei, as well as bi-nucleated cells, have been identified as potential indicators of genotoxicity [42]. While the mechanisms behind NA formation (shown in Figure 11b) are not fully understood, these abnormalities are regarded as indicators of genotoxic damage, complementing MN scoring in routine genotoxicity assessments.

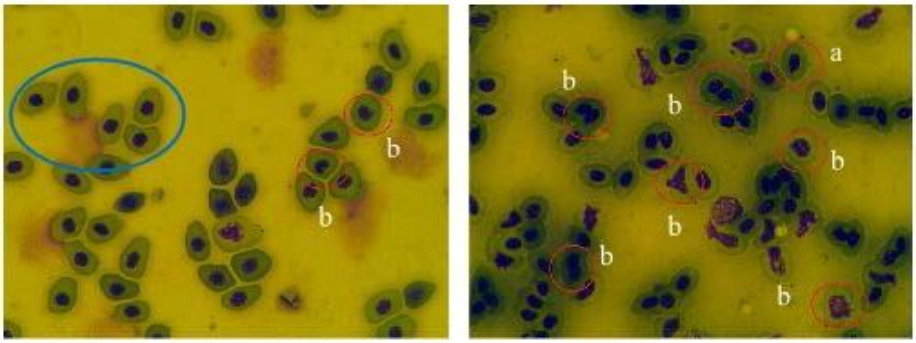

Figure 11. Erythrocytes were studied for the Environmental Genotoxicity test. Cells inside the blue circle are normal cells. Cells inside the red circles are (a) micronuclei and (b) nuclear abnormalities.

3.7.1 Micronuclei Test.

The average number of micronuclei (MN) varied across species and sampling sites, ranging from 0.111 to 3.667 per 1000 erythrocytes for *M. cephalus*, 0.000 to 0.0667 per 1000 erythrocytes for *T. lepturus*, 0.222 to 0.0889 per 1000 erythrocytes for *S. leiura*, and 0.778 to 2.556 per 1000 erythrocytes for *E. jonesi*. Elevated Cu concentrations were significantly correlated with increased MN formation ($R > 0.98$, $p < 0.05$), consistent with earlier reports linking Cu exposure to clastogenic and aneugenic effects in fish erythrocytes [43, 15]. The highest MN frequencies were observed in *M. cephalus* at Site 2 and *E. jonesi*, which aligns with their benthic feeding habits and higher accumulation of Cu and Zn.

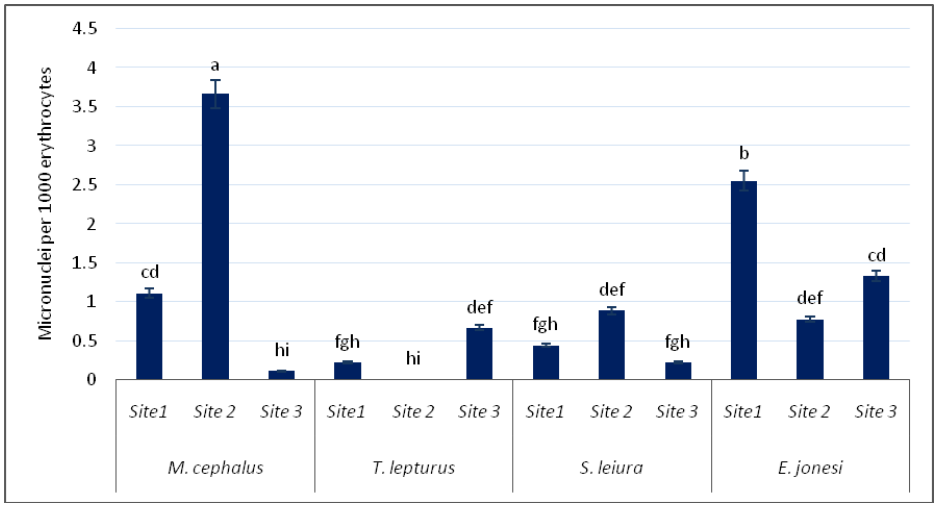

Figure 12. Frequency of MN in the erythrocytes of fish between the three sites. Data are expressed in the number of micronuclei formed per 100 erythrocytes. Different letters indicate significant differences in the number of micronuclei among species and sites.

Figure 12 illustrates the frequency of MN per 1000 erythrocytes, with the highest MN frequencies observed in *M. cephalus* at site 2 and *E. jonesi*, which aligns with the MT response and metal accumulation. The results show that as metal uptake increases, the MN frequency per 1000 erythrocytes also increases. These findings are consistent with those of Stankevičiūtė et al. [44], who reported a similar trend in Oncorhynchus mykiss exposed to Cu and Zn, where the highest MN frequency observed was 0.67 per 1000 erythrocytes, further confirming that higher metal accumulation correlates with increased MN formation.

3.7.2 Nuclear Abnormalities.

Figure 13 illustrates the impact of Cu concentration on nuclear abnormalities in fish, revealing significant differences between species and sampling sites. The study reveals that higher Cu concentrations are associated with a greater number of nuclear abnormalities, exhibiting a strong correlation ($R > 0.98$, $P < 0.05$). The frequency of nuclear abnormalities per 1000 erythrocytes ranged from 1.556 to 19.333 in *M. cephalus*,

1.222 to 1.556 in *T. lepturus*, 1.778 to 5.778 in *S. leiura*, and 4.778 to 11.889 in *E. jonesi*. NA frequencies were strongly correlated with Cu levels ($R > 0.98$, $p < 0.05$), reflecting higher sensitivity to metal stress. These findings are in agreement with previous studies that reported elevated NA frequencies under heavy metal exposure, often exceeding MN responses [44, 45].

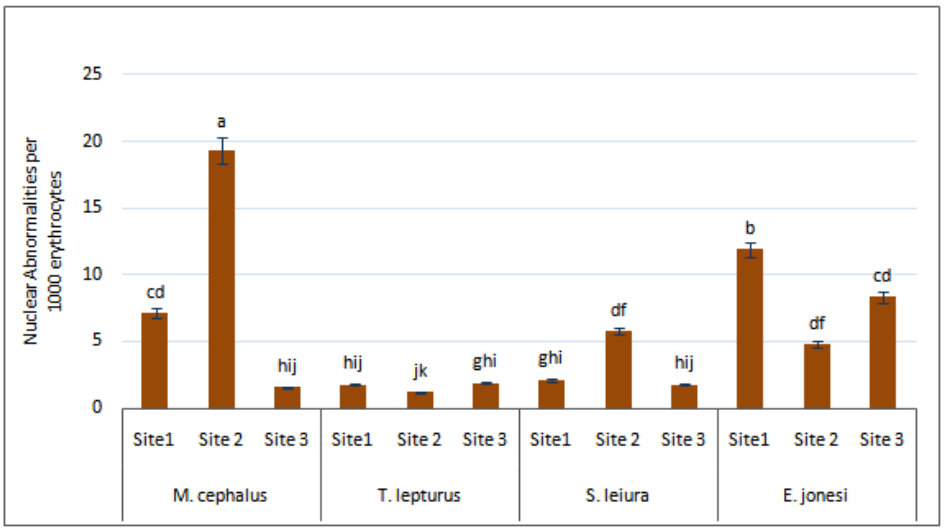

Figure 13. Frequency of NA in the erythrocytes of fish between the three sites. Data are expressed in the number of nuclear abnormalities per 100 erythrocytes. Different letters indicate significant differences in the number of nuclear abnormalities among species and sites.

The results in this study show that both MN and NA frequencies were significantly higher at higher Cu concentrations, which aligns with similar findings in other studies. For instance, Stankevičiūtė et al. [44] reported the highest NA frequency of 14.33 per 1000 erythrocytes in *Oncorhynchus mykiss* exposed to Cu and Zn, while [45] found the highest NA frequency of 6.22 per 1000 erythrocytes in *Parablennius sanguinolentus* exposed to heavy metals. These studies also observed that as metal uptake increased, so did the frequency of NA.

The present study also showed that the increase in MN and NA was more pronounced at higher Cu concentrations, with NA being more frequently observed than MN. This observation is consistent with previous studies, such as [45], where *Prochilodus scrofa* exposed to high Cu concentrations displayed elevated MN and NA frequencies. Both MN and NA frequencies showed a significant correlation with MT levels ($R > 0.98$, $P < 0.05$), indicating that the higher the MT levels, the greater the number of MN formed in the erythrocytes of the fish. This relationship likely stems from the correlation between MT and Cu levels; as Cu levels increase, so do MT levels, leading to a corresponding rise in MN formation.

Taken together, NA were consistently more frequent than MN across all species, suggesting that NA formation may be a more sensitive or earlier genotoxic indicator of heavy metal stress. While MN reflect permanent chromosomal damage caused by clastogenic or aneugenic events, NA are thought to result from disturbances in the mitotic spindle or nuclear envelope stability, which may occur more rapidly after exposure [42]. The predominance of NA in *M. cephalus* and *E. jonesi*, therefore, supports the idea that benthic feeders not only accumulate more metals but also manifest earlier cytogenetic stress responses. This comparative evidence highlights the utility of using both MN and NA assays together, with NA potentially serving as a more sensitive biomarker for detecting early genotoxic effects in metal-polluted environments.

4. Conclusions

This study demonstrated that the Sapangdaku River and its adjacent Tañon Strait coastline remain heavily influenced by mining-derived copper contamination, with pore water and sediment analyses confirming that copper is the dominant pollutant, followed by zinc and lead. Pore water Cu concentrations exceeded U.S. EPA, CCME, ANZG, and DENR criteria by more than an order of magnitude. At the same time,

sediment indices (Igeo, CF, PLI) consistently identified Cu as the primary driver of ecological risk, with localized contributions from Pb and Zn. In contrast, Cd and Cr remained close to background levels, indicating limited anthropogenic input and low bioavailability. Fish analyses revealed substantial bioaccumulation of Cu and Zn, particularly in benthic feeders such as *M. cephalus* and *E. jonesi*, which also exhibited the strongest biomarker responses. The induction of metallothionein in liver tissues and elevated frequencies of micronuclei and nuclear abnormalities in erythrocytes confirmed that metal contamination was biologically active, inducing detoxification mechanisms and genotoxic stress. Notably, nuclear abnormalities occurred more frequently than micronuclei, suggesting their utility as an earlier or more sensitive biomarker of heavy metal exposure. Overall, the integration of chemical and biological endpoints provides compelling evidence of ongoing ecological stress in the Sapangdaku River basin. The findings underscore the importance of ongoing biomonitoring and enhanced regulatory oversight to safeguard aquatic ecosystems and protect communities that rely on these resources. As *M. cephalus* emerged as a reliable sentinel species due to its sediment-feeding habits and consistent biomarker responses, its use in long-term monitoring could support environmental management and policy decisions aimed at mitigating the impacts of legacy mining and associated industrial activities in Toledo City. These findings also revealed the utility of MT, MN, and NA as sensitive indicators for assessing metal contamination and its potential ecological risks in aquatic environments.

5. Acknowledgements

The authors would like to thank the Department of Chemistry, University of San Carlos, Cebu City, Philippines, and the Biodiversity, Environment and Natural Resources Research Center, Cebu Technological University, Argao, Cebu, Philippines, for the technical support provided.

Author Contributions: Conceptualization, L.M.G. Villegas and R.P. Alburo; methodology, J.J.C. Leyson, L.M. Veloso, H.M. Alburo, , L.M.G. Villegas and R.P. Alburo.; software, J.J.C. Leyson; validation, J.J.C. Leyson and L.M.G. Villegas; formal analysis, J.J.C. Leyson and L.M.G. Villegas.; investigation, J.J.C. Leyson, L.M. Veloso, H.M. Alburo, , L.M.G. Villegas and R.P. Alburo.; resources, H.M. Alburo and R.P. Alburo; data curation, J.J.C. Leyson, L.M.G. Villegas and R.P. Alburo; writing— J.J.C. Leyson, L.M.G. Villegas and R.P. Alburo; writing— L.M.G. Villegas and R.P. Alburo, X.X.; visualization, J.J.C. Leyson; supervision, L.M.G. Villegas and R.P. Alburo; project administration, H.M. Alburo and R.P. Alburo; funding acquisition, H.M. Alburo and R.P. Alburo. All authors have read and agreed to the published version of the manuscript.

Funding: This research was funded by the BIODIVERSITY, ENVIRONMENTAL, AND NATURAL RESOURCES CENTER (BENRC) - CEBU TECHNOLOGICAL UNIVERSITY, ARGAO CAMPUS, CEBU, PHILIPPINES.

Conflicts of Interest: The authors declare no conflict of interest.

References

[1] Aggangan, N.; Pampolina, N.; Cadiz, N.; Raymundo, A. Assessment of Plant Diversity and Associated Mycorrhizal Fungi in the Mined-out Sites of Atlas Mines in Toledo City, Cebu for Bioremediation. *J. Environ. Sci. Manag.* **2015**, *18*(1), 71–86. https://doi.org/10.47125/jesam/2015_1/08

[2] Lo, J. M.; Sakamoto, H. Heavy metals distribution in the surface sediments from central west coast of Cebu, Philippines. *J. Sedimentol. Soc. Jpn.* **2005**, *62*(62), 31–41. https://doi.org/10.4096/jssj1995.62.31

[3] Sanchez, J. M. P.; Picardal, M.; Libres, M. T.; Pineda, H. A.; Paloma, M. L. B.; Librinca, J. M.; Raymund, R.; Ramayla, S. P.; Armada, R. L.; Picardal, J. P. Characterization of a river at risk: the case of Sapangdaku River in Toledo City, Cebu, Philippines. *AIMS Environ. Sci.* **2020**, *7*(6), 559–574. https://doi.org/10.3934/environsci.2020035

[4] Wiklund, J. A.; Hall, R. I.; Wolfe, B. B.; Edwards, T. W.; Farwell, A. J.; George Dixon, D. Use of pre-industrial floodplain lake sediments to establish baseline river metal concentrations downstream of Alberta oil sands: a new approach for detecting pollution of rivers. *Environ. Res. Lett.* **2014**, *9*(12), 124019. https://doi.org/10.1088/1748-9326/9/12/124019

[5] Mohiuddin, K. M.; Zakir, H. M.; Otomo, K.; Sharmin, S.; Shikazono, N. Geochemical distribution of trace metal pollutants in water and sediments of downstream of an urban river. *Int. J. Environ. Sci. Technol.* **2009**, *7*(1), 17–28. https://doi.org/10.1007/bf03326113

[6] van Leeuwen, C. J.; Dan, N. P.; Dieperink, C. The Challenges of Water Governance in Ho Chi Minh City. *Integr. Environ. Assess. Manag.* **2015**, *12*(2), 345–352. https://doi.org/10.1002/ieam.1664

[7] Ramayla, S.; Picardal, M.; Sanchez, J. M.; Librinca, J.; Pineda, H.; Libres, M.; Paloma, M. L.; Caturza, R. R.; Picardal, J. Phytoplankton Diversity and Macroinvertebrate Assemblage as Pollution Indicators in Sapangdaku River, Toledo City, Cebu, Philippines. *Int. J. Biosci.* **2021**, *18* (4), 38–46.

[8] Azcue, J. M.; Rosa, F.; Mudroch, A. Distribution of Major and Trace Elements in Sediments and Pore Water of Lake Erie. *J. Great Lakes Res.* **1996**, *22*(2), 389–402. https://doi.org/10.1016/s0380-1330(96)70964-4

[9] Kalnejais, L. H.; Martin, W. R.; Bothner, M. H. Porewater dynamics of silver, lead and copper in coastal sediments and implications for benthic metal fluxes. *Sci. Total Environ.* **2015**, *517*, 178–194. https://doi.org/10.1016/j.scitotenv.2015.02.011

[10] Sterckeman, T.; Douay, F.; Proix, N.; Fourrier, H. Vertical distribution of Cd, Pb and Zn in soils near smelters in the North of France. *Environ. Pollut.* **2000**, *107*(3), 377–389. https://doi.org/10.1016/s0269-7491(99)00165-7

[11] Louriño-Cabana, B.; Lesven, L.; Charriau, A.; Billon, G.; Ouddane, B.; Boughriet, A. Potential risks of metal toxicity in contaminated sediments of Deûle river in Northern France. *J. Hazard. Mater.* **2011**, *186* (2-3), 2129–2137. https://doi.org/10.1016/j.jhazmat.2010.12.124

[12] Liu, W. X.; Coveney, R. M.; Chen, J. L. Environmental quality assessment on a river system polluted by mining activities. *Appl. Geochem.* **2003**, *18*(5), 749–764. https://doi.org/10.1016/s0883-2927(02)00155-5

[13] Zhu, X.; Shan, B.; Tang, W.; Li, S.; Rong, N. Distributions, fluxes, and toxicities of heavy metals in sediment pore water from tributaries of the Ziya River system, northern China. *Environ. Sci. Pollut. Res. Int.* **2015**, *23*(6), 5516–5526. https://doi.org/10.1007/s11356-015-5709-7

[14] Islam, M. S.; Ahmed, M. K.; Raknuzzaman, M.; Habibullah -Al- Mamun, M.; Islam, M. K. Heavy metal pollution in surface water and sediment: A preliminary assessment of an urban river in a developing country. *Ecol. Indic.* **2015**, *48*, 282–291. https://doi.org/10.1016/j.ecolind.2014.08.016

[15] Bacolod, E. T.; Uno, S.; Tanaka, H.; Koyama, J. Micronuclei and other nuclear abnormalities induction in erythrocytes of marbled flounder, Pleuronectes yokohamae, exposed to dietary nitrated polycyclic aromatic hydrocarbons. *Kankyou Dokusei Gakkaishi/Kankyō Dokusei Gakkaishi* **2013**, *16*(2), 79–89. https://doi.org/10.11403/jset.16.79

[16] Al-Sabti, K.; Metcalfe, C. D. Fish micronuclei for assessing genotoxicity in water. *Mutat. Res. Genet. Toxicol.* **1995**, *343*(2-3), 121–135. https://doi.org/10.1016/0165-1218(95)90078-0

[17] Fenech, M.; Chang, W. P.; Kirsch-Volders, M.; Holland, N.; Bonassi, S.; Zeiger, E. HUMN project: detailed description of the scoring criteria for the cytokinesis-block micronucleus assay using isolated human lymphocyte cultures. *Mutat. Res. Genet. Toxicol. Environ. Mutagen.* **2003**, *534*(1-2), 65–75. https://doi.org/10.1016/s1383-5718(02)00249-8

[18] Linde, A. R.; Garcia-Vazquez, E. A simple assay to quantify metallothionein helps to learn about bioindicators and environmental health. *Biochem. Mol. Biol. Educ.* **2006**, *34*(5), 360–363. https://doi.org/10.1002/bmb.2006.494034052653

[19] Pulatsü, S.; Topçu, A. Review of 15 Years of Research on Sediment Heavy Metal Contents and Sediment Nutrient Release in Inland Aquatic Ecosystems, Turkey. *J. Water Resour. Prot.* **2015**, *07*(02), 85–100. https://doi.org/10.4236/jwarp.2015.72007

[20] Geolin, K. R. C.; Villegas, L. M. G.; Alburo, R. P. Metallothionein Response of Aninikad, Canarium Labiatum (Roding, 1798) to Heavy Metal Concentrations in Balamban Coastline, Cebu. *J. Agric. Technol. Manag.* **2021**, *24*(1), 1–12.

[21] Liu, W.; Wang, Z.; Wen, X.; Tang, H. The application of preliminary sediment quality criteria to metal contamination in the Le An River. *Environ. Pollut.* **1999**, *105*(3), 355–366. https://doi.org/10.1016/s0269-7491(99)00041-x

[22] Özşeker, K. Investigation of Sediment Pore Water Heavy Metal (Cu and Pb) Geochimistry in Deriner Dam Lake, Artvin, Turkey. *Süleyman Demirel Üniversitesi Eğirdir Su Ürünleri Fakültesi Dergisi* **2019**. https://doi.org/10.22392/egirdir.438914

[23] Wulan, D. R.; Marganingrum, D.; Yoneda, M. Distribution, source identification, and assessment of heavy metal pollution in the surface and pore waters of Cipeles River, West Java, Indonesia. *Environ. Sci. Pollut. Res.* **2020**, *27*(31), 39123–39134. https://doi.org/10.1007/s11356-020-09823-9

[24] Duman, F.; Kar, M. Temporal Variation of Metals in Water, Sediment and Tissues of the European Chup (Squalius cephalus L.). *Bull. Environ. Contam. Toxicol.* **2012**, *89*(2), 428–433. https://doi.org/10.1007/s00128-012-0679-7

[25] U.S. Environmental Protection Agency. Human Health Toxicity Values in Superfund Risk Assessments. 2015. https://www.epa.gov/risk/human-health-toxicity-values-superfund-risk-assessments (accessed 2025-09-27).

[26] Mehdizadeh, Y.; Karbassi, A. R.; Nasrabadi, T.; Sarang, A. Behavior, toxicity and diffusive flux of metals in a sediment core and pore-water from Anzali wetland. *Acta Geochim.* **2022**, *42*(2), 309–331. https://doi.org/10.1007/s11631-022-00578-3

[27] Gavriil, A. M.; Angelidis, M. O. Metal diagenesis in a shallow semi-enclosed marine system in the Aegean Sea, Greece. *Estuarine, Coastal Shelf Sci.* **2006**, *70*(3), 487–498. https://doi.org/10.1016/j.ecss.2006.06.029

[28] Müller, B.; Berg, M.; Yao, Z. P.; Zhang, X. F.; Wang, D.; Pfluger, A. How polluted is the Yangtze river? Water quality downstream from the Three Gorges Dam. *Sci. Total Environ.* **2008**, *402*(2), 232–247. https://doi.org/10.1016/j.scitotenv.2008.04.049

[29] Alburo, R. P.; Villegas, L. M. G. Ecological Risk Assessment of Heavy Metal Pollution in Surface Water and Sediment of Lahug River, Cebu, Philippines. *ASEAN J. Sci. Technol. Rep.* **2025**, *28*(3), e257492. https://doi.org/10.55164/ajstr.v28i3.257492

[30] Villacarlos, C. J. A.; Villegas, L. M. G.; Alburo, R. P. Metallothionein induction in bivalves exposed to heavy metals in sediment of the Balamban Coast, Cebu, Philippines. *Int. J. Aquat. Biol.* **2025**, *14*(2). https://doi.org/10.22034/ijab.v13i2.2425

[31] Kalay, M.; Canli, M. Elimination of Essential (Cu, Zn) and Non-Essential (Cd, Pb) Metals from Tissues of a Freshwater Fish Tilapia zilli. *TÜBİTAK Academic Journals* **2022**. https://journals.tubitak.gov.tr/zoology/vol24/iss4/11

[32] Cañete, R. C.; Villegas, L. M. G.; Castañares, J. M. Seasonal Bioaccumulation of Copper in Guppy, Poecilia reticulata (Peters) with Characterization of the Hydrophobic Fraction of Its Octanol - Water Emulsion. *KIMIKA* **2014**, *25*(1), 27–37. https://doi.org/10.26534/kimika.v25i1.27-37

[33] World Health Organization. Report on integrated risk assessment prepared for the WHO/UNEP/ILO International Programme on Chemical Safety. **2001**. https://www.who.int/publications/i/item/WHO-IPCS-IRA-01-12 (accessed 2021-11-9).

[34] Food and Agriculture Organization. Evaluation of certain food additives and contaminants. Joint FAO/WHO Expert Committee on Food additives. Geneva, World Health Organization. Report Series 922, **2000**. http://whqlibdoc.who.int/trs/WHO_TRS_922.pdf (accessed 2022-01-12).

[35] European Union. Commission Regulation as regards heavy metals, Directive, 2001/22/EC, No: 466, **2001**. https://www.ecolex.org/details/legislation/commission-regulation-ec-no-4662001-setting-maximum-levels-for-certain-contaminants-in-foodstuffs-lex-faoc034471/ (accessed 2020-10-18).

[36] Federal Environmental Protection Agency. Guidelines and standards for environmental pollution control in Nigeria. **2003**. https://leap.unep.org/en/countries/ng/national-legislation/interim-guidelines-and-standards-environmental-pollution-control (accessed 2020-10-18).

[37] Dhanakumar, S.; Solaraj, G.; Mohanraj, R. Heavy metal partitioning in sediments and bioaccumulation in commercial fish species of three major reservoirs of river Cauvery delta region, India. *Ecotoxicol. Environ. Saf.* **2015**, *113*, 145–151. https://doi.org/10.1016/j.ecoenv.2014.11.032

[38] Rajkowska, M.; Protasowicki, M. Distribution of metals (Fe, Mn, Zn, Cu) in fish tissues in two lakes of different trophy in Northwestern Poland. *Environ. Monit. Assess.* **2013**, *185*(4), 3493–3502. https://doi.org/10.1007/s10661-012-2805-8

[39] Yap, C. K.; Edward, F. B.; Emila, R. A. A.; Ainey, F. I.; Ismail, A.; Tan, S. G.; Sharizat, Y. Determination of contamination and bioavailabilities of heavy metals (Cu, Cd, Zn, Pb and Ni) in the Serdang urban lake by using guppy fish Poecilia reticulata. *Trends Appl. Sci. Res.* **2008**, *3*, 69–75. https://doi.org/10.3923/tasr.2008.69.75

[40] Carrasco, K. R.; Tilbury, K. L.; Myers, M. S. Assessment of the Piscine Micronucleus Test as an in situ Biological indicator of Chemical Contaminant Effects. *Can. J. Fish. Aquat. Sci.* **1990**, *47* (11), 2123–2136. https://doi.org/10.1139/f90-237

[41] Al-Sabti, K.; Metcalfe, C. D. Fish micronuclei for assessing genotoxicity in water. *Mutat. Res. Genet. Toxicol.* **1995**, *343* (2-3), 121–135. https://doi.org/10.1016/0165-1218(95)90078-0. [42] da Silva Souza, T.; Fontanetti, C. S. Micronucleus test and observation of nuclear alterations in erythrocytes of Nile tilapia exposed to waters affected by refinery effluent. *Mutat. Res. Genet. Toxicol. Environ. Mutagen.* **2006**, *605*(1-2), 87–93. https://doi.org/10.1016/j.mrgentox.2006.02.010

[42] Pandey, A. K.; Nagpure, N. S.; Trivedi, S. P. Evaluation of genotoxicity of profenofos to freshwater fish Channa punctatus (Bloch) using the micronucleus assay. *Afr. J. Biotechnol.* **2014**, *13*(39), 3985–3988. https://doi.org/10.5897/ajb2014.14095

[43] Stankevičiūtė, M.; Butrimavičienė, L.; Valskienė, R.; Greiciūnaitė, J.; Baršienė, J.; Vosylienė, M. Z.; Svecevičius, G. Analysis of nuclear abnormalities in erythrocytes of rainbow trout (Oncorhynchus mykiss) treated with Cu and Zn and after 4-, 8-, and 12-day depuration (post-treatment recovery). *Mutat. Res. Genet. Toxicol. Environ. Mutagen.* **2016**, *797*, 26–35. https://doi.org/10.1016/j.mrgentox.2016.01.003

[44] Ferrante, M.; Pappalardo, A. M.; Ferrito, V.; Pulvirenti, V.; Fruciano, C.; Grasso, A.; Sciacca, S.; Tigano, C.; Copat, C. Bioaccumulation of metals and biomarkers of environmental stress in Parablennius sanguinolentus (Pallas, 1814) sampled along the Italian coast. *Mar. Pollut. Bull.* **2017**, *122*(1-2), 288–296. https://doi.org/10.1016/j.marpolbul.2017.06.060

[45] Mazon, A. F.; Cerqueira, C. C. C.; Fernandes, M. N. Gill Cellular Changes Induced by Copper Exposure in the South American Tropical Freshwater Fish Prochilodus scrofa. *Environ. Res.* **2002**, *88*(1), 52–63. https://doi.org/10.1006/enrs.2001.4315.

ASEAN
Journal of Scientific and Technological Reports
Online ISSN:2773-8752

Research article

Linear Ensemble Algorithm: A Novel Meta-Heuristic Approach for Solving Constrained Engineering Problems

Phatnathee Wongsrisai[1], and Prompong Sugunnasil[2]

[1] Faculty of Engineering, Chiang Mai University, Chiang Mai, 50200, Thailand
[2] Faculty of Engineering, Chiang Mai University, Chiang Mai, 50200, Thailand
* Correspondence: prompong.sugunnasil@cmu.ac.th

Citation:
Wongsrisai, P.; Sugunnasil, P. Linear ensemble algorithm: A novel meta-heuristic approach for solving constrained engineering problems. *ASEAN J. Sci. Tech. Report.* **2025**, *28*(6), e257673. https://doi.org/10.55164/ajstr.v28i6.257673.

Article history:
Received: January 28, 2025
Revised: September 5, 2025
Accepted: September 10, 2025
Available online: October 14, 2025

Abstract: This research This study presents the Linear Ensemble Algorithm (LEAL), which couples evolutionary search with local, linear regression–based surrogates and a neighbor-guided linear combination scheme for constrained engineering problems and standard benchmarks. For single-objective problems, LEAL frequently attains or closely approaches global optima on multimodal functions such as Rastrigin and Griewank, yielding ~55–85% lower mean error than GA, DE, and PSO, and it can occasionally uncover best-known minima in engineering tasks (e.g., Pressure Vessel), indicating an ability to exploit intricate design trade-offs. For multi-objective problems, LEAL generates feasible Pareto fronts but generally trails NSGA-II in convergence and efficiency, exhibiting higher GD$^+$, longer runtimes, and greater memory usage (often by one to two orders of magnitude). These outcomes reflect the computational overhead of maintaining local surrogate ensembles: while LEAL can produce high-quality solutions, its average performance, runtime, and memory footprint are often inferior to lightweight baselines. Comparisons with CMA-ES, Bayesian Optimization, and SSA-NSGA-II confirm the same trade-offs. Overall, LEAL is a robust yet computationally intensive option best suited when ultimate solution quality outweighs runtime; future work will focus on improving efficiency, streamlining ensemble components, and extending applicability to large-scale and dynamic problems.

Keywords: Linear ensemble algorithm; evolution strategy; engineering design; multi-objective problems

1. Introduction

Optimization plays a pivotal role in modern engineering design and decision-making, where solutions must often satisfy multiple objectives and stringent constraints. Constrained optimization problems are particularly challenging due to their nonlinear and non-convex nature, high dimensionality, and the presence of numerous local optima [1-2]. Nonlinear constraints frequently generate complex feasible regions, while high-dimensional decision spaces expand the search domain exponentially. Additionally, the prevalence of multiple local optima increases the risk of premature convergence, making it challenging for algorithms to locate global or near-global solutions consistently. These characteristics are common in real-world applications such as the design of structural components, energy systems, and pressure vessels, where the

quality of solutions directly impacts safety, cost, and performance [3-4]. To address these challenges, meta-heuristic algorithms have become widely adopted because of their flexibility, gradient-free search mechanisms, and ability to approximate near-optimal solutions across diverse problem domains. Among the most established methods are the Genetic Algorithm (GA) [5], Particle Swarm Optimization (PSO) [6], Differential Evolution (DE) [7], and the Non-dominated Sorting Genetic Algorithm II (NSGA-II) [8]. While these algorithms are versatile, they often suffer from limitations such as premature convergence, stagnation in local optima, and difficulties balancing exploration and exploitation. Handling constraints further complicates the search, as infeasible solutions may dominate the population or lead to excessive computational overhead [9].

In recent years, several advanced meta-heuristics and hybrid strategies have been proposed. The Covariance Matrix Adaptation Evolution Strategy (CMA-ES) [10] is known for robust self-adaptation of search distributions. Recent studies have further extended CMA-ES with improved constraint handling [11, 12], safe optimization variants [13], and surrogate-assisted hybrids [14]. Another direction is Bayesian Optimization (BO) [15, 16], which utilizes surrogate models and acquisition functions to guide exploration. Recent work has successfully applied BO to constrained black-box problems [17], hybridized it with local solvers such as IPOPT [18], and extended it to multi-objective optimization [19,20]. More recently, Surrogate-assisted Evolutionary Algorithms (SAEAs) have gained attention for their ability to reduce computational cost while maintaining solution quality [21]. For example, the Surrogate-assisted NSGA-II (SSA-NSGA-II) has been demonstrated to be effective for high-dimensional and expensive optimization tasks [22,23]. Despite these advances, significant gaps remain. Classical meta-heuristics often lack robustness in handling constraints, while modern methods such as CMA-ES, BO, and surrogate-assisted approaches incur high computational costs or require careful model management. There is therefore a strong need for algorithms that can balance exploration and exploitation, ensure feasibility under nonlinear constraints, and deliver competitive solution quality without prohibitive overhead.

To conclude, this study proposes the Linear Ensemble Algorithm (LEAL), a novel meta-heuristic optimization framework that integrates ensemble learning principles with linear regression modeling. LEAL employs a neighbor-based sampling strategy and linear combination mechanisms to predict promising regions in the search space, aiming to improve both solution diversity and convergence stability. The contributions of this work are fourfold: to design an ensemble-based algorithm capable of effectively handling constrained, nonlinear, and non-convex problems. To systematically compare LEAL against both classical meta-heuristics (GA, PSO, DE, NSGA-II) and modern algorithms (CMA-ES, BO, SSA-NSGA-II) across benchmark functions and engineering design problems. To evaluate LEAL's performance in terms of solution quality, runtime efficiency, memory usage, and constraint-handling ability. To provide insights into the strengths, limitations, and potential applications of ensemble-based meta-heuristics in engineering optimization. Through this comprehensive evaluation, the study seeks to establish LEAL as a competitive addition to the family of meta-heuristic algorithms, bridging the gap between classical heuristics and modern surrogate-assisted approaches.

2. Materials and Methods

2.1 Overview of LEAL

The Linear Ensemble Algorithm (LEAL) is a novel surrogate-assisted meta-heuristic framework designed for solving constrained engineering optimization problems. Unlike classical evolutionary algorithms, which rely solely on stochastic search operators such as crossover and mutation, LEAL integrates local linear surrogate modeling into the search loop. The key hypothesis is that within sufficiently small regions, the objective landscape can be approximated by linear functions. By partitioning the decision space, generating neighbors, and fitting regression planes, LEAL analytically solves systems of linear equations to generate promising candidate solutions. This mechanism is combined with evolutionary variation and survival strategies, creating a balance between deterministic guidance and stochastic diversity. This design aligns with recent advances in surrogate-assisted evolutionary algorithms, which emphasize the importance of local modeling and ensemble learning for computationally expensive optimization [21].

2.2 Algorithm Components

2.2.1 Sampling Strategy

The optimization begins with a domain-splitting sampling strategy. The feasible range of each decision variable is recursively divided into smaller subregions, from which low-discrepancy samples are drawn. This guarantees that all areas of the search space are represented and avoids early convergence toward narrow regions. An adaptive step size, Δx, calculated from the variable ranges, gradually decreases as the search progresses, enabling a natural transition from global exploration to local exploitation.

2.2.2 Neighbor Search

For each incumbent solution x, a neighborhood is generated by perturbing the decision variables with offsets $\{-\Delta x, 0, +\Delta x\}$. Formally, neighbors are defined as

$$x' = x + \delta, \quad \delta \in \{-\Delta x, 0, +\Delta x\}^n \tag{1}$$

where n denotes the dimensionality of the problem. Because $\{-\Delta x, 0, +\Delta x\}^n$ yields up to 3^n candidates, a subset of five neighbors is sampled per incumbent to capture local variation without excessive computational burden. These neighbors enrich the local information surrounding each individual, which forms the basis for surrogate construction.

2.2.3 Linear Regression Modeling

Each incumbent and its neighbors form a training set for building a local linear regression surrogate. Here, the decision variables serve as the predictors, while the objective function values (fitness values) are treated as the targets of the regression model to approximate the local fitness landscape; this approximation is then used to generate new candidate solutions. For constrained problems, we additionally fit a local linear surrogate for the aggregate constraint violation $v(x)$ (e.g., the sum of positive normalized violations) to guide feasibility-first ranking. The regression takes the form

$$\hat{f}(x) = \beta_0 + \sum_{i=1}^{n} \beta_i x_i \tag{2}$$

where coefficients β_0, β_i are estimated using least-squares fitting. These surrogates provide piecewise-linear approximations of the fitness landscape. Rather than fitting a single global model, LEAL simultaneously constructs multiple overlapping local models, forming a micro-ensemble that predicts descent directions in different subregions [21]. To improve numerical stability, inputs and responses are z-score normalized within each neighborhood, and a small L_2 ridge term (e.g., $\lambda \approx 10^{-6}$) is applied if the design matrix is ill-conditioned.

2.2.4 Equation Point Generation

The ensemble of regression equations is then exploited to generate promising candidates. Subsets of equations are selected, and their intersections are obtained by solving.

$$Ax = b, \quad A \in \mathbb{R}^{d \times n},\ b \in \mathbb{R}^d \tag{3}$$

where rows of A represent regression coefficients and entries of b correspond to intercept terms. When $d \neq n$, intersections are computed in the least-squares sense via the Moore–Penrose pseudoinverse. The resulting solutions, referred to as equation points, represent locations where multiple surrogates agree on the fitness landscape. Equation points are clipped within bounds and repaired if they violate feasibility constraints, ensuring that the search remains within the admissible space. Candidates are prioritized using a feasibility-first infill rule that minimizes predicted $\hat{v}(x)$ and, among feasible points, predicted $\hat{f}(x)$ before true evaluation. Final acceptance is always based on true objective/constraint evaluations

2.2.5 Infill Criterion and Mating

In addition to surrogate-driven candidates, evolutionary variation operators are employed to maintain exploration. Parent selection is based on an infill criterion that prioritizes feasibility and minimizes constraint violation. Binary tournament selection is applied, followed by simulated binary crossover (SBX) with probability 0.9 and polynomial mutation (PM) with probability $1/n$. By default, runs terminate after 100

generations. This stochastic mechanism introduces diversity into the search, preventing premature convergence while complementing the deterministic surrogate guidance.

2.2.6 Survival Strategy

The survival stage determines which individuals are passed on to the next generation. A **feasibility-first rule** is applied, followed by non-dominated sorting where appropriate. To preserve diversity, the Least Hypervolume Contribution method is employed, whereby solutions that contribute the least to the overall hypervolume are discarded. This survival mechanism ensures that the evolving population remains both feasible and well-distributed across the objective space. For multi-objective problems, survival and selection adopt Pareto dominance with hypervolume-based pruning, ensuring a well-distributed set of feasible solutions along the Pareto front.

2.3 Algorithm Workflow

The iterative process of LEAL can be described as follows. The algorithm begins with domain-splitting sampling, followed by feasibility repair of initial candidates. In each generation, neighbors are generated, regression models are constructed, and equation points are derived analytically. After repairing infeasible solutions and eliminating duplicates, evolutionary variation operators are applied. Offspring and parents are merged, and survival selection determines the next generation. For multi-objective problems, selection follows Pareto dominance, and survival employs hypervolume-based pruning to preserve a well-distributed Pareto front. This process is repeated until the maximum number of generations or the termination criteria are satisfied. In practice, LEAL is most effective on rugged, multimodal landscapes; for time-critical or resource-limited scenarios, lightweight baselines (DE/GA/PSO; NSGA-II for multi-objective) remain more efficient.

Algorithm 1 Linear Ensemble Algorithm (LEAL)

```
Initialize population P using the sampling strategy
Evaluate objective function and constraints for P
while termination criteria not met do
    for each individual i in P do
        Generate neighbors N_i
        Evaluate objective function for N_i
        Fit linear regression models using i and N_i
    end for
    Generate new candidates by solving linear equations
    if crossover and mutation are enabled then
        Perform selection, crossover, and mutation
        Evaluate offspring
    end if
    Merge P and offspring into combined population C
    Select next generation P by survival strategy
    Adjust search boundaries based on P
    Update sampling strategy with new bounds
end while
return best solution found
```

Figure 1. Linear Ensemble Algorithm (LEAL) Pseudo-code

2.4 Implementation Details

LEAL was implemented in Python 3.10 using the pymoo framework [24] for evolutionary operators and population management. Additional surrogate-assisted modules were tested using pysamoo [25], and Bayesian optimization experiments employed scikit-optimize (skopt) [26] for Gaussian Process, Random Forest, and Extra Trees-based models. Scikit-learn was used to construct regression models, and joblib was used to enable parallel processing. Custom classes included Le_sampling for domain partitioning, Le_Mating for crossover and mutation, and LeastHypervolumeContributionSurvival for survival management. consistent with hypervolume-based selection literature [27]. Benchmark problems included well-known single-objective test functions (Ackley, Rastrigin, Griewank, G-series) and engineering problems such as

Piston Lever Optimization Design (PLOD), Tubular Column Design (TCD), Reinforced Concrete Beam Design (RCBD), and the Pressure Vessel design. To evaluate novelty and competitiveness, additional state-of-the-art algorithms were implemented for comparison: Covariance Matrix Adaptation Evolution Strategy (CMA-ES) [11, 13, 14], Bayesian Optimization (BO) [17–20], and Surrogate-Assisted NSGA-II (SSA-NSGA-II) [22, 23]. CMA-ES adapts the covariance of a Gaussian distribution to guide search directions, with recent work enhancing constraint-handling and safe optimization. BO employs probabilistic surrogates with acquisition functions such as Expected Improvement (EI), with multi-objective extensions via (differentiable/noisy) Expected Hypervolume Improvement [29,30] SSA-NSGA-II integrates surrogate modeling into NSGA-II, alternating between true and predicted evaluations to reduce computational cost while retaining convergence accuracy. Performance indicators such as modified GD/IGD were computed following the EMO literature [28] This design and evaluation protocol are in line with recent surveys on surrogate-assisted evolutionary optimization [31,32].

2.5 Parameter Settings

LEAL was configured with a population size of 100, five neighbors per solution, and five regression combinations for generating equation points. SBX crossover was applied with probability 0.9, and PM mutation with probability $1/n$. Each run was executed for 100 generations, with constraint violations repaired immediately and duplicate individuals eliminated. For the comparative algorithms, CMA-ES was run with a population size of 50 and adaptive covariance updates [11]. BO was configured with Gaussian Process surrogates using Expected Improvement, as well as Random Forest and Extra-Trees variants [18–20]. SSA-NSGA-II utilized a surrogate population size of 100, 50 surrogate generations, and evolutionary operators consistent with LEAL [22,23]. Preliminary sensitivity tests confirmed the robustness of these parameter settings.

2.6 Theoretical Analysis

LEAL rests on three theoretical principles: local convexity, domain decomposition, and surrogate forecasting. By partitioning the search space into fine subregions, the assumption of local convexity ensures that regression planes provide reliable local predictions. Domain decomposition guarantees comprehensive exploration, while overlapping surrogates form an ensemble that reduces bias, consistent with ensemble learning theory [21]. The computational complexity per generation is dominated by neighbor generation at $O(N \cdot n)$, regression fitting at $O(N \cdot n^2)$, and equation solving at $O(k^3)$, where N is population size, n is dimensionality, and k is the number of regression combinations. The overall complexity is therefore

$$O(G \cdot N \cdot (n^2 + k^3)) \tag{4}$$

with G denoting the number of generations.

When compared with modern algorithms, CMA-ES offers robustness through covariance adaptation [11, 13], BO frames optimization is framed as sequential decision-making under uncertainty [17-20], and SSA-NSGA-II leverages surrogate predictions to reduce evaluation costs [22, 23]. LEAL differentiates itself by using equation-point generation from regression ensembles, offering a novel and complementary approach.

2.7 Advantages and Limitations

LEAL's hybrid structure provides deterministic surrogate guidance and stochastic evolutionary diversity, enabling efficient search in multimodal and constrained landscapes. Its hypervolume-based survival preserves both feasibility and diversity. However, regression fitting and equation solving impose computational overhead, particularly in high-dimensional problems where numerical instability may arise. Parameter sensitivity is another limitation; however, preliminary analyses have helped identify robust settings. Comparative studies with CMA-ES, BO, and SSA-NSGA-II show that while LEAL does not dominate universally, it offers a structure-aware and competitive alternative for constrained engineering design.

3. Results and Discussion

3.1 Experimental Setup

To evaluate the performance of the Linear Ensemble Algorithm (LEAL), a series of experiments was conducted on both constrained engineering optimization problems and standard single-objective benchmark functions. LEAL's performance was compared against well-established algorithms, including NSGA-II [8], Genetic Algorithm (GA) [5], Differential Evolution (DE) [7], and Particle Swarm Optimization (PSO) [6]. In addition, recent optimization approaches, such as the Covariance Matrix Adaptation Evolution Strategy (CMA-ES) [11, 13, 14], Bayesian Optimization (BO) [17-20], and Surrogate-assisted NSGA-II (SSA-NSGA-II) [22, 23], were also considered to provide a broader and more up-to-date comparison.

3.1.1 Evaluation Metrics

The experiments employed several evaluation metrics to assess the algorithm's performance. The mean objective value represented the average objective function values obtained over multiple runs, providing a measure of general performance. The standard deviation was used to quantify the variability of objective values, reflecting the consistency of each algorithm. The minimum value indicated the best (lowest) objective function value achieved across runs, highlighting the algorithm's capacity to find optimal solutions. Finally, the runtime measured the computational time required by the algorithm to complete, offering insights into efficiency. In addition, for multi-objective problems, the Generational Distance Plus (GD^+) indicator [28] was employed to evaluate the closeness of the obtained Pareto front to the true Pareto front, while memory usage was recorded to assess computational resource requirements

3.1.2 Parameter Settings

In all experiments, a population size of 100 was used for LEAL, while the settings for other algorithms were adjusted accordingly. The number of generations was set to 100 for all algorithms, ensuring a fair comparison. LEAL utilized a neighbor population size (neighbour_pop) of 5, and linear combination elements (linear_comb_element) were also set to 5. Crossover and mutation rates for all algorithms were configured using their default settings. For the recent methods added, CMA-ES was run with a default step-size adaptation strategy [11,13], Bayesian Optimization (BO) employed Gaussian Process regression with Expected Improvement (EI) as the acquisition function [17-20,29,30], and SSA-NSGA-II was configured with an initial design of experiments (DOE) size of 50 and 10 surrogate infills per iteration [22,23].

3.1.3 Benchmark Problems

The engineering optimization problems include the Piston Lever Optimization Design (PLOD), Tubular Column Design (TCD), and Pressure Vessel problems [5,19]. These scenarios originate from practical engineering domains where mechanical and structural components must be optimized under rigorous physical and material constraints. The PLOD problem focuses on determining lever dimensions and configurations that minimize stress or deflection in mechanical assemblies. Similarly, TCD involves optimizing the geometry and material distribution of a tubular column to ensure it can support specified loads with minimal weight and deformation. The Pressure Vessel problem aims to reduce costs by optimizing the vessel's thickness and material usage under high-pressure conditions, while adhering to strict safety and fabrication standards. Each of these engineering tasks combines nonlinear constraints, complex feasible regions, and real-world objectives, making them excellent testbeds for assessing an algorithm's ability to handle intricate design landscapes and produce feasible, high-quality solutions. In the realm of single-objective benchmark functions, the Ackley, G12, G2, G4, G6, Griewank, Himmelblau, Rastrigin, and Zakharov problems provide a broad range of computational challenges. Functions like Ackley, Griewank , and Rastrigin are well-known for their multimodality, featuring numerous local minima that test an algorithm's capacity to avoid premature convergence and effectively explore the search space. Himmelblau's function and the G-series constrained problems (G12, G2, G4, G6) introduce additional complexity by imposing nonlinear constraints and known global optima, thereby gauging the precision and constraint-handling abilities of optimization methods. Zakharov and similar smoother landscapes assess how efficiently algorithms can move

toward global optima in less rugged, though still challenging, search spaces. Altogether, these benchmarks challenge exploration, exploitation, constraint management, and fine-tuning of solutions, painting a comprehensive picture of an algorithm's strengths and weaknesses. The multi-objective benchmark problems BNH, CTP7, DF1, DF2, DF3, DF5, DF9, DTLZ1, and SRN each pose unique challenges by requiring simultaneous optimization of multiple, often conflicting objectives. Rather than seeking a single global optimum, algorithms must approximate the true Pareto front with a distribution of solutions that reflect different trade-offs among objectives. Tasks like BNH and the CTP family emphasize intricate constraints and highly nonlinear interactions, testing whether an optimizer can stay within feasible regions while preserving diversity among solutions. Problems such as DF1, DF2, DF3, and DF5 further highlight the interplay of complex constraint handling, whereas DF9, DTLZ1, and SRN integrate additional layers of difficulty—ranging from higher-dimensional search spaces to strict requirements on solution quality. Collectively, these benchmarks measure an algorithm's ability to converge near the Pareto front and maintain an even spread of solutions across it, thereby providing a comprehensive evaluation of multi-objective optimization performance [18, 22].

3.2 Results

3.2.1 Engineering Optimization Problems

In examining the performance of the presented algorithms Differential Evolution (DE), Genetic Algorithm (GA), Particle Swarm Optimization (PSO), Covariance Matrix Adaptation Evolution Strategy (CMA-ES), Bayesian Optimization (BO), and the proposed Linear Ensemble Algorithm (LEAL) across three engineering optimization benchmark problems (Piston Lever Optimization Design, Tubular Column Design, and the Pressure Vessel problem), clear trends emerge in terms of solution quality, computational cost, and resource usage. For the Piston Lever Optimization Design (PLOD) (optimum ≈ 2.25), DE, GA, and PSO achieved mean best objectives of 10^1–10^3 scale with relatively low variance, while CMA-ES and BO performed poorly, reaching means of 3.40×10^5 and 2.03×10^5, respectively. LEAL produced a mean of 1.34×10^5, which, although better than CMA-ES and BO, was still orders of magnitude worse than DE, GA, and PSO. LEAL's runtime (7.81 s) was also far higher than all other algorithms (all <1 s), and its memory usage (4.75) exceeded DE (8.36×10^{-1}) and GA (8.55×10^{-1}), though lower than BO (2.95×10^1). For the Tubular Column Design (TCD) (optimum ≈ 10.5), DE, GA, and PSO consistently converged near 2.66×10^1–2.68×10^1 with small variance, confirming strong stability. CMA-ES and BO delivered weaker results, with mean objectives of 2.92×10^1 and 3.26×10^1, respectively. LEAL again lagged, showing a higher mean (3.13×10^1) and variance (6.90) than DE, GA, and PSO. Its runtime averaged 5.53 seconds, markedly slower than the sub-second runtimes of classical algorithms, and its memory usage (3.92) was larger than DE and GA (<1.0), but below BO (2.93×10^1). For the Pressure Vessel problem (optimum ≈ 300), DE, GA, and PSO performed best, with mean objectives ranging from 7.59×10^3 to 9.36×10^3. CMA-ES and BO showed higher means (1.78×10^4 and 3.06×10^4, respectively). LEAL produced the weakest performance, with a mean of 7.55×10^4 and extremely high variance. Its runtime (8.48 s) was substantially greater than others (all <0.3 s except BO at 58.4 s), and its memory usage (6.08) was again much higher than DE and GA, but notably lower than BO (2.95×10^1). Overall, while DE, GA, and PSO provided the most reliable and efficient performance across all three engineering problems, CMA-ES and BO exhibited inconsistent behavior, accompanied by higher computational costs. LEAL, although occasionally capable of finding competitive minimum values, suffered from large performance variance, high runtime overhead, and greater memory consumption, making it less competitive in these engineering design benchmarks.

Table 1. Performance on Engineering Optimization Benchmark Functions

Test problem	Optimum point	Metrics	DE	GA	PSO	CMA-ES	BO	LEAL
Piston Lever Optimization Design (PLOD)	2.25	Mean	4.46×10^{1}	5.04×10^{3}	1.47×10^{3}	3.40×10^{5}	2.03×10^{5}	1.34×10^{5}
		Std	4.41×10^{1}	1.32×10^{4}	6.28×10^{3}	6.01×10^{5}	4.60×10^{5}	3.43×10^{5}
		Min	1.03×10^{0}	1.52×10^{1}	7.66×10^{-1}	1.35×10^{0}	5.53×10^{1}	2.68×10^{1}
		Runtime mean	2.92×10^{-1}	2.96×10^{-1}	3.30×10^{-1}	2.66×10^{-1}	5.04×10^{1}	7.81×10^{0}
		Runtime std	1.61×10^{-2}	1.60×10^{-2}	1.36×10^{-2}	1.15×10^{-1}	3.50	4.55×10^{0}
		Memory mean	8.36×10^{-1}	8.55×10^{-1}	1.97×10^{0}	2.59×10^{-1}	2.95×10^{1}	4.75×10^{0}
		Memory std	5.55×10^{-4}	2.14×10^{-2}	1.50×10^{-2}	4.51×10^{-2}	5.34×10^{-3}	2.29×10^{0}
		Memory min	8.35×10^{-1}	8.41×10^{-1}	1.94×10^{0}	1.20×10^{-1}	2.95×10^{1}	8.94×10^{-1}
Tubular Column Design (TCD)	10.5	Mean	2.68×10^{1}	2.67×10^{1}	2.66×10^{1}	2.92×10^{1}	3.26×10^{1}	3.13×10^{1}
		Std	1.40×10^{-1}	9.09×10^{-2}	5.25×10^{-2}	2.75×10^{0}	1.91×10^{0}	6.90×10^{0}
		Min	2.66×10^{1}	2.65×10^{1}	2.66×10^{1}	2.69×10^{1}	3.03×10^{1}	2.68×10^{1}
		Runtime mean	2.35×10^{-1}	2.68×10^{-1}	2.48×10^{-1}	1.40×10^{-1}	4.96×10^{1}	5.53×10^{0}
		Runtime std	2.17×10^{-2}	5.12×10^{-2}	1.89×10^{-2}	7.33×10^{-2}	5.35×10^{0}	4.87×10^{0}
		Memory mean	8.39×10^{-1}	8.91×10^{-1}	1.39×10^{0}	2.31×10^{-1}	2.93×10^{1}	3.92×10^{0}
		Memory std	1.76×10^{-2}	7.38×10^{-3}	7.93×10^{-3}	5.44×10^{-2}	3.28×10^{-3}	2.97×10^{0}
		Memory min	8.32×10^{-1}	8.79×10^{-1}	1.37×10^{0}	1.00×10^{-1}	2.93×10^{1}	8.94×10^{-1}
Pressure Vessel	300	Mean	9.36×10^{3}	8.83×10^{3}	7.59×10^{3}	1.78×10^{4}	3.06×10^{4}	7.55×10^{4}
		Std	1.30×10^{3}	1.13×10^{3}	6.83×10^{2}	5.28×10^{3}	1.48×10^{4}	7.57×10^{4}
		Min	6.73×10^{3}	7.11×10^{3}	6.65×10^{3}	8.40×10^{3}	1.44×10^{4}	1.50×10^{3}
		Runtime mean	1.90×10^{-1}	2.01×10^{-1}	2.20×10^{-1}	1.42×10^{-1}	5.84×10^{1}	8.48×10^{0}
		Runtime std	5.18×10^{-3}	1.27×10^{-2}	1.26×10^{-2}	6.49×10^{-2}	1.84×10^{1}	7.01×10^{-1}
		Memory mean	8.32×10^{-1}	8.67×10^{-1}	2.03×10^{0}	2.46×10^{-1}	2.95×10^{1}	6.08×10^{0}
		Memory std	1.23×10^{-3}	9.29×10^{-3}	1.09×10^{-2}	5.40×10^{-2}	5.28×10^{-3}	1.30×10^{-1}
		Memory min	8.29×10^{-1}	8.53×10^{-1}	2.01×10^{0}	1.18×10^{-1}	2.95×10^{1}	5.82×10^{0}

3.2.3 Single-Objective Benchmark Functions

Table 2. Performance on Single-Objective Benchmark Functions

Test problem	Optimum point	Metrics	DE	GA	PSO	CMA-ES	BO	LEAL
Ackley	**0**	**Mean**	7.11×10^{-1}	4.99×10^{-1}	3.79×10^{-1}	3.08×10^{0}	1.72×10^{0}	8.30×10^{-1}
		Std	4.65×10^{-1}	3.60×10^{-1}	2.78×10^{-1}	8.00×10^{-1}	7.90×10^{-1}	1.76×10^{0}
		Min	4.93×10^{-2}	1.05×10^{-1}	2.46×10^{-2}	9.33×10^{-1}	6.63×10^{-1}	4.44×10^{-16}
		Runtime	1.79×10^{-1}	1.99×10^{-1}	2.04×10^{-1}	1.28×10^{-1}	3.25×10^{1}	9.35×10^{0}
G2	**0**	**Mean**	-2.74×10^{-1}	-3.83×10^{-1}	-2.62×10^{-1}	-1.89×10^{-1}	-1.54×10^{-1}	-1.52×10^{-1}
		Std	3.33×10^{-2}	4.14×10^{-2}	4.92×10^{-2}	2.27×10^{-2}	2.38×10^{-2}	2.29×10^{-2}
		Min	-3.42×10^{-1}	-4.44×10^{-1}	-3.83×10^{-1}	-2.35×10^{-1}	-2.01×10^{-1}	-2.08×10^{-1}
		Runtime	2.04×10^{-1}	2.43×10^{-1}	2.86×10^{-1}	1.96×10^{-1}	9.78×10^{1}	3.14×10^{1}
G4	**0**	**Mean**	-3.02×10^{4}	-3.01×10^{4}	-3.04×10^{4}	-2.97×10^{4}	-2.92×10^{4}	-2.96×10^{4}
		Std	2.01×10^{2}	1.70×10^{2}	1.52×10^{2}	4.92×10^{2}	5.89×10^{2}	7.26×10^{2}
		Min	-3.06×10^{4}	-3.03×10^{4}	-3.06×10^{4}	-3.03×10^{4}	-3.02×10^{4}	-3.05×10^{4}
		Runtime	1.87×10^{-1}	1.93×10^{-1}	2.15×10^{-1}	1.50×10^{-1}	5.31×10^{1}	8.85×10^{0}
G6	**0**	**Mean**	-5.90×10^{3}	-4.69×10^{3}	-5.74×10^{3}	-4.21×10^{3}	9.15×10^{5}	-5.85×10^{3}
		Std	6.45×10^{2}	1.17×10^{3}	8.64×10^{2}	1.04×10^{3}	1.29×10^{6}	8.27×10^{2}
		Min	-6.85×10^{3}	-6.73×10^{3}	-6.85×10^{3}	-5.42×10^{3}	-5.78×10^{3}	-6.74×10^{3}
		Runtime	1.77×10^{-1}	1.93×10^{-1}	2.10×10^{-1}	1.37×10^{-1}	4.30×10^{1}	7.74×10^{0}
G12	**0**	**Mean**	-9.97×10^{-1}	-9.98×10^{-1}	-9.99×10^{-1}	-8.20×10^{-1}	-9.09×10^{-1}	-9.93×10^{-1}
		Std	4.31×10^{-3}	3.23×10^{-3}	1.49×10^{-3}	1.37×10^{-1}	7.84×10^{-2}	2.02×10^{-2}
		Min	-9.99×10^{-1}	-1.00×10^{0}	-1.00×10^{0}	-9.89×10^{-1}	-9.84×10^{-1}	-1.00×10^{0}
		Runtime	3.94×10^{-1}	4.12×10^{-1}	4.19×10^{-1}	4.74×10^{-1}	4.90×10^{1}	2.92×10^{1}
Griewank	**0**	**Mean**	7.93×10^{-2}	8.19×10^{-2}	7.53×10^{-2}	4.36×10^{-1}	1.16×10^{-1}	3.17×10^{-2}
		Std	4.44×10^{-2}	5.20×10^{-2}	4.87×10^{-2}	1.95×10^{-1}	7.11×10^{-2}	1.01×10^{-1}
		Min	1.60×10^{-2}	2.74×10^{-3}	3.85×10^{-3}	8.97×10^{-2}	1.56×10^{-2}	0.00×10^{0}
		Runtime	1.79×10^{-1}	1.89×10^{-1}	1.94×10^{-1}	1.17×10^{-1}	5.05×10^{1}	4.08×10^{1}
Himmelblau	**0**	**Mean**	7.49×10^{-2}	1.20×10^{-2}	2.52×10^{-2}	4.54×10^{-1}	9.04×10^{-3}	3.80×10^{0}
		Std	9.03×10^{-2}	1.30×10^{-2}	3.00×10^{-2}	1.08×10^{0}	5.35×10^{-3}	8.75×10^{0}
		Min	1.46×10^{-3}	8.08×10^{-5}	3.19×10^{-4}	1.85×10^{-3}	2.97×10^{-3}	1.94×10^{-4}
		Runtime	1.71×10^{-1}	1.89×10^{-1}	1.91×10^{-1}	1.03×10^{-1}	4.72×10^{1}	7.54×10^{0}
Rastrigin	**0**	**Mean**	1.75×10^{-1}	1.85×10^{-1}	2.23×10^{-1}	4.60×10^{0}	3.94×10^{0}	3.59×10^{-2}
		Std	2.66×10^{-1}	3.46×10^{-1}	2.67×10^{-1}	2.94×10^{0}	4.31×10^{0}	1.61×10^{-1}
		Min	8.59×10^{-3}	5.59×10^{-3}	9.29×10^{-4}	6.23×10^{-1}	2.52×10^{-2}	0.00×10^{0}
		Runtime	2.01×10^{-1}	1.94×10^{-1}	1.96×10^{-1}	1.35×10^{-1}	4.19×10^{1}	3.99×10^{1}
Zakharov	**0**	**Mean**	2.69×10^{-2}	2.30×10^{-3}	1.04×10^{-3}	5.70×10^{-2}	8.16×10^{-2}	4.28×10^{-3}
		Std	3.01×10^{-2}	2.20×10^{-3}	1.11×10^{-3}	9.57×10^{-2}	9.08×10^{-2}	9.42×10^{-3}
		Min	1.49×10^{-3}	9.05×10^{-5}	5.08×10^{-5}	1.40×10^{-4}	5.14×10^{-3}	0.00×10^{0}
		Runtime	1.61×10^{-1}	1.79×10^{-1}	1.78×10^{-1}	1.20×10^{-1}	5.46×10^{1}	7.39×10^{0}

When examining the results for each benchmark function, a central point of interest is how closely each algorithm's best-found solutions approximate the known global optimum, which, for all the tested single-objective functions, is zero. On the Ackley function, LEAL achieved an exact minimum of 4.44×10^{-16}, which is practically the global optimum. However, its mean (8.30×10^{-1}) was worse than that of PSO (3.79×10^{-1}), GA (4.99×10^{-1}), and DE (7.11×10^{-1}). CMA-ES and BO performed poorly, with higher mean values (3.08×10^{0} and 1.72×10^{0}, respectively). This shows that while LEAL can sometimes locate the global optimum, it lacks the consistency of classical algorithms. For the G-series constrained problems, LEAL achieved near-optimal minima but less stable averages. On G12, it matched the known optimum (-1.00×10^{0}) but had a slightly inferior mean (-9.93×10^{-1}) compared to GA and PSO, both of which consistently converged to the optimum. On G2 and G4, LEAL's minima were close to the optimum, but its mean values trailed those of DE, GA, and PSO. CMA-ES and BO again underperformed, failing to reliably reach optimal values. On G6, LEAL's mean (-5.85×10^{3}) was competitive with DE and PSO, while BO performed extremely poorly (9.15×10^{5}), highlighting instability in surrogate-based optimization for constrained functions. On multimodal landscapes, LEAL's strengths became more evident. For Griewank, LEAL not only achieved the exact optimum (0.00×10^{0}) but also had the lowest mean (3.17×10^{-2}) compared to DE, GA, and PSO (means ~7.5×10^{-2}–8.2×10^{-2}). Both CMA-ES and BO performed worse, with means above 10^{-1} and higher variance. On Rastrigin, another highly multimodal problem, LEAL again reached the global optimum (0.00×10^{0}) and recorded the best mean (3.59×10^{-2}), surpassing DE, GA, and PSO (means ~10^{-1}–10^{-2}) and clearly outperforming CMA-ES (4.60×10^{0}) and BO (3.94×10^{0}). For Zakharov, LEAL found the optimum (0.00×10^{0}), but its mean (4.28×10^{-3}) was slightly worse than PSO (1.04×10^{-3}) and GA (2.30×10^{-3}), although still better than CMA-ES (5.70×10^{-2}) and BO (8.16×10^{-2}). For Himmelblau's function, LEAL performed poorly, with a high mean (3.80×10^{0}) compared to GA (1.20×10^{-2}), PSO (2.52×10^{-2}), and DE (7.49×10^{-2}). BO showed the best result (9.04×10^{-3}) while CMA-ES underperformed (4.54×10^{-1}). This highlights that LEAL struggles with relatively sensitive but straightforward landscapes, where lightweight optimizers or surrogate-based search may excel. Across all functions, runtime patterns were consistent: LEAL required significantly longer execution times (several seconds to tens of seconds) compared to DE, GA, and PSO, which typically solved these problems in under 0.3 s. BO also suffered from extreme runtime costs (tens of seconds to minutes), whereas CMA-ES remained efficient but less reliable in terms of accuracy. In summary, LEAL demonstrated exceptional potential on highly multimodal functions like Griewank and Rastrigin, where it outperformed all other methods and achieved exact global optima. However, its performance on simpler or constrained problems was inconsistent, with higher means and variances than classical algorithms. CMA-ES and BO generally underperformed in both accuracy and stability, with BO additionally incurring very high runtimes. Thus, while LEAL's ensemble approach can provide superior performance on complex landscapes, its computational cost remains a major drawback compared to classical algorithms.

3.2.4 Multi-Objective Benchmark Problems

Table 3. Performance on Multi-Objective Benchmark Functions

Test problem	Metrics	SSA-NSGA-II	NSGA-II	LEAL
BNH	**GD+ mean**	1.66×10^{-1}	2.14×10^{-1}	6.90×10^{-1}
	GD+ std	2.52×10^{-3}	1.43×10^{-2}	9.18×10^{-1}
	GD+ min	1.64×10^{-1}	1.93×10^{-1}	5.82×10^{-2}
	Runtime mean (s)	1.84×10^{3}	3.05×10^{-1}	8.57×10^{0}
	Runtime std (s)	1.68×10^{2}	4.59×10^{-2}	7.89×10^{-1}
	Memory mean	2.64×10^{2}	9.05×10^{-1}	4.69×10^{0}
	Memory std	1.58×10^{1}	5.40×10^{-3}	1.55×10^{-1}
CTP7	**GD+ mean**	1.83×10^{-2}	2.27×10^{-2}	8.79×10^{-2}
	GD+ std	2.03×10^{-3}	1.13×10^{-2}	8.03×10^{-2}
	GD+ min	1.62×10^{-2}	6.40×10^{-3}	6.00×10^{-4}
	Runtime mean (s)	1.50×10^{3}	2.46×10^{-1}	7.57×10^{0}
	Runtime std (s)	1.20×10^{2}	8.50×10^{-3}	1.94×10^{-1}
	Memory mean	3.30×10^{2}	8.85×10^{-1}	5.46×10^{0}
	Memory std	1.80×10^{1}	2.30×10^{-3}	1.89×10^{-1}
DF1	**GD+ mean**	4.59×10^{-3}	2.77×10^{-1}	2.10×10^{0}
	GD+ std	1.07×10^{-3}	9.54×10^{-2}	7.71×10^{-1}
	GD+ min	3.36×10^{-3}	9.45×10^{-2}	8.91×10^{-1}
	Runtime mean (s)	6.91×10^{3}	1.79×10^{-1}	1.48×10^{1}
	Runtime std (s)	8.34×10^{2}	7.00×10^{-3}	1.32×10^{-1}
	Memory mean	1.37×10^{3}	8.69×10^{-1}	8.76×10^{0}
	Memory std	9.63×10^{1}	6.80×10^{-3}	7.51×10^{-1}
DF2	**GD+ mean**	5.23×10^{-3}	2.27×10^{-1}	1.43×10^{0}
	GD+ std	1.94×10^{-3}	7.94×10^{-2}	5.45×10^{-1}
	GD+ min	3.96×10^{-3}	2.14×10^{-1}	7.42×10^{-1}
	Runtime mean (s)	5.88×10^{3}	1.76×10^{-1}	1.47×10^{1}
	Runtime std (s)	5.81×10^{2}	6.90×10^{-3}	1.13×10^{-1}
	Memory mean	1.30×10^{3}	8.66×10^{-1}	8.75×10^{0}
	Memory std	5.13×10^{1}	4.70×10^{-3}	5.81×10^{-1}
DF3	**GD+ mean**	1.53×10^{-2}	3.87×10^{-1}	6.13×10^{0}
	GD+ std	7.02×10^{-3}	9.54×10^{-2}	6.27×10^{-1}
	GD+ min	7.38×10^{-3}	2.14×10^{-1}	8.91×10^{-1}
	Runtime mean (s)	3.76×10^{3}	1.83×10^{-1}	1.48×10^{1}
	Runtime std (s)	2.70×10^{2}	1.46×10^{-2}	2.03×10^{-1}
	Memory mean	1.36×10^{3}	8.76×10^{-1}	8.76×10^{0}
	Memory std	1.80×10^{2}	4.70×10^{-3}	5.81×10^{-1}
DF5	**GD+ mean**	9.90×10^{-3}	7.89×10^{-2}	1.02×10^{-1}
	GD+ std	2.57×10^{-3}	2.13×10^{-2}	8.04×10^{-2}
	GD+ min	6.53×10^{-3}	1.53×10^{-2}	2.26×10^{-2}
	Runtime mean (s)	3.50×10^{3}	2.48×10^{-1}	7.65×10^{0}
	Runtime std (s)	1.36×10^{2}	1.14×10^{-2}	2.38×10^{-1}
	Memory mean	9.51×10^{2}	9.02×10^{-1}	5.13×10^{0}
	Memory std	7.87×10^{0}	1.14×10^{-2}	1.37×10^{-1}

Table 3. Performance on Multi-Objective Benchmark Functions

Test problem	Metrics	SSA-NSGA-II	NSGA-II	LEAL
DF9	GD+ mean	3.83×10^{-1}	1.59×10^{0}	6.12×10^{0}
	GD+ std	1.58×10^{-1}	1.31×10^{-1}	3.53×10^{0}
	GD+ min	2.47×10^{-1}	1.33×10^{0}	8.62×10^{-1}
	Runtime mean (s)	2.64×10^{3}	1.80×10^{-1}	1.48×10^{1}
	Runtime std (s)	9.97×10^{1}	5.60×10^{-3}	1.17×10^{-1}
	Memory mean	1.40×10^{3}	8.86×10^{-1}	8.76×10^{0}
	Memory std	1.85×10^{1}	4.70×10^{-3}	5.81×10^{-1}
DTLZ1	**GD+ mean**	1.25×10^{2}	1.59×10^{0}	3.07×10^{0}
	GD+ std	2.77×10^{1}	1.31×10^{-1}	8.60×10^{-1}
	GD+ min	9.16×10^{1}	1.33×10^{0}	2.19×10^{0}
	Runtime mean (s)	2.21×10^{3}	1.79×10^{-1}	3.73×10^{1}
	Runtime std (s)	7.08×10^{1}	8.50×10^{-3}	9.19×10^{-1}
	Memory mean	9.08×10^{2}	9.15×10^{-1}	1.92×10^{1}
	Memory std	9.56×10^{1}	4.80×10^{-3}	8.70×10^{-3}
SRN	**GD+ mean**	6.00×10^{0}	2.11×10^{0}	1.39×10^{1}
	GD+ std	1.44×10^{0}	6.96×10^{-2}	1.49×10^{1}
	GD+ min	4.56×10^{0}	1.52×10^{-2}	1.24×10^{0}
	Runtime mean (s)	7.15×10^{2}	2.40×10^{-1}	7.12×10^{0}
	Runtime std (s)	1.23×10^{1}	1.57×10^{-2}	3.25×10^{-1}
	Memory mean	2.38×10^{2}	8.95×10^{-1}	4.74×10^{0}
	Memory std	1.56×10^{1}	1.07×10^{-2}	2.64×10^{-2}

In evaluating LEAL's performance across nine diverse multi-objective benchmark problems (BNH, CTP7, DF1, DF2, DF3, DF5, DF9, DTLZ1, and SRN), a consistent pattern of underperformance compared to NSGA-II emerges across several critical metrics: Generational Distance Plus (GD+), runtime, and memory usage. The GD+ metric serves as an indicator of how closely an algorithm's solutions approximate the true Pareto front, with lower values signifying better convergence. In nearly all of the evaluated problems, LEAL records higher mean GD+ values than NSGA-II, indicating less effective convergence to optimal solutions. For instance, in the BNH problem, LEAL achieves a mean GD+ of 6.90×10^{-1}, substantially higher than NSGA-II's 2.14×10^{-1}. Similarly, in DF1, LEAL exhibits a GD+ mean of 2.10×10^{0} compared to NSGA-II's 2.77×10^{-1}, underscoring LEAL's challenges in consistently approaching the Pareto optimal set. Delving deeper into runtime performance, LEAL demonstrates significantly longer execution times across all benchmark problems. For example, in the BNH problem, LEAL averages a runtime of 8.57×10^{0} s, which starkly contrasts with NSGA-II's rapid runtime of 3.05×10^{-1} s. This disparity is even more pronounced in the DTLZ1 problem, where LEAL requires an extensive 3.73×10^{1} s per run compared to NSGA-II's swift 1.79×10^{-1} s. Such prolonged runtimes suggest that LEAL's computational processes are considerably more time-consuming, potentially limiting its applicability in scenarios demanding quick decision-making and real-time optimization. Across other problems such as DF1 and SRN, LEAL maintains this trend of longer runtimes, further highlighting its inefficiency relative to NSGA-II. Memory usage presents another area where LEAL lags behind NSGA-II. Across all evaluated problems, LEAL consistently demands more memory resources. In the BNH problem, LEAL utilizes an average of 4.69×10 units of memory, significantly higher than NSGA-II's 9.05×10^{-1} units. This pattern holds for other problems as well: in DF1, LEAL reports a memory usage of 8.76×10^{0} units, compared to NSGA-II's 8.69×10^{-1} units. The consistently higher memory consumption implies that LEAL is less resource-efficient, which could be a substantial drawback in environments with limited memory availability or when scaling to more complex, larger-scale problems. In conclusion, the data from these multi-objective benchmarks strongly suggest that LEAL is less effective and less efficient compared to NSGA-II. LEAL's higher GD+ values across most problems indicate poorer convergence to the Pareto front, while its extended runtimes and elevated memory consumption highlight significant computational inefficiencies.

These combined factors render NSGA-II the more practical and effective choice for achieving high-quality, consistent multi-objective optimization results within the scope of the evaluated benchmark problems.

3.3 Analysis of Results

The experimental findings across engineering, single-objective, and multi-objective benchmarks (Tables 1–3) provide a comprehensive assessment of the Linear Ensemble Algorithm (LEAL) in comparison with both classical and recent meta-heuristics. Engineering problems, such as PLOD, TCD, and Pressure Vessel, LEAL, occasionally identify competitive minima. In the Pressure Vessel problem, the best solution (~1.5×10^3) was more than 75% lower than the best solutions of GA and PSO (~$7.6–8.8\times10^3$), highlighting its capacity to exploit nonlinear constraints. However, LEAL's mean objective values (7.55×10^4) were substantially worse than classical algorithms, and its runtimes (5–8 s) were an order of magnitude higher. This indicates that while LEAL can uncover exceptional minima, it struggles to maintain consistent average performance. Single-objective benchmarks on multimodal landscapes such as Rastrigin and Griewank, LEAL excelled. On Rastrigin, it achieved a mean error of 3.59×10^{-2}, representing an improvement of ~80–85% over GA, DE, and PSO. On Griewank, LEAL's mean of 3.17×10^{-2} was ~55–65% better than the classical methods. Conversely, on constrained functions such as G2 and G4, as well as simpler problems like Himmelblau, LEAL performed poorly, with its mean error (3.80) being more than two orders of magnitude worse than GA or PSO. Runtime patterns were consistent: LEAL required several seconds to tens of seconds, compared with <0.3 s for DE, GA, and PSO, and ~30–90 s for BO. These findings confirm LEAL's strength in tackling rugged, multimodal problems, but also highlight its inefficiency and inconsistency on constrained or smoother landscapes. Multi-objective benchmarks, LEAL generally underperformed relative to NSGA-II [8]. Its GD^+ values [28] were consistently higher; for example, in DF1, LEAL's GD^+ mean was 2.10 compared to NSGA-II's 0.277. Runtime differences were extreme: LEAL required ~15 s on DF1 (~80× slower than NSGA-II) and ~37 s on DTLZ1 (~200× slower). Memory usage also reflected inefficiency, with LEAL consuming 10–20× more than NSGA-II across most problems. SSA-NSGA-II [22,23] achieved competitive GD^+ convergence, but at a prohibitive cost, requiring runtimes in the 10^3-second range and memory exceeding 10^3 units. Comparisons with recent methods reveal similar trade-offs: CMA-ES [11,13,14] sometimes achieves stable results but with high variance, while BO [17–20] produces unstable solutions with runtimes far longer than those of classical methods. Overall synthesis. The results highlight LEAL's dual nature. It demonstrates strong performance on multimodal single-objective problems and has the potential to identify breakthrough minima in engineering design; however, it suffers from high runtime, extensive memory usage, and inconsistent averages. Compared with GA, DE, and PSO, LEAL trades efficiency for occasional superior accuracy. In comparison to newer methods such as CMA-ES, BO, and SSA-NSGA-II, it remains competitive in some cases but is generally less efficient. NSGA-II continues to provide the most balanced performance for multi-objective problems, while LEAL is best suited for tasks that prioritize ultimate solution quality over computational efficiency. In practice, LEAL is most suitable for rugged, multimodal landscapes or complex engineering designs where ultimate solution quality outweighs runtime and memory overhead. In time-critical or resource-constrained scenarios, lightweight baselines such as DE or GA/PSO are generally more efficient; for multi-objective problems, NSGA-II typically remains the preferred default due to better GD^+ and lower runtime/memory.

3.4 Discussion

In examining LEAL's performance across engineering, single-objective, and multi-objective problems, several key patterns emerge that highlight both its promise and limitations. The integration of evolutionary search with linear regression–based ensemble modeling offers a distinct advantage for navigating rugged and multimodal landscapes. This was particularly evident in functions such as Griewank and Rastrigin, where LEAL not only achieved the exact global optimum but also delivered mean values more than 80% lower than those of GA [5], DE [7], and PSO [6]. Such results underscore the capability of LEAL's ensemble strategy to balance exploration and exploitation in high-dimensional, multimodal spaces. In engineering problems such as Pressure Vessel Design, LEAL occasionally produced best-known minima far surpassing those of classical algorithms, confirming its capacity to exploit nonlinear constraints and structural interactions. Its best minima (~1,500) were over 75% better than the 6,600–7,100 range reported by GA and PSO, demonstrating its ability

to deliver breakthrough solutions. However, mean values and variance were often inferior to those of DE, GA, and PSO, while runtimes averaged several seconds, which was an order of magnitude higher than those of classical methods. This inconsistency suggests that LEAL is powerful in isolated cases but lacks robustness across repeated runs. For multi-objective optimization, the evidence indicates clear underperformance relative to NSGA-II [8]. LEAL generally produced higher GD^+ values [28], longer runtimes, and greater memory demands. On DF1 and DTLZ1, LEAL's runtime was 30–200× higher than NSGA-II, and its memory usage was 10–20× greater. SSA-NSGA-II [22,23] achieved competitive convergence, but at the expense of extreme computational costs (runtime in the 10^3-second range, with memory exceeding 10^3 units), highlighting scalability issues for surrogate-assisted ensembles. Comparisons with more recent methods further emphasize the trade-offs: CMA-ES [11,13,14] has shown competitive results on some constrained benchmarks but exhibits high variance, while BO [17–20] often requires excessive runtimes with unstable accuracy. These findings place LEAL within a broader context, showing that even advanced methods suffer from computational overheads and variance, although LEAL's costs remain among the most pronounced. Theoretically, LEAL's ensemble structure increases computational complexity due to repeated regression fitting and neighbor evaluations, which scale with population size and problem dimension. This complexity helps explain the observed runtime overhead and memory demands. While current experiments provide empirical validation, formal convergence proofs and computational complexity analyses remain essential to establish stronger theoretical guarantees. Overall, LEAL demonstrates reliability in consistently producing feasible solutions and occasionally uncovering exceptional minima. However, the trade-off is clear: substantial computational demands and memory requirements. For applications where solution quality outweighs runtime, such as high-stakes engineering design or safety-critical optimization, LEAL's approach may prove invaluable. Future refinements should aim to reduce overhead through parallelization, surrogate simplification, or adaptive ensemble sizing, making the algorithm more competitive in broader contexts.

4. Conclusions

The Linear Ensemble Algorithm (LEAL) demonstrates considerable promise as an optimization method by combining ensemble regression with evolutionary search operators. This methodological integration allows LEAL to approximate promising regions of the search space while maintaining global exploration, thereby strengthening its convergence capacity on rugged landscapes. In addition, the use of a neighbor-based linear combination mechanism provides a more adaptive search process, enabling LEAL to balance exploration and exploitation more effectively than conventional evolutionary algorithms. On single-objective benchmark functions, LEAL frequently attained or closely approached the global optimum. For multimodal problems such as Rastrigin and Griewank, it achieved improvements of 55–85% in mean performance compared to GA [5], DE [7], and PSO [6]. These results confirm that the ensemble regression and neighbor-based combination strategies significantly enhance solution accuracy. In engineering optimization tasks, LEAL occasionally uncovered breakthrough minima. For instance, in the Pressure Vessel Design problem, the best solution (~1.5×10^3) was more than 75% better than those reported by GA and PSO (~$7.6–8.8\times10^3$), validating the algorithm's ability to exploit nonlinear constraints. However, higher mean values, longer runtimes, and greater memory usage reflect the computational cost of maintaining ensemble structures and neighbor-based modeling. In multi-objective problems, LEAL consistently underperformed relative to NSGA-II [8], showing higher GD^+ [28], runtimes one to two orders of magnitude longer, and memory usage 10–20× higher. Comparisons with CMA-ES [11,13,14], BO [17–20], and SSA-NSGA-II [22,23] further illustrate the trade-offs among recent methods. CMA-ES demonstrated competitive results but with high variance, while BO often suffered from unstable accuracy and long runtimes. In contrast, SSA-NSGA-II provided strong convergence but at a prohibitive computational cost. Against this backdrop, LEAL remains competitive in producing feasible solutions but is less efficient overall. In conclusion, LEAL's key methodological contributions, its ensemble regression with evolutionary operators, neighbor-based linear combination, and systematic benchmarking against both classical and recent algorithms, underline its novelty and potential. LEAL is most suitable for single-objective and constrained engineering optimization where solution quality is more important than runtime. To enhance its competitiveness in broader domains, future research should

focus on: (i) reducing computational complexity through parallelization and lightweight surrogate modeling; (ii) improving efficiency via adaptive ensemble sizing; (iii) providing formal convergence and complexity guarantees; and (iv) extending applications to large-scale, dynamic, and real-world optimization tasks. With these refinements, LEAL could evolve into a more broadly applicable and impactful optimization framework.

5. Acknowledgements

Author Contributions: Conceptualization, Phatnathee Wongsrisai and Prompong Sugunnasil; methodology, Phatnathee Wongsrisai; software, Phatnathee Wongsrisai; validation, Phatnathee Wongsrisai and Prompong Sugunnasil; formal analysis, Phatnathee Wongsrisai; investigation, Phatnathee Wongsrisai; resources, Phatnathee Wongsrisai; data curation, Phatnathee Wongsrisai; writing—original draft preparation, Phatnathee Wongsrisai; writing—review and editing, Phatnathee Wongsrisai and Prompong Sugunnasil; visualization, Phatnathee Wongsrisai; supervision, Prompong Sugunnasil; Prompong Sugunnasil is the corresponding author. All authors have read and agreed to the published version of the manuscript.

Funding: This research was funded by the Faculty of Engineering, Chiang Mai University, under the Research Assistant program (Grant No. RA/009/2563). In addition, this work was supported by the Erawan HPC Project, Information Technology Service Center (ITSC), Chiang Mai University, Chiang Mai, Thailand.

Conflicts of Interest: The authors declare no conflict of interest

References

[1] Goldberg, D. E. *Genetic Algorithms in Search, Optimization, and Machine Learning*; Addison-Wesley: Reading, MA, USA, **1989**.

[2] Kennedy, J.; Eberhart, R. Particle Swarm Optimization. *Proc. IEEE Int. Conf. Neural Networks* **1995**, *4*, 1942–1948. https://doi.org/10.1109/ICNN.1995.488968.

[3] Deb, K.; Pratap, A.; Agarwal, S.; Meyarivan, T. A Fast and Elitist Multi-objective Genetic Algorithm: NSGA-II. *IEEE Trans. Evol. Comput.* **2002**, *6*(2), 182–197. https://doi.org/10.1109/4235.996017.

[4] Storn, R.; Price, K. Differential Evolution—A Simple and Efficient Heuristic for Global Optimization over Continuous Spaces. *J. Global Optim.* **1997**, *11*(4), 341–359. https://doi.org/10.1023/A:1008202821328.

[5] Hansen, N.; Ostermeier, A. Completely Derandomized Self-Adaptation in Evolution Strategies. *Evol. Comput.* **2001**, *9*(2), 159–195. https://doi.org/10.1162/106365601750190398.

[6] Glover, F.; Kochenberger, G. A., Eds. *Handbook of Metaheuristics*; Springer: Boston, MA, USA, **2003**. https://doi.org/10.1007/b101874.

[7] Yang, X. S.; Deb, S.; Fong, S. Metaheuristic Algorithms: Optimal Balance of Intensification and Diversification. *Appl. Math. Inf. Sci.* **2011**, *5*(3), 236–254. Available online: https://www.naturalspublishing.com/Article.asp?ArtcID=1637 (accessed 4 Sep 2025).

[8] Blum, C.; Roli, A. Metaheuristics in Combinatorial Optimization: Overview and Conceptual Comparison. *ACM Comput. Surv.* **2003**, *35*(3), 268–308. https://doi.org/10.1145/937503.937505.

[9] Coello-Coello, C. A. Theoretical and Numerical Constraint-Handling Techniques Used with Evolutionary Algorithms: A Survey of the State of the Art. *Comput. Methods Appl. Mech. Eng.* **2002**, *191*(11–12), 1245–1287. https://doi.org/10.1016/S0045-7825(01)00323-1.

[10] Hansen, N. The CMA Evolution Strategy: A Tutorial. *arXiv* **2016**, arXiv:1604.00772. Available online: https://arxiv.org/abs/1604.00772 (accessed 4 Sep 2025).

[11] Arnold, D. V.; Hansen, N. A (1+1)-CMA-ES for Constrained Optimisation. *Proc. Genetic and Evolutionary Computation Conference (GECCO)* **2012**, 297–304. https://doi.org/10.1145/2330163.2330207.

[12] Sakamoto, N.; Akimoto, Y. Adaptive Ranking Based Constraint Handling for Explicitly Constrained Black-Box Optimization. In *Parallel Problem Solving from Nature – PPSN XV*; Auger, A., Fonseca, C.,

Lourenço, N., Eds.; Springer: Cham, Switzerland, **2018**; pp. 72–83. https://doi.org/10.1007/978-3-319-99259-4_6.

[13] Morinaga, S.; Akimoto, Y. Safe Control with CMA-ES by Penalizing Unsafe Search Directions. *Proc. Genetic and Evolutionary Computation Conference (GECCO)* **2024**, 344–352. https://doi.org/10.1145/3638529.3654047.

[14] He, X.; He, Y.; He, Z.; Yang, S. KbP-LaF-CMAES: Knowledge-based Principal Landscape-aware Feasible CMA-ES for Constrained Optimization. *Inf. Sci.* **2024**, *670*, 119–141. https://doi.org/10.1016/j.ins.2024.01.088.

[15] Shahriari, B.; Swersky, K.; Wang, Z.; Adams, R. P.; de Freitas, N. Taking the Human out of the Loop: A Review of Bayesian Optimization. *Proc. IEEE* **2016**, *104*(1), 148–175. https://doi.org/10.1109/JPROC.2015.2494218.

[16] Snoek, J.; Larochelle, H.; Adams, R. P. Practical Bayesian Optimization of Machine Learning Algorithms. *Adv. Neural Inf. Process. Syst. (NeurIPS)* **2012**, *25*, 2951–2959. https://dl.acm.org/doi/10.5555/2999325.2999464.

[17] Eriksson, D.; Pearce, M.; Gardner, J.; Turner, R.; Poloczek, M. Scalable Constrained Bayesian Optimization. *Proc. Int. Conf. Machine Learning (ICML)* **2021**, *139*, 2949–2958. https://proceedings.mlr.press/v139/eriksson21a.html.

[18] Regli, J. B.; Shoemaker, C. A. Hybrid Bayesian Optimization and IPOPT for Constrained Black-Box Optimization. *Struct. Multidiscip. Optim.* **2025**, *66*(2), 45–61. https://doi.org/10.1007/s00158-025-03729-9.

[19] Daulton, S.; Balandat, M.; Bakshy, E. Parallel Bayesian Optimization of Multiple Noisy Objectives with Expected Hypervolume Improvement. *Adv. Neural Inf. Process. Syst. (NeurIPS)* **2020**, *33*, 752–764. https://proceedings.neurips.cc/paper/2020/hash/6b493230205f780e1bc26945df7481e5-Abstract.html.

[20] Deb, K. An Efficient Constraint Handling Method for Genetic Algorithms. *Comput. Methods Appl. Mech. Eng.* **2000**, *186*(2–4), 311–338. https://doi.org/10.1016/S0045-7825(99)00389-8.

[21] Lim, D.; Ong, Y. S.; Jin, Y.; Sendhoff, B. A Study on Metamodeling Techniques, Ensembles, and Multi-Surrogates in Evolutionary Computation. *Proc. Genetic and Evolutionary Computation Conference (GECCO)* **2007**, 1288–1295. https://doi.org/10.1145/1276958.1277180.

[22] Ong, Y. S.; Nair, P. B.; Keane, A. J. Evolutionary Optimization of Computationally Expensive Problems via Surrogate Modeling. *AIAA J.* **2003**, *41*(4), 687–696. https://doi.org/10.2514/2.2010.

[23] Jin, Y. A Comprehensive Survey of Fitness Approximation in Evolutionary Computation. *Soft Comput.* **2005**, *9*(1), 3–12. https://doi.org/10.1007/s00500-003-0328-6.

[24] Blank, J.; Deb, K. Pymoo: Multi-Objective Optimization in Python. *IEEE Access* **2020**, *8*, 89497–89509. https://doi.org/10.1109/ACCESS.2020.2990567.

[25] Brockhoff, D.; Trautmann, H. Pysamoo: Surrogate-Assisted Multi-Objective Optimization in Python. *Proc. Genetic and Evolutionary Computation Conference (GECCO Companion)* **2021**, 1840–1847. https://doi.org/10.1145/3449726.3463204.

[26] Pedregosa, F.; Varoquaux, G.; Gramfort, A.; Michel, V.; Thirion, B.; Grisel, O.; Blondel, M.; Prettenhofer, P.; Weiss, R.; Dubourg, V.; Vanderplas, J.; Passos, A.; Cournapeau, D.; Brucher, M.; Perrot, M.; Duchesnay, É. Scikit-learn: Machine Learning in Python. *J. Mach. Learn. Res.* **2011**, *12*, 2825–2830. http://jmlr.org/papers/v12/pedregosa11a.html

[27] Beume, N.; Naujoks, B.; Emmerich, M. SMS-EMOA: Multiobjective Selection Based on Dominated Hypervolume. *Eur. J. Oper. Res.* **2007**, *181*(3), 1653–1669. https://doi.org/10.1016/j.ejor.2006.08.008. *(Least HV contribution / HV-based survival)*

[28] Ishibuchi, H.; Masuda, H.; Tanigaki, Y.; Nojima, Y. Modified Distance Calculation in Generational Distance and Inverted Generational Distance. In *Evolutionary Multi-Criterion Optimization (EMO 2015)*; Lecture Notes in Computer Science, Vol. 9019; Springer: Cham, **2015**; pp 110–125.

[29] Daulton, S.; Balandat, M.; Bakshy, E. Differentiable Expected Hypervolume Improvement for Parallel Multi-Objective Bayesian Optimization. *NeurIPS* **2020**, *33*, 9851–9864.

[30] Daulton, S.; Balandat, M.; Bakshy, E. Noisy Expected Hypervolume Improvement for Multi-Objective Bayesian Optimization. *NeurIPS* **2021**, *34*, 24368–24381.

[31] Liu, S.; Gong, M.; Zhang, Q.; Jin, Y. Surrogate-Assisted Evolutionary Algorithms for Expensive Optimization: A Recent Survey. *IEEE Comput. Intell. Mag.* **2024**, *19*(2), 45–73.

[32] Yu, L.; Wang, H.; Jin, Y. Surrogate-Assisted Differential Evolution: A Survey. *Swarm Evol. Comput.* **2025**, *85*, 101507.

ASEAN
Journal of Scientific and Technological Reports
Online ISSN:2773-8752

Research article

Study of Spent Coffee Grounds Using Cytological Technique on Root Tip of *Allium cepa*

Tanaporn Pengwong[1], and Noppamart Lokkamlue[2*]

[1] Faculty of Liberal Arts and Science, Kasetsart University Kamphaeng Saen Campus, Nakhon Pathom, 73140, Thailand
[2] Faculty of Liberal Arts and Science, Kasetsart University Kamphaeng Saen Campus, Nakhon Pathom, 73140, Thailand
* Correspondence: faasnmlo@ku.ac.th; (NL)

Citation:
Pengwong, T.; Lokkamlue, N. Study of Spent coffee grounds using cytological technique on root yip of *Allium cepa*. *ASEAN J. Sci. Tech. Report.* **2025**, *28*(6), e259706. https://doi.org/10.55164/ajstr.v28ix.259706.

Article history:
Received: June 12, 2025
Revised: September 5, 2025
Accepted: September 10, 2025
Available online: October 14, 2025

Abstract: Coffee is a widely consumed beverage that has a major impact on economies, markets, and industries; however, the postproduction of coffee drinks results in wasted or spent coffee grounds (SCG). SCG is used as a plant growth medium; however, its suitable level of use is uncertain. This research determined the optimal amount of SCG for root development and its effect on the cells of *Allium cepa*. The SCG was mixed with sand (S) in different ratios (SCG:S = 40:60, 50:50, 60:40, 70:30, 80:20, 90:10) to evaluate their effects on root growth and cytotoxicity on cells. Root number and length were measured to assess growth, while the mitotic index (MI) and chromosomal abnormalities were analyzed to determine cytotoxic effects. The 40:60 SCG:S mixture produced the highest root growth compared to controls, whereas higher SCG ratios (70:30, 80:20, 90:10) reduced the MI. Various chromosomal abnormalities were observed, such as micronuclei, c-mitosis, fragmented chromosomes, chromosome bridges, sticky chromosomes, and laggard chromosomes. Therefore, the chemical compounds in SCG affected cytotoxicity on *A. cepa* roots. The most beneficial use of SCG for addition to plant growth media resulted from a precisely defined mixture to balance growth enhancement with potential cytotoxic risk.

Keywords: Cell aberration; root tip; cell division; spent coffee grounds; growth media

1. Introduction

Coffee belongs to the family Rubiaceae and the tribe Coffeeae [1]. More than 100 species of the genus *Coffea* are known, with the two varieties *C. arabica* and *C. canephora* being the most economically exploited species [2]. Coffee is one of the most popular beverages globally and is the second most-traded commodity after petroleum. Due to high demand, the coffee industry generates a variety of by-products. The process of producing coffee begins with harvesting coffee cherries, which are either dry- or wet-processed to produce green coffee, the standardized trading form [3]. However, the industrial production of coffee yields large quantities of by-products, including cherry husks, cherry pulps, silver skin, and ultimately, spent coffee grounds (SCG) [4]. SCG refers to the solid waste generated in serving individual coffee consumers or during the industrial production of instant coffee and the roasting of coffee beans [5,6]. During instant coffee production, an estimated 6 million tonnes of SCG are generated worldwide annually [6]. Furthermore, the accumulation of coffee waste is increasing in line with the increase in coffee consumption [7]. Disposing of SCG in large quantities in landfills could lead to pollution of water resources and the release of CO_2, which contributes to climate change [5]. Therefore, the

large volume of SCG generated during coffee production highlights the increasing importance of effective recycling.

SCG is a valuable organic waste that can be repurposed for economic, commercial, and domestic agricultural applications. SCG contains polysaccharides, sugars, proteins, minerals, lipids, caffeine, acids, alkaloids, and polyphenols [8,9]. Ramalakshmi et al. [10] found that the primary antioxidant in SCG is 5-caffeoylquinic acid (~6%). Bravo et al. [11] also noted substantial levels of total caffeoylquinic acids (6–13 mg/g) and dicaffeoylquinic acids (3–6 mg/g). Due to its chemical composition, antioxidant, emulsifying, and emulsion properties, as well as its high lipid content (mostly fatty acids), SCG has the potential for incorporation into topical products such as creams and sun protectors [9]. Additionally, SCG can supply nutrients and promote plant growth, particularly in dry agricultural areas that require improved soil fertility [12]. SCG directly enhances the soil's physical, chemical, and biological structure by leaching various nutrients, including nitrogen, phosphorus, and potassium, into the soil through water [13]. Consistently, the application rate and plant species, as well as the application of raw SCG, have shown positive effects on physical and chemical soil properties such as moisture content, soil porosity, and bulk density [13]. However, the high moisture content of SCG can produce odors and harbor insects [5], while different types of SCG have varying effects on the toxicity of the plant [14]. The compounds in SCG may interfere with seed germination and root elongation, thus raising concerns about its safe use in crop production [15,16].

Although the agronomic potential of SCG as a soil amendment has been thoroughly investigated for various plant species, there has been no published information on the cytotoxicity of SCG in plant cells, particularly using the *Allium cepa* test. Cytological studies can provide insights into the mechanisms of SCG toxicity and better evaluate its suitability for sustainable agricultural applications. Currently, a cytological technique is used to examine chromosome abnormalities. The onion plant is an ideal model for studying chromosomal changes due to its moderate number of chromosomes (2n = 16), suitable size, low cost, high sensitivity, and reproducibility [17]. Therefore, analyzing *A. cepa* root tip cells is a convenient method for determining the cytotoxic impact of SCG on the growth of onion roots and chromosome aberrations under a microscope.

2. Materials and Methods

2.1 Preparation of aceto-orcein dye

A sample (1 g) of orcein dye powder was dissolved in 45 mL of acetic acid and 55 mL of distilled water. Then, the orcein solution was boiled until completely dissolved. After that, the solution was passed through Whatman filter paper and stored in dark bottles, where it was used as a 1% w/v aceto-orcein dye solution for chromosome staining.

2.2 Onion cultivation

Spent coffee grounds (SCG) were derived from roasted coffee powder that had been used to prepare coffee beverages, dried at 40°C, and then sieved to obtain a uniform particle size. A sample of 10 onion bulbs was placed in trays containing different treatments of sand combined with SCG for approximately 7 days, until the emergence of new roots at 25±2°C. For the root cytotoxicity assay, six treatments of each growth medium were varied in the following order: SCG:S, 40:60, 50:50, 60:40, 70:30, 80:20, and 90:10, and then compared to a positive control (100% SCG) and a negative control (100% S). The experiment was performed in triplicate for each SCG-to-sand ratio.

2.3 Measurements of the number and length of onion roots

After the cultivation period, the roots of the onions from each treatment were cleaned. The lengths and number of root tips were measured for three onion bulbs from each treatment. Subsequently, the remaining seven onion bulbs were transferred to a fixative solution containing ethanol and glacial acetic acid in a 3:1 ratio for 24 hours at 4°C. Then, the roots were transferred to 70% v/v alcohol at the same temperature. These treated roots were used in subsequent steps for preparing onion root cell slides.

2.4 Cytotoxicity assay on root cells

Once cut, the rootlets were soaked in a fixative solution for 24 hours at 4°C. The root tips (1–3 mm in length) were hydrolyzed in 1 N hydrochloric acid at room temperature for 5 minutes and then stained with aceto-orcein for 5 minutes. Following staining, they were squashed onto a glass slide to determine the mitotic phase for the percentage mitotic index (MI) and to assess for the percentage of chromosomal cell aberrations, using equations (1) and (2), respectively. This was done by viewing the slides under a light microscope (Olympus CX 23) with a 400× objective lens; 200 cells were considered per slide for three slides in each treatment.

$$\% \text{ MI} = \frac{\text{Number of cells in mitotic phases}}{\text{Total number of cells counted}} \times 100 \quad (1)$$

$$\% \text{ Cell aberration} = \frac{\text{Number of aberration cells}}{\text{Total number of cells counted}} \times 100 \quad (2)$$

2.5 Statistical analysis

The SPSS software program, version 29, was used to analyze the number and length of roots, as well as the number of cells. One-way analysis of variance with a 5% significance level ($p < 0.05$) was applied to compare the averages. All treatments were conducted in triplicate, with the data presented as the mean ± standard deviation (SD).

3. Results and Discussion

3.1 Effect of SCG on the growth of onion roots

SCG provides sufficient nutrients and supports plant growth, with numerous studies investigating its use as an alternative to chemical fertilizers for promoting plant growth. For example, Hechmi et al. [12] reported that raw SCG contained significant concentrations of organic matter (62.6%), nitrogen (2.4%), phosphorus (0.47%), and potassium (0.94%). SCG residues from instant coffee preparation could be distinguished by their fine particle size and relatively high humidity levels, ranging from 69.7% [18] to 80% [6]. Additionally, raw SCG had a high water-holding capacity (70–73 g per 100 g of SCG), which could supply water to the plant [19]. Furthermore, the pH of raw SCG was moderately acidic, ranging from 3.9 [14] to 5.52 [20], indicating its potential use as a bio-fertilizer for many plant species. These findings from other studies support the current results on onion root growth, based on different combinations of SCG and sand as the onion plant medium. The growth medium mixed with SCG resulted in greater root length and number of roots (2.07 ± 0.48 cm and 17.33 ± 2.31 roots, respectively) than the 100% sand-negative control group. The best effects on root length were observed when using the SCG:S ratios of 40:60 and 50:50 (4.61 ± 0.50 and 3.16 ± 0.44 cm, respectively). The number of roots for 40:60 was 31.00 ± 4.58 (Table 1). When the SCG-to-sand ratio exceeded 50, the length of the roots decreased. The mixtures with ratios of 60:40 and 70:30 were not significantly different from the negative control group (Table 1). Therefore, these ratios did not lead to improved growth of the onion roots. The ratios of 80:20 and 90:10 significantly reduced root length compared to the negative control group (0.90 ± 0.18 and 0.75 ± 0.19 cm, respectively). However, these ratios were consistent with the positive control group, where the growth medium was 100% SCG (1.11 ± 0.10 cm), suggesting that the presence of certain substances in the SCG may excessively inhibit root growth in such growth media (Figure 1 F–H). For the different mixtures of SCG and sand, ranging from 50:50 to 90:10, there was no significant increase in the number of roots compared to the control groups (Table 1), indicating that the specified ratios of SCG to sand did not affect the number of roots (Figure 1). Therefore, the optimal ratio of SCG-to-sand for promoting the growth of onion roots (both the length and number of roots) was 40:60 (Figure 1 B). Caliskan et al. [21] demonstrated that the application of 20% SCG + 80% sand media as the growth medium for stone pine (*Pinus pinea*) produced the greatest root collar diameter and number of lateral branches. However, higher SCG rates (30%) decreased the seedling height, maximum root length, total needle weight, stem weight, main root weight, and lateral root weight [21]. The current results for root growth of *A. cepa* showed that the 60% SCG rate resulted in decreased root length, suggesting that such higher SCG rates affected root development. Ribeiro et al. [16] anticipated that the presence of other chemicals in raw SCG, such

as caffeine (CFN) and phenolic compounds, inhibited seed germination. Raw (fresh and air/oven-dried) SCG generally contains significant concentrations of phenolic compounds [8] and tannin and CFN [16]. CFN can have positive and negative effects on small plants, as the caffeine found in coffee can affect them depending on its concentration. Using caffeine at an optimal concentration can accelerate root growth, increase the frequency of root formation, and increase the number of roots following root pruning in small plants [22]. CFN extracted using supercritical CO_2 from SCG corresponded to 18–48% of the extracted compounds from coffee beans and 8–31% from roasted coffee [21]. CFN concentrations exceeding 0.1% can harm plant tissue by slowing or stopping root formation and shoot growth, and causing tissue necrosis [23]. SCG generally contains high levels of polyphenols, which are induced mainly by phytotoxic chemicals in the raw material [8,24]. In addition, phytotoxicity may be due to the high tannin concentrations in SCG [25], which can be toxic to root formation. The roots play a crucial role in absorbing and transporting water and minerals. Additionally, SCG derivatives, such as biochar, contain carboxylic acids that exhibit phytotoxic effects by inhibiting seed germination in lettuce (*Lactuca sativa*) [26]. The primary mechanism by which SCG may inhibit plant growth is by reducing nitrogen release, which is related to the amount of chlorophyll [13]. Furthermore, the carbon-nitrogen ratio (C/N) of raw SCG ranges from 20 to 32, which is higher than the C/N ratio in most horticultural soils and far higher than that of soil microbial populations [13].

Table 1. Length and number of onion roots after 7 days of growth in different spent coffee grounds (SCG) and sand (S) mixtures

Growth medium (SCG:S)	Root length (cm)	Number of roots
0:100	2.07 ± 0.48^{c}	17.33 ± 2.31^{c}
40:60	4.61 ± 0.50^{a}	31.00 ± 4.58^{a}
50:50	3.16 ± 0.44^{b}	24.33 ± 3.31^{b}
60:40	2.00 ± 0.65^{c}	18.00 ± 1.73^{c}
70:30	1.91 ± 0.31^{c}	16.67 ± 2.08^{c}
80:20	0.90 ± 0.18^{d}	17.00 ± 2.65^{c}
90:10	0.75 ± 0.19^{d}	16.67 ± 5.51^{c}
100:0	1.11 ± 0.10^{d}	19.00 ± 1.00^{bc}

Note: Values (mean ± SD) with different lowercase superscripts in column indicate significant ($p<0.05$) differences.

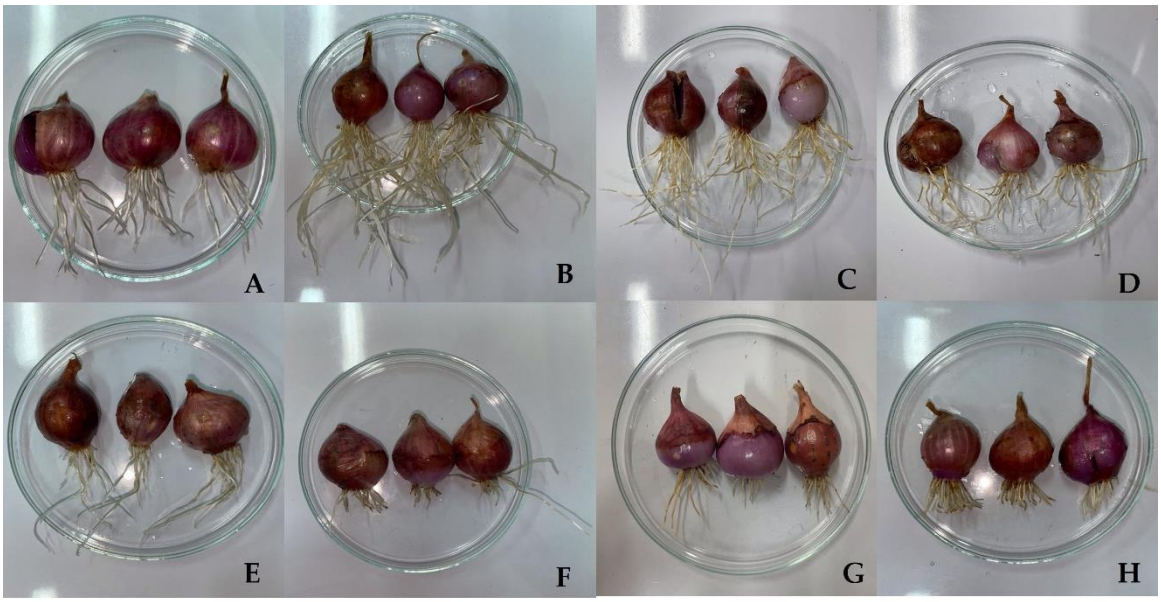

Figure 1. Onion bulb roots planted in various ratios of SCG-to-S for 7 days: (A) 0:100, (B) 40:60, (C) 50:50, (D) 60:40, (E) 70:30, (F) 80:20, (G) 90:10, (H) 100:0

3.2 Cytotoxicity of SCG on onion root cells

Examination of the amount of SCG that causes toxicity to cells and chromosomes in onion root cells identified that when SCG-exposed cells were examined, the MI decreased. Compared to the control group, the decrease in MI of dividing onion root tip cells leads to a corresponding increase in chromosomal abnormalities. This increase has been reported to be directly proportional to the chemical concentration and the duration of exposure to the onion roots [27]. After 7 days of growth, the growth medium consisting of large amounts of SCG mixed with sand (70:30 or higher) led to a significant decrease in the MI compared to the negative control group. However, the SCG:S mixture of 60:40 had lower toxicity than the 70:30 medium, although the MI values (37.67 ± 1.04 and 34.83 ± 1.15, respectively) were not significantly different. In contrast, the 60:40 mixture of SCG and sand had a significantly higher MI than the positive control group (Table 2), indicating that the 60:40 ratio began to affect the onion root cells, leading to an increase in abnormalities and inhibition of cell division at the root tip, resulting in a decrease in root length compared to the negative control group (Figure 1D). Furthermore, a correlation was observed between the number of abnormal cells and the decrease in MI (Table 2). In addition, the 40:60 and 50:50 growth media had MI values of 41.50 ± 2.65 and 40.67 ± 1.53, respectively. These ratios did not significantly impact the decrease in MI compared to the negative control group (Table 2). Hence, they were suitable for promoting cell division in onion roots, leading to increased root length (Figures 1B and C). However, the 100% SCG resulted in increased root length corresponding to the MI values for the 80:20 and 90:10 treatments. The cell abnormalities resulting from toxicity due to excessive mixing of SCG included micronuclei, c-mitosis, fragmented chromosomes, chromosome bridges, sticky chromosomes, and laggard chromosomes (Figure 2F–L). The number of these abnormalities varied with each set of growth media treatments. The mechanisms underlying these effects likely relate to the chemical composition of SCG, which contains caffeic acid, coumaric acid, and protocatechuic acid [28]. These compounds are known to produce reactive oxygen species (ROS), which leads to oxidative stress and the disruption of essential cellular enzymes [29]. Similar trends have been observed in studies where *A. cepa* was exposed to coffee extracts, resulting in dose-dependent declines in germination and mitotic activity [30]. The abnormalities observed in onion root cells can be attributed to the presence of CNF, as reported by Chandraker et al. [31]. They examined beverages containing CNF, such as coffee, tea, and Coca-Cola®, to observe their impact on the normality of *A. cepa* root cells. They observed that the concentration of the beverages and the duration of exposure to the onion roots led to the formation of abnormal cells with characteristics such as c-mitosis, stickiness, adherent chromosomes, and laggard chromosomes. Furthermore, *A. cepa* remains a reliable model for identifying cytogenetic disruptions caused by environmental pollutants due to its sensitivity and cost-effectiveness [17]. However, a limitation of the current study was the lack of chemical analysis of the SCG extracts to establish dose-response relationships and to determine the specific chemical or chemicals responsible for SCG toxicity. Nevertheless, this approach should support the development of safe and sustainable methods for using SCG in agriculture.

Table 2. Abnormal cells and MI values observed in onion root cells during mitotic cell division

Growth medium (SCG:S)	% MI	MN	CM	FC	CB	SC	LC	Cell aberration (number)	Cell aberration (%)
0:100	41.67 ± 0.76^{a}	10.33 ± 1.15^{ab}	4.00 ± 1.00^{cd}	7.00 ± 0.00^{a}	14.67 ± 1.53^{a}	22.67 ± 0.58^{d}	28.33 ± 2.08^{cd}	87.00 ± 1.00^{cd}	43.50 ± 0.50^{cd}
40:60	41.50 ± 2.65^{a}	12.00 ± 4.00^{a}	2.67 ± 2.08^{cd}	6.67 ± 3.21^{a}	12.67 ± 1.53^{a}	24.00 ± 2.65^{d}	26.67 ± 4.16^{d}	84.67 ± 6.11^{d}	42.33 ± 3.06^{d}
50:50	40.67 ± 1.53^{a}	6.33 ± 1.15^{bc}	5.00 ± 1.00^{bc}	10.33 ± 1.53^{a}	13.67 ± 2.08^{a}	26.33 ± 1.53^{cd}	27.67 ± 1.53^{d}	89.33 ± 3.15^{cd}	44.67 ± 1.76^{cd}
60:40	37.67 ± 1.04^{ab}	4.33 ± 2.08^{c}	3.33 ± 1.53^{cd}	6.33 ± 1.15^{a}	13.33 ± 1.53^{a}	31.00 ± 3.46^{bc}	35.00 ± 3.46^{abc}	93.33 ± 1.53^{bcd}	46.67 ± 0.76^{bcd}
70:30	34.83 ± 1.15^{bc}	10.33 ± 3.06^{ab}	4.33 ± 2.08^{cd}	8.67 ± 4.16^{a}	14.67 ± 2.08^{a}	27.00 ± 2.00^{cd}	29.67 ± 6.51^{bcd}	94.67 ± 1.53^{bc}	47.33 ± 0.76^{bc}
80:20	33.67 ± 1.89^{bc}	5.67 ± 1.53^{bc}	12.67 ± 1.15^{a}	9.00 ± 2.00^{a}	13.33 ± 1.53^{a}	30.00 ± 2.00^{bc}	32.00 ± 1.00^{abcd}	102.67 ± 3.79^{ab}	51.33 ± 1.89^{ab}
90:10	31.00 ± 4.77^{c}	6.00 ± 4.58^{bc}	7.67 ± 2.08^{b}	8.67 ± 2.52^{a}	15.00 ± 3.00^{a}	32.33 ± 4.73^{b}	38.33 ± 5.03^{a}	108.00 ± 11.27^{a}	54.00 ± 5.63^{a}
100:0	33.15 ± 0.87^{c}	5.00 ± 2.00^{c}	1.67 ± 0.58^{d}	6.67 ± 1.15^{a}	14.33 ± 2.08^{a}	37.33 ± 2.08^{a}	35.33 ± 1.15^{ab}	100.33 ± 3.51^{ab}	50.17 ± 1.76^{ab}

Note: Values (mean ± SD) with different lowercase superscripts in column indicate significant ($p<0.05$) differences. Abbreviations: MI = mitotic index, MN = micronucleus, CM = C-mitosis, FC = fragmented chromosome, CB = chromosome bridges, SC = sticky chromosomes, and LC = laggard chromosome.

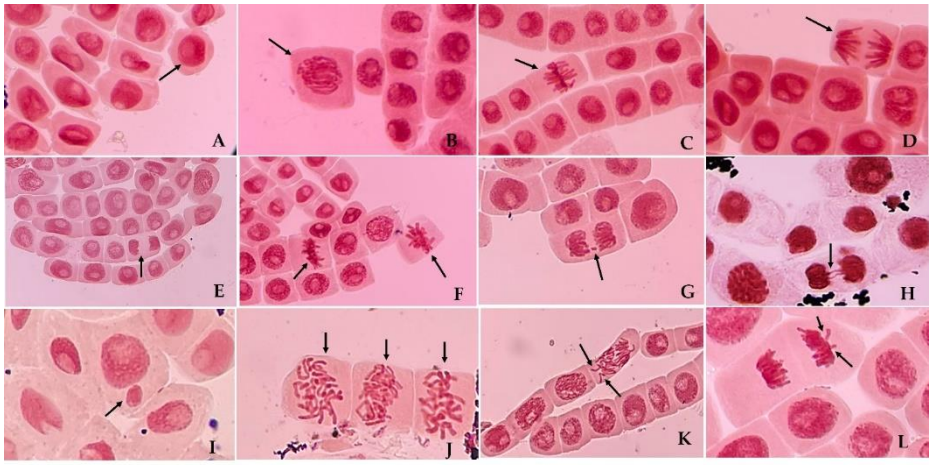

Figure 2. Characteristics of normal and abnormal cell division in onion root tip cells at 400× magnification: (A) Interphase, (B) Prophase, (C) Metaphase, (D) Anaphase, (E) Telophase, (F) Sticky chromosome, (G) Fragmented chromosome, (H) Chromosome bridges, (I) Micronucleus, (J) C-mitosis, (K and L) Laggard chromosome

4. Conclusions

Spent coffee grounds (SCG) can be utilized as a growth medium to promote plant growth. The experiments on onions demonstrated that the optimal SCG-to-sand ratio for influencing root growth was 40:60. During the onion root cell toxicity testing of SCG, it was observed that using a growth medium with a 60:40 ratio resulted in increased abnormalities in the onion root cells. This mixture inhibited cell division at the root tips, which was correlated with abnormal cells and a decrease in the MI. Using SCG in optimal amounts can promote root growth in plants, but excessive use may lead to cell toxicity and hinder growth. Consequently, SCG might be an alternative to organic amendments for plants. However, further research is needed to investigate the chemical profiling of SCG in relation to various plant species, as well as to conduct cytotoxic and physiological assessments. This would help clarify the dose-response relationships and toxicity mechanisms and facilitate the development of processes or tests for evaluating SCG in field conditions. Such a comprehensive approach could ultimately lead to the safe and sustainable incorporation of SCG in agricultural systems.

5. Acknowledgements

The Faculty of Liberal Arts and Science and Kasetsart University Kamphaeng Saen Campus, Thailand, provided a grant. The Genetics Division provided the necessary facilities.

Author Contributions: TP, technical assistance; NL, conceptualization, methodology, original draft preparation, review, editing, validation, resource; and wrote the manuscript. All authors have read and agreed to the published version of the manuscript.

Funding: This research received no external funding.

Conflicts of Interest: The authors declare no conflict of interest.

References

[1] Clifford, MN; Williams, T.; Bridson, D. Chlorogenic acids and caffeine as possible taxonomic criteria in *Coffea* and *Psilanthus*. *Phytochemistry.* **1989**, *28*, 829–838. https://doi.org/10.1016/0031-9422(89)80124-4

[2] Davis, A.P.; Govaerts, R.; Bridson, D.M.; Stoffelen, P. An annotated taxonomic conspectus of the genus *Coffea* (Rubiaceae). *Bot. J. Linn. Soc.* **2006**, *152*, 465–512. https://doi.org/10.1111/j.1095-8339.2006.00584.x

[3] Esquivel, P.; Jiménez, V.M. Functional properties of coffee and coffee by-products. *Food Res. Int.* **2012**, *46*, 488–495. https://doi.org/10.1016/j.foodres.2011.05.028

[4] de Melo Pereira, G.V.; de Carvalho Neto, D.P.; Júnior, A.I.M.; do Prado, F.G.; Pagnoncelli, M.G.B.; Karp, S.G.; Soccol, C.R. Chemical composition and health properties of coffee and coffee by-products. *Advances in Food and Nutrition Research.* **2020**, *91*, 65–96. https://doi.org/10.1016/bs.afnr.2019.10.002

[5] Murthy, P.S.; Naidu, M.M. Sustainable management of coffee industry by-products and value addition—A review. *Resources, Conservation and Recycling.* **2012**, *66*, 45–58. https://doi.org/10.1016/j.resconrec.2012.06.005

[6] Mussatto, S.I.; Carneiro, L.M.; Silva, J.P.A.; Roberto, I.C.; Teixeira, J.A. A study on chemical constituents and sugars extraction from spent coffee grounds. *Carbohyd. Polym.* **2011**, *83*, 368–374. https://doi.org/10.1016/j.carbpol.2010.07.063

[7] Colantoni, A.; Paris, E.; Bianchini, L.; Ferri, S.; Marcantonio, V.; Carnevale, M.; Palma, A.; Civitarese, V.; Gallucci, F. Spent coffee ground characterization, pelletization test and emissions assessment in the combustion process. *Sci. Rep.* **2021**, *11*, Article 5119. https://doi.org/10.1038/s41598-021-84772-y

[8] Santos, C.; Fonseca, J.; Aires, A.; Coutinho, J.; Trindade, H. Effect of different rates of spent coffee grounds (SCG) on composting process, gaseous emissions and quality of end-product. *Waste Manag.* **2017**, *59*, 37–47. https://doi.org/10.1016/j.wasman.2016.10.020

[9] dos Santos, É.M.; de Macedo, L.M.; Tundisi, L.L.; Ataide, J.A.; Camargo, G.A.; Alves, R.C.; Oliveira, M.B.P.P.; Mazzola, P.G. Coffee by-products in topical formulations: A review. *Trends Food Sci. Tech.* **2021**, *111*, 208–291. https://doi.org/10.1016/j.tifs.2021.02.064

[10] Ramalakshmi, K.; Rao, L.J.M.; Takano-Ishikawa, Y.; Goto, M. Bioactivities of low-grade green coffee and spent coffee in different in vitro model systems. *Food Chem.* **2009**, *115*, 79–85. https://doi.org/10.1016/j.foodchem.2008.11.063

[11] Bravo, J.; Juániz, I.; Monente, C.; Caemmerer, B.; Kroh, L.W.; de Peña, M.P.; Cid, C. Evaluation of spent coffee obtained from the most common coffeemakers as a source of hydrophilic bioactive compounds. *J. Agr. Food Chem.* **2012**, *60*, 12565–12573. https://doi.org /10.1021/jf3040594

[12] Hechmi, S.; Guizani, M.; Kallel, A.; Zoghlami1, R.I.; Zrig, E.B.; Louati, Z.; Jedidi, N.; Trabelsi, I. Impact of raw and pre-treated spent coffee grounds on soil properties and plant growth: a mini-review. *Clean Technol. Envi.* **2023**, *25*, 2831–2843. https://doi.org/10.1007/s10098-023-02544-w

[13] Hardgrove, S.J.; Livesley, S.J. Applying spent coffee grounds directly to urban agriculture soils greatly reduces plant growth. *Urban For. Urban Gree.* **2016**, *18*, 1–8. https://doi.org/10.1016/j.ufug.2016.02.015

[14] Cruz, R.; Cardoso, M.M.; Fernandes, L.; Oliveira, M.; Mendes, E.; Baptista, P.; Morais, S.; Casal, S. Espresso coffee residues: a valuable source of unextracted compounds. *J. Agr. Food Chem.* **2012**, *60*, 7777–7784. https://dx.doi.org/10.1021/jf3018854

[15] Kim, M-.S.; Min, H-.G.; Koo, N.; Park, J.; Lee, S-.H.; Bak, G-.I.; Kim, J-.G. The effectiveness of spent coffee grounds and its biochar on the amelioration of heavy metals-contaminated water and soil using chemical and biological assessments. *J. Environ. Manag.* **2014**, 146, 124–130. https://doi.org/10.1016/j.jenvman.2014.07.001

[16] Ribeiro, J.P.; Vicente, E.D.; Gomes, A.P.; Nunes, M.I.; Alves, C.; Tarelho, L.A. Effect of industrial and domestic ash from biomass combustion, and spent coffee grounds, on soil fertility and plant growth: experiments at field conditions. *Environ. Sci. Pollut. R.* **2017**, *24*, 15270–15277. https://doi.org/10.1007/s11356-017-9134-y

[17] Nicuță, D.; Grosu, L.; Patriciu, O.-I.; Voicu, R.-E.; Alexa, I.-C. The *Allium cepa* model: a review of its application as a cytogenetic tool for evaluating the biosafety potential of plant extracts. *Methods Protoc.* **2025,** 8, Article 88. https://doi.org/10.3390/mps8040088

ASEAN
Journal of Scientific and Technological Reports
Online ISSN:2773-8752

Research article

Effect of Storage Temperature on Degradation and Antioxidant Activity of Anthocyanin in Community–Produced Mao Juice from Sakon Nakhon Province, Thailand

Thitiya Sripakdee[1], Wuttichai Roschat[2, 3*], Thatphong Chaisura[4], and Aphisit Maiaka[5]

[1] Faculty of Science and Technology, Sakon Nakhon Rajabhat University, Sakon Nakhon, 47000, Thailand
[2] Faculty of Science and Technology, Sakon Nakhon Rajabhat University, Sakon Nakhon, 47000, Thailand
[3] Biomass Energy Research Laboratory, Center of Excellence on Alternative Energy, Research and Development Institution, Sakon Nakhon Rajabhat University, Sakon Nakhon, 47000, Thailand
[4] Faculty of Science and Technology, Sakon Nakhon Rajabhat University, Sakon Nakhon, 47000, Thailand
[5] Faculty of Science and Technology, Sakon Nakhon Rajabhat University, Sakon Nakhon, 47000, Thailand
* Correspondence: roschat1@gmail.com

Citation:
Sripakdee, T.; Roschat, W.; Chaisura, T.; Maiaka, A. Effect of storage temperature on the degradation and antioxidant activity of anthocyanin in community-produced Mao juice from Sakon Nakhon Province, Thailand. *ASEAN J. Sci. Tech. Report.* **2025**, *28*(6), e260077. https://doi.org/10.55164/ajstr.v28i6.260077.

Article history:
Received: June 30, 2025
Revised: September 7, 2025
Accepted: September 12, 2025
Available online: October 14, 2025

Abstract: This study examined the influence of storage temperature and duration on anthocyanin degradation and antioxidant activity in Mao juice, a community-produced beverage from *Antidesma thwaitesianum* in Sakon Nakhon Province, Thailand. Four commercial samples were stored at 4°C and 30°C for 35 days. Anthocyanin content was determined by the pH differential method, while antioxidant activity was assessed using ABTS and FRAP assays. Results showed that Sample A had the highest initial anthocyanin content at 4 °C (41.74 mg/L), decreasing slightly to 40.24 mg/L. At 30 °C, anthocyanin degradation was more pronounced, with Sample A declining from 36.06 to 33.89 mg/L, Sample B from 21.87 to 18.86 mg/L, and Samples C and D dropping from 1.03 to 0.70 mg/L and 0.76 to 0.53 mg/L, respectively. Degradation followed first-order kinetics, with rate constants ranging from 1.0×10^{-3} to 10.9×10^{-3} day^{-1} and half-lives between 99.0 and 9.1 weeks. Sample A was the most stable ($k = 1.0\times10^{-3}$ day^{-1} at 4°C), while Sample C degraded fastest at 30 °C. Antioxidant capacity was highest in Sample A at 4°C on day 0 (1,286.17 mg Trolox/100 mL, ABTS assay), decreasing to 1,240.16 mg by day 35, compared with 1,184.46 mg at 30°C. FRAP values showed parallel trends, with Sample A declining from 826.56 to 811.55 mg Trolox/100 mL at 4°C and from 770.80 to 750.38 mg at 30 °C. The greatest antioxidant loss occurred in Sample B at 30°C ($k = 10.0\times10^{-3}$ day^{-1}). Overall, cold storage was shown to preserve Mao juice stability and functional quality, providing practical guidance for local producers to extend shelf life.

Keywords: Mao juice; anthocyanin degradation; antioxidant activity; storage temperature; community product

1. Introduction

In recent years, a growing global trend toward health consciousness has emerged, particularly through the increasing consumption of natural products. This shift in consumer behavior has led to a substantial expansion of the functional beverage market, with fruit juices playing a prominent role. These beverages are often marketed for their purported health benefits, such as enhancing the immune system, delaying the signs of aging, reducing oxidative stress, and, notably, preventing chronic diseases, including cancer. These health-

promoting effects are primarily attributed to the presence of natural antioxidants found abundantly in fruits and vegetables. Among various antioxidants, anthocyanins have received significant attention due to their dual roles as both pigments and bioactive compounds. Anthocyanins are water-soluble flavonoid compounds responsible for the vivid red, purple, and blue hues in many fruits and vegetables. Their coloration varies with pH, appearing red in acidic environments and shifting to blue under alkaline conditions, making them not only valuable as functional food ingredients but also as natural pH indicators [1-3].

Beyond their aesthetic function, anthocyanins exhibit a range of biological activities, including anti-inflammatory, antimicrobial, and strong antioxidant properties, which contribute to cellular protection against oxidative stress and damage induced by free radicals. These mechanisms are closely linked to the prevention of non-communicable diseases (NCDs), including cardiovascular disease, diabetes, and certain types of cancer. As a result, anthocyanin-rich fruits such as berries, grapes, purple corn, black rice, and purple sweet potatoes have been increasingly incorporated into health-oriented food and beverage products. Ongoing research continues to explore their therapeutic potential, bioavailability, and stability under different processing conditions to enhance their application in functional foods and nutraceuticals [3-6].

Focusing on Sakon Nakhon province, one of the northeastern provinces of Thailand, it is recognized for its rich biodiversity and the presence of many endemic plant species unique to the region. One notable endemic plant is *Antidesma thwaitesianum*, a wild fruit found specifically in Sakon Nakhon. Commonly known as "Mao", this fruit is known to contain a variety of phytochemicals, including polyphenols and anthocyanins, which exhibit strong antioxidant properties [7-9]. In addition to its phytochemical richness, the Mao fruit plays a significant role in local traditions and the local economy. Local communities often process the fruit into ready-to-drink juices, which have become a well-known regional product. Mao–based beverages display a vibrant reddish–purple color due to their high anthocyanin content and are valued for both their flavor and health benefits [10-12]. Scientific studies report that consumption of drinks containing anthocyanin–rich extracts, such as Mao juice can lower postprandial blood glucose levels, suggesting potential applications in glycemic control [13-14]. Furthermore, Mao fruit extracts inhibit monosaccharide–induced protein glycation and suppress the activity of carbohydrate-hydrolyzing enzymes, including alpha-amylase [11, 13, 15-17]. These bioactivities indicate the potential of Mao fruit as a natural functional ingredient for developing products aimed at preventing and managing metabolic disorders, particularly type 2 diabetes. Utilization of Mao fruit in functional beverage development not only enhances the value of local agricultural produce but also provides a promising natural resource for innovations in health–promoting products.

However, the study also reported that the anthocyanins in Mao juice exhibit low stability and are prone to degradation, leading to the formation of colorless compounds. Various factors influence this instability during fruit processing, including temperature, heating duration, and the concentration of soluble solids. In addition to these variables, the storage conditions of anthocyanin–rich fruit juices also play a crucial role in determining the stability of these compounds. Research has shown that the stability of anthocyanins in fruit juices is significantly impacted by both the temperature and the type of fruit juice [18-19]. A study on the stability of anthocyanins in black carrot juice, for example, indicated that temperature fluctuations and the composition of the juice are key determinants of anthocyanin degradation. Furthermore, the degradation of anthocyanin pigments follows first-order kinetic reactions, suggesting a predictable pattern of degradation over time. These findings imply that the antioxidant capacity of Mao juice, along with its anthocyanin content, may alter during storage, especially under suboptimal conditions [20-22]. Such instability presents challenges for the commercialization and long-term storage of anthocyanin-rich products, such as Maqui juice. It is therefore critical to explore methods for enhancing the stability of anthocyanins, such as adjusting processing techniques, optimizing storage conditions, or utilizing stabilizing agents. Improving the shelf life and preserving the bioactive properties of anthocyanin–rich juices would not only enhance their therapeutic potential but also increase their commercial viability. Recent studies have explored several strategies to address these challenges, such as the use of encapsulation techniques, controlled atmosphere packaging, and the addition of natural antioxidants to stabilize anthocyanin pigments. For instance, research conducted by Rezazadeh and Ghasempour [23], Muche et al. [24], and Türkyılmaz and Özkan [25] highlights the role of encapsulation in improving anthocyanin stability in fruit juices under varying storage conditions.

Therefore, the primary objective of this study is to investigate the impact of temperature and storage time on the anthocyanin content and antioxidant capacity in Mao juice, a locally produced beverage from Sakon Nakhon Province. This research explicitly examines how varying temperatures affect the degradation rates of anthocyanins and antioxidants in Mao juice, as well as the influence of storage time on these bioactive compounds. The study focuses on evaluating the effect of temperature on anthocyanin degradation over 35 days, with samples stored under two conditions: room temperature (30 °C) and refrigeration (4 °C). These temperatures were selected to reflect common storage conditions, with 4°C representing typical refrigeration that slows microbial growth and chemical degradation, and 30 °C representing ambient conditions that the juice may encounter during transportation or storage without cooling, allowing for a comparison of anthocyanin stability under both conditions. Anthocyanin content is quantified using the pH Differential method, while antioxidant activity is assessed using the ABTS and FRAP assays. Additionally, the study tracks the rate of degradation of both anthocyanins and antioxidants over the storage period. The findings from this study are expected to provide valuable insights for local community-based Mao juice producers. The results will help identify key production and storage factors that influence the retention of vital compounds in the juice, ultimately offering guidance on best practices for maintaining product quality and optimizing the health benefits for consumers.

2. Materials and Methods

2.1 Materials

This study investigated four Mao juice samples, designated as Sample A, B, C, and D, sourced from different commercial brands in Sakon Nakhon Province, to evaluate the effects of storage temperature on anthocyanin degradation and antioxidant activity. Brand names have been omitted and replaced with sample codes to avoid potential commercial implications, as the findings regarding bioactive compound levels may influence consumer purchasing decisions and, consequently, impact the reputation or sales of the producers. To maintain experimental accuracy and reliability, a variety of chemicals were used. The key reagents included ethanol (C_2H_5OH), which was utilized for extraction; hydrochloric acid (HCl) and sodium acetate (CH_3COONa) for pH adjustments during the analysis; potassium chloride (KCl) and aluminum chloride ($AlCl_3$) for preparing various assay solutions; and antioxidants such as 2,2′-Azinobis-3-ethylbenzothiazoline-6-sulfonic acid (ABTS) and 2,4,6-Tri(2-pyridyl)-s-triazine (TPTZ), employed to assess antioxidant capacity. Additionally, potassium persulfate was used in the preparation of oxidizing agents. All chemicals were sourced from reputable suppliers, including Sigma–Aldrich, Fluka, QRëC, Merck, Acros Chemical Co. Ltd., and Carlo Erba, ensuring that high-quality reagents were utilized for precise and consistent experimental outcomes.

2.2 Sample preparation

Four commercially available Mao juice samples, designated as Samples A, B, C, and D, were utilized in this study. Each brand provided 500 mL of freshly produced juice, prepared in triplicate. The samples were stored at two different temperatures: refrigeration (4 °C) and ambient room temperature (30 °C). To prevent light-induced degradation, all sample bottles were wrapped in aluminum foil and stored in a dark environment. These temperatures were chosen to reflect common storage conditions: 4°C represents typical refrigeration, which slows microbial growth and chemical degradation, while 30 °C represents ambient conditions that the juice may encounter during transportation or storage without refrigeration. This setup enabled the evaluation of juice stability under both refrigerated and room-temperature conditions. Analyses were conducted over 35 days, with sampling on days 0 (baseline), 7, 14, 21, 28, and 35. At each sampling interval, the juice samples underwent filtration to remove pulp and particulate matter, followed by centrifugation at 3,000 rpm for 20 minutes to separate the sediments. The resulting supernatant was collected for subsequent analyses. For the extraction of anthocyanins and antioxidants, 1 mL of the clarified juice was mixed with 2 mL of ethanol acidified with 1% hydrochloric acid (v/v), achieving a 1:2 sample–to–solvent ratio. The mixture was incubated at room temperature for 2 h in the absence of direct sunlight to prevent degradation of sensitive compounds. Post–incubation, samples were centrifuged at 4,000 rpm for 10 min, and the clear supernatant was collected for the determination of anthocyanin content and antioxidant capacity.

This methodology aligns with established protocols for anthocyanin and antioxidant extraction, ensuring the stability and integrity of bioactive compounds during analysis [26-27].

2.3 Determination of anthocyanin content by the pH differential method

Total anthocyanin content (TAC) was determined using the pH differential method, following the procedures described by Chua et al. [28-9] and Handayani et al. [30]. This method is based on the principle that anthocyanin structures undergo reversible changes in response to pH variation, thereby altering their absorbance properties. In this technique, anthocyanin extracts were adjusted to pH levels of 1.0 and 4.5, and their absorbance was measured across a wavelength range of 260-700 nm. Anthocyanins typically exhibit maximum absorbance between 460 and 560 nm. At pH 1.0, anthocyanins predominantly exist in the colored oxonium form, resulting in high absorbance within this range. In contrast, at pH 4.5, anthocyanins transition to the colorless hemiketal form, leading to a loss of absorbance at these wavelengths. If other compounds that absorb at similar wavelengths are present, their absorbance values remain unchanged under both pH conditions. Thus, the absorbance difference between pH 1.0 and pH 4.5 is explicitly attributed to anthocyanins. To correct for sample turbidity or light scattering, absorbance at 700 nm was also recorded at both pH levels and subtracted from the measurements. Finally, the total anthocyanin content was calculated based on the corrected absorbance values using the appropriate formula, ensuring greater accuracy and precision of the results. The total anthocyanin content (TAC) in Mao juice samples was determined using the pH–differential method, adapted from the procedures described by Chua et al. [28-29] and Handayani et al. [30]. Initially, the Mao juice extracts were diluted 100-fold with distilled water to ensure that the absorbance readings fell within the optimal range for accurate measurement. The final volume of each diluted sample was adjusted to 100 mL. A preliminary absorbance measurement at 520 nm was conducted using a UV-Visible spectrophotometer to verify that the absorbance was within the desirable range of 0.2-0.8, which minimizes errors associated with instrumental sensitivity. Following the preliminary check, the diluted samples were prepared for pH–differential analysis by mixing 2 mL of the sample with 2 mL of 0.025 M potassium chloride buffer solution at pH 1.0 to form the first mixture. Similarly, 2 mL of the sample was mixed with 2 mL of 0.4 M sodium acetate buffer solution at pH 4.5 to form the second mixture. Both mixtures were allowed to equilibrate at room temperature for 15 min, protected from direct sunlight to prevent anthocyanin degradation.

After equilibration, the absorbance of each mixture was measured at two specific wavelengths: 520 nm, corresponding to the maximum absorption peak of anthocyanins, and 700 nm, used to correct for any turbidity or light scattering. Distilled water was used as the blank for all spectrophotometric measurements. The absorbance values were recorded separately for the mixtures at pH 1.0 and pH 4.5. The net absorbance (A) related to anthocyanin concentration was calculated using the following formula (1):

$$A = (A_{520} - A_{700})_{pH\ 1.0} - (A_{520} - A_{700})_{pH\ 4.5} \quad (1)$$

where A_{520} and A_{700} represent the absorbance values at 520 nm and 700 nm, respectively, under each pH condition. The monomeric anthocyanin content, expressed as milligrams of cyanidin-3-glucoside equivalents per liter (mg/L), was calculated according to the following equation (2):

$$\text{Monomeric anthocyanin (mg/L)} = \frac{A \times MW \times DF \times 1000}{\varepsilon \times l} \quad (2)$$

Where MW is the molecular weight of cyanidin-3-glucoside (449.2 g/mol), DF is the dilution factor (i.e., the ratio of the final volume to the initial volume of the diluted sample), ϵ is the molar absorptivity coefficient of cyanidin-3-glucoside in a pH 1.0 buffer (26,900 L/mol cm), and l is the path length of the cuvette (1 cm). As shown in Figure 1, the experimental procedure for determining anthocyanin content was carried out using the pH differential method. All measurements were performed in triplicate for each sample to ensure the precision and reliability of the results.

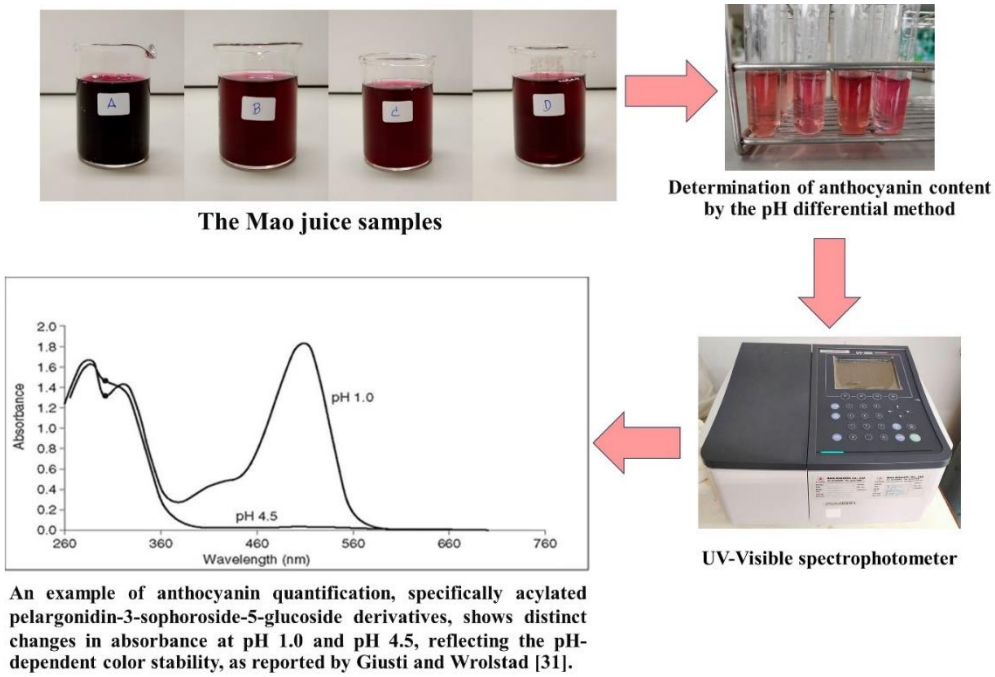

Figure 1. The experimental procedure for determining anthocyanin content using the pH differential method.

2.4 Antioxidant activity analysis

2.4.1 ABTS radical scavenging assay

The in vitro antioxidant activity was evaluated using a modified ABTS radical scavenging assay, following the methods described by Li et al. [31], Cai et al. [32], and Bai et al. [33]. The experimental procedure commenced with the collection of the Mao juice samples stored at refrigeration temperature (4 °C) and ambient room temperature (30 °C) on days 0 (baseline), 7, 14, 21, 28, and 35. The samples were prepared according to the method described in Section 2.2. For the ABTS radical scavenging assay, 7 mM ABTS stock solution and 2.45 mM potassium persulfate solution were prepared separately. Equal volumes of the two solutions were mixed and allowed to react in the dark at room temperature for 12–16 h to generate the $ABTS^{\bullet+}$ radical cation. The resulting $ABTS^{\bullet+}$ solution was subsequently diluted with ethanol to achieve an absorbance of 1.00 ± 0.02 at 734 nm. For the antioxidant assay, the Mao juice samples were diluted 500-fold and 100-fold with distilled water, depending on the expected antioxidant activity. An aliquot of 1 mL of the diluted sample was mixed with 3 mL of the prepared $ABTS^{\bullet+}$ working solution. After incubation at room temperature for 6 min in the dark, the absorbance at 734 nm was measured using a UV–Visible spectrophotometer (UV-1800, Shimadzu, Japan). Ethanol was used as a blank control. As displayed in Figure 2, the antioxidant activity of Mao juice samples was analyzed using a modified ABTS radical scavenging assay. The antioxidant capacity of each sample was quantified by comparing the percentage inhibition of $0ABTS^{\bullet+}$ with a standard curve of Trolox and expressed as milligrams of Trolox equivalents per 100 mL of sample (mg TE/100 mL). All measurements were performed in triplicate to ensure accuracy and reproducibility. This technique offers several advantages, including its ability to measure both hydrophilic and lipophilic antioxidant activity. It is also susceptible, rapid, and adaptable for use with a wide variety of sample types, including fruit juices. These strengths make the ABTS assay a robust and reliable method for antioxidant evaluation in complex food matrices.

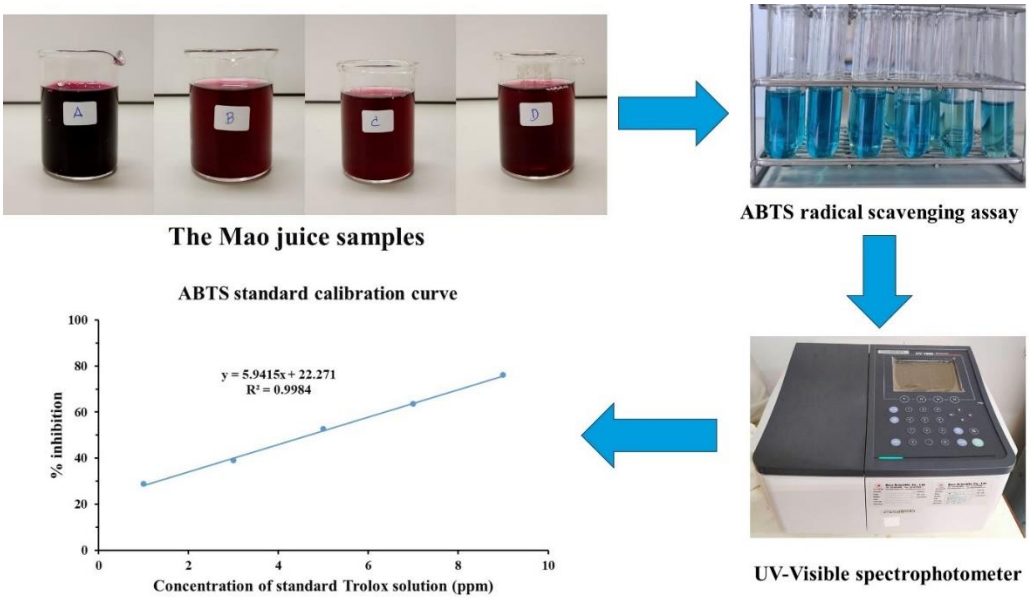

Figure 2. Analysis of antioxidant activity in Mao juice samples using a modified ABTS radical scavenging assay.

2.4.2 Ferric Reducing Antioxidant Power (FRAP) assay

The antioxidant capacity of Mao juice samples was evaluated using the Ferric Reducing Antioxidant Power (FRAP) assay, adapted with modifications based on the methods reported by Bamigbade et al. [34], Spiegel et al. [35], and Muthu et al. [36]. The FRAP reagent was freshly prepared before each analysis by mixing three solutions in the ratio of 10:1:1. These included (1) 300 mM acetate buffer (pH 3.6), (2) 10 mM 2,4,6-tripyridyl-s-triazine (TPTZ) solution dissolved in 40 mM hydrochloric acid, and (3) 20 mM ferric chloride hexahydrate ($FeCl_3 \cdot 6H_2O$) solution. The mixed reagent was pre-warmed to 37 °C in a water bath prior to use. For the calibration curve, 1 mL of Trolox standard solution at various concentrations was mixed with 3 mL of the FRAP reagent. The mixture was incubated at 37 °C for 10 minutes, and the absorbance was measured at 593 nm using a UV-visible spectrophotometer. A standard curve was constructed by plotting absorbance versus Trolox concentration (Figure 3) and used to determine the antioxidant capacity of Mao juice samples. The FRAP assay offers several advantages, including simplicity, rapidity, and low cost, making it ideal for routine antioxidant screening in food samples. It also measures the reducing ability of antioxidants, which is closely associated with their capacity to donate electrons—a fundamental mechanism of antioxidant action. Furthermore, the assay demonstrates high compatibility with aqueous extracts, making it suitable for evaluating fruit juices and other hydrophilic food matrices. The Mao juice samples, obtained from the extraction procedure described in Section 2.2, were initially diluted 100-fold with distilled water to ensure that the absorbance readings would fall within the linear range of the FRAP assay. An aliquot of 1 mL of each diluted extract was thoroughly mixed with 3 mL of the freshly prepared FRAP reagent. The mixture was incubated at 37 °C for 10 min to allow complete reaction, and the absorbance was subsequently measured at 593 nm using a UV-Visible spectrophotometer. Ethanol or distilled water was used as a blank control to calibrate the instrument prior to sample measurements. The antioxidant capacity was expressed as milligrams of Trolox equivalents per 100 mL of sample (mg TE/100 mL), based on interpolation from the Trolox calibration curve. All measurements were performed in triplicate to ensure accuracy and reproducibility.

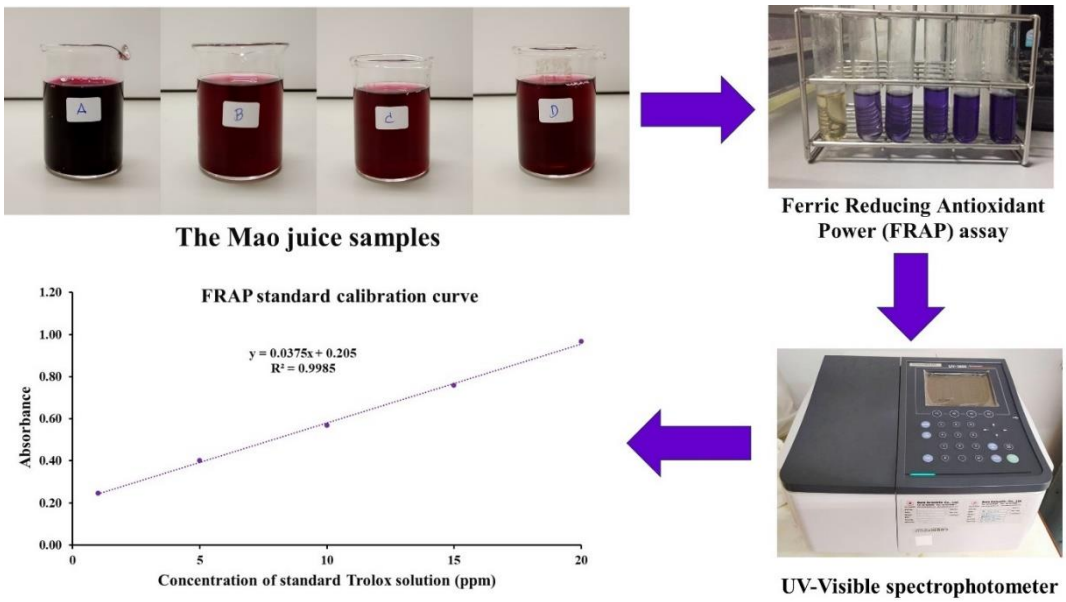

Figure 3. Determination of the antioxidant capacity of Mao juice samples using the Ferric Reducing Antioxidant Power (FRAP) assay.

2.4.3 Degradation kinetics and stability of anthocyanins and antioxidant activity in Mao juice

The degradation kinetics and stability of anthocyanins in Mao juice were investigated by monitoring samples stored at two temperature conditions—refrigeration (4 °C) and ambient room temperature (30 °C)—over a 35-day storage period. Mao juice samples were collected on days 0, 7, 14, 21, 28, and 35, and the total anthocyanin content (TAC) was quantified using the pH differential method, as described in Section 2.2. To evaluate the degradation behavior, a first-order kinetic model was applied, as described in the research reports of Hernandez (Prieto et al. [37] and Chen et al. [38]). The natural logarithm of the ratio of anthocyanin concentration at time (t) to the initial concentration, $\ln(C_t/C_0)$, was plotted against storage time (t), as shown in the following equation (3):

$$\ln(C_t/C_0) = -kt \quad (3)$$

Where C_t is the anthocyanin concentration at time (t), C_0 is the initial anthocyanin concentration, k is the first-order rate constant, and t is the storage time. A linear relationship between $\ln(C_t/C_0)$ and t confirmed that the degradation of anthocyanins followed first-order kinetics. The degradation rate constant (k) was calculated from the slope of the linear regression. The half-life ($t_{1/2}$) of anthocyanins was then determined using equation (3):

$$t_{1/2} = \frac{-\ln 0.5}{k} \approx \frac{0.693}{k} \quad (4)$$

This kinetic approach is widely used for evaluating the thermal sensitivity and oxidative degradation of anthocyanins in fruit-based products. It provides valuable insight into the stability of bioactive compounds under different storage conditions, facilitating optimization of product shelf life and quality preservation strategies.

2.5 Statistical Analysis

All experimental measurements were performed in triplicate, and results are presented as mean ± standard deviation (SD). The data in this study were reported as averages from repeated experiments, and both the standard deviation and percent error were taken into account. All results showed a percent error not exceeding 3%, indicating acceptable precision of the measurements. As this research represented a preliminary study, the four Mao juice samples (Samples A, B, C, and D) were obtained from different commercial brands in Sakon Nakhon Province, each with distinct production processes. Therefore, the study did not emphasize

detailed statistical comparisons among brands; instead, it focused on overall trends in the degradation of anthocyanin content—the principal bioactive compound—and on changes in antioxidant activity. In addition, degradation kinetics and stability analyses were employed to describe the behavior of anthocyanins and their antioxidant activity during storage at various temperatures, and the results were interpreted using basic statistical methods for experimental estimation.

3. Results and Discussion

3.1 Determination of total anthocyanin content using the pH differential method

The total anthocyanin content (TAC) of Mao juice from four commercial brands was monitored during storage at refrigeration temperature (4 °C) and ambient temperature (30 °C) using the pH differential method, with quantification based on comparison to a cyanidin-3-3-glucoside standard. As presented in Table 1, Sample A exhibited the highest initial anthocyanin concentration, followed by Samples B, C, and D, respectively. These differences are likely attributable to variability in raw material selection, cultivar types, harvest maturity, and post-harvest handling. Furthermore, processing methods such as pasteurization, extraction, and filtration may play a significant role in preserving or degrading heat-sensitive compounds, including anthocyanins. Storage temperature was found to have a notable influence on anthocyanin stability. A higher storage temperature (30 °C) accelerated the degradation of anthocyanins across all samples compared to refrigeration at 4 °C. This observation aligns with the known thermal sensitivity of anthocyanin pigments, which are susceptible to structural transformation and oxidation at elevated temperatures [4,27,37-40]. In addition, the anthocyanin content exhibited a gradual decline over time under both storage conditions, with a more pronounced decrease at 30 °C. The degradation pattern observed suggests that prolonged exposure to elevated temperatures exacerbates anthocyanin breakdown, possibly due to enhanced kinetic activity leading to hydrolysis and polymerization reactions. These results indicate that both temperature and storage duration are critical factors in maintaining anthocyanin stability in Mao juice, underscoring the importance of cold chain storage for extending shelf life and preserving the functional quality of anthocyanin-rich beverages.

Table 1. Total anthocyanin content (mg/L) of Mao juice from four commercial brands during storage at 4 °C and 30 °C.

Sample of Mao juice	Storage temperature	Total anthocyanin content (mg/L)					
		Day 0	Day 7	Day 14	Day 21	Day 28	Day 35
Sample A	4 °C	41.74	41.41	41.07	40.91	40.57	40.24
Sample B	4 °C	29.89	29.22	28.72	28.38	28.05	27.88
Sample C	4 °C	1.26	1.20	1.16	1.13	1.10	1.07
Sample D	4 °C	1.03	1.00	0.96	0.90	0.85	0.81
Sample A	30 °C	36.06	35.40	34.90	34.56	34.06	33.89
Sample B	30 °C	21.87	21.20	20.70	20.20	19.53	18.86
Sample C	30 °C	1.03	0.96	0.86	0.84	0.76	0.70
Sample D	30 °C	0.76	0.73	0.70	0.66	0.56	0.53

3.2 Degradation kinetics and stability of anthocyanins in Mao juice

The degradation behavior of anthocyanins in Mao juice under various storage conditions was analyzed by monitoring changes at 4 °C and 30 °C over 35 days. Figure 4 illustrates the linear relationship between the natural logarithm of the anthocyanin content ratio ($\ln(C_t/C_0)$) and storage time (t), confirming that anthocyanin degradation follows first-order reaction kinetics across all samples. The strong linearity (R^2 values approaching 1.0) at both temperatures further supports this kinetic model. From Figure 4, it is evident that the slope of the degradation curves increases with temperature, indicating a higher degradation rate at 30 °C compared to 4 °C. This trend is quantified in Table 2, where all samples exhibit higher degradation rate constants (k) and shorter half-lives ($t_{1/2}$) at elevated temperature. The thermal acceleration of anthocyanin breakdown aligns with known degradation mechanisms involving enhanced molecular mobility and oxidative reactions under heat.

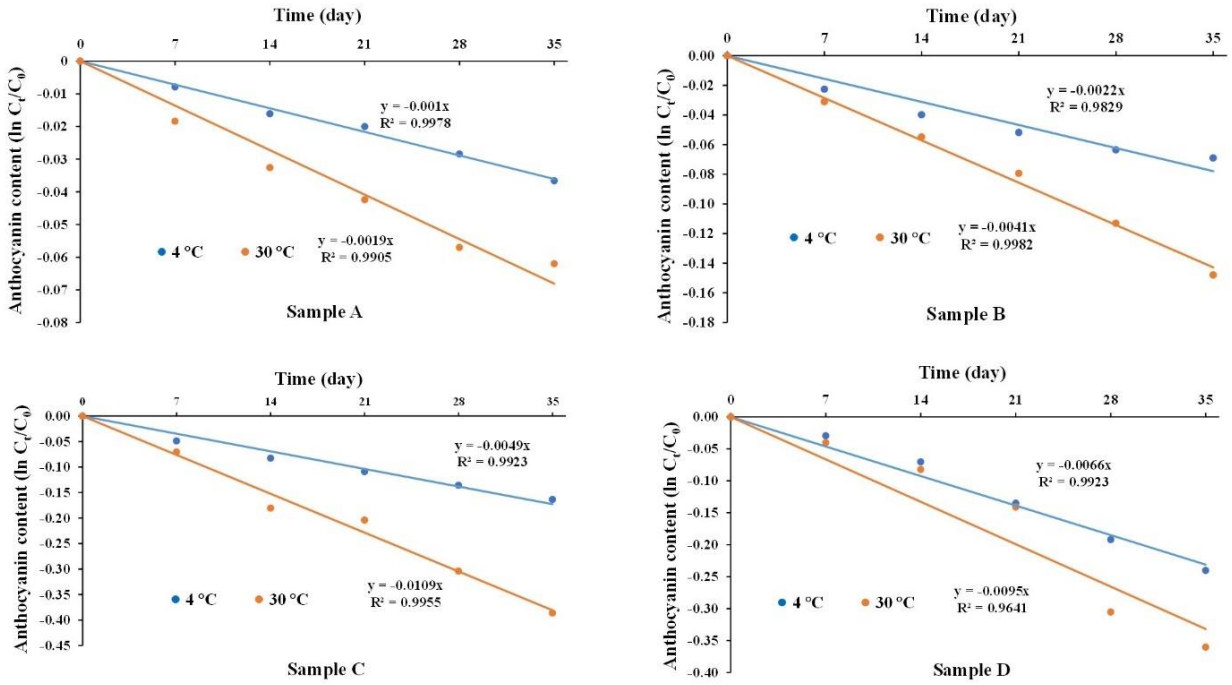

Figure 4. Degradation rate of anthocyanins in Mao juice stored at 4 °C and 30 °C over 35 days, analyzed using the pH–differential method.

Table 2. Degradation kinetics and half-life ($t_{1/2}$) of anthocyanins in Mao juice during storage at 4 °C and 30 °C, determined by the pH–differential method assuming first-order kinetics.

Sample of Mao juice	Storage temperature	Degradation rate constant k × 10^{-3} (day^{-1})	Half–life ($t_{1/2}$) (week)
Sample A	4 °C	1.0	99.0
Sample B	4 °C	2.2	45.0
Sample C	4 °C	4.9	20.2
Sample D	4 °C	6.6	15.0
Sample A	30 °C	1.9	52.1
Sample B	30 °C	4.1	24.1
Sample C	30 °C	10.9	9.1
Sample D	30 °C	9.5	10.3

Among the four samples, Sample A showed the most significant resistance to anthocyanin degradation, with the lowest k values (1.0 × 10^{-3} day^{-1} at 4 °C and 1.9 × 10^{-3} day^{-1} at 30 °C) and the most prolonged half-lives (99.0 and 52.1 weeks, respectively). This suggests that Sample A may contain more stable anthocyanin structures or protective components such as co-pigments or antioxidants. In contrast, Samples C and D exhibited significantly higher degradation rates at 30 °C (k = 10.9 × 10^{-3} and 9.5 × 10^{-3} day^{-1}) and shorter half-lives (9.1 and 10.3 weeks), highlighting their lower anthocyanin stability under ambient conditions. These differences may result from variations in juice composition, pH, enzymatic activity, or the presence of prooxidant compounds [5, 21, 32, 38-40]. These results highlight the critical role of low–temperature storage in preserving anthocyanin stability and extending the shelf life of Mao juice, in agreement with previous research on thermally sensitive bioactive compounds in fruit-based beverages.

3.3 Changes in antioxidant activity of Mao juice during storage

3.3.1 Effect of temperature and storage duration on the degradation rate of antioxidants in Mao juice using the ABTS method

The antioxidant activity of Mao juice stored at different temperatures was assessed using the ABTS radical cation decolorization assay, as displayed in Table 3. The results clearly demonstrated a time-dependent and temperature-sensitive decline in antioxidant capacity over a 35-day storage period. Samples stored at 30 °C exhibited a more rapid reduction in antioxidant activity compared to those stored at 4 °C, indicating that elevated temperatures accelerate oxidative degradation of phenolic compounds, including anthocyanins and other antioxidant constituents. Among the tested samples, Sample A consistently showed the highest antioxidant levels throughout the study, suggesting superior compositional or varietal stability. In contrast, Sample D exhibited the lowest antioxidant activity, particularly under higher temperature conditions, reflecting greater susceptibility to oxidative deterioration. The ABTS assay was selected for this study due to its sensitivity, reproducibility, and broad applicability in determining the total antioxidant capacity of complex mixtures. One of its key advantages lies in its ability to measure both hydrophilic and lipophilic antioxidant compounds, providing a comprehensive assessment of antioxidant potential. Moreover, the ABTS radical is stable in aqueous and organic solvents and can be generated enzymatically or chemically, making it suitable for routine analysis of food and beverage matrices. The findings underscore the critical role of cold storage (e.g., 4°C) in maintaining the antioxidant integrity of Mao juice, thereby helping to preserve its functional quality and extend its shelf life [31, 33, 41-42].

Table 3. Antioxidant content determined by the ABTS method in Mao juice stored at 4 °C and 30 °C over the storage period.

Sample of Mao juice	Storage temperature	Antioxidant content (mg Trolox / 100 mL)					
		Day 0	Day 7	Day 14	Day 21	Day 28	Day 35
Sample A	4 °C	1286.17	1279.10	1263.85	1253.59	1248.01	1240.16
Sample B	4 °C	162.04	159.81	158.48	156.35	155.71	153.61
Sample C	4 °C	147.56	147.09	145.68	143.05	140.95	139.85
Sample D	4 °C	125.21	124.33	123.11	122.63	120.01	118.24
Sample A	30 °C	1246.78	1235.36	1224.59	1214.30	1202.38	1184.46
Sample B	30 °C	150.19	147.36	146.06	143.86	142.22	140.52
Sample C	30 °C	137.73	136.18	132.98	130.15	129.14	124.15
Sample D	30 °C	124.60	122.99	119.89	116.99	115.72	113.68

The degradation kinetics of antioxidants in Mao juice, as evaluated by the ABTS method under the assumption of first-order kinetics, provide significant insights into the stability of antioxidant compounds during storage at two different temperatures: 4 °C and 30 °C. The degradation rate constants (k) and corresponding half-lives ($t_{1/2}$) presented in Table 4 and Figure 5 demonstrate the impact of storage temperature and sample variation on antioxidant stability. At 4 °C, all samples exhibited relatively lower degradation rate constants, ranging from 1.0 to 1.6 × 10^{-3} day^{-1}, corresponding to half-lives of approximately 62 to 99 weeks. Sample A exhibited the slowest degradation rate (k = 1.0 × 10^{-3} day^{-1}) and, consequently, the longest half-life (99 weeks), indicating superior antioxidant stability under refrigeration. Samples B, C, and D exhibited similar degradation rates (1.5-1.6 × 10^{-3} day^{-1}), resulting in shorter half-lives of approximately 62 to 66 weeks. This suggests minor variations in antioxidant composition or initial concentration among the samples, possibly due to differences in raw material quality, processing, or formulation.

Table 4. Degradation rate constants and half-life ($t_{1/2}$) of antioxidants in Mao juice during storage at 4 °C and 30 °C, determined by the ABTS method assuming first-order kinetics.

Sample of Mao juice	Storage temperature	Degradation rate constant $k \times 10^{-3}$ (day^{-1})	Half–life $t_{1/2}$ (week)
Sample A	4 °C	1.0	99.0
Sample B	4 °C	1.6	61.9
Sample C	4 °C	1.5	66.0
Sample D	4 °C	1.6	61.9
Sample A	30 °C	1.4	70.7
Sample B	30 °C	1.9	52.1
Sample C	30 °C	2.7	36.7
Sample D	30 °C	2.7	36.7

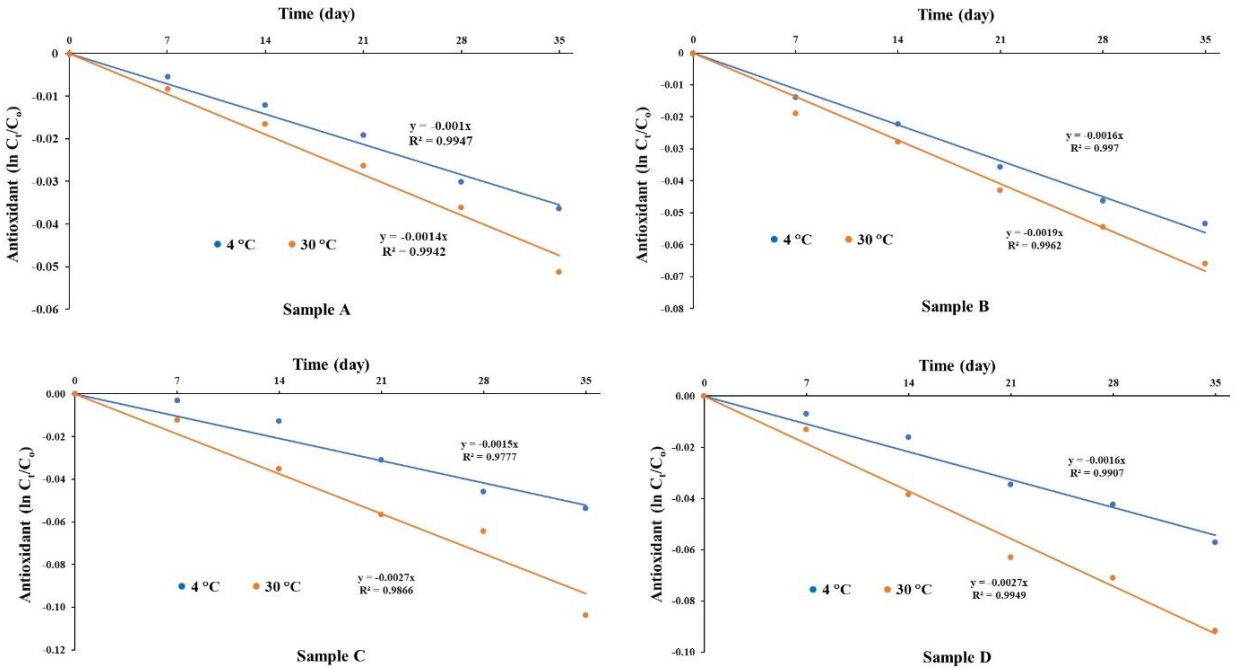

Figure 5. Degradation rate of antioxidants in Mao juice stored at 4 °C and 30 °C over 35 days, determined by the ABTS method.

When storage temperature increased to 30 °C, the degradation rates accelerated markedly, with k values increasing to between 1.4 and 2.7 × 10^{-3} day^{-1}. Correspondingly, the half-life shortened significantly to between 37 and 71 weeks. Sample A again demonstrated relatively better stability at elevated temperature with a degradation rate constant of 1.4 × 10^{-3} day^{-1} and a half–life of approximately 71 weeks, although this stability was noticeably reduced compared to storage at 4 °C. Samples C and D were the most susceptible to degradation at 30 °C, both exhibiting the highest rate constants (2.7 × 10^{-3} day^{-1}) and the shortest half–lives (36.7 weeks). This increase in degradation rate with temperature aligns well with the general understanding that antioxidant compounds are thermally labile and undergo accelerated oxidative degradation under higher thermal conditions [25, 37-38, 40-41]. The findings suggest that refrigeration significantly prolongs the antioxidant activity in Mao juice, potentially extending its functional shelf life. Conversely, storage at ambient or elevated temperatures compromises the antioxidant stability of the juice, potentially reducing its antioxidant effectiveness and overall quality. Moreover, the variability among samples highlights the importance of consistent raw material selection and processing controls to optimize antioxidant retention.

Therefore, controlling storage temperature is crucial for preserving antioxidant potency in Mao juice. The observed first-order degradation kinetics provide a helpful model for predicting shelf life under various storage conditions, which is valuable for both producers and consumers aiming to maximize the health benefits associated with antioxidants in Mao juice.

3.3.2 Effect of temperature and storage duration on the degradation rate of antioxidants in Mao juice using the FRAP assay

The results obtained from the FRAP assay, as presented in Table 5, clearly demonstrate that the antioxidant content in Mao juice declined over time at both storage temperatures, with a more pronounced degradation observed at 30 °C. Sample A, which initially exhibited the highest antioxidant capacity at 4 °C (826.56 mg Trolox/100 mL), showed a gradual decrease throughout the 35-day storage period, dropping to 811.55 mg Trolox/100 mL. In contrast, at 30 °C, the antioxidant content in the same sample started at a lower level (770.80 mg Trolox/100 mL) and declined more rapidly to 750.38 mg Trolox/100 mL, confirming the negative impact of elevated temperature on antioxidant retention.

Table 5. Antioxidant content determined by the FRAP assay in Mao juice stored at 4 °C and 30 °C over the storage period.

Sample of Mao juice	Storage temperature	Antioxidant content (mg Trolox / 100 mL)					
		Day 0	Day 7	Day 14	Day 21	Day 28	Day 35
Sample A	4 °C	826.56	824.58	820.00	816.50	812.94	811.55
Sample B	4 °C	152.41	152.11	151.97	150.65	150.14	149.85
Sample C	4 °C	107.05	106.46	106.14	105.56	105.27	105.11
Sample D	4 °C	105.74	105.14	104.96	104.26	103.96	103.67
Sample A	30 °C	770.80	767.11	764.24	757.64	754.12	750.38
Sample B	30 °C	149.56	147.96	147.38	146.07	145.34	145.05
Sample C	30 °C	106.27	105.54	105.35	104.52	104.10	103.94
Sample D	30 °C	104.04	103.57	102.80	102.42	101.90	101.43

Table 6. Degradation rate constants and half-life ($t_{1/2}$) of antioxidants in Mao juice during storage at 4 °C and 30 °C, determined by the FRAP assay assuming first-order kinetics.

Sample of Mao juice	Storage temperature	Degradation rate constant $k \times 10^{-3}$ (day^{-1})	Half–life $t_{1/2}$ (week)
Sample A	4 °C	6.0	165.0
Sample B	4 °C	5.0	198.0
Sample C	4 °C	6.0	165.0
Sample D	4 °C	6.0	165.0
Sample A	30 °C	8.0	126.6
Sample B	30 °C	10.0	99.0
Sample C	30 °C	8.0	126.6
Sample D	30 °C	7.0	141.4

The degradation kinetics of antioxidants in Mao juice conformed to a first-order model, as illustrated in Figure 6 and summarized in Table 6. The rate constants (k) ranged from 5.0×10^{-3} to 10.0×10^{-3} day^{-1}, with the most rapid degradation observed in Sample B stored at 30 °C ($k = 10.0 \times 10^{-3}$ day^{-1}), corresponding to the shortest half-life of 99.0 weeks. In contrast, the slowest degradation was observed in the same sample kept at 4°C ($k = 5.0 \times 10^{-3}$ day^{-1}), exhibiting the longest half-life of 198.0 weeks. These findings suggest that the antioxidant compounds present in Mao juice, particularly in Sample B, may exhibit varying thermal stability, which differences could influence formulation, extraction efficiency, or matrix composition. Compared to the ABTS method, which also indicated a gradual loss of antioxidant capacity, the FRAP assay provided a more apparent distinction between storage temperatures in terms of degradation kinetics. While both assays revealed the stability advantage of refrigeration, the FRAP results particularly emphasized the susceptibility

of ferric–reducing antioxidants to heat–induced oxidation over time. This may imply differences in the types of antioxidants each method measures, with FRAP primarily detecting compounds capable of reducing Fe^{3+}, which are often more sensitive to thermal stress. The findings reinforce the necessity of cold storage to preserve the antioxidant integrity of Mao juice. Furthermore, combining insights from both FRAP and ABTS assays offers a more comprehensive understanding of antioxidant stability, as the two methods reflect different antioxidant mechanisms—electron transfer in FRAP versus radical scavenging in ABTS [38-42].

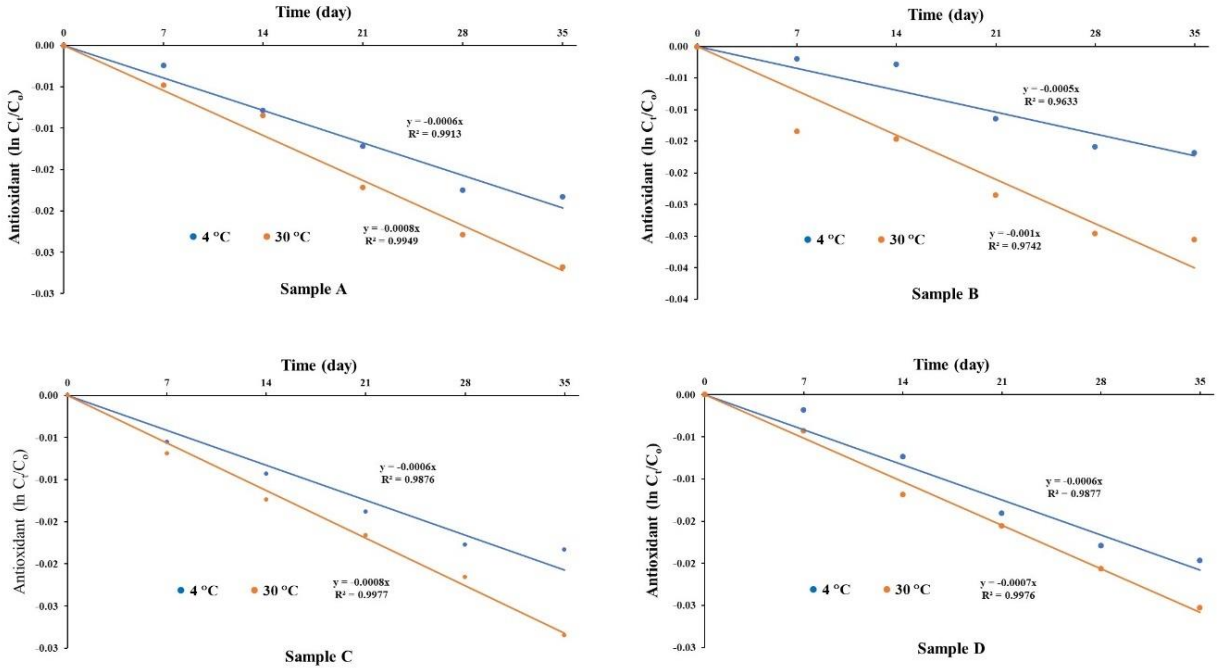

Figure 6. Degradation rate of antioxidants in Mao juice stored at 4 °C and 30 °C over 35 days, determined by the FRAP assay.

4. Conclusions

In summary, this study demonstrated that storage temperature and duration significantly affect the degradation of anthocyanins and the antioxidant activity in Mao juice, a community-produced beverage derived from *Antidesma thwaitesianum*. Among four commercial samples evaluated, Sample A stored at 4 °C exhibited the highest initial anthocyanin content (41.74 mg/L), which declined only slightly to 40.24 mg/L over 35 days. In contrast, at 30 °C, anthocyanin levels in the same sample decreased more rapidly, from 36.06 mg/L to 33.89 mg/L. Samples C and D, which had lower starting values (1.03 mg/L and 0.76 mg/L, respectively), exhibited marked degradation, dropping to 0.70 mg/L and 0.53 mg/L, respectively, at 30 °C. The degradation followed first–order kinetics, with rate constants ranging from 1.0×10^{-3} day^{-1} (Sample A at 4 °C) to 10.9×10^{-3} day^{-1} (Sample C at 30 °C), corresponding to half–lives between 99.0 and 9.1 weeks. Antioxidant activity, measured by the ABTS assay, confirmed these trends. Sample A exhibited the highest initial antioxidant level at 4 °C (1286.17 mg Trolox/100 mL), decreasing to 1240.16 mg after 35 days; however, at 30 °C, the decline was more pronounced, reaching 1184.46 mg. The FRAP assay supported this observation: Sample A decreased from 826.56 to 811.55 mg Trolox/100 mL at 4 °C and from 770.80 to 750.38 mg at 30 °C. The most rapid antioxidant degradation occurred in Sample B at 30 °C, with a rate constant of 10.0×10^{-3} day^{-1} and a half–life of 99.0 weeks (FRAP). These findings highlight the critical role of cold storage in preserving the nutritional and functional properties of Mao juice. Refrigeration at 4 °C not only slowed anthocyanin and antioxidant degradation but also extended product stability compared to storage at 30 °C. These insights are particularly relevant for local producers aiming to maintain product quality and extend shelf life. To further enhance stability and commercial viability, future development may focus on utilizing encapsulation technologies to protect bioactive compounds from oxidation and thermal stress. The addition of natural stabilizers or co-

pigments could help reduce degradation by enhancing the resilience of the pigment. Refinement of thermal or non-thermal processing methods, such as optimized pasteurization or high-pressure processing (HPP), may offer additional benefits. Moreover, selecting packaging with enhanced oxygen and light barrier properties can prevent premature degradation. Continued research into the bioavailability and health impacts of Mao juice under varying storage conditions will be essential for supporting its position as a functional beverage with regional and commercial significance.

5. Acknowledgements

This research was supported by the Chemistry Program and the Innovation in Chemistry for Community Research Unit at the Faculty of Science and Technology, as well as the Biomass Energy Research Laboratory within the Center of Excellence on Alternative Energy, Research and Development Institute at Sakon Nakhon Rajabhat University, Thailand. These institutions provided the necessary equipment and resources for the study.

Author Contributions: Conceptualization, T.S. and W.R.; methodology, T.S. and W.R.; validation, T.S. and W.R.; formal analysis, T.S., W.R., T.C., A.M.; investigation, T.C. and A.M.; resources, T.C. and A.M.; data curation, T.S. and W.R.; writing—original draft preparation, T.S. and W.R.; writing—review and editing, W.R.; visualization, T.S. and W.R.; funding acquisition, T.S. All authors have read and agreed to the published version of the manuscript.

Funding: This research was funded by the Chemistry Program and the Innovation in Chemistry for Community Research Unit at the Faculty of Science and Technology, Sakon Nakhon Rajabhat University, Thailand.

Conflicts of Interest: The authors declare no conflict of interest.

Declarations: Declaration of generative AI and AI–assisted technologies in the writing process.

References

[1] Khoo, H.E.; Azlan, A.; Tang, S.T.; Lim, S.M. Anthocyanidins and anthocyanins: Colored pigments as food, pharmaceutical ingredients, and the potential health benefits. *Food & Nutrition Research* **2017**, *61*, 1361779. https://doi.org/10.1080/16546628.2017.1361779

[2] Gonzalez de Mejia, E.; Zhang, Q.; Penta, K.; Eroglu, A.; Lila, M.A. The colors of health: Chemistry, bioactivity, and market demand for colorful foods and natural food sources of colorants. *Annual Review of Food Science and Technology* **2020**, *11*, 145–182. https://doi.org/10.1146/annurev-food-032519-051729

[3] Tan, J.; Han, Y.; Han, B.; Qi, X.; Cai, X.; Ge, S.H.X. Extraction and purification of anthocyanins: A review. *Journal of Agriculture and Food Research* **2022**, *8*, 100306. https://doi.org/10.1016/j.jafr.2022.100306

[4] Huang, H.; Ying, P.; Wang, Y.; Wu, Q.; Wang, L.; Fu, X. Temperature dependent convection induced incremental extraction of anthocyanins from *Melastoma dodecandrum* Lour. based on recyclable natural deep eutectic system. *Food Chemistry* **2025**, *484*, 144331. https://doi.org/10.1016/j.foodchem.2025.144331

[5] Laila, U.; Yuliyanto, P.; Hariyadi, S.; Juligani, B.; Indrianingsih, A.W.; Kristanti, D.; Ariani, D.; Herawati, E.R.N.; Iwansyah, A.C.; Anwar, M.; Ginting, E.; Pangestu, A.; Andriana, Y.; Purwaningsih, H.; Indrasari, S.D.; Nurmahmudi, N.; Hariadi, H.; Hoo, A.W.; Wardhani, R. Incorporation of low−pH purple−fleshed sweet potato (*Ipomoea batatas* L.) anthocyanin extract into a sucrose matrix: Characterization and application in powdered beverage. *Food and Bioproducts* Processing **2025**, *151*, 172–188. https://doi.org/10.1016/j.fbp.2025.03.008

[6] Lv, G.; Zhao, J. Molecular mechanism of differences in anthocyanin components between pericarp and red hairy root of early maturing litchi cultivars. *Plant Physiology and Biochemistry* **2025**, *223*, 109895. https://doi.org/10.1016/j.plaphy.2025.109895

[7] Sripakdee, T.; Manochai, K.; Singkhan, P.; Jandaruang, J.; Arthan, S.; Siriwong, K.; Poomsuk, N. Fermentation kinetic and alpha–amylase inhibition studies of Mao wine fermented by three commercial Saccharomyces cerevisiae yeasts. *Trends in Sciences* **2024**, *21*, 7462. https://doi.org/10.48048/tis.2024.7462

[8] Suravanichnirachorn, W.; Haruthaithanasan, V.; Suwonsichon, S.; Sukatta, U.; Maneeboon, T.; Chantrapornchai, W. Effect of carrier type and concentration on the properties, anthocyanins and antioxidant activity of freeze–dried Mao (*Antidesma bunius* (L.) Spreng) powders. *Agricultural and Natural Resources* **2018**, *52*, 354–360. https://doi.org/10.1016/j.anres.2018.09.011

[9] Rosruen, T.; Vadhanasindhu, V.; Phuwapraisirisan, P. Anthocyanin and polyphenol contents of *Antidesma thwaitesianum* Müll. Arg. berry juice being stabilized by protein matrices. *International Journal of Agricultural Technology* **2021**, *17*, 685–696.

[10] Krongyut, O.; Sutthanut, K. Phenolic profile, antioxidant activity, and anti–obesogenic bioactivity of Mao Luang fruits (*Antidesma bunius* L.). *Molecules* **2019**, *24*, 4109. https://doi.org/10.3390/molecules24224109

[11] Ngamlerst, C.; Udomkasemsab, A.; Kongkachuichai, R.; Kwanbunjan, K.; Chupeerach, C.; Prangthip, P. The potential of antioxidant–rich Maoberry (*Antidesma bunius*) extract on fat metabolism in liver tissues of rats fed a high–fat diet. *BMC Complementary and Alternative Medicine* **2019**, *19*, 294. https://doi.org/10.1186/s12906-019-2716-0

[12] Castro–Acosta, M.L.; Smith, L.; Miller, R.J.; McCarthy, D.I.; Farrimond, J.A.; Hall, W.L. Drinks containing anthocyanin–rich blackcurrant extract decrease postprandial blood glucose, insulin and incretin concentrations. *Journal of Nutritional Biochemistry* **2016**, *38*, 154–161. https://doi.org/10.1016/j.jnutbio.2016.09.002

[13] Aksornchu, P.; Chamnansilpa, N.; Adisakwattana, S.; Thilavech, T.; Choosak, C.; Marnpae, M.; Mäkynen, K.; Dahlan, W.; Ngamukote, S. Inhibitory effect of *Antidesma bunius* fruit extract on carbohydrate digestive enzymes activity and protein glycation in vitro. *Antioxidants* **2021**, *10*, 32. https://doi.org/10.3390/antiox10010032

[14] Picot, C.M.N.; Subratty, A.H.; Mahomoodally, M.F. Inhibitory potential of five traditionally used native antidiabetic medicinal plants on α–amylase, α–glucosidase, glucose entrapment, and amylolysis kinetics in vitro. *Advances in Pharmacological Sciences* **2014**, *2014*, 739834. https://doi.org/10.1155/2014/739834

[15] Jorjong, S.; Butkhup, L.; Samappito, S. Phytochemicals and antioxidant capacities of Mao–Luang (*Antidesma bunius* L.) cultivars from Northeastern Thailand. *Food Chemistry* **2015**, *181*, 248–255. https://doi.org/10.1016/j.foodchem.2015.02.093

[16] Kukongviriyapan, U.; Kukongviriyapan, V.; Pannangpetch, P.; Donpunha, W.; Sripui, J.; Sae–Eaw, A.; Boonla, O. Mamao pomace extract alleviates hypertension and oxidative stress in nitric oxide deficient rats. *Nutrients* **2015**, *7*, 6179–6194. https://doi.org/10.3390/nu7085275

[17] Udomkasemsab, A.; Ngamlerst, C.; Kwanbunjun, K.; Krasae, T.; Amnuaysookkasem, K.; Chunthanom, P.; Prangthip, P. Maoberry (*Antidesma bunius*) improves glucose metabolism, triglyceride levels, and splenic lesions in high–fat diet–induced hypercholesterolemic rats. *Journal of Medicinal Food* **2019**, *22*, 29–37. https://doi.org/10.1089/jmf.2018.4203

[18] Xue, H.; Zhao, J.; Wang, Y.; Shi, Z.; Xie, K.; Liao, X.; Tan, J. Factors affecting the stability of anthocyanins and strategies for improving their stability: A review. *Food Chemistry: X* **2024**, *24*, 101883. https://doi.org/10.1016/j.fochx.2024.101883

[19] Gençdağ, E.; Özdemir, E.E.; Demirci, K.; Görgüç, A.; Yılmaz, F.M. Copigmentation and stabilization of anthocyanins using organic molecules and encapsulation techniques. *Current Plant Biology* **2022**, *29*, 100238. https://doi.org/10.1016/j.cpb.2022.100238

[20] Saini, A.; Hamid, A.; Shams, R.; Dash, K.K.; Shaikh, A.M.; Kovács, B. Anthocyanin extraction from black carrot: Health promoting properties and potential applications. *Journal of Agriculture and Food Research* **2025**, *19*, 101533. https://doi.org/10.1016/j.jafr.2024.101533

[21] Toklucu, A.K.; Özkan, M.; Cemeroğlu, B. Effects of temperature, solid content and pH on the stability of black carrot anthocyanins. *Food Chemistry* **2007**, *101*, 212–218. https://doi.org/10.1016/j.foodchem.2006.01.019

[22] Toklucu, A.K.; Özkan, M.; Cemeroğlu, B. Stability of black carrot anthocyanins in various fruit juices and nectars. *Food Chemistry* **2006**, *97*, 598–605. https://doi.org/10.1016/j.foodchem.2005.05.036

[23] Rezazadeh, A.; Ghasempour, Z. Anthocyanin stabilization in beverages. In: Mérillon, J.M.; Rivière, C.; Lefèvre, G. (Eds.), Natural Products in Beverages, Reference Series in Phytochemistry; *Springer: Cham*, **2025**; pp. 178. https://doi.org/10.1007/978-3-031-38663-3_178

[24] Muche, B.M.; Speers, R.A.; Rupasinghe, H.P.V. Storage temperature impacts on anthocyanins degradation, color changes, and haze development in juice of "Merlot" and "Ruby" grapes (*Vitis vinifera*). *Frontiers in Nutrition* **2018**, *5*, 100. https://doi.org/10.3389/fnut.2018.00100

[25] Türkyılmaz, M.; Özkan, M. Kinetics of anthocyanin degradation and polymeric colour formation in black carrot juice concentrates during storage. *International Journal of Food Science and Technology* **2012**, *47*, [no pagination given]. https://doi.org/10.1111/j.1365-2621.2012.03098.x

[26] Tena, N.; Asuero, A.G. Up−to−date analysis of the extraction methods for anthocyanins: Principles of the techniques, optimization, technical progress, and industrial application. *Antioxidants* **2022**, *11*, 286. https://doi.org/10.3390/antiox11020286

[27] Khezri, S.; Ghanbarzadeh, B.; Ehsani, A. Barberry anthocyanins: Recent advances in extraction, stability, biological activities, and utilisation in food systems—A review. *International Journal of Food Science and Technology* **2025**, *60*, vvaf031. https://doi.org/10.1093/ijfood/vvaf031

[28] Chua, L.S.; Thong, H.Y.; Soo, J. Effect of pH on the extraction and stability of anthocyanins from jaboticaba berries. *Food Chemistry Advances* **2024**, *5*, 100835. https://doi.org/10.1016/j.focha.2024.100835

[29] Chua, L.S.; Abd Wahab, N.S. Drying kinetic of jaboticaba berries and natural fermentation for anthocyanin−rich fruit vinegar. *Foods* **2023**, **12**, 65. https://doi.org/10.3390/foods12010065

[30] Handayani, L.; Aprilia, S.; Arahman, N.; Bilad, M.R. Identification of the anthocyanin profile from butterfly pea (*Clitoria ternatea* L.) flowers under varying extraction conditions: Evaluating its potential as a natural blue food colorant and its application as a colorimetric indicator. *South African Journal of Chemical Engineering* **2024**, *49*, 151–161. https://doi.org/10.1016/j.sajce.2024.04.008

[31] Li, J.L.; Yu, J.H.; Li, W.Z.; Deng, D.J.; Xin, Y.; Reaney, M.J.T.; Cai, Z.Z.; Wang, Y. Optimized two−step flash chromatography method for large−scale isolation of linusorb and its antioxidant capacity evaluation. *Food Research International* **2025**, *207*, 116082. https://doi.org/10.1016/j.foodres.2025.116082

[32] Cai, W.W.; Hu, X.M.; Wang, Y.M.; Chi, C.F.; Wang, B. Bioactive peptides from skipjack tuna cardiac arterial bulbs: Preparation, identification, antioxidant activity, and stability against thermal, pH, and simulated gastrointestinal digestion treatments. *Marine Drugs* **2022**, *20*, 626. https://doi.org/10.3390/md20100626

[33] Bai, H.; Wang, S.; Wang, Z.M.; Zhu, L.L.; Yan, H.B.; Wang, Y.B.; Wang, X.Y.; Peng, L.; Liu, J.Z. Investigation of bioactive compounds and their correlation with the antioxidant capacity in different functional vinegars. *Food Research International* **2024**, *184*, 114262. https://doi.org/10.1016/j.foodres.2024.114262

[34] Bamigbade, G.B.; Subhash, A.; Abdin, M.; Jarusheh, H.; Abu−Jdayil, B.; Liu, S.Q.; Palmisano, G.; Ali, A.; Eldin, A.K.; Ayyash, M. Date pomace polysaccharides−capped selenium nanoparticles: Biosynthesis, optimization, physicochemical characterization, biological activities, stability and gut microbiota modulation. *Food Hydrocolloids for Health* **2025**, *7*, 100198. https://doi.org/10.1016/j.fhfh.2025.100198

[35] Spiegel, M.; Kapusta, K.; Kołodziejczyk, W.; Saloni, J.; Żbikowska, B.; Hill, G.A.; Sroka, Z. Antioxidant activity of selected phenolic acids–Ferric reducing antioxidant power assay and QSAR analysis of the structural features. *Molecules* **2020**, *25*, 3088. https://doi.org/10.3390/molecules25133088

[36] Muthu, S.; Altemimi, A.B.; Lakshmikanthan, M.; Krishnan, K.; ALKaisy, Q.H.; Awlqadrf, F.H.; Hesarinejad, M.A. Phycocolloids from *Sargassum microcystum*: Immunomodulatory and antioxidant activities of alginic acid and fucoidan. *Food Hydrocolloids for Health* **2025**, *7*, 100209. https://doi.org/10.1016/j.fhfh.2025.100209

[37] Hernandez–Prieto, D.; Salar, F.J.; Garre, A.; Fernandez, P.S.; García–Viguera, C.; Fría, J. Kinetic modelling of anthocyanins and vitamin C degradation in a maqui–citrus beverage during storage for different sweeteners and pasteurization treatments. *LWT – Food Science and Technology* **2024**, *199*, 116082. https://doi.org/10.1016/j.lwt.2024.116082

[38] Chen, J.Y.; Du, J.; Li, M.L.; Li, C.M. Degradation kinetics and pathways of red raspberry anthocyanins in model and juice systems and their correlation with color and antioxidant changes during storage. *LWT – Food Science and Technology* **2020**, *128*, 109448. https://doi.org/10.1016/j.lwt.2020.109448

[39] Kechinski, C.P.; Guimarães, P.V.R.; Noreña, C.P.Z.; Marczak, L.D.F. Degradation kinetics of anthocyanin in blueberry juice during thermal treatment. *Journal of Food Science* **2010**, *75*, C173–C176. https://doi.org/10.1111/j.1750-3841.2009.01479.x

[40] Wu, X.; Lin, Q.; Belwal, T.; Huang, H.; Zou, L.; Lv, W.; Luo, Z. Effect of advanced/hybrid oxidation process involving ultrasonication and ultraviolet radiation (sonophotolysis) on anthocyanin stability: Degradation kinetics and mechanism. *Food Chemistry* **2022**, *370*, 131083. https://doi.org/10.1016/j.foodchem.2021.131083

[41] Dawidowicz, A.L.; Olszowy, M. Antioxidant properties of BHT estimated by ABTS assay in systems differing in pH or metal ion or water concentration. *European Food Research and Technology* **2011**, *232*, 837–842. https://doi.org/10.1007/s00217-011-1451-7

[42] Xu, B.; Dong, Q.; Yu, C.; Chen, H.; Zhao, Y.; Zhang, B.; Yu, P.; Chen, M. Advances in research on the activity evaluation, mechanism and structure–activity relationships of natural antioxidant peptides. *Antioxidants* **2024**, *13*, 479. https://doi.org/10.3390/antiox13040479

ASEAN
Journal of Scientific and Technological Reports
Online ISSN:2773-8752

Research article

Sustainable Bio-Bitumen Formulation Using a Grey Relational Taguchi Approach with Waste Oils and Biochar

Penki Ramu[1, 2*], Subrat Kumar Rout[3], and Aditya Kumar Das[4]

[1] Civil Engineering, GMR Institute of Technology, Rajam, Vizianagaram, 532127, India
[2] Department of Civil Engineering, Siksha 'O' Anusandhan University, Bhubaneswar, 751030, India
[3] Department of Civil Engineering, Siksha 'O' Anusandhan University, Bhubaneswar, 751030, India
[4] Department of Civil Engineering, National Institute of Technology Rourkela, Odisha, 769008, India
* Correspondence: ramu.p@gmrit.edu.in

Citation:
Ramu, P.; Rout, S.K.; Das, A.K. Sustainable bio-bitumen formulation: A grey relational taguchi approach with waste oils and biochar additives. *ASEAN J. Sci. Tech. Report.* **2025**, *28*(6), e259576. https://doi.org/10.55164/ajstr.v28i6.259576.

Article history:
Received: May 30, 2025
Revised: August 26, 2025
Accepted: September 6, 2025
Available online: October 19, 2025

Abstract: Pavement binder properties play a crucial role in road durability, yet conventional bitumen relies on depleting crude oil resources. This study explores a sustainable alternative by modifying 60/70 penetration grade bitumen with biochar (BC), waste engine oil (WEO), waste cooking oil (WCO), and phthalic anhydride (PA). A hybrid optimization framework combining Taguchi-based Grey Relational Analysis (GRA) with Principal Component Analysis (PCA) was applied using an L16 orthogonal array to evaluate multiple performance responses. The optimal formulation, consisting of 5% BC, 2% WEO, 1% WCO, and 0% PA, achieved a penetration of 102 dmm, ductility of 63 cm, a softening point of 50 °C, and an elastic recovery of 100%, meeting the standard requirements. While PA individually improved certain properties such as moisture resistance, its combined effect with other modifiers reduced overall performance, likely due to antagonistic interactions or chemical incompatibility. These findings underscore the need for advanced optimization methods that can address both synergistic and antagonistic effects in multi-component systems. The proposed PCA–Grey–Taguchi approach provides a systematic pathway for designing high-performance bio-bitumen, demonstrating the potential of waste-derived modifiers to deliver cost-effective, environmentally sustainable, and technically viable pavement binders for future road infrastructure.

Keywords: Bio-bitumen; biochar; waste engine oil; waste cooking oil; grey relational analysis

1. Introduction

The global infrastructure industry increasingly demands resilient and environmentally responsible materials that also meet stringent performance requirements [1]. Asphalt concrete remains a key component in road construction, providing durable and long-lasting surfaces [2]. Conventional asphalt mixtures primarily consist of aggregates, asphalt binders, and mineral fillers [3]. However, the transportation sector contributes significantly to greenhouse gas (GHG) emissions, with road traffic and construction activities accounting for 74% of the sector's emissions, which represent 32% of global totals [4]. The Sustainable Development Goals (SDGs), the Convention on Biological Diversity, and the Paris Agreement are just a few of the conventions that the Green Roads Toolkit will ensure roads comply with. It will also incorporate green road elements beyond the current hallmark of conventional

roads, which are connectivity, safety, and affordability [5-6]. In addition, extracting natural aggregates and disposing of construction waste impose substantial environmental burdens. Consequently, researchers are increasingly exploring sustainable alternatives, including the incorporation of waste-derived materials into asphalt mixtures, to reduce environmental impact and enhance pavement performance [3]. This study contributes to the development of "Green Roads," including climate-resilient, sustainable, and environmentally friendly pavement systems.

Bitumen is a black binding material used with aggregates in road construction. Due to its dark color, it contributes to the urban heat island effect under extreme temperatures, thereby exacerbating climate change, since it is derived from fossil fuels [7]. Bitumen is processed through fractional distillation and oxidation. Oxidation plays a vital role in producing various paving grades, and it must be carefully controlled to ensure that the cohesion and adhesion properties of bitumen conform to standards [8]. Its production is hazardous due to its low dielectric/micro-permittivity constant, high levels of polycyclic aromatic hydrocarbons (PAHs), and the presence of hydrogen sulfide and bromine [9]. Bitumen deposits are often located at relatively shallow depths, ranging from 0 to 500 m below the Earth's surface, which leads to subsurface water contamination and poses risks to human health and the environment. Moreover, extraction is cumbersome, complex, and time-consuming [10]. Global bitumen reserves are being consumed at an alarming rate of 100 million metric tonnes annually and are projected to last only another 46 years, since it is a non-renewable finite resource [11]. Another major factor challenging the future of bitumen is the decline in crude oil reserves and the associated fluctuations in cost. To meet increasing demands for strength under evolving wheel loads and resilience to thermal susceptibility, modification of bitumen is therefore essential. Polymer-modified bitumen (PMB) refers to the incorporation of elastomeric polymers into bitumen to reduce heat susceptibility and deformation under load [12]. PMBs are widely applied in high-performance pavement projects worldwide, particularly in areas requiring enhanced rutting resistance, elasticity, and durability [13]. However, their higher cost and potential for premature failure when interacting with certain hydrocarbon oils can limit broader adoption, especially in resource-constrained regions [12]. This study, therefore, aims to develop a cost-effective and sustainable alternative to traditional residual bitumen and PMB systems, addressing both performance and environmental objectives.

In this research, conventional 60/70 penetration grade bitumen is modified with biochar (BC), waste engine oil (WEO), waste cooking oil (WCO), and phthalic anhydride (PA) using a Taguchi-based design of experiments. These materials were selected to promote sustainability and circular economy principles in line with the Sustainable Development Goals, with the aim of mitigating climate change impacts. Biochar, an end-product of the thermochemical conversion of biomass waste, is produced globally in significant quantities. Its porous, irregular surface has been reported to enhance physicochemical bonding with bitumen, improving stiffness and stability [14]. WEO has been shown to act as a fluxing agent, reducing viscosity and improving workability, but may increase susceptibility to permanent deformation at high dosages. WCO can improve low-temperature flexibility but may reduce moisture resistance due to its polar compounds. While individual studies have examined these modifiers separately, limited research has optimized them in combination to capture synergistic benefits while mitigating antagonistic effects. This study addresses that gap by systematically evaluating their interactions, balancing performance, cost, emissions, and workability. Large volumes of solid biomass wastes, such as sugarcane bagasse, coconut copra, rice husks, and palm oil residues, are generated in Southeast Asia. Due to their low economic value, these wastes are often managed inefficiently, primarily through burning or uncontrolled decomposition, both of which contribute to environmental pollution [15]. Similarly, most WCO and WEO are disposed of in open dumps, causing serious environmental problems by releasing foul odors and contaminating soil and water with hazardous liquids [16-[17]. The above-mentioned issues can be effectively addressed by employing these waste materials in bio-bitumen production. Process efficiency in material development is best achieved through optimisation, as traditional approaches that vary one factor at a time often overlook the interaction effects between components, increasing both cost and testing time. To address these challenges, statistical strategies such as the Design of Experiments (DoE) have been adopted to identify cause–and–effect relationships between variables and performance outcomes [18]. In this study, a Grey–Taguchi multi-objective optimisation approach was selected for its ability to handle multiple performance criteria, capture interaction effects, and determine the most effective

combination of bio-based modifiers for bitumen [19-20]. The method is implemented using Minitab software, which enables the design, statistical analysis, and ranking of factor levels to achieve optimal binder properties, incorporating a detailed experimental design and the integration of Taguchi, Grey Relational Analysis, and Principal Component Analysis.

A limited amount of research has examined the combined effects of biochar, waste cooking oil, and waste engine oil on key performance parameters, including penetration, ductility, softening point, and elastic recovery, using a Grey-Taguchi optimization approach with Principal Component Analysis (PCA) integration. Previous studies have examined the use of various additives in bio-bitumen formulations. By combining waste cooking oil, waste engine oil, and waste biochar in the synthesis of bio-bitumen and utilizing the Grey-Taguchi approach integrated with PCA, this work seeks to close this gap. By analyzing the crucial performance factors, this research aims to identify the optimal additive combination for producing high-performing and sustainable bio-bitumen formulations.

2. Methodology

2.1 Taguchi Analysis

The Taguchi method, developed by Genichi Taguchi, is a statistical design of experiments (DoE) framework that improves process robustness by systematically analysing factor effects through orthogonal arrays [27]. Its foundation lies in fractional factorial design, signal-to-noise (S/N) ratios as quality metrics, and the Quality Loss Function, which relates deviation from the target to performance loss [28-29]. In this framework, the S/N ratio is a key indicator, expressed either as a logarithmic measure of mean-to-variance [30] or as the ratio of wasted to required energy [31]. Regression analysis is further employed to evaluate relationships between input and output variables [31]. In this study, an L16 orthogonal array (OA) was employed to evaluate four factors—biochar (BC), waste engine oil (WEO), waste cooking oil (WCO), and phthalic anhydride (PA), each at four levels (4^4). Factor ranges were defined as BC (0–15%), WEO (0–3%), WCO (0–3%), and PA (0–15%), based on prior literature and preliminary tests to balance stiffness, rutting resistance, workability, and fatigue performance [32]. The final ranges ensured that BC content did not induce brittleness, WEO/WCO avoided excessive softening, and PA levels provided sufficient reactivity without binder hardening. The L16 OA ensured equal representation of factor–level combinations, with all 16 trials conducted in randomised order to minimise experimental bias. Each test was carried out once per response, consistent with the Taguchi method's robustness. Binder properties were evaluated using standard protocols: Penetration (ASTM D5/IS 1203), Ductility (ASTM D113/IS 1208), Softening Point (ASTM D36/IS 1205), and Elastic Recovery (ASTM D6084). The S/N ratios were calculated using the "smaller-the-better" (STB) and "larger-the-better" (LTB) formulations shown in (1) and (2), where n denotes the number of trials and Y the measured response:

$$K_{ij} = -10\log_{10}\left(\frac{1}{n}\sum_{j=1}^{n} Y_{ij}^2\right) \text{STB} \quad (1)$$

$$K_{ij} = -10\log_{10}\left(\frac{1}{n}\sum_{j=1}^{n} \frac{1}{Y_{ij}^2}\right) \text{LTB} \quad (2)$$

The factors and their corresponding levels are summarised in Table 1, and the complete L16 orthogonal array with experimental responses is presented in Table 2.

2.2 Grey–Taguchi Analysis (Multi-objective Optimization)

Grey Relational Analysis (GRA) was adopted in this study to overcome the limitation of the Taguchi method, which is restricted to single-objective optimization. Since the present work involves multiple performance characteristics—penetration, ductility, softening point, and elastic recovery—a hybrid Taguchi–GRA–Principal Component Analysis (PCA) framework was employed. In this approach, PCA was utilized to objectively assign weights to each response parameter, thereby avoiding arbitrary assumptions. By ensuring that each characteristic's contribution to the overall optimization is proportional to its statistical significance,

PCA provides a more robust weighting system. PCA performs an orthogonal transformation that converts correlated variables into a set of uncorrelated variables, known as principal components (PCs), which retain most of the variance in the dataset [12]. This methodology is widely adopted in multi-response optimization problems in engineering, as it effectively reduces dimensionality while preserving essential information, thereby enabling accurate Grey Relational Grading. In the present study, a hybrid Taguchi–GRA–PCA approach was adopted (Figure 1) to facilitate the multi-objective optimization of bio-bitumen formulations.

Table 1 Factors and their levels used in the Taguchi L16 orthogonal array

FACTORS	BC	WEO	WCO	PA
LEVEL 1	0	0	0	0
LEVEL 2	5	1	1	5
LEVEL 3	10	2	2	10
LEVEL 4	15	3	3	15

Table 2 L16 orthogonal array with factor–level combinations for all 16 experimental trials

Run	BC	WEO	WCO	PA	Penetration (dmm)	Ductility (cm)	Softening Point (^{0}c)	Elastic Recovery (%)
1	0	0	0	0	52.3	70	50	97
2	0	1	1	5	106	31.3	62	98
3	0	2	2	10	122	36.8	65	97
4	0	3	3	15	51	26.8	58	94
5	5	0	1	10	149	30.2	50	93
6	5	1	0	15	156.3	33	52	92
7	5	2	3	0	161	49.5	60	95
8	5	3	2	5	151	41.5	52	95
9	10	0	2	15	66	35	58	94
10	10	1	3	10	80	55	46	96
11	10	2	0	5	80	58	45	96
12	10	3	1	0	102	63	50	100
13	15	0	3	5	78.33	51.2	59	91
14	15	1	2	0	78	53	56	99
15	15	2	1	15	105.33	33.5	62	95
16	15	3	0	10	127.66	33.8	60	96

Although the Taguchi method provides an optimal factor setting for single-response optimisation, it is limited when multiple performance criteria must be satisfied simultaneously. To address this limitation, the S/N ratios derived here were further processed using Grey Relational Analysis (GRA) integrated with Principal Component Analysis (PCA).

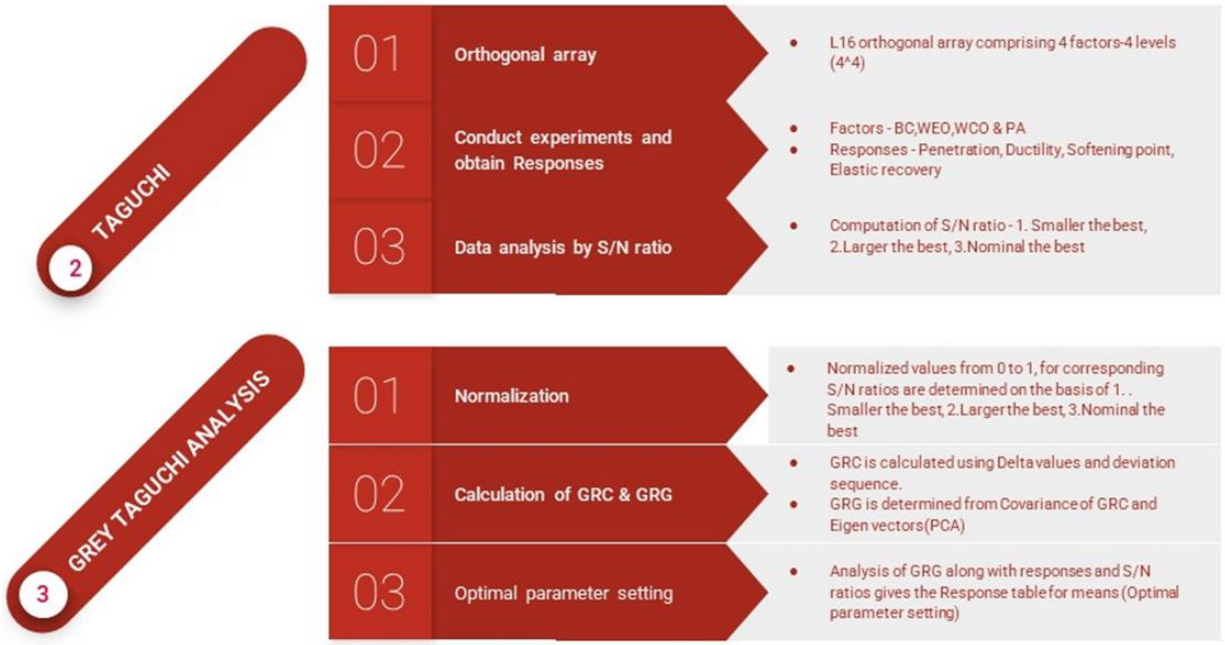

Figure 1. Roadmap for optimization of bio-bitumen using Grey-Taguchi technique

2.2.1 Optimization Using GRA

The signal-to-noise (S/N) ratios obtained from the Taguchi design (Section 2.1) were first normalized to a range of 0 to 1. For the "smaller-the-better" characteristic (penetration), normalization was performed using Equation (3):

$$X_i^*(k) = \frac{maxX_i^o(k) - X_i^o(k)}{maxX_i^o(k) - minX_i^o(k)} \quad (3)$$

For the "larger-the-better" characteristics (ductility, softening point, and elastic recovery), normalization was performed using Equation (4):

$$X_i^*(k) = \frac{X_i^o(k) - minX_i^o(k)}{maxX_i^o(k) - minX_i^o(k)} \quad (4)$$

The normalized results are presented in **Table 3**.

The deviation sequence from the ideal value (1) was calculated as:

$$\Delta_{oi}(k) = |X_o^*(k) - X_i^o(k)| \quad (5)$$

The Grey Relational Coefficient (GRC) was then computed using Equation (6):

$$\xi_i(k) = \frac{\Delta_{min} + \psi \cdot \Delta_{max}}{\Delta_{oi}(k) + \psi \cdot \Delta_{max}} \quad (6)$$

Where ψ is the distinguishing coefficient (taken as 0.5), and Δmin and Δmax are the minimum and maximum deviation sequences, respectively.

Finally, the Grey Relational Grade (GRG) for each trial was obtained as:

$$\gamma_i(GRG) = \sum_{k=1}^{n} \omega_k \cdot \xi_i(k) \quad (7)$$

where ωk represents the weight for the k-th response, determined from PCA eigenvectors.

Table 3. Normalized values for the deviation sequence

RUN ORDER	NORMALIZED VALUES			
	PENETRATION	DUCTILITY	SOFTENING POINT	ELASTIC RECOVERY
1	0.02	1.00	0.29	0.68
2	0.64	0.16	0.87	0.79
3	0.76	0.33	1.00	0.68
4	0.00	0.00	0.69	0.34
5	0.93	0.12	0.29	0.23
6	0.97	0.22	0.39	0.12
7	1.00	0.64	0.78	0.46
8	0.94	0.46	0.39	0.46
9	0.22	0.28	0.69	0.34
10	0.39	0.75	0.06	0.57
11	0.39	0.80	0.00	0.57
12	0.82	0.89	0.29	1.00
13	0.37	0.67	0.74	0.00
14	0.37	0.71	0.59	0.89
15	0.63	0.23	0.87	0.46
16	0.80	0.24	0.78	0.57

Table 4. Grey Relational Grading and Grey Relational Coefficient

Grey Relational Coefficient						
Run Order	Penetration	Ductility	Softening Point	Elastic Recovery	GRG	Rank
1	0.34	1.00	0.41	0.61	0.65	3
2	0.58	0.37	0.80	0.70	0.54	10
3	0.67	0.43	1.00	0.61	0.62	4
4	0.33	0.33	0.62	0.43	0.39	16
5	0.88	0.36	0.41	0.39	0.54	11
6	0.95	0.39	0.45	0.36	0.58	7
7	1.00	0.58	0.70	0.48	0.72	2
8	0.90	0.48	0.45	0.48	0.61	5
9	0.39	0.41	0.62	0.43	0.44	15
10	0.45	0.67	0.35	0.54	0.53	12
11	0.45	0.72	0.33	0.54	0.55	9
12	0.73	0.82	0.41	1.00	0.75	1
13	0.44	0.61	0.65	0.33	0.53	13
14	0.44	0.63	0.55	0.82	0.58	6
15	0.58	0.39	0.80	0.48	0.53	14
16	0.71	0.40	0.70	0.54	0.56	8

The calculated GRG values and their corresponding rankings are shown in Table 4. The trial with the highest GRG value represents the optimal parameter combination. The response analysis and S/N ratio plots for the GRG, generated in Minitab, are summarized in Table 5 and Figure 2. Eigen Analysis of the covariance matrix was performed to extract the principal components, which quantify the contribution of each performance characteristic to the total variance. The resulting eigenvalues and eigenvectors (Tables 6 and 7) were used as weighting factors (ω_k) in Eq. (7) for Grey Relational Grade computation.

Table 5. Input factors, responses, and corresponding S/N ratios

Input factors		Responses							Signal-to-noise ratios			
Run	**Penetration (dmm)**	**SNRA1**	**SNRA2**	**SNRA3**	**SNRA4**	**WEO**	**WCO**	**PA**	**SNRA1**	**SNRA2**	**SNRA3**	**SNRA4**
1	52.3	-34.37	36.90	33.98	39.74	0	0	0	-34.37	36.90	33.98	39.74
2	106	-40.51	29.91	35.85	39.82	1	1	5	-40.51	29.91	35.85	39.82
3	122	-41.73	31.32	36.26	39.74	2	2	10	-41.73	31.32	36.26	39.74
4	51	-34.15	28.56	35.27	39.46	3	3	15	-34.15	28.56	35.27	39.46
5	149	-43.46	29.60	33.98	39.37	0	1	10	-43.46	29.60	33.98	39.37
6	156.3	-43.88	30.37	34.32	39.28	1	0	15	-43.88	30.37	34.32	39.28
7	161	-44.14	33.89	35.56	39.55	2	3	0	-44.14	33.89	35.56	39.55
8	151	-43.58	32.36	34.32	39.55	3	2	5	-43.58	32.36	34.32	39.55
9	66	-36.39	30.88	35.27	39.46	0	2	15	-36.39	30.88	35.27	39.46
10	80	-38.06	34.81	33.26	39.65	1	3	10	-38.06	34.81	33.26	39.65
11	80	-38.06	35.27	33.06	39.65	2	0	5	-38.06	35.27	33.06	39.65
12	102	-42.32	35.99	33.98	40.00	3	1	0	-42.32	35.99	33.98	40.00
13	78.33	-37.88	34.19	35.42	39.18	0	3	5	-37.88	34.19	35.42	39.18
14	78	-37.84	34.49	34.96	39.91	1	2	0	-37.84	34.49	34.96	39.91
15	105.33	-40.45	30.50	35.85	39.55	2	1	15	-40.45	30.50	35.85	39.55
16	127.66	-42.12	30.58	35.56	39.65	3	0	10	-42.12	30.58	35.56	39.65

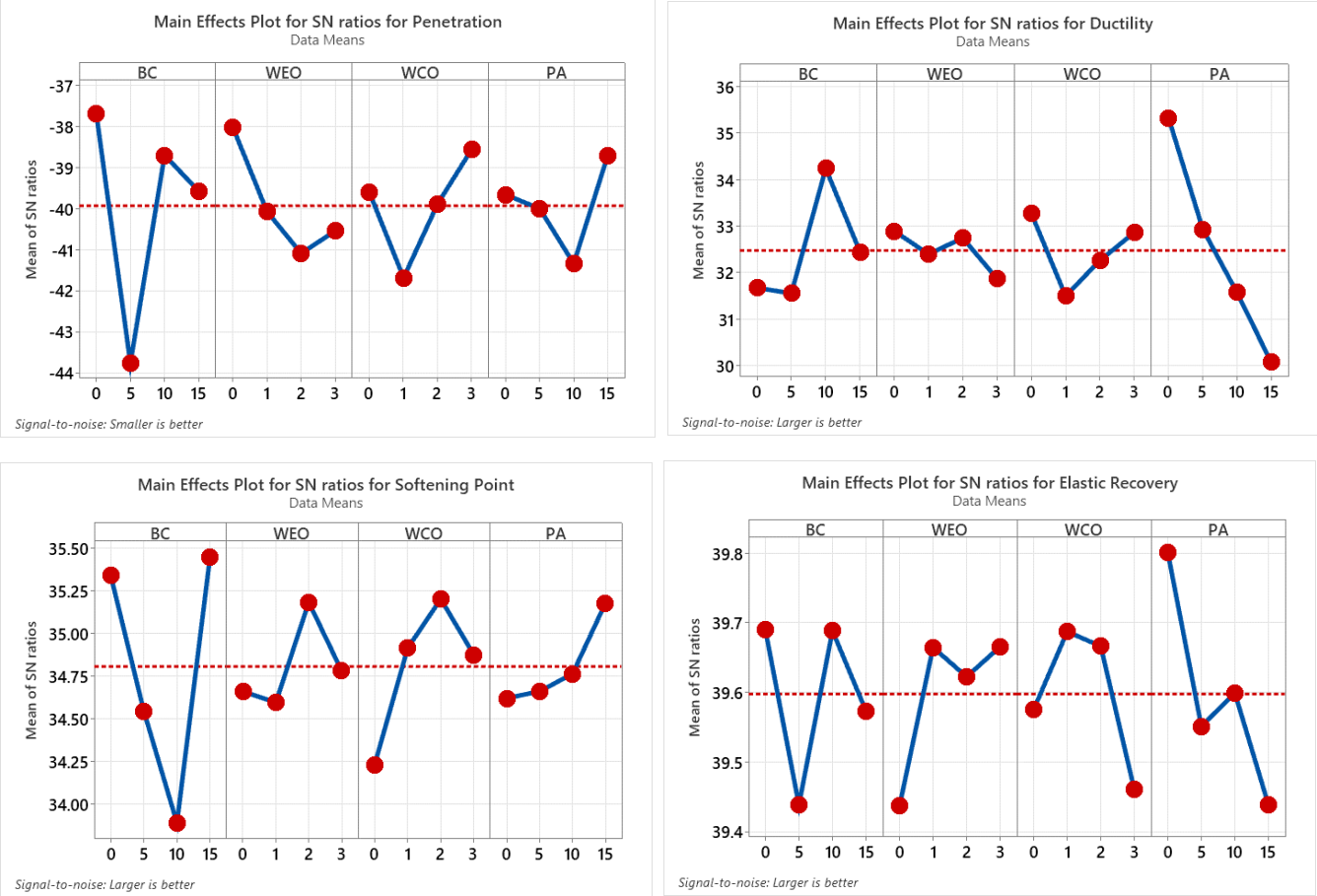

Figure 2. S/N ratio plots for responses

Table 6. Eigen vectors

Eigenvectors Variable	PC1	PC2	PC3	PC4
C1	0.57	-0.78	-0.20	0.159
C2	-0.63	-0.29	-0.12	0.709
C3	0.40	0.53	-0.57	0.48
C4	-0.34	-0.15	-0.79	-0.493

Table 7. Eigen analysis of the Covariance Matrix

Principal Component	PC1	PC2	PC3	PC4
Eigenvalue	0.068374	0.044395	0.030729	0.010365
Proportion	0.444	0.289	0.2	0.067
Cumulative	0.444	0.733	0.933	1

3. Results and Discussions

The levels of the input parameters or factors are determined through a combination of insights from literature reviews and laboratory experimentation on conventional bitumen. This process involves evaluating each input parameter or factor individually, one at a time. This study would require 256 (4^4) experimental

runs because it has 4 components at 4 levels each. Fractional factorials offer a quicker option, but they require statistical knowledge that is not always available. A more effective approach is provided by orthogonal arrays, which enable smaller, less expensive tests with excellent reproducibility rates. In just 16 experimental runs, this research with 4 factors at 4 levels each can be completed with the right orthogonal array. For these 16 experimental runs, the laboratory tests were conducted to determine the following responses: Penetration, Ductility, Softening point, and Elastic recovery. Later, these values are analyzed in Minitab software to calculate S/N ratios for each response and are tabulated in Table 4. S/N ratios are calculated from Eq. 1. For instance, the S/N ratio for the first run order of Penetration, where the objective is "smaller-the-better," is required.

$$S/N = -10\log(52.32) = -34.37$$

Similarly, for the remaining responses, S/N ratios are calculated as "larger-the-better" using Eq. 2. For instance, the S/N ratio of the first run order of Ductility.

$$S/N = -10\log(1/702) = 36.90$$

S/N Ratio graphs are plotted for all 4 responses. The optimal value of the response can be determined from the graph that possesses the highest mean SNR. These graphs are shown in Figure 2. It has been found that for Penetration, the highest SNR is obtained at BC & WEO at 0%, WCO at 3%, and PA at 15%. For Ductility, the highest SNR was obtained at BC-10 %, WEO, WCO, and PA at 0%. For Softening Point, the highest SRN is obtained at BC – 15%, WEO – 2%, WCO 2%, and PA – 15%. Elastic recovery showed the highest SNR at BC – 0% & 10%, WEO – 3%, WCO – 1% and PA – 0%. Multiple regression analysis has been performed to examine these optimized outcomes further. The analysis indicates that binder composition significantly affects performance characteristics. For penetration, a higher BC content increases binder stiffness and reduces softness, while WEO functions as a fluxing agent, lowering viscosity. The inclusion of WCO at around 3% enhances plasticity without causing excessive softening, and PA at 15% contributes to elasticity while maintaining a relatively softer consistency. In terms of ductility, a BC content of 10% improves stiffness without resulting in excessive embrittlement. The absence of oils helps avoid over-softening, and the exclusion of PA prevents potential incompatibility issues. Regarding softening point, higher BC content (15%) enhances stiffness and thermal resistance, whereas small quantities of oils aid dispersion without compromising thermal stability. For elastic recovery, low PA content minimizes phase separation, and the combined effects of selected oil dosages promote chain mobility, thereby improving elasticity. Regression analysis can be used to establish a mathematical relationship between specific independent variables (response) and a dependent variable (predictor). As demonstrated, functions of independent variables may be used to express dependent variables in multiple regression.

$$\mathbf{Z = a_0 + a_1x_1 + a_2x_2 + a_3x_3 + \ldots + a_nx_n}$$

Where X1 to Xn are the independent variables, Z is the dependent variable, and a0 to an are the equation parameters for the linear relation. The coefficient of determination, also known as R^2, can be used to assess how well a linear model fits a particular set of observable data. To establish a link between the dependent and independent variables, statistical linear regression was performed in this study using MINITAB. Below is a discussion of the outcomes that were reached.

The relation between Penetration and the input parameters BC, WEO, WCO, and PA is given by the equation below.

$$PENETRATION = 104.9 - 0.43\ BC + 9.80\ WEO - 5.29\ WCO - 0.33\ PA$$

From this model, BC was identified as the most influential factor, accounting for 61.06% of the variation in penetration (calculated from the ANOVA sum of squares).

For ductility: DUCTILITY=57.28+0.383 BC−1.46 WEO−0.71 WCO−1.739 PA

PA had the greatest influence on ductility, contributing 59.29%.

For softening point: SOFTENING POINT=50.96−0.045 BC+0.63 WEO+1.38 WCO+0.225 PA

BC was the dominant factor for softening point, contributing 44.32%.

For elastic recovery: ELASTIC RECOVERY=96.92−0.0200 BC+0.700 WEO−0.400 WCO−0.2300 PA
PA contributed 38.07% to the variation in elastic recovery.

These results demonstrate that the parameters influencing each response differ, making single-objective optimization insufficient. To obtain an optimal combination that meets all performance criteria, Grey Relational Analysis (GRA) was applied to the S/N ratios from Taguchi (Table 5).

3.1 Normalization

The first step in this process is to normalize the data of all response characteristics using Equations 3 and 4. The normalized values and deviation sequence are tabulated in Table 3. The calculation of normalized values is given below for run order 1,

$$X_{iP}^{*}(1) = \frac{maxX_i^o(k) - X_i^o(k)}{maxX_i^o(k) - minX_i^0(k)} = \frac{-34.15 - (-34.37)}{-34.15 - (-44.14)} = 0.02$$

$$X_{iD}^{*}(1) = \frac{X_i^o(k) - minX_i^o(k)}{maxX_i^o(k) - minX_i^o(k)} = \frac{(36.90) - (28.56)}{(36.90) - (28.56)} = 1.00$$

$$X_{iSP}^{*}(1) = \frac{X_i^o(k) - minX_i^o(k)}{maxX_i^o(k) - minX_i^o(k)} = \frac{(33.98) - (33.06)}{(36.26) - (33.06)} = 0.29$$

$$X_{iER}^{*}(1) = \frac{X_i^o(k) - minX_i^o(k)}{maxX_i^o(k) - minX_i^o(k)} = \frac{(39.74) - (39.18)}{(40) - (39.18)} = 0.68$$

The deviation sequences have been computed using Eq. 5, as a prerequisite for GRCs. Both the normalized values and the deviation sequence are tabulated and given in Table 3. The deviation sequence for run order 1 of all responses is computed as shown below:

$$\Delta_{oiP}(1) = |X_o^*(k) - X_i^o(k)| = |1 - 0.02| = 0.98$$

$$\Delta_{oiD}(1) = |X_o^*(k) - X_i^o(k)| = |1 - 1| = 0.00$$

$$\Delta_{oiSP}(1) = |X_o^*(k) - X_i^o(k)| = |1 - 0.29| = 0.71$$

$$\Delta_{oiER}(1) = |X_o^*(k) - X_i^o(k)| = |1 - 0.68| = 0.32$$

3.2 Computation of GRCs and GRGs

The GRC was calculated for each response characteristic using Equation 6 and the values of the deviation sequences listed in Table 3. In Equation 6, the value of the distinguishing coefficient, φ = 0:5, was substituted. Equation 7 was used to compute the GRGs after integrating the PCA methodology. Table 5 reports the calculated grey relation coefficients. The following is an example of the GRC calculation for run order 1:

$$\xi_{iP}(1) = \frac{\Delta_{min} + \psi \cdot \Delta_{max}}{\Delta_{oi}(k) + \psi \cdot \Delta_{max}} = \frac{0 + 0.5 * 1}{0.98 + 0.5 * 1} = 0.34$$

$$\xi_{iD}(1) = \frac{\Delta_{min} + \psi \cdot \Delta_{max}}{\Delta_{oi}(k) + \psi \cdot \Delta_{max}} = \frac{0 + 0.5 * 1}{0.00 + 0.5 * 1} = 1.00$$

$$\xi_{iSP}(1) = \frac{\Delta_{min} + \psi \cdot \Delta_{max}}{\Delta_{oi}(k) + \psi \cdot \Delta_{max}} = \frac{0 + 0.5 * 1}{0.71 + 0.5 * 1} = 0.41$$

$$\xi_{iER}(1) = \frac{\Delta_{min} + \psi \cdot \Delta_{max}}{\Delta_{oi}(k) + \psi \cdot \Delta_{max}} = \frac{0 + 0.5 * 1}{0.32 + 0.5 * 1} = 0.61$$

In Grey Relational Analysis (GRA), Principal Component Analysis (PCA) was applied to determine the relative importance of each performance characteristic objectively. PCA was performed on the normalized S/N ratio matrix by decomposing the covariance matrix into eigenvalues and eigenvectors (Table 3). The first two principal components were retained, explaining 90.3% of the total variance (PC1: 67.9%, PC2: 22.4%), which justifies their use for weighting. The weights for each response were calculated from the normalized square of the PC1 eigenvector loadings, as PC1 accounts for the majority of the data variance. These weights

were then applied to the Grey Relational Coefficients (GRCs) to compute the Grey Relational Grades (GRGs), integrating multi-response optimization effectively within the GRA framework. The array's constituents for each of the several performance attributes, as listed in Table 5, display the GRCs for each performance characteristic. Each eigenvalue's corresponding eigenvector is listed in Table 7, and the square of the principal component values of the respective eigenvectors yields the weighted contribution of each performance attribute. Furthermore, Table 7 indicates that up to 67.9% of the variation is attributed to the first main component, which accounts for the three performance criteria. Equation 7, which calculates the weighted value of each performance indicator, is used to compute grey relation grades (GRGs) with the introduction of PCA. Table 6 provides information about the GRGs and their corresponding ranks. The following is an example of a GRG calculation for experiment number 1 using Equation 7:

$$\gamma_i(GRG) = 0.34 * 0.32 + 1 * 0.40 + 0.41 * 0.16 + 0.61 * 0.12 = 0.65$$

The values of all the grey relational grades range from 0 to 1. A strong association is observed between the reference sequence and the comparability sequence as the GRG value approaches the maximum. The maximum GRG value in this study is obtained for the 12th run order with BC-10%, WEO – 3%, WCO – 1%, and PA – 0%. The corresponding test results are Penetration – 102 dmm, Ductility – 63cm, Softening point – 50 °C, and Elastic recovery – 100%. Furthermore, the optimum parameter setting for each factor is derived from the Response table for means. The optimum parameter setting (BC-5%, WEO-2%, WCO-1%, and PA-0%) has undergone a confirmatory test to assess the accuracy of the inquiry for penetration, Ductility, Softening point, and Elastic recovery.

4. Conclusion

This study presents a novel approach to developing sustainable, high-performance bio-bitumen binders by integrating waste oils and biochar, optimized using Grey-Taguchi analysis. The maximum Grey Relational Grade (GRG) was observed for the 12th run (BC-10%, WEO-3%, WCO-1%, PA-0%), achieving a penetration of 102 dmm, ductility of 63 cm, a softening point of 50°C, and an elastic recovery of 100%. An alternative "optimal" parameter set from the response table (BC-5%, WEO-2%, WCO-1%, PA-0%) was also validated, showing balanced improvements. While the 12th run showed slightly better individual properties, the chosen optimal set represents a practical compromise considering overall performance and process stability. The optimized binders meet existing standard specifications, demonstrating their potential for practical pavement use. Key limitations include the absence of long-term aging data and in-depth chemical analysis. The Grey-Taguchi results highlight that, despite all modifiers individually improving properties, PA at 0% was optimal due to possible antagonistic interactions with other additives. Future work should focus on detailed rheological, chemical, and durability studies, alongside cost and environmental assessments, to enable widespread application of bio-bitumen as a sustainable alternative in pavement construction.

Author Contributions: Penki Ramu: Conceptualization, Methodology, Investigation, Data curation, Formal analysis, Writing – Original Draft, Project administration. Subrat Kumar Rout: Supervision, Methodology, Validation, Resources, Writing – Review & Editing. Aditya Kumar Das: Data Analysis, Visualization, Validation, Writing – Review & Editing. All authors have read and approved the final manuscript.

Funding: This research received no external funding

Conflicts of Interest: The authors declare no conflict of interest

References

[1] Zhou, Y.; Wang, H.; Zhang, X.; Sun, Y. Chemical modification of bio-oil with phthalic anhydride for hydrophobic bio-bitumen. *Constr. Build. Mater.* **2020**, *263*, 120–129.

[2] Li, M.; Chen, Z.; Xu, J. Environmental impacts of waste engine oil and waste cooking oil: Challenges and opportunities. *Waste Manag.* **2019**, *85*, 387–399.

[3] Jegan, A.; Ramesh, S.; Kumar, P. Characterization of coconut shell derived biochar for engineering applications. *J. Anal. Appl. Pyrolysis* **2020**, *152*, 104960.

[4] Lu, Y.; Zhang, X.; Li, Q.; Wu, H. Waste engine oil modified bitumen with organic montmorillonite: Fatigue and self-healing properties. *J. Cleaner Prod.* **2023**, *406*, 136–247.
[5] Kim, J.; Lee, H.; Park, D. Principal component analysis in multi-response optimization: Applications in materials engineering. *Mater. Des.* **2012**, *39*, 1–10.
[6] Freddi, R.; Salmon, P. Grey relational analysis integrated with the Taguchi method for process optimization: A case study. *Int. J. Adv. Manuf. Technol.* **2019**, *102*(5–8), 1705–1715.
[7] Mathew, S.; Rajendrakumar, P. Optimization of machining parameters using Grey relational analysis. *J. Mater. Process. Technol.* **2011**, *209*(1), 367–371.
[8] Venkatesh, K.; Sharma, A.; Singh, P. Hybrid Taguchi–Grey–PCA approach for multi-objective optimization in composite material processing. *Mater. Today: Proc.* **2021**, *45*, 1372–1379.
[9] Agrawal, P.; Gupta, R.; Kumar, N. Application of Grey relational analysis with PCA weighting for optimization of drilling process. *J. Manuf. Processes* **2020**, *54*, 310–321.
[10] Zhang, Y.; Liu, X.; Wang, L. Biochar in asphalt modification: A review of performance and mechanisms. *Renewable Sustainable Energy Rev.* **2021**, *146*, 111179.
[11] Guo, X.; Huang, L.; Zhao, Y. Effect of waste cooking oil on low-temperature properties of bio-asphalt. *Fuel* **2020**, *278*, 118298.
[12] Ahmad, J.; Tiwari, A.; Singh, N. Waste engine oil as rejuvenator in aged bitumen: Performance evaluation. *Constr. Build. Mater.* **2021**, *312*, 125372.
[13] Chen, M.; Wang, H.; Xu, Y. Moisture resistance of phthalic anhydride modified bio-asphalt. *Int. J. Pavement Eng.* **2022**, *23*(12), 3987–3996.
[14] Liu, T.; He, J.; Wu, S. Grey relational analysis for evaluating asphalt mixture performance. *Road Mater. Pavement Des.* **2020**, *21*(4), 1031–1046.
[15] Sun, X.; Zhang, F.; Li, K. Multi-objective optimization of asphalt binder properties using Grey relational analysis. *J. Traffic Transp. Eng.* **2020**, *7*(5), 593–602.
[16] Zhang, B.; Ma, Y. Application of PCA in material property optimization. *J. Mech. Sci. Technol.* **2020**, *34*(11), 4557–4566.
[17] Zhao, L.; Tang, H.; Wu, G. Performance of waste cooking oil-modified asphalt binder. *Fuel Process. Technol.* **2020**, *210*, 106572.
[18] Singh, S.; Kumar, R.; Mishra, V. Recycling of waste lubricating oils for sustainable bitumen modification. *Sustainable Mater. Technol.* **2020**, *26*, e00215. https://doi.org/10.1016/j.susmat.2020.e00215
[19] Gupta, M.; Jain, H. Taguchi method and Grey relational analysis for multi-response optimization: A review. *Int. J. Eng. Res. Technol.* **2020**, *9*(7), 561–567.
[20] Wu, J.; Li, H.; Fang, C. Synergistic effects of biochar and waste oils in asphalt modification. *Constr. Build. Mater.* **2021**, *289*, 123196. https://doi.org/10.1016/j.conbuildmat.2021.123196
[21] Patel, R.; Shah, D.; Desai, K. Optimization of bio-bitumen formulation using Grey-Taguchi method. *J. Cleaner Prod.* **2022**, *334*, 130255.
[22] Chen, K.; Wang, J. Eigenvector weighting in multi-objective optimization of composites. *Composite Struct.* **2021**, *255*, 112939.
[23] Bhat, A. N.; Reddy, P. Circular economy applications of waste oils in road construction. *Resour. Conserv. Recycl.* **2021**, *168*, 105437.
[24] Zhou, S.; Fang, L.; Li, X. Moisture resistance of bio-oil modified bitumen using chemical additives. *J. Mater. Civ. Eng.* **2021**, *33*(4), 04021035.
[25] Li, G.; Zhang, X.; Liu, P. Experimental study on biochar-modified asphalt binder. *Fuel* **2020**, *280*, 118653. https://doi.org/10.1016/j.fuel.2020.118653
[26] Kumar, H.; Singh, S.; Mishra, R. Grey relational analysis for optimizing bitumen properties. *Mater. Today: Proc.* **2022**, *49*, 2506–2513.
[27] Wang, C.; Li, Y.; Sun, L. Application of multi-response optimization in pavement material design. *Constr. Build. Mater.* **2021**, *314*, 125661.
[28] Sharma, P.; Yadav, D. Influence of waste cooking oil and waste engine oil on rheological properties of bitumen. *J. Mater. Res. Technol.* **2021**, *15*, 1839–1848.

[29] Mishra, R. K.; Gupta, A.; Kumar, V. Role of biochar in improving rutting resistance of asphalt binders. *J. Transp. Eng., Part B: Pavements* **2021**, *147*(2), 04021008.
[30] He, X.; Yang, Z.; Liu, M. Multi-criteria optimization of asphalt mix design using Taguchi–Grey–PCA. *Int. J. Pavement Res. Technol.* **2021**, *14*, 624–635.
[31] Banerjee, S.; Prasad, K.; Joshi, R. Integration of PCA and Grey relational analysis for multi-performance material optimization. *Procedia CIRP* **2021**, *99*, 205–210.
[32] Ramu, P.; Rout, S. K.; Das, A. K. Optimizing bio-bitumen mixes through response surface methodology. *Ecocycles* **2024**, *10*(1), 68–83. https://doi.org/10.19040/ecocycles.v10i1.413.

ASEAN
Journal of Scientific and Technological Reports
Online ISSN:2773-8752

Academic article

Effects of Dietary Insect Powder Supplementation on Hematological Parameters of Common Carp (*Cyprinus carpio*) Fry

Hadeel Mohammed Joda[1], and Abbas Kazim Hamza[2*]

[1] Department of Biology, College of Education, University of Al-Qadisiyah, Iraq
[2] Department of Biology, College of Education, University of Al-Qadisiyah, Iraq
* Correspondence: Abbas.hamza@qu.edu.iq

Citation:
Jodam, M.H.; Hamza, K.A. Effects of dietary insect powder supplementation on hematological parameters of common carp (*Cyprinus carpio*) fry. *ASEAN J. Sci. Tech. Report.* **2025**, *28*(6), e260795. https://doi.org/10.55164/ajstr.v28i6.260795

Article history:
Received: August 11, 2025
Revised: September 9, 2025
Accepted: September 18, 2025
Available online: October 24, 2025

Abstract: The increasing demand for sustainable protein sources in aquaculture has driven research into insect meal as an alternative to fishmeal for fish nutrition. This study evaluated the effects of dietary insect powder supplementation on blood parameters and liver enzymes in common carp (*Cyprinus carpio*) fry to assess both efficacy and safety of this protein source. Seventy-two common carp fry (average weight 16.65±0.01 g) were randomly distributed into four treatments with six fish per replicate: T0 (control diet), T1 (1% insect powder), T2 (2% insect powder), and T3 (3% insect powder). The insect powder consisted of equal proportions of dried grasshopper and mealworms mixed with a commercial floating diet (30% crude protein, 412 kcal/g gross energy). After 60 days of feeding, blood samples were collected to analyze hematological parameters including red blood cells, hemoglobin, hematocrit, mean corpuscular volume (MCV), mean corpuscular hemoglobin (MCH), mean corpuscular hemoglobin concentration (MCHC), platelets, and white blood cells, as well as liver enzymes aspartate aminotransferase (AST), alanine aminotransferase (ALT), and alkaline phosphatase (ALP). All insect powder supplementation treatments significantly improved blood parameters compared to the control, with treatment effectiveness following the order T3 > T2 > T1 > T0. Treatment T3 achieved the highest values for red blood cells, hemoglobin, and hematocrit. Notably, liver enzyme levels showed no significant differences between treatments, indicating the absence of hepatotoxicity. The results demonstrate that insect powder supplementation, particularly at 3% inclusion level, effectively enhances hematological parameters in common carp fry without causing liver damage, supporting its potential as a safe and beneficial alternative protein source in aquaculture feeds.

Keywords: Common carp; insect meal; hematological parameters; alternative protein; aquaculture nutrition

1. Introduction

Aquaculture has emerged as the fastest-growing food production sector globally, contributing significantly to meeting the increasing demand for protein-rich foods [1]. However, the industry faces substantial challenges regarding sustainable feed ingredients, particularly the reliance on fishmeal as a primary protein source [2]. Fishmeal, derived from wild-caught fish, is characterized by its exceptional nutritional profile, featuring a high protein content, a balanced amino acid composition, and excellent palatability [3]. Nevertheless, the ongoing reliance on fishmeal poses significant challenges related to environmental sustainability, resource depletion, and economic feasibility, particularly as global fishmeal production has stagnated while aquaculture production continues to rise [4-5]. The urgent need for alternative protein sources has driven extensive research into various substitutes, including plant-based proteins, single-cell proteins, and, more recently, insect meal [6, 7].

Among these alternatives, insect meal has garnered considerable attention due to its superior nutritional characteristics, including a high protein content (40-70%), a favorable amino acid profile, essential fatty acids, vitamins, and minerals [8-9]. Insects such as black soldier fly larvae, mealworms, crickets, and grasshoppers have shown promising results as replacements for fishmeal in various aquaculture species [10-11]. Additionally, insect production offers environmental advantages, including lower greenhouse gas emissions, reduced land and water requirements, and the ability to utilize organic waste streams [12].

Although many studies have investigated the effects of insect meal on growth performance and feed utilization in fish [13-14], there remains a limited understanding of the physiological responses, specifically hematological parameters and liver function, which serve as crucial indicators of fish health and nutritional status [15]. Blood parameters, including red blood cell count, hemoglobin concentration, and hematocrit, reflect the oxygen-carrying capacity and overall physiological condition of fish [16]. Similarly, liver enzymes such as aspartate aminotransferase (AST), alanine aminotransferase (ALT), and alkaline phosphatase (ALP) serve as sensitive biomarkers for hepatotoxicity and metabolic stress [17-18]. The common carp (Cyprinus carpio) is one of the most important aquaculture species globally, accounting for a significant portion of freshwater fish production [19]. Despite its economic importance, research on the effects of insect meal supplementation on blood parameters and liver function in common carp remains limited. Therefore, the primary objective of this study was to investigate the impact of dietary insect powder (a mixture of grasshopper and mealworm) supplementation at varying inclusion levels on hematological parameters and liver enzymes in common carp fry, thereby providing insights into both the nutritional benefits and safety of insect-based feeds.

2. Materials and Methods

2.1 Experimental Design and Fish Management

2.1.1 Experimental Fish

A total of 72 common carp (*Cyprinus carpio* L.) fry were obtained from a private hatchery in Al-Mahawil District, Babil Governorate, Iraq. The fish had an initial average weight of 16.65 ± 0.01 g. Upon arrival at the experimental facility, fish were gradually thermally acclimated and subsequently treated with a 0.3% saline bath for 5 minutes to eliminate potential pathogens that could interfere with the experimental outcomes. Following treatment, the fish were maintained in storage tanks before being randomly distributed into experimental units.

2.1.2 Experimental Setup

The fish were randomly assigned to four experimental treatments, with three replicates per treatment and six fish per replicate, following a completely randomized design (CRD). The experimental treatments were: T0 (control diet without insect powder supplementation), T1 (basal diet + 1% insect powder), T2 (basal diet + 2% insect powder), and T3 (basal diet + 3% insect powder).

2.2 Rearing System and Environmental Conditions

2.2.1 Facility Description

The growth experiment was conducted at the Animal House Laboratory, Al-Qadisiyah University, College of Education, Department of Biology, from March 17, 2025, to May 15, 2025. The experimental system consisted of 12 glass aquariums with dimensions of 50 cm × 50 cm × 50 cm, providing a volume of 0.125 m^3 and a capacity of 125 liters each. The aquariums were arranged in a U-shaped configuration and covered with plastic mesh to prevent fish from escaping.

2.2.2 Water System and Equipment

Each aquarium was equipped with a 25-watt aeration pump and a 50-watt water heater to maintain optimal environmental conditions. The water supply was provided through 3/4-inch diameter pipes connected to a 1/2 horsepower water pump, which was linked to a 500-liter plastic storage tank. Water was allowed to stand for more than 8 hours before use to facilitate the removal of chlorine. An additional 1,000-liter tank served as a secondary water storage and supply reservoir. Water drainage was accomplished

through hand pumps connected to 1-inch diameter pipes, which led to a main drainage system. The facility was equipped with an electrical inverter to ensure a continuous power supply during potential outages.

2.2.3 Water Quality Monitoring

The following physicochemical parameters were monitored throughout the experimental period: water temperature, dissolved oxygen concentration, pH, salinity, and total hardness. Measurements were conducted using standard protocols to ensure optimal environmental conditions for the growth and development of common carp.

2.3 Experimental Diets and Feed Preparation

2.3.1 Basal Diet

A commercial floating diet (Fardaneh brand, Iranian origin) was used as the basal diet. The diet contained 30% crude protein, 18% fat, 9% crude fiber, 9% ash, 22% nitrogen-free extract, 1.5% phosphorus, and had a gross energy content of 412 kcal/g. Vitamin supplementation included 250 mg vitamin C, 200 mg vitamin E, 2000 I.U. vitamin D3, and 8000 I.U. vitamin A per kilogram of feed.

2.3.2 Insect Powder Preparation

Commercial dried grasshopper and mealworm powder, typically used for feeding ornamental birds and fish, was obtained from local markets. The two insect types were mixed in equal proportions and continuously blended to ensure homogeneity. The mixture was then finely ground, and samples were submitted to laboratories affiliated with the Ministry of Science and Technology for analysis of their chemical composition. The insect powder contained 41.26% crude protein, 12.06% fat, 7.15% crude fiber, 3.65% ash, and 29.14% nitrogen-free extract on a dry matter basis (93.26%).

2.3.3 Experimental Diet Formulation

The basal Fardaneh diet was ground into a fine powder, and 10-kg portions were allocated for each experimental treatment. Insect powder was incorporated according to the experimental design at inclusion levels of 0%, 1%, 2%, and 3% for treatments T0, T1, T2, and T3, respectively. Each mixture was thoroughly blended to ensure homogeneous distribution of the insect powder. Water was added at a rate of 350-400 ml per kg until a solid paste consistency was achieved. The mixture was then processed through a National-type grinding machine with 2-3 mm holes to form feed pellets. The pellets were air-dried and exposed to sunlight until completely dry, then stored in sealed bags until use.

Table 1. The chemical composition of the Fardaneh diet

Elements	Unit
Dry matter (%)	88
Crude protein (%)	30
Fat (%)	18
Crude fiber (%)	9
Ash (%)	9
Nitrogen-free extract (%)	22
Phosphor (%)	1.5
Vit. C (mg)	250
Vit. E (mg)	200
Vit. D3 (I.U.)	2000
Vit. A (I.U.)	8000
Gross energy (Kcal/g)*	412

*Total energy = (% protein x 5.4) + (% fat x 9) + (% nitrogen-free extract x 4)

2.4 Sample Collection and Analysis

2.4.1 Blood Sampling

After 60 days of experimental feeding, blood samples were collected from two fish per treatment. Blood was drawn from the caudal vein using 3 ml plastic syringes, with sample volumes ranging from 0.5 to 1.0 ml per fish. For hematological analysis, blood samples were immediately transferred to tubes containing ethylenediaminetetraacetic acid (EDTA) as an anticoagulant. For serum biochemical analysis, separate blood samples were collected in vacuum gel tubes without anticoagulants to facilitate the separation of serum.

Table 2. Powder of insect mixture

Element	Percentage (%)
Dry matter	93.26
Crude protein (N*6.25)	41.26
Fat	12.06
Crude fiber	7.15
Ash	3.65
Nitrogen-free extract	29.14
Total	100%

2.4.2 Hematological and Biochemical Analysis

Hematological parameters analyzed included red blood cell count, white blood cell count, hemoglobin concentration, hematocrit, mean corpuscular volume (MCV), mean corpuscular hemoglobin (MCH), mean corpuscular hemoglobin concentration (MCHC), and platelet count. Serum biochemical analysis focused on liver enzyme activities, specifically aspartate aminotransferase (AST), alanine aminotransferase (ALT), and alkaline phosphatase (ALP). All analyses were performed at the Zoo Center using a Seamaty Hematology Analyzer (SMT 120 VP, China).

2.5 Statistical Analysis

Data were analyzed using SPSS software version 26 following a completely randomized design (CRD). Significant differences between treatment means were determined using Duncan's multiple range test [20] at a significance level of $p \leq 0.05$. Results are presented as means ± standard error.

3. Results and Discussion

3.1 Environmental Parameters

Throughout the 60-day experimental period, all monitored water quality parameters remained within optimal ranges for common carp cultivation. Water temperature ranged between 20-21°C, dissolved oxygen levels were maintained at 7.1-7.4 mg/L, pH values recorded between 7.1-7.23, salinity ranged from 1.27-1.8 g/L, and total hardness values were between 450-455.2 mg/L. These environmental conditions are consistent with established requirements for common carp aquaculture [21, 22], ensuring that any observed differences in physiological parameters could be attributed to dietary treatments rather than environmental stress factors. According to established guidelines, common carp can tolerate temperature ranges of 3-35°C [23], minimum dissolved oxygen levels of 3 mg/L [24], salinity levels up to 14 g/L [25], pH ranges of 6.5-9.5 [26], and total hardness up to 620 mg $CaCO_3$/L [27]. The recorded parameters in this study were well within these acceptable ranges, confirming optimal rearing conditions throughout the experimental period.

3.2 Hematological Parameters

3.2.1 Red Blood Cell Parameters

The incorporation of insect powder in common carp diets resulted in significant improvements in red blood cell-related parameters (Table 3). Treatment T3 (3% insect powder) demonstrated the highest red blood cell count ($1.94 \pm 0.05 \times 10^6$ cells/mL), followed by T2 ($1.24 \pm 0.01 \times 10^6$ cells/mL), T1 ($0.95 \pm 0.05 \times 10^6$ cells/mL), and T0 ($0.78 \pm 0.02 \times 10^6$ cells/mL), with all supplemented treatments showing significant differences ($p \leq 0.05$) compared to the control. Similarly, hemoglobin concentrations followed the same pattern, with T3 achieving the highest value (11.05 ± 0.05 g/dL), significantly exceeding T2 (10.50 ± 0.29 g/dL), T1 (9.70 ± 0.20 g/dL), and

T0 (7.85 ± 0.55 g/dL). Hematocrit values also demonstrated dose-dependent improvements, with T3 recording 24.91 ± 0.41%, compared to 22.83 ± 0.17%, 21.75 ± 0.25%, and 19.94 ± 0.05% for T2, T1, and T0, respectively. The enhancement in erythropoietic parameters can be attributed to the rich nutritional profile of the insect powder mixture. Grasshoppers and mealworms are excellent sources of vitamin B_{12} [28], which plays a crucial role in erythropoiesis and red blood cell maturation [29]. Additionally, these insects contain substantial amounts of iron and B-complex vitamins [30, 31], which are essential cofactors in the synthesis of hemoglobin and the formation of red blood cells [32].

3.2.2. Red Blood Cell Indices

Mean corpuscular volume (MCV), mean corpuscular hemoglobin (MCH), and mean corpuscular hemoglobin concentration (MCHC) showed similar dose-dependent improvements across treatments. Treatment T3 recorded the highest MCV (161.50 ± 0.50 μL), MCH (32.12 ± 0.09 pg/mL), and MCHC (33.59 ± 0.28%), all of which were significantly higher than those in the control treatment. These improvements in red blood cell indices suggest enhanced erythropoietic activity and the formation of larger, more hemoglobin-rich erythrocytes [33]. The superior amino acid profile of insect protein, particularly the presence of essential amino acids such as leucine, valine, histidine, methionine, lysine, and tyrosine [30, 34], likely contributed to improved hemoglobin synthesis and red blood cell quality. Recent research has demonstrated that amino acid supplementation, particularly leucine, valine, and histidine, significantly influences red blood cell production, while methionine, lysine, and tyrosine contribute directly to hemoglobin synthesis [35].

3.2.3. White Blood Cell and Platelet Counts

White blood cell counts showed significant improvements in treatments T2 (94.96 ± 0.54 × 10^3/mL) and T3 (96.40 ± 0.40 × 10^3/mL) compared to T0 (89.58 ± 0.51 × 10^3/mL) and T1 (91.61 ± 0.61 × 10^3/mL), although no significant difference was observed between T2 and T3. Platelet counts demonstrated a clear dose-response relationship, with T3 achieving the highest count (99.55 ± 0.44 × 10^3/μL), followed by T2, T1, and T0. The enhancement in white blood cell counts suggests improved immune function, likely attributed to the presence of antimicrobial peptides (AMPs) in insect meal [36]. These bioactive compounds, along with chitin derivatives, have been shown to modulate immune responses in aquatic organisms [37]. Furthermore, insect meals contain lauric acid, a medium-chain fatty acid with demonstrated antimicrobial and immunostimulatory properties [38, 39]. The improved platelet counts indicate enhanced hemostatic function and potentially improved stress resistance in fish fed insect-supplemented diets.

Table 3. Some of the studied blood parameters (mean ± standard error) of common carp fry fed on a mixture of insect powder during the duration of the experiment.

Studied parameters	Experimental treatments				Significant level
	T0	T1	T2	T3	
R.B.C (10^6cell/ml)	0.78 ± 0.02^{d}	0.95 ± 0.05^{c}	1.24 ± 0.01^{b}	1.94 ± 0.05^{a}	0.05
Hemoglobin (g/dL)	7.85 ± 0.55^{c}	9.70 ± 0.20^{b}	10.50 ± 0.29^{ab}	11.05 ± 0.05^{a}	0.05
Hematocrit (%)	19.94 ± 0.05^{d}	21.75 ± 0.25^{c}	22.83 ± 0.17^{b}	24.91 ± 0.41^{a}	0.05
M.C.V (μL)	159.50 ± 0.50^{b}	160.30 ± 0.10^{ab}	160.40 ± 0.09^{ab}	161.50 ± 0.50^{a}	0.05
M.C.H (pg/mL)	29.05 ± 0.05^{c}	29.71 ± 0.38^{bc}	31.15 ± 0.85^{ab}	32.12 ± 0.09^{a}	0.05
M.C.H.C (%)	30.59 ± 0.49^{b}	31.65 ± 0.65^{b}	33.80 ± 0.20^{a}	33.59 ± 0.28^{a}	0.05
Platelets (10^3/ μL)	88.50 ± 0.50^{d}	90.81 ± 0.21^{c}	95.51 ± 0.51^{b}	99.55 ± 0.44^{a}	0.05
W.B.C (10^3/ml)	89.58 ± 0.51^{b}	91.61 ± 0.61^{b}	94.96 ± 0.54^{a}	96.40 ± 0.40^{a}	0.05

3.3 Liver Enzyme Activities

3.3.1 Hepatic Safety Assessment

Liver enzyme analysis revealed no significant differences ($p > 0.05$) between treatments for aspartate aminotransferase (AST), alanine aminotransferase (ALT), and alkaline phosphatase (ALP) activities (Table 4). AST values ranged from 67.47 ± 0.47 to 68.75 ± 0.25 I.U./L, ALT values from 13.00 ± 0.99 to 14.65 ± 0.45 I.U./L, and ALP values from 25.60 ± 0.60 to 27.50 ± 0.50 I.U./L across all treatments. These results are particularly

significant as they demonstrate the hepatic safety of insect powder supplementation at the tested inclusion levels. Liver enzymes, particularly AST and ALT, serve as sensitive biomarkers for hepatocellular damage and metabolic stress [40, 41]. The absence of elevated enzyme activities indicates that insect powder supplementation did not induce hepatotoxicity or liver dysfunction, even at the highest inclusion level of 3%.

3.3.2. Metabolic Implications

The maintained liver enzyme activities within normal physiological ranges suggest that insect protein was efficiently utilized without causing metabolic stress. This finding is consistent with previous studies demonstrating the safety of moderate insect meal inclusion in fish diets [42, 43]. The absence of hepatotoxic effects may be attributed to the high digestibility and bioavailability of insect proteins, which reduces the metabolic burden on the liver compared to some plant-based protein sources that may contain anti-nutritional factors.

Table 4. Studied Liver enzymes (mean ± standard error) of common carp fry fed on a mixture of insect powder during the duration of the experiment.

Studied parameters	Experimental treatments				Significant level
	T0	T1	T2	T3	
A.S.T (I.U./L)	67.75 ± 0.75	68.50 ± 0.50	67.47 ± 0.47	68.75 ± 0.25	NS
A.L.T (I.U./L)	13.75 ± 0.75	13.00 ± 0.99	13.65 ± 0.65	14.65 ± 0.45	NS
A.L.P (I.U./L)	25.60 ± 0.60	26.50 ± 0.49	27.50 ± 0.50	27.25 ± 0.25	NS

3.4 Dose-Response Relationships and Optimal Inclusion Levels

The study demonstrated clear dose-dependent responses across most measured parameters, with treatment effectiveness following the order T3 > T2 > T1 > T0. This pattern suggests that within the tested range (0-3%), higher inclusion levels of insect powder provided greater physiological benefits without compromising fish health or liver function. The superior performance of the 3% inclusion level may be attributed to the cumulative effects of enhanced protein quality, improved micronutrient availability, and the presence of bioactive compounds. However, future studies should investigate higher inclusion levels to determine the optimal supplementation rate and identify potential threshold effects beyond which benefits may plateau or adverse effects may occur.

3.5 Mechanistic Considerations and Future Research Directions

The observed improvements in hematological parameters likely result from multiple synergistic mechanisms. The high-quality protein and essential amino acids in insect meal support enhanced protein synthesis for hemoglobin and cellular components. The presence of bioactive compounds, such as antimicrobial peptides and chitin derivatives, may contribute to improved gut health and enhanced nutrient absorption, thereby indirectly supporting a better physiological status [44-45]. Future research should focus on investigating the underlying molecular mechanisms responsible for these improvements, including gene expression studies related to erythropoiesis and immune function. Additionally, longer-term studies are needed to evaluate the sustained effects of insect meal supplementation and to determine optimal feeding strategies for different growth stages of common carp. The environmental sustainability implications of insect meal utilization in aquaculture also warrant further investigation, particularly regarding life cycle assessments and economic feasibility compared to conventional protein sources. Integration of insect farming with aquaculture operations could potentially create circular production systems that enhance overall sustainability and resource efficiency.

4. Conclusions

This study investigated the hypothesis that dietary insect powder supplementation would enhance hematological parameters in common carp fry without causing hepatotoxicity. The results conclusively demonstrate that incorporating a mixture of grasshopper and mealworm powder at inclusion levels of 1%, 2%, and 3% significantly improved blood parameters in a dose-dependent manner, with the 3% inclusion level yielding optimal results. The most significant findings include substantial improvements in red blood cell count, hemoglobin concentration, hematocrit, and red blood cell indices (MCV, MCH, MCHC) across all

supplemented treatments compared to the control. Additionally, white blood cell and platelet counts were enhanced, suggesting improved immune function and hemostatic capacity. Critically, liver enzyme activities (AST, ALT, ALP) remained within normal physiological ranges across all treatments, confirming the hepatic safety of insect powder supplementation at the tested inclusion levels. This research contributes valuable evidence to the growing body of knowledge supporting insect meal as a safe and effective alternative protein source in aquaculture. The findings demonstrate that insect powder not only serves as a nutritionally adequate fishmeal substitute but also actively enhances physiological performance indicators in common carp fry. The absence of hepatotoxic effects addresses significant safety concerns regarding novel feed ingredients in aquaculture. Several limitations should be acknowledged, including the relatively short experimental duration (60 days), the limited range of inclusion levels tested (0-3%), and the focus on a single fish species and life stage. Additionally, the study did not investigate the underlying molecular mechanisms responsible for the observed physiological improvements. Future research directions should include longer-term feeding trials to assess sustained effects and potential cumulative benefits, investigation of higher inclusion levels to determine optimal supplementation rates, evaluation across different fish species and life stages, and molecular-level studies to elucidate the mechanisms underlying enhanced hematological performance. Economic feasibility analyses and life cycle assessments would further support the practical implementation of insect meal in commercial aquaculture operations. Overall, this study provides compelling evidence that insect powder supplementation represents a promising strategy for enhancing fish health while supporting sustainable aquaculture development.

5. Acknowledgements

The authors would like to thank the University of Al-Qadisiyah, College of Education, Department of Biology, for its assistance and facilities. The authors acknowledge, in particular, those at the Animal House Laboratory and the Zoo Center for experimentation and analysis, as well as the Ministry of Science and Technology laboratories for chemical composition analyses. We are also grateful to the private hatchery in Al-Mahawil/Babil for providing the common carp fry.

Author Contributions: Conceptualization, H.M.J. and A.K.H..; methodology, H.M.J. and A.K.H...; software, H.M.J. and A.K.H..;; validation, H.M.J. and A.K.H...; formal analysis, H.M.J. and A.K.H...; investigation, H.M.J. and A.K.H..; resources, H.M.J. and A.K.H...; data curation, H.M.J. and A.K.H..; writing—original draft preparation, H.M.J. and A.K.H..; writing—review and editing, H.M.J. and A.K.H..; visualization, H.M.J. and A.K.H..; supervision, H.M.J. and A.K.H..

Conflicts of Interest: This work has no conflicts of interest.

References

[1] FAO. The State of World Fisheries and Aquaculture 2022. Towards Blue Transformation; FAO: Rome, Italy, **2022**.

[2] Tacon, A.G.J.; Metian, M. Global overview on the use of fish meal and fish oil in industrially compounded aquafeeds: Trends and future prospects. *Aquaculture* **2008**, *285*, 146-158. https://doi.org/10.1016/j.aquaculture.2008.08.015

[3] Olsen, R.L.; Hasan, M.R. A limited supply of fishmeal: Impact on future increases in global aquaculture production. *Trends Food Sci. Technol.* **2012**, *27*, 120-128. https://doi.org/10.1016/j.tifs.2012.06.003

[4] Shepherd, C.J.; Jackson, A.J. Global fishmeal and fish-oil supply: inputs, outputs and markets. *J. Fish Biol.* **2013**, *83*, 1046-1066. https://doi.org/10.1111/jfb.12224

[5] Naylor, R.L.; Hardy, R.W.; Buschmann, A.H.; Bush, S.R.; Cao, L.; Klinger, D.H.; Little, D.C.; Lubchenco, J.; Soto, D.; Troell, M. A 20-year retrospective review of global aquaculture. *Nature* **2021**, *591*, 551-563. https://doi.org/10.1038/s41586-021-03308-6

[6] Gatlin, D.M.; Barrows, F.T.; Brown, P.; Dabrowski, K.; Gaylord, T.G.; Hardy, R.W.; Herman, E.; Hu, G.; Krogdahl, Å.; Nelson, R.; et al. Expanding the utilization of sustainable plant products in aquafeeds: A review. *Aquac. Res.* **2007**, *38*, 551-579. https://doi.org/10.1111/j.1365-2109.2007.01704.x
[7] Makkar, H.P.S.; Tran, G.; Heuzé, V.; Ankers, P. State-of-the-art on use of insects as animal feed. *Anim. Feed Sci. Technol.* **2014**, *197*, 1-33. https://doi.org/10.1016/j.anifeedsci.2014.07.008
[8] van Huis, A.; Van Itterbeeck, J.; Klunder, H.; Mertens, E.; Halloran, A.; Muir, G.; Vantomme, P. Edible insects: Future prospects for food and feed security. *FAO For. Pap.* **2013**, *171*, 1-201.
[9] Henry, M.; Gasco, L.; Piccolo, G.; Fountoulaki, E. Review on the use of insects in the diet of farmed fish: Past and future. *Anim. Feed Sci. Technol.* **2015**, *203*, 1-22. https://doi.org/10.1016/j.anifeedsci.2015.03.001
[10] Barroso, F.G.; de Haro, C.; Sánchez-Muros, M.J.; Venegas, E.; Martínez-Sánchez, A.; Pérez-Bañón, C. The potential of various insect species for use as food for fish. *Aquaculture* **2014**, *422-423*, 193-201. https://doi.org/10.1016/j.aquaculture.2013.12.024
[11] Sankian, Z.; Khosravi, S.; Kim, Y.O.; Lee, S.M. Effects of dietary inclusion of yellow mealworm (*Tenebrio molitor*) meal on growth performance, feed utilization, body composition, plasma biochemical indices, selected immune parameters and antioxidant enzyme activities of mandarin fish (*Siniperca scherzeri*) juvenile. *Aquaculture* **2018**, *496*, 79-87. https://doi.org/10.1016/j.aquaculture.2018.07.012
[12] Oonincx, D.G.A.B.; van Itterbeeck, J.; Heetkamp, M.J.W.; van den Brand, H.; van Loon, J.J.A.; van Huis, A. An exploration on greenhouse gas and ammonia production by insect species suitable for animal or human consumption. *PLoS ONE* **2010**, *5*, e14445. https://doi.org/10.1371/journal.pone.0014445
[13] Gasco, L.; Finke, M.; van Huis, A. Can diets containing insects promote animal health? *J. Insects Food Feed* **2018**, *4*, 1-4. https://doi.org/10.3920/JIFF2018.x001
[14] Nogales-Mérida, S.; Gobbi, P.; Józefiak, D.; Mazurkiewicz, J.; Dudek, K.; Rawski, M.; Kierończyk, B.; Józefiak, A. Insect meals in fish nutrition. *Rev. Aquac.* **2019**, *11*, 1080-1103. https://doi.org/10.1111/raq.12281
[15] Haney, D.C.; Hursh, D.A.; Mix, M.C.; Winton, J.R. Physiological and hematological changes in chum salmon artificially infected with erythrocytic necrosis virus. *J. Aquat. Anim. Health* **1992**, *4*, 48-57. https://doi.org/10.1577/1548-8667(1992)004<0048:PAHCIC>2.3.CO;2
[16] Fazio, F. Fish hematology analysis as an important tool of aquaculture: A review. *Aquaculture* **2019**, *500*, 237-242. https://doi.org/10.1016/j.aquaculture.2018.10.030
[17] Luskova, V. Annual cycles and normal values of hematological parameters in fishes. *Acta Sci. Nat. Brno* **1997**, *31*, 70.
[18] Gabriel, U.U.; Akinrotimi, O.A.; Bekibele, D.O.; Onunkwo, D.N.; Anyanwu, P.E. Locally produced fish feed: Potentials for aquaculture development in sub-Saharan Africa. *Afr. J. Agric. Res.* **2007**, *2*, 287-295.
[19] FAO. Cyprinus carpio (Linnaeus, 1758). *Cultured Aquatic Species Information Programme*; FAO: Rome, Italy, **2023**.
[20] Duncan, D.B. Multiple range and multiple F tests. *Biometrics* **1955**, *11*, 1-42. https://doi.org/10.2307/3001478
[21] Boyd, C.E.; Tucker, C.S. *Pond Aquaculture Water Quality Management*; Springer: Boston, MA, USA, 1998. https://doi.org/10.1007/978-1-4615-5407-3
[22] Hargreaves, J.A.; Tucker, C.S. Managing ammonia in fish ponds. *SRAC Publ.* **2004**, *4603*, 1-8.
[23] Froese, R.; Pauly, D. FishBase. *World Wide Web Electronic Publication*; **2011**. www.fishbase.org
[24] Salman, M.H.M.A. *The Basics of Fish Farming and Production*, 2nd ed.; University of Basra Press: Basra, Iraq, **2000**; p. 396.
[25] Salman, N.A.; Al-Mahdawi, G.J.; Kittan, S.A.; Al-Rudaing, A.M.; Habah, M.K. Accilimation of common carp, Bunni and Gattan to the drainage water Saddam's River using concrete ponds. *Mar. Mesopotamica* **1993**, *8*, 190-201.
[26] Food and Agriculture Organization (FAO). Report of the symposium on new developments in the utilization of heated effluent and of recirculation system for intensive aquaculture, Stavanger, 29-30 May 1980. *EIFAC/T39*; FAO: Rome, Italy, **1981**.
[27] Al-Dubaikal, A.Y. A Nutritional and Metabolic Study of Young Brown Carp *Barbus sharpeyi*, Catfish *B. xanthopterus*, and Common Carp *Cyprinus carpio* L. under Laboratory Conditions. Ph.D. Thesis, University of Basra, Basra, Iraq, **1996**.

[28] Schmidt, A.; Call, L.; Macheiner, L.; Mayer, H.K. Determination of vitamin B12 in four edible insect species by immunoaffinity and ultra-high performance liquid chromatography. *Food Chem.* **2018**, *281*, 124-129. https://doi.org/10.1016/j.foodchem.2018.12.039

[29] Koury, M.J.; Ponka, P. New insights into erythropoiesis: The roles of folate, vitamin B12, and iron. *Annu. Rev. Nutr.* **2004**, *24*, 105-131. https://doi.org/10.1146/annurev.nutr.24.012003.132306

[30] Jauncey, K.; Ross, B. A Guide to Tilapia Feeds and Feeding Ins. Aquaculture, Univ. Sterling, FK94 La, Scotland, U. K. **1982**; p 111.

[31] Hanif, N.I.; Apriantini, N.A.; Endrawati, N.Y.C. Review: Nutritional contents and bioactive compounds of mealworm (*Tenebrio molitor*) as edible insect. *J. Ilmu Prod. Teknol. Hasil Peternak.* **2023**, *11*, 153-162. https://doi.org/10.29244/jipthp.11.3.153-162

[32] Tiglis, M.; Grintescu, I.C.; Neagu, T.P.; Grintescu, I.M. Iron and erythropoiesis – Optimizing the link. *Mod. Med.* **2020**, *27*, 1-8. https://doi.org/10.31689/rmm.2020.27.2.91

[33] Hrubec, T.C.; Smith, S.A. Hematology of fishes. In *Schalm's Veterinary Hematology*, 6th ed.; Weiss, D.J., Wardrop, K.J., Eds.; Blackwell Publishing Ltd.: Singapore, **2010;** pp. 994-1003.

[34] Rumpold, B.A.; Schlüter, O.K. Nutritional composition and safety aspects of edible insects. *Mol. Nutr. Food Res.* **2013**, *57*, 802-823. https://doi.org/10.1002/mnfr.201200735

[35] Binns, H.C.; Alipour, E.; Sherlock, C.E.; Nahid, D.S.; Whitesides, J.F.; Cox, A.O.; Furdui, C.M.; Marrs, G.S.; Kim-Shapiro, D.B.; Cordy, R.J. Amino acid supplementation confers protection to red blood cells before *Plasmodium falciparum* bystander stress. *Blood Adv.* **2024**, *8*, 2552-2564. https://doi.org/10.1182/bloodadvances.2023010820

[36] Wang, S.; Zeng, X.; Yang, Q.; Qiao, S. Antimicrobial peptides as potential alternatives to antibiotics in food animal industry. *Int. J. Mol. Sci.* **2016**, *17*, 603. https://doi.org/10.3390/ijms17050603

[37] Mousavi, S.; Zahedinezhad, S.; Loh, J.Y. A review on insect meals in aquaculture: The immunomodulatory and physiological effects. *Int. Aquat. Res.* **2020**, *12*, 100-115.

[38] Lieberman, S.; Enig, M.G.; Preuss, H.G. A review of monolaurin and lauric acid: Natural virucidal and bactericidal agents. *Altern. Complement. Ther.* **2006**, *12*, 310-314. https://doi.org/10.1089/act.2006.12.310

[39] Zhan, W.; Peng, H.; Xie, S.; Deng, Y.; Zhu, T.; Cui, Y.; Cao, H.; Tang, Z.; Jin, M.; Zhou, Q. Dietary lauric acid promoted antioxidant and immune capacity by improving intestinal structure and microbial population of swimming crab (*Portunus trituberculatus*). *Fish Shellfish Immunol.* **2024**, *151*, 109739. https://doi.org/10.1016/j.fsi.2024.109739

[40] Balint, T.; Ferenczy, J.; Katai, F.; Kiss, I.; Kroazc, L.; Lang, G.; Polyhos, C.; Szabo, I.; Nemesok, J. Similarities and differences between the massive eel (*Anguilla anguilla*) devastation that occurs in lake Balaton in 1991 and 1995. *Ecotoxicol. Environ. Saf.* **1997**, *37*, 17-23. https://doi.org/10.1006/eesa.1996.1509

[41] Al-Ghanim, K.A. Effect of cypermethrin toxicity on enzyme activities in the freshwater fish *Cyprinus carpio* L. *Afr. J. Biotechnol.* **2014**, *13*, 1169-1173. https://doi.org/10.5897/AJB12.1724

[42] Madibana, M.J.; Mwanza, M.; Lewis, B.R.; Fouché, C.H.; Toefy, R.; Mlambo, V. Black soldier fly larvae meal as a fishmeal substitute in juvenile dusky kob diets: Effect on feed utilization, growth performance, and blood parameters. *Sustainability* **2020**, *12*, 9460. https://doi.org/10.3390/su12229460

[43] Zou, Q.; Huang, Y.; Cao, J.; Zhao, H.; Wang, G.; Li, Y.; Pan, Q. Effects of replacing fishmeal with American cockroach meal on growth performance, digestive enzyme activities, and hepatic antioxidant capacity in juvenile common carp (*Cyprinus carpio*). *Aquac. Nutr.* **2024**, *30*, 1-12.

[44] Lu, D.; Geng, T.; Hou, C.; Huang, Y.; Qin, G.; Guo, X. *Bombyx mori* cecropin A has a high antifungal activity to entomopathogenic fungus *Beauveria bassiana*. *Gene* **2016**, *583*, 29-35. https://doi.org/10.1016/j.gene.2016.02.045

[45] Gasco, L.; Finke, M.; van Huis, A. Can diets containing insects promote animal health? *J. Insects Food Feed* **2018**, *4*, 1-4. https://doi.org/10.3920/JIFF2018.x001

ASEAN
Journal of Scientific and Technological Reports
Online ISSN:2773-8752

Research article

Edible Mushroom Extracts: Evaluating Phenolic Content, Antioxidant Capacity, and Anticancer Effects

Chompoonuth Porncharoennop[1*] and Thornthan Sawangwan[2]

[1] Faculty of Science, Ramkhamhaeng University, Bangkok, 10240, Thailand
[2] Faculty of Science, Ramkhamhaeng University, Bangkok, 10240, Thailand
* Correspondence: chompoonuth.p@rumail.ru.ac.th

Citation:
Porncharoennop, C.; Sawangwan, T. Edible mushroom extracts: Evaluating phenolic content, antioxidant capacity, and anticancer effects. *ASEAN J. Sci. Tech. Report.* **2025**, 28(6), e260401. https://doi.org/10.55164/ajstr.v28i6.260401.

Article history:
Received: July 18, 2025
Revised: September 11, 2025
Accepted: September 18, 2025
Available online: October 19, 2025

Abstract: Edible mushrooms have also been recognized as valuable sources of bioactive compounds with potential therapeutic benefits. Although several edible mushrooms have demonstrated anticancer effects, limited studies have investigated their impact on colorectal cancer cells. Furthermore, it is of interest to further examine the relationship between the total phenolic content, antioxidant activity, and anticancer potential of edible mushroom extracts. Therefore, this study aimed to evaluate the anticancer effects of ethanolic extracts from eight edible mushrooms sourced from Wang Nam Khiao Farm on HT-29 cells and to investigate the relationship between their total phenolic content, antioxidant capacity, and anticancer activity. Total phenolic content was the highest in *Lentinus edodes.* The strongest antioxidant property was observed in *Pleurotus ostreatus*. Based on anticancer results, the mushrooms were classified into three groups: vigorous activity (*P. ostreatus*, *Auricularia auricular-judae*, *Pleurotus djamor*, and *Pleurotus sajor-caju*), moderate activity (*Tremella fuciformis* and *Volvariella volvacea*), and low activity (*Flammulina velutipes* and *L. edodes*). A positive relationship was generally observed between total phenolic content, antioxidant activity, and anticancer efficacy, suggesting that phenolic compounds may play a role in mediating anticancer effects. Interestingly, *L. edodes* was an exception, exhibiting elevated total phenolic content and antioxidant capacity, yet demonstrating low anticancer activity, indicating that additional bioactive compounds or mechanisms may contribute to its anticancer effects. These findings highlight the promising role of edible mushrooms as potential sources of natural antioxidants and anticancer agents for the prevention of colon cancer. Further chemical characterization and mechanistic studies are required to elucidate the compounds responsible for the biological activities.

Keywords: Edible mushroom; phenolic compound; antioxidant activity; anticancer activity

1. Introduction

Mushrooms can be divided into three main groups: medicinal mushrooms, such as *Cordyceps militaris*, *Ganoderma lucidum*, and *Schizophyllum commune*; edible mushrooms, including *Auricularia auricular-judae*, *Tremella fuciformis*, *Pleurotus sajor-caju*, and *Volvariella volvacea*; and poisonous mushrooms, such as *Amanita phalloides* and *Cortinarius rubellus* [1–2]. However, numerous edible mushrooms have long been appreciated not only as nutritious food but also as valuable sources of bioactive compounds with potential health

benefits [3,4]. Numerous studies have demonstrated that mushrooms possess antioxidant, anti-inflammatory, antimicrobial, and anticancer properties, primarily due to the presence of secondary metabolites such as polysaccharides, terpenoids, and phenolic compounds [5–6]. However, the amount of these active ingredients in each mushroom varies according to the species, environmental conditions, cultivation techniques, and the stage of growth at the time of harvest [7–12]. Phenolic compounds, in particular, have been extensively studied for their antioxidant activity, which involves eliminating reactive oxygen species and preserving cellular integrity against oxidative stress [13–16]. The total phenolic content is often correlated with antioxidant capacity in natural products, including those of mushroom extracts [16–18]. Since oxidative stress plays a crucial role in carcinogenesis, antioxidants derived from edible mushrooms are considered promising agents for cancer prevention and therapy [19].

Several edible mushrooms have demonstrated the ability to kill human cancer cells, particularly breast cancer cells, through interfering with cancer cell growth, for example, by stopping the cell cycle and triggering apoptosis [20–30]. Few studies have examined the impact of mushroom extracts on colorectal carcinoma cells, and none have investigated the relationship between the total phenolic content, antioxidant ability, and the anticancer effect of edible mushroom extracts [31–34]. Our study includes *A. auricular-judae*, which is a widely consumed edible mushroom; however, research on its specific biological activities, such as anticancer effects, is significantly less extensive than that of other edible mushroom species. Hence, this research aims to evaluate the potential of various edible mushroom extracts to inhibit the proliferation of colon cancer cells while also investigating the relationship between the total phenolic content, antioxidant capacities, and anticancer efficiency exhibited by these extracts. It was hypothesized that edible mushroom extracts could inhibit the proliferation of colon cancer cells by exhibiting a positive relationship with total phenolic content and antioxidant ability. The findings from this study could lead to molecular-level studies of the cancer cell inhibition mechanisms of mushroom extracts, potentially resulting in the development of healthy food products from edible mushrooms in the future.

2. Materials and Methods

2.1 Preparation of edible mushroom extracts

Eight edible mushrooms (*Auricularia auricular-judae*, *Flammulina velutipes*, *Lentinus edodes*, *Pleurotus djamor*, *Pleurotus ostreatus*, *Pleurotus sajor-caju, Tremella fuciformis*, and *Volvariella volvacea*) were purchased from Wang Nam Khiao Farm, an organic mushroom farm in Nakhon Ratchasima Province, Thailand. The mushroom identities were confirmed morphologically by referring to the literature [35]. The mushrooms were cleaned by rinsing them with clean water and then air-dried until they were slightly moist. They were subsequently chopped into small pieces and then dried at 60°C for 24 hours in a hot-air oven to a constant weight. Then, the samples were ground into a fine powder using a blender. To prepare the extracts, 30 g of each sample was added to 150 mL of a 1:4 (v/v) water and 95% ethanol. The mixtures were then incubated in a shaker for 4 h at 80°C and 150 rpm. The supernatant was separated by centrifugation at 5,000 rpm for 15 min. The solvent was then evaporated using a rotary evaporator heated to 60°C, as modified from Sawangwan et al. [36]. The obtained crude extract was stored at -20ºC until further investigation.

2.2 Determination of total phenolic content

The total phenolic content of eight edible mushroom extracts was determined using the Folin–Ciocalteu colorimetric method adapted from Seephonkai et al. [37]. Briefly, 10 μL of the extract was mixed with 50 μL of Folin–Ciocalteu reagent (Sigma-Aldrich, Saint Louis, USA) and 65 μL of distilled water in a 96-well plate. After incubation at room temperature for 8 minutes, 125 μL of 7.5% (w/v) sodium carbonate was added to the mixture. The reaction was allowed to proceed in the dark at room temperature for 2 h. The absorbance was measured at 765 nm using a microplate reader (Synergy H1, BioTek Instruments, Inc., Winooski, VT, USA). Gallic acid was used as a standard to construct a standard curve.

2.3 Determination of antioxidant activity

The antioxidant activity of the mushroom extracts was determined using the DPPH radical scavenging assay, modified from the method of Loypimai et al. [38]. Briefly, 50 μL of mushroom extract (0–5 mg/mL) was combined with 150 μL of 0.3 mM 2,2-diphenyl-1-picrylhydrazyl (DPPH, Sigma-Aldrich, Saint Louis, USA) solution prepared in methanol in a 96-well microplate. For half an hour, the reaction mixture was kept in the dark at room temperature. The absorbance was then measured at 517 nm using a microplate reader. The percentage of DPPH radical inhibition was calculated using the following equation.

$$\% \text{ DPPH radical inhibition} = (\text{Mean OD}_{\text{blank}} - \text{Mean OD}_{\text{sample}}) / \text{Mean OD}_{\text{blank}} \times 100$$

A graph was plotted to show the relationship between the percentage of DPPH radical inhibition and the concentrations of mushroom extract. The effective concentration required to scavenge 50% of DPPH radicals (EC_{50}) was calculated from the linear regression equation obtained from the dose–response curve. The EC_{50} value reflects the concentration of the antioxidant required to decrease the initial DPPH concentration by 50%.

2.4 Cell culture

The HT-29 human colon cancer cell line (HT-29 cells) was purchased from iCell Bioscience Inc. (China). Cells were propagated and maintained in DMEM enriched with 10% FBS and 1% (v/v) antibiotic-antimycotic solution (all from Gibco, Thermo Fisher Scientific Inc., USA). The incubator provided a humidified atmosphere of 5% CO_2 and a temperature of 37°C.

2.5 Evaluation of anticancer activity

The anticancer activity of edible mushroom extracts against HT-29 cells was assessed by colorimetric 3-(4,5-dimethylthiazol-2-yl)-2,5-diphenyl tetrazolium bromide (MTT Sigma-Aldrich, Saint Louis, USA) assay. The experiment included untreated HT-29 cells as a control and culture medium as a blank control. HT-29 cells were seeded in triplicate into 96-well plates at a density of 5 × 10^4 cells/well and incubated for 24 hours to allow for cell adhesion. Subsequently, these cells were treated with edible mushroom extracts for 48 h. The extracts were prepared across six concentrations (5 to 0.156 mg/mL) using a two-fold serial dilution method. After treatment, the MTT solution was added to the wells, and the plates were incubated for 4 hours. Subsequently, the solution was removed, and 100% DMSO was added to dissolve the formazan crystals. Cell cytotoxicity was assessed by measuring absorbance at 570 nm with a microplate reader. The percentage of viable cells was then calculated based on the following equation.

$$\text{Cell viability (\%)} = \text{Mean OD}_{\text{sample}} / \text{Mean OD}_{\text{blank}} \times 100$$

Cell viability was calculated as a percentage relative to the untreated control. The half-maximal inhibitory concentration (IC_{50}) was then determined using a nonlinear regression equation.

2.6 High-performance liquid chromatography (HPLC) analysis of phenolic compounds

Quantification of gallic acid, tannic acid, and caffeic acid was analyzed using an HPLC system (HP 1100, Hewlett-Packard, Germany) with a UV–Vis detector and a reverse-phase C18 column (4.6 × 250 mm, 5 μm) at 30 °C. The mobile phase consisted of 5% acetic acid (A) and acetonitrile (B), delivered isocratically at a flow rate of 1.0 mL/min. Gallic and tannic acids were detected at 280 nm, while caffeic acid was detected at 320 nm [39].

2.7 Statistical analysis

The data, reported as mean ± standard error of the mean (SEM), from three independent experiments were statistically analyzed using SPSS for Windows, version 21 (SPSS, Chicago, IL, USA). A completely randomized design (CRD) was employed. Normally distributed data were subjected to one-way analysis of variance (ANOVA), with statistical significance set at $p < 0.05$.

3. Results and Discussion

Eight edible mushrooms (*A. auricular-judae*, *F. velutipes*, *L. edodes*, *P. djamor*, *P. ostreatus*, *P. sajor-caju*, *T. fuciformis*, and *V. volvacea*) were extracted using ethanol and investigated for their total phenolic content, antioxidant activity, anticancer effect, and some phenolic compound content.

3.1 Total phenolic content of edible mushroom extracts

Phenolic compounds, a significant class of secondary metabolites, are crucial for antioxidant activity and are known to help prevent cancer. Their antioxidant potential is primarily due to their ability to scavenge free radicals, reduce transition metal ions, and inhibit lipid peroxidation [14,40]. To examine the total phenolic content of eight edible mushroom extracts, a Folin-Ciocalteu reagent was used in this study. As shown in Figure 1, *L. edodes* exhibited the highest concentration of total phenolic content at 1.53 mg/mL, followed by *V. volvacea* at 1.27 mg/mL, *P. sajor-caju* at 1.24 mg/mL, *P. ostreatus* at 1.17 mg/mL, *P. djamor* at 1.15 mg/mL, and *A. auricular-judae* at 1.08 mg/mL. *T. fuciformis* and *F. velutipes* exhibited low levels of total phenolic content at 0.43 mg/mL and 0.56 mg/mL, respectively.

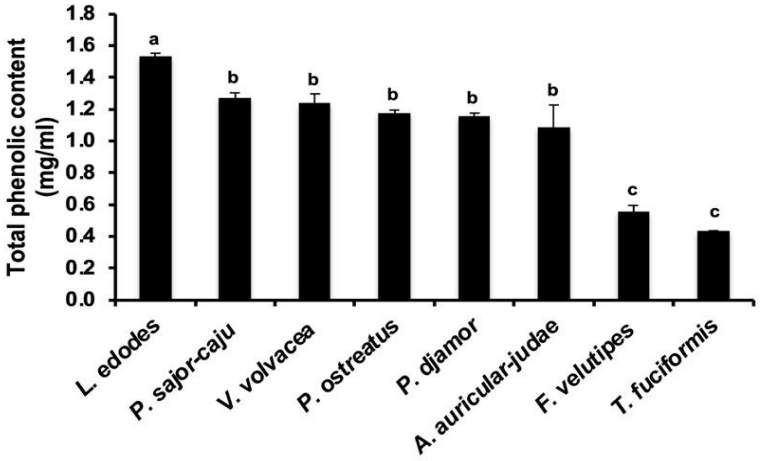

Figure 1. Total phenolic content of eight edible mushroom extracts using Folin-Ciocalteu reagent. Values presented are mean ± SEM derived from three independent experiments. Bars with different letters (a, b, c) indicate statistically significant differences from each other ($P < 0.05$).

Cheung et al. [14] compared the total phenolic content of two edible mushrooms (*L. edodes* and *V. volvacea),* which were extracted by four extractants (petroleum ether, ethyl acetate, methanol, and distilled water). They found that both *L. edodes* and *V. volvacea* had similar maximum total phenolic content when using ethyl acetate (0.10 mg GAEs/mg of extract for *L. edodes* and 0.09 mg GAEs/mg of extract for *V. volvacea*) and water (0.08 mg GAEs/mg of extract for *L. edodes* and 0.10 mg GAEs/mg of extract for *V. volvacea*) as an extractant, respectively. Their results were consistent with our results, which showed comparable total phenolic content in *L. edodes* and *V. volvacea*.

Boonsong et al. [13] investigated the total phenolic content of five edible mushrooms in Thailand (*L. edodes, V. volvacea, P. eous, P. sajor-caju, and A. auricular-judae),* which were extracted using three different solvents (ethanol, diethyl ether, and distilled water). The highest total phenolic content was found in the condition using distilled water as an extractant. In addition, *L. edodes* had the highest total phenolic content in all extractants, followed by *V. volvacea, P. eous, P. sajor-caju, and A. auricular-judae*, respectively. Their results corresponded with our findings, which indicated that the highest total phenolic content was observed in *L. edodes*, and the ranking of total phenolic content in other mushrooms was similar.

3.2 Antioxidant activity of edible mushroom extracts

Since the association between total phenolic content and antioxidant activity was reported in much research [7, 10–12, 41], the antioxidant activity of eight edible mushroom extracts was investigated in this study by DPPH radical scavenging assay. As shown in Figure 2, all mushroom extracts demonstrated a dose-dependent increase in antioxidant activity. When the EC_{50} values of all mushroom extracts were compared, the data are shown in Figure 3 and Table 1. *P. ostreatus*, *L. edodes*, *A. auricular-judae*, *P. djamor*, *P. sajor-caju*, and *V. volvacea* exhibited high antioxidant activity, indicated by their low EC_{50} values. *F. velutipes* displayed the lowest antioxidant activity, indicated by the highest EC_{50} value, followed by *T. fuciformis*.

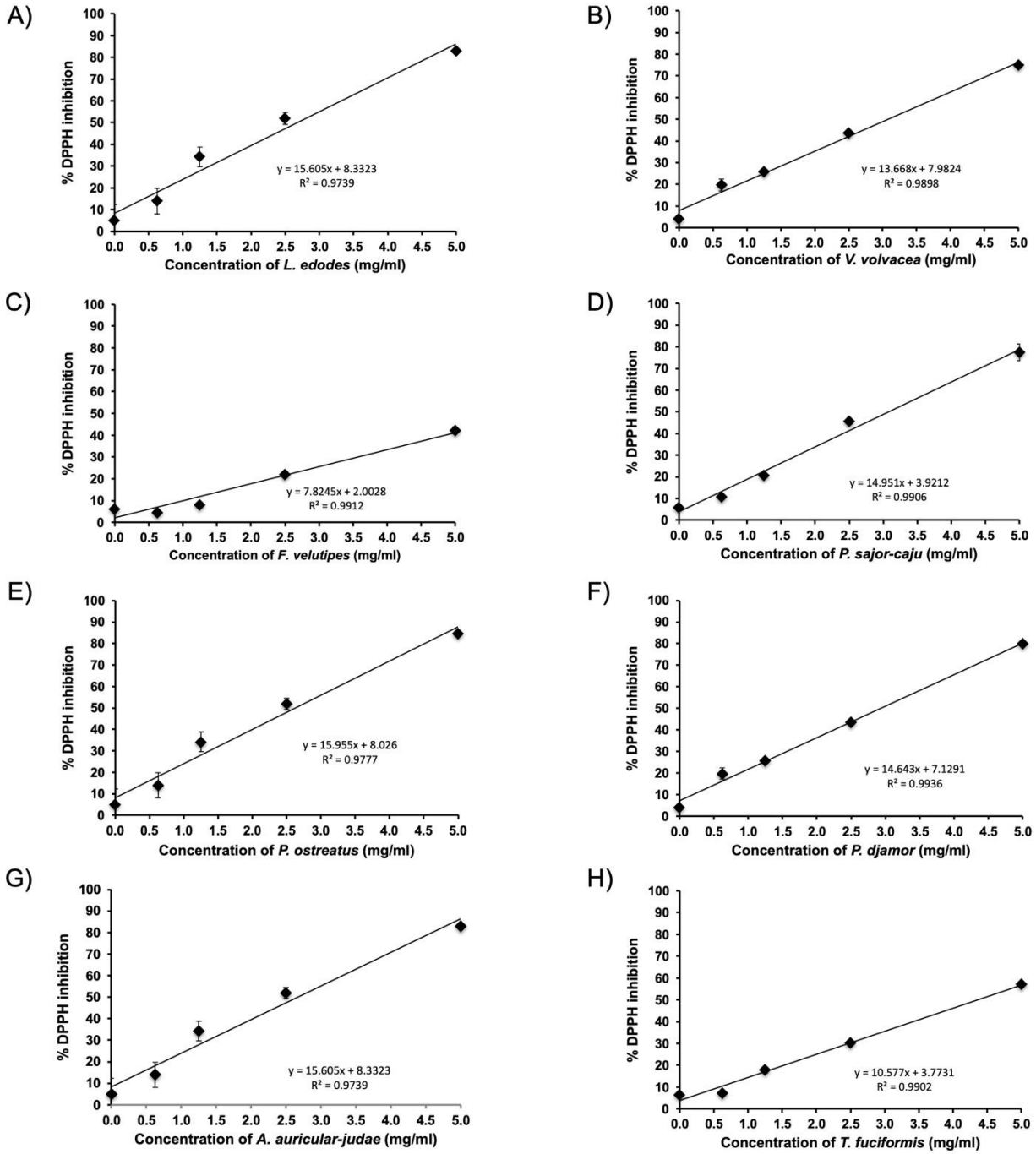

Figure 2. Percentage of DPPH inhibition of eight mushroom extracts by DPPH assay. *L. edodes* (A), *V. volvacea (B),* F. *velutipes* (C), *P. sajor-caju* (D), *P. ostreatus* (E), *P. djamor* (F), *A. auricular-judae* (G), and *T. fuciformis* (H). Values presented are mean ± SE derived from three independent experiments.

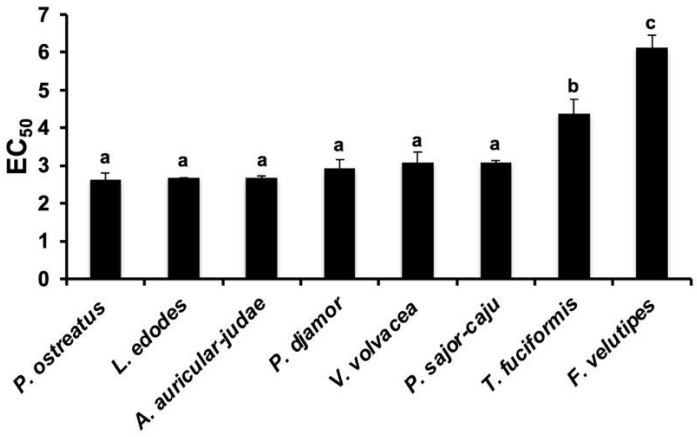

Figure 3. Half maximal effective concentration (EC_{50}) of eight mushroom extracts. These data were obtained from Figure 2, which shows the concentration of each mushroom extract required for 50% DPPH inhibition. Values presented are mean ± SEM derived from three independent experiments. Bars with different letters (a, b, c) indicate statistically significant differences from each other ($P < 0.05$).

Table 1. Comparison of IC_{50}, EC_{50}, and total phenolic content of eight mushroom extracts.

Mushroom extracted	IC_{50} (mg/mL)	EC_{50} (mg/mL)	Total phenolic content (mg/mL)
A. auricular-judae	0.15 ± 0.03^{a}	2.67 ± 0.05^{a}	1.08 ± 0.12^{b}
F. velutipes	0.94 ± 0.07^{c}	6.13 ± 0.38^{c}	0.56 ± 0.06^{c}
L. edodes	1.04 ± 0.08^{c}	2.67 ± 0.01^{a}	1.53 ± 0.05^{a}
P. djamor	0.20 ± 0.02^{a}	2.93 ± 0.22^{a}	1.15 ± 0.06^{b}
P. ostreatus	0.11 ± 0.01^{a}	2.63 ± 0.18^{a}	1.17 ± 0.12^{b}
P. sajor-caju	0.26 ± 0.02^{a}	3.07 ± 0.06^{a}	1.24 ± 0.11^{b}
T. fuciformis	0.49 ± 0.06^{b}	4.37 ± 0.33^{b}	0.43 ± 0.04^{c}
V. volvacea	0.53 ± 0.03^{b}	3.08 ± 0.29^{a}	1.27 ± 0.04^{b}

Data were expressed as mean ± SEM.
Means with different letters (a, b, c) within a column of each group are statistically significant differences from each other ($P<0.05$).

Our findings align with those of Hussein et al. [42], who reported that *A. auricular-judae* extracted using methanol demonstrated the highest antioxidant activity (EC_{50} = 0.08 mg/mL) among seven wild edible mushrooms (*Polyporus tenuiculus, L. sajor-caju* W, *L. squarrosulus, Macrolepiota procera, Panus conchatus, A. auricular-judae,* and *L. sajor-caju D*). Oke & Aslim [43] also displayed that *A. auricular-judae* extracted using distilled water (EC_{50} = 0.309 mg/mL) exhibited greater antioxidant activity compared to *P. eryngii* (EC_{50} = 0.545 mg/mL). lkay Koca & Gençcelep [44] conducted a study on the antioxidant activity of 24 wild edible mushrooms, including *P. ostreatus*, which is also utilized in our experiment. The EC_{50} values of the same mushroom reported by various research groups exhibit inconsistency. The observed variation may be attributed to the differing extraction methods and extractants utilized in the experiment [13,14]. Furthermore, it has been noted that the substrate utilized for mushroom cultivation and the maturation stages of fruiting bodies may affect the antioxidant content in mushrooms, potentially resulting in variations in antioxidant activity among the same mushroom across different studies [42].

Boonsong et al. [13] studied the antioxidant activity of five edible mushrooms in Thailand (*L. edodes*, *V. volvacea*, *P. sajor-caju*, *A. auricular-judae*, and *P. eous*) using three different extractants (ethanol, diethyl ether, and distilled water). The findings indicated that ethanol served as the most effective extractant, with *L. edodes* exhibiting the highest antioxidant activity, followed by *V. volvacea*, *P. eous*, *P. sajor-caju*, and *A. auricular-judae*, in that order. The findings contrast with our study, which indicated that *L. edodes* and *A. auricular-judae* extracted with ethanol exhibited comparable antioxidant activity. Despite the application of the same

extractant, this inconsistency may be due to differences in the extraction method and other factors, as mentioned earlier. Turning now to the comparison of antioxidant activity and total phenolic content, antioxidant activity was observed to increase with total phenolic content in this study. A group of mushrooms that had high total phenolic content exhibited high antioxidant activity. For instance, *L. edodes* and *P. ostreatus,* classified within the group with the highest total phenolic content, exhibited significant antioxidant activity. In contrast, *T. fuciformis* and *F. velutipes,* placed in the low total phenolic content group, displayed low antioxidant activity, as expected. Thus, it can be summarized that there is a positive relationship between total phenolic content and antioxidant activity. This finding is consistent with the results of Boonsong et al. [13], Cheung et al. [14], Heleno et al. [45], and Hussein et al. [42], who reported that the antioxidant activity of mushrooms is positively correlated with their phenolic compound content.

3.3 Anticancer activity of edible mushroom extracts on HT-29 cells

To assess the anticancer effect of mushroom extracts on colon cancer cells, six concentrations of a two-fold serial dilution of edible mushroom extracts (5 to 0.156 mg/mL) were incubated with HT-29 cells for 48 h, and the MTT assay was used to assess cell viability. The results, as illustrated in Figure 4, indicated that all mushroom extracts enhanced the anticancer effect in a dose-dependent manner. Upon comparing the IC_{50} values across all mushroom extracts, it was evident that these extracts could be classified into three groups (Figure 5). The first group demonstrated a significant anticancer effect, characterized by low IC_{50} values: *P. ostreatus* (0.11 mg/mL), *A. auricular-judae* (0.15 mg/mL), *P. djamor* (0.20 mg/mL), and *P.* sajor-*caju* (0.26 mg/mL). The second group, exhibiting a moderate anticancer effect, consisted of *T. fuciformis* (0.49 mg/mL) and *V. volvacea* (0.53 mg/mL). The third group, demonstrating a low anticancer effect, included *F. velutipes* (0.94 mg/mL) and *L. L. edodes* (1.038 mg/mL). The results suggest that the observed impact may be attributed to the elevated levels of total phenolic content and antioxidant activity present in these mushroom extracts (Table 1).

Interestingly, *A. auricular-judae*, an under-researched species, exhibited a more potent anticancer effect than the more extensively studied mushrooms, such as *L. edodes*. While *L. edodes* exhibited high total phenolic content and antioxidant activity, it demonstrated low anticancer activity. Similarly, Elhusseiny et al. [46] indicated that aqueous extracts of *L. edodes* exhibited significant antioxidant activity while displaying only moderate cytotoxicity against various cancer cell lines. However, this discrepancy may be attributed to several factors. First, although phenolic compounds are well known for their antioxidant properties through free radical scavenging, not all phenolic constituents exhibit direct cytotoxic effects on cancer cells. The type of phenolic compounds present in *L. edodes* may contribute more to antioxidant activity than to mechanisms associated with antiproliferation of cancer cells, such as apoptosis induction or cell cycle arrest. Nam et al. [47] highlighted that phenolic compounds contribute significantly to the antioxidant activity in L. edodes, but their anticancer activity is context-dependent and influenced by the type of compound and cellular targets. Roszczenko et al. [48] indicated that while antioxidants, such as phenolics, protect against oxidative stress, anticancer effects require mechanisms like apoptotic induction or cell-cycle arrest, which are not generally provided by all phenolics. Second, the cancer cell line used in this study may not be sensitive to the specific bioactive compounds in *L. edodes*, highlighting the importance of cell-type specificity in anticancer evaluations. Silva et al. [49] reported that elevated levels of phenolic content and antioxidant activity exhibit significant potential for cancer prevention; however, the response is determined by the specific type of phenolic and the type of cancer cells involved. This result suggests that high phenolic content and antioxidant activity do not necessarily translate to strong anticancer properties, particularly if the compounds do not induce apoptosis or inhibit cell proliferation.

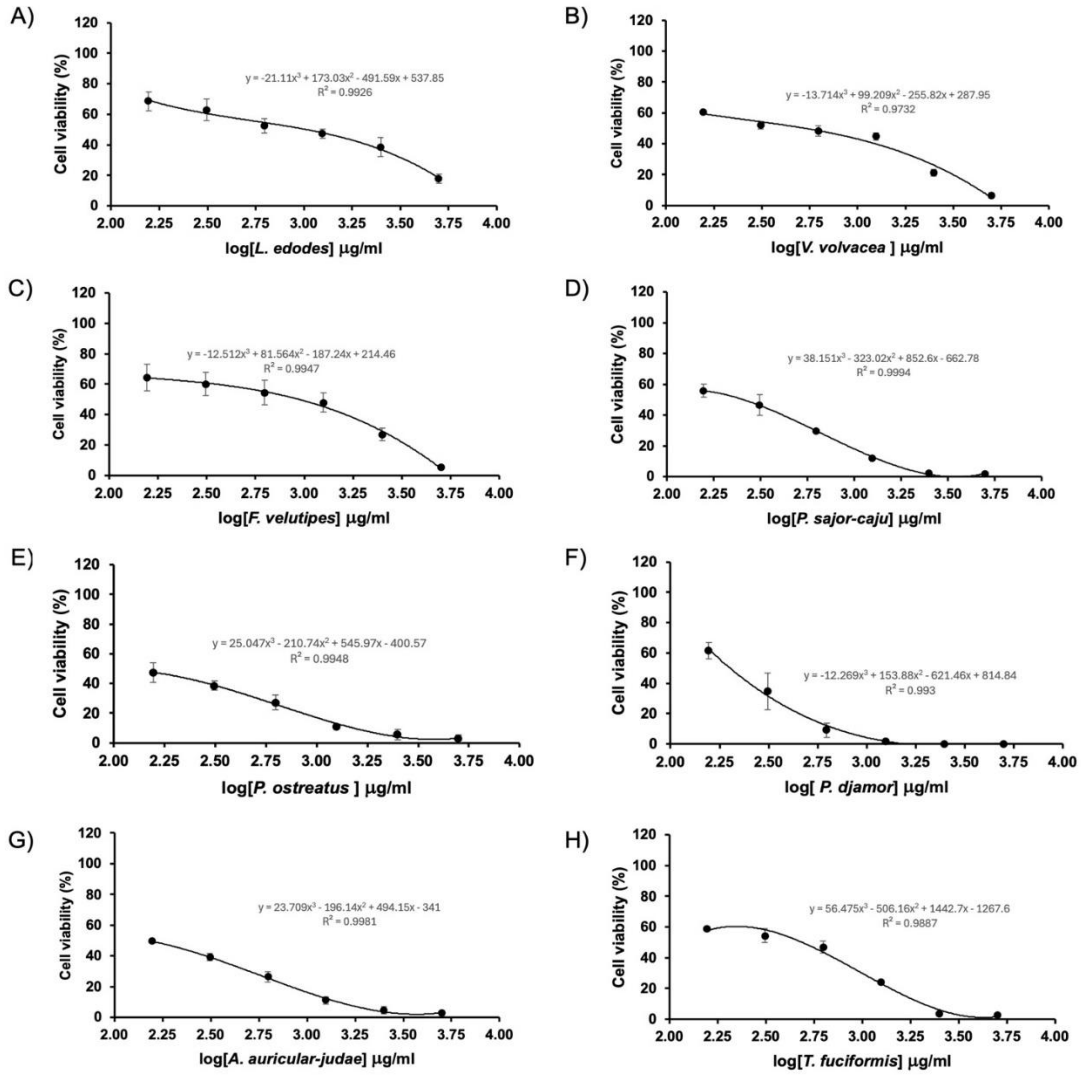

Figure 4. Cell viability of HT-29 cells toward eight mushroom extracts. Varying concentrations of eight mushroom extracts were tested with HT-29 cells by using the MTT assay. *L. edodes* (A), *V. volvacea* (B), *F. velutipes* (C), *P. sajor-caju* (D), *P. ostreatus* (E), *P. djamor* (F), *A. auricular-judae* (G), and *T. fuciformis* (H). Values presented are mean ± SEM derived from three independent experiments.

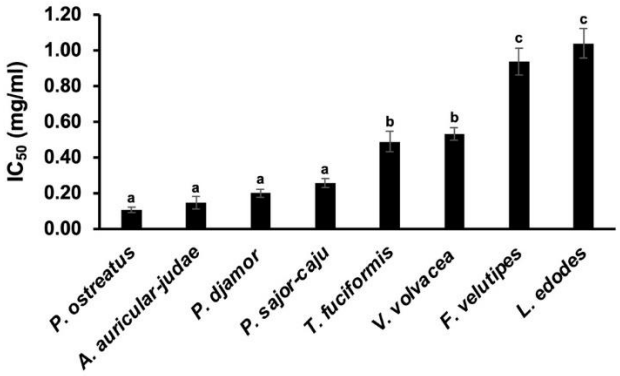

Figure 5. Half maximal inhibitory concentration (IC_{50}) of eight mushroom extracts. These data were obtained from Figure 4, which was the concentration of each mushroom extract at 50% viability of HT-29 cells. Values presented are mean ± SEM derived from three independent experiments. Bars with different letters (a, b, c) indicate statistically significant differences from each other ($P < 0.05$).

To date, edible mushrooms have demonstrated potential anticancer properties in various studies; however, specific research on their effects on colon cancer cells is limited. The extracts of *L. edodes* demonstrated minimal impact on the proliferation of HT-29 cells, in contrast to *P. ostreatus*, which notably inhibited their growth [50]. The dichloromethane extract of *A. auricular-judae* showed potent antitumor effects against HT-29 cells, with an IC_{50} of 0.73 mg/mL [51]. An aqueous extraction of *P. ostreatus* was shown to inhibit cell proliferation in COLO-205 colon cancer cells with an IC_{50} of 0.812 mg/mL [52]. Compounds isolated from *P. djamor*, such as ergosta-5,7,22-trien-3β-ol, have shown significant cytotoxic effects against HT-29 cells [53]. Lectins extracted from *P. ostreatus* exhibited anticancer activity toward HT-29 cells with an IC_{50} of 0.27 mg/mL [54]. Lentinan from *L. edodes* demonstrated significant anticancer effects on HT-29 cells by inhibiting cell proliferation, reducing migration, and inducing cell death [55]. The ethanol extract of *V. volvacea*, when combined with cetuximab, significantly reduced cell viability in HT-29 cells [56].

3.4 HPLC Analysis of phenolic compounds in mushroom extracts

Phenolic compounds have been reported to exhibit antioxidant and anticancer activities. Thus, in this experiment, we analyzed the quantities of three specific phenolic compounds (gallic acid, tannic acid, and caffeic acid) using HPLC techniques to evaluate the relationship between bioactive substances in edible mushrooms and their antioxidant activity, as well as their effect on inhibiting the growth of HT-29 cells. The results are shown in Table 2. Gallic acid was present in the minimum quantity among the phenolic components detected in the edible mushroom extracts. *L. edodes* exhibited the highest concentration of gallic acid (0.118 mg/mL), which contains more gallic acid than other types of mushrooms by more than three times, whereas *P. ostreatus* showed no detectable levels of gallic acid. The mushrooms with the highest concentration of tannic acid were *P. sajor-caju* at 11.69 mg/mL, followed by *F. velutipes* at 6.94 mg/mL, *A. auricular-judae* at 4.19 mg/mL, and *V. volvacea* at 3.27 mg/mL, while *L. edodes* showed no detectable levels of tannic acid. *A. auricular-judae* possessed the most excellent content of caffeic acid (335.32 mg/mL), which demonstrated a significantly higher concentration of caffeic acid relative to other mushroom extracts. This aligns with the findings of Oke & Aslim [43], who reported that *A. auricular-judae* exhibited significantly higher concentrations of caffeic acid compared to other mushrooms. Palacios et al. [57] discovered that *P. ostreatus* contained the highest concentration of gallic acid when compared to other mushrooms, while no caffeic acid was detected. This contrasts with our finding, in which gallic acid was not detected; however, a small amount of caffeic acid was detected in *P. ostreatus*. The concentration of phenolic compounds in mushrooms can fluctuate based on various factors, including the mushroom species, cultivation nutrients, growing conditions, the growth stage of the mushrooms, and the age of the fresh samples [58,59].

Table 2. HPLC analyzed the quantity of phenolic compounds in eight mushroom extracts.

Samples	Phenolic compounds (mg/mL)		
	Gallic acid	**Tannic acid**	**Caffeic acid**
A. auricular Judae	0.02 ± 0.002^{c}	4.19 ± 0.65^{c}	335.32 ± 94.45^{a}
F. velutipes	0.01 ± 0.001^{d}	6.94 ± 0.77^{b}	1.00 ± 0.01^{b}
L. edodes	0.12 ± 0.003^{a}	0.00^{f}	1.98 ± 0.13^{b}
P. djamor	0.03 ± 0.002^{b}	0.79 ± 0.05^{e}	2.65 ± 0.13^{b}
P. ostreatus	0.00^{e}	1.05 ± 0.11^{e}	1.07 ± 0.01^{b}
P. sajor-caju	0.02 ± 0.00^{c}	11.69 ± 0.15^{a}	1.20 ± 0.08^{b}
T. fuciformis	0.02 ± 0.003^{c}	0.97 ± 0.04^{e}	1.05 ± 0.04^{b}
V. volvacea	0.01 ± 0.002^{d}	3.27 ± 0.19^{d}	6.06 ± 0.43^{b}

Data were expressed as mean ± SEM.
Means with different letters (a, b, c, d, e, f) within a column of each group are statistically significant differences from each other ($P<0.05$).

Interestingly, no clear relationship was observed between the concentrations of gallic acid, tannic acid, and caffeic acid and the anticancer activity of the mushroom extracts against HT-29 cells. For instance, *L. edodes*, which exhibited the lowest anticancer activity, contained the highest amount of gallic acid among the eight

mushroom extracts. In contrast, *P. ostreatus*, *A. auricular-judae*, *P. djamor*, and *P. sajor-caju*, which demonstrated strong antiproliferative effects, had very low gallic acid levels. Additionally, when considering the amount of tannic acid, it was found that F. *velutipes*, which belongs to the low anticancer activity group, has a higher amount of tannic acid than other mushrooms in the high anticancer activity group, except for *P. sajor-caju*. Furthermore, *A. auricular-judae*, categorized among the group exhibiting elevated anticancer activity, contained the highest concentration of caffeic acid, whereas other mushrooms in this group possessed markedly lower levels of caffeic acid. These findings suggest that phenolic acid content alone is not a determining factor for anticancer activity in these mushroom extracts. Other bioactive components, such as polysaccharides, terpenoids, or synergistic interactions among various compounds, may contribute more significantly to the observed biological effects. This result is consistent with previous studies in other plants, which reported that the presence of phenolic acids does not always directly translate to high anticancer activity [60–63]**.**

4. Conclusions

This study evaluated total phenolic content, antioxidant properties, and the anticancer activity of eight edible mushroom extracts. According to their cytotoxic effects against HT-29 cells, the mushrooms could be classified into three groups. The first group, exhibiting pronounced anticancer activity, included *P. ostreatus*, *A. auricular-judae*, *P. djamor*, and *P. sajor-caju*. The second group, demonstrating moderate anticancer effect, comprised *T. fuciformis* and *V. volvacea*. The third group, showing a low anticancer effect, included *F. velutipes* and *L. edodes*. A positive relationship was generally observed between total phenolic content, antioxidant activity, and anticancer efficacy, supporting the role of phenolic compounds in mediating bioactivity. It is worth noting that *L. edodes* presented an exception to this trend, as it exhibited high total phenolic content and antioxidant activity but low anticancer activity. It can be suggested that while phenolic compounds and antioxidant potential may contribute to anticancer effects, other factors or bioactive compounds are likely involved in mediating the anticancer effects. Moreover, not all phenolic constituents exhibit direct antiproliferative effects on cancer cells. These findings suggest that edible mushrooms could serve as promising natural sources of antioxidants and anticancer agents. The results may support future development of mushroom-derived nutraceuticals for colon cancer prevention. Further research is required to identify the bioactive compounds and unravel the molecular mechanisms, such as apoptosis or cell cycle arrest, that contribute to their anticancer effects. Specifically, further studies should focus on identifying the specific compounds or mechanisms unique to *L. edodes* to better understand why it exhibits potent antioxidant but weak anticancer activity. A statistical correlation analysis would also be necessary in the future to confirm the relationship between phenolic content and biological activities. Moreover, it would be beneficial to evaluate the activity of these extracts against various cancer cell lines, as well as non-cancerous normal cell lines, to assess their selectivity and toxicity. Future *in vivo* studies are also needed to verify the anticancer effects of the extracts in an animal model.

5. Acknowledgements

The authors would like to thank Dr. Sithiruk Roytrakul from the National Center for Genetic Engineering and Biotechnology (BIOTEC), NSTDA, for generously supplying the HT-29 cell line used in this research. The financial support provided by the Research and Development Institute of Ramkhamhaeng University is gratefully appreciated.

Author Contributions: Conceptualization: C. P. and T. S.; resources: C. P. and T. S.; formal analysis: C.P.; investigation: C.P.; visualization: C.P.; validation: C. P. and T.S.; writing – original draft: C.P.; writing – review & editing: C.P. and T.S.; supervision: T.S.; project administration: C.P.; funding acquisition: C.P. All authors have read and agreed to the published version of the manuscript.

Funding: This research was funded by the Research and Development Institute of Ramkhamhaeng University.

Conflicts of Interest: The authors declare no conflict of interest. The funders had no role in the study's design, data collection, analysis, or interpretation, nor in the writing of the manuscript or the decision to publish the results.

References

[1] Kozarski, M.; Klaus, A.; Jakovljevic, D.; Todorovic, N.; Vunduk, J.; Petrović, P.; Niksic, M.; Vrvic, M. M.; Van Griensven, L. Antioxidants of Edible Mushrooms. *Molecules* **2015**, *20*(10), 19489. https://doi.org/10.3390/molecules201019489

[2] Wasser, S. Medicinal Mushrooms as a Source of Antitumor and Immunomodulating Polysaccharides. *Appl. Microbiol. Biotechnol.* **2002**, *60*(1–2), 10–23. https://doi.org/10.1007/s00253-002-1076-7

[3] Ferreira, I. C. F. R.; Barros, L.; Abreu, R. M. V. Antioxidants in Wild Mushrooms. *Curr. Med. Chem.* **2009**, *16*(12), 1543–1565. https://doi.org/10.2174/092986709787909587

[4] Valverde, M. E.; Hernández-Pérez, T.; Paredes-López, O. Edible Mushrooms: Improving Human Health and Promoting Quality Life. *Int. J. Microbiol.* **2015**, *2015*, 376387. https://doi.org/10.1155/2015/376387

[5] Wasser, S. P. Medicinal Mushroom Science: Current Perspectives, Advances, Evidences, and Challenges. *Biomed. J.* **2014**, *37*(6), 345–356. https://doi.org/10.4103/2319-4170.138318

[6] Roupas, P.; Keogh, J.; Noakes, M.; Margetts, C.; Taylor, P. The Role of Edible Mushrooms in Health: Evaluation of the Evidence. *J. Funct. Foods* **2012**, *4*(4), 689–702. https://doi.org/10.1016/j.jff.2012.05.003

[7] Boonsong, S.; Klaypradit, W.; Wilaipun, P. Antioxidant Activities of Extracts from Five Edible Mushrooms Using Different Extractants. *Agric. Nat. Resour.* **2016**, *50*(2), 89–93. https://doi.org/10.1016/j.anres.2015.07.002

[8] Hirasawa, M.; Shouji, N.; Neta, T.; Fukushima, K.; Takada, K. Three Kinds of Antibacterial Substances from *Lentinus Edodes* (Berk.) Sing. (Shiitake, an Edible Mushroom). *Int. J. Antimicrob. Agents* **1999**, *11*(2), 151–157. https://doi.org/10.1016/S0924-8579(98)00084-3

[9] Jeong, S. C.; Jeong, Y. T.; Yang, B. K.; Islam, R.; Koyyalamudi, S. R.; Pang, G.; Cho, K. Y.; Song, C. H. White Button Mushroom (*Agaricus Bisporus*) Lowers Blood Glucose and Cholesterol Levels in Diabetic and Hypercholesterolemic Rats. *Nutr. Res.* **2010**, *30*(1), 49–56. https://doi.org/10.1016/j.nutres.2009.12.003

[10] Mau, J. L.; Chao, G. R.; Wu, K. T. Antioxidant Properties of Methanolic Extracts from Several Ear Mushrooms. *J. Agric. Food Chem.* **2001**, *49*(11), 5461–5467. https://doi.org/10.1021/jf010637h

[11] Moradali, M. F.; Mostafavi, H.; Ghods, S.; Hedjaroude, G. A. Immunomodulating and Anticancer Agents in the Realm of Macromycetes Fungi (Macrofungi). *Int. Immunopharmacol.* **2007**, *7*(6), 701–724. https://doi.org/10.1016/j.intimp.2007.01.008

[12] Ren, L.; Perera, C.; Hemar, Y. Antitumor Activity of Mushroom Polysaccharides: A Review. *Food Funct.* **2012**, *3*(5), 473–490. https://doi.org/10.1039/c2fo10279j

[13] Boonsong, S.; Klaypradit, W.; Wilaipun, P. Antioxidant Activities of Extracts from Five Edible Mushrooms Using Different Extractants. *Agric. Nat. Resour.* **2016**, *50*(2), 89–93. https://doi.org/10.1016/j.anres.2015.07.002

[14] Cheung, L. M.; Cheung, P. C. K.; Ooi, V. E. C. Antioxidant Activity and Total Phenolics of Edible Mushroom Extracts. *Food Chem.* **2003**, *81* (2), 249–255. https://doi.org/10.1016/S0308-8146(02)00419-3

[15] Mwangi, R. W.; Macharia, J. M.; Wagara, I. N.; Bence, R. L. The Antioxidant Potential of Different Edible and Medicinal Mushrooms. *Biomed. Pharmacother.* **2022**, *154*, 112621. https://doi.org/10.1016/j.biopha.2022.112621

[16] Puttaraju, N. G.; Venkateshaiah, S. U.; Dharmesh, S. M.; Urs, S. M. N.; Somasundaram, R. Antioxidant Activity of Indigenous Edible Mushrooms. *J. Agric. Food Chem.* **2006**, *54*(26), 9764–9772. https://doi.org/10.1021/jf0615707

[17] Abdelshafy, A. M.; Belwal, T.; Liang, Z.; Wang, L.; Li, D.; Luo, Z.; Li, L. A Comprehensive Review on Phenolic Compounds from Edible Mushrooms: Occurrence, Biological Activity, Application and Future Prospective. *Crit. Rev. Food Sci. Nutr.* **2022**, *62*(7), 1775–1799. https://doi.org/10.1080/10408398.2021.1898335

[18] Becker, E. M.; Nissen, L. R.; Skibsted, L. H. Antioxidant Evaluation Protocols: Food Quality or Health Effects. *Eur. Food Res. Technol.* **2004**, *219* (1), 2–11. https://doi.org/10.1007/s00217-004-1012-4

[19] Li, X.; Wu, Q.; Xie, Y.; Ding, Y.; Du, W. W.; Sdiri, M.; Yang, B. B. Ergosterol Purified from Medicinal Mushroom *Amauroderma Rude* Inhibits Cancer Growth in Vitro and in Vivo by Up-Regulating Multiple Tumor Suppressors. *Oncotarget* **2015**, *6* (19), 17208–17223. https://doi.org/10.18632/oncotarget.4026

[20] Deng, G.; Lin, H.; Seidman, A.; Fornier, M.; D'Andrea, G.; Wesa, K.; Yeung, S.; Cunningham-Rundles, S.; Vickers, A. J.; Cassileth, B. A Phase I/II Trial of a Polysaccharide Extract from *Grifola Frondosa*

(Maitake Mushroom) in Breast Cancer Patients: Immunological Effects. *J. Cancer Res. Clin. Oncol.* **2009**, *135* (9), 1215–1221. https://doi.org/10.1007/s00432-009-0562-z

[21] Elbatrawy, E. N.; Ghonimy, E. A. A.; Alassar, M. M.; Wu, F. S. Medicinal Mushroom Extracts Possess Differential Antioxidant Activity and Cytotoxicity to Cancer Cells. *Int. J. Med. Mushrooms* **2015**, *17*(5), 449–455. https://doi.org/10.1615/IntJMedMushrooms.v17.i5.70

[22] Fang, N.; Li, Q.; Yu, S.; Zhang, J.; He, L.; Ronis, M. J. J.; Badger, T. M. Inhibition of Growth and Induction of Apoptosis in Human Cancer Cell Lines by an Ethyl Acetate Fraction from Shiitake Mushrooms. *J. Altern. Complement. Med.* **2006**, *12*(2), 125–132. https://doi.org/10.1089/acm.2006.12.125

[23] Hu, H.; Ahn, N. S.; Yang, X.; Lee, Y. S.; Kang, K. S. *Ganoderma Lucidum* Extract Induces Cell Cycle Arrest and Apoptosis in MCF-7 Human Breast Cancer Cell. *Int. J. Cancer* **2002**, *102*(3), 250–253. https://doi.org/10.1002/ijc.10707

[24] Israilides, C.; Kletsas, D.; Arapoglou, D.; Philippoussis, A.; Pratsinis, H.; Ebringerová, A.; Hříbalová, V.; Harding, S. E. In Vitro Cytostatic and Immunomodulatory Properties of the Medicinal Mushroom *Lentinula Edodes*. *Phytomedicine* **2008**, *15*(6–7), 512–519. https://doi.org/10.1016/j.phymed.2007.11.029

[25] Jiang, J.; Sliva, D. Novel Medicinal Mushroom Blend Suppresses Growth and Invasiveness of Human Breast Cancer Cells. *Int. J. Oncol.* **2010**, *37*(6), 1529–1536. https://doi.org/10.3892/ijo-00000806

[26] Li, X.; Wu, Q.; Xie, Y.; Ding, Y.; Du, W. W.; Sdiri, M.; Yang, B. B. Ergosterol Purified from Medicinal Mushroom *Amauroderma Rude* Inhibits Cancer Growth in Vitro and in Vivo by Up-Regulating Multiple Tumor Suppressors. *Oncotarget* **2015**, *6*(19), 17208–17223. https://doi.org/10.18632/oncotarget.4026

[27] Shin, A.; Kim, J.; Lim, S. Y.; Kim, G.; Sung, M. K.; Lee, E. S.; Ro, J. Dietary Mushroom Intake and the Risk of Breast Cancer Based on Hormone Receptor Status. *Nutr. Cancer* **2010**, *62*(4), 476–483. https://doi.org/10.1080/01635580903441212

[28] Soares, R.; Meireles, M.; Rocha, A.; Pirraco, A.; Obiol, D.; Alonso, E.; Joos, G.; Balogh, G. Maitake (D Fraction) Mushroom Extract Induces Apoptosis in Breast Cancer Cells by BAK-1 Gene Activation. *J. Med. Food* **2011**, *14*(6), 563–572. https://doi.org/10.1089/jmf.2010.0095

[29] Xue, Z.; Li, J.; Cheng, A.; Yu, W.; Zhang, Z.; Kou, X.; Zhou, F. Structure Identification of Triterpene from the Mushroom *Pleurotus Eryngii* with Inhibitory Effects Against Breast Cancer. *Plant Foods Hum. Nutr.* **2015**, *70*(3), 324–328. https://doi.org/10.1007/s11130-015-0492-7

[30] Min, Z.; Jian, H.; Xing, X.; Holman, C. D. A. J. Dietary Intakes of Mushrooms and Green Tea Combine to Reduce the Risk of Breast Cancer in Chinese Women. *Int. J. Cancer* **2009**, *124*(6), 1435–1439. https://doi.org/10.1002/ijc.24047

[31] Durgo, K.; Koncar, M.; Komes, D.; Belscak-Cvitanovic, A.; Franekic, J.; Jakopovich, I.; Jakopovich, N.; Jakopovich, B. Cytotoxicity of Blended versus Single Medicinal Mushroom Extracts on Human Cancer Cell Lines: Contribution of Polyphenol and Polysaccharide Content. *Int. J. Med. Mushrooms* **2013**, *15*(5), 459–472. https://doi.org/10.1615/IntJMedMushr.v15.i5.20

[32] Lee, H. S.; Kim, E. J.; Kim, S. H. Ethanol Extract of *Innotus Obliquus* (Chaga Mushroom) Induces G1 Cell Cycle Arrest in HT-29 Human Colon Cancer Cells. *Nutr. Res. Pract.* **2015**, *9*(2), 111–115. https://doi.org/10.4162/nrp.2015.9.2.111

[33] Šeklić, D. S.; Stanković, M. S.; Milutinović, M. G.; Topuzović, M. D.; Štajn, A.; Marković, S. D. Cytotoxic, Antimigratory, pro-and Antioxidative Activities of Extracts from Medicinal Mushrooms on Colon Cancer Cell Lines. *Arch. Biol. Sci.* **2016**, *68* (1), 131–141. https://doi.org/10.2298/ABS150427131S

[34] Yoshikawa, R.; Yanagi, H.; Hashimoto-Tamaoki, T.; Morinaga, T.; Nakano, Y.; Noda, M.; Fujiwara, Y.; Okamura, H.; Yamamura, T. Gene Expression in Response to Anti-Tumour Intervention by Polysaccharide-K (PSK) in Colorectal Carcinoma Cells. *Oncol. Rep.* **2004**, *12*(6), 1287–1292. https://doi.org/10.3892/or.12.6.1287

[35] Hall, I. R.; Buchanan, P. K.; Stephenson, S. L.; Yun, W. *Edible and Poisonous Mushrooms of the World*; Timber Press: Portland, OR, USA, **2022**.

[36] Sawangwan, T.; Wansanit, W.; Pattani, L.; Noysang, C. Study of Prebiotic Properties from Edible Mushroom Extraction. *Agric. Nat. Resour.* **2018**, *52*(6), 572–578. https://doi.org/10.1016/j.anres.2018.11.020

[37] Seephonkai, P.; Samchai, S.; Thongsom, A.; Sunaart, S.; Kiemsanmuang, B.; Chakuton, K. DPPH Radical Scavenging Activity and Total Phenolics of Phellinus Mushroom Extracts Collected from Northeast of Thailand. *Chin. J. Nat. Med.* **2011**, *9*(6), 441–446. https://doi.org/10.3724/SP.J.1009.2011.00441

[38] Loypimai, P.; Moonggarm, A.; Chottanom, P. Effects of Ohmic Heating on Lipase Activity, Bioactive Compounds and Antioxidant Activity of Rice Bran. *Aust. J. Basic Appl. Sci.* **2009**, *3*(4), 3824–3831.

[39] Mradu, G.; Saumyakanti, S.; Sohini, M.; Arup, M. HPLC Profiles of Standard Phenolic Compounds Present in Medicinal Plants. *Int. J. Pharmacogn. Phytochem. Res.* **2012**, *4*(3), 114–119.

[40] Yoon, K. N.; Alam, N.; Lee, K. R.; Shin, P. G.; Cheong, J. C.; Yoo, Y. B.; Lee, T. S. Antioxidant and Antityrosinase Activities of Various Extracts from the Fruiting Bodies of *Lentinus Lepideus*. *Molecules* **2011**, *16*(3), 2334–2347. https://doi.org/10.3390/molecules16032334

[41] Becker, E. M.; Nissen, L. R.; Skibsted, L. H. Antioxidant Evaluation Protocols: Food Quality or Health Effects. *Eur. Food Res. Technol.* **2004**, *219*(1), 2–11. https://doi.org/10.1007/s00217-004-1012-4

[42] Hussein, J. M.; Tibuhwa, D. D.; Mshandete, A. M.; Kivaisi, A. K. Antioxidant Properties of Seven Wild Edible Mushrooms from Tanzania. *Afr. J. Food Sci.* **2015**, *9*(9), 488–493. https://doi.org/10.5897/ajfs2015.1328

[43] Oke, F.; Aslim, B. Protective Effect of Two Edible Mushrooms against Oxidative Cell Damage and Their Phenolic Composition. *Food Chem.* **2011**, *128* (3), 675–680. https://doi.org/10.1016/j.foodchem.2011.03.036

[44] lkay Koca, A. K. İ.; Gençcelep, H. Antioxidant Properties of Wild Edible Mushrooms. *J. Food Process Technol.* **2011**, *02*(06). https://doi.org/10.4172/2157-7110.1000130

[45] Heleno, S. A.; Ferreira, R. C.; Antonio, A. L.; Queiroz, M. J. R. P.; Barros, L.; Ferreira, I. C. F. R. Nutritional Value, Bioactive Compounds and Antioxidant Properties of Three Edible Mushrooms from Poland. *Food Biosci.* **2015**, *11*, 135–141. https://doi.org/10.1016/j.fbio.2015.04.006

[46] Elhusseiny, S. M.; El-Mahdy, T. S.; Awad, M. F.; Elleboudy, N. S.; Farag, M. M. S.; Yassein, M. A.; Aboshanab, K. M. Proteome Analysis and in Vitro Antiviral, Anticancer and Antioxidant Capacities of the Aqueous Extracts of *Lentinula Edodes* and *Pleurotus Ostreatus* Edible Mushrooms. *Molecules* **2021**, *26*(15), 4623. https://doi.org/10.3390/molecules26154623

[47] Nam, M.; Choi, J. Y.; Kim, M. S. Metabolic Profiles, Bioactive Compounds, and Antioxidant Capacity in *Lentinula Edodes* Cultivated on Log versus Sawdust Substrates. *Biomolecules* **2021**, *11*(11), 1654. https://doi.org/10.3390/biom11111654

[48] Roszczenko, P.; Szewczyk-Roszczenko, O. K.; Gornowicz, A.; Iwańska, I. A.; Bielawski, K.; Wujec, M.; Bielawska, A. The Anticancer Potential of Edible Mushrooms: A Review of Selected Species from Roztocze, Poland. *Nutrients* **2024**, *16*(17), 2849. https://doi.org/10.3390/nu16172849

[49] Silva, G. B. da; Rocha, K. G.; Bagatini, M. D.; Kempka, A. P. Anticancer Properties of Phenolic Acids and Cell Death Signaling Pathways: A 20-Year Bibliometric Analysis (2003–2023). *Food Biosci.* **2025**, *64*, 105741. https://doi.org/10.1016/j.fbio.2024.105741

[50] Jedinak, A.; Sliva, D. *Pleurotus Ostreatus* Inhibits Proliferation of Human Breast and Colon Cancer Cells through P53-Dependent as Well as P53-Independent Pathway. *Int. J. Oncol.* **2008**, *33*(6), 1307–1313. https://doi.org/10.3892/ijo00000122

[51] Reza, M. A.; Hossain, M. A.; Lee, S. J.; Yohannes, S. B.; Damte, D.; Rhee, M. H.; Jo, W. S.; Suh, J. W.; Park, S. C. Dichlormethane Extract of the Jelly Ear Mushroom *Auricularia Auricula-Judae* (Higher Basidiomycetes) Inhibits Tumor Cell Growth in Vitro. *Int. J. Med. Mushrooms* **2014**, *16*(1), 77–84. https://doi.org/10.1615/IntJMedMushr.v16.i1.40

[52] Arora, S.; Tandon, S. Mushroom Extracts Induce Human Colon Cancer Cell (COLO-205) Death by Triggering the Mitochondrial Apoptosis Pathway and Go/G1-Phase Cell Cycle Arrest. *Arch. Iran. Med.* **2015**, *18* (5), 329–335. https://doi.org/0151805/AIM.006

[53] Jagadeesh, R.; Babu, G.; Lakshmanan, H.; Oh, O. M.-J.; Jang, J. K.-Y.; Kong, K. W.-S.; Raaman, N. Bioactive Sterol Derivatives Isolated from the *Pleurotus Djamor* Var. *Roseus* Induced Apoptosis in Cancer Cell Lines. *Cardiovasc. Hematol. Agents Med. Chem.* **2020**, *18*(2), 127–134. https://doi.org/10.2174/1871525718666200303123557

[54] Kamel, I. M.; Khalil, N. M.; Atalla, S. M. M.; Seleem, S. M. Purification, Molecular And Biochemical Characterization And Biological Applications Of Hemagglutinating Lectin With Anticancer Activities

From *Pleurotus Ostreatus*. *Plant Arch.* **2021**, *21*(Suppliment-1), 384–391. https://doi.org/10.51470/plantarchives.2021.v21.s1.065

[55] Park, G. S.; Shin, J.; Hong, S.; Gopal, J.; Oh, J. W. Anticarcinogenic Potential of the Mushroom Polysaccharide Lentinan on Gastric and Colon Cancer Cells: Antiproliferative, Antitumorigenic, Mu-2-Related Death-Inducing Gene, MUDENG Ramifications. *J. Ind. Eng. Chem.* **2024**, *135*, 36–47. https://doi.org/10.1016/j.jiec.2024.01.024

[56] Permana, S.; Nabilahasna, E. A.; Meilany, F. A.; Ilmiyah, S. Z.; Widodo, E.; Norahmawati, E.; Kawamoto, Y.; Endrawati, H.; Endharti, A. T. Enhanced Anticancer Effect of Cetuximab Combined with Ethanol Extract of *Volvariella Volvacea* in Colorectal Cancer Targeted TOP2A and PPARγ. *J. Pharm. Pharmacogn. Res.* **2024**, *12*(6), 1129–1142. https://doi.org/10.56499/jppres23.189512.6.1129

[57] Palacios, I.; Lozano, M.; Moro, C.; D'Arrigo, M.; Rostagno, M. A.; Martínez, J. A.; García-Lafuente, A.; Guillamón, E.; Villares, A. Antioxidant Properties of Phenolic Compounds Occurring in Edible Mushrooms. *Food Chem.* **2011**, *128*(3), 667–674. https://doi.org/10.1016/j.foodchem.2011.03.085

[58] Kim, M. Y.; Seguin, P.; Ahn, J. K.; Kim, J. J.; Chun, S. C.; Kim, E. H.; Seo, S. H.; Kang, E. Y.; Kim, S. L.; Park, Y. J.; Ro, H. M.; Chung, I. M. Phenolic Compound Concentration and Antioxidant Activities of Edible and Medicinal Mushrooms from Korea. *J. Agric. Food Chem.* **2008**, *56*(16), 7265–7270. https://doi.org/10.1021/jf8008553

[59] Miles, P. G.; Chang, S. T. *Mushroom Biology Concise Basics and Current Development*; World Scientific: Singapore, **1997**; 193.

[60] Ismail, M.; Bagalkotkar, G.; Iqbal, S.; Adamu, H. A. Anticancer Properties and Phenolic Contents of Sequentially Prepared Extracts from Different Parts of Selected Medicinal Plants Indigenous to Malaysia. *Molecules* **2012**, *17*(5), 5745–5756. https://doi.org/10.3390/molecules17055745

[61] Wang, X.; Sankarapandian, K.; Cheng, Y.; Woo, S. O.; Kwon, H. W.; Perumalsamy, H.; Ahn, Y. J. Relationship between Total Phenolic Contents and Biological Properties of Propolis from 20 Different Regions in South Korea. *BMC Complement. Altern. Med.* **2016**, *16*(1), 108. https://doi.org/10.1186/s12906-016-1043-y

[62] Milella, R. A.; De Rosso, M.; Gasparro, M.; Gigante, I.; Debiase, G.; Forleo, L. R.; Marsico, A. D.; Perniola, R.; Tutino, V.; Notarnicola, M.; Velasco, R.; Flamini, R. Correlation between Antioxidant and Anticancer Activity and Phenolic Profile of New Apulian Table Grape Genotypes (*V. Vinifera* L.). *Front. Plant Sci.* **2023**, *13*, 1064023. https://doi.org/10.3389/fpls.2022.1064023

[63] Rao, Y. K.; Geethangili, M.; Fang, S. H.; Tzeng, Y. M. Antioxidant and Cytotoxic Activities of Naturally Occurring Phenolic and Related Compounds: A Comparative Study. *Food Chem. Toxicol.* **2007**, *45*(9), 1727–1736. https://doi.org/10.1016/j.fct.2007.03.012.

ASEAN
Journal of Scientific and Technological Reports
Online ISSN:2773-8752

Research article

One-Day Trip Itinerary Planning for Visitors to Songkhla City

Somsak Kaewploy[1*], Chatchai Waiyapattanakorn[2] Watchanachai Joompha[3], and Kulyuth Boonseng[4]

[1] Faculty of Industrial Technology, Songkhla Rajabhat University, Songkhla, 90000, Thailand
[2] Faculty of Industrial Technology, Songkhla Rajabhat University, Songkhla, 90000, Thailand
[3] Faculty of Integrated Engineering and Technology, Rajamangala University of Technology Tawan-Ok, Chanthaburi, 22210, Thailand
[4] Faculty of Industrial Technology, Songkhla Rajabhat University, Songkhla, 90000, Thailand
* Correspondence: somsak.ka@skru.ac.th

Citation:
Kaewploy, S.; Waiyapattanakorn, C.; Joompha, W.; Boonseng, K One-day trip itinerary planning for visitors to Songkhla city. *ASEAN J. Sci. Tech. Report*. **2025**, *28*(6), e259060. https://doi.org/10.55164/ajstr.v28i6.259060.

Article history:
Received: April 30, 2025
Revised: September 11, 2025
Accepted: September 18, 2025
Available online: October 19, 2025

Abstract: One-day trip itinerary planning has gained increasing attention in secondary cities such as Songkhla, which is renowned for its rich cultural heritage and natural attractions. However, systematic approaches to designing itineraries under strict time constraints remain limited. This study aims to evaluate the effectiveness of three routing methods for one-day itinerary planning in Songkhla City: (1) Nearest Neighbor Heuristic (NNH), (2) Saving Algorithm (SA), and (3) a mathematical optimization model solved using LINGO software. The analysis utilizes real-world data from ten prominent tourist destinations in Songkhla City. Results indicate that all three methods successfully generated two sub-routes, each constrained to a maximum duration of 360 minutes. Among them, the mathematical model yielded the most optimal solution, minimizing the total travel distance to 56.20 kilometers and total travel time to 619 minutes. The Saving Algorithm (SA) achieved near-optimal results (57.68 kilometers, 625 minutes), while the Nearest Neighbor Heuristic (NNH) method, although slightly less accurate (57.72 kilometers, 671 minutes), proved advantageous in terms of computational efficiency and implementation simplicity. These findings highlight the trade-off between optimality and computational effort, emphasizing the importance of selecting suitable methods based on problem scale and constraints. The study provides strategic insights into developing efficient and sustainable itinerary planning frameworks for tourism in emerging secondary cities.

Keywords: One-day trip; heuristics; mathematical model; itinerary planning

1. Introduction

The tourism industry plays a pivotal role in driving Thailand's economic development, particularly in the southern region, which is endowed with rich natural and cultural resources. Key provinces, such as Phuket, Krabi, and Surat Thani, have emerged as internationally renowned destinations, contributing significantly to the national service sector's gross domestic product [1]. However, the concentration of tourists in these popular areas has exerted pressure on natural resources, while high-potential provinces like Songkhla, Nakhon Si Thammarat, and Trang remain underdeveloped and insufficiently promoted [2]. Songkhla, a coastal province, is notable for its rich historical and cultural heritage, particularly in the Songkhla Old Town area, where Chinese, Thai, and Western architectural styles coexist, reflecting the region's prosperous past [3]. The city also features a variety of attractions that integrate natural and cultural assets, such as Samila Beach with its iconic Golden Mermaid sculpture,

Tang Kuan Hill with panoramic city views, and Ko Yo Island, which is home to cultural landmarks and temples situated on the shores of Songkhla Lake.

In 2024, Songkhla recorded more than 6.9 million visitors, representing a 24.53% increase from 2023, and generated over 50 billion baht in tourism revenue. The majority of international visitors originated from Malaysia, Indonesia, Singapore, Laos, and China [4]. Despite the consistent growth in tourist numbers, effective itinerary planning, particularly for one-day trips catering to tourists with limited time, remains underdeveloped. Efficient route sequencing, time management, and the incorporation of time window constraints are critical components that directly affect tourists' experiences. However, there is a noticeable lack of comprehensive research on these aspects specific to Songkhla. Previous studies have predominantly focused on major tourist destinations, such as Phuket or Chiang Mai, utilizing mathematical models and engineering-based approaches, including the traveling salesman problem (TSP) and the vehicle routing problem (VRP), to optimize tourism routes [5, 6]. Nonetheless, these approaches often lack flexibility and fail to address the local context and constraints of secondary cities like Songkhla. Furthermore, the integration of heuristic techniques, such as the Nearest Neighbor Heuristics (NNH) and the Saving Algorithm (SA), which are noted for their computational speed and ease of use with explicit time-based constraints, remains limited, despite their potential in enhancing real-world decision-making for tourists [7-9].

This research article presents a one-day trip itinerary planning framework for exploring Songkhla City, applying both heuristic methods and a mathematical model under time window constraints. The heuristic methods adopted include the Nearest Neighbor Heuristic (NNH) and the Saving Algorithm (SA) Method, which are known for reducing computational time and offering practically efficient routes. The primary objective of this study is to support tourists in planning effective and personalized one-day itineraries in Songkhla that align with both temporal constraints and individual preferences. The findings aim to contribute strategically to the enhancement of tourism management in Songkhla City, ultimately promoting more efficient and sustainable tourism development in the future.

2. Application of Heuristics Method and Mathematical Models

Efficient tourism route planning is a crucial factor in enhancing tourist satisfaction, particularly in the context of one-day trips, which are constrained by limited time. The application of heuristic techniques and mathematical models has gained popularity as an effective approach to solving tourism routing problems, as these methods can provide high-quality solutions within a limited timeframe [10].

2.1 Nearest Neighbor Heuristics (NNH) Method

The NNH is a widely used technique in tourism route planning due to its simplicity and efficiency in generating initial solutions. Although it does not guarantee the optimal solution, it serves as a practical starting point for itinerary design [11]. The procedure for applying the NNH method to tourism route planning consists of the following steps:

(1) Begin by defining the starting point of the trip, which serves as the reference location for searching nearby attractions. This starting point may be a hotel, bus terminal, airport, or any other relevant location. Identify the tourist attraction that is closest to the reference point.

(2) Select the nearest tourist attraction and add it to the main route. Then, update this attraction as the new reference point for future searches.

(3) Identify the next unvisited tourist attraction that is closest to the current reference point. Estimate the cumulative travel and visit time if this attraction is added to the route. If the total time does not exceed the allowed trip duration, include the selected attraction in the main route.

(4) If the cumulative time exceeds the trip duration, terminate the current route. Then, check whether there are any remaining unvisited attractions. If so, repeat steps 1 to 3 until all attractions are assigned to one or more feasible routes.

2.2 Saving Algorithm (SA) Method

The SA method, originally proposed by Clarke and Wright [12], is one of the most widely adopted heuristic techniques used for minimizing travel distances and transportation costs. This approach is based on

the concept of calculating savings generated by merging travel routes between pairs of tourist attractions. The methodology can be described in the following steps [11–13]:

(1) Select a starting point or reference location for the tour. Initially, this results in separate routes from the starting point to each tourist attraction.

(2) Calculate the travel time, distance, and cost savings (referred to as the saving value) using Equation (1):

$$S_{ij} = D_{0i} + D_{0j} - D_{ij} \quad (1)$$

Where:

i, j denote the tourist attractions
0 represents the starting point or reference location
S_{ij} is the distance saved by combining the routes to i and j
D_{0i} is the distance from the starting point to attraction i
D_{oj} is the distance from the starting point to attraction j
D_{ij} is the distance between attractions i and j

(3) Sort the values of S_{ij} in descending order.

(4) Construct tourism routes by pairing attractions i and j that yield the highest saving values.

(5) Repeat the process iteratively until all tourist attractions are included in the route(s), subject to travel constraints such as the total tour duration, which must not exceed the maximum allowable time as defined in the itinerary plan. The concept of savings is illustrated in Figure 1. The SA is a well-established theoretical framework in tourism route planning. Its logic is straightforward, and its implementation is relatively simple. The saving value (S_{ij}) represents the potential reduction in travel distance between two attractions. A higher saving value indicates a greater potential to reduce the total route distance.

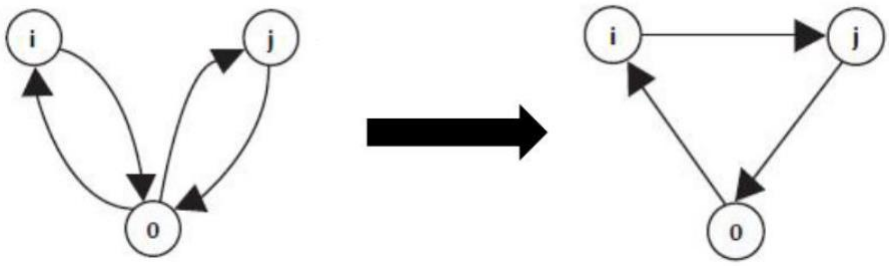

Figure 1. Conceptual of savings value. [11]

2.3 Mathematical Model

A mathematical model is a structured approach for solving allocation and resource optimization problems that involve relationships among multiple variables. The primary objective is to identify the optimal solution or the most beneficial course of action for a given system, considering the specified constraints or limitations. The standard components of a mathematical model include [13]: (1) decision variables and parameters, (2) constraints or restrictions, and (3) an objective function. In this research, the proposed mathematical model is formulated as a time-constrained tourism routing problem, also known as the time-window constrained traveling problem. The route starts and ends at the exact location, involving a visit to 10 tourist attractions within Songkhla City. The model is designed to reflect real-world scenarios of one-day tourism, where all selected attractions must be visited within a limited time frame and under predefined time windows [14]. Currently, various software tools are available for solving linear programming problems, such as Excel Solver and LINGO. This study employs LINGO software to solve the proposed model [15]. LINGO, developed by LINDO Systems in the United States, enables users to input mathematical expressions directly or define models using conventional mathematical notation. In the latter case, all variables and parameters must be declared explicitly, followed by the formulation of the objective function and constraints in LINGO syntax to obtain the optimal solution. This study presents a one-day trip itinerary planning approach for

visiting Songkhla City, employing a mathematical modeling framework to identify the optimal solution under constraints of time and distance. The primary objective of the model is to minimize the total travel distance while ensuring that all selected tourist attractions are accessible within the designated time window. The model is designed to capture the essential decision-making components of the routing problem and incorporates the following elements:

(1) Decision variables

X_{ijk} = 1 if the route travels from node i to j in route k

X_{ijk} = 0 otherwise

Y_{ik} = 1 if tourist attraction i is visited in route k

Y_{ik} = 0 otherwise

$U_i \geq 0$: auxiliary variable used for subtour elimination (miller-tucker-zemlin (MTZ) formulation)

(2) Parameters

D_{ij} : distance between node i and node j (km)

t_i : visiting time at node i (minutes), with:

$t_0 = 0$ (Start and end at node Ho)

$t_1 = 120$, $t_2 = 40$, $t_3 = 30$, $t_4 = 90$, $t_5 = 30$,

$t_6 = 30$, $t_7 = 30$, $t_8 = 30$, $t_9 = 40$, $t_{10} = 120$

v = 60 km/h = 1 km/min

T_{max} = 360 minutes (maximum time per route)

N = 10: number of tourist attraction

M = 2: number of available routes

Index sets: $i, j \in \{0, 1, \ldots, N\}$, $k \in \{1, 2\}$

(3) Objective function

minimize the total travel distance across both routes: using Equation (2)

$$\text{Min} \quad \sum_{i=0}^{N}\sum_{j=0}^{N}\sum_{k=1}^{M} D_{ij} X_{ijk} \tag{2}$$

(4) Constraints

(4.1) Coverage constraint: each tourist attraction must be visited exactly once in one of the two routes: using Equation (3)

$$\sum_{i=1}^{M} Y_{ij} = 1 \qquad \forall i \in \{1, \ldots, N\} \tag{3}$$

(4.2) Flow conservation: for every node in a route, the number of incoming and outgoing edges must match: using Equation (4) and (5)

$$\sum_{j=0}^{N} X_{ijk} = Y_{ik} \qquad \forall i \in \{1, \ldots, N\}, \forall k \in \{1, 2\} \tag{4}$$

$$\sum_{i=0}^{N} X_{ijk} = Y_{jk} \qquad \forall j \in \{1, \ldots, N\}, \forall k \in \{1, 2\} \tag{5}$$

(4.3) Start and end at depot (node 0): each route must start and end at the depot node (Ho): using Equation (6) and (7)

$$\sum_{j=1}^{N} X_{0jk} = 1 \qquad \forall k \in \{1, 2\} \tag{6}$$

$$\sum_{i=1}^{N} X_{i0k} = 1 \qquad \forall k \in \{1, 2\} \tag{7}$$

(4.4) Time constraint: total time (travel time + visiting time) must not exceed the maximum allowed time per route: using Equation (8)

$$\sum_{i=0}^{N}\sum_{j=0}^{N} \frac{D_{ij}}{v} . X_{ijk} + \sum_{i=1}^{N} t_i . Y_{ik} \leq T_{max} \qquad \forall k \in \{1, 2\} \tag{8}$$

(4.5) Subtour elimination (MTZ constraints): using Equation (9)

$$U_i - U_j + N \, . \, X_{ijk} \leq N\text{-}1 \qquad \forall i \neq j \in \{1, \ldots, N\}, \forall k \in \{1, 2\} \tag{9}$$

(5) Variable conditions: using Equation (10-12)

$$X_{ijk} \in \{0, 1\} \qquad \forall i,j \in \{0, \ldots, N\}, \forall k \in \{1, 2\} \tag{10}$$

$$Y_{ik} \in \{0, 1\} \qquad \forall i \in \{1, \ldots, N\}, \forall k \in \{1, 2\} \tag{11}$$

$$U_i \geq 0 \qquad \forall i \in \{1, \ldots, N\} \tag{12}$$

The one-day trip itinerary planning for visiting Songkhla City was conducted using a mathematical model developed and solved through Lingo software. The primary objective was to determine the most efficient travel plan in terms of minimizing the total travel distance, while simultaneously satisfying time constraints and ensuring that all designated tourist attractions were visited.

3. Results and Discussion

3.1 Data Collection

This study focuses on developing a one-day trip itinerary for visiting the city of Songkhla, incorporating ten popular tourist attractions. Private vehicles or rental cars were assumed to be the primary mode of transportation, with an average travel speed of 60 km/h. The researcher collected the geographic coordinates of major tourist sites in Songkhla for routing purposes. The BP Samila Beach and Resort (Ho) was selected as both the starting and ending point of the trip, as it is a popular accommodation choice among tourists. This location is situated at a latitude of 7.2140266 and a longitude of 100.5968600, according to Google Maps.

Table 1. Coordinates and visiting times for tourist attractions in Songkhla City.

Code	Tourist attraction	Coordinates (Latitude, Longitude)	Visiting time (minutes)
TA1	Koh Yo	7.1625439264314630, 100.54359928526166	120
TA2	General Prem Tinsulanonda Historical Park	7.1490522083543380, 100.56137037928802	40
TA3	Khao Kao Seng (Khao Kao Seng Temple)	7.1830935997878465, 100.61764270196703	30
TA4	Chalatat Beach-Samila Beach	7.2151756617667290, 100.59531766011072	90
TA5	Songkha City Park	7.2125770570205600, 100.59687456627293	30
TA6	Song Thale Park	7.2278169984735910, 100.57749037521063	30
TA7	Tangkuan Hill	7.2112713194156230, 100.58933755176975	30
TA8	Khao Noi	7.2109748113266940, 100.59274018229340	30
TA9	Songkhla National Museum	7.2025028068605340, 100.58850537794254	40
TA10	Songkhla Old Town	7.1953756321492170, 100.58999283805554	120

The coordinates and estimated visiting times for each tourist attraction are presented in Table 1. These data were used to evaluate the most appropriate travel routes, considering both the distances between tourist attractions and the distance from each attraction to the starting point. The pairwise distance matrix is provided in Table 2, which supports the optimal determination of routes.

Table 2. Distance matrix between tourist attractions (unit: kilometers).

Point	Ho	TA1	TA 2	TA 3	TA4	TA5	TA6	TA7	TA8	TA9	TA10
Ho	0.00	19.85	16.95	4.74	1.24	0.49	3.51	1.46	0.95	2.42	3.16
TA1	19.85	0.00	5.29	17.31	19.05	18.50	12.24	18.30	18.29	17.63	16.87
TA2	16.95	5.29	0.00	14.24	15.98	15.43	17.76	15.24	15.22	14.56	9.91
TA3	4.74	17.31	14.24	0.00	5.61	4.50	7.80	5.71	5.32	4.95	4.32
TA4	1.24	19.05	15.98	5.61	0.00	0.63	3.22	1.17	0.66	2.39	2.97
TA5	0.49	18.50	15.43	4.50	0.63	0.00	3.47	1.42	0.91	2.37	3.23
TA6	3.51	12.24	17.76	7.80	3.22	3.47	0.00	2.68	2.91	3.30	4.75
TA7	1.46	18.30	15.24	5.71	1.17	1.42	2.68	0.00	0.54	1.35	2.23
TA8	0.95	18.29	15.22	5.32	0.66	0.91	2.91	0.54	0.00	1.34	2.21
TA9	2.42	17.63	14.56	4.95	2.39	2.37	3.30	1.35	1.34	0.00	0.96
TA10	3.16	16.87	9.91	4.32	2.97	3.23	4.75	2.23	2.21	0.96	0.00

Note: Ho = BP Samila Beach and Resort

3.2 Nearest Neighbor Heuristics (NNH)

The NNH method was applied to plan a one-day tourism route for visiting the city of Songkhla. This approach constructs a travel route by iteratively selecting the next unvisited tourist attraction that is closest in distance to the current location. The process begins at the starting point (Ho) and continues until all designated destinations have been visited, concluding with a return to the origin. Based on the implementation results, as shown in Table 3, the itinerary was effectively divided into two main routes. Route 1 includes visits to seven attractions: TA5, TA4, TA8, TA7, TA9, TA6, and TA3, resulting in a total travel distance of 19.51 kilometers and an overall duration of 325 minutes. Route 2 covers three attractions: TA10, TA2, and TA1, with a total distance of 38.21 kilometers and a total travel time of 5 hours and 46 minutes. Both routes were designed to comply with the one-day travel constraint of a maximum of 360 minutes per route, thereby demonstrating the feasibility of using the NNH method for time-constrained tourism planning.

Table 3. Tourism route results using the NNH method.

Route	Tourist Attractions Visited	Distance (km)	Time (minutes)
1	Ho - TA_5 - TA_4 - TA_8 - TA_7 - TA_9 - TA_6 - TA_3 - Ho	19.51	325
2	Ho - TA_{10} - TA_2 - TA_1 - Ho	38.21	346

3.3 Saving Algorithm (SA)

The one-day tourism route planning for visiting Songkhla City was conducted using the SA method, which aims to determine an efficient sequence of travel that minimizes both the total travel distance and duration. This optimization is subject to a time constraint of no more than 360 minutes per route. The outcome of the implementation was divided into two main routes, as detailed in Table 4. Route 1 consists of visits to seven tourist attractions: TA9, TA6, TA7, TA8, TA4, TA5, and TA3. This route starts and ends at the origin point (Ho), covering a total distance of 19.47 kilometers and requiring a total travel time of 4 hours and 39 minutes. Route 2 includes three tourist attractions: TA1, TA2, and TA10, and also starts and ends at Ho. This route has a total distance of 38.21 kilometers and a total travel time of 5 hours and 46 minutes. Both routes fully comply with the 360-minute time constraint, ensuring feasibility for a one-day trip itinerary.

Table 4. Tourism route results using the SA method.

Route	Tourist Attractions Visited	Distance (km)	Time (minutes)
1	Ho - TA_9 - TA_6 - TA_7 - TA_8 - TA_4 – TA_5 - TA_3 - Ho	19.47	279
2	Ho - TA_1 – TA_2 – TA_{10} - Ho	38.21	346

3.4 Mathematical Model

The results obtained from solving the mathematical model with LINGO are presented in Table 5. The model generated two feasible travel routes. The first route starts from the origin (Ho), continues through tourist attractions TA6, TA1, TA2, and TA10, and returns to the origin. This route covers a total distance of 34.11 kilometers and takes 277 minutes. The second route begins at Ho, proceeds through TA3, TA9, TA7, TA8, TA4, and TA5, and returns to Ho, covering a distance of 13.36 kilometers in 342 minutes.

Table 5. Results of tourism route planning using the mathematical model with Lingo software

Route	Tourist Attractions Visited	Distance (km)	Time (minutes)
1	Ho - TA_6 - TA_1 – TA_2 - TA_{10} - Ho	34.11	277
2	Ho – TA_3 – TA_9 - TA_7 - TA_8- TA_4- TA_5 - Ho	13.36	342

These results demonstrate the model's capability to generate effective travel plans under real-world constraints, specifically time limitations and comprehensive coverage of all attractions. This highlights the potential of mathematical modeling as a robust tool for addressing tourism-related route optimization problems within a logistics context.

In summary, the mathematical model executed via Lingo software yielded the optimal solution for this small-scale problem. It can serve as a benchmark for comparison with heuristic methods in subsequent analyses or in studies involving larger and more complex problem instances.

3.5 Comparative Results of Route Planning Methods

This study applied three different methods to develop a one-day tourism itinerary for visiting Songkhla City: (1) Nearest Neighbor Heuristics (NNH), (2) the Saving Algorithm (SA), and (3) a mathematical model implemented using LINGO software. The outcomes derived from each method are summarized and compared in Table 6 and Figure 2.

Table 6. Comparison of tourism route planning results.

Method	Route	Tourist attractions	Distance (km)	Total Distance (km)	Time (min)	Total Time (min)
Nearest Neighbor Heuristics (NNH)	1	Ho - TA_5 - TA_4 - TA_8 - TA_7 - TA_9 - TA_6 - TA_3 - Ho	19.51	57.72	325	671
	2	Ho - TA_{10} - TA_2 - TA_1 - Ho	38.21		346	
Saving Algorithm (SA)	1	Ho - TA_9 - TA_6 - TA_7 - TA_8 - TA_4 - TA_5 - TA_3 - Ho	19.47	57.68	279	625
	2	Ho - TA_1 - TA_2 - TA_{10} - Ho	38.21		346	
Mathematical Model	1	Ho - TA_3 - TA_9 - TA_6 - TA_7 - TA_8 - TA_4 - TA_5 - Ho	17.99	56.2	277	619
	2	Ho - TA_1 - TA_2 - TA_{10} - Ho	38.21		342	

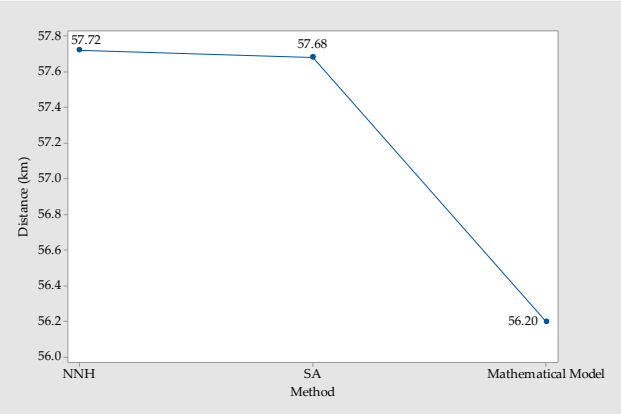

(a) Comparison of total distance per method.

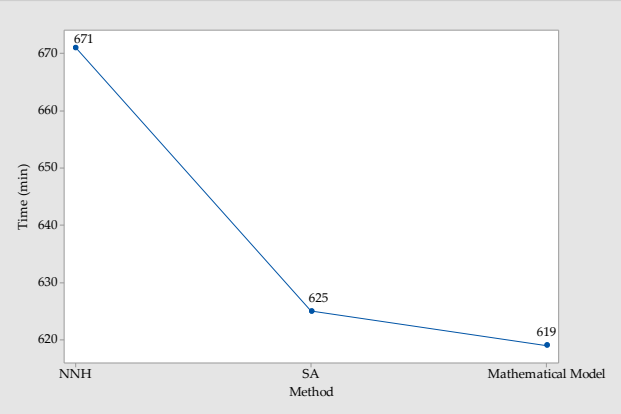

(b) Comparison of total time per method.

Figure 2. Comparison of results for each method.

According to Table 6, the mathematical model solved with LINGO provided the most optimal results in terms of both travel distance and total time. Based on the analysis in Figure 2(a), the mathematical model yielded the optimal result, with the shortest total travel distance of 56.20 kilometers. In contrast, the two heuristic methods produced similar but higher results: the SA recorded a near-optimal total distance of 57.68 kilometers, while the NNH had the highest total distance at 57.72 kilometers. This result clearly indicates that for the small-scale problem under consideration, the mathematical model can accurately determine the optimal solution in terms of distance. In terms of total time (Figure 2(b)), the mathematical model again yielded the best result, with the shortest total time of 619 minutes. The SA followed closely at 625 minutes, exhibiting performance remarkably similar to that of the mathematical model. In contrast, the NNH had a significantly higher total time of 671 minutes. Although NNH is the simplest and quickest method for computation, it proved to be the least efficient in terms of total travel time and visiting time. These comparative results confirm that the mathematical model can provide the optimal solution for small-scale routing problems, serving as a benchmark against which other methods can be compared. However, the heuristic methods demonstrated their practical value, particularly the SA, which delivered near-optimal results for both distance and time. Although the mathematical model provides a perfect solution, it comes at the cost of higher processing time, which may be impractical for large-scale problems. Conversely, while heuristic methods do not guarantee optimality, they offer greater speed and flexibility, making them a highly suitable alternative for large-scale problems or real-time planning. Therefore, the choice of method depends on the problem's context and the trade-off between the demand for accuracy and the constraints of computational resources. Therefore, as the problem size increases (e.g., more tourist sites or complex constraints), the mathematical model may become less practical due to time and resource limitations. In such contexts, heuristic methods become more suitable in practice. A high-level conceptual comparison of each method is summarized in Table 7.

Table 7. Conceptual comparison of routing methods.

Comparison criteria	Mathematical model	Nearest Neighbor Heuristics	Saving Algorithm
Method type	Exact (mathematical)	Heuristic	Heuristic
Solution quality	Optimal	Suboptimal	Near-optimal
Computational time	High	Very low	Low
Suitability for small problems	High	Moderate	High
Suitability for large problems	Low (time-intensive)	High	High
Ease of development/use	Moderate to difficult	Very easy	Moderate

In conclusion, for small-scale problems where high accuracy is critical, the mathematical model is the most appropriate choice. However, for large-scale scenarios or applications requiring real-time responsiveness, heuristic methods such as NNH or SA are more practical alternatives.

3.6 Discussion

The findings of this study present a comparative analysis of three routing approaches: NNH, the SA, and a mathematical model solved via LINGO for a one-day trip itinerary for visitors in Songkhla City under time window constraints. Among the three methods, the mathematical model yielded the optimal results in terms of minimizing both total travel distance (56.2 kilometers) and total travel time (619 minutes), aligning with previous studies [6, 11] suggesting that exact methods are well-suited for small-scale, constraint-intensive routing problems [14]. However, heuristic approaches offer significant advantages in terms of computational speed and ease of implementation. The SA, in particular, produced near-optimal results (57.68 kilometers, 625 minutes), demonstrating its effectiveness in consolidating routes based on the principle of distance savings. Meanwhile, the NNH, though providing a slightly less optimal outcome (57.72 kilometers, 671 minutes), was the fastest and simplest method, making it highly suitable for real-time applications or large-scale systems [13, 15]. These findings underscore the inherent trade-off between accuracy and efficiency. While mathematical models can guarantee optimality, heuristic methods provide the flexibility and practicality needed in scenarios constrained by time or computational resources. This hybrid analysis provides strategic insights into tourism route planning, particularly in secondary cities like Songkhla, where both logistical efficiency and feasibility of implementation must be considered. Moreover, this research contributes to bridging existing gaps in the literature and supports the advancement of sustainable tourism by promoting improved accessibility and equitable distribution of tourist flows across urban areas [7]. The integration of mathematical and heuristic approaches presents a balanced framework for optimizing travel itineraries in real-world tourism contexts.

4. Conclusions

This study focused on planning one-day trip itineraries for visitors to Songkhla City. Songkhla is a secondary city in Thailand with significant tourism potential but lacks efficient routing strategies, particularly under time window constraints. The research aimed to compare the performance of three primary route planning methods: (1) the Nearest Neighbor Heuristic (NNH), (2) the Saving Algorithm (SA), and (3) a mathematical model developed and solved using LINGO software. The findings revealed that the mathematical model provided the most accurate and optimal solution for small-scale problems, yielding the shortest total travel distance (56.20 kilometers) and travel time (619 minutes), while satisfying the time constraint of no more than 360 minutes per route. Meanwhile, both heuristic methods demonstrated rapid computation and practical applicability, particularly in cases involving a larger number of tourist attractions or where real-time planning is required. Although heuristic methods do not guarantee optimality, they offer substantial benefits in flexibility and efficiency. Specifically, the comparative evaluation showed that: (1) the mathematical model delivered the most precise results but required the longest computation time, (2) Nearest Neighbor Heuristics (NNH) offered the most straightforward implementation and the lowest processing time but yielded suboptimal solutions, and (3) the Saving Algorithm (SA) achieved near-optimal performance, closely approximating the results of the mathematical model while maintaining low computation time. In summary, the choice of routing method should be guided by the problem context. For small-scale problems that demand high accuracy, the mathematical model is the most suitable. In contrast, for large-scale problems requiring rapid decision-making, heuristic methods offer a more practical solution. This research contributes to the development of strategic frameworks for tourism route planning in secondary cities such as Songkhla and provides a foundation for more efficient and sustainable tourism management in the future.

5. Acknowledgements

The authors would like to express their sincere appreciation to the Bachelor of Engineering Program in Logistics Engineering, Faculty of Industrial Technology, Songkhla Rajabhat University, for providing essential academic and technical support throughout the completion of this research.

Author Contributions: Conceptualization, S.K., C.W. and W.J.; methodology, S.K., C.W., W.J. and K.B.; software and coding, S.K. and W.J.; analysis and visualization, S.K., C.W. and W.J.; validation, S.K., C.W. and W.J.; writing-original draft preparation, S.K., C.W. and W.J.; writing-review and editing, S.K. and W.J. All authors have read and agreed to the published version of the manuscript.

Conflicts of Interest: The authors declare no conflict of interest.

References

[1] Tourism Authority of Thailand. *Tourism Statistics Report 2023*; Ministry of Tourism and Sports: Bangkok, **2023**. Retrieved from https://www.mots.go.th/more_news_new.php?cid=521 (accessed April 2, 2025).

[2] Tourism Authority of Thailand. *Southern Thailand Tourism Development Strategy 2024–2027*; TAT Strategy Division: Bangkok, **2024**. Retrieved from https://www.tatstrategy.org/plan/southern-strategy-2024-2027.pdf (accessed April 2, 2025).

[3] Songkhla Provincial Public Relations Office. TAT Hat Yai Office Organizes "GO Songkhla by Tuk Tuk" Caravan to Promote Tourism Vibrancy. *Songkhla Provincial Public Relations Office*, **2024**, December 21. Retrieved from https://songkhla.prd.go.th/th/content/category/detail/id/9/iid/349754 (accessed April 2, 2025).

[4] Matichon Online. TAT Aims to Promote Songkhla as a World-Class Tourist City with Three Highlight Campaigns. *Matichon Online*, 2025. Retrieved from https://www.matichon.co.th/economy/news_5058427 (accessed April 2, 2025).

[5] Ran, W.; Liu, L.; Yang, G. A Hybrid Ant Colony Algorithm for Tour Route Optimization with Time Window Constraints. *Inf. Technol. J.* **2013**, *12*, 5701–5706. https://doi.org/10.3923/itj.2013.5701.5706.

[6] Xu, Y.; Zhang, J.; Zhang, C. Multi-objective Itinerary Planning for Tourist Route Design. *Expert Syst. Appl.* **2018**, *93*, 28–38. https://doi.org/10.1016/j.eswa.2017.09.039.

[7] Pongponrat, K.; Pongquan, S. Community Participation in a Local Tourism Planning Process: A Case Study of Nathon Community on Samui Island, Thailand. *Asia-Pac. J. Rural Dev.* **2007**, *17*(2), 27–46. https://doi.org/10.1177/1018529120070202

[8] Patil, S.; Jaybhaye, R. Tourism Development in South Asia Region: Challenges and Opportunities. *Turizam* **2023**, *27*(4), 212–227. https://doi.org/10.5937/turizam27-43676.

[9] United Nations World Tourism Organization. *Tourism for Inclusive Growth*; UNWTO: 2021. Retrieved from https://www.unwto.org/wtd2021 (accessed April 2, 2025).

[10] Gutin, G.; Punnen, A. P., Eds. The Traveling Salesman Problem and Its Variations. *Combinatorial Optimization Series*, **2007**, *12*. https://doi.org/10.1007/b101971

[11] Suksee, S.; Meecharoen, T. Minimization of Transportation Cost by Applying the Vehicle Routing Problem: A Case Study of Car Accessory Company. *Kasem Bundit Eng. J.* **2019**, *9*(1), 69–84.

[12] Clarke, G.; Wright, J. W. Scheduling of Vehicles from a Central Depot to a Number of Delivery Points. *Oper. Res.* **1964**, *12*(4), 568–581. https://doi.org/10.1287/opre.12.4.568.

[13] Pitakaso, R. *Differential Evolution Approach for Solving Logistics Transportation Problems*; Ubon Ratchathani University: Ubon Ratchathani, Thailand, **2013**.

[14] Laporte, G. Fifty Years of Vehicle Routing. *Transp. Sci.* **2009**, *43*(4), 408–416. https://doi.org/10.1287/trsc.1090.0301.

[15] LINDO Systems. *Optimization Modeling Software*. Retrieved from https://www.lindo.com/ (accessed April 12, 2025).

ASEAN
Journal of Scientific and Technological Reports
Online ISSN:2773-8752

Academic article

Quality Characteristics of Pregelatinized Cassava Flour and Its Application in Frozen Dough for Artisan Pizza

Endang Yuli Purwani[1*], Wayan Trisnawati[2], I Putu Wardana[3], Saktyanu Kristyantoadi Dermoredjo[4], Agus Syarip Hidayat[5], Mutaqin[6], Sahat Marulitua Pasaribu[7], Bambang Sayaka[8], Made Oka Adnyana[9], Renny Rochani[10], Erliana Ginting[11], Eka Rahayu[12], Dian Adi Anggraeni Elisabeth[13], and Diana Nur Afifah[14, 15]

[1] Organization for Agriculture and Food, National Research and Innovation Agency (NRIA), Tangerang Selatan, 15310, Indonesia
[2] Organization for Agriculture and Food, National Research and Innovation Agency (NRIA), Tangerang Selatan, 15310, Indonesia
[3] Research Organization for Economic of Industry, Services, and Trade, National Research and Innovation Agency (NRIA), Jakarta, 12710, Indonesia
[4] Research Organization for Economic of Industry, Services, and Trade, National Research and Innovation Agency (NRIA), Jakarta, 12710, Indonesia
[5] Research Organization for Economic of Industry, Services, and Trade, National Research and Innovation Agency (NRIA), Jakarta, 12710, Indonesia
[6] Research Organization for Economic of Industry, Services, and Trade, National Research and Innovation Agency (NRIA), Jakarta, 12710, Indonesia
[7] Research Organization for Economic of Industry, Services, and Trade, National Research and Innovation Agency (NRIA), Jakarta, 12710, Indonesia
[8] Research Organization for Economic of Industry, Services, and Trade, National Research and Innovation Agency (NRIA), Jakarta, 12710, Indonesia
[9] Research Organization for Economic of Industry, Services, and Trade, National Research and Innovation Agency (NRIA), Jakarta, 12710, Indonesia
[10] Industrial Engineering Department, Sebelas Maret University, Surakarta, 57126, Indonesia
[11] Research Organization for Agriculture and Food, National Research and Innovation Agency (NRIA), Yogyakarta, 55861, Indonesia
[12] Research Organization for Agriculture and Food, National Research and Innovation Agency (NRIA), Yogyakarta, 55861, Indonesia
[13] Research Organization for Economic of Industry, Services, and Trade, National Research and Innovation Agency (NRIA), South Jakarta – Jakarta, 12710, Indonesia
[14] Faculty of Medicine, Universitas Diponegoro, Semarang, 50275, Indonesia
[15] Center of Research and Service – Diponegoro University (CORES-DU), Universitas Diponegoro, Semarang, 50275, Indonesia
* Correspondence: eypdata@gmail.com

Citation:
Purwani, E.Y.; Trisnawati, W.; Wardana, I.P.; Dermoredjo, S.K.; Hidayat, A.S.; Mutaqin; Pasaribu, S.M.; Sayaka, B.; Adnyana, M.O.; Rochani, R.; Ginting, E.; Rahayu, E.; Elisabeth, D.A.A.; Afifah, D.N. Quality characteristics of pregelatinized cassava flour and its application in frozen dough for artisan pizza. *ASEAN J. Sci. Tech. Report.* **2025**, *28*(6), e258754. https://doi.org/10.55164/ajstr.v28i6.258754.

Article history:
Received: April 12, 2025
Revised: September 15, 2025
Accepted: September 27, 2025
Available online: October 20, 2025

Abstract: Cassava has played a significant role in Indonesia, serving as a cultural identifier and symbol of tradition. It has undergone various modern adaptations by transforming into pregelatinized cassava flour (PCF). This study reports on the characteristics of PCF produced by small entrepreneurs, evaluates the suitability of PCF frozen dough for fusion dishes like PCF-pizza, and assesses consumer acceptability of PCF-pizza. PCF-pizza combined the elements of Indonesian ethnic cuisine, such as cassava, with the popular Western dish of pizza. For these purposes, a PCF producer was interviewed, followed by PCF sampling, which was then further formulated into a dough. The dough was developed in a laboratory, and it was stored in a freezer at a temperature of -20 + 2 °C for 0, 14, and 28 days. An artisan baker was intensively coached to develop the dough for the production of PCF-pizza, which was then delivered to the end consumer. Standard methods were applied to analyze the PCF characteristics. A questionnaire was used to explore the consumers acceptability of the PCF-pizza. The study revealed that PCF has suitable characteristics for dough preparation of PCF-pizza. The dough could expand and form pores upon baking, indicating that the dough protected the yeast cells during frozen storage. The PCF frozen dough, stored for 14 days, was still suitable for producing PCF-pizza. Consumers accepted the PCF-pizza texture, taste, and aroma, and the price was feasible for the artisanal bakery industry. This study demonstrated that the scientific and technological innovation of PCF, supported by public investment, presents opportunities for improved cassava utilization, thereby encouraging the development of smallholder agro-industries.

Keywords: Cassava; flour; fusion dish; pregelatinized; PCF-pizza

1. Introduction

Cassava (*Manihot esculenta* Crantz) played an important role in Indonesian culinary traditions, serving as a cultural identifier and symbol of traditions [1–3]. This tuber was incorporated into many traditional foods, savory snacks, and sweet desserts. This tuber crop can be grown in various types of agroecosystems throughout the archipelago and can become an income-generating crop. Cassava has several attributes that make this crop attractive for both economic and health reasons[4]. Cassava is processed into starch to be utilized as an ingredient in the food industry, such as tapioca pearls, mochi, etc. Currently, cassava has undergone various modern adaptations by the food industry. The development of pregelatinized cassava flour (PCF) is a breakthrough in cassava transformation. The process involves washing, peeling, chipping, heat or extrusion treatment, and fine grinding [5]. This processing helped reduce post-harvest loss of cassava and even out fluctuations in seasonal supply. The cassava flour has been incorporated into the development of high-fiber, low-sugar snacks [6], artificial rice [7–9], a matrix for turmeric encapsulation [10], and noodles [11–12]. It was also blended with rice flour and sago starch to produce gluten-free wafers [13].

In Malang, East Java, Indonesia, there is a type of staple food made from dried cassava (also known as gaplek), which is ground into flour and then steamed or boiled. This type of food is popular as Tiwul and is a beloved ethnic dish that showcases the region's rich culinary heritage. Pizza is a popular and versatile dish that originated in Italy but has become beloved worldwide. Pizza is incredibly adaptable, allowing for endless combinations of flavors and styles to suit personal tastes and regional preferences. It was reported that pizza dough was successfully developed from PCF [14–15]. The use of PCF for pizza was a fusion that combines elements of Indonesian ethnic cuisine with the popular Western dish. This fusion dish was named PCF-pizza, which was produced as an artisanal food product. An artisan food product was all about high-quality, handcrafted, traditional, and locally sourced ingredients. Currently, artisanal food products are rapidly being produced by smallholder enterprises worldwide. Despite these facts, the potential for commercializing PCF-pizza has not been fully tapped due to a lack of appropriate information concerning PCF technology and its characteristics, as well as the acceptability of PCF-pizza. On the other hand, frozen dough has been widely applied in the bakery industry, which is reported to enhance productivity, streamline operations, and improve product quality. This study is distinctive in documenting the production of PCF by small-scale entrepreneurs, characterizing its properties, and demonstrating its application in frozen dough for an innovative product, PCF-pizza. The work uniquely integrates local cassava-based ingredients with a globally popular dish, highlighting both scientific innovation and socio-cultural value. The objectives of this study were to report the characteristics of PCF produced by small entrepreneurs, to assess the suitability of PCF for preparing frozen dough, and to evaluate the consumers' acceptability of PCF-pizza produced by an artisanal bakery.

2. Materials and Methods

2.1. Materials

Sweet cassava was supplied by a farmers' association in Warungkiara District, Sukabumi Regency, West Java Province. PCF was produced by a small entrepreneur (PT Infiad Indonesia) at Cigombong District, Bogor Regency, West Java Province. PCF-pizza was produced by the artisanal baking shop of Roti Boss at Kendal Payak District, Malang Regency, East Java Province. Figure 1 shows the area covered in this study. All baking ingredients, such as yeast, sugar, and margarine, were purchased from the local market. Chemicals of analytical grade, such as HCl, H_2SO_4, and PDA, were purchased from Indonesian distributors.

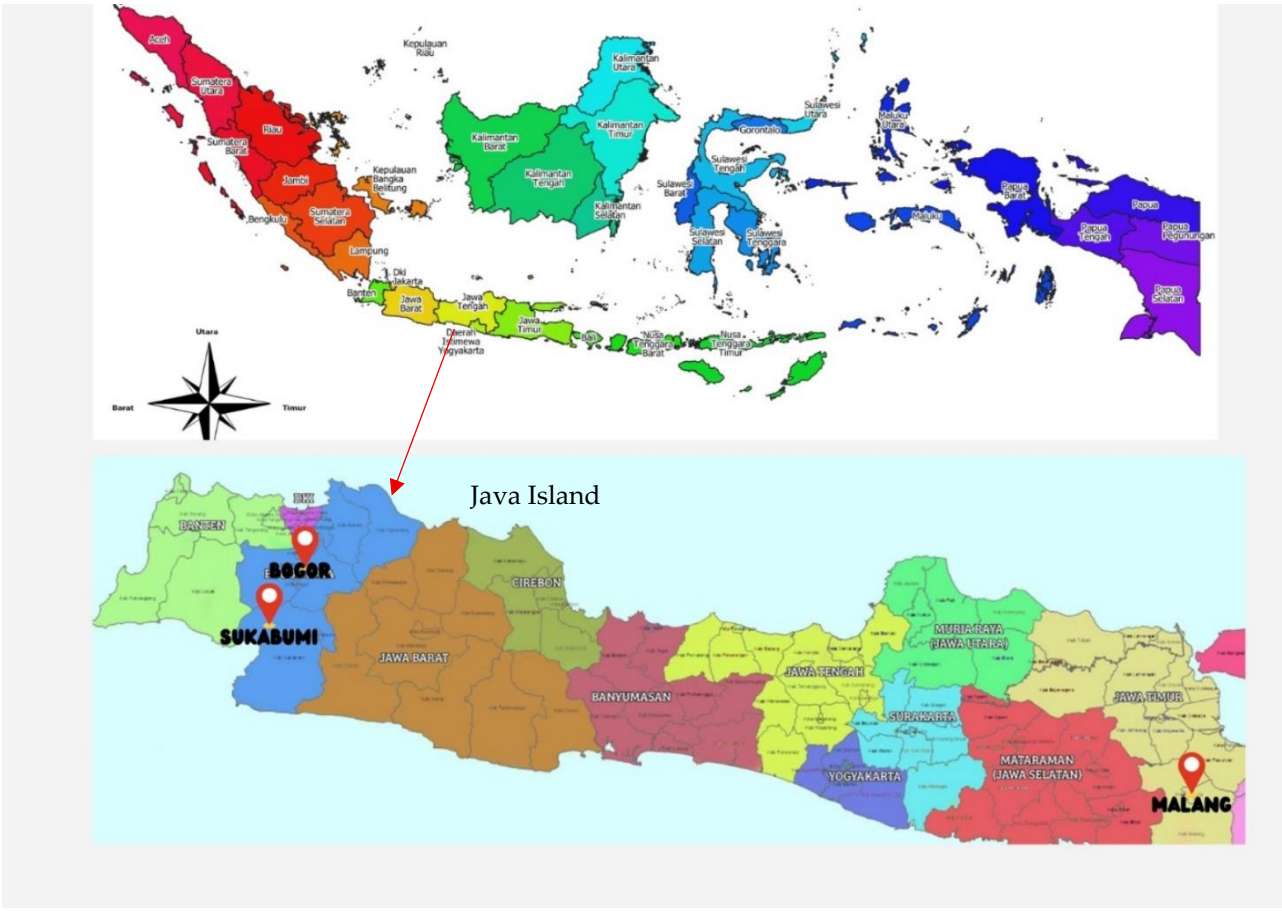

Figure 1. Geographical map of the study area

2.2. Survey and sampling of PCF

A survey conducted at PT Infiad Indonesia (Bogor, West Java) documented the PCF production technology, including descriptions of the machinery and its functions. PCF was taken for sample analysis and pizza formulation. It was packed in high-density polyethylene (HDPE) bags, placed in carton boxes, and delivered by car to the laboratory and an artisanal bakery. The ethical clearance No. 402/KE.01/SK/06/2023 was approved by the Ethics Commission on Social and Humanities, National Research and Innovation Agency, Republic of Indonesia.

2.3. Preparation of PCF-Based Dough and Artisanal Production of PCF-pizza.

The PCF (produced by PT Infiad Indonesia) was blended with rice flour and sago starch, with a weight proportion of 5:4:1, respectively. The basic recipe of the dough consisted of 200 g blended PCF flour, 3 g of xanthan gum, 0.6 g of bread improver, 3 g of yeast, 20 g of sugar, 40 g of margarine, 25 g of full-cream milk powder, 50 g of whole egg, and 250 mL of water. All ingredients were mixed in a bread maker machine (RB Bread RB250C). Mixing for 15 minutes, fermentation-proofing, and resting for 2 hours were automatically established by the machine. The dough was placed in a covered plastic container and immediately stored in a freezer at a temperature of -20 + 2 °C. After frozen storage for 0, 14, and 28 days, the dough was thawed at 25 °C for 1 hour. The dough was divided into 50 g pieces, molded, and then baked in a baking oven for about 10-15 minutes at 220 °C + 10 °C. The artisan baker of Roti Boss was asked to join in this study. She was selected due to her regularity, quantity in production, and experience with cassava flour utilization. She was intensively coached to produce PCF-pizza. The production process was followed step by step, from the dough preparation to the finished food (Figure 2). The baker was located in Malang, East Java Province.

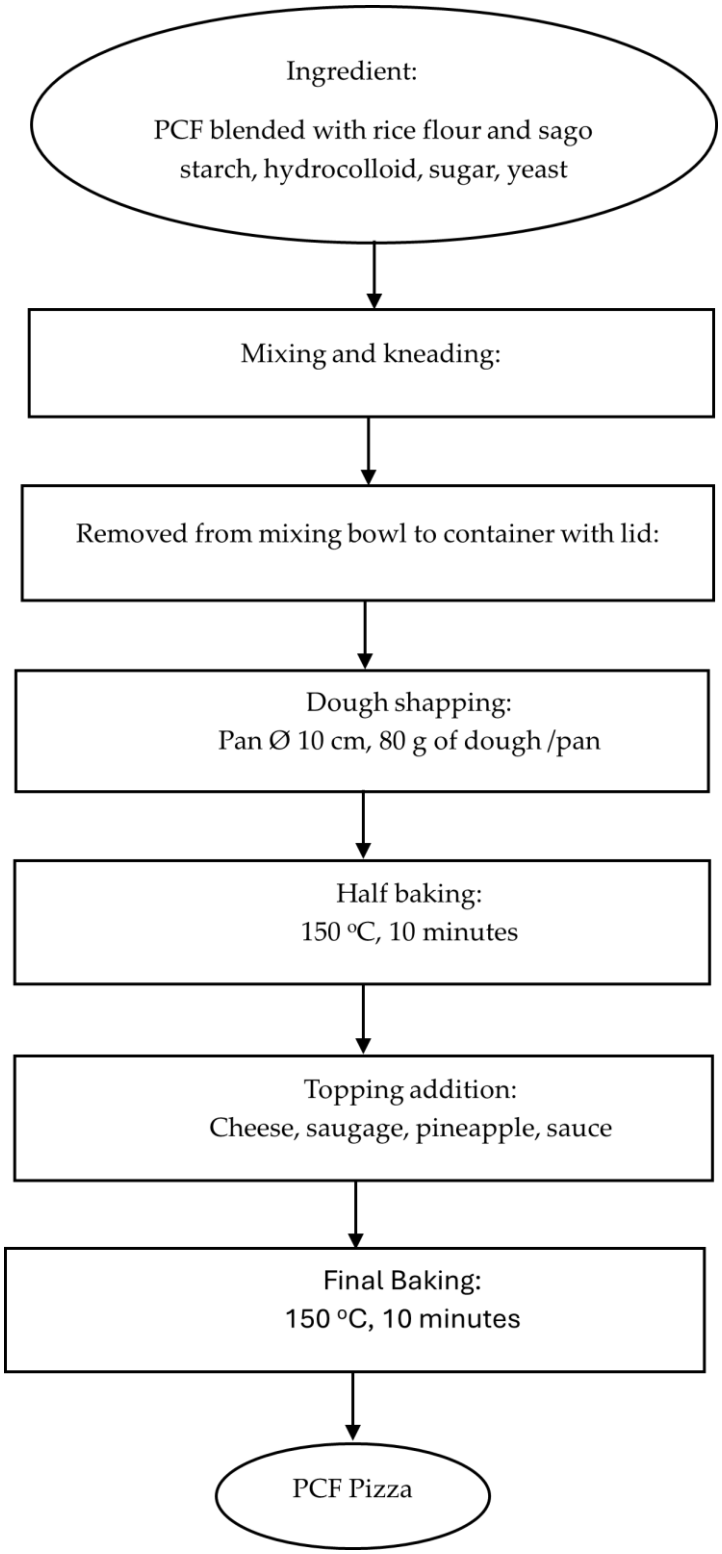

Figure 2. Overview of the production of PCF-Pizza

2.4. Physicochemical and Sensory Analysis

The national standard method, SNI 7622:2011 [17], was used for the analysis of moisture content, fat, protein, and microbiological contaminants. The polarized light microscope and Scanning Electron Microscope

(Zeissevoima-10) were applied to the observed starch granule of PCF [18]. The particle distribution was analyzed on a set of sieves [19]. The pasting properties were recorded by Rapid Visco Analyzer (Perten, Newport Scientific, Australia) [20]. Dough was analyzed for the viability of yeast (PDA method) and baking volume [14]. A picture was taken to observe crumb formation after the dough was baked. Sensory evaluation was conducted on PCF-pizza produced by an artisanal baker. A form was distributed to 69 of the selected consumers who attended the Roti Boss bakery shop. They were asked to evaluate the quality attributes of PCF-pizza in terms of color, texture, and taste. The evaluation was carried out in 3 categories (1: Dislike, 2: Neutral, 3: Like). They were also asked to state the reason for preferring PCF-pizza and the maximum price they were willing to pay for PCF-pizza.

2.5. Data Analysis

A single treatment factor was applied in the experiment on frozen dough storage. The data were analyzed using a two-way ANOVA with a single factor for the storage period, followed by Duncan's multiple range test at the $P < 0.05$ level. Data on consumer evaluation and the socio-economic characteristics of consumers were summarized, and descriptive statistics (percentages) were generated using Excel pivot tables.

3. Results and Discussion

3.1. Production technology and characteristics of PCF

Cassava flour contains starch, fiber, sugars, and small amounts of lipids and other components. It has different properties compared to cassava starch, which forms a more cohesive paste when cooked. Pregelatinized flour is flour that has undergone partial or complete gelatinization. The typical method for the pre-gelatinization process includes spray drying, extrusion, and drum drying [21]. This means that the starch in the flour was heat-treated with the availability of suitable water. According to Indonesian Regulation Number 13/2023 [22], PCF was categorized under No. 06.2.1 and thus could be used as a raw material by food processors. PCF was produced by a small entrepreneur (PT. Infiad Indonesia), located in Cigombong village, Bogor Regency, West Java Province. Dehydrated cassava chips as raw material were supplied by a farmers' association in Sukabumi Regency, West Java Province, located approximately 80 km south of Bogor. Farmers who supply cassava implement good agricultural practices (GAP). GAP implementation was important because the PCF processor required a consistent and high-quality raw material supply. GAP implementation on cassava has already been reported [23]. The dehydrated cassava chips were used as raw materials. The production of PCF on a commercial scale has been made possible through research in new cassava processing innovations, including the designs of machinery and partnerships between the government and small enterprises. In the case of PCF production, the Indonesian government invested in machinery that consisted of a pin mill, mixer machine, extruder, dryer, and pulverizer. The equipment was installed in accordance with the Good Manufacturing Practice (GMP) standard. The general steps of PCF production were described in Patent No.IDP000084586, published in Indonesia [24]. Table 1 summarizes the principal processing machinery for PCF production. It was reported that approximately 5 tons of PCF were produced in 2021, which was about 25% of the full capacity.

Table 1. General overview of PCF production

Step	Description	Equipment
Preparation	Dried cassava was selected as the raw material. The size of the cassava chip was reduced to a small size or milled into coarse flour.	Pinmill
Moisture Adjustment	Water was added to the flour to achieve a moisture content of 25%.	Mixer
Extrusion	The hydrated flour was subjected to heat and pressure. The screw in the extruder forces the material through a heated barrel at 60 °C to 90 °C, with screw speed at 45 Hz, causing the starch granules to gelatinize partially.	Twin screw extruder
Cooling	The material exits the extruder, and it is then rapidly cooled to stabilize the gelatinized structure. This cooling process was achieved using air.	Cooling Conveyor
Drying	The extrudate needs to be dried further to reduce its moisture content to a desired level (less than 12%), in order to prevent microbial growth and prolong its shelf life.	Drying oven
Grinding	The dried extrudate was ground into a fine powder	Pulverizer
Packaging & Storage	The pregelatinized flour was tested for quality control. It was then packaged into a plastic bag for storage and distribution.	Packaging machine

At the early stage of production, the PCF was delivered to the end user in the Bogor area. It was further processed by the food industry for use in making wafers and artisanal bakery shops [6, 13]. In this study, PCF was delivered to the end user of Roti Boss artisan bakery in Malang, East Java. With excellent transportation facilities, especially on Java Island, this technology has facilitated mass production and enabled PCF applications to be more intensive. Figure 1 shows the location of cassava farmers, PCF producers, and the PCF end user in this study. The technology for PCF production has provided opportunities for smallholder farmers to experiment with new ways of accessing more profitable markets. Cassava machinery and flour processing can be adopted by development agencies, NGOs, and research centers to enhance household food security, reduce food and raw material imports, and expand market options for smallholder farmers. Figure 3 presents the diagram of the PCF supply chain from farmer to end user.

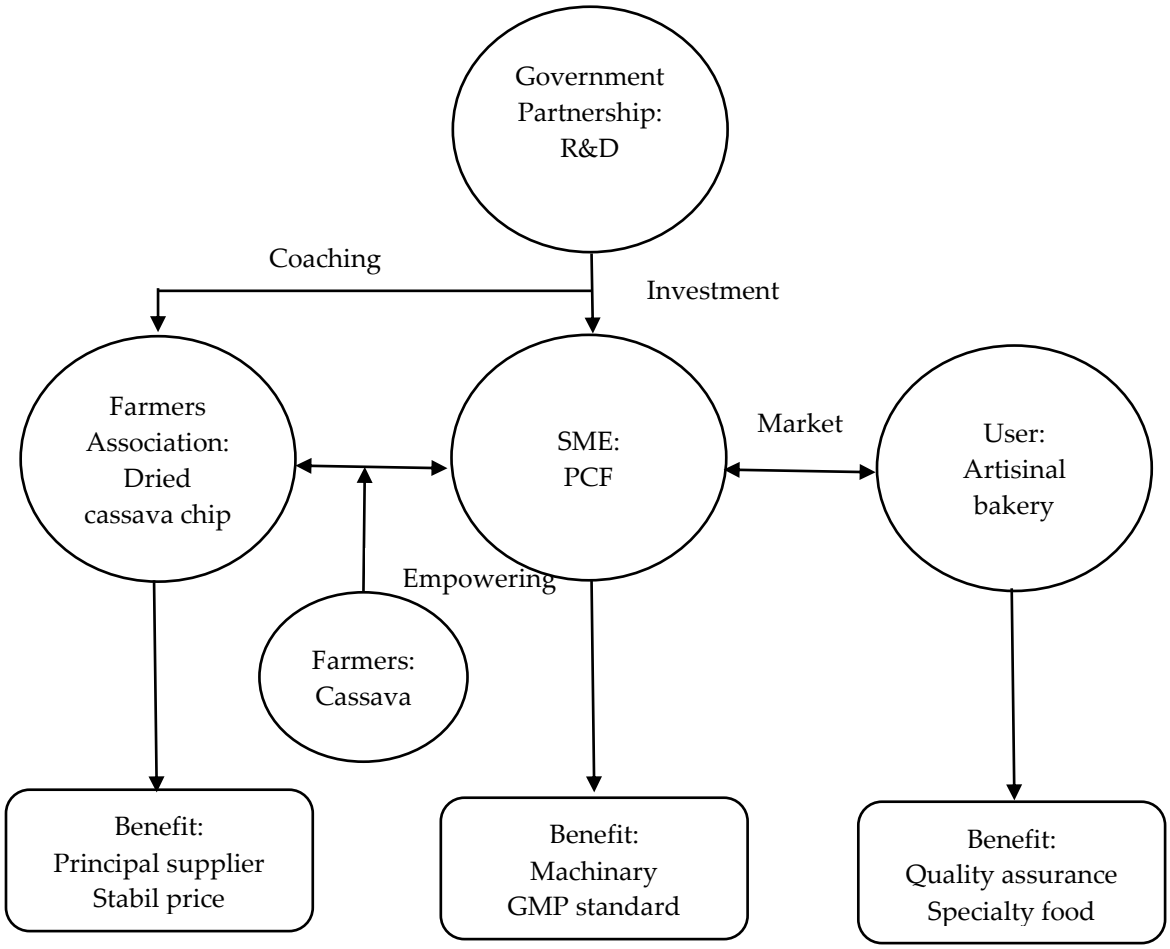

Figure 3. Diagram of cassava supply from farmers to the PCF processor and user

Table 2 shows the general characteristics of PCF produced by the small entrepreneurs at Cigombong. Low moisture content in PCF contributes to a longer shelf life. Extrusion technology has proven to be versatile in generating materials with distinct characteristics, particularly in the food production industry. Extrusion was also applicable for tuber flour refining [25]. At Cigombong, extrusion was conducted using a twin-screw extruder (local brand) with an initial temperature of 60 °C, a final temperature of 90 °C, a screw rotation speed of 44.7 Hz, and a cutter speed of 16 Hz.

Table 2. Characteristics of PCF

No	Characteristic	Value
1	Moisture (%)	9.74
2	Protein (%)	2.34
3	Fat (%)	0.28
4	HCN (ppm)	< 40
5	Microbiological contaminant or Total Plate Count (CFU)	1.2×10^4
6	Sensory properties:	White creamy color, tasteless, odorless

The application of the extrusion process for cassava flour resulted in a partially pre-cooked starch structure. The starch granules of native flour exhibit a characteristic of maltese cross pattern due to their crystalline structure, while those of PCF had a loss of birefringence. The extrusion process disrupted the

crystalline structure; therefore, fragmented granules and irregular shapes were observed. Figure 4 presents the photomicrograph of starch granules in PCF.

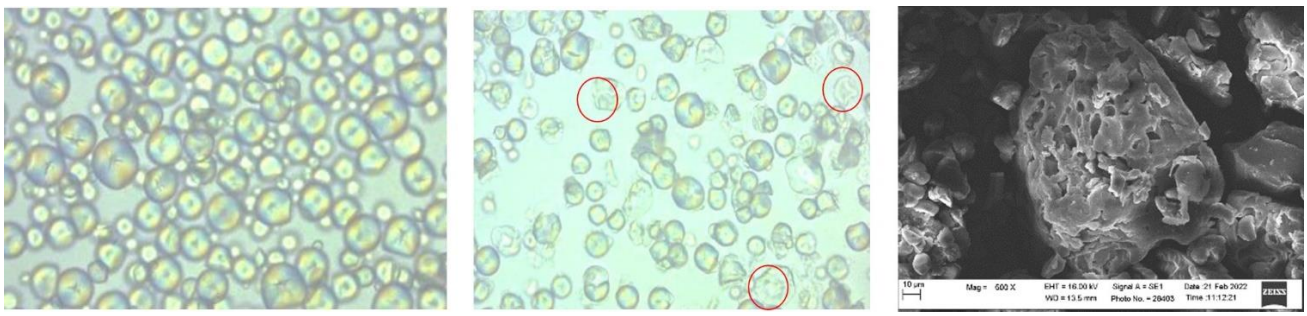

Figure 4. Starch granula (a) in native cassava flour under polarized light microscope, (b) PCF under polarized light microscope, (c) in PCF under scanning electron microscope.

The particle size, or granularity, is considered a key parameter for determining the quality of the flour after milling. The PCF was shown to have fine-sized particles (Figure 5). At least 95% of the flour passed through a 100-mesh sieve, and more than 90% passed through a 200-mesh sieve. This was comparable to the characteristics of wheat flour, where at least 98% of the flour passes through a 212-μm sieve [26]. The mesh number refers to the U.S. Standard Sieve Mesh number, which represents the number of openings per linear inch (2.54 cm) of the mesh. The mesh numbers 80, 100, 200, and 300 corresponded to particle sizes of approximately 177 μm, 149 μm, 74 μm, and 48 μm, respectively. The distribution of the flour's particle size would significantly affect the final product performance in terms of content uniformity, dissolution, thermal properties, and stability. The particle size distribution also affected the physical properties of the food powder, including bulk density, compressibility, and flowability [27,28]. It was reported that finer flours increased water-holding capacity and solubility [29]. Therefore, the PCF will have opportunities to fulfil the food ingredient market's requirements with its functional properties. It was stated that the specific functional properties of heat-processed pregelatinized cassava flours could facilitate their incorporation into various product formulations, such as baked goods and gluten-free functional foods. This could enhance the utilization of local starch sources and potentially reduce costs by substituting imported ingredients [30].

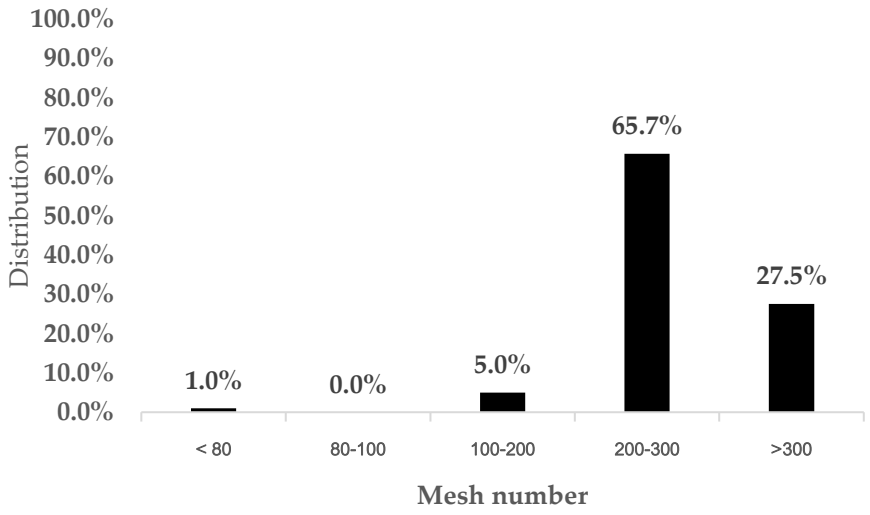

Figure 5. Particle size distribution of PCF

Pasting properties were important for controlling viscosity behavior during the processing and storage of several food systems. The PCF exhibited lower hot viscosity and higher cold viscosity than the non-PCF, due to the starch granules being pregelatinized (Figure 6). A significant decrease in the pasting profile

of extruded cassava flour was previously reported [12,31]. It reflects a higher degree of gelatinization, coupled with starch degradation, due to the net effect of heat, moisture, and echanical energy applied during the extrusion process [31].

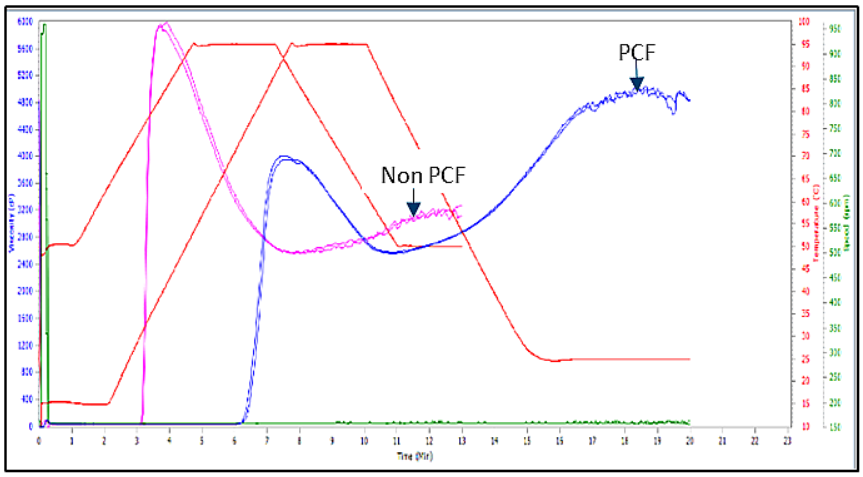

Figure 6. Pasting the profile of PCF and non-PCF

The food industry should benefit from pregelatinized cassava flour. Migration toward the application of this type of flour will encourage farmers to diversify their production. Not only will cassava use increase, but also the use of other roots and tuber crops, gluten-free cereals, and edible palms. It also provides an opportunity to revitalize the cassava flour market at a time when cassava consumption is continuously decreasing due to the adoption of Western lifestyle foods and the neglect of traditional recipes.

3.2 PCF-Based Dough Characteristics and Consumers' Acceptability of PCF-pizza

In recent years, frozen dough has gained widespread adoption in the bakery industry. The development of frozen dough has brought numerous benefits to companies, including convenient storage and transportation, as well as an extended shelf life. Frozen dough was a cost-efficient choice as bakeries can employ fewer skilled in-store bakers since base bread dough is already prepared and ready to use. It also allows bakeries to be more responsive to consumer needs, avoiding occurrences of running out of stock or over-stocking, which leads to wastage. Moreover, frozen dough helps create new market opportunities. Bakers can expand their distribution area and product range to introduce new bread products consistently. Expanding a product range is made easier by the flexibility of frozen dough, as the same frozen base dough can be customized to suit different consumer preferences in terms of shape, size, fillings, and toppings. In this study, frozen dough was preliminarily developed, and the results are presented in Table 3. The viability of yeast cells declined after 14 days and 28 days of frozen storage. However, a survival rate of more than 90% was observed in yeast. Under frozen conditions, yeast cells were susceptible to dying because of the rapid formation of ice crystals in the environment. Without the proper cryoprotectant, the yeast cell membrane can rupture, rendering biological functionality unfeasible after the thawing process [32]. Our study indicated that the yeast cells were well protected during the frozen storage of the dough. It was speculated that the freezing tolerance of yeast cells was closely associated with the presence of xanthan gum. Xanthan gum affects the water absorption properties of the food matrix and thus limits the freezing water content. This occurs due to the connection of free water; in this way, the migration of water through the intracellular medium decreases, which reduces the formation of ice crystals and promotes a decrease in the freezing point [21,33].

Table 3. Quality attribute of frozen dough during storage for 0, 14, and 28 days storage

Attribute	0 Day	14 Days	28 Days
Viability (CFU/g)	$1.1 \times 10^8 + 2.83^{a}$	$9.2 \times 10^6 + 7.07^{b}$	$6.1 \times 10^6 + 18.38^{b}$
Volume (cm^3)	$15.05 + 1.26^{a}$	$7.06 + 0.11^{b}$	$5.82 + 0.55^{c}$

Volume was commonly used to indicate consumer preferences for bakery products. The volume of frozen dough baked samples decreased as the storage time prolonged. The volume of bread was strongly related to the gas production of yeast cells and the retention capacity of the gluten-like network provided by xanthan gum. This finding aligns with the study reported by [21]. Crumb refers to the inner part of a bakery product. It should be open and airy, with uniform distribution of pores or holes. This characteristic could be achieved through proper fermentation, kneading, and baking. Figure 7 shows the appearance of the sectional structure of the baked product derived from PCF-based dough. It was found that the pore size was not uniform. The pore appearance did not differ significantly among the samples. Frozen storage produced many ice crystals, which mechanically disrupted the structural integrity of starch, causing the double helix structure of starch to break and rearrange [21]. Based on the volume and crumb properties, frozen dough stored for 14 days was still suitable for producing PCF-pizza.

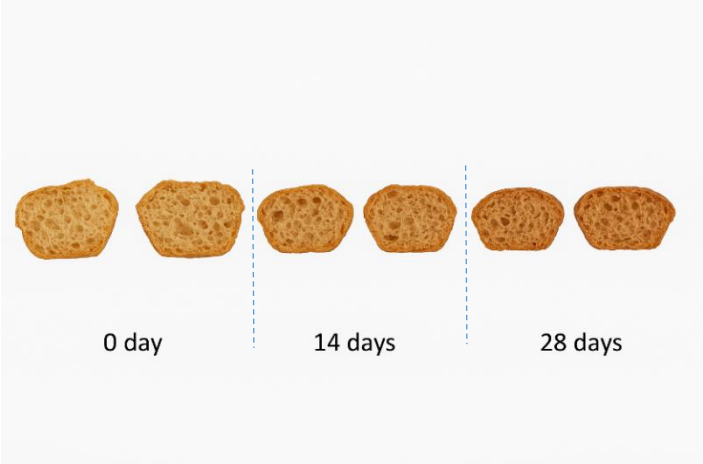

Figure 7. Pore/crumb of baked products derived from dough after frozen storage

This study was carried out through contact with artisan bakers who have experience in making artisan bakery products, including pizza, in Malang Regency, East Java. The baker used wheat flour to make pizza, and she had no experience making pizza with non-wheat flour. Most artisan bakers lacked the experience to handle frozen dough. It is worth noting that the fusion dish of PCF-pizza was categorized as a gluten-free bakery. The baking conditions were assessed thanks to the experience of the artisan bakers. The formulation involved adjusting the composition of the ingredients to meet not only the technological requirements of the pizza but also the nutritional and organoleptic needs of the consumer. The mixture of PCF flour and all ingredients, including sugar, water, and commercial yeast, was well-kneaded in a standing mixer to homogenize the dough. The dough was then incubated for 2 hours before being shaped. The shaping of the dough was manually carried out using a pan (diameter Ø 10 cm) filled with 80 g of dough. The shaped dough was partially baked in the baking oven at 150°C for 10 minutes. They were then placed on a table at room temperature for additional topping. The dough was further baked at 150 °C for 10 minutes. Dough preparation and baking of the PCF-pizza were carried out successively in a short time. It was noticed that PCF-pizza has a similar appearance to regular pizza (Figure 8).

Figure 8. PCF-Pizza (left) half-baked and (right) fully baked

The characteristics of 69 respondents participating in this study are presented in Table 4. The participant number meets international ISO recommendations of (30–100). A larger panel provides more accurate and consumer-representative sensory results. It was noted that of the total 69 respondents, 78% were female, and 22% were male. Most of the respondents were > 20 < 50 years old. Based on their employment status, about 46% of the respondents were entrepreneurs, 27.5% were public servants, and the remaining 26% were students.

Table 4. Characteristics of respondents

Description	N	%
Gender		
•Female	54	78.3%
•Male	15	21.7%
Age		
•< 20-year-old	8	11.6%
•> 20 - < 30-year-old	27	39.1%
•> 30 - < 40	19	27.5%
•> 40 - < 50	12	17.4%
•> 50	3	4.3%
Employment status		
•Entrepreneurs	32	46.4%
•Public servants	19	27.5%
•Student	18	26.1%
Having experience in gluten-free bakery consumption		
•No	40	58.0%
•Yes	28	40.6%
Consider the importance of gluten-free products		
•No	8	11.6%
•Neutral	14	20.3%
•Yes	47	68.1%

The respondents' preferences for PCF-pizza are summarized in Figures 9, 10, and 11. About 40.6% of respondents have experience in gluten-free bakery consumption. However, most of the respondents (68.1%) considered the importance of gluten-free products. In general, the fusion dish of PCF-pizza was well accepted by respondents. Sensory attributes such as taste, texture, and color were preferred by 42.0%, 34.8%, and 36.2% of respondents, respectively. In addition, most respondents (63.8%) stated that the maximum price was IDR 30000 – 35000 for a medium-sized PCF-pizza (Ø 22 cm). These results suggest that PCF-pizza could be a viable option in the potential market of Malang Regency. It also agreed with the previous study [16]. Therefore, it was recommended that efforts be made to ensure market availability.

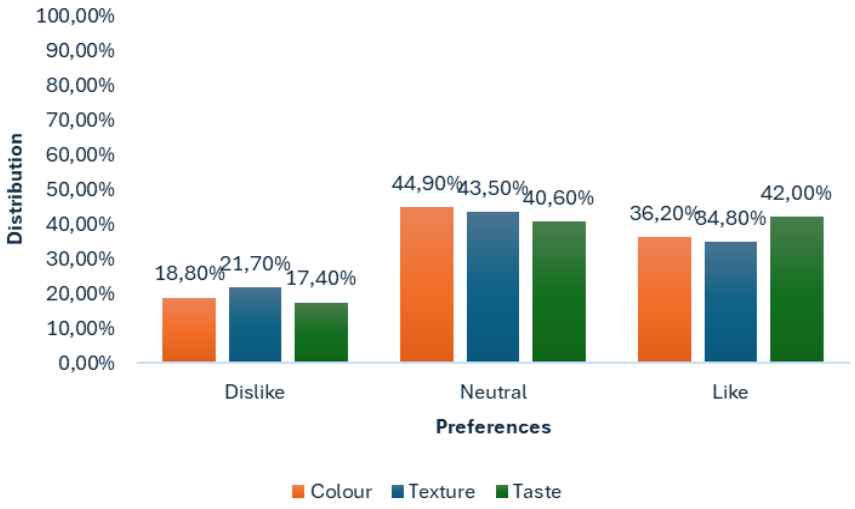

Figure 9. Consumers preferences on color, texture, and taste of PCF-Pizza

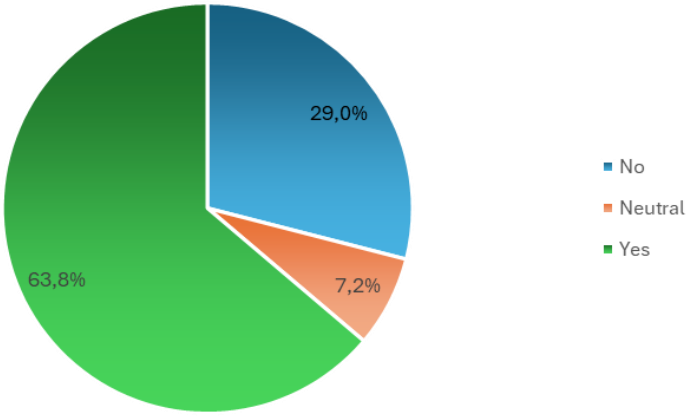

Figure 10. Consumers Willingness to Pay for PCF-Pizza

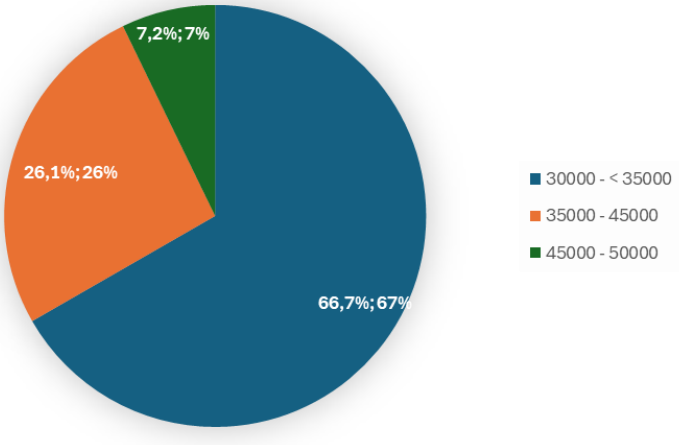

Figure 11. Consumers preference for price (IDR) of PCF-Pizza

The originality of this study lies in its combined focus on smallholder-produced PCF, frozen dough technology, and consumer acceptance of PCF-pizza. To our knowledge, no prior work has systematically linked cassava flour innovation with frozen dough applications and artisan-level product development. By bridging traditional cassava utilization with contemporary food trends, the study provides novel insights into the functional properties of PCF and its role in enhancing the competitiveness of local agro-industrial products.

4. Conclusions

PCF was considered a new cassava processing innovation, achieved by combining extrusion cooking with milling using a pulverizer. This process ensures that the PCF has a unique characteristic, including the special structure and fine texture of the pre-cooked starch. Overall, the findings provide valuable insights into the PCF's contribution to the development of the acceptable fusion dish, PCF-pizza, especially in Malang, East Java. It was found that frozen dough stored for 14 days was still suitable for producing PCF-pizza. PCF-pizza's potential market was available in the Malang Regency, as approximately 63% of the respondents accepted the color, texture, and taste of PCF-pizza.

5. Acknowledgments

The authors would like to express their gratitude to the Farmers Association of Sukabumi Regency, West Java Province, and the owner of Roti Boss, an artisanal bakery in Malang Regency, East Java Province, for their participation in this study.

Author Contributions: Conceptualization, E.Y.P., I.P.W., and R.R.; methodology, S.K.D., E.R., and E.G.; software, W.T.; validation, S.K.D., B.S., and M.O.A.; formal analysis, E.R. and E.G.; investigation, E.G., D.A.A.E., and M.; resources, R.R.; data curation, S.K.D., B.S., and M.O.A.; writing—original draft preparation, E.Y.P., I.P.W., and W.T.; writing—review and editing, E.Y.P., S.K.D., B.S., A.S.H., and S.M.P.; visualization, M.; supervision, S.M.P.; project administration, I.P.W.; funding acquisition, E.Y.P., I.P.W., and D.N.A. All authors have read and agreed to the published version of the manuscript.

Funding: This research was funded by RISPRO-LPDP under grant number PRJ-14/LPDP/2021, with co-funding from the National Research and Innovation Agency (BRIN) under grant number CRC-RP2A BRIN 2023. The Article Processing Charge (APC) was supported by Diponegoro University, under grant number 229/UN7.A/HK/IV/2024.

Conflicts of Interest: The authors declare no conflict of interest.

References

[1] Cempaka, L. Peuyeum: Fermented Cassava from Bandung, West Java, Indonesia. *J. Ethn. Foods* **2021**, *8*(3), 3. https://doi.org/10.1186/s42779-021-00079-3

[2] Ardiansyah, A.; Sihabudin, A.; Dua, M. Pseudo Identity in Cassava Rice as A Traditional Religious Identity Struggle Against Contemporary Religious Discrimination. *Indonesian J. Soc. Sci. Res.* **2024**, *5*(1), 20–29. https://doi.org/10.11594/ijssr.05.01.03

[3] Wae, V. P. S. M.; Priska, M.; Daud, M. H. Ethnoscientific Study of the Making of Traditional Uwi Kaju Ndota and Alu Ndene Food in Ende Regency. *J. Penelit. Pendidik. IPA* **2024**, *10*(4), 1969–1975. https://doi.org/10.29303/jppipa.v10i4.6293

[4] Andrade Neves, E. C.; Nascimento, G. C.; Ferreira, A. R.; Neves, D. A.; Fukushima, A. R.; Baffile Leoni, L. A.; Silva Clerici, M. T. P. Classification, Nutritional and Technological Characteristics of Cassava Flour Marketed in Belém, Pará, Brazil. *Braz. J. Food Technol.* **2020**, *23*, e2019143. https://doi.org/10.1590/1981-6723.14319

[5] Purwani Endang Yuli; Syamsuri Prayudi; Budianto Renny; Farid Bachtir; Nuning Argo Subekti. Pengembangan Teknologi produksi Tepung Pregelatinisasi Ubikayau sebagai Bahan Baku Inovatif Industri Pangan Nasional; **2022**.

[6] Afifah, D. N.; Ayustaningwarno, F.; Febriyanti, F.; Nadia, I. P.; Ratri, L. K.; Rahadiyanti, A.; Purwanti, R.; Wijayanti, H. S.; Nuryanto, N.; Ardiaria, M.; Murwani, R.; Zhu, F.; Pratiwi, S. N. Characteristics of Red Bean-Mocaf Biscuits as Alternative High-Fiber Low-Sugar Snacks. *Prog. Nutr.* **2024**, *26*(1), e2024040. https://doi.org/10.23751/pn.v26i1.15427

[7] Sumardiono, S.; Pudjihastuti, I.; Poerwoprajitno, A. R.; Suswadi, M. S. Physichocemical Properties of Analog Rice from Composite Flour: Cassava, Green Bean and Hanjeli. *World Appl. Sci. J.* **2014**, *32*(6), 1140–1146. https://doi.org/10.5829/idosi.wasj.2014.32.06.708

[8] Wahjuningsih, S. B.; Susanti, S. Chemical, Physical, and Sensory Characteristics of Analog Rice Developed from the Mocaf, Arrowroof, and Red Bean Flour. In *IOP Conference Series: Earth and Environmental Science*; Institute of Physics Publishing, **2018**, *102*, 012015. https://doi.org/10.1088/1755-1315/102/1/012015

[9] Putri, E. C. J.; Sumardiono, S. Fiber Content of Analog Rice Production from Composite Flour: Cassava, Avocado Seeds, and Tofu Waste. In *Journal of Physics: Conference Series*; Institute of Physics Publishing, **2020**, *1517*, 012027. https://doi.org/10.1088/1742-6596/1517/1/012027

[10] Febrianta, H.; Yunianto, V. D.; Nurwantoro, N.; Bintoro, V. P. Freeze-Drying Microencapsulation of Turmeric (*Curcuma Longa* l.) Using an Amorphous Matrix of Maltodextrin, Modified Cassava Flour and Skim Milk. *Ann. Univ. Dunarea Jos Galati Fascicle VI: Food Technol.* **2020**, *44*(2), 26–42. https://doi.org/10.35219/FOODTECHNOLOGY.2020.2.02

[11] Al-Baarri, A. N.; Legowo, A. M.; Rizqiati, H.; Widayat; Septianingrum, A.; Sabrina, H. N.; Arganis, L. M.; Saraswati, R. O.; Mochtar, R. C. P. R. Application of Iota and Kappa Carrageenans to Traditional Several Food Using Modified Cassava Flour. In *IOP Conference Series: Earth and Environmental Science*; Institute of Physics Publishing, **2018**, *102*, 012056. https://doi.org/10.1088/1755-1315/102/1/012056

[12] Parassih, E. K.; Purwani, E. Y.; Kiyat, W. El. Optimisation of Cassava Dried Noodle Using Hydrocolloid and Protein Isolates: A Tropical Noodle. *Future Food: J. Food, Agric. Soc.* **2020**, *8*(4). https://doi.org/10.17170/kobra-202010131943

[13] Haliza, W.; Kusuma, A.; Purwani, E.; Wardana, I. Consumer Acceptability of Special Wafer Made from Pregelatinized Cassava Flour. In *Proceedings ofthe 6th Food Ingredient Asia Conference (6th FiAC 2020) - Food Science, Nutrition and Health*; Scitepress, **2022**; pp 88–91. https://doi.org/10.5220/0010529600003108

[14] Ratnaningsih; Nilasari, R.; Purwani, E. Y. Bread Quality of Pregelatinized Cassava Flour with Frozen Storage. In *IOP Conference Series: Earth and Environmental Science*; Institute of Physics Publishing, **2019**; 309, p 012051. https://doi.org/10.1088/1755-1315/309/1/012051

[15] Fatihati, H. S.; Palupi, N. S.; Ratnaningsih, R.; Purwani, E. Y. Effect of Mannitol and Sago Starch on the Qualities of Frozen Dough Pizza from Rice-Pregelatinized Cassava Flour. *Food Res.* **2024**, *8*(S2), 108–118. https://doi.org/10.26656/FR.2017.8(S2).69

[16] Wardana, I. P.; Purwani, E. Y.; Dermoredjo, S. K.; Mutaqin; Sayaka, B.; Pasaribu, S. M.; Rochani, R.; Ginting, E.; Elisabeth, D. A. A. Business Model Strategy for Utilization of Pregelatinized Cassava Flour (PCF) by Micro-Small-Medium Enterprise (MSME). In *Proceedings of the 8th International Conference of Food, Agriculture and Natural Resources & the 2nd International Conference of Sustainable Industrial Agriculture (IC-FANRes-IC-SIA 2023)*; **2023**; pp 211–218. https://doi.org/10.2991/978-94-6463-451-8_19

[17] Badan Standardisasi Nasional (BSN). *Tepung mokaf*. SNI 7622:2011; BSN: Jakarta, **2011**; pp 1–43.

[18] Diyono, W.; Budiyanto, A.; Purwani, E. Y.; Aulia, S.; Rumaisha; Widaningrum. Physical Properties of Physico-Enzymatically Modified Sago Starch Originated from Papua: A Preliminary Study. In *IOP Conference Series: Earth and Environmental Science*; Institute of Physics, **2022**, *1024*, 012045. https://doi.org/10.1088/1755-1315/1024/1/012045

[19] Sonaye, S.; Baxi, R. N. Particle Size Measurement And Analysis Of Flour. *Int. J. Eng. Res. Appl.* **2012**, *2*(3), 195–200.

[20] Purwani Endang Yuli; Budianto Agus; Setyawan Nurdi; Yahya, D. R.; Ahza, A. B. Proceedings The 14 Th International Sago Symposium SAGO 2023 TOKYO. In *Proceedings The 14th International Sago Symposium SAGO 2023 TOKYO The Role of Sago in Achieving the Sustainable Development Goals*; The Society of Sago Palm Studies: Tokyo, **2023**; pp 41–45.

[21] Ma, H.; Liu, M.; Liang, Y.; Zheng, X.; Sun, L.; Dang, W.; Li, J.; Li, L.; Liu, C. Research Progress on Properties of Pregelatinized Starch and Its Application in Wheat Flour Products. *Grain Oil Sci. Technol.* **2022**, *5*(2), 87–97. https://doi.org/10.1016/j.gaost.2022.01.001

[22] Badan Pengawasan Obat dan Makanan (BPOM). *2023-Peraturan BPOM Nomor 13 Tahun 2023_231005_191921_katagori Pangan*. Decree No 13; Kementerian Kesehatan: Jakarta, **2023**.

[23] Subekti, N. A.; Purwanto, O. D.; Purwani, E. Y.; Taufiq, A.; Ramadhan, R. P.; Putu Wardana, I.; Damardjati, D. S.; Rochani, R.; Sasmita, P.; Syamsuri, P. Evaluating Cassava Best Management Practices towards Low Fertility Soil in West Java, Indonesia. In *IOP Conference Series: Earth and Environmental Science*; IOP Publishing Ltd, **2021**, *911*, 012028. https://doi.org/10.1088/1755-1315/911/1/012028

[24] Syamsuri, P.; Purwani, E. Y.; Budiyanto, A.; Diyono, W.; Rahayu, E.; Mulyono, E.; Damardjati, D. S.; Budijanto, M.; Subekti, N. A.; Wardana, I. P.; Ramadhan, R. P.; Purwano, O. D.; Wahyudi, M.; Danuarsa. KEMENTERIAN HUKUM DAN HAK ASASI MANUSIA REPUBLIK INDONESIA. IDP000084586, **2022**.

[25] Kumoro, A. C.; Retnowati, D. S.; Ratnawati, R. Chemical Compositions Changes during Hot Extrusion at Various Barrel Temperatures for Porang (*Amorphophallus Oncophyllus*) Tuber Flour Refining. In *Journal of Physics: Conference Series*; Institute of Physics Publishing, **2019**, *1175*, 012279. https://doi.org/10.1088/1742-6596/1175/1/012279

[26] CODEX ALIMENTARIUS. *STANDARD FOR WHEAT FLOUR*. Codex Alimentarius International Food Standards; FAO-WHO, **2023**.

[27] Suhag, R.; Kellil, A.; Razem, M. Factors Influencing Food Powder Flowability. *Powders* **2024**, *3*(1), 65–76. https://doi.org/10.3390/powders3010006

[28] Akbar, U.; Rasane, P.; Mondol, M. S. A.; Singh, J.; Nanda, V.; Kiliçgün, H.; Kaur, S. Impact of Particle Size on Physical and Functional Characteristics of Baby Corn Powder. *Turk. J. Agric. For.* **2025**, *49*(1), 75–88. https://doi.org/10.55730/1300-011X.3250

[29] Lu, M.; Yang, W.; Zhang, H.; Yu, Y.; Chen, F.; Hao, Y. Study on the Characteristics of Fine Rice Flour by Micro-Crushing and Its Effects on the Quality Improvement of Rice Cakes. *Foods* **2024**, *13*(22), 3565. https://doi.org/10.3390/foods13223565

[30] Krishnakumar, T.; Sajeev M. S.; Giri, N. Pre-Gelatinised Cassava Flour: Potential Applications in Food Industries. *Food Beverage News*. Kerala, June 9, **2020**.

[31] Fayose F, T.; Huan, Z. Pasting Characteristics of Cassava at Different Extrusion Conditions. *Agric. Eng. Today* **2014**, *1*(38), 6–11.

[32] Bhattacharya, S. Cryopretectants and Their Usage in Cryopreservation Process. In *Cryopreservation Biotechnology in Biomedical and Biological Sciences*; IntechOpen, **2018**. https://doi.org/10.5772/intechopen.80477

[33] Maity, T.; Saxena, A.; Raju, P. S. Use of Hydrocolloids as Cryoprotectant for Frozen Foods. *Crit. Rev. Food Sci. Nutr.* **2018**, *58*(3), 420–435. https://doi.org/10.1080/10408398.2016.1182892.

ASEAN
Journal of Scientific and Technological Reports
Online ISSN:2773-8752

Research article

Green Extraction of Bioactive Compounds from Tomato Pomace Using Fatty Acid Ethyl Esters Derived from Krabok Seed Oil

Sumana Tawil[1], Wuttichai Roschat[2, 3*], Sunti Phewphong[2, 3], Achiraya Srisai[4], Warinyupha Yathongchai[5], Praphatsara Hanchai[6], Ruchira Wiangpati[7], Butsabong Pongcomsing[8], and Tappagorn Leelatam[3, 9]

[1] Faculty of Science and Technology, Sakon Nakhon Rajabhat University, Sakon Nakhon, 47000, Thailand
[2] Faculty of Science and Technology, Sakon Nakhon Rajabhat University, Sakon Nakhon, 47000, Thailand
[3] Research and Development Institution, Sakon Nakhon Rajabhat University, Sakon Nakhon, 47000, Thailand
[4] Faculty of Science and Technology, Sakon Nakhon Rajabhat University, Sakon Nakhon, 47000, Thailand
[5] Faculty of Science and Technology, Sakon Nakhon Rajabhat University, Sakon Nakhon, 47000, Thailand
[6] Faculty of Science and Technology, Sakon Nakhon Rajabhat University, Sakon Nakhon, 47000, Thailand
[7] Faculty of Science and Technology, Sakon Nakhon Rajabhat University, Sakon Nakhon, 47000, Thailand
[8] Faculty of Science and Technology, Sakon Nakhon Rajabhat University, Sakon Nakhon, 47000, Thailand
[9] Faculty of Science and Technology, Sakon Nakhon Rajabhat University, Sakon Nakhon, 47000, Thailand
* Correspondence: roschat1@gmail.com

Citation:
Tawil, S.; Roschat, W.; Phewphong, S.; Srisai, A.; Yathongchai, W.; Hanchai, P.; Wiangpati, R.; Pongcomsing, B.; Leelatam, T. Green extraction of bioactive compounds from tomato pomace using fatty acid ethyl esters derived from Krabok seed oil. *ASEAN J. Sci. Tech. Report.* **2025**, *28*(6), e260061. https://doi.org/10.55164/ajstr.v28i6.260061.

Article history:
Received: June 30, 2025
Revised: September 12, 2025
Accepted: September 27, 2025
Available online: October 19, 2025

Abstract: Tomato pomace, a byproduct of food processing, is rich in bioactive carotenoids such as lycopene and β-carotene, which are valued for their antioxidant properties but typically extracted using toxic organic solvents. This study aimed to develop an environmentally friendly approach for extracting and quantifying these compounds using fatty acid ethyl esters (FAEE) derived from Krabok seed oil, in comparison with hexane. Conventional maceration extraction (ME) and ultrasonic-assisted extraction (UAE) were applied, and the extracts were analyzed for lycopene and β-carotene content, antioxidant activity, and storage stability. The results showed that the UAE was more efficient than ME, while hexane provided higher extraction yields due to its lower viscosity, with lycopene and β-carotene contents of 67.97–75.33 and 10.51–11.50 mg/100 g dry weight (DW), respectively. FAEE extraction yielded slightly lower amounts (59.92–63.60 mg/100 g DW lycopene and 1.63–7.01 mg/100 g DW β-carotene) but exhibited superior antioxidant activity, with DPPH inhibition up to 92.05% when combined with the extracted compounds. Stability tests further revealed that FAEE-extracted carotenoids were more resistant to degradation, retaining up to 90% lycopene and 85% β-carotene after 56 days, whereas hexane-extracted compounds degraded rapidly. Overall, FAEE demonstrates strong potential as a sustainable, non-toxic solvent for the recovery of bioactive carotenoids from tomato pomace, supporting applications in the food and cosmetic industries.

Keywords: Fatty acid ethyl esters (FAEE); green technique; lycopene; β–Carotene; antioxidant activity

1. Introduction

Tomatoes (*Lycopersicon esculentum* Mill.) are a significant economic and industrial crop in Thailand, widely consumed across the country. Sakon Nakhon Province leads the Northeast region in tomato production, with a total cultivation area of 5,232 rai. Tomatoes are rich in carotenoids, primarily lycopene

and β−carotene, which are red−orange pigments. Lycopene, abundant in red tomatoes, serves as a potent antioxidant. β−carotene, predominantly found in orange tomatoes, is a precursor for vitamin A synthesis, which is essential for maintaining healthy vision [1]. In addition to carotenoids, tomatoes are an excellent source of vitamins and minerals beneficial to human health, including vitamin C, vitamin A, and vitamin E [2]. Vitamin E, in particular, functions as an antioxidant, playing a critical role in supporting liver health and blood functions while combating free radicals [3]. Fresh tomatoes are commonly processed into products like juice and sauce, generating by−byproducts such as skins, peels, and seeds, which account for 10–15% of the fresh weight of the original tomatoes. These residual tomato pomace are typically extracted through maceration or ultrasonic extraction. In maceration, bioactive compounds are extracted by immersing the plant material in a suitable solvent, allowing passive diffusion of solutes across cell walls, followed by filtration and squeezing. While this method avoids heat degradation, it is solvent-intensive and time-consuming. In contrast, ultrasonic-assisted extraction relies on acoustic cavitation, where alternating high- and low-pressure sound waves (20–100 kHz) generate microbubbles that collapse violently, disrupting cell walls and enhancing solvent penetration. This accelerates mass transfer, reduces solvent usage, and improves extraction efficiency. Common solvents include water or organic solvents like hexane, which, while effective for non-polar compounds, pose environmental and health risks due to their volatility [5–6].

Many previous studies have highlighted the use of environmentally friendly extraction methods in place of chemicals. For instance, Sharma et al. [7] investigated the valorization of seabuckthorn pomace for extracting bioactive carotenoids using green extraction techniques. They applied ultrasonic and microwave−assisted extractions combined with green solvents like edible oils, aiming to improve extraction efficiency while minimizing environmental impact. This study advocates for sustainable methods to recover valuable carotenoids from by-products, offering an eco-friendlier alternative to conventional extraction processes in the food and pharmaceutical industries. Yara−Varón et al. [8] explored the use of vegetable oils as eco−friendly solvents for extracting and developing food and natural products. Oils like olive and coconut oil effectively and safely extract compounds such as phenols and carotenoids, reducing reliance on toxic synthetic solvents. This sustainable approach minimizes environmental impact and enhances the industrial value of vegetable oils. Despite challenges in cost and efficiency, it presents a promising alternative for safe, sustainable production. Diacon et al. [9] investigated fatty acid ethyl esters (FAEE) as a green solvent for extracting carotenoids from tomato waste. FAEE achieved up to 90% carotenoid recovery compared to hexane, reducing toxic chemical use and promoting sustainable practices. This efficient process adds value to agricultural waste and aligns with the goals of the circular economy.

The research report above highlights that vegetable oils and their derivatives, such as FAEE, are gaining attention as solvents for extracting bioactive carotenoids. This approach offers a promising alternative for developing environmentally friendly and safe green solvents for applying extracts in various fields. From the previous research report of our research group, it was found that the oil from Krabok seed (*Irvingia malayana*) contains major fatty acids, with lauric acid ($C_{12:0}$) and myristic acid ($C_{14:0}$) making up approximately 52% and 35% by weight, respectively. This places it in the category of oils with small molecules. Additionally, the oil demonstrates important chemical properties, including high oxidation stability and a low acid number [10]. Additionally, our research on the synthesis of FAEE from Krabok seed oil demonstrated its excellent potential for use in herbal massage oil. The process achieved a high yield of 99.83 ± 0.17% under optimal conditions. The FAEE primarily contained lauric acid ($C_{12:0}$) and myristic acid ($C_{14:0}$), with 97 wt.% saturated fatty acids. Its physicochemical properties included a viscosity of 1.73 ± 0.03 cSt/s, density of 0.8199 ± 0.0049 g/cm^3, cloud point of +4 °C, and pour point of −1 °C. Additionally, it exhibited good acidity and oxidation stability, making it a sustainable and promising ingredient for cosmetic applications [11]. The low viscosity of FAEE enables better penetration into plant matrices, thereby enhancing mass transfer and improving extraction efficiency. Its high oxidation stability also prevents degradation of sensitive carotenoids during extraction. Moreover, as it is derived from renewable sources and biodegradable, FAEE aligns with the principles of green chemistry, offering a safer and more sustainable alternative to conventional organic solvents such as hexane.

Although previous studies have explored various green solvents and extraction methods for recovering carotenoids from plant by-products, there is limited research on the use of FAEE derived from locally available Krabok seed oil as an eco–friendly solvent for tomato pomace. Therefore, this study investigates extraction techniques and quantification of bioactive compounds from tomato pomace, a waste byproduct of processing, employing environmentally sustainable methods. Solvent extraction methods, including conventional maceration and ultrasonic–assisted extraction, were utilized. FAEE derived from the transesterification of Krabok seed oil was evaluated as a solvent and compared to hexane, given that both lycopene and β-carotene are non–polar and fat–soluble. FAEE demonstrated efficacy as a solvent. The bioactive compounds, specifically lycopene and β–carotene, were quantified using ultraviolet–visible spectroscopy. Additionally, antioxidant activity was assessed using the DPPH assay, providing critical insights for optimizing extraction techniques and laying the groundwork for potential applications in food or cosmetic products.

2. Materials and Methods

2.1 Materials

The tomato pomace was sourced from the Royal Food Processing Factory No. 3, located in Tao Ngoi Subdistrict, Tao Ngoi District, Sakon Nakhon Province, Thailand. The preparation process involved drying the pulp at 50 °C for 8 h, followed by fine grinding and sieving. The processed pulp was then stored in a −40 °C freezer to maintain its quality and prevent mold growth by avoiding exposure to humidity. Fatty acid ethyl esters (FAEE) derived from the transesterification of Krabok seed oil were obtained from the Biomass Energy Laboratory, Research and Development Institute, Sakon Nakhon Rajabhat University, Thailand. The physicochemical properties of FAEE were investigated and reported in the study by Thangthong et al. [11]. The main chemicals used in this research included hexane (C_6H_{14}), ethanol (C_2H_5OH), acetone (C_3H_6O), 2,2–diphenyl–1–picrylhydrazyl (DPPH), lycopene standard ($C_{40}H_{56}$), and β–carotene standard (β–carotene; $C_{40}H_{56}$). All chemicals were of AR grade and sourced from RCI Lab Scan, QREC, Aldrich, and Sigma–Aldrich brands.

2.2 Study of the Efficiency of Extraction Techniques

The study of the efficiency of bioactive compound extraction techniques in this research includes simple maceration extraction (ME) and ultrasonic–assisted extraction (UAE) using hexane and FAEE as solvents. For the simple maceration extraction, about 1 g of dried tomato pomace is weighed (with the exact weight recorded) and placed in a brown bottle. Then, 10 mL of hexane is pipetted into the bottle, and the mixture is shaken using a shaker for 1 min. The bottle is then placed in a hot water bath at 50 °C for 60 min. These extraction temperatures and durations were selected to optimize carotenoid recovery while minimizing thermal degradation, as reported in previous studies [5–6]. Although carotenoids such as lycopene and β-carotene are heat-sensitive, these conditions have been shown to preserve the majority of compounds, ensuring reliable quantification. After the heating period, the solution is centrifuged at 3,000 rpm for 10 min. The resulting solution is stored in a brown bottle and kept in a refrigerator at −20 °C until further analysis. This process is repeated twice more. The same experiment is then conducted, but with FAEE replacing hexane as the solvent. The ultrasonic extraction process began by accurately weighing 1 g of dried tomato pomace (recording the exact weight) and placing it in a brown bottle. Next, 10 mL of hexane was added, and the mixture was shaken for 1 min using a shaker. The sample was then subjected to ultrasonic treatment in an ultrasonic cleaner at 50 °C and 40 kHz with an ultrasonic power of 120 W (power density ≈ 12 W/100 mL) for 60 min, following conditions reported in previous studies [5–7]. After ultrasonic-assisted extraction, the solution was centrifuged at 3,000 rpm for 10 min. The resulting supernatant was transferred to a brown bottle and stored in a refrigerator at −20 °C for further analysis. The experiment was repeated two more times under the same conditions. Subsequently, the procedure was repeated using FAEE as the solvent instead of hexane. All experiments were performed in triplicate (n = 3), and results are expressed as mean ± SD.

2.3 Determination of lycopene and β–carotene content in tomato pomace extracts

The analysis was performed following methods modified from Diacon et al. [9] and Fish [12]. The procedure began with creating an equation for calculating the amount of lycopene. A lycopene standard

solution was prepared by weighing 0.0050 g of lycopene standard (containing 6.4% lycopene), dissolving it in hexane, and diluting it to 50 mL in a volumetric flask to achieve a concentration of 6.4 mg/L. The standard solution was freshly prepared and used immediately. The subsequent steps involved repeating the process using FAEE as the solvent in place of hexane. A series of lycopene solutions with varying concentrations was then prepared by pipetting 1.5, 3.0, 4.5, 6.0, and 7.5 mL of the 6.4 mg/L lycopene standard solution into separate volumetric flasks and diluting each to 10 mL with hexane. This produced solutions with lycopene concentrations of 0.96, 1.92, 2.88, 3.84, and 4.8 mg/L, respectively. These solutions were used to construct standard curves at wavelengths of 450 and 503 nm. The experimental procedure was then repeated with FAEE as the solvent instead of hexane for comparative analysis.

The β−carotene standard solution was prepared by weighing 0.0050 g of β−carotene standard (containing 97.5% β−carotene), dissolving it in hexane, and adjusting the volume to 50 mL in a volumetric flask. This resulted in a β−carotene standard solution with a concentration of 97.5 mg/L, which was freshly prepared and used immediately. The experiment was repeated using FAEE as the solvent instead of hexane. The β−carotene solutions at various concentrations were then prepared as follows:

1) The standard graph at 450 nm (hexane and FAEE as solvents): The β−carotene standard solution (97.5 mg/L) was pipetted in volumes of 0.1, 0.2, 0.3, 0.4, and 0.5 mL, and the volume was adjusted to 10 mL with the respective solvent (hexane or FAEE). This yielded solutions with concentrations of 0.975, 1.95, 2.925, 3.9, and 4.875 mg/L.

2) the standard graph at 503 nm (hexane as solvent): The β−carotene standard solution was pipetted in volumes of 0.1, 0.5, 1.0, 1.5, and 2.0 mL, with the volume adjusted to 10 mL using hexane. The resulting concentrations were 0.975, 4.875, 9.75, 14.625, and 19.5 mg/L.

3) The standard graph at 503 nm (FAEE as solvent): The β−carotene standard solution was pipetted in volumes of 0.1, 0.3, 0.5, 0.7, and 0.9 mL, and the volume was adjusted to 10 mL using FAEE. This produced solutions with concentrations of 0.975, 2.925, 4.875, 6.825, and 8.775 mg/L.

These prepared solutions were used to construct β−carotene standard graphs at the specified wavelengths for comparative analysis between hexane and FAEE solvents. All prepared solutions were analyzed for absorbance using a UV−Visible spectrophotometer at the specified wavelengths of 450 and 503 nm. The measured absorbance values were used to construct standard curves by plotting absorbance against concentration (mg/L). Linear equations were derived from each curve, and the absorptivity values (ε) were calculated. These absorptivity values were then applied to the following equations for further analysis:

$$A_{503} = A_{lyc\text{-}503}\cdot[lyc] + A_{\beta\text{-}car\text{-}503}\cdot[\beta - car] \quad (1)$$

$$A_{450} = A_{lyc\text{-}450}\cdot[lyc] + A_{\beta\text{-}car\text{-}450}\cdot[\beta - car] \quad (2)$$

In addition, the concentration ranges selected for the calibration curves were justified based on preliminary assays and the expected analyte concentrations in the tomato extracts after applying the dilution factors. For lycopene, the calibration range (0.96–4.80 mg/L) was sufficient to cover the calculated concentrations of the extracts, which were approximately 1.75 mg/L for hexane extracts (df = 40) and 2.80 mg/L for FAEE extracts (df = 25), based on a lycopene content of ~70 mg/100 g DW. For β-carotene, the calibration ranges (0.975–4.875 mg/L at 450 nm; 0.975–19.5 mg/L at 503 nm; and 0.975–8.775 mg/L in FAEE) were also appropriate, although lower concentrations in some extracts (e.g., ~0.28 mg/L for hexane) required adjusting dilution factors to ensure that the measured concentrations fell within the validated linear ranges. Thus, the selected calibration ranges ensured accurate quantification while maintaining linearity and sensitivity.

In this study, the absorbance values at wavelengths of 503 nm and 450 nm, denoted as A_{503} and A_{450}, respectively, were measured. The absorptivity coefficients for lycopene and β−carotene at these wavelengths were also determined. Specifically, $A_{lyc\text{-}503}$ represents the absorptivity of lycopene at 503 nm, while $A_{lyc\text{-}450}$ represents the absorptivity of lycopene at 450 nm. In this study, the absorptivity coefficients are expressed in liters per milligram (L/mg) because the sample concentration was calculated in mg/L and the path length of the cuvette used in the UV−visible spectrophotometer was 1 cm. Therefore, the path length term (cm^{-1}) in the

conventional unit (L/mg·cm) is omitted, as it equals unity under these experimental conditions. Similarly, $A_{\beta\text{-car-503}}$ and $A_{\beta\text{-car-450}}$ represent the absorptivity of β−carotene at 503 nm and 450 nm, respectively. Using these values, the concentrations of lycopene and β−carotene, denoted as [lyc] and [β−car] (in mg/L), were calculated by substituting the absorbance and absorptivity values into the corresponding equations. This approach ensured accurate quantification of the pigments based on their distinct spectral characteristics.

The determination of lycopene and β−carotene content in tomato pomace samples extracted using various techniques was carried out by measuring the absorbance of the sample solutions with a UV−Visible spectrophotometer at wavelengths of 450 nm and 503 nm. The recorded absorbance values were then used to calculate the concentrations of lycopene and β−carotene in mg/L using the equations derived from the standard curves. Finally, the amounts of lycopene and β−carotene were reported in terms of mg per 100 g of dry weight (mg/100 g DW) using the following equations:

$$\text{Lycopene or β−carotene content (mg/100 g DW)} = [(C/1000) \times df \times (V/W)] \times 100 \quad (3)$$

Where: C is the concentration of lycopene or β-carotene in the sample solution (mg/L), df is the dilution factor of the sample, V is the volume of the extract used for the analytical measurement (mL), and W is the weight of the dry sample (g). The determination of lycopene and β−carotene content in tomato pomace samples extracted using these techniques was carried out in three replicates to ensure accuracy and reliability of the results. The absorbance measurements were taken for each replicate, and the concentrations of lycopene and β−carotene were calculated using the corresponding equations. The results were then averaged to obtain the final values for lycopene and β−carotene content in the samples. All experiments were performed in triplicate (n = 3), and results are expressed as mean ± SD.

2.4 Antioxidant activity test by DPPH method

The DPPH antioxidant activity assay was adapted from the method of Chu et al. [13], Preecharram et al. [14], and Phewphong et al. [15]. The experimental procedure began by preparing a 0.3 mM DPPH solution. This was done by weighing 0.0059 g of 2,2−diphenyl−1−picrylhydrazyl (DPPH radical), dissolving it in ethanol, and adjusting the volume to 50 mL in a volumetric flask (the solution should be prepared and used immediately). Next, a 5−fold diluted sample extract was prepared by pipetting 5 mL of the sample extract into a volumetric flask and adjusting the volume with hexane to 25 mL. The experiment was repeated as described, but the sample extract was replaced with FAEE. For the antioxidant activity test, 3 mL of the diluted sample solution was pipetted into a test tube, followed by the addition of 1.5 mL of DPPH solution. The solution was mixed by shaking for 10 seconds with a vortex mixer and then left in the dark for 15 min. The concentration of extracts used in the DPPH assay corresponded to a 5-fold dilution of the crude extracts, ensuring that absorbance values were within the measurable range of the assay. The absorbance of the solution was measured using a UV−Visible spectrophotometer at a wavelength of 540 nm. The absorbance values were then used to calculate the percentage of DPPH inhibition (% DPPH inhibition) using the following equation:

$$\%\ \text{DPPH inhibition} = [A_0 - (A - A_b)/A_0] \times 100 \quad (4)$$

Where: A_0 is the absorbance of the DPPH solution without the sample. A is the absorbance of the DPPH solution with the sample. A_b is the absorbance of the sample without DPPH. This equation measures the effectiveness of the sample in inhibiting the DPPH radical, reflecting its antioxidant activity. All experiments were performed in triplicate (n = 3), and results are expressed as mean ± SD.

2.5 Stability study of lycopene and β-carotene

The stability of lycopene and β-carotene in tomato pomace extracts obtained via ultrasound-assisted extraction (UAE) using FAEE as a solvent was evaluated over a period of 56 days. For the study, all extracts were stored in opaque amber glass containers to prevent light-induced degradation. The containers were tightly sealed to minimize oxygen exposure and evaporation. Samples were kept at a controlled temperature of 4 °C in a refrigerator with relative humidity below 60%. At predetermined intervals (0, 7, 14, 21, 28, 42, and 56 days), aliquots were taken to measure the concentrations of lycopene and β-carotene, as well as the DPPH

radical scavenging activity, following the procedures described in Section 2.4. These controlled storage conditions ensured reproducibility of the stability study. All experiments were performed in triplicate (n = 3), and results are expressed as mean ± SD.

2.6 Statistical analysis

The analysis of variance (ANOVA) was conducted using a one–way ANOVA to assess differences between experimental groups. Post–hoc comparisons were made using Duncan's multiple range test at a 95% confidence level. All statistical analyses were performed using the Statistical Package for the Social Sciences (SPSS) software.

3. Results and Discussion

3.1 Physical characteristics of extracts from tomato pomace

The bioactive compounds were extracted from tomato pomace obtained from the Royal Project Food Factory 3, Tao Ngoi District, Sakon Nakhon Province. The tomato pomace was pretreated by baking at 50 °C for 8 h, followed by fine grinding and sieving. Two extraction techniques were employed: maceration extraction (ME) and ultrasonic–assisted extraction (UAE), using hexane and fatty acid ethyl esters (FAEE) as extraction solvents. The physical characteristics of the resulting extracts are presented in Figure 1(a) and (b). For ME, the extracts obtained with hexane as the solvent (tubes 1, 2, and 3) were observed as clear orange liquids. In comparison, extracts obtained using FAEE as the solvent (tubes 4, 5, and 6) exhibited a darker orange hue than those obtained with hexane. Similarly, the UAE method produced extracts with hexane (tubes 7, 8, and 9) and FAEE (tubes 10, 11, and 12) that displayed physical characteristics consistent with those obtained through the ME method. This suggests that the solvent type had a more pronounced effect on the coloration of the extracts than the extraction method employed. The darker orange hue observed in extracts obtained with FAEE is attributed to its higher solubilization capacity for non-polar carotenoids, thereby enhancing pigment extraction compared to hexane. FAEE itself exhibits a slightly pale yellow color, indicating that the observed coloration primarily reflects the concentration of extracted bioactive compounds rather than the solvent's inherent color. This suggests that solvent selection can significantly influence both the yield and apparent intensity of carotenoid–containing extracts. It is worth noting that the color evaluation in this study was based on visual observation. Quantitative colorimetric analysis, such as using the CIE Lab* color space, could provide a more objective comparison; however, visual assessment combined with measured carotenoid content provides a reasonable indication of extraction efficiency and solvent performance.

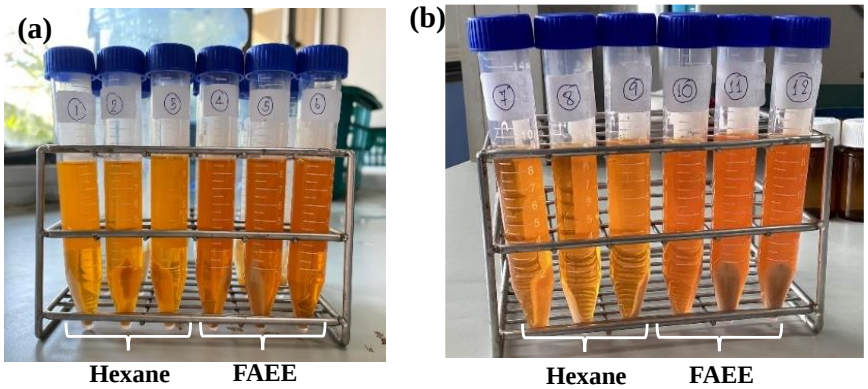

Figure 1. Physical characteristics of the extracts obtained using hexane and FAEE solvents: (a) maceration extraction (ME) and (b) ultrasonic–assisted extraction (UAE).

3.2 Development and validation of equations for lycopene and β–carotene quantification

Tomatoes are a rich source of carotenoids, particularly lycopene and β–carotene. These compounds are critical bioactive substances with overlapping absorption spectra, although their maximum absorption wavelengths (λ_{max}) differ. Accurate quantification of these compounds in tomato samples requires

consideration of their overlapping absorption. To address this, the relationship between the absorbance values at the λ_{max} of both compounds must be utilized for precise calculation, in accordance with Beer–Lambert's law. The law states that absorptivity is a constant specific to each substance under defined conditions, but can vary with changes in wavelength or external factors such as temperature and pH. This characteristic enables the formulation of equations for determining the concentrations of lycopene and β–carotene. The construction of these equations involved preparing standard solutions of lycopene and β–carotene at varying concentrations and analyzing their absorbance using a spectrophotometer at wavelengths of 450 nm and 503 nm, corresponding to their respective λ_{max}. Standard curves were generated, and the absorptivity values obtained from these curves, specific to the solvents used, were employed to develop equations for accurately quantifying lycopene and β–carotene in the samples [9, 12].

The quantification equation for lycopene and β–carotene in hexane was developed by analyzing standard solutions of these compounds at varying concentrations using Ultraviolet–Visible spectroscopy at wavelengths of 450 nm and 503 nm. The absorbance values and corresponding concentrations of the standard solutions were plotted to generate standard curves, as illustrated in Figure 2 (a), (b), (c) and (d). The results indicated that the standard curves for lycopene and β–carotene in hexane were linear, with coefficients of determination (R^2) ranging from 0.9973 to 1.0, demonstrating a strong linear relationship. The linear equations derived from these standard curves were used to calculate the absorptivity values, which are summarized in Table 1. In the case of hexane, the absorptivity values indicate that lycopene is more sensitive at 503 nm (0.1989 L/mg) than at 450 nm (0.1413 L/mg), whereas β-carotene is more sensitive at 450 nm (0.2540 L/mg) than at 503 nm (0.0402 L/mg). A higher absorptivity value implies greater sensitivity, meaning that small concentration changes produce more pronounced absorbance differences. This confirms that 503 nm is optimal for lycopene quantification, while 450 nm is preferred for β-carotene in hexane solvent. These absorptivity values serve as critical parameters for accurately determining the concentrations of lycopene and β–carotene in samples. The absorptivity values presented in Table 2 were substituted into equations (1) and (2), which led to the formation of equations (5) and (6) for lycopene and β–carotene, respectively. By combining these two equations, a unified equation was developed to calculate the concentrations of both compounds in hexane solvent. The resulting equations, as shown in Table 2, provide a comprehensive method for accurately quantifying lycopene and β–carotene based on their absorbance at the specified wavelengths.

$$A_{503} = 0.1989_{L/mg}\,[lyc]_{mg/L} + 0.0402_{L/mg}\,[\beta - car]_{mg/L} \quad (5)$$

$$A_{450} = 0.1413_{L/mg}\,[lyc]_{mg/L} + 0.254_{L/mg}\,[\beta - car]_{mg/L} \quad (6)$$

Table 1. Absorptivity values of lycopene and β–carotene in hexane and FAEE solvent.

Solvent	Wavelength (nm)	Absorptivity (L/mg)	
		Lycopene	β–Carotene
Hexane	503	0.1989	0.0402
	450	0.1413	0.2540
FAEE	503	0.2223	0.0997
	450	0.2256	0.2232

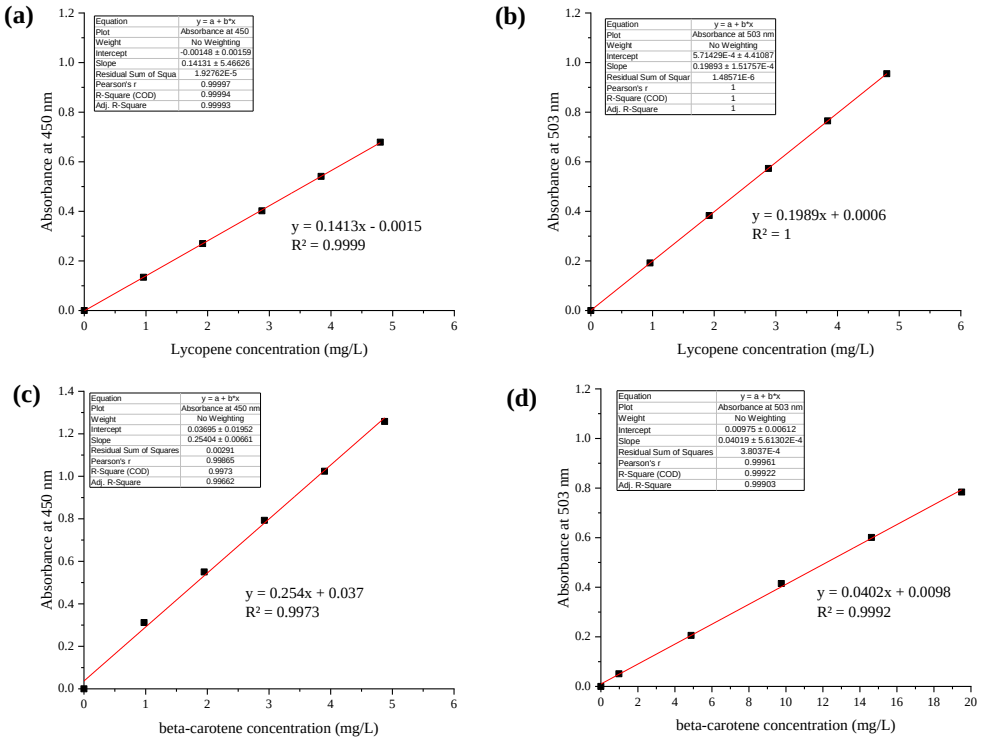

Figure 2. Standard curves for lycopene and β–carotene in hexane solvent: (a) lycopene at 450 nm, (b) lycopene at 503 nm, (c) β–carotene at 450 nm, and (d) β–carotene at 503 nm.

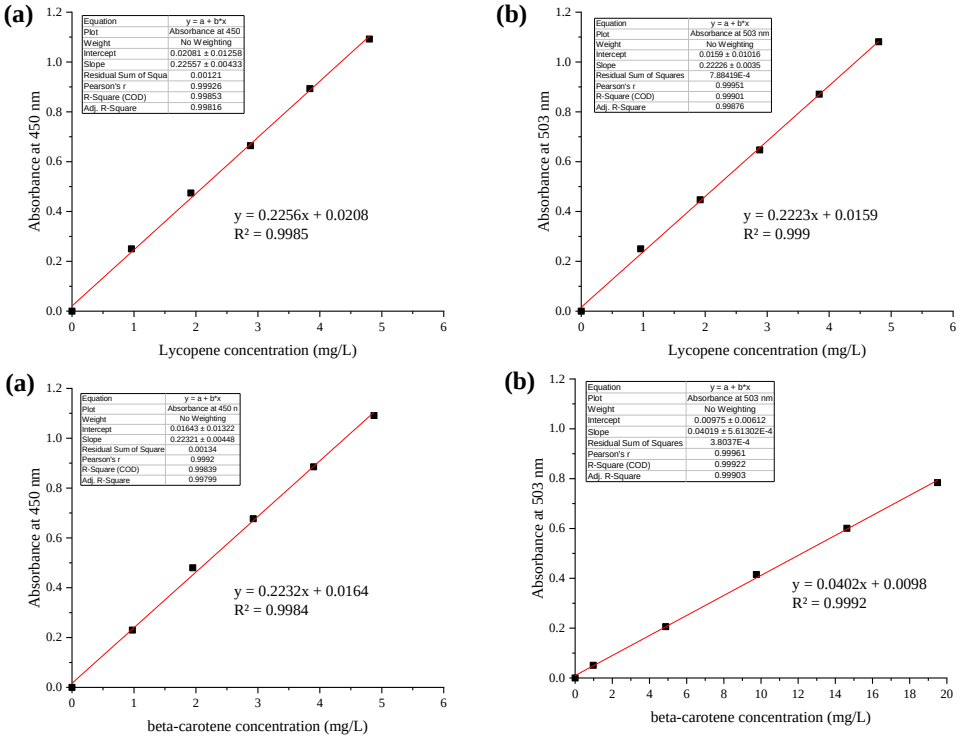

Figure 3. Standard curves for lycopene and β–carotene in FAEE solvent: (a) lycopene at 450 nm, (b) lycopene at 503 nm, (c) β–carotene at 450 nm, and (d) β–carotene at 503 nm.

Similarly, the calculation equations for lycopene and β−carotene content in FAEE solvent were developed by analyzing standard solutions of lycopene and β−carotene at various concentrations using UV−Visible spectroscopy at wavelengths of 450 nm and 503 nm. The absorbance values and corresponding concentrations of the standard solutions were used to generate standard curves, as shown in Figure 3 (a), (b), (c), and (d). The standard curves for both lycopene and β−carotene in FAEE solvent, measured at wavelengths of 450 nm and 503 nm, exhibited linear relationships with R^2 values ranging from 0.9984 to 0.9992. From these straight−line equations, the absorptivity values were determined, as presented in Table 1. When FAEE was used as the solvent, the absorptivity values of lycopene were relatively similar at 503 nm (0.2223 L/mg) and 450 nm (0.2256 L/mg), suggesting that either wavelength could be effectively employed. For β-carotene, absorptivity was also reasonably high at both wavelengths (0.0997 L/mg at 503 nm and 0.2232 L/mg at 450 nm), although 450 nm provided better sensitivity. These findings highlight solvent-dependent spectral characteristics that were subsequently incorporated into Equations (7) and (8), summarized in Table 2. These absorptivity values were then substituted into equations (1) and (2), resulting in equations (7) and (8), respectively. By combining equations (7) and (8), a unified set of equations for calculating the concentrations of lycopene and β−carotene in FAEE solvent was derived, as shown in Table 2. The experimental results demonstrated that the equations for determining lycopene and β−carotene concentrations from spectral data in hexane were consistent with and closely aligned with the findings reported by Fish [12] and Diacon et al. [16]. Similarly, the equations for lycopene and β−carotene determination in FAEE derived from the transesterification of Krabok seed oil exhibited results comparable to those reported by Diacon et al. [16] for FAEE obtained from the transesterification of sunflower oil. Notably, this study represents the first to utilize FAEE derived from Krabok seed oil as a solvent for extracting lycopene and carotene from tomato pomace.

$$A_{503} = 0.223_{L/mg}[lyc]_{mg/L} + 0.0997_{L/mg}[\beta - car]_{mg/L} \quad (7)$$

$$A_{450} = 0.2256_{L/mg}[lyc]_{mg/L} + 0.2232_{L/mg}[\beta - car]_{mg/L} \quad (8)$$

Table 2. Equations for the quantitative determination of lycopene and β−carotene in hexane solvent (mg/L).

Solvent	Lycopene (mg/L)	β−Carotene (mg/L)
Hexane	$[lyc] = 5.662\ A_{503} - 0.896\ A_{450}$	$[\beta-car] = 4.433\ A_{450} - 3.150\ A_{503}$
FAEE	$[lyc] = 8.183\ A_{503} - 3.655\ A_{450}$	$[\beta-car] = 8.176\ A_{450} - 8.272\ A_{503}$

Note: A refers to the absorbance value.

3.3 Quantification of lycopene and β−carotene in tomato extracts

Based on the analysis of lycopene and β-carotene extracted using conventional maceration extraction (ME) and ultrasonic-assisted extraction (UAE) with hexane and FAEE solvents, the hexane-extracted samples were diluted 40-fold, and the FAEE-extracted samples 25-fold before measurement. The different dilution factors were necessary to ensure that absorbance values fell within the linear range of the calibration curves. Because hexane extracts contained higher initial concentrations of lycopene and β-carotene than FAEE extracts, a greater dilution factor (40-fold) was applied, while only a 25-fold dilution was sufficient for FAEE. The absorbance values were then substituted into the equations provided in Table 2 to calculate the lycopene content in mg/L, and the results were subsequently expressed as mg/100 g dry weight (DW), as shown in Figure 4 (a) and (b). Statistical analysis confirmed that these differences were significant ($p < 0.05$), as indicated by the letter annotations in Figure 4. Overall, the extraction efficiency depends on the solvent properties, particularly viscosity, which affects the dissolution of bioactive compounds and the cavitation process in UAE [7, 17]. When comparing the two extraction methods using hexane and FAEE solvents, it was observed that the lycopene content extracted with hexane ranged from 67.97 ± 1.14 to 75.33 ± 4.02 mg/100 g DW, whereas the FAEE solvent yielded a range of 59.92 ± 0.58 to 63.60 ± 1.86 mg/100 g DW. Similarly, the β−carotene content extracted with hexane ranged from 10.512 ± 0.34 to 11.499 ± 0.79 mg/100 g DW, while the FAEE solvent yielded 1.629 ± 0.13 to 7.013 ± 0.68 mg/100 g DW.

To provide clearer evidence of the comparative extraction performance, quantitative differences between maceration extraction (ME) and ultrasonic-assisted extraction (UAE) were evaluated. UAE with hexane improved lycopene yield by approximately 10% and β-carotene yield by 9% relative to ME, while UAE with FAEE increased lycopene yield by about 7%. Notably, the UAE with FAEE enhanced β-carotene yield by nearly 340% compared to ME, highlighting the substantial benefit of sonication in overcoming the limitations of FAEE's higher viscosity. These results quantitatively confirm that UAE is more efficient than ME in recovering both lycopene and β-carotene. These findings suggest that hexane is more efficient in extracting lycopene and β−carotene than FAEE. The higher extraction efficiency of hexane may be attributed to its lower viscosity (0.44 cSt) compared to FAEE (1.73 cSt). The lower viscosity of hexane facilitates better dissolution of bioactive compounds during the maceration extraction process. Furthermore, in ultrasonic−assisted extraction, the higher viscosity of FAEE can hinder the cavitation process, which is crucial for effective extraction. Cavitation requires the sound pressure during the expansion phase to overcome the intermolecular forces of the liquid. As viscosity increases, the intermolecular attraction becomes stronger, making cavitation more difficult. Consequently, the higher viscosity of FAEE reduces its efficiency as a solvent compared to hexane [18–20].

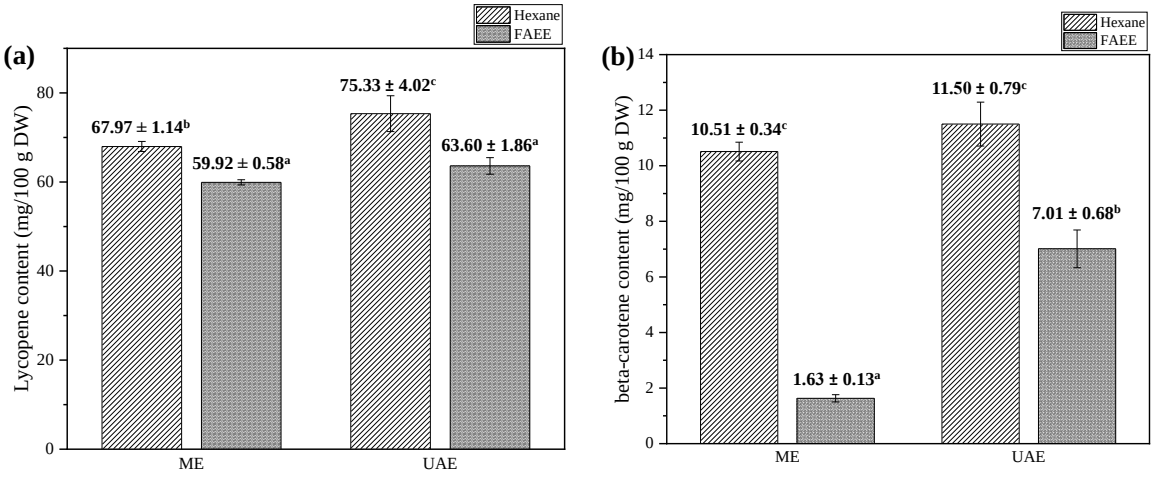

Figure 4. (a) Amount of lycopene extracted from tomato pomace and (b) amount of β−carotene extracted from tomato pomace using conventional maceration extraction (ME) and combined ultrasonic extraction (UAE) with hexane and FAEE solvents. Note: The values represent the mean of three replicates. Different letters within the same column indicate statistically significant differences at the 95% confidence level.

3.4 Antioxidant activity of tomato pomace extracts measured by the DPPH method

The antioxidant activity of tomato pomace extracts was evaluated using DPPH radical inhibition, as described in Section 2.4. In this assay, the DPPH solution without any sample (A_0) was used as the positive control to provide a reference for maximum radical activity and to validate the effectiveness of the extracts in scavenging free radicals. Two extraction methods—conventional maceration extraction (ME) and ultrasonic-assisted extraction (UAE)—were compared using FAEE and hexane as solvents (Figure 5(a)). The results showed that FAEE performed better than hexane in both methods. Specifically, ME with FAEE yielded a DPPH inhibition of 70.29 ± 0.35%, while UAE with FAEE produced 77.16 ± 4.44%, significantly higher than hexane ($p < 0.01$). The distinct polarity of FAEE allows the simultaneous extraction of both non-polar carotenoids and polar phenolic compounds. However, the observed DPPH inhibition did not correlate directly with the measured carotenoid content of lycopene and β-carotene. This discrepancy may arise from the combined antioxidant effect of multiple bioactive compounds, including phenolics, which can act synergistically with carotenoids. Therefore, the higher antioxidant activity observed with FAEE likely reflects the contribution of both carotenoids and phenolic compounds rather than carotenoids alone. The combined antioxidant activity of FAEE* and the extracted compounds was evident, with DPPH inhibition reaching 91.65

± 0.50% (ME) and 92.06 ± 0.89% (UAE), showing a statistically significant synergistic effect compared to FAEE-based extracts alone ($p < 0.05$). Additionally, UAE further improved extraction efficiency by disrupting plant cell walls, facilitating better solvent penetration, and increasing the rate of mass transfer, resulting in higher extraction of bioactive compounds. Beyond the performance, FAEE also offers an environmentally friendly alternative to hexane, as it is less harmful and does not evaporate during extraction, supporting a more sustainable process [21–25].

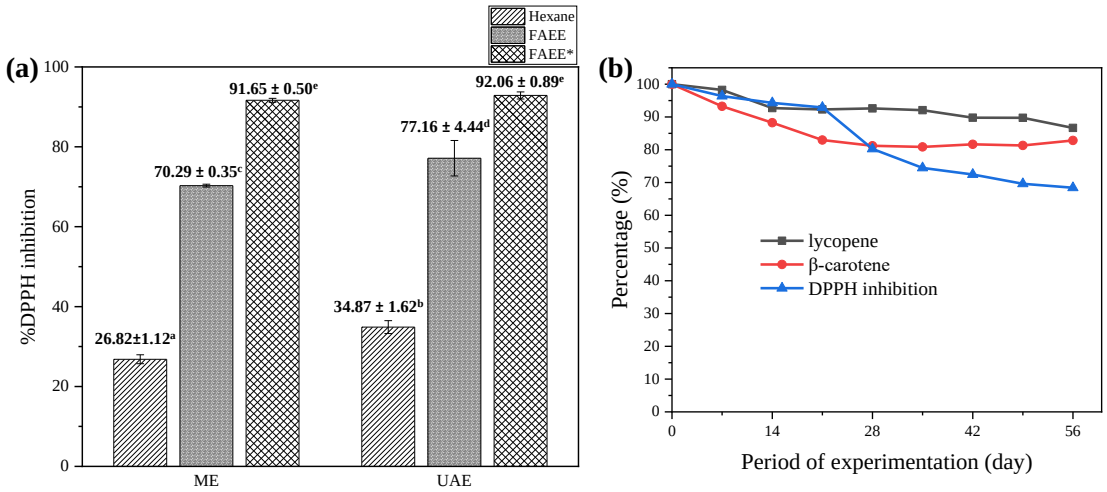

Figure 5. (a) Percentage of DPPH radical inhibition in tomato pomace extracts produced using different techniques. The positive control (DPPH solution without sample, A_0) was used to indicate maximum radical activity, and the calculation method is described in Section 2.4 (Equation 4). (b) A study on the stability of lycopene and β–carotene, along with the percentage inhibition of DPPH radicals, at different time intervals for tomato pomace extracts obtained using the UAE technique with FAEE as the solvent. Note: The values represent the mean of three independent replicates. Different letters within the same column indicate statistically significant differences at the 95% confidence level. *FAEE** Indicates the total antioxidant activity of FAEE.

3.5 A study on the stability of lycopene and β–carotene

The stability of lycopene and β-carotene in tomato pomace extracts obtained through ultrasound-assisted extraction (UAE) using fatty acid ethyl esters (FAEE) as a solvent was assessed over a 56-day period at 4 °C. The results showed that both compounds experienced an initial decline over the first 28 days, after which their levels stabilized. By day 56, lycopene had decreased by approximately 10%, and β-carotene by 15%, as shown in Figure 5(b). This study was conducted as a preliminary investigation with triplicate measurements (n = 3) at each time point. The reported reductions in lycopene (~10%) and β-carotene (~15%) over 56 days are presented as mean ± SD and should therefore be interpreted descriptively. Due to the limited sample size, formal inferential testing (e.g., repeated-measures ANOVA with post hoc comparisons) was not conducted in this work. Such analyses will be applied in future, larger-scale studies to confirm statistical significance and to report p-values and 95% confidence intervals. This indicates that while FAEE, derived from Krabok seed oil, is slightly less efficient than hexane in initial extraction, it offers considerable advantages in preserving the stability of these sensitive compounds. In contrast, hexane-extracted samples degraded rapidly, becoming unquantifiable after just 7 days. The enhanced stability observed in FAEE extracts can be attributed to its slight polarity, which provides stronger solute–solvent interactions than non-polar hexane. These weak dipole interactions and hydrogen bonding can protect carotenoids from pro-oxidant environments, thereby slowing oxidative degradation [16, 21, 22]. Moreover, FAEE derived from Krabok seed oil may contain endogenous bioactive compounds, such as tocopherols and phenolics, which can act synergistically with carotenoids to enhance antioxidant stability. Our previous study confirmed the synthesis and applicability of Krabok-derived FAEE as a functional, slightly polar solvent [11]. These properties likely contributed to the improved preservation of carotenoids compared to hexane.

The study further revealed a gradual decrease in antioxidant activity, with a more pronounced decline observed after the 21st day. Despite this, antioxidant efficiency remained above 70% by the 56th day. This suggests that, in addition to lycopene and β-carotene, other bioactive compounds might have degraded over time, with FAEE effectively mitigating the degradation and maintaining overall stability. These observations suggest that, in addition to lycopene and β-carotene, other minor bioactive compounds such as phenolics, flavonoids, and endogenous antioxidants present in the tomato pomace extracts may contribute significantly to the overall radical scavenging activity. The gradual decline in DPPH inhibition over time, despite relatively small losses in lycopene and β-carotene, suggests that these additional compounds are likely more susceptible to degradation under the applied storage conditions. FAEE, due to its slight polarity and ability to form weak dipole interactions and hydrogen bonds, may help stabilize these labile compounds, thereby mitigating the overall loss of antioxidant activity. Moreover, the protective effect of FAEE could be synergistic, where carotenoids and other bioactive compounds act together to preserve their radical scavenging capacity. This reinforces the importance of solvent selection not only for extraction efficiency but also for the long-term stability of complex mixtures of bioactive compounds, particularly when valorizing food waste for nutraceutical or functional food applications. Future studies incorporating correlation analyses between individual bioactive contents and antioxidant activity would provide quantitative insights into these synergistic effects and further substantiate the role of FAEE in maintaining extract stability.

These findings align with prior research indicating that antioxidants such as lycopene and β-carotene are prone to degradation under suboptimal storage conditions, and that the choice of solvent significantly impacts their stability [11, 16, 21, 22]. In addition, the UAE has been shown to improve extraction efficiency and compound stability by breaking cell walls and enhancing solvent penetration, as corroborated by the studies of Sharma et al. [7], León-López et al. [23], and da Silva Lima et al. [26]. Thus, employing FAEE for the extraction of lycopene and β-carotene from tomato waste offers a sustainable and eco-friendly alternative to conventional solvents. Combined with the UAE, this approach achieves higher extraction yields and better stability of bioactive compounds, supporting the sustainable valorization of tomato waste for applications in natural colorants, nutraceuticals, and functional foods. These results indicate that tomato pomace extracts obtained via FAEE-based UAE not only retain significant antioxidant activity over extended storage periods but also offer a practical and sustainable source of stable bioactive compounds. Such extracts have potential applications in the production of natural colorants, nutraceutical ingredients, and functional food products, providing value-added utilization of tomato waste while supporting environmentally friendly and cost-effective manufacturing processes.

4. Conclusions

In summary, this study demonstrates that fatty acid ethyl esters (FAEE) derived from Krabok seed oil are an effective and environmentally friendly solvent for extracting bioactive compounds, specifically lycopene and β–carotene, from tomato pomace. The ultrasonic–assisted extraction (UAE) method outperformed conventional maceration extraction (ME) in terms of efficiency, and FAEE provided superior antioxidant activity compared to hexane. Stability tests revealed that FAEE–extracted compounds maintained their integrity over a longer period, showing minimal degradation, while hexane–extracted samples deteriorated rapidly. These findings highlight the potential of FAEE as a sustainable and efficient solvent for the extraction of valuable bioactive compounds, contributing to the development of eco–friendly methods for utilizing tomato by–products in the food and cosmetic industries. Future research could focus on optimizing the extraction conditions further and exploring the scalability of this method for industrial applications.

5. Acknowledgements

This research was supported by the Chemistry Program and the Innovation in Chemistry for Community Research Unit at the Faculty of Science and Technology, as well as the Biomass Energy Research Laboratory within the Center of Excellence on Alternative Energy, Research and Development Institute at Sakon Nakhon Rajabhat University, Thailand. These institutions provided the necessary equipment and resources for the study.

Author Contributions: Conceptualization, S.T. and W.R.; methodology, S.T., W.R.; validation, S.T., W.R. and S.P.; formal analysis, S.T., W.R., A.S., W.Y., P.H., R.W., B.P.; investigation, S.P., A.S., W.Y., P.H., R.W., B.P., T.L.; resources, S.P. and T.L.; data curation, S.T and W.R.; writing—original draft preparation, S.T and W.R.; writing—review and editing, W.R; visualization, S.T and W.R.; funding acquisition, S.T. All authors have read and agreed to the published version of the manuscript.

Funding: This research was funded by the Chemistry Program and the Innovation in Chemistry for Community Research Unit at the Faculty of Science and Technology, Sakon Nakhon Rajabhat University, Thailand.

Conflicts of Interest: The authors declare no conflict of interest.

Declarations: Declaration of generative AI and AI–assisted technologies in the writing process.

References

[1] Kutrasaeng, N.; Prapatigul, P.; Martwanna, N. Pesticide application behaviors in tomato production of farmers in Sakon Nakhon Province. *Journal of Agriculture* **2017**, *33*, 235–244.

[2] Yosying, S.; Choenkwan, S.; Phumchantuk, P.; Palinthorn, F. Fresh tomato production of small–scale farmers along the Mekong River in the northeastern region of Thailand. *KKU Research Journal (Graduate Studies)* **2022**, *22*, 61–74.

[3] Przybylska, S.; Tokarczyk, G. Lycopene in the prevention of cardiovascular diseases. *International Journal of Molecular Sciences* **2022**, *23*, 1957. https://doi.org/10.3390/ijms23041957

[4] Leh, H.E.; Lee, L.K. Lycopene: A potent antioxidant for the amelioration of type II diabetes mellitus. *Molecules* **2022**, *27*, 2335. https://doi.org/10.3390/molecules27072335

[5] Eslami, E.; Carpentieri, S.; Pataro, G.; Ferrari, G.A. Comprehensive overview of tomato processing by–product valorization by conventional methods versus emerging technologies. *Foods* **2023**, *12*, 166. https://doi.org/10.3390/foods12010166

[6] Flais, D.; Oroian, M. Extraction of bioactive compounds from oxheart tomato pomace (*Lycopersicon esculentum* L.) using different solvents: Characterization of extracts. *Applied Sciences* **2024**, *14*, 7143. https://doi.org/10.3390/app14167143

[7] Sharma, M.; Hussain, S.; Shalima, T.; Aav, R.; Bhat, R. Valorization of seabuckthorn pomace to obtain bioactive carotenoids: An innovative approach of using green extraction techniques (ultrasonic and microwave–assisted extractions) synergized with green solvents (edible oils). *Industrial Crops and Products* **2022**, *175*, 114257. https://doi.org/10.1016/j.indcrop.2021.114257

[8] Yara–Varón, E.; Li, Y.; Balcells, M.; Fabiano–Tixier, A.S.; Chemat, F. Vegetable oils as alternative solvents for green oleo–extraction, purification, and formulation of food and natural products. *Molecules* **2017**, *22*, 1474. https://doi.org/10.3390/molecules22091474

[9] Diacon, A.; Călinescu, I.; Vinatoru, M.; Chipurici, P.; Vlaicu, A.; Boscornea, A.C.; Mason, T.J. Fatty acid ethyl esters (FAEE): A new, green, and renewable solvent for the extraction of carotenoids from tomato waste products. *Molecules* **2021**, *26*, 4388. https://doi.org/10.3390/molecules26144388

[10] Roschat, W.; Phewphong, S.; Pholsupho, P.; Namwongsa, K.; Wongka, P.; Moonsin, P.; Yoosuk, B.; Promarak, V. The synthesis of a high–quality biodiesel product derived from Krabok (*Irvingia malayana*) seed oil as a new raw material of Thailand. *Fuel* **2022**, *308*, 122009. https://doi.org/10.1016/j.fuel.2021.122009

[11] Thangthong, A.; Roschat, W.; Hachai, C.; Inthikhot, K.; Kiinti, K.; Thammayod, A.; Phewphong, S.; Leelatam, T.; Tawil, S.; Moonsin, P.; Promarak, V. Synthesis of the fatty acid ethyl esters (FAEE) from Krabok (*Irvingia malayana*) seed oil for use as the main ingredient in the production of herbal massage oil. *Trends in Sciences* **2024**, *21*(11), 8444. https://doi.org/10.48048/tis.2024.8444

[12] Fish, W.W. Refinements of the attending equations for several spectral methods that provide improved quantification of β–carotene and/or lycopene in selected foods. *Postharvest Biology and Technology* **2012**, *66*, 16–22. https://doi.org/10.1016/j.postharvbio.2011.08.007

[13] Chu, C.C.; Hasan, Z.A.B.; Chua, S.K.; Nyam, K.L. Formulation and characterization of novel nanostructured lipid carriers with photoprotective properties made from carnauba wax, beeswax, pumpkin seed oil, and UV filters. *Journal of the American Oil Chemists' Society* **2020**, *97*(5), 531–542. https://doi.org/10.1002/aocs.12340

[14] Preecharram, S.; Phosri, S.; Theansungnoen, T.; Roschat, W.; Arthan, S.; Lasopha, S.; Jandaruang, J. Nutritional values and their potential applications in food products of Krabok seed (*Irvingia malayana*). *Trends in Sciences* **2024**, *21*(1), 7316. https://doi.org/10.48048/tis.2024.7316

[15] Phewphong, S.; Roschat, W.; Namwongsa, K.; Wonam, A.; Kaisri, T.; Duangpakdee, P.; Leelatam, T.; Moonsin, P.; Promarak, V. Evaluation of the nutritional, minerals, and antioxidant potential of Roselle (*Hibiscus sabdariffa* Linn.) seeds from Roi Et Province in the Northeastern Region of Thailand. *Trends in Sciences* **2023**, *20*(6), 6664. https://doi.org/10.48048/tis.2023.6664

[16] Diacon, A.; Călinescu, I.; Vinatoru, M.; Chipurici, P.; Vlaicu, A.; Boscornea, A.C.; Mason, T.J. Fatty acid ethyl esters (FAEE): A new, green and renewable solvent for the extraction of carotenoids from tomato waste products. *Molecules* **2021**, *26*(14), 4388. https://doi.org/10.3390/molecules26144388

[17] Sharma, M.; Bhat, R. Extraction of carotenoids from pumpkin peel and pulp: Comparison between innovative green extraction technologies (ultrasonic and microwave−assisted extractions using corn oil). *Foods* **2021**, *10*(4), 787. https://doi.org/10.3390/foods10040787

[18] Li, J.; Pettinato, M.; Casazza, A.A.; Perego, P. A comprehensive optimization of ultrasound−assisted extraction for lycopene recovery from tomato waste and encapsulation by spray drying. *Processes* **2022**, *10*(2), 308. https://doi.org/10.3390/pr10020308

[19] Carneiro, C.R.; Alhaji, A.M.; da Silva, C.A.S.; de Sousa, R.C.S.; Monteiro, S.; Coimbra, J.S.R. Potential challenges of the extraction of carotenoids and fatty acids from Pequi (Caryocar brasiliense) oil. *Foods* **2023**, *12*(9), 1907. https://doi.org/10.3390/foods12091907

[20] Chaudhary, K.; Khalid, S.; Zahid, M.; Ansar, S.; Zaffar, M.; Hassan, S.A.; Naeem, M.; Maan, A.A.; Aadil, R.M. Emerging ways to extract lycopene from waste of tomato and other fruits: A comprehensive review. *Journal of Food Process Engineering* **2024**, *47*(9), e14720. https://doi.org/10.1111/jfpe.14720

[21] Campos−Lozada, G.; Pérez Marroquín, X.A.; Callejas−Quijada, G.; Campos−Montiel, R.G.; Morales Peñaloza, A.; León−López, A.; Aguirre−Álvarez, G. The effect of high−intensity ultrasound and natural oils on the extraction and antioxidant activity of lycopene from tomato (Solanum lycopersicum) waste. *Antioxidants* **2022**, *11*, 1404. https://doi.org/10.3390/antiox11071404

[22] Rahimi, S.; Mikani, M. Lycopene green ultrasound−assisted extraction using edible oil accompanied with response surface methodology (RSM) optimization performance: Application in tomato processing wastes. *Microchemical Journal* **2019**, *146*, 1033–1042. https://doi.org/10.1016/j.microc.2019.02.039

[23] León−López, A.; Fuentes−Jiménez, L.; Hernández−Fuentes, A.D.; Campos−Montiel, R.G.; Aguirre−Álvarez, G. Hydrolysed collagen from sheepskins as a source of functional peptides with antioxidant activity. *International Journal of Molecular Sciences* **2019**, *20*, 3931. https://doi.org/10.3390/ijms20153931

[24] Rattanabun, W.; Keawbankrud, W.; Pimpila, S.; Roekudomsak, K.; Phocharoen, C.; Suthiporn, P.; Nantakarat, S. Hair treatment products containing pigeon pea oil as chemical properties and anti−oxidant activity. *Creative Science* **2024**, *16*(3), 256828. https://doi.org/10.55674/cs.v16i3.256828

[25] Sanmanoch, W.; Surapat, W.; Phosri, S.; Yaraksa, N. Antioxidant activity and cytotoxicity against the cervical epithelial carcinoma (HeLa) cell line of crude Ganoderma lucidum mycelial extracts: Antioxidant activity and cytotoxicity of crude Ganoderma lucidum mycelial extracts. Creative Science **2024**, *16*(1), 254094. https://doi.org/10.55674/cs.v16i1.254094

[26] da Silva Lima, R.; Nunes, I.L.; Block, J.M. Ultrasound−assisted extraction for the recovery of carotenoids from guava's pulp and waste powders. *Plant Foods for Human Nutrition* **2020**, *75*(1), 63–69. https://doi.org/10.1007/s11130-019-00784-0

ASEAN
Journal of Scientific and Technological Reports
Online ISSN:2773-8752

Research article

Manufacturing Design and Cost Analysis for Customer-oriented Rubber Mat Product using Abrasive Waterjet Cutting

Kunlapat Thongkaew[1, 5*], Supapan Chaiprapat[2, 5], Chukree Daesa[3, 5], and Zaleha Mustafa[4]

[1] Faculty of Engineering, Prince of Songkla University, Songkhla, 90110, Thailand
[2] Faculty of Engineering, Prince of Songkla University, Songkhla, 90110, Thailand
[3] Faculty of Engineering, Prince of Songkla University, Songkhla, 90110, Thailand
[4] Faculty of Industrial and Manufacturing Technology and Engineering, Universiti Teknikal Malaysia Melaka, 76100, Malaysia
[5] Smart Industrial Research Center, Faculty of Engineering, Prince of Songkla University, Songkhla, 90110, Thailand
* Correspondence: kunlapat.t@psu.ac.th

Citation:
Thongkaew, K.; Chaiprapat, S.; Deasa, C.; Mustafa, Z. Manufacturing design and cost analysis for customer-oriented rubber mat product using abrasive waterjet cutting. *ASEAN J. Sci. Tech. Report.* **2025**, *28*(6), e259644. https://doi.org/10.55164/ajstr.v28i6.259644.

Article history:
Received: June 5, 2025
Revised: September 20, 2025
Accepted: September 27, 2025
Available online: October 19, 2025

Abstract: Molding is a widely used technique for large-scale manufacturing of rubber products, ensuring profitability for companies. Advances in rubber-based products have significantly improved consumer satisfaction by fostering direct engagement between manufacturers and customers. This study aims to develop a framework for transforming a blank rubber mat into a custom-designed jigsaw rubber mats using abrasive waterjet (AWJ) cutting. Customers can design their own rubber mats and submit digital images, which are then processed and cut by a waterjet machine to create jigsaw rubber mats. The optimal cutting path was developed based on the number of cutting points and the similarity index to ensure precise cutting operations. The production cost was subsequently analyzed, as the uniqueness of each design influences it. The evaluation of toolpath optimization and AWJ cutting application revealed that the number of cutting points could be reduced by more than 50% compared to the original fine cutting points while maintaining a similarity index above 99%. This reduction significantly shortened cutting time. The manufacturing of customized jigsaw rubber mats incurs only a minor additional cost, approximately 13% of the overall manufacturing cost of regular rubber mats. These findings suggest that this approach could provide manufacturers with a competitive advantage by enabling the production of customer-oriented products that are both responsive and economically feasible.

Keywords: Customer-oriented design; rubber products; image processing; waterjet cutting; cost analysis

1. Introduction

Natural rubber is a key agricultural commodity in Thailand, a major exporter that supplies over a billion dollars' worth of raw materials and finished rubber goods worldwide [1]. As a polymer, rubber possesses unique structural properties that make it highly elastic and versatile, making it suitable for a wide range of applications, including tires, footwear, and seals. Typically, rubber products are manufactured through molding processes, including compression molding, transfer molding, and injection molding. Compression molding is ideal for simple-shaped products that require less precision, such as O-rings, oil seal rubber caps, and rubber mats. In contrast, injection molding is more suitable for complex products that demand higher accuracy [2]. Transfer molding is another

option for manufacturers, as it requires a lower investment while still maintaining acceptable quality. In many cases, conducting a heat transfer analysis or computational fluid dynamics simulation is necessary to obtain critical data before mold design. The molding process relies on advanced technologies and highly skilled operators to ensure product quality and process efficiency [2]. However, the significant resources and effort required for mold manufacturing drive up costs considerably, including the high expense of mold materials. As a result, for molding to be economically viable, a substantial number of molded items must be produced to achieve economies of scale, a principle known as mass manufacturing [3].

As modern marketing strategies increasingly prioritize individual demands, mass production is gradually being replaced by the emerging system of mass customization. Mass-customized products effectively cater to consumers' desire for originality and uniqueness while allowing manufacturers to achieve profitable margins by adding sentimental value to their products [4]. Given the small production lot sizes—sometimes as small as a single unit for personalized premium products—agility and flexibility are crucial for business success. Customer involvement in product design has become a key competitive strategy to enhance product appeal. To accommodate diverse customer requirements, manufacturers must prepare their production processes in advance. Recognizing the inefficiencies of conventional mass production, industrialists are actively seeking more adaptive and agile production solutions. Technologies such as computer numerical control (CNC) machines, flexible manufacturing, and computer-integrated systems are being implemented to transition from mass production to mass customization, resulting in increased productivity, lower costs, and a wider range of product offerings [5]. Customizing rubber products presents a significant challenge due to the limitations of molding processes, which require large-scale manufacturing to be economically viable [6]. Alternative automated technologies can be considered, but their applicability must be carefully evaluated. In a typical production line, after the primary blanking process, a secondary post-cutting process is introduced to transform mass-produced items into more specific or customized products.

Manual cutting, often performed using a box cutter or bladed knife, is the simplest method for cutting industrial rubber products [7-9]. While this approach may appear cost-effective, manufacturers often overlook the hidden costs associated with rework and material waste resulting from poor cut quality. Additionally, manual cutting restricts each unit to a single, predetermined size. In contrast, die cutting requires a significantly higher initial investment, as dies must be custom-made for each application. The feasibility of die cutting should be assessed based on various cost factors, including machine operations, die design and production, maintenance, and potential reproduction. If the benefits of fast cutting outweigh the associated costs, die cutting becomes a desirable alternative. Non-conventional cutting techniques are gaining popularity in the industry due to their ability to handle complex materials and produce intricate shapes. Selecting the appropriate cutting process and machining operation is crucial for ensuring overall production success [10]. Mizzi et al. [11] investigated the use of laser cutting for manufacturing microstructure/auxetic rubber sheets. These structures have varying ligament thicknesses, which complicate the laser-cutting process and increase susceptibility to manufacturing issues, such as residual stress effects. Previous studies have explored the mechanism of abrasive waterjet (AWJ) cutting for rubber, revealing that material removal in rubber differs from that of metallic or brittle materials [12]. Rubber is primarily removed through shear and tensile forces created by the high-pressure waterjet, resulting in smooth cuts. Tangwarodomnukun et al. [13] developed a low-cost, sheet-based rapid prototyping technique for rubber sheets, utilizing a low-pressure waterjet to construct three-dimensional rubber sheet configurations layer by layer. The resulting prototype closely resembled the intended design.

AWJ cutting is emerging as a highly suitable automated technology for rubber cutting due to its distinct advantages, including the absence of thermal damage to the target material, high machining flexibility, and minimal environmental impact [14]. This technology enables the cutting of freeform shapes and produces smooth machined surfaces with high integrity [15]. Furthermore, unlike die cutting, AWJ cutting does not require tooling, which helps reduce costs, accelerate prototyping, and shorten production lead times. Although AWJ machining technology accommodates a wide range of materials, limited research has focused on the economic aspects of system investment and operational costs when applied to rubber [16-21]. Generally, abrasive particles account for approximately 60-70% of the total cost, while cutting speed has the most

significant impact on output efficiency [16]. However, there has been minimal focus on analyzing the cutting factors that influence machining performance and cost for specific rubber materials.

Most rubber producers in Thailand are small to medium-sized businesses, and there is still a lack of awareness regarding custom-oriented rubber products. Additionally, accurate cost estimation for custom rubber mats remains limited or poorly documented. Therefore, the objective of this study is to provide a framework for manufacturing customized jigsaw rubber mats, particularly for manufacturers seeking to reduce costs by adopting post-cutting with abrasive waterjet (AWJ) technology instead of creating a new mold. This approach allows manufacturers to optimize their resources, enhance industry competitiveness, and ensure long-term viability in a dynamic market. In this study, a mass-produced blank rubber mat was transformed into a personalized jigsaw rubber mat using a post-cutting procedure. The customer's design was processed to generate an optimal tool path using CNC code for AWJ cutting, which is well-suited for rubber cutting applications. A mathematical optimization model was developed to minimize manufacturing costs while maintaining cutting performance standards. This enhanced flexibility in accommodating diverse customer demands provides a significant competitive advantage for manufacturers.

2. Materials and Methods

2.1 Rubber Mat Manufacturing Process

Rubber mats are typically made from natural rubber compounds and are widely used as flooring overlays in kindergartens and nursing homes to provide a soft and continuous surface. These overlays play a crucial role in preventing injuries in the event of accidents. Figure 1 illustrates a typical production line for rubber blanks. The production process begins with a series of rubber compound processing steps, including procuring dried rubber sheets, mixing them with additives to achieve the desired properties, and calendaring the compound into rubber sheets. The rubber compound samples are then tested for polymerization properties, such as curing temperature and curing time, to determine the appropriate forming parameters in accordance with the Thai Industrial Standard Institute (TISI) 2377-2008 [22]. After testing, the rubber sheets are cut into smaller pieces and placed into molds, where they are shaped into rubber blanks with interlocking edges using compression molding.

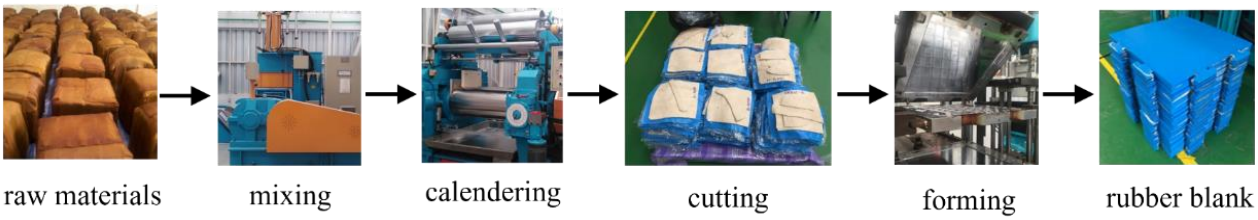

Figure 1. A rubber mat blank forming line.

2.2 Customized Rubber Mats Manufacturing Design and Cost Analysis

In this system, customers can create their own cutting designs for jigsaw rubber mats, resulting in unique, value-added products. A dedicated production line has been established specifically for this customized product, where rubber blanks are mass-produced and custom cutting is performed using automated and flexible machinery, as shown in Figure 2. A CNC abrasive waterjet cutting machine (Figure 2) is classified as soft automation, capable of cutting various materials using a high-pressure water jet stream. This machine effectively carves cured rubber sheets into customer-designed patterns with precision and efficiency.

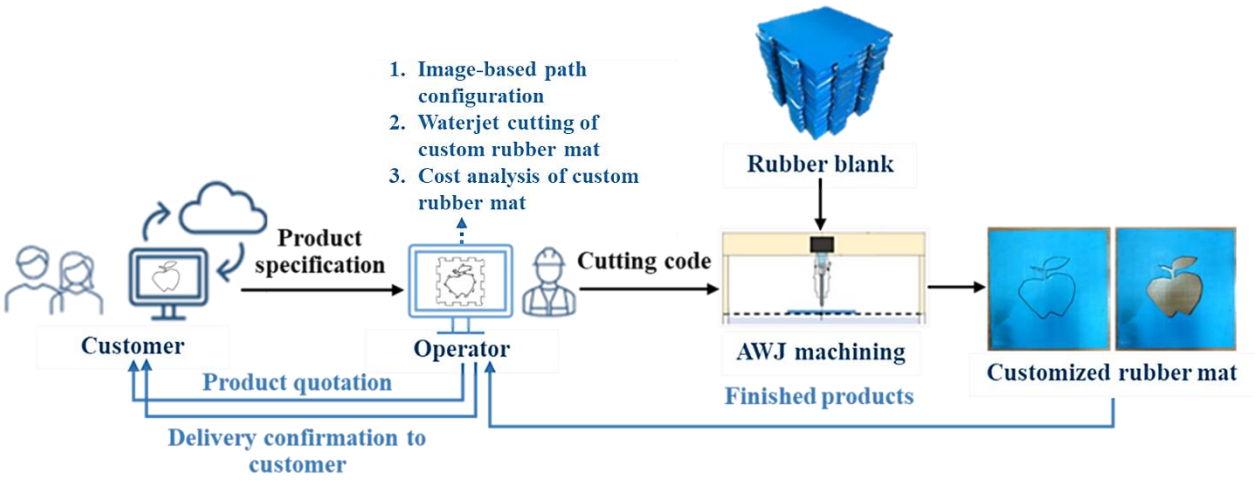

Figure 2. A proposed production line for customized rubber mats.

According to Figure 2, customers submit scribbled images along with product specifications, such as cutting dimensions, to an operator for the generation of cutting codes for the abrasive waterjet machine. Before setting the cutting paths based on the scribbled images, the operator enhances image quality using image processing techniques. To ensure that the cutting quality closely matches the original design, this method considers variables such as tolerance and spacing. Additionally, cost optimization is performed before selecting the cutting path and generating the NC code for the AWJ machine used to produce the customized rubber mats. The details of this process are explained in the following sections.

2.2.1 Image Pre-processing and Configuration of Cutting Paths

Customers can submit their design directly to the manufacturer for cutting on the rubber blank (Figure 3). If necessary, image pre-processing techniques such as resizing, filtering, and noise reduction can be applied to enhance image quality. The number of data points, or the points that the scribble passes through, can be substantial and will increase with higher resolution. These data points are used to configure the cutting path, which is established based on the image coordinate system [row (r), column (c)]. Although laser scanners and coordinate measuring devices already incorporate some pre-processing to extract data points from images, the resulting discrete data remain numerous and scattered in structure [23]. These raw data are not practically feasible for the cutting tool to follow, so they are selectively filtered to generate a set of consecutive edge data points.

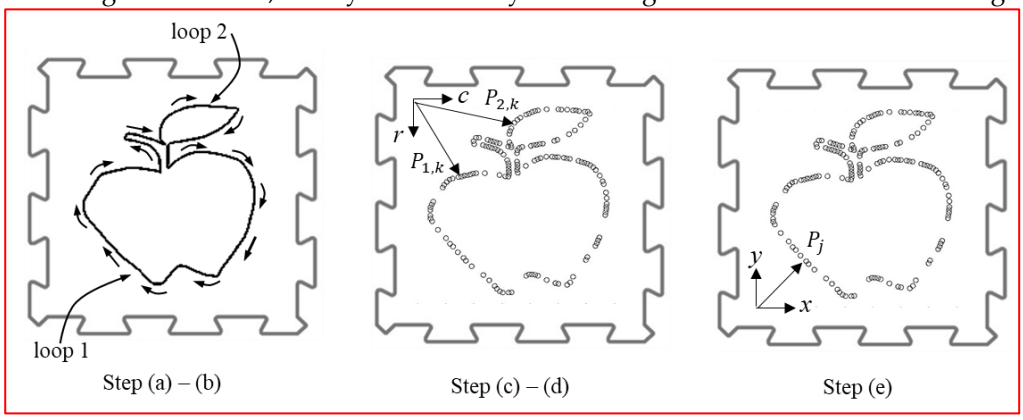

Figure 3. A sample of a cutting path configuration

Since rubber is elastic and flexible, machining errors can be more tolerable compared to other industrial materials. The cutting path can be determined through the following steps (Figure 3):

(a) Define path loop: Cluster the data points into different path loops.

(b) Create skeleton of the scribble: Within each loop, the data points are thinned to a one-pixel width spine. They are viewed as a skeleton of the scribble. The authors applied the skeletonization function in MATLAB 2023a to a binary image via the *bwmorph* function [24].

(c) Create data points: Although a band of the data points is compressed into a single pixel, the total number of points remains large, and their positions are very close to another. It is not technically and economically viable for the tool to follow, and the number of points must be reduced using a spacing factor. For any loop m at the i^{th} order, cutting points P can be explained by Eq. (1).

$$P_{m,i} \in C_{m1} \; if \; i = 1, 2s, 3s, ... \tag{1}$$

When s is a spacing factor

$C_{m,1}$ is a set of cutting points of the m^{th} loop after applying a spacing factor.

The scribble now becomes a series of connected linear segments. Their collinearity is evaluated to determine the redundancy of the points along the segment chain. The next point will be included in a set of cutting points if the deviation falls within a specified tolerance. This process is repeated until no points can be skipped further.

$$P_{m,k} \in C_{m2} \quad if \left\| (P_{m,k} - P_{m,k-1}) \times \frac{P_{m,k+1} - P_{m,k-1}}{\|P_{m,k+1} - P_{m,k-1}\|} \right\| \geq \mathrm{t} \tag{2}$$

When C_{m2} is the final set of cutting points of the m^{th} loop, and t is a specified tolerance

The tolerance t must be deliberately imposed. It is one of the cost drivers. Increasing the tolerance reduces the number of cutting points, thereby shortening the tool travel distance and machining time. However, if the tolerance is too wide, the number of cutting points will be fewer, resulting in the scribble becoming too rigid, less curvy, and deviating from the original image.

(d) Create image coordinate points: $P_{m,k}$, currently in the image coordinate space, is transformed into the machine coordinate system (Figure 3) using Eq. (2).

$$P^{M}_{m,k} = [T]P_{m,k} + V \tag{3}$$

$$T = \begin{bmatrix} 0 & 1 \\ -1 & 0 \end{bmatrix} \tag{4}$$

where T is a transformation matrix and V is a translational vector indicating a position of the image coordinate space's origin with respect to the machine coordinate system.

(e) Create real coordinate points: This set of coordinates will subsequently need to be scaled to the real-world dimensioning.

At this stage, the total distance (D) that the tool will travel to complete the scribble can be calculated from

$$D = \sum_{i=1}^{n_m} \sum_{j=1}^{n_{pm}-1} \left| P_{j+1} - P_j \right| ; \quad P_j \in C_{m2} \tag{5}$$

when P_j is a vector of the cutting point j, n_m is the number of loops, and n_{pm} is the number of points in the m^{th} loop

The points along the cutting path are formatted into cutting code (CNC code). To ensure smooth cutting of the rubber mat, a header and additional commands are required. The most critical aspect of the cutting code is the selection of machining parameters. The following section will discuss the selection of

appropriate waterjet machine parameters in relation to cutting quality and cost. An example of CNC code used for the cutting machine.

2.2.2 Abrasive Waterjet Cutting for Customized Rubber Mats

Abrasive Waterjet (AWJ) technology was adopted for post-cutting rubber jigsaw customization due to its distinct advantages, including the absence of thermal damage to target materials, high machining flexibility, and minimal environmental impact [25]. The investigation of AWJ cutting parameters affecting machining performance on rubber mats was conducted based on a preliminary study by Kirdwan et al. [26]. The feasible ranges of the parameters for through-cutting rubber mats were found to be 100-300 MPa of water pressure, 2000-4000 mm/min of cutting speed, 2 mm of standoff distance between the nozzle and the mat, and 350-370 g/min of abrasive mass flow rate of abrasive Garnet mesh 80. These parameters were configured on the Sunrise CUX400-SQ1313AWJ machine, which features an orifice diameter of 0.33 mm and a nozzle diameter of 1.02 mm, as shown in Figure 4(a). The AWJ machining technique operates by pumping ultra-high-pressure water through an aperture to create a jet beam, which is then mixed with abrasive particles in a mixing chamber, as illustrated in Figure 4(b). The AWJ travels through a focusing tube or nozzle, reshaping the jet beam before performing the cutting operation.

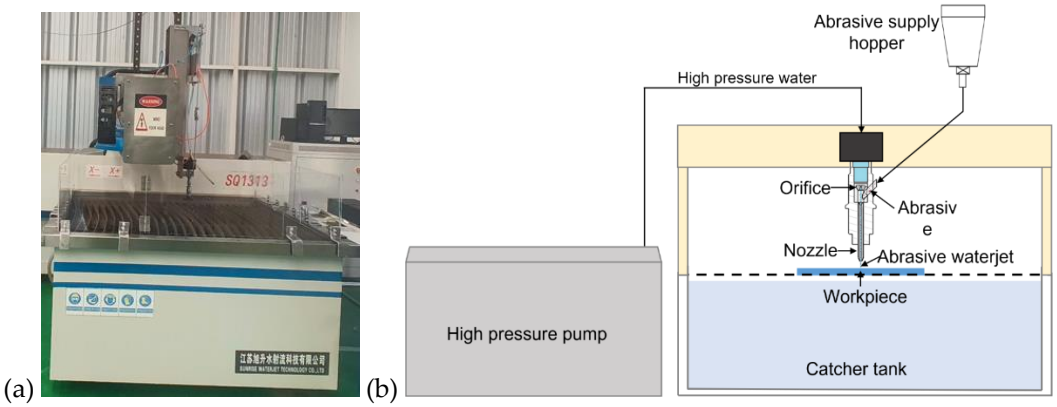

Figure 4. (a) an AWJ machine and (b) an AWJ machining system.

Two rubber mat sizes with the same rubber compound were selected for the experiments: a small mat measuring 200 mm × 200 mm × 5 mm and a large mat measuring 330 mm × 330 mm × 7 mm. The experimental setup for AWJ cutting on rubber mats is shown in Figure 5. The cutting performance indicators, including kerf width, kerf wall inclination angle, and cut surface roughness, were also evaluated.

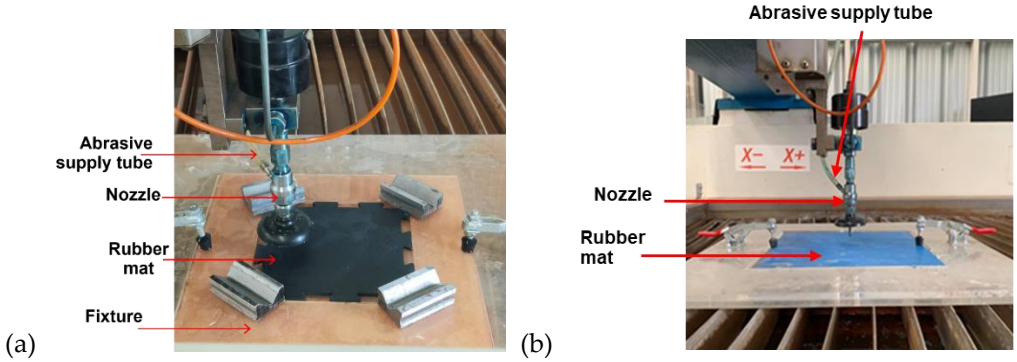

Figure 5. (a) a small mat and (b) a large mat.

The experiment involving the cutting of twelve rubber mat samples revealed that higher water pressure increased jet kinetic energy, resulting in a higher material removal rate and an increased kerf width. Conversely, a faster nozzle traverse speed resulted in reduced kerf width and depth but caused greater taper

and surface roughness. Additionally, both the abrasive mass flow rate and standoff distance influenced kerf width and surface roughness. The rubber cutting removal mechanism is primarily caused by elastic deformation resulting from tensile and shear forces generated by the dynamic jet impact. During the initial cutting stage, the surface of the rubber mat was crushed when deformation exceeded its maximum threshold. A worn-down edge was observed at the kerf top edge (Figure 6(a)), and visible scratches appeared on the cut surface (Figure 6(b)), with the upper section being smoother than the lower section. As the depth of cut increased, jet impact energy decreased, resulting in varying degrees of rupture in the rubber's chemical bonds, leading to a rougher cut surface in the bottom zone [12]. A detailed analysis of the cutting mechanism can be found in Kirdwan et al. [26]. However, based on the cutting parameters considered in this study, the average machined surface roughness was measured at 3.15 μm, which was deemed acceptable for producing a jigsaw rubber mat with high-quality cuts.

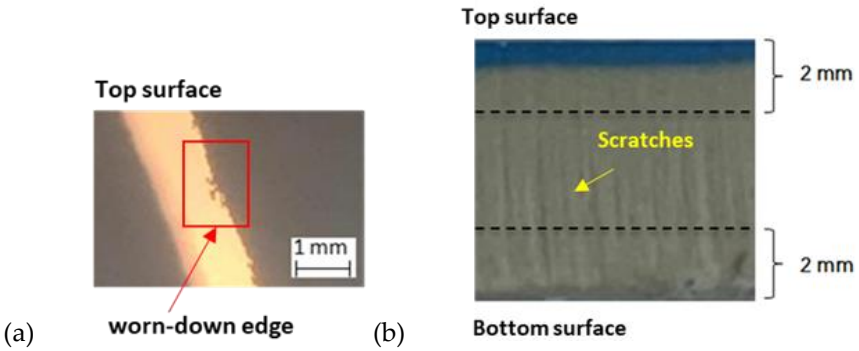

Figure 6. (a) A worn-down edge at the kerf top edge and (b) Scratches on the cut surface [27].

2.2.3 Cost Analysis for Customized Rubber Mats

Cost analysis is one of the key challenges in custom product manufacturing, as variations in unit features from one production lot to another often complicate the determination of overall product costs, particularly those related to cutting processes. Without accounting for these costs, manufacturers may struggle to establish competitive pricing necessary for market survival. In general, the cost of manufacturing jigsaw rubber mats is driven by two main activities: producing rubber blank jigsaws and performing AWJ post-cutting [26]. It is a well-known fact in manufacturing economics that costs can be broadly categorized into fixed and variable costs [28]. In the case of AWJ cutting, fixed costs are primarily influenced by expenses related to machine operations, the jet nozzle, maintenance, and parts replacement [27]. Meanwhile, changes in process parameters—such as water pressure, cutting speed, and abrasive flow rate—significantly impact variable costs. The calculation of AWJ cutting costs per hour was developed in a previous study [27]. That can be expressed as:

$$C_{T,awj} = C_1 + \left(c_{wa} \times \frac{\pi d^2}{4} \times \sqrt{\frac{2P_w}{\rho_w}}\right) + (c_{ab} \times m_{ab}) \quad (6)$$

where the first term of C_1 is the accumulated constant value, including the fixed cost of the AWJ machine system, the cost of tooling, labour, and electricity, as detailed in Table 1. The second and third terms represent the material costs associated with water and abrasive consumption, respectively. In these terms, c_{wa} and c_{ab} are the unit costs of water and abrasive, m_{ab} is the mass flow rate of abrasive consumption, d is the orifice diameter, Pw is the water pressure, and ρ_w is the water density. In this study, d and ρ_w are assumed at 0.33 mm and 997.05 kg/m^3 at 25 ºC, respectively.

From Equation (6), the cost of cutting ($C_{T,awj}$) is expressed in terms of cost per hour (currency unit/hr), which is not applicable in this study, where the variation from one design to another is so high. The cutting cost per piece ($C_{p,awj}$) is rather conclusive. It can be computed as a function of cutting speed and cutting length [27].

$$C_{p,awj} = L_t \times \left(C_{T,awj}/v\right) \quad (7)$$

where L_t is the cutting length (m) and v is the cutting speed (m/h). $C_{T,awj}$ can be determined in terms of the cutting cost per meter ($C_{m,awj}$). The constant values in Equation (6) can be obtained from the case study factory, as shown in Table 1, where a detailed analysis of AWJ cutting costs is discussed in Thongkaew et al. [27]. Thus, the cutting cost per meter under the condition of the case study factory can be expressed as:

$$C_{m,awj} = \frac{C_{T,awj}}{v} = \frac{1}{v}\left(5.05 + 2.49 \times 10^{-9} \cdot \sqrt{P_w} + 0.18 m_{ab}\right) \quad (8)$$

Table 1. Cost elements of the AWJ cutting from the case study factory [27]

Cost Element	Value	Cost	Note
- AWJ machining system cost (C_s)	2.00	USD / hr	
- Tooling cost (C_t)	1.66	USD / hr	The accumulated constant
- Labor cost (C_l)	1.30	USD / hr	value (C1) from Eq. (6)
-Electricity cost (C_e)	0.99	USD / hr	
-Unit cost of water (c_{wa})	0.63	USD / m^3	
-Unit cost of abrasive (c_{ab})	0.18	USD / kg	

Based on Equation (8), it is evident that the cutting cost is primarily influenced by cutting speed, water pressure, and the abrasive mass flow rate. Adjusting these parameters directly impacts cutting quality, as previously discussed. The interdependencies among these parameters can complicate cost analysis; however, an optimal solution exists and can be determined using Equation (9).

The minimum cutting cost function is constrained by a set of process parameters and is solved using the built-in *fmincon* function in MATLAB 2023a Optimization Toolbox [29], which allows for the minimization of a nonlinear multivariable equation under specified constraints.

- Objective function

$$min\, C_{m,awj} = \frac{1}{v}\left(5.05 + 2.49 \times 10^{-9} \cdot \sqrt{P_w} + 0.18 m_{ab}\right) \quad (9)$$

- Constraints

(a) $120 \leq v \leq 240$ (m/h) (Constraint of cutting speed)
(b) $100 \times 10^6 \leq P_w \leq 300 \times 10^6$ (Pa) (Constraint of water pressure)
(c) $20.99 \leq m_{ab} \leq 22.21$ (kg/h) (Constraint of abrasive mass flow rate)
(d) $6.315 + 0.000332v - 0.000613P_w - 0.01065\, m_{ab} \leq 4$ (Constraint of surface roughness)
(e) $-1.087 - 0.00027v - 0.000674P_w + 0.00776 m_{ab} \leq 2$ (Constraint of kerf width)

3. Results and Discussion

3.1 Customized Rubber Mats: Cutting Path Configuration

The spacing factor and tolerance of the cutting paths directly impact the number of cutting points and the cutting length. A larger spacing factor and higher tolerance result in fewer cutting points. However, this reduction can cause the processed image to deviate from the original design submitted by the customer. Therefore, selecting an appropriate spacing factor and tolerance is crucial to preserving the originality of the image while maintaining a cost-effective number of cutting points. In this study, a similarity index obtained from the *ssim* function in MATLAB 2023a was used to evaluate how closely the processed image matched the original design. The study considered the effects of cutting patterns, spacing factors, and tolerances. The spacing factor ranged from 2 to 10, while the tolerance was set between 0 and 1, as shown in Table 2. Table 2 presents the number of cutting points, cutting length, and similarity index for three cutting patterns—an apple, the letter "A," and the letter "R" (Figure 7)—in relation to variations in spacing factor and tolerance.

Table 2. The number of cutting points and similarity indices as affected by the spacing factors and the tolerances.

Spacing Factor (*s*)	Tolerance (*t*)	Apple		A		R	
		Cutting Points	Similarity	Cutting Points	Similarity	Cutting Points	Similarity
2	0	518	0.9948	507	0.9978	817	0.9977
2	0.5	517	0.9949	507	0.9978	817	0.9977
2	0.7	517	0.9949	507	0.9978	817	0.9977
2	0.8	360	0.9835	232	0.9726	720	0.9936
2	0.85	358	0.9831	231	0.9722	720	0.9936
2	0.9	56	0.9567	57	0.9656	72	0.9597
2	0.95	55	0.9562	57	0.9656	68	0.9587
2	1	45	0.9553	40	0.9641	52	0.958
3	0	387	0.9935	410	0.997	577	0.9968
3	0.5	340	0.9935	376	0.9969	445	0.9968
3	0.7	339	0.9935	376	0.9969	445	0.9968
:	:	:	:	:	:	:	:
8	0.85	153	0.9905	109	0.984	247	0.9943
8	0.9	143	0.9895	102	0.9802	237	0.994
8	0.95	130	0.9888	81	0.9788	186	0.9926
8	1	94	0.9851	73	0.9786	93	0.9865
10	0	161	0.9888	142	0.9941	222	0.9936
10	0.5	159	0.9888	133	0.9941	212	0.9936
10	0.7	157	0.9888	133	0.9941	212	0.9936
10	0.8	145	0.9883	106	0.9873	210	0.9935
10	0.85	140	0.9879	97	0.9854	209	0.9936
10	0.9	131	0.9871	79	0.9796	201	0.9932
10	0.95	126	0.9869	75	0.9804	156	0.9928
10	1	88	0.9859	66	0.9801	90	0.9851

Table 2 illustrates that the resulting tool paths undergo physical changes in response to adjustments in the spacing factor and tolerance. As these parameters increase, the number of cutting points decreases, simplifying both calculation and machining. However, this also causes the path to deviate significantly from the original scribble. Figure 8 further demonstrates the cutting routes generated with different spacing factors and tolerances.

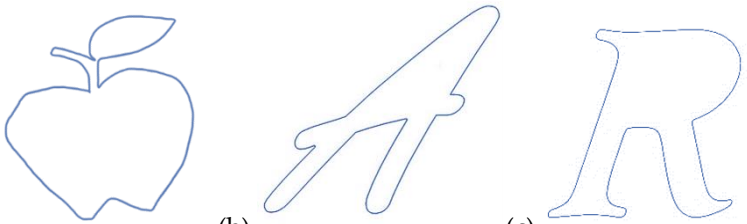

(a) (b) (c)

Figure 7 (a) an apple, (b) the letter A, and (c) the letter R.

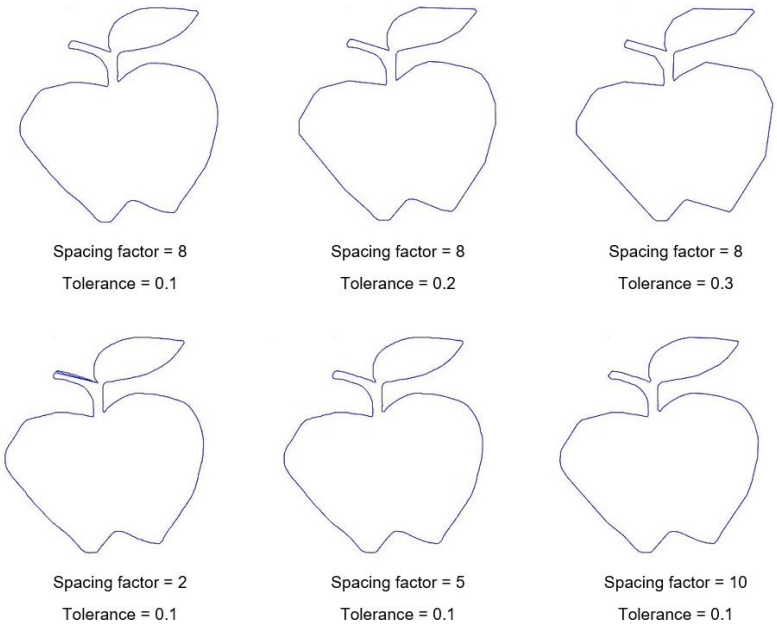

Figure 8. Examples of cutting paths at different spacing factors and tolerances.

However, as the degree of simplification increases, the similarity to the original design decreases. The number of cutting points and the similarity index were plotted across different spacing factors and tolerances to determine the optimal balance. Figure 9 highlights the optimal cutting points for each distinct cutting pattern (an apple, the letter "A," and the letter "R"). The optimal condition is identified at the point where the graph transitions abruptly to an almost horizontal line, indicating that further increasing the number of cutting points would provide only a marginal improvement in similarity. The recommended number of cutting points for the apple was 153, yielding a similarity index of 0.9905, with a spacing factor of 8 and a tolerance of 0.85. This represents a significant reduction from the original 2,040 cutting points while maintaining a high level of accuracy.

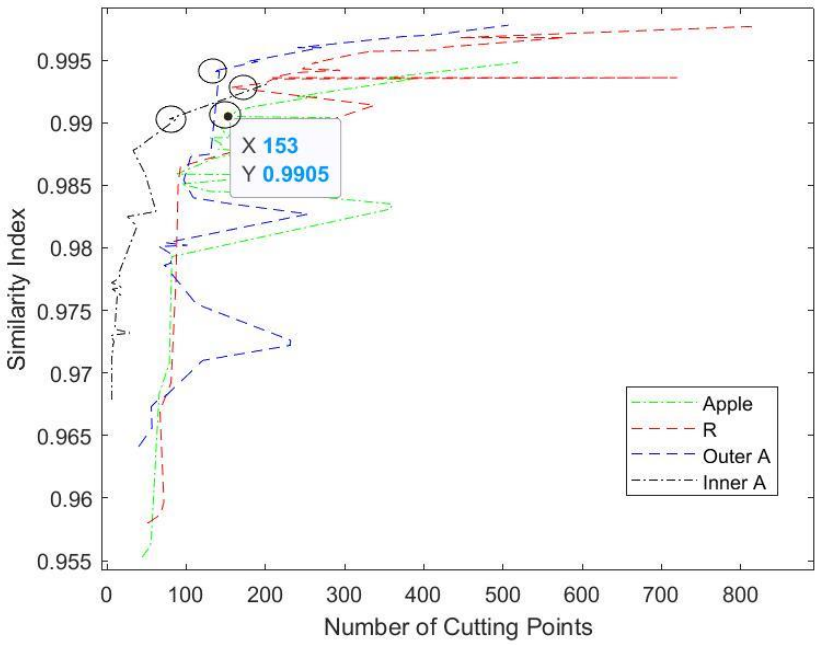

Figure 9. Similarity indices vs. No. of cutting points corresponding to spacing factor and tolerance.

The number of cutting points is initially reduced by adjusting the spacing factor. As the spacing factor increases, the path appears more like a chain of linear segments, resulting in a lower similarity index. As shown in Table 2, when the tolerance is small, most cutting points (pixel-wise) are retained, leading to a very high similarity. However, when the tolerance is increased, some points can be excluded as long as they remain within the allowable range.

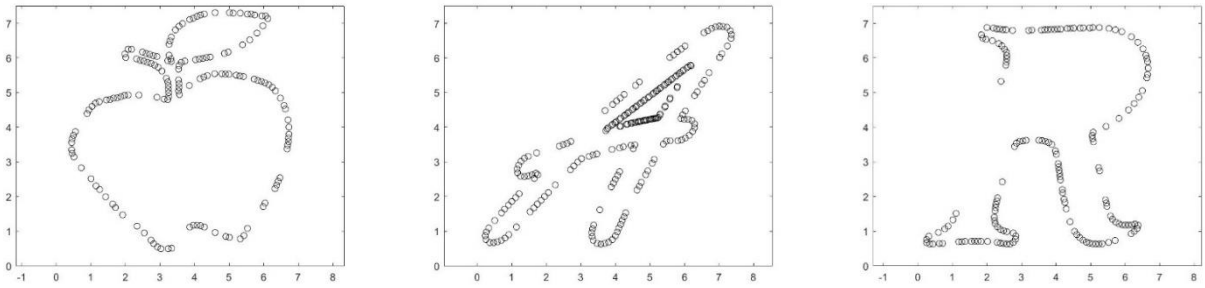

(a) (b) (c)

Figure 10. The cutting paths of (a) the apple, (b) the letter A, and (c) the letter R.

The points are more concentrated in areas where the curve changes direction abruptly, as observed in Figure 10. The selected tool paths for the apple, the letter "A," and the letter "R" demonstrate a significant reduction in the number of cutting points from their initial values, resulting in fewer than 200 points. Although the letter "A" appears to be composed mainly of straight lines, some segments gradually change direction, resulting in more cutting points than expected. Using the similarity index helps identify the optimal parameters for generating an efficient tool path.

3.2 Samples of Customized Rubber Mats: Cutting Cost Analysis

After determining the optimal cutting path, a cost analysis of the cutting process was conducted, taking into account economic considerations. Using the *fmincon* function to solve Equation (9) for the minimum cutting cost, the optimal cutting parameters were established as follows: 100 MPa water pressure, 4000 mm/min (or 240 m/hr) cutting speed, and an abrasive mass flow rate of 350 g/min (or 20.99 kg/h). Under these conditions, the unit cutting cost per meter ($C_{m,avj}$) was calculated using Equation (8), resulting in a cost of 0.37 USD/m. In addition to similarity considerations, the number of cutting points also influences the cutting length, which directly affects the cutting cost. Table 3 provides an example of the cutting cost for the apple at different numbers of cutting points. The apple, the letter "A," and the letter "R" were all cut to create customized jigsaw rubber mats using the recommended tool paths and cutting parameters shown in Figure 11.

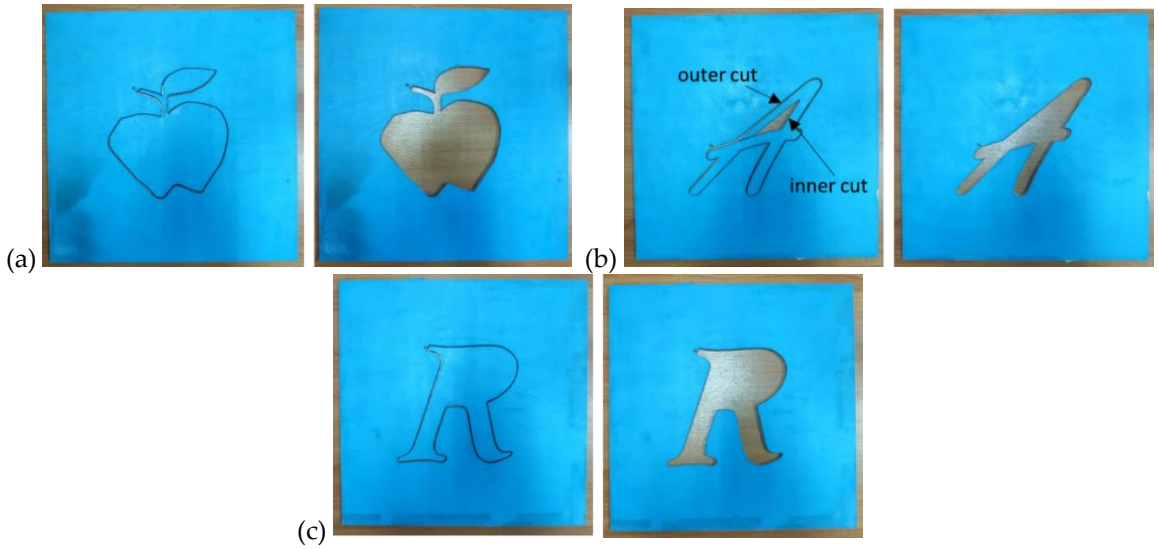

Figure 11. (a) apple shape, (b) A letter, and (c) an R letter.

Table 3. Cutting costs are affected by the cutting point and cutting distance of the apple.

Spacing Factor	Tolerance	Cutting Point	Cutting Length (mm)	Similarity	Cutting Time (s)	Cutting Cost (USD)
2	0	518	828.04	0.9948	12.4206	0.3064
2	0.5	517	828.04	0.9949	12.4206	0.3064
2	0.7	517	828.04	0.9949	12.4206	0.3064
2	0.8	360	824.99	0.9835	12.3749	0.3052
2	0.85	358	824.99	0.9831	12.3749	0.3052
2	0.9	56	814.32	0.9567	12.2148	0.3013
2	0.95	55	814.32	0.9562	12.2148	0.3013
2	1	45	813.56	0.9553	12.2034	0.3010
:	:	:	:	:		:
8	0.85	153	745.49	0.9905	11.1824	0.2758
8	0.9	143	745.49	0.9895	11.1824	0.2758
8	0.95	130	745.24	0.9888	11.1786	0.2757
8	1	94	744.98	0.9851	11.1747	0.2756
10	0	161	742.44	0.9888	11.1366	0.2747
:	:	:	:	:		:
		Average	792.3031	0.9817	11.8845	0.2932
		Std. Dev.	39.4897	0.0151	0.5923	0.0288

Table 4 presents the cutting time and cutting cost for each design, calculated using Equation (9), with cutting parameters set at a water pressure of 100 MPa, a cutting speed of 4000 mm/min, and an abrasive mass flow rate of 350 g/min. According to a previous study, the estimated production cost of a rubber blank mat was 2.90 USD per piece [27]. With the recommended cutting parameters, the post-AWJ process yielded a jigsaw rubber mat at an estimated cost of 0.37 USD per piece, adding only 12.76% to the overall manufacturing cost of the blank mat. Additionally, this cutting process operates at a very high speed, requiring less than 12 seconds per piece, making it a commercially viable option for typical industrial applications.

Table 4. Cutting time and cutting the cost of each scribble with selected parameters.

Scribble	Spacing Factor	Tolerance	Cutting Point	Cutting Length (mm)	Similarity	Cutting Time (s)	Cutting Cost (USD)
Apple	8	0.85	153	745.490	0.99	11.182	0.2758
A	10	0.7	133	702.82	0.99	10.542	0.2600
R	10	0.95	156	771.40	0.99	11.571	0.2854

Based on the analysis, personalized jigsaw rubber mats can be efficiently produced using AWJ cutting in a short time, incurring only an additional cost of approximately 13% of the total production cost of blank rubber mats. This remarkably low cost is achieved through the flexibility and agility of soft automation. The combination of imaging techniques for generating AWJ tool paths and optimizing cutting parameters has proven to be an economically viable solution for meeting custom demands. While this approach is designed to simplify the design and manufacturing processes of custom rubber mats, it also accommodates a wide range of product configurations at a competitive cost, comparable to that of mass-produced goods.

3.3 Manufacturing Cost Comparison of Customized Rubber Mats

Figure 12 presents a comparative analysis of the production costs for customized jigsaw rubber mats manufactured using three different techniques: molding, die cutting, and AWJ cutting. The costs of these manufacturing methods are displayed in relation to the quantity of finished products. The cost of traditional molding was calculated based on the fixed cost of a new mold, approximately $ 3,600, along with the variable cost of producing a rubber blank mat, which was $ 2.90 per unit [27]. The cost of die post-cutting was estimated

by combining the total unit cost of manufacturing a blank rubber mat with the cost of die post-cutting, which includes expenses for a swing arm machine, labor, and electricity. The cost per piece for die cutting was approximately 9.15 USD. The cost of AWJ post-cutting was determined by adding the total unit cost of manufacturing a blank rubber mat to the AWJ post-cutting cost, which was 0.37 USD per piece.

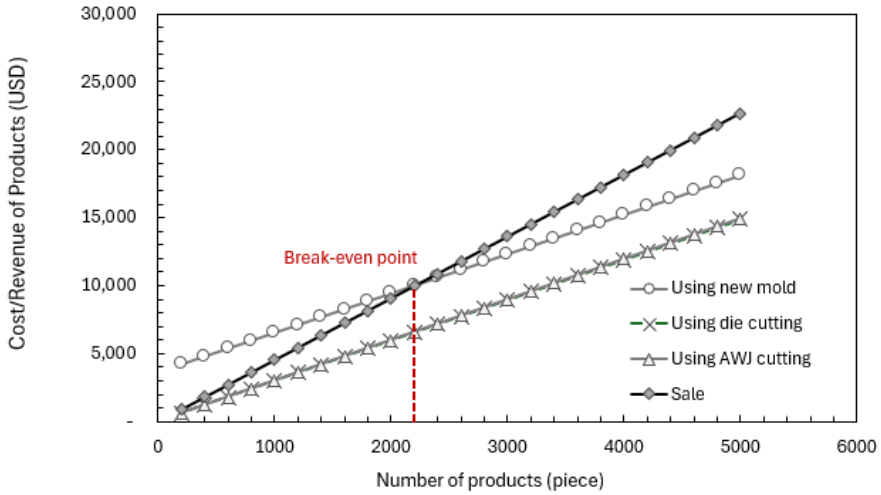

Figure 12. Customized rubber mat production costs of molding, die cutting, and AWJ cutting.

It was assumed that the unit sale price of a jigsaw rubber mat was 50% higher than its manufacturing cost, resulting in an estimated sale price of approximately 4.54 USD. According to Figure 12, the breakeven point for using the molding method was around 2,200 pieces, whereas both die cutting and AWJ cutting could generate a profit from the very first piece. However, die cutting required additional time for the production of a new die by a subcontractor, which could take up to a week. Thus, the findings indicate that AWJ post-cutting is a more suitable method for producing small quantities of customized products, offering a rapid response time and lower manufacturing costs without the need for new mold or die investments.

4. Conclusions

In this study, abrasive waterjet (AWJ) cutting was employed to transform a blank rubber mat into a custom-designed jigsaw rubber mat. This approach enhances the competitiveness of small enterprises by enabling them to offer more value-added products tailored to specific or personalized customer requirements. Once a customer's design is submitted, an AWJ cutting plan is automatically generated, along with an estimate of the production cost. To preserve the originality of the design, it is essential for manufacturers to carefully control tool path parameters, such as the spacing factor and tolerance, as these vary depending on the design. The findings of this study indicate that the additional cost of post-cutting with AWJ to produce customized jigsaw rubber mats was only approximately 13% of the total production cost. This is relatively low in comparison to the conventional method of creating a new mold. The comparative analysis further confirmed that post-AWJ cutting is well-suited for producing small to medium quantities of customized rubber mats, due to its rapid response time and lower manufacturing costs, which are achieved by eliminating the need for new mold investments. Additionally, automated machining processes, such as AWJ cutting, have become increasingly affordable in recent years. Therefore, the approach demonstrated in this study holds significant potential for small manufacturers, enabling them to leverage agility and responsiveness to remain competitive.

5. Acknowledgements

This research was financially supported by the Natural Rubber Innovation Research Institute, Prince of Songkla University (Grant No ENG62010975). The authors would also like to thank the Faculty of Engineering, Prince of Songkla University, for facility support, as well as Pornteap Kirdwan for operational support, and Rattaphum Agricultural Cooperative Ltd. for providing resources for AWJ machine rubber blanks.

Author Contributions: Conceptualization, K.T. and S.C.; methodology, K.T. and S.C.; validation, C.D. and S.C.; formal analysis, K.T.; data curation, K.T.; writing—original draft preparation, K.T.; writing—review and editing, Z.M. and S.C. All authors have read and agreed to the published version of the manuscript.

Funding: This research was funded by the Natural Rubber Innovation Research Institute, Prince of Songkla University (Grant No ENG62010975).

Conflicts of Interest: The authors declare no conflict of interest.

References

[1] Bank of Thailand. Thailand Exports: Agriculture: Rubber. CEIC Data. https://www.ceicdata.com/en/thailand/exports-by-product-group/exports-agriculture-rubber (accessed 2022-01-26).

[2] Isayev, A. I. *Injection and Compression Molding Fundamentals*; Marcel Dekker Inc.: New York and Basel, **1987**. https://doi.org/10.1201/9780203750810

[3] Murthy, B. S.; Eifler, T.; Howard, T. J.; McMahon, C. Mass Production Tools and Process Readiness for Uniform Parts—Injection Molding Application. *J. Polym. Compos.* **2017**, *5*(3), 311–320.

[4] Fogliatto, F. S.; Silveira, G. J. C.; Borenstein, D. The mass customization decade: An updated review of the literature. *Int. J. Prod. Econ.* **2012**, *138*(1), 14–25. https://doi.org/10.1016/j.ijpe.2012.03.002

[5] Wang, Y.; Ma, H. S.; Yang, J. H.; Wang, K. S. Industry 4.0: a way from mass customization to mass personalization production. *Adv. Manuf.* **2017**, *5*(4), 311–320. https://doi.org/10.1007/s40436-017-0204-7

[6] Doner, R.; Abonyi, G. Upgrading Thailand's Rubber Industry: Opportunities and Challenges. *Thammasat Econ. J.* **2013**, *31*(4), 44–66.

[7] Mitsomwang, P.; Nagasawa, S.; Kuroiwa, H.; Fukushima, Y. Deformation Analysis of Silicone Rubber Sheet Subjected to Keen WC Blade Indentation. *Int. J. Autom. Technol.* **2024**, *8*(5), 761–772. https://doi.org/10.20965/ijat.2014.p0761

[8] Kojima, M.; Nagasawa, S.; Igarashi, Y. Cutting Characteristics of Silicone Rubber Sheet with Respect to Indentation Velocity of Keen Wedge Blade. *J. Jpn. Soc. Technol. Plast.* **2020**, *61*(708), 1–6. https://doi.org/10.9773/sosei.61.1

[9] Mispan, M. S.; Mustafa, A. H.; Sarkawi, H.; Jidin, A. Z. Low-cost and portable automatic sheet cutter. *Int. J. Electr. Comput. Eng.* **2020**, *10*(5), 5139–5146. https://doi.org/10.11591/ijece.v10i5.pp5139-5146

[10] Mizzi, L.; Salvati, E.; Spaggiari, A.; Tan, J. C.; Korsunsky, A. M. Highly stretchable two-dimensional auxetic metamaterial sheets fabricated via direct-laser cutting. *Int. J. Mech. Sci.* **2020**, *167*, 105242. https://doi.org/10.1016/j.ijmecsci.2019.105242

[11] Mizzi, L.; Salvati, E.; Spaggiari, A.; Tan, J. C.; Korsunsky, A. M. A decision guidance framework for non-traditional machining processes selection. *Ain Shams Eng. J.* **2018**, *9*(1), 203–214. https://doi.org/10.1016/j.asej.2015.10.013

[12] Hu, Y.; Kang, Y.; Wang, X. C.; Li, X. H.; Long, X. P.; Zhai, G. Y.; Huang, M. Mechanism and Experimental Investigation of Ultra High-Pressure Water Jet on Rubber Cutting. *J. Precis. Eng. Manuf.* **2014**, *15*(9), 1973–1978. https://doi.org/10.1007/s12541-014-0553-0

[13] Tangwarodomnukun, V.; Koomsap, P.; Chowdhary, A. A Preliminary Study of Applying Waterjet for Rapid Prototyping. Presented at The 11th Asia Pacific Industrial Engineering and Management Systems Conference, Melaka, Malaysia, **2010**.

[14] Natarajana, Y.; Murugesan, P. K.; Mohan, M.; Khan, S. A. L. A. Abrasive water jet machining process: a state of art of review. *J. Manuf. Processes* **2020**, *49*, 271–322. https://doi.org/10.1016/j.jmapro.2019.11.030

[15] Chen, J. F.; Yuan, Y. M.; Gao, H.; Zhou, T. Y. Smoothing strategy for corner of small curvature radius by abrasive waterjet machining. *Adv. Manuf.* **2023**, *11*(2), 390–406. https://doi.org/10.1007/s40436-023-00443-3

[16] Andersson, U.; Holmqvist, G. Strategies for Cost- and Time-effective Use of Abrasive Waterjet Cutting. Presented at WJTA American Waterjet Conference, Houston, Texas, **2005**.

[17] Radovanovic, M. Abrasive waterjet cutting cost. *Nonconventional Technol. Rev.* **2007**, *1*(1), 97–102.

[18] Radovanović, M. Cost optimization of abrasive water jet cutting using GA. *Tribol. J. BULTRIB* **2013**, *3*(3), 70–75.

[19] Ciupan, E.; Ciupan, C.; Lungu, F. The cost estimation of a water jet cutting process using artificial neural networks. *Nonconventional Technol. Rev.* **2018**, *22*(4), 26–30.
[20] Radovanovic, M. Multi-Objective Optimization of Abrasive Water Jet Cutting Using MOGA. In *23rd International Conference on Material Forming (ESAFORM 2020)*; Elsevier: Amsterdam, **2020**, *47*, 781–787. https://doi.org/10.1016/j.promfg.2020.04.241
[21] Kuagoolkijgarn, P.; Koomsap, P. Applying Image Processing for Rapid Customization of Multi-Color Nested Pattern Products. In *New World Situation: New Directions in Concurrent Engineering. Advanced Concurrent Engineering*; Springer: London, **2010**; pp 401–414. https://doi.org/10.1007/978-0-85729-024-3_40.
[22] Thai Industrial Standard Institute. Rubber Flooring: TIS 2377-2008; Thai Industrial Standard: Thailand, **2008**.
[23] Feng, H. Y.; Teng, Z. Iso-planar piecewise linear NC tool path generation from discrete measured data points. *Comput.-Aided Des.* **2005**, *37*(1), 55–64. https://doi.org/10.1016/j.cad.2004.04.001
[24] MathWorks. *Image Processing Toolbox User Guide*; The MathWorks, Inc: **2023**.
[25] Wang, J. *Abrasive Waterjet Machining of Engineering Materials*; Trans Tech Publications Inc, **2003**. https://doi.org/10.4028/www.scientific.net/MSFo.19
[26] Kirdwan, P.; Thongkaew, K.; Daesa, C.; Chaiprapat, S. Influence of Abrasive Waterjet Cutting on Efficiency of Cutting Rubber Floor Mats. *J. King Mongkut's Univ. Technol. North Bangkok* **2025**, *35*(1), 1–12. https://doi.org/10.14416/j.kmutnb.2024.09.004
[27] Thongkaew, K.; Naemsai, T.; Mustafa, Z. Cost Estimation for Post Abrasive Waterjet Cutting on Customized Jigsaw Rubber Mats. *J. Adv. Manuf. Technol.* **2023**, *1*(1), 1–16.
[28] Krachangphiphop, P.; Wannasin, J.; Meemongkol, N. Process-based cost modelling for gas induced semi-solid-processed below-knee prosthesis. *Int. J. Prod. Res.* **2018**, *56*(4), 1361–1368. https://doi.org/10.1080 00207543.2017.1364441
[29] MathWorks. *Optimization Toolbox User Guide*; The MathWorks, Inc: **2023**.

ASEAN
Journal of Scientific and Technological Reports
Online ISSN:2773-8752

Research article

Optimization of Hydrogen and Methane Co-production from Co-digestion of Canned Seafood Wastewater with Glycerol Waste in a Two-stage Continuous System: Comparing CSTR-PFR and CSTR-CSTR Reactors

Tussanee Srimachai[1, 6, 7, 8], Mathavee Thipmunee[2], Yakob Longsoh[2], Peemanas Manaswin[4], and Kiattisak Rattanadilok Na Phuket[5, 6, 7, 8*]

[1] College of Innovation and Management, Songkhla Rajabhat University, Songkhla, 90000, Thailand
[2] Biofuel and Biocatalysis Innovation Research Unit, Mahidol University, Nakhonsawan Campus, 60130, Thailand;
[3] La-ngu Industrial and Community Education College, Satun, 91100, Thailand
[4] College of Innovation and Management, Songkhla Rajabhat University, Songkhla, 90000, Thailand
[5] College of Innovation and Management, Songkhla Rajabhat University, Songkhla, 90000, Thailand
[6] Faculty of Science and Technology, Songkhla Rajabhat University, Songkhla, 90000, Thailand
[7] Microbial Resources and Utilization Center SKRU, Songkhla Rajabhat University, Songkhla, 90000, Thailand
[8] Community Innovation Learning and Transfer Center "Thung Yai Sarapee Model" Songkhla Rajabhat University, Satun, 91100, Thailand
* Correspondence: kiattisak.pa@skru.ac.th

Citation:
Srimachai, T.; Thipmunee, M., Longsoh, Y.; Manaswin, P., Rattanadilok Na Phuket, K. Optimization of hydrogen and methane Co-production from Co-digestion of canned seafood wastewater with glycerol waste in a two-stage continuous wystem: comparing CSTR-PFR and CSTR-CSTR reactors. *ASEAN J. Sci. Tech. Report.* **2025**, *28*(6), e259743. https://doi.org/10.55164/ajstr.v28i6.259743.

Article history:
Received: July 26, 2025
Revised: September 20, 2025
Accepted: September 27, 2025
Available online: October 19, 2025

Abstract: The challenge posed by canned seafood wastewater (CSW) involves a low COD of 6.80 g/L and a high protein concentration of 3.56 g/L, making it unsuitable for hydrogen and methane production. Consequently, the potential return on investment for establishing a commercial system remains inadequate. To address this issue, a two-stage anaerobic digestion system incorporating co-digestion with glycerol waste (GW) was implemented. The two-stage co-digestion of CSW with GW, at various mixing ratios of 99:1, 98:2, 97:3, 96:4, and 95:5% (v/v), resulted in hydrogen yields of 15.6, 33.6, 38.7, 65.0, and 6.3 ml H_2/g COD, respectively, while methane yields were measured at 311, 320, 326, 345, and 99 ml CH_4/g COD, correspondingly. The ideal conditions for achieving the highest yields of hydrogen and methane from the anaerobic co-digestion of CSW with GW were found to be at a mixing ratio of 96:4% (v/v). The ongoing production of hydrogen and methane in a two-stage process utilizing CSTR-PFR and CSTR-CSTR reactors can yield hydrogen and methane at rates of 27.44 and 163.61 L/L of wastewater, and 20.41 and 145.35 L/L of wastewater, respectively. Anaerobic co-digestion of CSW with GW could enhance the production of hydrogen and methane from a two-stage anaerobic digestion system.

Keywords: Hydrogen; methane; canned seafood wastewater; glycerol waste; two-stage anaerobic digestion system

1. Introduction

Hydrogen and methane are types of renewable energy from the decomposition of organic waste, such as sewage and industrial waste, used in the production of hydrogen (Hydrolysis, Acidogenesis) and methane production (Methanogenesis). The microorganism was divided into two phases. Acidogenic bacteria produce a pH of 5-6 and a hydraulic retention time (HRT) of 2 days in the system. As part of the methane production process, the

methanogen requires different conditions from the acid-producing bacteria. The pH value in this stage ranges from 7 to 8 and takes about 15–20 days. Separating the two microorganisms will help to degrade the substance. Single digestion and co-digestion to balance nutrients. It allows the degradation process to occur completely, and it could harvest hydrogen and methane [1]. Bertasini et al. [2] reported that hydrogen-methane co-production is achieved through anaerobic fermentation using a two-stage biological process. In the first stage, known as dark fermentation, microorganisms break down biomass feedstocks to produce hydrogen and volatile fatty acids (VFAs). In the second stage, methanogenic microorganisms are added to the effluent from the first stage, which utilizes anaerobic fermentation to convert the VFAs produced during hydrogen production into methane [3].

Sillero et al. [4] reported that the agri-food industry generates numerous waste streams of different origins and compositions, which are susceptible to pollution sources. Canned seafood wastewater represents a significant industry that provides advantages for Thailand. The process of seafood canning consumes a substantial amount of water, resulting in high levels of effluent ranging from 14 to 20 cubic meters per ton of material [5]. The chemical makeup of canned seafood wastewater (CSW) includes nitrogen concentrations between 80 and 1,000 mg/l, COD levels from 1,000 to 18,000 mg/l, and BOD values ranging from 100 to 3,000 mg/l [6]. Anaerobic digestion is less popular than the problem of organic nitrogen and high sodium concentrations. This substance inhibits microbial activity in anaerobic systems [7]. Canned seafood processing wastewater contains high levels of protein and fat, which tend to degrade ammonia quickly in anaerobic conditions. The tiny amount of biogas generated as a result of these limitations makes the expense of building an anaerobic treatment system unjustified. Most seafood processing plants do not use an anaerobic digestion system for wastewater treatment. Most factories prefer to use aeration systems instead because they are easier to manage, but they also have higher energy costs. However, the problem can be solved by using a common fermentation technology. Co-digestion technology is the use of wastewater from fermented canned seafood processing plants in combination with other organic carbon sources. The advantage of joint fermentation technology is the concentration of organic matter in the effluent, expressed as COD. Dissolved toxins reduce the effect of methane-producing microorganisms in wastewater, resulting in higher methane yield [8].

Approximately 10% of the raw materials used in biodiesel manufacturing are glycerol wastes, which are byproducts of the process [9]. In 2011, the world's total glycerol waste was about 3,000,000 metric tons. It is expected to increase to 4,600,000 tons by 2020, based on the expansion of biodiesel production [10]. The advantages of using glycerol waste include an easy-to-digest fermentation process during the decomposition process, which enhances the C: ratio due to its high carbon content, and dilutes the poison in the system [11]. The use of glycerol waste as a co-fermentation medium has been reported to increase methane production by 50-200% due to the optimal use of suitable fermentation media, which promotes the fermentation process to yield positive synergies. Therefore, it is possible to utilize fermentation technology to develop and apply it to canned seafood processing factories. This is a waste treatment process that can add value to waste by converting it into energy. It is interesting because it has the potential to develop into a sustainable source of energy in the future. The study focused on optimizing the production of hydrogen and methane through the single digestion of canned seafood wastewater and glycerol waste, as well as the co-digestion of these two waste streams. Additionally, it examined continuous hydrogen and methane production by comparing the reactor's performance in methane processes using a two-stage anaerobic method.

2. Materials and Methods

2.1 Feedstock and inocula

Canned seafood wastewater from Siam International Food Company, Songkhla, Thailand. Inocula from the biogas system of Chotiwat Hatyai, trading frozen food, Songkhla, Thailand. Characteristics of canned seafood wastewater and glycerol waste are shown in Table 1. Anaerobic sludge was collected from the biogas system. The sludge was treated by heating, where it was boiled at 100 °C for 1 h [12] to remove methanogenic bioactivity from the hydrogen inoculum. Before using the hydrogen, the inoculum was starved for 1 week to minimize the effects of organic materials contained in the microbial sludge before starting the system. The methane inoculum was incubated at pH 7 under mesophilic conditions (37°C).

2.2 Batch reactor

Hydrogen and methane production from single digestion of canned seafood wastewater (CSW 50, 60, 70, 80, 90 and 100% (v/v)), glycerol waste (GW 1, 2, 3, 4, and 5% (v/v)) and co-digestion canned seafood wastewater with glycerol waste was tested at different mixing ratios were determined in batch assays under the mesophilic condition as described previously. The first stage was operated in a batch test under an initial pH of 5.5. Hydrogen effluent was investigated for methane production in the second stage under an initial pH of 7. A two-stage batch fermentation system, comprising hydrogen fermentation in the first stage and methane fermentation in the second stage, was established in 500 mL serum bottles with a working volume of 200 mL. Two-stage anaerobic co-digestion of CSW with GW at concentrations of 99:1, 98:2, 97:3, 96:4, and 95:5% (v/v). The system was flushed with nitrogen gas to generate anaerobic conditions. During the fermentation experiment, total gas volume and composition were periodically monitored by gas counters and gas chromatography, respectively.

2.3 Continuous reactor

Continuous anaerobic co-digestion of CSW with GW was operated by comparing the continuous stirred-tank reactor (CSTR) to the plug-flow reactor (PFR), R1, and the continuous stirred-tank reactor (CSTR) to the continuous stirred-tank reactor (CSTR), R2. Working volumes are 1 L (1-stage) and 5 L(2-stage), respectively. The continuous experiment was operated under the optimal conditions determined from the batch test. Experiment reactors were operated at HRTs of 2, 3, 4, and 5 days for the hydrogen stage (1-stage) and HRTs of 10, 15, 20, and 25 days for the methane stage (2-stage) under mesophilic conditions. The biogas production was measured by water displacement (using a gas counter) every day. Biogas composition analysis by GC-TCD.

2.4 Microorganism community analysis by DGGE

Polymerase chain reaction-denaturing gradient gel electrophoresis (PCR-DGGE) was employed in this study to analyze the microbial community structure, following the methodology described by Kongjan et al. [13]. The PCR products obtained from the experiment were purified and sequenced by Macrogen Inc. (Seoul, Korea). The closest matches for the partial 16S rRNA gene sequences were determined by performing database searches in GenBank using BLAST [14].

2.5 Analytical methods

The protein, carbohydrate, lipid content, pH, volatile fatty acids (VFAs), and alkalinity of CSW and GW were assessed. Standard procedures for examining wastewater were applied to single digestion of canned seafood wastewater, glycerol waste, and co-digestion of wastewater with glycerol waste. The amount of biogas produced daily for each test was noted using the water displacement technique [15]. Gas chromatography with thermal conductivity detectors (TCD) was employed to analyze the composition of the biogas. Methane, carbon dioxide, hydrogen, and nitrogen were evaluated using a GC-TCD equipped with a 3.3 ft stainless steel column packed with Shin Carbon (60/80 mesh). Argon served as the carrier gas at a flow rate of 14 mL/min. The temperatures for the injection port, oven, and detector were set at 120 °C, 40 °C, and 100 °C, respectively [16]. A 1 mL gas sample was injected in two separate trials for H_2 (1-stage) and CH_4 (2-stage). The theoretical methane potential was calculated based on the elemental composition of carbon, hydrogen, nitrogen, and oxygen using Bushwell's formula, which is derived from the stoichiometric conversion of the compound to methane [17]. The energy yield from biogas was estimated using energy factors of 12.9 J per mL of H_2 and 40.1 J per mL of CH_4 [18].

3. Results and Discussion

3.1 Substrate and co-substrate characterization

The CSW was sourced from Siam International Food Company, located in Songkhla, Thailand. The primary components of CSW included a pH of 7.3, 6.8 g/l of total chemical oxygen demand (COD), 2.48 g/l of total solids, 1.23 g/l of volatile solids, 0.57 g/l of total nitrogen, 3.56 g/l of protein, 0.19 g/l of carbohydrate, and 1.55 g/l of fat. Following its collection, the CSW was kept at -20 ºC until needed. The glycerol waste (GW) was

obtained from the biodiesel facility at Prince of Songkhla University's Hat-Yai campus in southern Thailand. The key components of GW were as follows: a pH of 8.7, 1,082 g/l of total chemical oxygen demand (COD), 279.53 g/l of total solids, 254.96 g/l of volatile solids, 0.26 g/l of total nitrogen, 1.65 g/l of protein, 845 g/l of carbohydrate, and 63.76 g/l of fat. The details regarding the composition of canned seafood wastewater and glycerol waste are presented in Table 1.

Table 1. Characteristics of canned seafood wastewater, glycerol waste, and inoculum composition

Compositions	Substrates		
	CSW	GW	Inoculum
pH	7.3	8.7	7.2
TS (g/L)	2.48	309.41	77.45
VS (g/L)	1.23	284.25	67.06
Ash (g/L)	1.24	24.57	10.39
COD (g/L)	6.80	1,082	ND
VFA (mg/L)	1,216	2,080	7.140
Carbohydrate (g/L)	0.89	20.82	0.25
Protein (g/L)	3.56	1.65	16.87
Nitrogen (g/L)	0.57	0.26	2.7
Lipid (g/L)	0.11	88.65	9.24
C: N	11.93	416.00	ND

ND: Not Determined

3.2 Hydrogen and methane production from single digestion of CSW and GW

Two-stage anaerobic single digestion of CSW at a concentration of 50, 60, 70, 80, 90, and 100% (v/v) has H_2 yield of 5.6, 8.3, 8.8, 9.5, 10.7, and 18.0 mL H_2/g COD, respectively (Figure 1) and methane yield was 274, 323, 345, 333, 328 and 321 mL CH_4/g COD, respectively (Figure 2). Glycerol waste (GW) had a high COD of 1,082 g/L. Two-stage anaerobic single digestion of GW at a concentration of 1, 2, 3, 4, and 5% (v/v) has H_2 yield of 10.9, 24.3, 37.2, 23.6, and 2.5 ml H_2/g COD, respectively (Figure 3) and methane yield was 179, 299, 336, 228, and 147 CH_4/g COD, respectively (Figure 4). The single digestion at 3% GW yields high hydrogen, and 70% CSW yields high methane. Results agreed with [6] CSW is a type of wastewater protein that rapidly decomposes into ammonia nitrogen, particularly during anaerobic digestion. High concentrations of such compounds can directly inhibit the activity of methanogens [19]. The anaerobic breakdown of these types of waste during the acidification stage occurs more quickly than the methanogenic stage, resulting in the accumulation of volatile fatty acids (VFAs) in the reactor. This accumulation results in a gradual decrease in pH, which subsequently hinders the performance of methanogenic archaea. Therefore, co-digestion contributes to balancing the C: N ratio in the system.

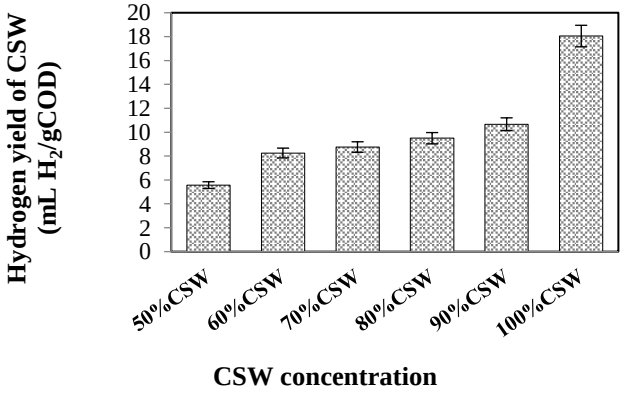

Figure 1. Hydrogen yield of CSW

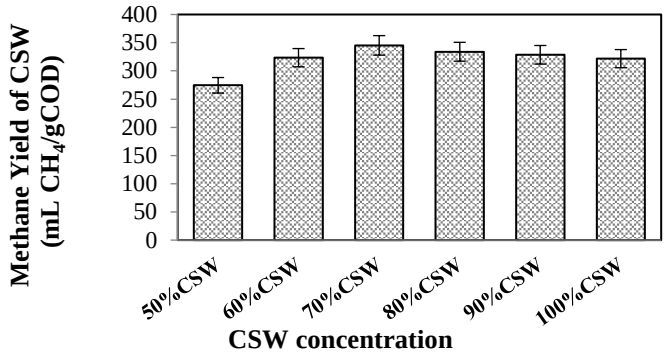

Figure 2. Methane yield of CSW

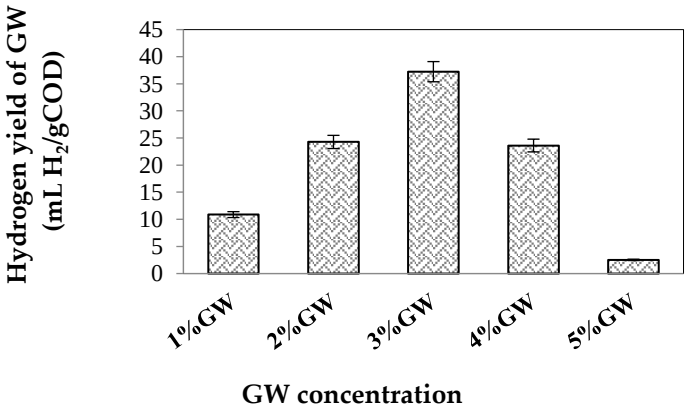

Figure 3. Hydrogen yield of GW

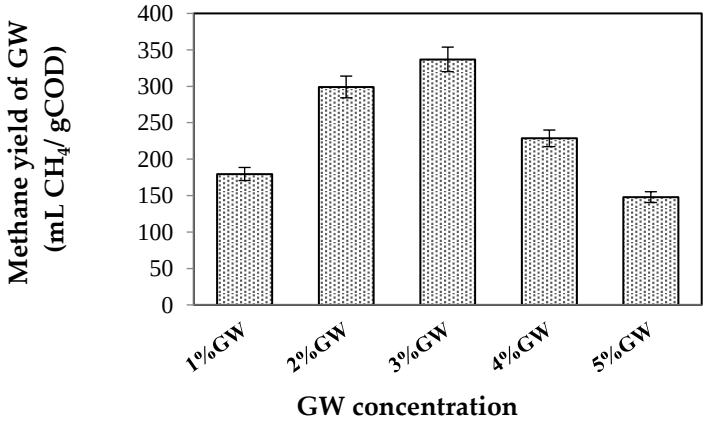

Figure 4. Methane yield of GW

3.3 Hydrogen and methane production from co-digestion of CSW and GW

Two-stage anaerobic co-digestion of CSW with GW at mixing ratios of 99:1, 98:2, 97:3, 96:4, and 95:5% (v/v) has H_2 yield of 15.63, 33.66, 38.79, 65.00, and 6.33 ml H_2/g COD, respectively (Figure 5) and methane yield was 311.57, 320.18, 340.26, 345.08 and 99.39 ml CH_4/g COD respectively (Figure 6). The maximum hydrogen and methane yields from anaerobic co-digestion of CSW with GW were achieved at a mixing ratio of 96:4% (v/v). The C: N ratio of 34.32 was more effective in biodegradation, resulting in higher hydrogen and methane yields (Table 2). The C: N ratio is a primary factor that indicates the presence of appropriate nutrients in the anaerobic system [20]. Additionally, optimizing the C: N ratio between 20 and 35 is practical for creating

synergies during co-substrate digestion [21]. The degradation efficiency of co-digestion CSW with GW was higher than 10% in the hydrogen stage (1-stage) and 90% in the methane stage (2-stage), as shown in Table 2. Increasing the C:N ratio resulted in biodegradation rates higher than 14.44% and 98.59%, respectively. For biodegradation efficiency calculated by 1 - C/C_0 * 100, where C_0 is the initial COD concentration and C is the COD concentration after a specific time.

Table 2. The effect of the ratio CSW to GW on the C: N ratio, hydrogen and methane yield, and biodegradation

Condition	C: N ratio	Yield (mL/g COD)		Biodegradation (%)	
		H_2	CH_4	H_2	CH_4
99% CSW+1%GW	21.10	15.63	311.57	3.47	89.02
98% CSW+2%GW	25.20	33.66	320.18	7.48	91.48
97% CSW+3%GW	30.65	38.79	340.06	8.62	97.15
96%CSW+4%CW	34.32	65.00	345.08	14.44	98.59
95%CSW+5%CW	40.21	6.33	99.39	1.40	28.39

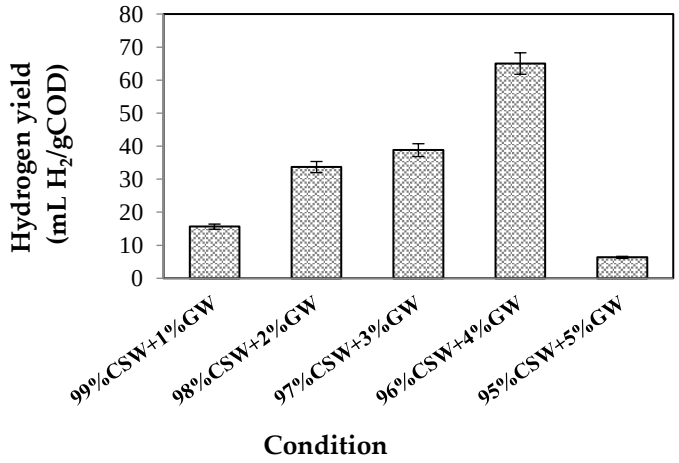

Figure 5. Hydrogen yield of CSW: GW

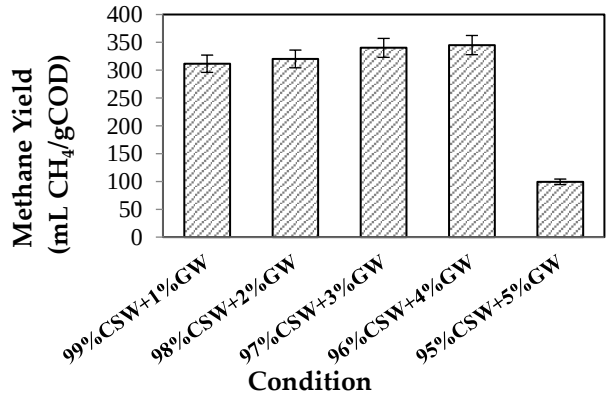

Figure 6. Methane yield of CSW: GW

The hydrogen energy of 0.018 kWh/kg COD in the first stage and 3.03 kWh/kg COD in the second stage is shown in Figure 7. Biodegradation resulted in a significant decrease at 5% GW, leading to reduced hydrogen and methane production. Results agreed with. Panpong et al. [22] demonstrated that incorporating GW as a co-substrate alongside CSW could significantly boost biogas production potential. GW can improve the carbon supply from CSW, thereby reducing toxicity. The concentration of ammonia nitrogen increased, as indicated by the rise in the C:N ratio. The system demonstrated good adaptability to the mixed substrate, resulting in increased production of hydrogen and methane.

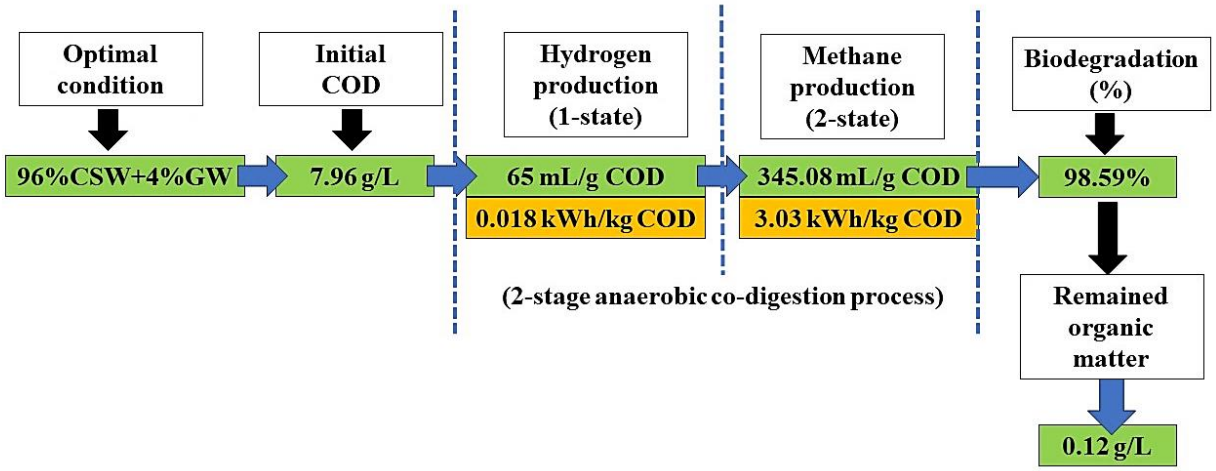

Figure 7. Mass and energy balance

3.4 Continuous hydrogen and methane production of co-digestion CSW with GW, and comparing between R1 and R2 reactors

A mixing ratio of 96:4% (v/v) was determined to be the optimal condition from a batch test; it will continue to be operated in a continuous system. Continuous hydrogen and methane production from co-digestion of CSW with GW of mixing ratio of 96:4% (v/v) by two-stage CSTR-PFR (R1) and CSTR-CSTR (R2) was investigated. R1 and R2 reactors had maximum hydrogen and methane yield (Hydrogen and methane production rate) of 25.2 mL H_2/L/day, 150 mL CH_4/L/day, 18.76 mL H_2/L/day, and 133.60 mL CH_4/L/day, respectively. Wongarmat et al. [23] reported that a hydrogen production rate of 193.6 mL H_2/L/day at an optimal hydraulic retention time (HRT) of 3 days and a methane production rate of 422.0 mL CH_4/L/day with an HRT of 20 days from co-digesting filter cake (FC), biogas effluent (BE), and anaerobic sludge (AS) from the sugar and ethanol industry. The reason why the hydrogen and methane production rate in co-digesting FC, BE, and AS from the sugar and ethanol industry is higher when compared to the co-digested canned seafood industry with glycerol waste due to the high COD value of FC, BE, and AS (290.03, 58.56, and 78.85 g/L) [23]. The canned seafood industry had 6.80 g/L of COD, resulting in a higher hydrogen and methane production rate than wastewater from the canned seafood industry. Hydrogen and methane production from the Two-stage R1 and R2 reactors were 27.44 and 163.61 L/L wastewater, 20.41 and 145.35 L/L wastewater, respectively. Hydrogen reactor production increased when the HRT was increased to 4 days, decreased after the HRT was reduced to 3 days, and then recovered to 4 days of HRT, indicating that 4 days of HRT is the maximum HRT (Figure 8). While reactor methane production increased when the HRT was extended to 20 days, the trend decreased after reducing the HRT to 15 and 10 days, and then recovered within 20 days of the original HRT, indicating that 20 days of HRT was the optimal HRT for methane production (Figure 9). Sillero et al. [4] reported that a maximum hydrogen yield was obtained in the acidogenic phase and mesophilic methanogenic phase at 5 and 12 days of HRT, respectively, from sewage sludge and waste from the agri-food sector (poultry manure and vinasse). The results from the experiment showed that methane production from the PFR reactor had a higher yield than the CSTR reactor. Corresponding to the result of Ting Sun et al. [24], the increased organic loading rate brought more substrate into the anaerobic digestion system and enhanced the concentration of substrate. When the organic loading rate increased to a high level, the overloading substrate for biogas/methane production was inhibited. The advantage of the PFR reactor was that it was fed slowly, due to its long pipe system, resulting in the PFR being able to obtain a higher organic loading rate compared to the CSTR reactor [25]. Consequently, it results in the microorganisms in the system being more stable and resistant to chemicals and changes than those in the CSTR reactor. PFR reactors provided flexibility to the system even with increased feed solid concentration, and therefore, are more stable than CSTR systems. Therefore, the R1 reactor (CSTR+PFR) was the optimal continuous system for producing hydrogen and methane from CSW through co-digestion with GW in a two-stage anaerobic digestion system. In addition, co-digestion results in controlling the C/N ratio, enhancing the elimination of organic compounds, decreasing

inhibitors, and preserving moisture content [26] to make the Hydrogen and Methane Co-production system balanced and efficient. The optimal results showed that the 1-stage (H_2) in R1 contained a microorganism community of a total of 14 dominant species, which were dominated by *Pseudofulvimonas sp., Clostridium sp., Burkholderia sp., Thermanaerovibrio sp., Sphingomicrobium sp., and Thermococcoides sp.* at HRT 4 days (HRT 4), is the best organic retention period for hydrogen production for the CSTR-PFR reactor (R1) (Figure 10). Meanwhile, the archaea community in the 2-stage reactor (CH_4) was dominated by *Methanobacterium sp., Methanoculleus sp., Methanosarcina sp., and Methanosaeta sp.* at HRT 20 days (Figure 10). Most archaea communities form a methyl group in the acetate molecule, from which methane is formed in more than 70 percent of cases.

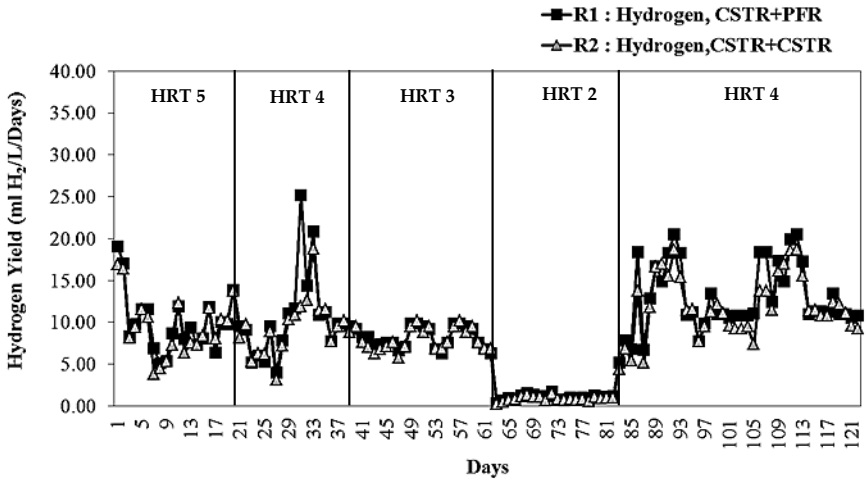

Figure 8. Hydrogen yield of different reactors and different HRTs

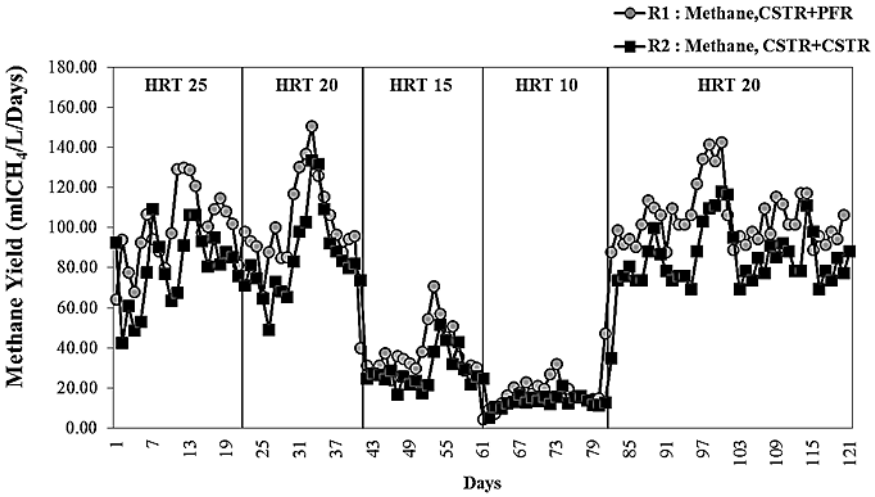

Figure 9. Methane yield of different reactors and different reactor HRTs

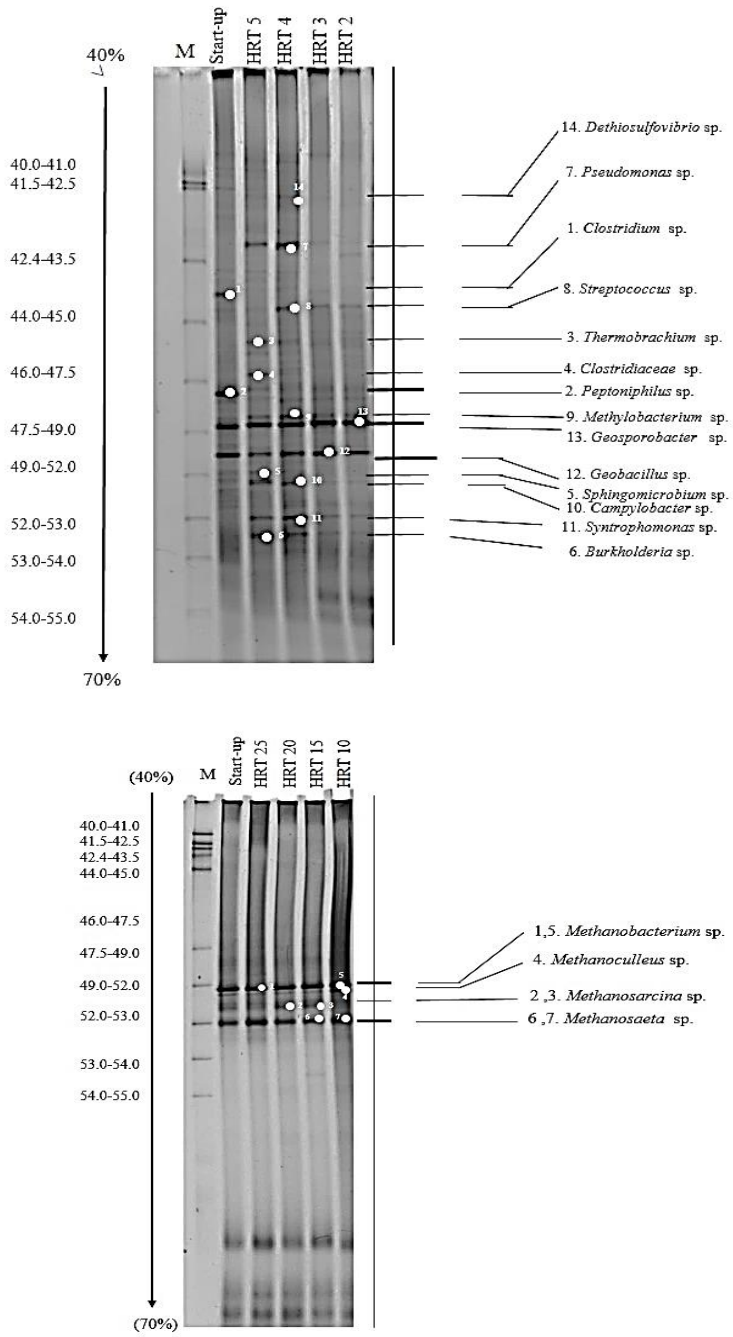

Figure 9. DGGE profiles of 16S rRNA gene fragments for sludge samples from 1-stage (H_2 production) (A), and 2-stage (CH_4 production) of CSW+4%GW co-digestion by two-stage CSTR-PFR (R1)

4. Conclusions

Optimization of conditions to achieve maximum hydrogen and methane yields from two-stage anaerobic co-digestion of CSW with GW was achieved at a mixing ratio of 96:4% (v/v), resulting in yields of 65.00 mL H_2/g COD and 345.08 mL CH_4/g COD. 4% GW was the optimal co-substrate for CSW upgrading, enhancing hydrogen and methane quality and yielding positive synergies in effective biodegradation for a two-stage digestion process. Additionally, GW can dilute toxic compounds within CSW and offers low prices due to the waste generated from biodiesel production. Continuous systems of CSW with a GW of mixing ratio of 96:4% (v/v) by two-stage CSTR-PFR (R1) and CSTR-CSTR (R2) were investigated. R1 and R2 had maximum hydrogen and methane production of 27.44 and 163.61 L/L wastewater and 20.41 and 145.35 L/L wastewater

at HRT 20 days. CSTR-PFR (R1) reactor was an optimal continuous process for productive hydrogen and methane from CSW because PFR is a long pipe system, resulting in a higher organic loading rate when compared with the CSTR reactor, resulting in the microorganisms in the system being stable, more resistant to chemicals and changes than the CSTR reactor. Pseudofulvimonas sp., Clostridium sp., Burkholderia sp., *Thermanaerovibrio* sp., *Sphingomicrobium* sp., and *Thermococcoides* sp dominated the microorganism community of hydrogen production. Meanwhile, the archaea community in methane production was dominated by *Methanobacterium* sp., *Methanoculleus* sp., Methanosarcina sp., and *Methanosaeta* sp.

5. Acknowledgments

We are thankful to Siam International Food Company. Songkhla, Thailand, for providing the inoculum and wastewater in this study. Moreover, thank you to Songkhla Rajabhat University and Thaksin University for their support in workplace research.

Author Contributions: Conceptualization, T.S. and K.R.; methodology, M.T., Y.L., T.S., and K.R.; formal analysis, M.T., T.S., and P.M.; investigation, Y.L., and T.S.; writing—original draft preparation, K.R.; writing—review and editing, K.R.

Funding: This research was financially supported by the Energy Policy and Planning Office (EPPO).

Conflicts of Interest: The authors declare no conflict of interest.

References

[1] Liu, X.; Li, R.; Ji, M.; Han, L. Hydrogen and methane production by co-digestion of waste activated sludge and food waste in the two-stage fermentation process substrate conversion and energy yield. *Bioresource Technol.* **2013**, *146*, 317–323. https://doi.org/10.1016/j.biortech.2013.07.096

[2] Bertasini, D.; Battista, F.; Mancini, R.; Frison, N.; Bolzonella, D. Hydrogen and methane production through two stage anaerobic digestion of straw residues. *Environ. Res.* **2024**, *247*, 118101. https://doi.org/10.1016/j.envres.2024.118101

[3] Dong, Z.; Cao, S.; Zhao, B.; Wang, Y.; Wang, L.; Li, N. Optimization of hydrogen-methane co-production from corn stover via enzymatic hydrolysis: Process intensification, microbial community dynamics, and life cycle assessment. *Bioresource Technol.* **2025**, *426*, 132367. https://doi.org/10.1016/j.biortech.2025.132367

[4] Sillero, L.; Perez, M.; Solera, R. Optimisation of anaerobic co-digestion in two-stage systems for hydrogen, methane and biofertiliser production. *Fuel* **2024**, *365*, 131186. https://doi.org/10.1016/j.fuel.2024.131186

[5] Palenzuela-Rollon, A. *Anaerobic Digestion of Fish Processing Wastewater with Special Emphasis on Hydrolysis of Suspended Solids*; Taylor and Francis: London, **1999**.

[6] Chowdhury, P.; Viraraghavan, T.; Srinivasan, A. Biological treatment processes for fish processing wastewater: A review. *Bioresource Technol.* **2010**, *101*(2), 439–449. https://doi.org/10.1016/j.biortech.2009.08.065

[7] Chen, Y.; Cheng, J. J.; Creamer, K. S. Inhibition of anaerobic digestion process: A review. *Bioresource Technol.* **2008**, *99* (10), 4044–4064. https://doi.org/10.1016/j.biortech.2007.01.057

[8] Kangle, K. M.; Kore, S. V.; Kore, V. S.; Kulkarni, G. S. Recent trends in anaerobic co-digestion. *Environ. Res. Technol.* **2012**, *2*(4), 210–219.

[9] Yazdani, S. S.; Gonzalez, R. Anaerobic fermentation of glycerol: A path to economic viability for the biofuels industry. *Curr. Opin. Biotechnol.* **2007**, *18*(3), 213–219. https://doi.org/10.1016/j.copbio.2007.05.002

[10] Viana, M. M.; Freitas, A. V.; Leitao, R. C.; Pinto, G. A. S.; Santaella, S. T. Anaerobic digestion of crude glycerol a review. *Environ. Technol. Rev.* **2012**, *1*(1), 81–92. https://doi.org/10.1080/09593330.2012.692723

[11] Fountoulakis, M. S.; Manios, T. Enhanced methane and hydrogen production from municipal solid waste and agro-industrial by-products co-digested with crude glycerol. *Bioresource Technol.* **2009**, *100*(11), 3043–3047. https://doi.org/10.1016/j.biortech.2009.01.016

[12] Ginkel, S.; Sung, S. Biohydrogen production as a function of pH and substrate concentration. *Environ. Sci. Technol.* **2001**, *35*(23), 4726–4730. https://doi.org/10.1021/es001979r

[13] Kongjan, P.; O-Thong, S.; Angelidaki, I. Performance and microbial community analysis of two-stage process with extreame thermophiliclic hydrogen and thermophilic methane production from hydrolysate in UASB reactors. *Bioresource Technol.* **2012**, *102*(4), 4028–4035. https://doi.org/10.1016/j.biortech.2010.12.009

[14] Altschul, S. F.; Madden, T. L.; Schäffer, A. A.; Zhang, J.; Zhang, Z.; Miller, W.; David, J.; Lipman, D. Gapped BLAST and PSI-BLAST: a new generation of protein database search programs. *Nucleic Acids Res.* **1997**, *25*(17), 3389–3402. https://doi.org/10.1093/nar/25.17.3389

[15] Yan, Z.; Son, Z.; Li, D.; Yuan, Y.; Liu, X.; Zheng, T. The effects of initial substrate concentration, C/N ratio, and temperature on solid-state anaerobic digestion from composting rice straw. *Bioresource Technol.* **2015**, *177*, 266–273. https://doi.org/10.1016/j.biortech.2014.11.089

[16] Mamimin, C.; Thongdumyu, P.; Hniman, A.; Prasertsan, P.; Imai, T.; O-Thong, S. Simultaneous thermophilic hydrogen production and phenol removal from palm oil mill effluent by *Thermoanaerobacterium*-rich sludge. *Int. J. Hydrogen Energy* **2012**, *37*(20), 15598–15606. https://doi.org/10.1016/j.ijhydene.2012.04.062

[17] Symons, G. E.; Buswell, A. M. The methane fermentation of carbohydrates. *J. Am. Chem. Soc.* **1933**, *55* (5), 2028–2036. https://doi.org/10.1021/ja01332a039

[18] Kongjan, K.; O-Thong, S.; Angelidaki, I. Biohydrogen production from desugared molasses (DM) using thermophilic mixed cultures immobilized on heat treated anaerobic sludge granules. *Int. J. Hydrogen Energy* **2011**, *36*(22), 14261–14269. https://doi.org/10.1016/j.ijhydene.2011.06.130

[19] Siegert, I.; Banks, C. The effect of volatile fatty acid additions on the anaerobic digestion of cellulose and glucose in batch reactors. *Process Biochem.* **2005**, *40*(10), 3412–3418. https://doi.org/10.1016/j.procbio.2005.01.025

[20] Sani, K.; Jariyaboon, R.; O-Thong, S.; Cheirsilp, B.; Kaparaju, P.; Raketh, M.; Kongjan, P. Deploying two-stage anaerobic process to co-digest greasy sludge and waste activated sludge for effective waste treatment and biogas recovery. *J. Environ. Manag.* **2022**, *316*, 115307. https://doi.org/10.1016/j.jenvman.2022.115307

[21] Cremonez, P. A.; Teleken, J. G.; Weiser Meier, T. R.; Alves, H. J. Two-stage anaerobic digestion in agroindustrial waste treatment: A review. *J. Environ. Manag.* **2021**, *281*, 111854. https://doi.org/10.1016/j.jenvman.2020.111854

[22] Panpong, K.; Srimachai, T.; Nuithitikul, K.; Kongjan, P.; O-Thong, S.; Mai, T.; Kaewthong, N. Anaerobic co-digestion between canned sardine wastewater and glycerol waste for biogas production: Effect of different operating processes. *Energy Procedia* **2017**, *138*, 260–266. https://doi.org/10.1016/j.egypro.2017.10.050

[23] Wongarmat, W.; Sittijunda, S.; Imai, T.; Reungsang, A. Co-digestion of filter cake, biogas effluent, and anaerobic sludge for hydrogen and methane production: Optimizing energy recovery through two-stage anaerobic digestion. *Carbon Resour. Convers.* **2025**, *8*, 100248. https://doi.org/10.1016/j.crcon.2024.100248

[24] Ting Sun, M.; Lei Fan, X.; Zhao, X.; Fu, S. F.; He, S.; Manasa, M. R. K.; Guo, B. Effects of organic loading rate on biogas production from microalgae: Performance and microbial community structure. *Bioresource Technol.* **2017**, *235*, 292–300. https://doi.org/10.1016/j.biortech.2017.03.075

[25] Namsree, P.; Suvajittanont, W.; Puttanlek, C.; Uttapap, D.; Rungsardthong, V. Anaerobic digestion of pineapple pulp and peel in a plug-flow reactor. *J. Environ. Manag.* **2012**, *110*, 40–47. https://doi.org/10.1016/j.jenvman.2012.05.017

[26] Rabii, A.; Aldin, S.; Dahman, Y.; Elbeshbishy, E. A review on anaerobic co-digestion with a focus on the microbial populations and the effect of multi-stage digester configuration. *Energies* **2019**, *12*(6), 1106. https://doi.org/10.3390/en12061106.

ASEAN
Journal of Scientific and Technological Reports
Online ISSN:2773-8752

Research article

Comprehensive Pharmacognostic Analysis and Quality Control Parameters of *Cannabis sativa* L. subsp. *sativa*: Evaluating Leaves and Flowers for Medicinal Applications

Lukman Sueree[1,2*], Fameera Madaka[2], Suchada Jongrungruangchok[3], Niran Vipunngeun[4], and Thanapat Songsak[5]

[1] Faculty of Science and Technology, Hatyai University, Songkhla, 90110, Thailand
[2] Drug and Herbal Product Research and Development Center, College of Pharmacy, Rangsit University, Pathum Thani, 12000, Thailand
[3] College of Pharmacy, Rangsit University, Pathum thani, 12000, Thailand
[4] College of Pharmacy, Rangsit University, Pathum thani, 12000, Thailand
[5] College of Pharmacy, Rangsit University, Pathum thani, 12000, Thailand
* Correspondence: lukman.su@hu.ac.th

Citation:
Sueree, L.; Madaka, F.; Jongrungruangchok, S.; Vipunngeun, N.; Songsak, T. Comprehensive pharmacognostic analysis and quality control prarameters of C*annabis sativa* L. subsp. *sativa*: Evaluation leaves and flowers for medicinal applications. *ASEAN J. Sci. Tech. Report.* **2025**, *28*(6), e259515. https://doi.org/10.55164/ajstr.v28i6.259515.

Article history:
Received: May 26, 2025
Revised: September 29, 2025
Accepted: October 1, 2025
Available online: October 20, 2025

Abstract: This study establishes pharmacognostic specifications and quality control parameters for *Cannabis sativa* L. subsp. *sativa* leaves and flowers. Microscopic examination revealed distinctive structures, including stomata, trichomes, and vascular tissues. Physicochemical analysis quantified key parameters: leaf samples showed loss on drying (5.12 ± 0.13%), total ash (14.41 ± 0.43%), acid-insoluble ash (1.21 ± 0.08%), ethanol-soluble extractives (3.24 ± 0.06%), and water-soluble extractives (21.75 ± 0.38%), while flower samples yielded values of 5.25±0.01%, 12.61 ± 0.14%, 1.08 ± 0.08%, 4.06 ± 0.02%, and 19.51 ± 0.27%, respectively. TLC fingerprinting using silica gel 60 GF254 with hexane:acetate (9:1) identified four distinct spots with hRf values of 10-12, 18-20, 22-24, and 42-44. Phytochemical screening confirmed the presence of alkaloids (+++), cardiac glycosides (+), tannins (+), and flavonoids (+) in both plant parts, with saponins detected only in flowers. The microbial analysis demonstrated contamination levels within acceptable limits, with total aerobic counts (8.4×10^3 CFU/g) and yeast/mold counts (1.4×10^4 and 8.0×10^3 CFU/g for leaves and flowers, respectively), indicating a complete absence of pathogenic bacteria. Heavy metal concentrations were significantly below safety thresholds: arsenic (0.05-0.11 ppm), cadmium (≤0.01 ppm), lead (0.17-0.84 ppm), and mercury (0.09-0.23 ppm). These comprehensive parameters establish a scientific foundation for quality assessment and standardization of *Cannabis sativa* L. subsp. *sativa*, supporting its safe and consistent application in medicinal preparations.

Keywords: *Cannabis sativa* L. subsp. *sativa*; thin-layer chromatography (TLC); pharmacognostic investigation; physicochemical parameters

1. Introduction

Cannabis sativa L. has been utilized for millennia across diverse cultures for medicinal, industrial, and ritualistic purposes. Archaeological evidence suggests that cannabis cultivation dates back to approximately 5000 BCE, with medicinal applications documented in ancient Chinese pharmacopeias as early as 2700 BCE [1]. Traditional medical systems across Asia, the Middle East, and Africa have employed various cannabis preparations for conditions including

pain, inflammation, epilepsy, and gastrointestinal disorders [2]. The plant's historical significance extends beyond medicine to textile production, with hemp fibers used for the manufacture of rope, clothing, and paper throughout human civilization [3].

The medicinal properties of *Cannabis sativa* derive from its complex phytochemical profile, particularly its cannabinoid content. Primary bioactive compounds include Δ9-tetrahydrocannabinol (THC), cannabidiol (CBD), and cannabinol (CBN), alongside terpenes, flavonoids, and other secondary metabolites that contribute to its therapeutic effects [4]. Recent scientific research has validated many traditional applications, demonstrating cannabis efficacy for chronic pain, muscle spasticity, chemotherapy-induced nausea, and certain forms of epilepsy [5]. Despite increasing recognition of cannabis therapeutic potential, significant challenges persist in ensuring the quality, consistency, and safety of cannabis-derived products. The standardization of medicinal plant materials is a critical aspect of modern herbal medicine, particularly for botanicals with complex chemical compositions, such as *Cannabis sativa* [6]. Standardization encompasses parameters such as botanical identification, physicochemical assessment, chemical fingerprinting, and contaminant screening, all of which are essential for establishing quality specifications [7]. The World Health Organization emphasizes these quality control measures as fundamental prerequisites for safely integrating traditional medicines into contemporary healthcare systems [8]. The lack of comprehensive pharmacognostic specifications for *Cannabis sativa* L. subsp. *sativa* impedes both research progress and clinical applications. Current commercial cannabis products demonstrate substantial variability in chemical composition, potency, and purity, undermining both therapeutic outcomes and safety profiles [9]. Pharmacognostic standardization addresses these concerns by providing objective criteria for authenticating botanical identity, assessing quality, and detecting adulteration or contamination [10].

This study aims to establish detailed pharmacognostic specifications for *Cannabis sativa* L. subsp. *sativa* leaves and flowers through a comprehensive evaluation of macroscopic and microscopic characteristics, physicochemical parameters, phytochemical constituents, and safety indicators, including microbial load and heavy metal content. The resulting standardization will provide essential quality control benchmarks for researchers, manufacturers, and regulatory authorities, facilitating consistency in scientific investigations and therapeutic applications. Furthermore, this research contributes to the growing body of scientific evidence supporting the integration of properly standardized cannabis preparations into evidence-based healthcare frameworks.

2. Materials and Methods

2.1 Plant Collection and Authentication

Dried samples of *Cannabis sativa* L. subsp. *Sativa plants were harvested from Tak province, Thailand, under approved cultivation protocols that complied* with Thailand's Narcotics Act B.E. 2562 amendment [11]. Plant materials were authenticated by a taxonomic expert using standard botanical keys and voucher specimens (Pharm.RSU.30) and deposited at the Department of Pharmacognosy, Rangsit University. Samples were cleaned to remove foreign materials, air-dried at 45±2°C until a constant weight was achieved, and powdered using a mechanical grinder (mesh size 60) according to the methods described by Chandra et al. [12].

2.2 Macroscopic Evaluation

According to WHO guidelines for the quality assessment of herbal medicine, organoleptic evaluation was conducted on intact dried leaf and flower materials [13]. Macroscopic characteristics, including size, shape, color, texture, fracture properties, and odor, were documented using descriptive terminology consistent with pharmacognostic standards [14]. Digital photographs were captured using a Nikon D750 camera with a macro lens under controlled lighting conditions to document morphological features.

2.3 Microscopic Analysis

Microscopic examination was performed on powdered samples using the techniques described by Evans [15]. Samples were prepared by treating them with a chloral hydrate solution and then mounted in glycerin. Clearing agents were employed for specific tissue identification, including 5% NaOH and 5% KOH. Powder characteristics were observed using an Olympus BX53 microscope at magnifications of 100×, 400×, and 1000×, with photomicrographs captured using an Olympus DP74 digital camera. Diagnostic features,

including stomata, trichomes, epidermal cells, and vascular elements, were identified in accordance with anatomical reference standards [16].

2.4 Physicochemical Parameter Determination

2.4.1 Loss on Drying

The loss on drying was determined according to the method described in the United States Pharmacopeia [17]. Triplicate samples (3 g) of powdered material were accurately weighed in pre-dried, tarred crucibles and dried at 105°C for 6 hours until a constant weight was achieved. Results were calculated as percentage weight loss and expressed as mean ± standard deviation.

2.4.2 Total Ash and Acid-Insoluble Ash

Total ash and acid-insoluble ash were determined according to WHO guidelines [13]. For total ash, triplicate samples (3 g) were incinerated in silica crucibles at 500°C for 5 hours until carbon-free ash was obtained. For acid-insoluble ash determination, the total ash was boiled with 25 mL of 2N HCl for 5 minutes, filtered through ashless filter paper, and the residue was incinerated at 500°C to constant weight. Results were expressed as percentage weight by weight (% w/w).

2.4.3 Extractive Values (Water and Ethanol)

Water-soluble and ethanol-soluble extractive values were determined using the cold maceration method described in the Indian Pharmacopoeia of 2018 [18]. Accurately weighed powdered samples (5 g) were macerated with 100 mL of water or 95% ethanol in stoppered flasks for 24 hours with frequent agitation. The extracts were filtered, and 20 mL aliquots were evaporated to dryness in pre-weighed dishes at 105°C and weighed. Extractive values were calculated as percentage yield and expressed as mean ± standard deviation of triplicate determinations.

2.5 TLC Fingerprinting

Thin-layer chromatography (TLC) was performed using the method described by Wagner and Bladt [19] with modifications. Ethanolic extracts were prepared by macerating 1 g of powdered sample with 20 mL of 95% ethanol for 24 hours, filtering, and concentrating. The extracts (3 µL) were spotted on silica gel 60 GF254 plates (Merck, Germany) alongside reference standards of cannabidiol (CBD), cannabinol (CBN), and tetrahydrocannabinol (THC) (Sigma-Aldrich, USA). Plates were developed in a hexane: acetate (9:1) mobile phase in pre-saturated chambers to a distance of 8 cm. The developed plates were visualized under UV light (254 nm and 365 nm) and subsequently sprayed with anisaldehyde-sulfuric acid reagent, followed by heating at 105°C for 5 minutes. RF values were calculated, and chromatographic profiles were documented.

2.6 Phytochemical Screening

Preliminary phytochemical screening was conducted on ethanolic and aqueous extracts following standard procedures described by Harborne [20] and Tiwari et al. [21]. Tests were performed for the detection of alkaloids (Dragendorff's, Hager's, Marme's, Mayer's, Valser's, and Wagner's reagents), anthraquinones (Kedde test), saponins (foam test), cardiac glycosides (Keller-Kiliani test), tannins (gelatin, ferric chloride, and lead acetate tests), and flavonoids (Shinoda and Pew tests). Results were recorded as strongly positive (+++), positive (++), weakly positive (+), or negative (-) based on the intensity of reactions.

2.7 Microbial Contamination Assessment

Microbial analysis was performed according to the United States Pharmacopeia [17] and WHO guidelines [6]. Samples were tested for total aerobic microbial count (TAMC) using plate count agar, yeast, and mold count using potato dextrose agar, and specific pathogens, including *Escherichia coli*, *Salmonella* spp., *Staphylococcus aureus*, *Pseudomonas aeruginosa*, and *Clostridium* spp. using selective media and enrichment techniques. Microbial enumeration was performed using the pour plate method with appropriate dilutions, and results were expressed as colony-forming units per gram (CFU/g) of dried material.

2.8 Heavy Metal Analysis

Heavy metal analysis was conducted according to AOAC International methods [22] using atomic absorption spectrophotometry (AAS). Powdered samples (1 g) were digested with 20 mL of concentrated nitric

acid using a microwave digestion system (MARS 6, CEM Corporation). The digested solutions were filtered, diluted to 50 mL with deionized water, and analyzed for arsenic (As), cadmium (Cd), lead (Pb), and mercury (Hg) using a Perkin Elmer PinAAcle 900T atomic absorption spectrometer. Calibration curves were prepared using certified reference standards (Merck, Germany), and results were expressed as parts per million (ppm).

3. Results and Discussion

3.1 Macroscopic characteristics of leaves and flowers

The macroscopic examination of *Cannabis sativa* L. subsp. *Sativa revealed distinctive morphological features that facilitate* its authentication and quality assessment (Table 1, Fig. 1). The leaves exhibited a characteristic palmate compound structure with 5-7 lanceolate leaflets radiating from a central point, consistent with taxonomic descriptions by Small and Cronquist [23]. Leaf specimens measured 5-9 cm long with serrated margins containing 9-13 teeth per cm. The adaxial surface displayed bright to dark green coloration, while the abaxial surface appeared slightly paler, aligning with observations reported by Upton et al. [16]. Trichome distribution, a critical taxonomic and chemotypes marker in *Cannabis*, was evident macroscopically as a fine, crystalline appearance on leaf surfaces, particularly concentrated along the veins. This feature aligns with findings by Mahlberg and Kim [24], who noted that trichome density is an indicator of cannabinoid content. The dried leaves exhibited a distinctive aromatic odor and a brittle texture with irregular fracture patterns when crushed, properties that Beutler and Der Marderosian [25] associate with the adequate preservation of volatile terpenes. Flower specimens are presented as compact, resinous clusters, measuring 2-4 cm in length, with bright to dark green coloration interspersed with yellowish pistillate structures. The floral material exhibited significantly higher trichome density than leaf samples, appearing as a crystalline coating visible to the naked eye. This characteristic aligns with Potter [26] observation that glandular trichomes, particularly capitate-stalked trichomes, concentrate in floral structures and contain the highest proportion of cannabinoids and terpenes. The dense trichome coverage on flowers corresponds to their traditionally higher medicinal value, as noted by Hazekamp et al. [27]. The organoleptic evaluation revealed that the flower samples possessed a more intense, pungent aroma than the leaf material, consistent with the higher levels of monoterpenes and sesquiterpenes documented by Fischedick et al. [28]. When fractured, the flowers exhibited a fibrous, somewhat sticky texture, even in a dried state, indicating the preservation of resins and essential oils. These macroscopic characteristics collectively provide reliable preliminary identification parameters when comparing *Cannabis sativa* L. subsp. *sativa* to other *Cannabis* varieties or potential adulterants. The visual and organoleptic profile documented in this study represents authenticated *Cannabis sativa* L. subsp. *sativa* from controlled cultivation, establishing a reference standard for quality assessment following pharmacopoeial requirements [29]. As noted by Lata et al. [30], environmental factors significantly influence the macroscopic characteristics of *Cannabis*; therefore, these findings provide baseline data specific to plants cultivated in Thailand's climate conditions.

Table 1. Macroscopic Characteristics of *Cannabis sativa* L. subsp. *sativa* Leaves and Flowers

Characteristic	Leaves	Flowers
Color	Bright to dark green	Bright to dark green with yellowish tints
Size	5-9 cm in length	2-4 cm in length
Shape	Palmate, 5-7 lobed	Compact, clustered
Texture	Papery when dry, slightly rough	Resinous, sticky when fresh
Odor	Characteristic, aromatic	Strong, pungent, aromatic
Margin	Serrated	-
Trichome density	Moderate	High
Surface	Glandular, hairy	Densely glandular
Fracture	Brittle	Fibrous

Figure 1. Macroscopic features of *Cannabis sativa* L. subsp. *sativa*: (A) Dried leaves showing palmate structure with 5-7 leaflets; (B) Dried flower clusters showing dense trichome coverage. Scale bar = 2 cm.

3.2 Microscopic features and diagnostic cellular elements

Microscopic analysis of *Cannabis sativa* L. subsp. *sativa* leaf and flower powders revealed distinct histological characteristics essential for authentication and quality assessment (Table 2, Figure 2). The leaf powder displayed several diagnostic elements, most notably the anomocytic stomata on the lower epidermis, which Patel et al. [31] identified as a distinguishing taxonomic feature of the Cannabaceae family. These stomata, measuring 20-25 μm in diameter, were irregularly distributed and surrounded by 4-6 subsidiary cells with no specific arrangement pattern. Trichomes observed in the leaf powder were predominantly non-glandular, covering trichomes with a unicellular base and an elongated apex, measuring 150-300 μm in length. These findings align with Stearn [32] botanical characterization of *Cannabis* species. Cystolithic trichomes containing calcium carbonate deposits were also observed, consistent with Hammond and Mahlberg's [33] detailed classification of trichomes. Glandular trichomes were less abundant in leaf material than in flower samples, supporting Mahlberg and Kim [24] observations regarding differential trichome distribution across plant organs. Vascular elements in leaf powder included lignified xylem vessels with helical and annular thickenings, measuring 15-25 μm in diameter, alongside thin-walled phloem elements. Mesophyll fragments appeared as clusters of chlorenchyma cells with irregular surfaces, and occasional calcium oxalate crystals (rosette type, 10-15 μm diameter) were observed, consistent with Andre et al. [34] anatomical descriptions. The flower powder exhibited more abundant glandular trichomes than leaf material, particularly capitate-stalked trichomes with globular heads measuring 50-80 μm in diameter. This observation corresponds with Potter [26] findings that these structures contain the highest concentration of cannabinoids and terpenes. The flower epidermal fragments displayed numerous trichome bases and occasional stomata, while vascular elements included pitted vessels and lignified fibers with narrow lumens. A distinctive feature of the flower powder was the presence of resin glands, which appeared as spherical structures with a yellowish content. This corresponds with Happyana et al. [35] description of cannabinoid-rich secretory structures. Pollen grains, measuring 25-35 μm in diameter with a smooth exine, were occasionally observed in male flower samples, exhibiting the characteristic morphology described by Heslop-Harrison et al. [36]. Comparative analysis of leaf and flower powder microscopy revealed that while both plant parts share certain cellular elements, the flower material consistently displayed a higher density of glandular trichomes and secretory structures. This correlates with chemical analysis data, which show higher concentrations of cannabinoids in floral tissue [37]. The microscopic profiles documented here provide reliable diagnostic markers for authenticating *Cannabis sativa* L. subsp. *sativa* and enable the detection of potential adulterants or substitutions. Importantly, the

microscopic features observed in this study align with specifications provided in pharmacopoeial references [38-39], confirming the identity and quality of the plant material. These findings establish a comprehensive microscopic profile that can serve as a reference standard for quality control purposes in medicinal cannabis research and production.

Table 2. Microscopic Characteristics of *Cannabis sativa* L. subsp. *sativa* Leaf and Flower Powders

Diagnostic Element	Leaf Powder	Flower Powder
Trichomes	Covering trichomes, non-glandular	Covering trichomes with dense glandular heads
Epidermis	Lower epidermis with anomocytic stomata	Epidermis with abundant trichome bases
Vascular elements	Simple xylem vessels, fibers	Pitted vessels, spiral vessels
Mesophyll	Palisade cells in sectional view	Palisade mesophyll in surface view
Calcium oxalate	Rosette crystals (10-15 μm)	Rosette crystals (8-12 μm)
Secretory cells	Sparse oil cells	Abundant resin glands
Fibers	Thin-walled, elongated	Thick-walled with a narrow lumen

3.3 Physicochemical parameter values and comparison with standards

The physicochemical parameters of *Cannabis sativa* L. subsp. *sativa* leaves and flowers were systematically evaluated to establish quality specifications and ensure consistency (Table 3, Figure 3). These parameters serve as critical indicators of purity, identity, and stability, providing objective criteria for quality control, as emphasized by various pharmacopoeial authorities [13, 38]. The loss-on-drying values for the leaf (5.12±0.13%) and flower (5.25±0.01%) samples were comparable and significantly below the pharmacopoeial limit of 10.0%. These findings suggest that proper drying and storage conditions minimize the risk of microbial contamination and hydrolytic degradation of cannabinoids. Hazekamp et al. [40] noted that moisture content below 10% is essential for preserving the stability of cannabinoids, particularly THC, which can degrade to CBN in the presence of excessive moisture and oxygen. Total ash content, representing the inorganic residue after complete incineration, was determined to be 14.41±0.43% and 12.61±0.14% for leaves and flowers, respectively. These values fall within the acceptable limit of 15.0% established by the WHO [13] for herbal materials. The slightly higher ash content in leaves compared to flowers corresponds with findings by Radwan et al. [41], who attributed this difference to higher mineral accumulation in foliar tissue. The acid-insoluble ash values (1.21±0.08% for leaves, 1.08±0.08% for flowers) were well below the 2.0% limit, indicating minimal contamination with siliceous materials and soil particles, thus confirming the high quality of the harvested material. Water-soluble extractives were notably high for both leaves (21.75±0.38%) and flowers (19.51±0.27%), exceeding the minimum requirement of 18.0% specified in the Indian Pharmacopoeia [18] for medicinal plants. This parameter indicates the presence of substantial water-soluble compounds, including polysaccharides, certain flavonoids, and amino acids, which contribute to the plant's therapeutic properties. The higher water-soluble extractive value in leaves aligns with Chandra et al. [12] observation that leaves contain more significant water-soluble components than flowers. Ethanol-soluble extractives, indicative of bioactive compounds such as cannabinoids, terpenes, and resins, were measured at 3.24±0.06% for leaves and 4.06±0.02% for flowers. Both values exceed the minimum requirement of 3.0% established for medicinal cannabis in the European Pharmacopoeia [29]. The higher ethanol-soluble extractive value in flowers correlates with their more significant concentration of cannabinoids and terpenes, consistent with findings by Fischedick et al. [28]. This differential is clinically relevant, as noted by Upton et al. [16], who emphasized the higher therapeutic potency of floral material due to the presence of enriched ethanol-extractable compounds. The comparative analysis of these physicochemical parameters against pharmacopoeial standards (Figure 3) confirms that leaf and flower materials meet or exceed quality requirements. The consistency of these parameters across replicate samples (n = 3) further attests to the uniformity of the plant material. As Kunle et al. [7] emphasized, such standardization is essential for ensuring batch-to-batch consistency in herbal medicines, particularly for regulated therapeutic products. The physicochemical profile established in this study serves

as a reference standard for future quality assessment of *Cannabis sativa* L. subsp. *sativa* cultivated under similar conditions. While specific to the Thai-cultivated samples examined, these parameters provide valuable comparative data for global cannabis research and contribute to the ongoing development of international quality standards for medicinal cannabis [42].

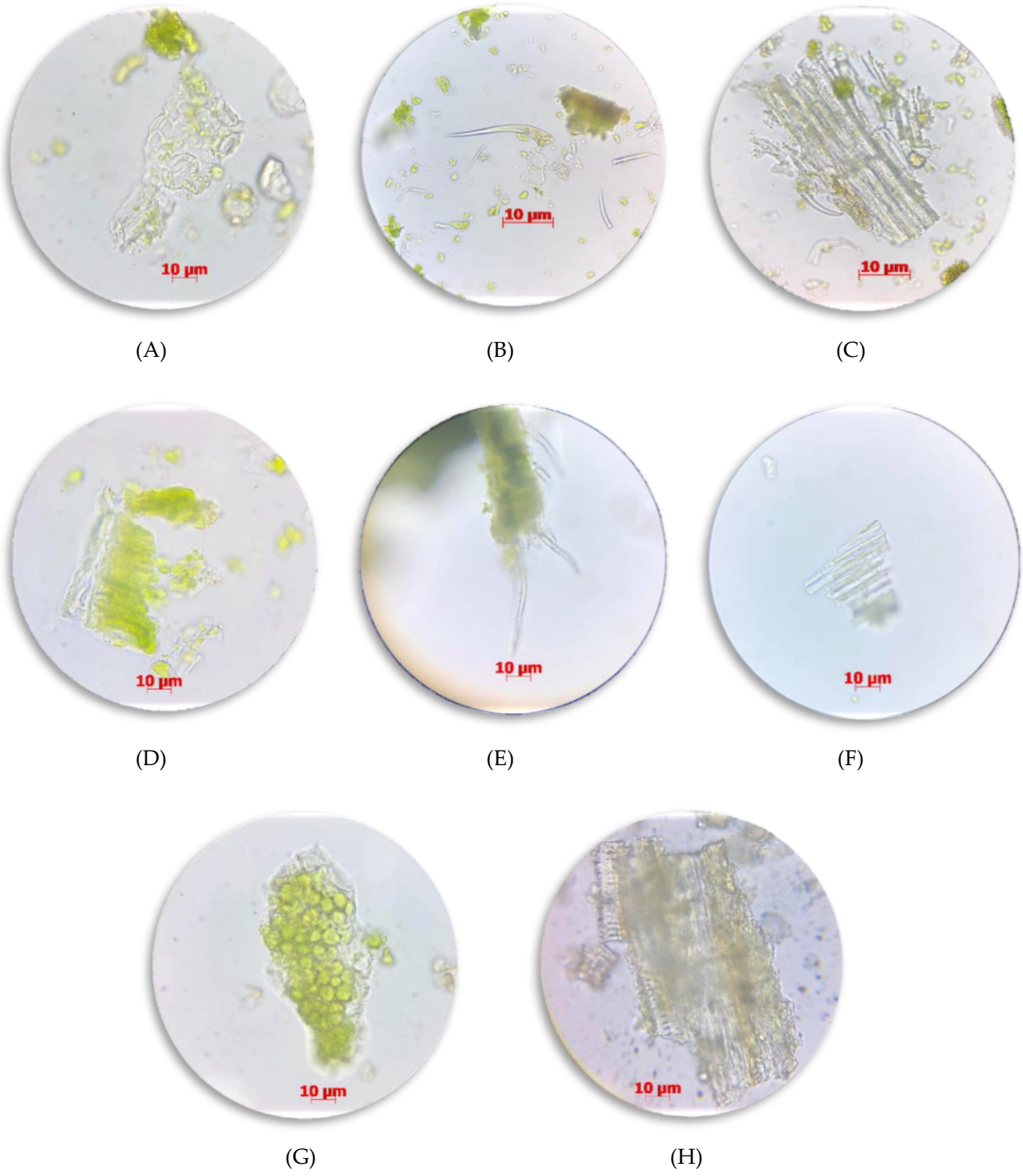

Figure 2. Microscopic characteristics of *Cannabis sativa* L. subsp. *sativa*: (A-D) Leaf powder showing: (A) Lower epidermis with anomocytic stomata, (B) Covering trichome, (C) Fragment of fiber, (D) Fragment of mesophyll in sectional view; (E-H) Flower powder showing: (E) Epidermis with covering trichome, (F) Fragment of fiber, (G) Palisade mesophyll in surface view, (H) Pitted vessel and fiber. Scale bar = 10 µm.

Table 3. Physicochemical Parameters of *Cannabis sativa* L. subsp. *sativa* Compared to Pharmacopoeial Standards

Parameter	Leaves (% w/w)	Flowers (% w/w)	Pharmacopoeial Standards (% w/w)*	Compliance
Loss on drying	5.12 ± 0.13	5.25 ± 0.01	NMT 10.0	Compliant
Total ash	14.41 ± 0.43	12.61 ± 0.14	NMT 15.0	Compliant
Acid-insoluble ash	1.21 ± 0.08	1.08 ± 0.08	NMT 2.0	Compliant
Water-soluble extractives	21.75 ± 0.38	19.51 ± 0.27	NLT 18.0	Compliant
Ethanol-soluble extractives	3.24 ± 0.06	4.06 ± 0.02	NLT 3.0	Compliant

*Standards from WHO guidelines, EP, and USP monographs for herbal materials: NMT = Not More Than; NLT = Not Less Than. Values expressed as mean ± standard deviation (n=3)

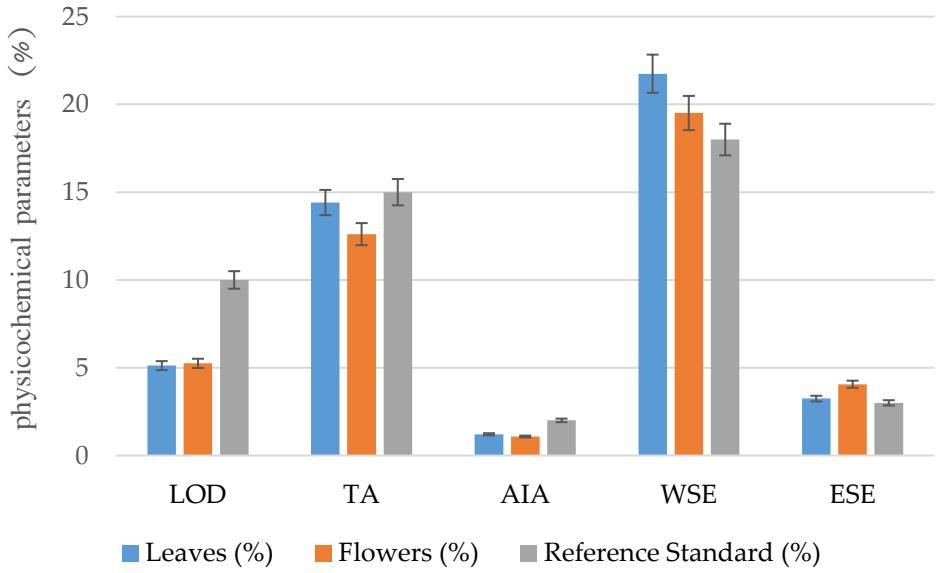

Figure 3. Comparison of physicochemical parameters between *Cannabis sativa* L. subsp. *sativa* leaves and flowers relative to pharmacopoeial standards. Values represent mean ± SD (n=3). LOD = loss on drying; TA = total ash; AIA = acid-insoluble ash; WSE = water-soluble extractives; ESE = ethanol-soluble extractives.

3.4 TLC profiles and chromatographic fingerprints

Thin-layer chromatography (TLC) analysis provided distinct chemical fingerprints of *Cannabis sativa* L. subsp. *sativa* leaf and flower extracts, enabling phytochemical characterization and comparison with reference cannabinoid standards (Table 4, Figure 4). The TLC system, employing silica gel 60 GF254 plates with a hexane: acetone (9:1) mobile phase, effectively separated the major constituents, yielding reproducible chromatographic profiles. Four prominent spots were consistently observed in leaf and flower extracts with hRf values of 10-12, 18-20, 22-24, and 42-44. Comparative analysis with reference standards indicated that spots with hRf values 10-12, 22-24, and 42-44 corresponded to cannabidiol (CBD), cannabinol (CBN), and Δ9-tetrahydrocannabinol (THC), respectively. These identifications align with previous chromatographic characterizations by Hazekamp et al. [43], who established similar relative migration patterns for these cannabinoids in comparable solvent systems. The visualization under different conditions provided complementary information about the chemical constituents. Under UV light at 254 nm, cannabinoids appeared as dark quenching spots against the fluorescent background, with THC and CBD showing powerful absorption. This observation corresponds with findings by Wagner and Bladt [19], who noted the characteristic UV absorption of cannabinoids due to their aromatic ring structures. Under UV 365 nm, spots

corresponding to THC and CBN displayed distinctive blue-violet fluorescence, consistent with Fischedick et al. [28] description of cannabinoid fluorescence properties.

Post-derivatization with anisaldehyde reagent revealed characteristic color reactions, further confirming the identity of the major constituents. The spot corresponding to THC developed a distinctive red-orange coloration (hRf 42-44), while CBD and CBN exhibited violet hues (hRf 10-12 and 22-24, respectively). These color reactions match those documented in the American Herbal Pharmacopoeia cannabis monograph [16] and confirm cannabinoid identity beyond retention factor comparison. The spot at hRf 18-20, which developed a violet color with an anisaldehyde reagent but did not correspond to the reference standards, may represent other cannabinoids or terpenes in the extracts. As suggested by Brenneisen [44], this spot could potentially be cannabigerol (CBG) or cannabichromene (CBC), which exhibit similar chromatographic behavior and color reactions. Further analysis with additional reference standards would be required for definitive identification. A comparative analysis of leaf and flower extracts revealed similar qualitative profiles, but with notable quantitative differences. The spots corresponding to THC and CBD appeared more intense in flower extracts than leaf extracts, indicating higher concentrations in floral material. This observation is consistent with Small and Naraine [45] findings that cannabinoid content is significantly higher in female flowers compared to leaf tissue, particularly in drug-type cannabis varieties. The differential distribution of cannabinoids across plant organs has significant implications for medicinal applications, as noted by Russo [46], who emphasizes the importance of selecting the appropriate plant part for specific therapeutic outcomes. The TLC fingerprints established in this study provide a reliable method for the authentication and quality control of *Cannabis sativa* L. subsp. *sativa*. The combination of retention factors, UV visualization characteristics, and color reactions after derivatization creates a distinctive profile that can identify and differentiate this plant material from potential adulterants. As emphasized by the European Medicines Agency [47], chromatographic fingerprinting is essential to the quality control framework for herbal medicinal products. Furthermore, the established TLC method offers advantages in simplicity, cost-effectiveness, and accessibility compared to more sophisticated techniques such as HPLC or GC-MS, making it particularly valuable for routine quality control in resource-limited settings. Nevertheless, as Amin et al. [48] recommended, these preliminary TLC findings should be complemented with quantitative analysis using instrumental methods for comprehensive phytochemical standardization.

Table 4. TLC Profile of *Cannabis sativa* L. subsp. *sativa* Extracts

Spot No.	hRf Value	Leaves Extract	Flowers Extract	Reference Standards	Color Reaction with Anisaldehyde
1	10-12	+	+	CBD	Violet
2	18-20	+	+	-	Violet
3	22-24	+	+	CBN	Violet
4	42-44	+	+	THC	Red-orange

3.5 Bioactive compound profile

Phytochemical screening revealed diverse bioactive constituents in *Cannabis sativa* L. subsp. *sativa* leaf and flower extracts (Table 5, Fig. 5). Both plant parts demonstrated similar qualitative profiles with notable quantitative differences, providing insights into their therapeutic potentials. Alkaloids were strongly detected in leaf and flower samples, particularly evident through positive reactions with Dragendorff's and Wagner's reagents. These findings align with Flores-Sanchez and Verpoorte's [49] characterization of cannabinoid alkaloids as a prominent chemical class in *the Cannabis genus*. The intense reactions suggest significant concentrations of major cannabinoids, which constitute the primary pharmacologically active compounds responsible for the plant's therapeutic effects [4]. As Brenneisen [44] noted, these nitrogen-containing compounds contribute significantly to the medicinal properties of cannabis, including analgesic, anti-inflammatory, and anticonvulsant effects. Saponins were detected exclusively in flower extracts, albeit at low concentrations, as indicated by a weak positive foam test. The absence of saponins in leaf material corresponds with findings by Pollastro et al. [50], who reported differential distribution of triterpenoid saponins across

cannabis plant organs. The presence of saponins in flowers may contribute to their enhanced biological activities, as these compounds have demonstrated immunomodulatory, anti-inflammatory, and antimicrobial properties [51]. This differential distribution represents a potentially valuable marker for distinguishing flower-derived preparations from leaf-based products.

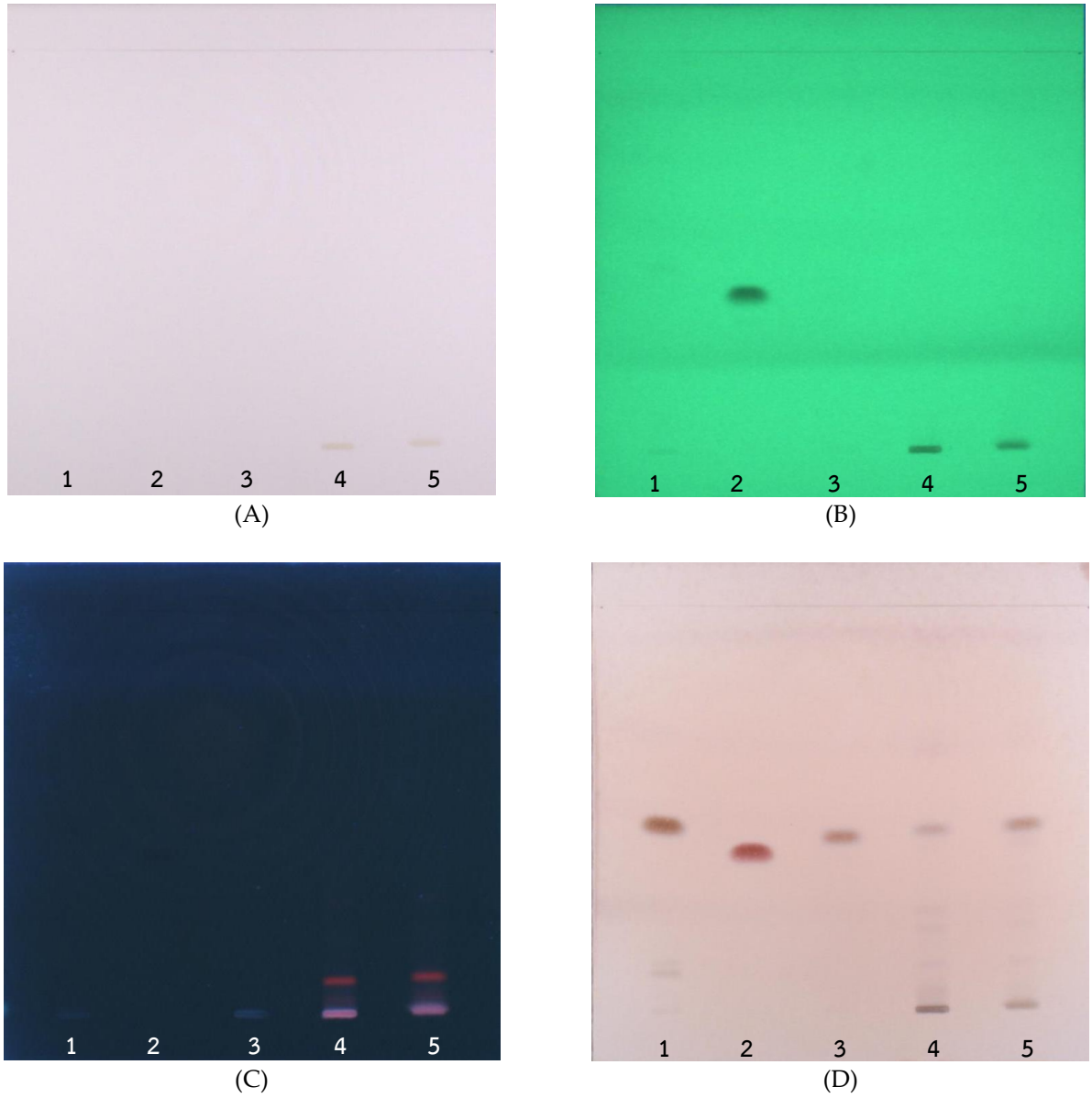

Figure 4. TLC fingerprint of *Cannabis sativa* L. subsp. *sativa* extracts developed in hexane:acetate (9:1). Lanes: 1 = CBD standard, 2 = CBN standard, 3 = THC standard, 4 = leaf extract, 5 = flower extract; Detection: A = visible light, B = UV 254 nm, C = UV 365 nm (fluorescence), D = anisaldehyde reagent.

Cardiac glycosides were weakly detected in both plant parts, as indicated by positive reactions in the Kedde and Keller-Kiliani tests. This observation aligns with Audu et al. [52] detection of cardiac glycosides in cannabis extracts, though their physiological significance in cannabis therapeutics remains inadequately characterized. As noted by Hollman [53], these compounds may contribute to the cardiovascular effects occasionally reported with cannabis consumption, warranting further investigation into their specific structures and bioactivities. Tannins were identified in leaf and flower extracts through positive reactions with lead acetate and ferric chloride, while tests with gelatin solution yielded negative results. This pattern indicates

the presence of hydrolyzable tannins rather than condensed tannins, consistent with the phytochemical characterization of cannabis by Andre et al. [34]. According to Russo [46], these polyphenolic compounds may contribute to the antioxidant and anti-inflammatory properties of cannabis preparations, potentially enhancing their therapeutic efficacy through synergistic interactions with cannabinoids. Flavonoids were detected in both plant parts through positive Shinoda and Pew tests, though at relatively low concentrations. Cannabis flavonoids, particularly cannflavins A and B, have been identified as pharmacologically active constituents with anti-inflammatory properties exceeding those of aspirin in some assays [54]. The presence of these compounds contributes to what Russo [55] described as the "entourage effect," wherein multiple phytochemicals act synergistically to enhance therapeutic outcomes beyond what could be achieved with isolated cannabinoids. Notably, anthraquinones were not detected in either plant part, which is consistent with previous phytochemical analyses by Radwan et al. [41] and provides a useful negative marker for authentication purposes. This finding also indicates that cannabis preparations are unlikely to exert the laxative effects commonly associated with anthraquinone-containing botanicals. The overall phytochemical profile (Figure 5) reveals that, while both plant parts contain similar classes of bioactive compounds, their relative concentrations differ, particularly in the case of alkaloids and saponins. These differences may explain the historically distinct applications of leaf and flower preparations in traditional cannabis therapeutics, as documented by Zuardi [2]. The comprehensive phytochemical screening results establish a foundation for quality control standards and provide direction for further investigation into specific bioactive constituents using more targeted analytical techniques. The observed phytochemical profile supports previous findings by Hazekamp and Fischedick [37] regarding the complex chemical composition of cannabis and its implications for therapeutic standardization. This complexity underscores the importance of comprehensive phytochemical characterization beyond cannabinoid content alone, particularly when evaluating cannabis for specific medicinal applications or developing standardized pharmaceutical preparations.

Table 5. Phytochemical Screening Results of *Cannabis sativa* L. subsp. *sativa* Extracts

Phytochemical Class	Test Method	Leaves	Flowers
Alkaloids	Dragendorff's reagent	+++	+++
	Hager's reagent	+	+
	Marme's reagent	+	+
	Mayer's reagent	+	++
	Valser's reagent	++	+
	Wagner's reagent	+++	+++
Anthraquinones	Kedde test	-	-
Saponins	Foam test	-	+
Cardiac glycosides	Kedde test	+	+
	Keller-Kiliani test	+	+
Tannins	3% gelatin solution	-	-
	1% lead acetate	+	+
	1% ferric chloride	+	+
Flavonoids	Shinoda test	+	+
	Pew test	+	+

+++ = Strong positive; ++ = Positive; + = Weak positive; - = Not detected

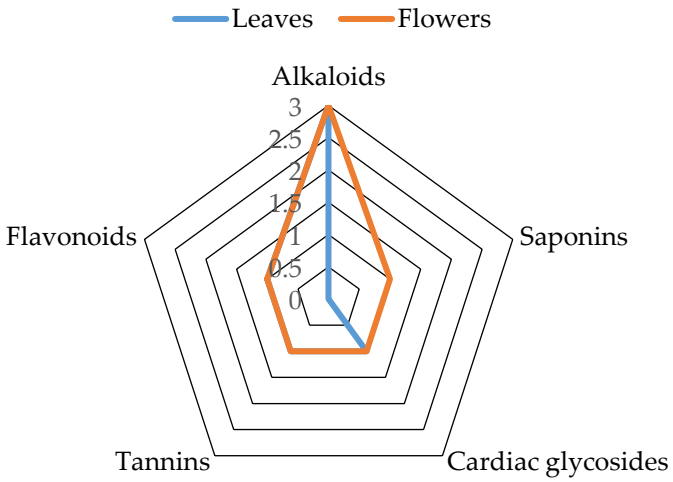

Figure 5. Phytochemical profile comparison between *Cannabis sativa* L. subsp. *sativa* leaf and flower extracts. Intensity scale: 0 = not detected, 1 = weak positive, 2 = positive, 3 = strong positive.

3.6 Microbial safety evaluation

Microbial contamination assessment of *Cannabis sativa* L. subsp. *sativa* samples revealed contamination levels within acceptable pharmacopoeial limits (Table 6, Fig. 6). The total aerobic microbial count (TAMC) for both leaf and flower samples was 8.4×10^3 CFU/g, significantly below the maximum permissible limit of 2×10^5 CFU/g established by the World Health Organization [6] and European Pharmacopoeia [29] for herbal medicines intended for internal use. The yeast and mold counts showed slight variation between plant parts, with leaf samples (1.4×10^4 CFU/g) containing marginally higher fungal contamination than flower samples (8.0×10^3 CFU/g). Both values remained compliant with the pharmacopoeial limit of 2×10^4 CFU/g. This differential may be attributed to the higher resin content in flowers, which Fischedick et al. [28] noted possesses natural antimicrobial properties that may inhibit fungal colonization. The observed microbial loads concur with findings from Hazekamp [56], who reported similar baseline contamination levels in properly handled medicinal cannabis. Pathogenic bacteria, including *Escherichia coli*, *Clostridium* spp., *Salmonella* spp., *Staphylococcus aureus*, and *Pseudomonas aeruginosa*, were not detected in any of the samples, indicating adherence to good agricultural and collection practices (GACP). The absence of these indicator organisms is particularly significant as they represent potential sources of gastrointestinal illness, respiratory infections, and other adverse health outcomes in immunocompromised patients who may use cannabis medicinally [57]. These results demonstrate microbiological quality within acceptable standards for pharmaceutical use, consistent with findings by Ruchlemer et al. [58], who emphasized the importance of microbial safety in cannabis intended for medicinal applications, particularly for immunocompromised patients. Implementing appropriate post-harvest processing techniques, including controlled drying at 45±2°C as employed in this study, likely contributed to microbial reduction, as supported by Holmes et al. [59], who demonstrated the efficacy of proper drying conditions in reducing microbial contamination in herbal materials. While the samples meet current pharmacopoeial requirements, ongoing microbiological monitoring is advisable throughout the production and storage phases. Jerushalmi et al. [60] noted that environmental factors during cultivation and storage can significantly influence microbial contamination levels in cannabis. Implementation of the Hazard Analysis Critical Control Point (HACCP) principles, as recommended by the American Herbal Products Association [61], would further ensure consistent microbial quality and safety. The observed results establish baseline microbiological specifications for *Cannabis sativa* L. subsp. *sativa* cultivated under the conditions described in this study. These findings contribute to the development of comprehensive quality standards for medicinal cannabis, addressing one of the primary safety concerns in botanical medicine, as emphasized by Sachs et al. [62] in their review of quality control parameters for medicinal cannabis preparations.

Table 6. Microbial Contamination Analysis of *Cannabis sativa* L. subsp. *Sativa*

Microorganism	Leaves (CFU/g)	Flowers (CFU/g)	Pharmacopoeial Limit (CFU/g)*	Compliance
Total aerobic count	8.4×10^3	8.4×10^3	NMT 2×10^5	Compliant
Yeasts and molds	1.4×10^4	8.0×10^3	NMT 2×10^4	Compliant
Escherichia coli	ND	ND	Absent/g	Compliant
Clostridium spp.	ND	ND	Absent/g	Compliant
Salmonella spp.	ND	ND	Absent/10g	Compliant
Staphylococcus aureus	ND	ND	Absent/g	Compliant
Pseudomonas aeruginosa	ND	ND	Absent/g	Compliant

*Based on WHO, USP, and EP requirements for herbal medicinal products for internal use, ND = Not detected; NMT = Not more than

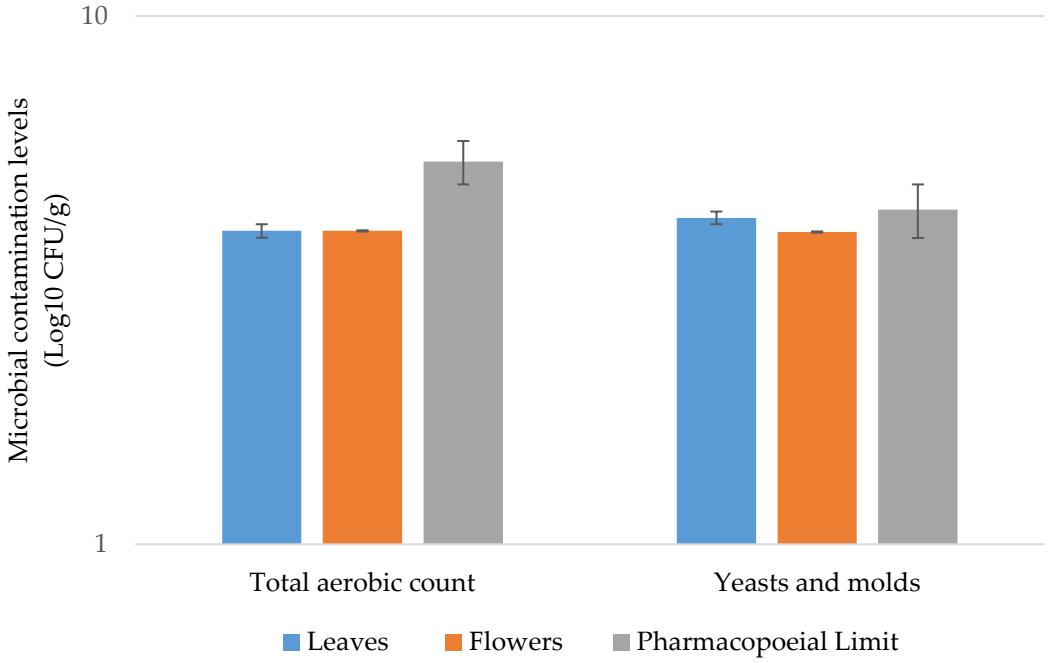

Figure 6. Microbial contamination levels in *Cannabis sativa* L. subsp. *sativa* leaves and flowers compared to pharmacopoeial limits. Bars represent mean values (n=3). No pathogenic bacteria were detected in any samples.

3.7 Heavy metal content assessment

The assessment of heavy metal content in *Cannabis sativa* L. subsp. *sativa* revealed concentrations well below established safety thresholds for most elements (Table 7, Fig. 7). Atomic absorption spectrophotometry analysis revealed that leaf and flower samples contained minimal levels of toxic metals, with most values significantly below the international permissible limits for herbal medicinal products. Arsenic concentrations were determined to be 0.05 ppm in leaves and 0.11 ppm in flowers, substantially below the WHO [6] permissible limit of 4.0 ppm. This finding aligns with Zerihun et al. [63], who reported similarly low arsenic levels in cannabis cultivated in non-contaminated soils. The slightly higher arsenic content in flowers compared to leaves corresponds with McPartland and McKernan's [64] observation that cannabis inflorescence can concentrate certain trace elements more efficiently than vegetative tissues. Cadmium levels were minimal in both plant parts (0.01 ppm in leaves, <0.01 ppm in flowers), representing less than 4% of the permissible limit of 0.3 ppm. These values are comparable to those reported by Linger et al. [65], who found cadmium concentrations below 0.05 ppm in cannabis grown in uncontaminated agricultural soil. The low cadmium content is particularly significant given the capacity of cannabis to accumulate this metal, as

demonstrated in phytoremediation studies by Citterio et al. [66]. Lead content was measured at 0.84 ppm in leaves and 0.17 ppm in flowers, well below the permissible limit of 10.0 ppm. The higher concentration in leaf tissue aligns with Eboh and Thomas [67] findings that lead predominantly accumulate in the vegetative parts of plants rather than reproductive structures. The observed lead levels pose minimal risk to consumers, representing less than 10% of the safety threshold established by international regulatory bodies [29].

Mercury concentrations were determined to be 0.09 ppm in leaves and 0.23 ppm in flowers. The leaf content falls comfortably below the WHO [6] permissible limit of 0.2 ppm, whereas the flower content marginally exceeds this threshold. However, as Dryburgh et al. [68] noted, the United States Pharmacopeia establishes a higher limit for mercury (0.5 ppm) in herbal materials, a standard that both samples meet. Flowers' slightly elevated mercury content warrants monitoring in future harvests, though it does not present an immediate safety concern based on current regulatory frameworks. The observed differential in heavy metal distribution between leaves and flowers supports. Nascimento et al. [69] findings regarding tissue-specific accumulation patterns in medicinal plants. The generally higher metal content in flowers for arsenic and mercury, contrasted with higher lead and cadmium levels in leaves, reflects the complex translocation mechanisms that vary by element, as Prasad [70] described in his comprehensive review of metal transport in plants. These results indicate that the cannabis samples analyzed were cultivated in environments with minimal heavy metal contamination and present negligible risk to consumers when used as intended. The findings align with Yang et al. [71] assessment of heavy metals in medicinal cannabis, which similarly found concentrations well below safety thresholds in properly cultivated material. The heavy metal profile documented here contributes to establishing baseline quality specifications for *Cannabis sativa* L. subsp. *sativa* and demonstrates compliance with international safety standards for medicinal plants. Regular monitoring of heavy metal content remains advisable, particularly in cannabis intended for medical applications, as emphasized by Russo [72] in his review of cannabinoid pharmacology and quality considerations. Environmental conditions, including soil composition and agricultural practices, can significantly influence metal uptake and accumulation [73], necessitating ongoing quality control measures throughout the cultivation and production processes.

Table 7. Heavy Metal Analysis of *Cannabis sativa* L. subsp. *Sativa*

Heavy Metal	Leaves (ppm)	Flowers (ppm)	Permissible limit (ppm)*	Compliance
Arsenic (As)	0.05	0.11	4.00	Compliant
Cadmium (Cd)	0.01	<0.01	0.30	Compliant
Lead (Pb)	0.84	0.17	10.0	Compliant
Mercury (Hg)	0.09	0.23	0.20	Non-compliant**

*Based on WHO (2007) guidelines for medicinal plants. **Flower mercury content slightly exceeds the WHO limit but falls within the USP limit (0.5 ppm)

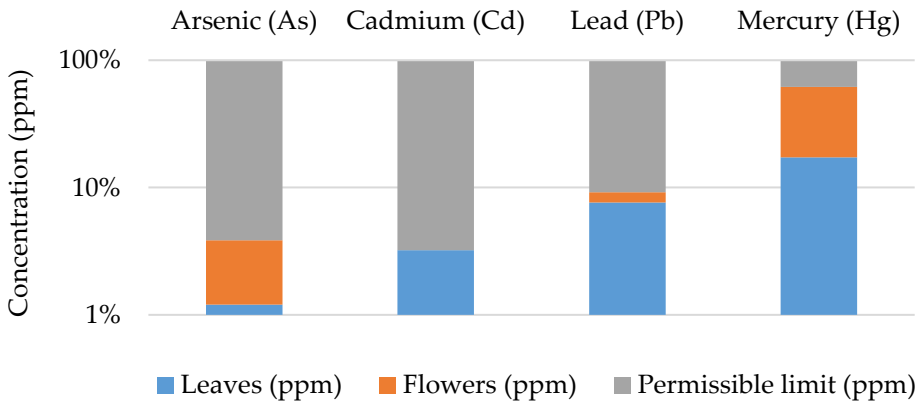

Figure 7. Heavy metal concentrations in *Cannabis sativa* L. subsp. *sativa* leaf and flower samples compared to international permissible limits. Note: logarithmic scale used for visualization purposes.

4. Conclusion

This comprehensive pharmacognostic investigation of *Cannabis sativa* L. subsp. *Sativa leaves and flowers establish detailed quality specifications for standardizing medical applications*. The study revealed distinctive macroscopic and microscopic characteristics that provide reliable identification parameters, including palmate leaf structure, serrated margins, and dense trichome coverage on flowers. Microscopically, the presence of anomocytic stomata, cystolithic trichomes, and specific vascular elements provides definitive diagnostic markers for authentication. Physicochemical parameters demonstrated compliance with international pharmacopoeial standards, with the loss on drying, total ash, and acid-insoluble ash values falling within acceptable limits. The higher water-soluble extractives in leaves (21.75±0.38%) compared to flowers (19.51±0.27%) contrasted with higher ethanol-soluble extractives in flowers (4.06±0.02%) versus leaves (3.24±0.06%), reflecting their distinct phytochemical compositions. TLC fingerprinting revealed four primary spots corresponding to major cannabinoids, with characteristic color reactions providing reliable chemical markers for quality assessment. Phytochemical screening confirmed the presence of alkaloids, cardiac glycosides, tannins, and flavonoids in both plant parts, with saponins detected exclusively in flowers. This differential distribution of bioactive compounds supports distinct therapeutic applications for leaf and flower preparations. The safety evaluation demonstrated microbial contamination within acceptable limits and heavy metal content substantially below regulatory thresholds, except for marginally elevated mercury levels in flowers, which still meet USP standards. These findings establish critical quality control parameters for ensuring consistency, safety, and efficacy of *Cannabis sativa* L. subsp. *sativa* in pharmaceutical applications. Implementing these specifications in regulatory frameworks would facilitate standardization across production batches, enabling reliable therapeutic outcomes. We recommend incorporating these pharmacognostic parameters into relevant pharmacopeias and establishing appropriate manufacturing protocols based on these specifications. Future research should focus on correlating specific phytochemical profiles with therapeutic efficacy, investigating seasonal and geographical variations in quality parameters, and developing simplified field tests for rapid authentication and verification. Additionally, exploring the relationship between cultivation conditions and cannabinoid/terpene profiles would provide valuable insights for optimizing medicinal cannabis production. Ultimately, this standardization contributes significantly to the evidence-based integration of cannabis into modern healthcare systems.

5. Acknowledgements

The authors gratefully acknowledge the financial support from the Research Institute of Rangsit University under grant number 110/2561. Additionally, we extend our sincere appreciation to the Faculty of Science and Technology, Hatyai University, Hatyai, Songkhla, Thailand, and the Herbal Medicinal Products Research and Development Center, Faculty of Pharmacy, Rangsit University, Thailand, for their invaluable support in providing materials and equipment essential to this research.

Author Contributions: Conceptualization, L.S., and F.M.; methodology, L.S.; software, F.M.; validation, L.S., F.M., and S.J.; formal analysis, L.S.; investigation, L.S.; resources, N.V.; data curation, L.S.; writing-original draft preparation, L.S.; writing-review and editing, N.V.; visualization, T.S.; supervision, L.S. All authors have read and agreed to the published version of the manuscript.

Funding: The financial support provided by the Research Institute of Rangsit University under grant number 110/2561

Conflicts of Interest: The authors declare no conflict of interest.

References

[1] Russo, E. B. History of cannabis and its preparations in saga, science, and sobriquet. *Chemistry & biodiversity*. **2007**, *4*(8), 1614-1648. https://doi.org/10.1002/cbdv.200790144

[2] Zuardi, A.W. History of cannabis as a medicine: a review. *Braz. J. Psychiatry*. **2006**, *28*, 153-157. https://doi.org/10.1590/S1516-44462006000200015

[3] Small, E. ; Marcus, D. Hemp: A new crop with new uses for North America. *Trends in new crops and new uses*. **2002**, *24*(5), 284-326.
[4] ElSohly, M.A.; Slade, D. Chemical constituents of marijuana: The complex mixture of natural cannabinoids. *Life Sci.* **2005**, *78*, 539-548. https://doi.org/10.1016/j.lfs.2005.09.011
[5] Whiting, P.F.; Wolff, R.F.; Deshpande, S.; Di Nisio, M.; Duffy, S.; Hernandez, A.V.; Keurentjes, J.C.; Lang, S.; Misso, K.; Ryder, S. Cannabinoids for medical use: a systematic review and meta-analysis. *JAMA* **2015**, *313*, 2456-2473. https://doi.org/10.1001/jama.2015.6358
[6] WHO. *WHO Guidelines for Assessing Quality of Herbal Medicines with Reference to Contaminants and Residues*; World Health Organization: Geneva, Switzerland, **2007**.
[7] Kunle, O.F.; Egharevba, H.O.; Ahmadu, P.O. Standardization of herbal medicines - A review. *Int. J. Biodivers. Conserv.* **2012**, *4*, 101-112. https://doi.org/10.5897/IJBC11.163
[8] WHO. *WHO Traditional Medicine Strategy: 2014-2023*; World Health Organization: Geneva, Switzerland, **2013**.
[9] Vandrey, R.; Raber, J. C.; Raber, M. E.; Douglass, B.; Miller, C.; Bonn-Miller, M. O.. Cannabinoid dose and label accuracy in edible medical cannabis products. *Jama.* **2015**, *313*(24), 2491-2493. https://doi.org/10.1001/jama.2015.6613
[10] Jackson, B.P.; Snowden, D.W.; Sharpe, S.A.; Upton, R. Authentication of botanical ingredients in dietary supplements: Methods of identification and the regulatory landscape. *J. AOAC Int.* **2021**, *104*, 1-8. https://doi.org/10.1093/jaoacint/qsab003
[11] Thailand Ministry of Public Health. Narcotics Act B.E. 2562 Amendment (No. 7). *Royal Thai Government Gazette* **2019**, *136*, Part 19.
[12] Chandra, S.; Lata, H.; ElSohly, M.A. *Cannabis sativa L.—Botany and Biotechnology*; Springer: Cham, Switzerland, **2017**. https://doi.org/10.1007/978-3-319-54564-6
[13] WHO. *Quality Control Methods for Herbal Materials*; World Health Organization: Geneva, Switzerland, **2011**.
[14] Jackson, B.P.; Snowden, D.W. *Atlas of Microscopy of Medicinal Plants, Culinary Herbs and Spices*; Belhaven Press: London, UK, 2012.
[15] Evans, W.C. *Trease and Evans' Pharmacognosy*, 16th ed.; Saunders Elsevier: Edinburgh, UK, **2009**.
[16] Upton, R.; Craker, L.; ElSohly, M.; Romm, A.; Russo, E.; Sexton, M. *Cannabis Inflorescence: Cannabis spp. Standards of Identity, Analysis, and Quality Control*; American Herbal Pharmacopoeia: Scotts Valley, CA, USA, **2014.**
[17] United States Pharmacopeia (USP-42). *United States Pharmacopeia and National Formulary*; United States Pharmacopeial Convention: Rockville, MD, USA, **2019**.
[18] Indian Pharmacopoeia, 8th ed.; Indian Pharmacopoeia Commission: Ghaziabad, India, **2018**.
[19] Wagner, H.; Bladt, S. *Plant Drug Analysis: A Thin Layer Chromatography Atlas*, 2nd ed.; Springer-Verlag: Berlin, Germany, **2009.**
[20] Harborne, J.B. *Phytochemical Methods: A Guide to Modern Techniques of Plant Analysis*, 3rd ed.; Chapman and Hall: London, UK, **2012**.
[21] Tiwari, P.; Kumar, B.; Kaur, M.; Kaur, G.; Kaur, H. Phytochemical screening and extraction: A review. *Int. Pharm. Sci.* **2011**, *1*, 98-106.
[22] Association of Official Analytical Chemists. Offcial Methods of Analysis of AOAC International. Gaithersburg, MD, USA, **2016.**
[23] Small, E.; Cronquist, A. A practical and natural taxonomy for Cannabis. *Taxon* **2003**, *25*, 405-435. https://doi.org/10.2307/1220524
[24] Mahlberg, P.G.; Kim, E.S. Accumulation of cannabinoids in glandular trichomes of Cannabis (Cannabaceae). *J. Ind. Hemp* **2004**, *9*, 15-36. https://doi.org/10.1300/J237v09n01_04
[25] Beutler, J.A.; Der Marderosian, A.H. Chemotaxonomy of Cannabis I. Crossbreeding between *Cannabis sativa* and *C. ruderalis*, with analysis of cannabinoid content. *Econ. Bot.* **2008**, *32*, 387-394. https://doi.org/10.1007/BF02907927

[26] Potter, D.J. A review of the cultivation and processing of cannabis (*Cannabis sativa* L.) for production of prescription medicines in the UK. *Drug Test. Anal.* **2014**, *6*, 31-38. https://doi.org/10.1002/dta.1531

[27] Hazekamp, A.; Fischedick, J. T.; Díez, M. L.; Lubbe, A.; Ruhaak, R. L. 3.24—Chemistry of cannabis. *Comprehensive natural products II*. **2010,** 3, 1033-1084. https://doi.org/10.1016/B978-008045382-8.00091-5

[28] Fischedick, J.T.; Hazekamp, A.; Erkelens, T.; Choi, Y.H.; Verpoorte, R. Metabolic fingerprinting of *Cannabis sativa* L., cannabinoids and terpenoids for chemotaxonomic and drug standardization purposes. *Phytochemistry* **2010**, *71*, 2058-2073. https://doi.org/10.1016/j.phytochem.2010.10.001

[29] European Pharmacopoeia, 10th ed.; European Directorate for the Quality of Medicines & Healthcare: Strasbourg, France, **2020**.

[30] Lata, H.; Chandra, S.; Khan, I.A.; ElSohly, M.A. Cannabis cultivation: methodological issues for obtaining medical-grade product. *Epilepsy Behav.* **2017**, *70*, 302-312. https://doi.org/10.1016/j.yebeh.2016.11.029

[31] Patel, B.; Patel, M.; Nagar, A. Microscopic evaluation as a tool for authentication of medicinal plant Canabis sativa Linn. *Int. J. Recent Sci. Res.* **2019**, *10*, 34110-34113. https://doi.org/10.24327/ijrsr.2019.1008.3825

[32] Stearn, W.T. The Cannabis plant: botanical characteristics. In *The Botany and Chemistry of Cannabis*; Joyce, C.R.B., Curry, S.H., Eds.; J. & A. Churchill: London, UK, **1970**; pp. 1-10.

[33] Hammond, C.T.; Mahlberg, P.G. Morphology of glandular hairs of *Cannabis sativa* from scanning electron microscopy. *Am. J. Bot.* **1973**, *60*, 524-528. https://doi.org/10.1002/j.1537-2197.1973.tb05953.x

[34] Andre, C.M.; Hausman, J.F.; Guerriero, G. *Cannabis sativa*: The plant of the thousand and one molecules. *Front. Plant Sci.* **2016**, *7*, 19. https://doi.org/10.3389/fpls.2016.00019

[35] Happyana, N.; Agnolet, S.; Muntendam, R.; Van Dam, A.; Schneider, B.; Kayser, O. Analysis of cannabinoids in laser-microdissected trichomes of medicinal *Cannabis sativa* using LCMS and cryogenic NMR. *Phytochemistry* **2013**, *87*, 51-59. https://doi.org/10.1016/j.phytochem.2012.11.001

[36] Heslop-Harrison, J.; Heslop-Harrison, Y.; Shivanna, K.R. The evaluation of pollen quality, and a further appraisal of the fluorochromatic (FCR) test procedure. *Theor. Appl. Genet.* **1973**, *43*, 109-118. https://doi.org/10.1007/BF00273915

[37] Hazekamp, A.; Fischedick, J.T. Cannabis - from cultivar to chemovar. *Drug Test. Anal.* **2012**, *4*, 660-667. https://doi.org/10.1002/dta.407

[38] United States Pharmacopeia (USP). *United States Pharmacopeia and National Formulary*; United States Pharmacopeial Convention: Rockville, MD, USA, **2022**.

[39] British Pharmacopoeia Commission. *British Pharmacopoeia*; The Stationery Office: London, UK, **2019**.

[40] Hazekamp, A. Evaluating the effects of gamma-irradiation for decontamination of medicinal cannabis. *Front. Pharmacol.* **2016**, *7*, 108. https://doi.org/10.3389/fphar.2016.00108

[41] Radwan, M.M.; ElSohly, M.A.; Slade, D.; Ahmed, S.A.; Wilson, L.; El-Alfy, A.T.; Khan, I.A.; Ross, S.A. Non-cannabinoid constituents from a high potency *Cannabis sativa* variety. *Phytochemistry* **2015**, *78*, 14-27. https://doi.org/10.1016/j.phytochem.2012.02.002

[42] WHO. Critical Review Report: Cannabis and cannabis resin. Expert Committee on Drug Dependence, World Health Organization: Geneva, Switzerland, **2018.**

[43] Hazekamp, A.; Peltenburg, A.; Verpoorte, R.; Giroud, C. Chromatographic and spectroscopic data of cannabinoids from *Cannabis sativa* L. *J. Liq. Chromatogr. Relat. Technol.* **2009**, *28*, 2361-2382. https://doi.org/10.1080/10826070500187558

[44] Brenneisen, R. Chemistry and analysis of phytocannabinoids and other Cannabis constituents. In *Marijuana and the Cannabinoids*; ElSohly, M.A., Ed.; Humana Press: Totowa, NJ, USA, **2007**; pp. 17-49.

[45] Small, E.; Naraine, S.G.U. Size matters: evolution of large drug-secreting resin glands in elite pharmaceutical strains of *Cannabis sativa* (marijuana). *Genet. Resour. Crop Evol.* **2016**, *63*, 349-359. https://doi.org/10.1007/s10722-015-0254-2

[46] Russo, E.B. Taming THC: potential cannabis synergy and phytocannabinoid-terpenoid entourage effects. *Br. J. Pharmacol.* **2011**, *163*, 1344-1364. https://doi.org/10.1111/j.1476-5381.2011.01238.x

[47] European Medicines Agency. Guideline on specifications: test procedures and acceptance criteria for herbal substances, herbal preparations and herbal medicinal products/traditional herbal medicinal products. EMA/CPMP/QWP/2820/00 Rev. 2. **2011**.

[48] Amin, M.R.; Mondol, R.; Habib, M.R.; Hossain, M.T. Antimicrobial and cytotoxic activity of three bitter plants *Enhydra fluctuans*, *Andrographis paniculata* and *Clerodendrum viscosum*. *Adv. Pharm. Bull.* **2012**, *2*, 207-211.

[49] Flores-Sanchez, I.J.; Verpoorte, R. Secondary metabolism in cannabis. *Phytochem. Rev.* **2008**, *7*, 615-639. https://doi.org/10.1007/s11101-008-9094-4

[50] Pollastro, F.; Minassi, A.; Fresu, L.G. Cannabis phenolics and their bioactivities. *Curr. Med. Chem.* **2018**, *25*, 1160-1185. https://doi.org/10.2174/0929867324666170810164636

[51] Sparg, S.G.; Light, M.E.; Van Staden, J. Biological activities and distribution of plant saponins. *J. Ethnopharmacol.* **2004**, *94*, 219-243. https://doi.org/10.1016/j.jep.2004.05.016

[52] Audu, B.S.; Ofojekwu, P.C.; Ujah, A.; Ajima, M.N.O. Phytochemical, proximate composition, amino acid profile and characterization of Marijuana (*Cannabis sativa* L.). *J. Phytopharmacol.* **2014**, *3*, 35-43.

[53] Hollman, Peter CH. Absorption, bioavailability, and metabolism of flavonoids. Pharmaceutical biology. 42.sup1. 2004, 74-83.

[54] Werz, O.; Seegers, J.; Schaible, A.M.; Weinigel, C.; Barz, D.; Koeberle, A.; Allegrone, G.; Pollastro, F.; Zampieri, L.; Grassi, G.; Appendino, G. Cannflavins from hemp sprouts, a novel cannabinoid-free hemp food product, target microsomal prostaglandin E2 synthase-1 and 5-lipoxygenase. *Pharma Nutrition* **2014**, *2*, 53-60. https://doi.org/10.1016/j.phanu.2014.05.001

[55] Russo, E.B. The case for the entourage effect and conventional breeding of clinical cannabis: No "strain," no gain. *Front. Plant Sci.* **2019**, *9*, 1969. https://doi.org/10.3389/fpls.2018.01969

[56] Hazekamp, A.; Tejkalová, K.; Papadimitriou, S. Cannabis: from cultivar to chemovar II—a metabolomics approach to Cannabis classification. *Cannabis Cannabinoid Res.* **2016**, *1*, 202-215. https://doi.org/10.1089/can.2016.0017

[57] McKernan, K.; Spangler, J.; Zhang, L.; Tadigotla, V.; Helbert, Y.; Foss, T.; Smith, D. Cannabis microbiome sequencing reveals several mycotoxic fungi native to dispensary grade Cannabis flowers. *F1000Research* **2016**, *4*, 1422. https://doi.org/10.12688/f1000research.7507.2

[58] Ruchlemer, R.; Amit-Kohn, M.; Raveh, D.; Hanuš, L. Inhaled medicinal cannabis and the immunocompromised patient. *Support. Care Cancer* **2015**, *23*, 819-822. https://doi.org/10.1007/s00520-014-2429-3

[59] Holmes, M.; Vyas, J.M.; Steinbach, W.; McPartland, J. *Microbiological Safety Testing of Cannabis*; Cannabis Safety Institute: Portland, OR, USA, **2015.**

[60] Jerushalmi, S.; Maymon, M.; Dombrovsky, A.; Freeman, S. Fungal pathogens affecting the production and quality of medical cannabis in Israel. *Plants* **2020**, *9*, 882. https://doi.org/10.3390/plants9070882

[61] American Herbal Products Association. *Cannabis Laboratory Operations and Testing: Recommendations for Regulators of Cannabis Testing Laboratories*; American Herbal Products Association: Silver Spring, MD, USA, **2014.**

[62] Sachs, J.; McGlade, E.; Yurgelun-Todd, D. Safety and toxicology of cannabinoids. *Neurotherapeutics* **2015**, *12*, 735-746. https://doi.org/10.1007/s13311-015-0380-8

[63] Zerihun, A.; Chandravanshi, B.S.; Debebe, A.; Mehari, B. Levels of selected metals in leaves of *Cannabis sativa* L. cultivated in Ethiopia. *Springer Plus* **2015**, *4*, 359. https://doi.org/10.1186/s40064-015-1145-x

[64] McPartland, J.M.; McKernan, K.J. Contaminants of concern in cannabis: microbes, heavy metals and pesticides. In *Cannabis sativa L. - Botany and Biotechnology*; Chandra, S., Lata, H., ElSohly, M.A., Eds.; Springer: Cham, Switzerland, **2017**; pp. 457-474.

[65] Linger, P.; Müssig, J.; Fischer, H.; Kobert, J. Industrial hemp (*Cannabis sativa* L.) growing on heavy metal contaminated soil: fibre quality and phytoremediation potential. *Ind. Crops Prod.* **2002**, *16*, 33-42. https://doi.org/10.1016/S0926-6690(02)00005-5

[66] Citterio, S.; Santagostino, A.; Fumagalli, P.; Prato, N.; Ranalli, P.; Sgorbati, S. Heavy metal tolerance and accumulation of Cd, Cr and Ni by *Cannabis sativa* L. *Plant Soil* **2003**, *256*, 243-252. https://doi.org/10.1023/A:1026113905129

[67] Eboh, L.O.; Thomas, B.E. Analysis of heavy metal content in Cannabis leaf and seed cultivated in southern part of Nigeria. *Pak. J. Nutr.* **2005**, *4*, 349-351. https://doi.org/10.3923/pjn.2005.349.351

[68] Dryburgh, L.M.; Bolan, N.S.; Grof, C.P.L.; Galettis, P.; Schneider, J.; Lucas, C.J.; Martin, J.H. Cannabis contaminants: sources, distribution, human toxicity and pharmacologic effects. *Br. J. Clin. Pharmacol.* **2018**, *84*, 2468-2476. https://doi.org/10.1111/bcp.13695

[69] Nascimento, S.S.; Silva, E.D.C.; Martins, G.L.; Albuquerque, J.F.S.; Silva, K.M.B.; Lima, N.B. Heavy metals in medicinal plants widely used in the Cariris Velhos, Paraíba, Brazil. *Semin. Cienc. Agrar.* **2014**, *35*, 2433-2444. https://doi.org/10.5433/1679-0359.2014v35n5p2433

[70] Prasad, M.N.V. *Heavy Metal Stress in Plants: From Biomolecules to Ecosystems*, 2nd ed.; Springer-Verlag: Berlin, Germany, **2004.**

[71] Yang, Y.; Deng, C.; Xu, X. Investigation of heavy metals in Chinese therapeutic herbs. *Am. J. Chin. Med.* **2017**, *45*, 1303-1318. https://doi.org/10.1142/S0192415X17500732

[72] Russo, E.B. Current therapeutic cannabis controversies and clinical trial design issues. *Front. Pharmacol.* **2016**, *7*, 309. https://doi.org/10.3389/fphar.2016.00309

[73] Kharytonov, M.; Pidlisnyuk, V.; Stefanovska, T.; Babenko, M.; Martynova, N.; Rula, I. The estimation of Ukrainian agricultural soils pollution with heavy metals. *Environ. Res. Eng. Manag.* **2019**, *75*, 47-56. https://doi.org/10.5755/j01.erem.75.3.23323

ASEAN
Journal of Scientific and Technological Reports
Online ISSN:2773-8752

Research article

Designing and Developing Quality Control of Processes Using the Failure Mode and Effects Analysis Method and Machine Learning

Sirirat Pungchompoo[1*], Nikorn Sirivongpaisal[2], Rakkrit Duansoithong[3], and Aree Teeraparbseree[4]

[1] Faculty of Engineering, Prince of Songkla University, Songkhla, 90112, Thailand
[2] Faculty of Engineering, Prince of Songkla University, Songkhla, 90112, Thailand
[3] Faculty of Engineering, Prince of Songkla University, Songkhla, 90112, Thailand
[4] Faculty of Engineering, Prince of Songkla University, Songkhla, 90112, Thailand
* Correspondence: sirirat.pu@psu.ac.th

Citation:
Pungchompoo, S.; Sirivongpaisal, N.; Duansoithong, R.; Teeraparbseree, A. Designing and developing quality control of processes using the failure mode and effects analysis method and machine learning. *ASEAN J. Sci. Tech. Report.* **2025**, *28*(6), e259345. https://doi.org/10.55164/ajstr.v28i6.259345.

Article history:
Received: May 15, 2025
Revised: September 15, 2025
Accepted: September 27, 2025
Available online: October 20, 2025

Abstract: Medium-density fiberboard (MDF) production involves multiple intricate stages. Uneven thickness formation, large volumes of dynamic data from automated systems, and rapidly evolving technologies create substantial challenges for maintaining consistent quality control. Conventional approaches rely heavily on expert judgment and lack predictive capability, leaving a critical gap in timely and accurate risk assessment. This study addresses these challenges by integrating Failure Mode and Effects Analysis (FMEA) with machine learning techniques to evaluate and predict risks throughout the MDF production process. Real production data from an industrial facility were used to ensure practical relevance. Domain experts first assessed the Severity (S), Occurrence (O), and Detection (D) parameters using the PFMEA method. Predictive models—including K-Nearest Neighbors, Support Vector Machine, Neural Network, and an Ensemble Method—were then developed to estimate risk scores. The findings show that the Neural Network and Ensemble Method achieved the highest overall accuracy. This integrated approach reduces subjective bias, enhances predictive precision, and supports informed decision-making for quality control and risk mitigation in industrial MDF production.

Keywords: Failure mode and effects analysis (FMEA); machine learning; data driven quality control

1. Introduction

The medium-density fiberboard (MDF) industry plays a significant role in the production of furniture and construction materials. In Thailand, the abundance of rubberwood makes it an ideal raw material for MDF manufacturing. Despite its potential, industrial MDF production continues to face challenges related to quality control, real-time data processing from automated systems, and adaptation to emerging technologies within the context of Industry 4.0. A case study identified inconsistency in board thickness as a major issue, mainly caused by fluctuations in temperature and pressure during the continuous hot press (CHP) process. This inconsistency reduces product quality, increases production costs, and affects customer confidence. Moreover, the large volume of complex, time-dependent data generated by modern

manufacturing equipment makes it difficult to conduct timely analysis without an effective risk assessment system.

Failure Mode and Effects Analysis (FMEA) is a widely used method for identifying and ranking potential risks in manufacturing processes. It uses a Risk Priority Number (RPN), calculated based on severity (S), occurrence (O), and detection (D), to help manage quality problems. However, traditional FMEA has some limitations. It is typically static, heavily dependent on expert opinions, and cannot adapt to real-time changes. As a result, many recent studies have combined FMEA with other techniques, such as Statistical Process Control (SPC), fuzzy logic, and artificial intelligence (AI), to improve its effectiveness.

For example, one study introduced a dynamic FMEA model using data from CNC machine operations and maintenance to reduce reliance on expert judgment and increase risk evaluation accuracy [1]. In another case, combining SPC with FMEA helped detect severe defects in hollow steel production, where poor machine setup led to an RPN of 360 [2]. In the chemical industry, this integration reduced process variation by 63% [4], while in furniture manufacturing, the use of Fuzzy-FMEA with SPC revealed that worker inexperience was the primary cause of product defects [3]. To overcome the limitations of traditional FMEA, machine learning methods are being increasingly utilized. One study applied a Fuzzy Adaptive Resonance Theory (Fuzzy ART) model to classify failure modes without fixed thresholds [5]. Another developed a fuzzy-based FMEA that used expert input and linguistic terms. This model was applied to a Load-Haul-Dump (LHD) machine in underground mining and showed that the electrical system had the highest fuzzy RPN of 117 [6]. AI-based methods have also widened the use of FMEA. For instance, chatbot-driven Social FMEA was used to assess socially responsible product designs [7]. In sustainable construction, a hybrid framework combining Artificial Neural Networks (ANN), fuzzy logic, and the Internet of Things (IoT) reached 92.7% prediction accuracy and adapted well to noisy and changing data [8]. In addition, optimization methods also help improve risk assessment. A two-stage optimization model for household energy systems lowered user costs by 30% and increased energy efficiency by 4.8% [9]. Furthermore, Random Forest has outperformed traditional logistic regression in several fields, including education [10] and political studies [11]. Logistic regression has also helped rank risks in solar power plants [12]. Finally, linking IoT with FMEA is a promising trend. Real-time sensor data, such as temperature, humidity, thickness, and pressure, can update RPN scores and support predictive models. This helps build proactive, data-driven quality control systems that meet the complex needs of today's production environments.

This highlights a clear research gap. Although Fuzzy FMEA and SPC-FMEA have been applied in risk assessment, both approaches show notable limitations in the context of MDF manufacturing, where real production data are complex, non-linear, and imbalanced. Fuzzy FMEA helps reduce ambiguity in expert scoring but relies on predefined membership functions and rule sets, which makes it challenging to adapt to changing data conditions. SPC-FMEA effectively tracks statistical fluctuations but lacks the flexibility to predict S, O, and D in advance. In contrast, integrating PFMEA with machine learning enables the model to learn directly from actual production data, handle class imbalance and non-linear relationships more effectively, and predict S, O, and D with greater accuracy. This integration enables systematic and timely RPN calculation and risk prioritization, particularly well-suited to the challenges of MDF production.

Therefore, this study aims to develop a data-driven quality control model for MDF manufacturing by integrating FMEA, IoT sensor data, and machine learning algorithms. The conceptual framework consists of two main components. The first focuses on identifying risk factors using FMEA and developing predictive models with methods such as Random Forest, XGBoost, and Neural Networks. The second introduces an Inverted Process Model that utilizes predictive outputs to recommend optimal process parameters, reduce the RPN, and enhance product quality. As illustrated in Figure 1, the proposed framework comprises three main stages: (1) Data Collection from automated systems, (2) Data Access and Preparation, and (3) Smart Data and Modeling through machine learning. By combining risk analysis with intelligent prediction, this approach facilitates the development of an intelligent quality control system that aligns with Industry 4.0.

2. Materials and Methods

This study aims to develop an integrated approach for analyzing and forecasting risks in the production process of medium-density fiberboard (MDF). The method combines expert-based Failure Mode

and Effects Analysis (FMEA) with quantitative techniques, including statistical analysis and machine learning algorithms. The objective is to improve the accuracy of assessing severity (S), occurrence (O), and detection (D), which are then used to calculate the Risk Priority Number (RPN) systematically. The outcome is to implement the model in a web application designed for practical use in industrial settings. The research methodology consists of two main stages.

Stage 1: Risk Evaluation Using PFMEA Based on Expert Judgments

The initial risk assessment used the Process FMEA (PFMEA) method, drawing on evaluations from three to five experts at an MDF manufacturing facility. These experts—engineers, production supervisors, and quality control staff—assigned scores independently for S, O, and D to potential failure modes within the production process. Scoring followed the standard FMEA 1–10 scale: Severity (S) ranged from 1 (negligible effect on product quality) to 10 (catastrophic failure affecting safety or compliance); Occurrence (O) from 1 (failure unlikely to occur) to 10 (failure almost inevitable to occur); and Detection (D) from 1 (failure almost inevitable to be detected) to 10 (failure improbable to be detected). The scores were averaged across experts, and RPN values were calculated (RPN = S × O × D). These data were then used to prioritize risk areas and provided the basis for developing predictive machine learning models in the next phase.

Stage 2: Development and Evaluation of Machine Learning Models

To address the non-linear and imbalanced nature of real production data, machine learning techniques were applied to predict S, O, and D values. The dataset was divided into 80% for training and 20% for testing. Within the training set, stratified 5-fold cross-validation (k = 5) was used to tune and evaluate models while preserving class proportions. No repeated cross-validation was applied. All variables were standardized and normalized prior to training to minimize the effects of different units and scales.

Because the data were complex and imbalanced across classes, oversampling techniques (RandomOverSampler/SMOTE) were applied only to the training set, with the test set kept untouched to preserve the original distribution. The Ensemble Method, combined with Bagging and Decision Trees, was also selected to reduce bias and variance, as well as to handle class imbalance effectively.

Severity (S), Occurrence (O), and Detection (D) were classified into 10 classes (Class 1–Class 10) following the standard FMEA scoring scale. The actual production data showed an imbalanced distribution—for example, S had the highest frequency in Class 1 (103 records) and fewer in higher classes; O was concentrated in Classes 1–3 (100–103 records); and D peaked in Class 6 (215 records) with some classes having no records. This imbalance was explicitly taken into account in model selection and data preprocessing.

Four algorithms were selected for model development, with the following key settings: K-Nearest Neighbors (KNN), k = 10 neighbors; Euclidean distance metric; squared inverse distance weight; and standardized data. Support Vector Machine (SVM): cubic kernel; kernel scale automatic; box constraint level 1; multiclass coding one-vs-one; standardized data. Neural Network (NN): one fully connected hidden layer; 100 neurons; ReLU activation; iteration limit 1000; regularisation strength (lambda) 0; standardized data. Ensemble Method (Bagging + Decision Trees): 30 learners; decision tree base learners; maximum number of splits 479; all predictors sampled.

Model development included data preprocessing, training, and tuning with stratified 5-fold cross-validation on the training set, followed by final performance evaluation on the 20% hold-out test set. Performance was assessed using classification metrics—Accuracy, Balanced Accuracy, Precision, Recall, and Macro-F1 Score—as well as regression-style indicators (R^2, RMSE, MAE) for comparison. A feature importance analysis was also conducted to identify key factors influencing risk. The predicted S, O, and D values were then used to compute new RPN scores, which were applied to guide process improvements and risk mitigation efforts.

The PFMEA focused specifically on four upstream processes that precede the Refiner stage, where initial observations indicated premature blade damage. This issue appeared to be caused by upstream conditions, including raw material contamination and technical inconsistencies. Therefore, four critical production processes were selected for detailed analysis.

- Debarking involves removing bark and foreign materials from logs. The process begins with log alignment using a vibration conveyor, followed by the removal of stones and metals via a roller stone trap. Logs are then transferred through handling systems to the debarking drum, which removes 60–80% of the bark.

- Chipping converts debarked logs into wood chips within a size range of 4–40 millimeters. The material is conveyed through a chain conveyor, bark separator, and belt conveyor to the chipper. Blade performance is continuously monitored through current (ampere) measurements to prevent damage.

- Chip washing reduces impurities and moisture in the wood chips. Chips are moved using a twin-screw system through a roller screen to classify size, washed with water, and dewatered using a screw press and plug screw. The moisture content is finally adjusted in a surge bin to meet the process requirements.

- Digesting softens the wood chips using high-pressure steam. The digester regulates both chip size and steam pressure within optimal ranges, ensuring the material is conditioned correctly before entering the refiner.

3. Results and Discussion

This section may be divided by subheadings. It should provide a concise and precise description of the experimental results, their interpretation, and the conclusions that can be drawn from the experiment. Authors should discuss the results and how they can be interpreted in light of previous studies and the working hypotheses. The findings and their implications should be discussed in the broadest context possible. Future research directions may also be highlighted.

3.1 PFMEA Assessment

The risk analysis of the MDF production process, conducted prior to the Refiner stage using the PFMEA method, revealed that the primary causes of premature Refiner blade wear are related to the presence of contaminants, unsuitable moisture levels, and a lack of effective defect detection, which still relies primarily on visual inspection. The PFMEA results are illustrated in Figure 1. During the debarking process, issues were observed with the vibration conveyor and roller conveyor trap, where wood stacking and the presence of foreign materials, such as stones and soil, frequently interrupted the material flow. This resulted in a high RPN score of 128. In the chipping process, particularly involving the chain conveyor, accumulated bark often caused the chipper to stop, leading to the highest recorded RPN of 192. This was attributed to the severity of the issue and the absence of an automated detection system. In the chip washing stage, residual contaminants and excessive moisture levels were found. These problems were linked to ineffective washing and dewatering operations, resulting in RPN values ranging from 120 to 126. These factors were shown to contribute to blade wear in the refiner. Overall, the key risks identified were related to poor control of contamination, suboptimal moisture management, and inaccurate detection methods. These findings suggest the need for process improvement through the implementation of automated sensor systems and enhanced filtering and conveying mechanisms to minimize equipment damage and stabilize the production process.

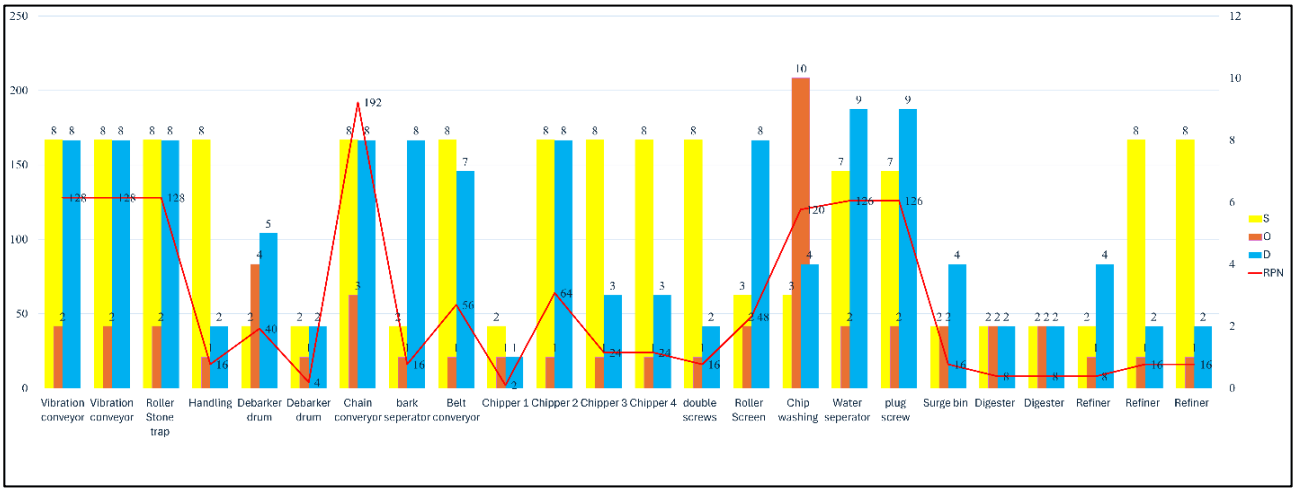

Figure 1. PFMEA Assessment Results

3.2.Development of Linear Models and Statistical Analysis

To validate the results of the PFMEA assessment, a statistical analysis was conducted using 354 actual production records collected between January 2023 and mid-May 2024. The study focused on the wear of the Refiner blade (Wear) and the specific energy consumption (SEC), which is directly associated with wear, in relation to several independent variables. These included chip types (Fine Chip, Good Chip, and Oversize Chip), the amount of bark in the process, both during debarking and before entering the roller screen, as well as the moisture content.

As illustrated in the matrix plot in Figure 2, the analysis revealed clear correlations between these variables and blade wear. The statistical results demonstrated that moisture content was significantly correlated with both the wear of the Refiner blade and the SEC values. Notably, the correlation coefficient between SEC and Wear reached a value of 0.908, indicating a strong direct relationship between energy consumption and the degree of blade deterioration during the production process. Moreover, moisture content was also found to be significantly related to chip type—particularly Fine Chip and Good Chip—as well as to the presence of bark contaminants during the debarking stage and prior to the roller screen. These findings reinforce the PFMEA results, which identified contamination and improper moisture levels as primary causes of equipment wear before the refining process. Additionally, the study confirmed that the current reliance on visual inspection for anomaly detection is insufficient for early identification and prevention of damage.

In summary, the results indicate that moisture content, chip type, and the level of contamination in both conveying and washing processes are key factors contributing to Refiner blade wear. The integration of statistical data analysis with PFMEA evaluation confirms that the development of automated detection systems and data-driven predictive models is essential for minimizing damage and systematically improving the efficiency and reliability of MDF production processes.

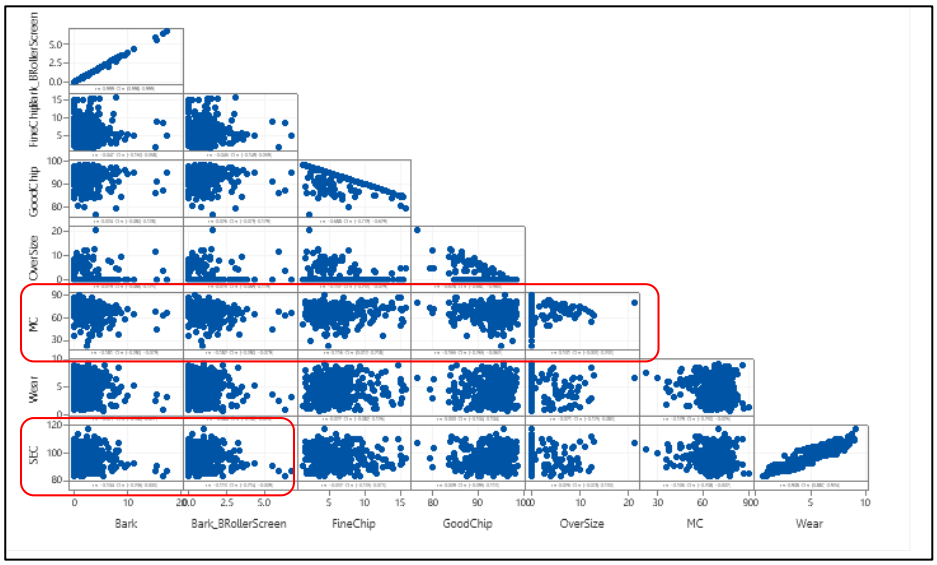

Figure 2. Matrix Plot for Pair Pearson Correlation Analysis

Under the variables analyzed through the PFMEA process, the values of severity (S), occurrence (O), and detection (D) were used as key factors in developing a predictive model for the Risk Priority Number (RPN) through multiple linear regression (MLR). The resulting MLR equation used to forecast the RPN is as follows:

RPN = -66.18 + 28.29 * O + 22.32 * S + 21.18 * D + 1.76 * 2.5<Wear<4 + 1.40 * Over size <5% + 0.28 * 80<SEC<130 + -0.45 * Bark + -0.48 * %MC < 80% + -0.48 * Good chip >80% + -1.76 * Fine chip <15% + -10.70 * Chip Washing_pH < 5 + -10.91 * Chip Washing_Solid < 7

However, the implementation of PFMEA evaluation and the subsequent statistical validation revealed several limitations. While Pearson correlation analysis provided an initial indication of linear relationships among variables, it was insufficient for capturing deeper or non-linear associations. Similarly, the use of

Multiple Linear Regression (MLR) presented constraints in accurately predicting RPN values from real-world production data, which are often complex and asymmetrical in nature. Therefore, it is necessary to develop more flexible machine learning models capable of accurately predicting the values of severity (S), occurrence (O), and detection (D), while minimizing the bias typically associated with expert-based assessments.

3.3 Risk Analysis and Prediction in Manufacturing Processes Using a Data-Driven Approach

The dataset used in this study consists of ten independent variables that reflect the characteristics of wood chips and key stages of the MDF production process, all of which are related to the wear and degradation of equipment in the production line. These variables were employed to develop predictive models and conduct systematic and practical risk analysis, focusing on their relationship with blade wear and overall process efficiency. Detailed descriptions of the variables are presented in Table 1.

Table 1. Key Variables Used in the Study

Variable	Definition
Fine chip <15%	Proportion of fine wood particles, accounting for less than 15% of total chips.
Good chip >80%	Proportion of high-quality wood chips exceeding 80% of the total chip volume.
Over size <5%	Proportion of oversized wood chips, not exceeding 5% of the total.
Bark	Amount of bark separated from the wood chips.
Bark Before Roller Screen	Bark is removed before the screening process using a roller screen.
%MC <80%	Moisture content in wood chips is maintained below 80%.
Chip Washing_pH <5	pH level of the water used in chip washing, where pH is less than 5.
Chip Washing_Solid <7	The concentration of solid particles in chip washing water is maintained at a level below 7%.
2.5 < Wear < 4	Degree of equipment wear ranging between 2.5 and 4.
80 < SEC < 130	Specific Energy Consumption (SEC) within the range of 80 to 130.

The dataset used in this study consists of ten independent variables, each with a considerably different range of values. For instance, some variables have values below 10, while others exceed 100. Without applying proper scaling or standardization prior to analysis, such disparities could adversely affect the performance of predictive models. Moreover, the dataset exhibits a non-linear relationship among variables and a notable degree of class complexity. As illustrated in Figure 3, the scatter plot shows overlapping distributions among Classes 1, 2, 3, and 4, indicating a high level of difficulty in distinguishing between these classes. In contrast, Class 8 is clearly separated from the others, demonstrating a distinct distribution pattern. These findings highlight the challenges in class classification and emphasize the importance of appropriate data preprocessing techniques.

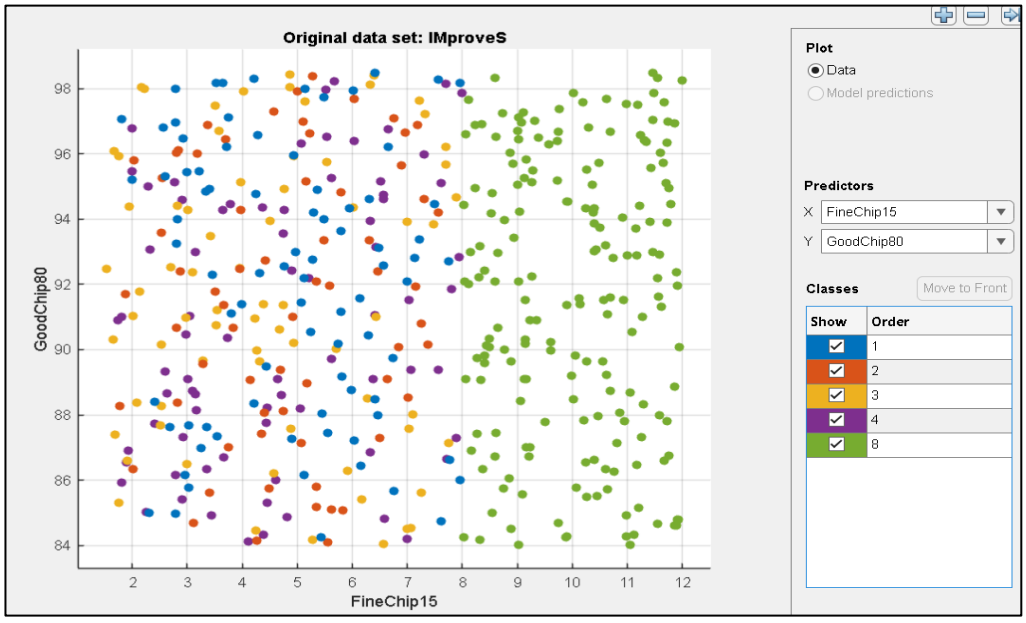

Figure 3. Scatter plot showing the distribution of data across different classes

For this reason, it was necessary to select models capable of handling non-linear relationships, varying data scales, and class complexity. Accordingly, four suitable machine learning models were considered, along with appropriate hyperparameter settings. This study involved the analysis and development of predictive models for risk assessment in MDF manufacturing, based on the principles of Failure Mode and Effects Analysis (FMEA) and using actual industrial data. The dataset presented notable challenges, including non-linearity, class overlap, and variation in the range of independent variables—especially within the S = 1–4 class group, which proved difficult to classify using conventional methods. To address these limitations, four machine learning algorithms were developed: K-Nearest Neighbors (KNN), Support Vector Machine (SVM), Neural Network (NN), and an Ensemble Method (Bagging with Decision Trees). Prior to model training, appropriate data preprocessing was performed, including hyperparameter tuning and standardization, to enhance model performance. The effectiveness of each model in predicting the three FMEA indicators—Severity (S), Occurrence (O), and Detection (D)—was evaluated using accuracy scores derived from the test datasets. Because the dataset was imbalanced, the Precision, Recall, and F1-Score reported in the tables are Weighted Averages calculated according to the proportion of samples in each class. The model achieving the highest accuracy for each target variable was identified and compared to determine which model performed best across all three dimensions.

For Severity (S) prediction, K-Nearest Neighbor (KNN) achieved the highest accuracy of 85.8%, followed closely by the Neural Network model at 85.0%. The Ensemble Method achieved an accuracy of 84.2%, while the Support Vector Machine (SVM) yielded the lowest accuracy at 83.3% (Table 2). In addition to accuracy, KNN also yielded substantial weighted precision (86.4%), recall (85.8%), and F1-score (85.5%), indicating consistent classification performance across severity levels, as shown in Table 2.

Table 2. Accuracy of Models in Predicting Severity (S)

Model	Accuracy (%)	Precision (%)	Recall (%)	F1 Score (%)
K-Nearest Neighbor	85.8	86.4	85.8	85.5
Neural Network	85.0	87.9	87.5	875
Ensemble Method	84.2	83.7	83.3	83.4
Support Vector Machine	83.3	84.5	83.3	83.5

In terms of Occurrence (O) prediction, the Neural Network model demonstrated the highest accuracy at 81.7%, followed by the Ensemble Method at 79.2%. SVM produced an accuracy of 76.7%, while KNN yielded the lowest accuracy at 75.8% (Table 3). Although the Ensemble Method achieved slightly lower accuracy than the Neural Network, it maintained relatively high weighted precision (81.5%) and recall (81.7%), resulting in a weighted F1-score of 81.2%, as shown in Table 3.

Table 3. Accuracy of Models in Predicting Occurrence (O)

Model	Accuracy (%)	Precision (%)	Recall (%)	F1 Score (%)
K-Nearest Neighbor	75.8	77.3	77.5	77.2
Neural Network	81.7	79.8	80.0	79.8
Ensemble Method	79.2	81.5	81.7	81.2
Support Vector Machine	76.7	75.7	75.0	75.2

For Detection (D) prediction, the SVM model achieved the highest accuracy at 85.0%, outperforming the Ensemble Method (80.8%), the Neural Network (80.8%), and KNN (79.2%) (Table 4). While SVM led in overall accuracy, the Ensemble Method showed the most balanced weighted metrics—precision (82.5%), recall (82.5%), and F1-score (82.3%)—reflecting consistent detection capability across classes, as shown in Table 4.

Table 4. Accuracy of Models in Predicting Detection (D)

Model	Accuracy (%)	Precision (%)	Recall (%)	F1 Score (%)
K-Nearest Neighbor	79.2	80.0	79.2	79.3
Neural Network	80.8	82.1	81.7	81.7
Ensemble Method	80.8	82.5	82.5	82.3
Support Vector Machine	85.0	83.3	80.8	81.2

3.4 Analysis and Prediction of Risk in MDF Manufacturing Using a Data-Driven Approach

The findings indicated that no single model achieved the highest accuracy across all target variables. However, when considering the overall performance, the Neural Network model consistently produced high accuracy levels and achieved the best results in predicting the occurrence (O) variable. Similarly, the Ensemble Method showed the highest accuracy in predicting detection (D) and performed comparably to the Neural Network in predicting both S and O. In contrast, although the KNN model delivered strong performance in predicting severity (S), it had the lowest accuracy in predicting occurrence and detection, highlighting its limitations in broader applications. Meanwhile, the Support Vector Machine (SVM) demonstrated slightly lower accuracy compared to other models, yet maintained consistent and acceptable results. Therefore, it can be concluded that both Neural Network and Ensemble Method models show strong potential for practical use in predicting all three FMEA indicators and should be further improved through hyperparameter tuning, data augmentation, and class balancing to increase overall prediction accuracy.

3.5 Recommendations for Improving MDF Production to Minimize Risk and RPN

Based on the PFMEA evaluation and data analysis from an actual manufacturing facility, the major risk factors contributing to Refiner blade wear and high RPN values include the proportion of fine chips, moisture content of raw materials, pH control in the chip washing process, and blade wear itself. These findings were supported by statistical analyses and machine learning model results, which identified these variables as significantly influencing severity (S), occurrence (O), and detection (D) scores. Thus, the following recommendations are proposed to improve the production process:

- Control of Fine Chips (FineC_weight) To maintain chip size within standard ranges, it is recommended to optimize cutting speed and feed rate in the Chipper process. Implementing a preventive maintenance plan can also help minimize blade wear, a major cause of uneven cutting and excessive fine chips, thereby reducing the risk in subsequent steps.

- Moisture Control Automatic moisture control systems should be installed in production areas, such as dehumidifiers or temperature regulation systems, to keep moisture levels within acceptable limits. Regular moisture measurements should be carried out using sensors and automated alerts. In addition, raw material storage areas should be improved to ensure better environmental control.

- pH Control in Chip Washing Frequent monitoring of pH levels in the washing process is necessary, and appropriate chemical adjustments should be made when values deviate from acceptable ranges. Effective control of wash water quality can help reduce residual substances that cause equipment damage and compromise chip quality.

- Reduction of Blade Wear (Wear). Scheduled tool maintenance, along with the use of high-durability materials, is essential. Additionally, the use of high-precision cutting equipment can help reduce the occurrence of oversized chips and improve the overall efficiency of the production process.

- Enhanced Detection Systems PFMEA results indicated that visual inspection has significant limitations. The development of automated detection systems using sensors—such as vibration, moisture, and electric current—can enhance real-time problem analysis and reduce the risk of human error.

- Use of Statistical Process Control (SPC) Control charts should be implemented to monitor the stability of the process after improvements. This approach enables real-time monitoring of deviations in the production process, thereby minimizing damage and enhancing long-term product quality.

3.6 Discussion

The risk analysis of the MDF production process using PFMEA, supported by actual operational data, revealed that the primary factors contributing to premature wear of critical equipment—particularly the Refiner blades—were contamination (e.g., stones, soil, and bark), excessive moisture content, and limited fault detection, which still relied mainly on visual inspection. High RPN scores reinforced these findings in several key processes, including the chipping stage with the chain conveyor (RPN = 192), the Debarking stage (RPN = 128), and the Chip Washing stage (RPN = 120–126). Statistical analysis using Pearson correlation confirmed significant positive relationships between moisture content and both blade wear and specific energy consumption (SEC), an indicator of process efficiency. Moisture content also correlated with chip types (Fine Chip and Good Chip) and the amount of bark present in the system, further supporting the PFMEA results that these variables substantially contribute to process risks. However, conventional statistical techniques, such as Pearson correlation and multiple linear regression, demonstrated limitations in capturing non-linear relationships and managing complex, imbalanced data distributions. As a result, machine learning models were introduced to improve predictive performance. Four models—K-Nearest Neighbors (KNN), Support Vector Machine (SVM), Neural Network (NN), and an Ensemble Method—were developed with appropriate data standardization and hyperparameter tuning prior to training. The comparative results indicated that no single model consistently outperformed others across all target variables. Nevertheless, the Neural Network achieved the highest accuracy in predicting occurrence (81.7%) and maintained consistent performance across all indicators, while the Ensemble Method attained the best accuracy in predicting detection (85.0%) and showed strength in handling imbalanced class distributions. Although the KNN model performed best in predicting severity (85.8%), its overall accuracy was lower in other variables, suggesting limited generalizability. Meanwhile, the SVM model offered stable results but achieved the lowest overall accuracy. Taken together, these findings indicate that both the Neural Network and Ensemble Method hold the most significant potential for future application in predictive risk analysis.

Compared with previous FMEA studies, this research demonstrates clear advantages. Keskin and Özkan [5] proposed the fuzzy ART algorithm as an alternative to traditional FMEA scoring; however, they did not test it with real-time production data. Balaraju et al. [6] applied a fuzzy-FMEA risk evaluation to a Load–Haul–Dump (LHD) machine in the mining sector, which performed well but still relied heavily on expert judgment. Spreafico and Sutrisno [7] developed a Social FMEA assisted by artificial intelligence to support sustainable product design, extending FMEA to social and environmental issues. Góes et al. [8] proposed a hybrid AI-based risk assessment framework combining ANN, fuzzy logic, and IoT for sustainable construction. In contrast, the present study integrates PFMEA with several machine learning algorithms directly on real MDF production data. It identifies key risk factors, such as the chipping process with an RPN of 192, and shows that the Neural Network and Ensemble Method achieve higher predictive accuracy. This integrated approach not only reduces subjectivity but also provides a practical framework that is ready for future integration with IoT sensors and transfer learning to enhance industrial applications.

Moreover, process improvement strategies can be guided by these findings. Priority should be given to controlling the proportions of fine chips and moisture, as identified in the Pareto analysis, while also managing pH levels during chip washing and minimizing blade wear. These objectives can be achieved by optimizing cutting speed and raw material feeding rates, implementing automated moisture control systems, continuously monitoring pH values, and replacing visual inspection with sensor-based detection. Integrating statistical process control (SPC) with machine learning—particularly through a web application for real-time monitoring and alerts—offers an effective strategy for enhancing predictive accuracy. Finally, increasing the volume of training data, balancing class distributions, and refining model parameters are essential steps to support more reliable and scalable risk management solutions in MDF production.

4. Conclusions

This study aimed to assess and predict risks in the medium-density fiberboard (MDF) production process by integrating Failure Mode and Effects Analysis (FMEA) with data analytics and machine learning techniques. The PFMEA effectively identified key risk factors in the pre-Refiner stages, particularly those

associated with contamination and improper moisture levels, with the chipping process showing the highest Risk Priority Number (RPN) at 192. Statistical analysis confirmed that moisture content was significantly correlated with blade wear, specific energy consumption (SEC), chip types, and bark contamination. However, traditional methods, such as Pearson correlation and multiple linear regression, were inadequate for capturing complex, non-linear patterns and managing class imbalance. Four machine learning models—the K-Nearest Neighbor (KNN), Support Vector Machine (SVM), Neural Network (NN), and an Ensemble Method—were therefore developed and tested with data standardization and hyperparameter tuning. The KNN model achieved the highest accuracy in predicting severity (S), while the Neural Network performed strongly for occurrence (O). The Ensemble Method excelled in detection (D) and handled imbalanced data more robustly. In addition to model performance, this approach enables factories to adjust process parameters more precisely, reduce defects and waste, lower production costs, and minimize downtime, while providing a data-driven basis for engineering decisions and continuous improvement. The findings suggest that implementing these recommendations could reduce defect rates, improve process stability and yield, and lower maintenance costs. In addition, future work will focus on enhancing the model's performance and practical applicability. First, additional data will be collected through data augmentation to increase the diversity and representativeness of the training set. Second, the system will be connected to the Internet of Things (IoT) infrastructure, enabling real-time data acquisition from sensors installed at each stage of the production process, ranging from the debarking stage to the refinery. This real-time data stream enables continuous model updating and monitoring, thereby reducing latency between data collection and risk prediction. Finally, transfer learning techniques will be explored to leverage pre-trained models for faster adaptation and improved accuracy on new datasets.

5. Acknowledgments

The authors gratefully acknowledge the financial support provided by Thailand Science Research and Innovation (TSRI) under the Fundamental Fund (FF), fiscal year 2024, through the government budget of Thailand (Project Reference Code: 24463; Research Project Code: ENG6701262M). The authors would also like to extend their appreciation to the Smart Industrial Research Center, the Faculty of Engineering, and Prince of Songkla University for their support and provision of research resources and facilities.

Author Contributions: Conceptualization, Sirirat Pungchompoo and Nikorn Sirivongpaisal; Methodology, Sirirat Pungchompoo; Validation, Sirirat Pungchompoo; Formal analysis, Sirirat Pungchompoo; Investigation, Sirirat Pungchompoo, Nikorn Sirivongpaisal, Rakkrit Duansoithong, and Aree Teeraparbseree; Resources, Sirirat Pungchompoo; Data curation, Sirirat Pungchompoo, Nikorn Sirivongpaisal, Rakkrit Duansoithong, and Aree Teeraparbseree; Writing – original draft preparation, Sirirat Pungchompoo; Writing – review and editing, Sirirat Pungchompoo; Visualization, Sirirat Pungchompoo; Supervision, Sirirat Pungchompoo and Nikorn Sirivongpaisal; Project administration, Sirirat Pungchompoo and Nikorn Sirivongpaisal; Funding acquisition, Sirirat Pungchompoo. All authors have read and agreed to the published version of the manuscript.

Funding: This research was funded by Thailand Science Research and Innovation (TSRI) under the Fundamental Fund (FF), fiscal year 2024, grant number ENG6701262M. The APC was funded by Thailand Science Research and Innovation (TSRI).

Conflicts of Interest: The authors declare no conflict of interest. The funders had no role in the design of the study, in the collection, analysis, or interpretation of data, in the writing of the manuscript, or in the decision to publish the results.

References

[1] Jiang, S.; Liu, Z.; Chen, J. A Dynamic Failure Mode and Effect Analysis (FMEA) Method for CNC Machine Tool in Service. *J. Phys.: Conf. Ser.* **2023**, *2483*, 012047. https://doi.org/10.1088/1742-6596/2483/1/012047

[2] Bangun, C. S.; Maulana, A.; Rasjidin, R.; Rahman, T. Application of SPC and FMEA Methods to Reduce the Level of Hollow Product Defects. *J. Tek. Ind.* **2022**, *8*(1), 12–16. https://doi.org/10.24014/jti.v8i1.16681

[3] Nurdaningsih, N. W.; Yunitasari, E. W.; Ma'arif, S. Statistical Process Control (SPC) and Fuzzy-Failure Mode and Effect Analysis (F-FMEA) Approaches to Reduce Reject Products in Wine Bottle Rack Production Process at PT Alis Jaya Ciptatama. *Opsi* **2022**, *15*(2), 274–283. https://doi.org/10.31315/opsi.v15i2.7567

[4] Appollis, L.-L. M.; van Dyk, W. A.; Matope, S. Using Failure Modes and Effects Analysis as a Problem-Solving Guideline When Implementing SPC in a South African Chemical Manufacturing Company. *S. Afr. J. Ind. Eng.* **2020**, *31*(1), 157–169. https://doi.org/10.7166/31-1-2294

[5] Keskin, G. A.; Özkan, C. An Alternative Evaluation of FMEA: Fuzzy ART Algorithm. *Qual. Reliab. Eng. Int.* **2009**, *25* (6), 647–661. https://doi.org/10.1002/qre.984

[6] Balaraju, J.; Govinda Raj, M.; Murthy, C. S. Fuzzy-FMEA Risk Evaluation Approach for LHD Machine – A Case Study. *J. Sustain. Min.* **2019**, *18*(4), 257–268. https://doi.org/10.1016/j.jsm.2019.08.002

[7] Spreafico, C.; Sutrisno, A. Artificial Intelligence Assisted Social Failure Mode and Effect Analysis (FMEA) for Sustainable Product Design. *Sustainability* **2023**, *15*(11), 8678. https://doi.org/10.3390/su15118678

[8] Góes, A. L. B.; Kazmi, R.; Aqsa, A.; Nuthakki, S. A Hybrid AI-Based Risk Assessment Framework for Sustainable Construction: Integrating ANN, Fuzzy Logic, and IoT. *Int. J. Adv. Comput. Sci. Appl.* **2025**, *16*(3), 46–56.

[9] Lu, Q.; Zeng, W.; Guo, Q.; Lü, S. Optimal Operation Scheduling of Household Energy Hub: A Multi-Objective Optimization Model Considering Integrated Demand Response. *Energy Rep.* **2022**, *8*, 15173–15188. https://doi.org/10.1016/j.egyr.2022.11.047

[10] Doz, D.; Cotič, M.; Felda, D. Random Forest Regression in Predicting Students' Achievements and Fuzzy Grades. *Mathematics* **2023**, *11*(19), 4129. https://doi.org/10.3390/math11194129

[11] Muchlinski, D.; Siroky, D.; He, J.; Kocher, M**.** Comparing Random Forest with Logistic Regression for Predicting Class-Imbalanced Civil War Onset Data. *Political Analysis* **2016**, *24*(1), 87–103. https://doi.org/10.1093/pan/mpv024

[12] Program, D. F.; Prijadi, R. FMEA-Based Logistic Regression Model for the Evaluation of Photovoltaic Power Plant Risk. *Quant. Econ. Manag. Stud.* **2024**, *5*, 644-657. https://doi.org/10.35877/454RI.qems2645

ASEAN
Journal of Scientific and Technological Reports
Online ISSN:2773-8752

Research article

Growth and Fiber Yield of Red Spanish Pineapple (*Ananas comosus* L.) through Fertilizer Management and Planting Density in Aklan, Philippines

Evelyn Vedasto[1*] and Neil Adrian Alegria[1]

[1] College of Agriculture, Forestry and Environmental Science, Aklan State University, Banga, Aklan, ,5601, Philippines
[2] College of Agriculture, Forestry and Environmental Science, Aklan State University, Banga, Aklan, ,5601, Philippines
* Correspondence: epvedasto@asu.edu.ph

Citation:
Vedasto E.; Alegria, N.A. Growth and fiber yield of red spanish pineapple (*Ananas comosus* L.) through fertilizer management and planting density in Aklan, Philippines. *ASEAN J. Sci. Tech. Report.* **2025**; *28*(6), e258793. https://doi.org/10.55164/ajstr.v28i6.258793.

Article history:
Received: April 15, 2025
Revised: September 19, 2025
Accepted: September 27, 2025
Available online: October 20, 2025

Abstract: The Red Spanish Pineapple (*Ananas comosus* L.) is a natural fiber-producing crop primarily cultivated for its *piña* fiber and is deemed the "Queen of Philippine Fabrics" and "Mother of all Phillippine Textiles". The Aklan province is the center and top producing *piña* fiber in the country and holds historical significance for *piña* weaving using traditional handlooms. However, proper fertilization of this crop has not yet been explored to optimize its potential to directly influence fiber leaves and fruits. This study analyzed the growth dynamics of RSP using planting density and fertilizer treatments. The study experimented to analyze the growth dynamics of the RSP using three planting densities (80 × 50 × 30 cm, 60 × 30 cm, and 30 × 30 cm) and five fertilizer treatments (control, STK recommendation 55-40-50, ASU recommendation 56-56-56, 20 t/ha vermicompost, and 40 t/ha vermicompost). The study showed that 20 tons per hectare of vermicompost consistently exhibited a significant influence on the growth performance of the RSP, while STK recommendations (55-40-50) also showed a significant effect on growth performance. In contrast, the ASU recommendation (56-56-56) exhibited moderate influence but had a lesser impact compared to other treatments. Meanwhile, planting distance demonstrated minimal influence; therefore, the growth performance of RSP was not as effective as that of fertilizer management. The results of this study provide relevant information and address the scarcity of data, sustain tradition, and optimize RSP to meet the demand for high-quality fiber locally and internationally.

Keywords: Agronomic practices; crop spacing; fertilizer application, growth enhancement, *Piña*

1. Introduction

The Red Spanish Pineapple (*Ananas comosus* L.) is a tropical plant from *Bromeliaceae* and is widely cultivated in the Philippines, particularly in the Province of Aklan. This natural fiber-producing crop is valued in the country not only for its sweet edible fruit for consumption but also primarily due to the fiber known as *Piña* silk, which contributes to the textile industry. Red Spanish Pineapple Silk is deemed the "Queen of Philippine Fabrics", "Mother of all Phillippine Textiles", and the finest Philippine fabric primarily due to its delicate silk and cream color. Aklan province is the center of *piña* weaving in the country. Likewise, this province holds historical significance for *piña* weaving using traditional handlooms, which were passed down to family and community

generations [1]. In fact, Aklan's *piña* handloom was recognized by UNESCO as an intangible cultural heritage of humanity in the country [2]. These fibers are known for their fine texture, dye-holding capacity, creamy white color, sat tolerant resistance, and high tensile strength. It is very popular in the local and international scenes due to its distinct, unique, and texture qualities, making it an export product of the country. However, the supply of planting materials and fibers cannot sustain the increasing demand for *piña* fibers and requires immediate attention for the sustainable production of RSP fibers in the country [3].

One of the key challenges in addressing this concern is the lack of standardized nutrient management practices for fiber production. Most of the varieties for pineapple fruit production have recommended planting distances, fertilizer rates (such as in the Soil Test Kit), and local formulations (ASU recommendation 56-56-56). Furthermore, vermicomposting has been shown to significantly improve plant growth and yield performance [4]. However, these protocols are rarely applied in RSP to determine and evaluate its fiber traits. Additionally, comprehensive studies determining the fiber yield of RSP using these protocols are lacking. Fertilization is one of the factors responsible for the quality of the fruit, especially in relation to the weight achieved. Furthermore, the macronutrients required by pineapple for growth and development are N, P, K, and Ca [5]. Several factors, such as nutrient availability, cultural practices, and fertilization, influence the quality and quantity of RSP leaf fiber. These practices enhance overall quality and quantity of the fiber, such as tensile strength, color, number of fibers extracted, and length. RSP is cultivated primarily for its fiber rather than fruit, and limited studies were conducted to determine the relationship between fertilizer application, planting density, and fiber yield in RSP [6-7]. The government recognizes and research initiatives have been conducted to support RSP production. In 2004, Aklan researchers created a tissue culture method for RSP to mass-produce planting materials for future plantation growth to satisfy the market for *piňa* fibers [8]. The growth performance of the RSP is influenced by the nutrients in the soil, which ensure optimal pineapple productivity. Pineapples require a proper supply of nutrients to sustain their growth, development, yield, and quality of fruit and fiber. Nitrogen and other macronutrients play an important role in the growth performance of pineapple, particularly in photosynthetic activity and overall fertility [9-12]. Moreover, it is vital to ensure optimum pineapple growth and productivity through the balanced use of fertilizers [13]. Proper fertilization enhances leaf quality and directly influences fiber and fruit quality, thereby increasing the income of growers and farmers [6].

The Red Spanish Pineapple has significant economic value not only in the Province of Aklan but throughout the entire country. Unlike other varieties (Queen Formosa and MD2) that are sweeter, this is the only pineapple variety mainly cultivated for its high-quality fibers for luxury fabrics, such as barong tagalog and filipinana. Moreover, news reported that pineapple (all varieties) produced an average of 580-600 US dollars per metric ton in recent years, and exported roughly 787.12 million U.S. dollars in 2024, with fresh/dried pineapple $428.74 million. But there were challenges, and many issues/concerns regarding RSP in relation to RSP's low production [15]. Despite its economic significance, there has been a significant decrease in production due to several challenges, leading to an inadequate fiber supply [16]. Hence, there is a need to address the problem of the decline of *piňa* fibers and optimize the potential of the RS pineapples [3]. Furthermore, RSP is still understudied, and there is limited information on the growth dynamics of this crop, specifically on cultural management, which is crucial for optimizing the fiber yield and fruit production of RSP. Hence, this research seeks to establish optimal planting density, implement an effective fertilizer program, and other cultural practices to enhance the production of quality fibers from tissue-cultured RSP. The conducted research fills a crucial gap in the industry by focusing on sustaining the tradition and livelihoods linked to the Red Spanish Pineapple and meeting the demand for high-quality fiber locally and internationally [17-18].

2. Materials and Methods

2.1 Research design

This research employed an experimental design and was laid out in Split Plot Design to accommodate two variables: planting density (main plot) and fertilizer management (sub-plot). The main plot was composed

off three types of plant spacing and was divided into subplots composed of five fertilizer treatments with three replications. The treatments included the following:

MAIN PLOT: Planting Density
- Treatment 1 (A_1) – 80 x 50 x 30 cm
- Treatment 2 (A_2) – 60 x 30 cm
- Treatment 3 (A_3) – 30 x 30 cm

SUB-PLOT: Fertilizer Management
- Treatment 1 (B_1) – 0 fertilizer (control)
- Treatment 2 (B_2) – STK Recommendation (55-40-50)
- Treatment 3 (B_3) – ASU Recommendation (56-56-56)
- Treatment 4 (B_4) – Vermicompost (20 t/ha)
- Treatment 5 (B_5) – Vermicompost (40 t/ha)

2.2 Location of the study

The study was conducted at the Diversified Field Crops Production Project at the Aklan State University—Main Campus in Banga, Aklan. Banga, Aklan, is situated in the central plain of Aklan, at approximately 11° 38' North, 122° 20' East, on the island of Panay. It is 21.3 meters (69.9 feet) above sea level with a level to nearly level (0-8%) and categorized as a hot and humid tropical climate, with an average temperature of 27.68 ºC, 243.85 (mm) monthly rainfall, and 78.77 relative humidity as of 2024, according to the Philippine Atmospheric, Geophysical and Astronomical Services Administration.

2.3 Selection and collection of planting materials

Quality tissue-cultured planting materials (slips) were sourced from a laboratory greenhouse. Disease-free and uniform-in-size planting materials were collected from the source to contribute to the high probability of survival when planted in the field.

2.4 Clearing of the area

Before land preparation, the area was cleared of previous crop debris and other foreign objects that might hinder land preparation. Weeds of various kinds were removed/cut using a grass cutter. Cut grasses were then piled in a specific area of the field to allow decomposition or compost to be returned later to the soil.

2.5 Land preparation

A land area of 700 sq m was prepared by plowing and harrowing. Each main plot measured 5 m × 10 m (50 m^2) and was divided into five subplots, each measuring 1 m × 10 m (10 m^2). Plowing was performed using animal-drawn implements to aerate the soil, reduce weeds and other pests, and incorporate crop residues into the soil. This was accomplished to ensure that the soil was in good tilth for better establishment of tissue-cultured RS pineapple to be planted in the area as experimental crops.

A week after plowing, the area was harrowed twice to reduce the potential weed population by preventing them from germinating, and plots and pathways were constructed after plowing and harrowing. After the land had been thoroughly prepared, plots were laid out, and staking followed using bamboo sticks to mark each designated hill where the plantlets were planted. Staking ensured the proper distance between plants, as this was one of the treatment variables of the study.

2.6 Planting Distance and Selection of Sample Plants

RSP plants were planted at different planting distances. For treatment 1 (A1 – 80 × 50 × 30 cm), plants were planted at a spacing of 80 cm between rows, 50 cm between plants within a row, and 30 cm between successive planting points or diagonal spacing. Meanwhile, treatment 2 (A2 – 60 × 30 cm) was planted at a planting distance of 60 cm between rows and 30 cm within the row. Lastly, for treatment 3 (A3 – 30 × 30 cm), the plants were properly distance at at 30 cm between rows and 30 cm between plants within the row.

In selecting the sample plants, ten representative plant samples were randomly assigned for data gathering by staking or marking the plants. Missing hills were immediately replanted as soon as the mortality of tissue-cultured plantlets was observed.

2.7 Fertilizer application

Fertilizer management was one of the treatment variables of the study, hence the fertilizers applied were: no fertilizer (B1, control), STK recommendation (B2, 55-40-50 at 3.5 g/plant), ASU recommendation (B3, 56-56-56 at 5 g/plant), vermicompost at 20 t/ha (B4, 180 g/plant), and vermicompost at 40 t/ha (B5, 360 g/plant). This was done only once, four months after transplanting, and the fertilizer materials were applied as bands around the base of the plant. This was then covered with fine soil to minimize the volatilization of dissolved nutrients, especially during intense sunlight.

2.8 Leaf harvesting and processing

Leaf harvesting (manual) commenced 18 months after planting (MAP). Harvested leaves were processed following the manner of leaf processing for RSP, such as hand scraping, washing, beating, combing, and drying. This was done to gather the necessary data on the yield parameters of the fibers processed from the experimental plants. Two kinds of fiber were extracted from the leaf—the *liniuan* and *bastos* fiber.

2.9 Data gathering

Data were obtained from 10 randomly identified sample plants, preferably growing at the center of the plot. The uniformity of sample plants was considered to avoid bias in data gathering. These sample plants were identified and marked, and the desired data on growth and fiber yield were measured. Appropriate equipment and instruments were used to gather or obtain the needed data that would contribute to the attainment of the specified objectives. It is worth noting that the RSP fiber is split into two classifications: *bastos* (which is strong and coarse), and *liniuan* (which is very fine and is suitable for weaving cloth). The following data were gathered at specified times throughout the study duration:

The height (cm) of the Red Spanish Pineapple (RSP) was obtained by measuring the plants from the base to the tip of the growing point using a meter stick in centimeters (cm). The mean difference between the final and initial data was used for analysis. The total number of fully developed leaves was manually counted and subtracted from the number of initially developed leaves. The length of the leaves was measured from the base of the leaf up to the highest tip using a meter stick in centimeters (cm). The leaf width (cm) was measured in the widest part of the leaf, particularly in the middle using a meter stick in centimeters (cm). Meanwhile, the fiber length of *linuan* and *bastos* was measured from both ends using a meter stick in centimeters (cm). The number of *liniuan* and *bastos* fibers extracted was manually counted, while the number of *liniuan* and *bastos* fibers strands was measured using a weighing scale in grams (g).

2.10 Statistical analysis

Data gathered were subjected to Analysis of Variance following Split Plot Design using STAR software. A pairwise comparison of treatment means was performed using the Least Significant Difference. Significant differences were declared at P-value <0.05.

3. Results and Discussion

3.1 Plant height

Table 1 depicts the mean plant height (in centimeters) of tissue-cultured Red Spanish Pineapple (RSP) as influenced by different fertilizer management at different planting distances. Results revealed that notable differences were observed in the plant height of the tissue cultured RSP by both fertilizer management and distance of planting. Moreover, statistics show that treatments with 20 tons vermicompost per hectare and STK Recommendation (55-40-50) showed comparable results of 101.63 and 101.59 cm, respectively, and yielded the tallest plants among all treatments applied. Moreover, the ASU recommendations (56-56-56) and treatments with vermicompost (40 tons per hectare) were comparable to each other, with values of 100.52 and 98.96 cm, respectively. In contrast, the lowest plant height was observed in the control group (without treatment), at 96.60 cm (Figure 1a).

STK recommendations may have provided well-balanced essential nutrients enhancing the growth performance of the RSP particularly on its plant height. A specific percentage of macronutrients, such as NPK, might have met the RSP nutrition needs, resulting in good plant height performance. Vermicompost enhances the growth, yield, and intake of some basic plant nutrients (NPK) and increases plant height by about 50% [19].

Additionally, vermicompost treatment likely enriched the soil organic content, positively impacting plant growth. Studies, like Rekha *et al.* [20], affirm that vermicompost-treated plants experienced substantial growth. Vermicompost aids nutrient uptake by providing readily available nutrients, as supported by Mahmud *et al.* (2020), who noted reduced soil acidity and increased macro and micronutrient levels in both soil and plants [21]. Nonetheless, excessive application of vermicompost, especially at 40 tons per hectare, may hinder plant growth and cause nutrient imbalance, as cautioned by Chamani *et al.* [22].

Numerous studies have been conducted on balanced nutrient management. For instance, ASU's recommendations focus on using well-balanced amounts to optimize plant growth and development. Fertilizer application increased the amount of NPK available in the root zone, which increased the plant's ability to absorb nutrients. Numerous studies have shown that the increased leaf photosynthetic capability resulting from this nutrient increase contributes to the buildup of plant biomass [23-24]. However, excessive fertilizer application can cause plant stunting due to insufficient water availability caused by high osmotic conditions in the soil [25].

Therefore, in terms of encouraging optimal growth, the ASU Recommendation (56-56-56), while balanced, may not have been as successful as the STK Recommendation. In contrast, the shorter plants in the control group demonstrated the importance of additional nutrients and proper fertilizer administration for RSP growth and development. Fertilizer recommendations contain several important factors, including fertilizer form, source, application timing, placement, and irrigation management. Another important aspect of fertilizer recommendation is the amount of a particular nutrient to be applied. The optimum fertilizer amount is determined from extensive field experimentation conducted for several years, at multiple locations, with several varieties, etc. [26]. It is essential to emphasize that the fertilizer rate aims to ascertain the precise quantity of fertilizer required to attain a commercially viable crop yield of satisfactory quality, which is economically viable for Red Spanish Pineapple growers.

Spacing between pineapple plants during cultivation can significantly impact their growth, fruit development, and overall performance due to competition for nutrients, water, and sunlight [27]. Certain studies have indicated that increasing planting density, such as up to 78,000 plants per hectare, can lead to increased plant height and reduced width of the D-leaf (the longest leaf in a pineapple plant), as well as a decrease in the percentage of plants responding to flowering induction after artificial flowering induction [28-29]. However, findings regarding the specific planting distances show variations in mean plant height, ranging from 98.71 cm to 100.66 cm. It was concluded that the planting distance did not have a significant impact on plant height during this experiment involving Red Spanish Pineapple cultivation.

The specific alterations made in fertilizer application and distance of planting might not have exerted a considerable impact on the growth conditions of the plants. The variation in the combined ranges probably did not lead to significant differences in height. It seems that the fertilizer might have influenced the height independently rather than in conjunction with distance. Each factor may have individually influenced plant growth to a certain degree, but their combined effects during simultaneous investigation may not have been notably impactful.

3.2 Number of leaves

The leaf count serves as a critical measure reflecting the Red Spanish pineapple's vegetative growth and leaf development. Pineapple leaf fiber (PALF) is a natural fiber with specific strength, rigidity, flexural resistance, and torsional resistance similar to jute fibers [30]. The analysis of mean leaf count demonstrated no substantial interaction effect between fertilizer management and planting distance (refer to Table 1). This suggests that the combined influence of these factors did not notably affect the leaf count. Notably, only the fertilizer management factor had a significant effect across all planting distance variations.

The findings revealed that plants treated with 40 tons of vermicompost per hectare exhibited the highest leaf count (104 pcs), as shown in Figure 2b. This indicates superior leaf development under this specific fertilizer management for RSP. Conversely, the 55-40-50 STK Recommendation resulted in a comparable leaf count (103 pcs), highlighting its efficacy in supporting leaf production at varying planting distances. However, lower levels of organic fertilizer, such as 20 tons/ha of vermicompost and the ASU Recommendation (56-56-56), yielded slightly fewer leaves (102 pcs), suggesting a limited impact on RSP leaf development. The control

treatment recorded the lowest leaf count (97 pcs), aligning with previous studies emphasizing vermicompost's role in bolstering leaf productivity. These results corroborated with Balan, *et al.,* 2019 and Joshi *et al. (*2010), who revealed that the application of vermicompost increased the productivity of leaves in the plants [31-32]. Regarding planting distance, mean leaf count ranged from 101 pcs (for 60 x 30 cm spacing) to 102 pieces (both for 80 x 50 x 30 cm and 30 x 30 cm spacing). However, planting distance did not significantly affect the plant height during this experiment.

The study underscores the significance of specific nutrient management, particularly the application of 40 tons/ha of vermicompost, in enhancing leaf growth in RSP. It also emphasizes the role of fertilizer composition in supporting leaf productivity, elucidating the intricate link between fertilizer application, planting distance, and leaf count per square meter in the Red Spanish pineapple variety grown in the region. While each factor individually contributed to higher leaf counts, their combined influences might not have been notable due to diverse influences or differing experimental conditions.

3.3 Length of the leaves

As depicted in Table 1, the mean leaf length of tissue-cultured RSP was affected by fertilizer management. The findings indicated that employing vermicompost at 20 tons per hectare resulted in the most extended leaf length at 74.19 cm across varied planting distances, surpassing other applied treatments. Following closely were the STK (55-40-50) and ASU (56-56-56) recommendations, achieving 73.15 cm and 72.37 cm, respectively, slightly trailing the 20 t/ha vermicompost. In contrast, vermicompost at 40 t/ha and the control group exhibited the shortest leaf lengths at 71.25 cm and 69.48 cm, respectively.

Vermicompost is widely used because it contains high nutrient content, specifically macro and micronutrients, to enhance the growth performance of crops. According to Mahmud et al. (2018), fertilization plays an important role in crop management to increase growth potential and crop yield [33]. Pineapple plants have a large nutrient uptake demand, especially for potassium, followed by nitrogen, calcium, magnesium, sulfur, and phosphorus [34].

Pineapple plants have a large nutrient uptake demand, especially for potassium (K), followed by nitrogen (N), sulfur (S), calcium (Ca), magnesium (Mg), and phosphorus (P) [35]. Macro- and micronutrients can be obtained by supplementing inorganic or organic fertilizers, such as vermicompost. Vermicompost is a slow-release fertilizer and is rich with essential plant nutrients produced by the joint action of certain species of earthworms (especially *Eisenia fetida* or *Eudriculus eugeniae*) and microorganisms in the decomposition of organic waste such as agro-wastes, sewage sludge and food wastes [36-38]. Several studies have shown that vermicompost amendment can directly increase plant production by increasing available plant nutrients and indirectly promote soil quality by improving soil structure and stimulating microbial activities, relative to conventional chemical fertilization [39,40].

The results showed that the interaction of planting distance and fertilizer management had a considerable effect on leaf length, most noticeably for 60 × 30 cm and 30 × 30 cm spacings with STK fertilizer, and the application of 20 t/ha of vermicompost, which produced the longest leaves (74–75 cm). Meanwhile, the shortest leaves were observed on the control treatments (68–70 cm) among all planting densities as shown in Figure 2c. This highlights the narrow distance of planting supplied with balanced fertilizer results and longer leaves due to the competition for light [41].

3.4 Width of the leaves

The examination of leaf width averages in tissue cultured RSP, detailed in Table 1, suggests the absence of a substantial interaction between fertilizer management and planting distance. However, a notable impact was evident in terms of fertilizer management across all planting distance variations. The widest leaves were observed in plants subjected to the 55-40-50 STK Recommendation, measuring 2.80 cm. The study emphasized that the STK recommendation provided a well balance nutrient blend with specific rations of nitrogen, phosphorus, and potassium resulting in significantly wider lead of RSP. According to Chen *et al.,* 2021, balanced fertilization could provide benefits starting from increasing productivity and quality of crop yields and can increase yield by 3–7% with less fertilizer input [42]. Balanced use of nutrients has been proven to improve crop yield and organic matter in soil [43].

The widest leaves were observed in plants subjected to the 55-40-50 STK Recommendation, measuring 2.80 cm. Slightly narrower widths were recorded in plants treated with the 56-56-56 ASU Recommendation, measuring 2.67 cm. The control group displayed a width of 2.44 cm, akin to the leaf widths observed in plants treated with 40 tons (2.38 cm) and 20 tons (2.37 cm) per hectare of vermicompost (Figure 2d). Plant spacing influences the leaf width of pineapple plants. According to Kaamoga, 2018, in his study, there were significant differences between plants in plant height and width, leaf length, and leaf width at different spacing in pineapple plants as affected by plant spacing and nutrient source on growth and yield of pineapple [44].

These variations were influenced by both plant spacing and nutrient sources, highlighting their impact on pineapple growth and yield. In contrast, no significant influence was detected on RSP, with mean values ranging from 2.41 cm for the 30 × 30 cm spacing to 2.63 cm for the 60 × 30 cm spacing. The results revealed that well-balanced fertilizer management can significantly influence the width of leaves in tissue-cultured RSP. The STK Recommendation notably contributed to the widest leaves, indicating its substantial effect. While planting distance accounted for some differences in leaf width, its influence was comparatively modest when contrasted with the use of fertilizers. These findings signify the noteworthy impact of the chosen fertilizer management on leaf width, while the studied planting distances did not exhibit a substantial effect on this aspect.

3.5 Number of liniuan fibers

The findings indicated that there was an interaction effect between the management of fertilizer and *liniuan* fiber strands. Statistical analysis demonstrated that all treatments applied with a planting distance of 80 x 50 x 30 cm yielded comparable results, with Treatment 5 (Vermicompost at 40 t/ha) exhibiting the highest average count of 31 pieces. Hence, the study shows that specific planting distance and the amount of vermicompost at 40 t/ha significantly influenced the *linuan* fiber strand, as shown in Table 1 and Figure 2e.

There was also an interaction effect between fertilizer management and *the liniuan* fiber strand at a planting distance of 60 × 30, but it was slightly different compared to an 80 × 50 × 30 planting distance. However, similar results show that all treatments are comparable. Treatment 3 (ASU recommendations) exhibited the highest number of *liniuan* fiber strands with 30 pcs, followed by T2 (STK Recommendation) and T4 (Vermicompost at 40 t/ha). The study suggests that vermicomposting using ASU recommendations is suitable for *liniuan* fiber strand production at planting of 60 x 30 cm.

Furthermore, there were interactions between fertilizer management and *the effects of the liniuan* fiber strands at a 30 × 30 cm planting distance. However, this time treatment 4 (vermicompost at 20 t/ha) shows the highest mean of *liniuan* fiber strands (31 pieces) followed by STK recommendation (30 pcs), treatment 5 (vermicompost at 40/ha), and treatment 3 (ASU recommendations). Results exhibited that using the 30 x 30 planting distance, lower rate application of vermicompost may produce good number *liniuan* fiber strands compared to other fertilizer management approaches. Moreover, the study revealed that there is an interaction effect between fertilizer management and distance of planting in RSP resulting in higher *liniuan* fiber strands. Vermicompost with higher rates significantly influences the *liniuan* fiber strands and specific fertilizer management can yield a better number of *liniuan* fiber strands depending on the planting distance.

Production of *liniuan* fiber strands would be affected to an extent by planting distance and fertilizer management, given the variety of connected factors like soil nutrition or spacing's influence on growth patterning in plants. Each element could also have a different effect due to differences among nutrients that are taken up differently into roots at varying rates.

Soil conditions vary with planting distances, affecting the availability of nutrients and root distribution. Several studies have demonstrated that planting distance influences crop performance [45-46]. The purpose of changing the planting distance is to provide each individual with sufficient room for growth. This has a great impact on the efficiency of light use, plant density, and interplant competition for water and nutrients (and hence overall crop productivity) [47].

Proper planting distance enhances growth performance by minimizing nutrient competition, thus reaching optimal growth [48-49]. On the other hand, a shorter distance of planting may cause stunted growth and a decrease in yield, thus hindering the optimal growth performance and reducing production. The planting density intertwines with plant population per area and, hence, significantly influences the essential factors in the growth performance of the plant such as sunlight, nutrients, plants, and space [50]. Moreover,

nutrients in the soil are crucial for enhancing the growth and fiber development of RSP; thus, it relies largely on the approach of fertilizer management and distance of planting. Improper application of synthetic fertilizers may affect the pH in soils, causing them to be vulnerable to acidification, pests, diseases, and crusting of soils. These significant changes can result in a decrease in organic matter in the soil and a reduction in beneficial organisms. However, it will negatively affect growth performance, reduce yield, and potentially release greenhouse gas emissions, resulting in climate change [51,52]. Moreover, the management of combining planting distance and proper fertilization can significantly increase root expansion thus absorbing more nutrients and may produce more fiber yield.

According to Omotoso and Akirinde in 2013 [53], pineapple growth and yield performance increased due to the proper use of fertilizers. Fiber production, planting distance, and fertilizer management may be related because they affect the distribution of nutrients in the soil. Similarly, researchers proved that fertilization influenced high-quality fibers in plants. The fiber properties suggested that fertilization was an essential attribute of fiber growth. Moreover, the notable interaction may have resulted from the interplay between the factors affecting nutrients in the soil, plant growth, and fiber production, which were influenced by both planting interval and fertilizer application strategies.

3.6 Number of bastos fibers

Results showed that a significant interaction between planting distance and fertilizer management was absent in the number of *bastos* fibers produced by RSP (Table 1). Individually, the fertilizer management factor significantly affected the number of *bastos* fiber strands, with the highest mean from plants that received the 56-56-56 ASU Recommendation (33 pcs), followed by those with the 55-40-50 STK Recommendation and application of 40 tons and 20 tons of vermicompost per hectare (32 pcs). The least number (31 pcs) of *bastos* fiber strands was observed in the control treatment, where no fertilizer was applied. The different planting distances also had no significant effect on this parameter across all the fertilizer management treatments, with the same mean value of 32 pieces recorded (Figure 2f).

Certain types of pineapples, particularly the Red Spanish variety, possess a natural ability to adapt to various planting distances. The pineapple plant employs a unique photosynthetic process known as Crassulacean Acid Metabolism (CAM). This adaptation is particularly beneficial because it enables the plant to efficiently preserve moisture. Pineapples exhibit the capacity to thrive in diverse soil types provided there is proper drainage and aeration. Different pineapple varieties possess inherent strengths in terms of resistance and adaptability to varied environments; however, this broad adaptability might lead to a decline in quality [54]. Their response to different spacing suggests that within this range, the plant adjusts its growth rate and fiber production instead of reacting distinctly to varied space patterns.

Pineapples excel at efficiently utilizing resources such as nutrients, water, and light. In this scenario, the plants might have equalized spacing differences by optimizing resource utilization, resulting in similar fiber quantities across the tested distances. The utilization of vermicompost, rich in organic matter and beneficial microorganisms, influenced *the production of bastos fiber* by enhancing soil structure, increasing water retentionn, and improving the delivery of minerals to the plants. This implies that employing specific nutrient ratios from recommended fertilizers (56-56-56 and 55-40-50) might have precisely met the pineapple's nutritional requirements during fiber development.

The interaction effect showed that the ASU fertilizer recommendation (56-56-56) exhibited the largest number of bastos fiber strands counted (33) regardless of the planting distance, whereas the control showed the least number of bastos fiber strands counted (31). This highlights that balanced fertilizer produces more fiber strands. Further, it's notable that wider planting distance (80 × 50 × 30 cm) produced significantly more fibers as the pineapple plants had more room and less competition [55]

3.7 Weight if liniuan fibers

The interaction of planting distance and fertilizer management did not greatly affect the weight of *liniuan* fiber strands. The data in Table 1 also showed that the main effects of both factors did not influence the weight of *liniuan* fiber strands, where the mean weight ranged from 0.23 g to 0.25 g at 80 x 50 x 30 cm planting distance, 0.23 g to 0.26 g at 60 x 30 cm planting distance, and 0.22 g to 0.26 g at 30 x 30 cm planting distance.

Although the mean weight differences between the treatments were minimal, there were noticeable variations within individual treatments and specific spacing intervals within certain planting distances. For instance, the mean weights of plants subjected to the STK Recommendation and Vermicompost (20 t/ha) treatments were higher than those at other planting distances.

The study showed that RSP responded differently to different fertilizers. At a certain distance, the nutrient ratio or specific components of STK Recommendation or Vermicompost (20 t/ha) were more aligned with the plants' nutritional needs, which resulted in slightly lighter fiber weights than for other treatments. Thus, despite some of the treatments not statistically differing in mean weights, these cellular weights from plants grown at the same planting distance are indicative of the dynamics of the soil and nutrients, the environment, and the responses of the plants. These significant differences in the weight of fiber per treatment with distance indicate the sensitivity of pineapple growth to various management practices and the environmental effects generated through management practices. These differences in the fiber weight of the treatments were significantly lower relative to environmental variations such as fertilization or spacing [56]. However, vermicomposting in organic amendments promotes soil fertility and structure, and thus performs better than spacing [57].

Minimal differences in the weight of the fibers from all treatments were observed. According to studies and analyses, these differences depend more on the weight and length of the leaves than on external factors such as fertilization and spacing [44]. On the other hand, vermicomposting as organic amendments outperforms spacing, as it improves fertility as well as the structure of soil [57]. *Liniuan* fiber weight had no significant effect because it had less effect on the distance of planting and fertilizer management. The impact of genetics, leaf morphology, and time of harvest are key contributing factors that need to be examined further to elucidate the effect on the fiber development of RSP [56,57].

3.8 Weight of bastos fibers

The results showed that there is no significant interaction between planting distance and fertilizer management in the weight of *bastos* fibers produced by RSP. The data presented in Table 1 also show that of these two factors, only fertilizer management had a significant effect on this parameter across all planting distance settings. The heaviest fiber strands were recorded in plants treated with the 55-40-50 STK Recommendation (0.32 g). Comparable to this value were those applied with vermicompost at rates of 20 tons (0.31 g) and 40 tons (0.30 g) per hectare, and the control (0.30 g). The lightest fiber strands were those with the 56-56-56 ASU Recommendation (0.28 g). The different planting distances also had no significant effect on this parameter across all the fertilizer management treatments, with the mean values ranging from 0.30 g at 60 x 30 cm and 30 x 30 cm planting distances to 0.31 g at 80 x 50 x 30 planting distance. When it comes to planting distance's impact on fiber weight, while it does play a role, its influence is notably weaker compared to the significant effects resulting from diverse fertilizer management practices. Factors such as nutrient distribution in the soil or root development might be influenced by planting distance, but these effects pale in comparison to the direct impact of fertilizer on available nutrients and plant growth.

Fertilizers have different nutrient compositions and proportions, which are essential for plant fiber growth and quality. For example, the ASU Recommendation (56-56-5) lacks specific element necessary for strong fiber formation, which can result in low weight in *bastos* fibers. On the other hand, the STK recommendation with heavy fibers showed a more balanced nutrient fertilization ratio (N, P, K), hence contributing to creating an ambiance for a strong formation of fiber. This fertilization enhances lignin deposition and secondary fiber cell walls [38]. Potassium (K) is among the most critical nutrients for metabolic function and strong fiber. This nutrient is involved in regulating stomatal opening and translocation of carbohydrates [58]. Compared an organic amendment of vermicompost (20–40 tons/ha) and STK (20 tons/ha), results were similar with improved fertility, mineralization, and root development affecting the water weight of fiber *bastos* [59]. Planting distance affected fiber weight to some degree, but the actual differences between treatments (planting distance) were not as pronounced as the differences occurring due to the different effects of the fertilizer. However, specific ratios have slight variations. Nutrient-specific formulations of macroelements (N, P, K) have been demonstrated to significantly influence the yield of fiber as well as its characteristics through regulation of photosynthesis, elongation, and wall strengthening of fiber cells and lignin biosynthesis [59-60].

Results revealed a significant interaction in the weight of bastos fiber strands, indicating that fiber weight varies depending on both fertilizer type and planting distance. Plants spaced at 80 × 50 × 30 cm and applied with 20 t/ha or 40 t/ha vermicompost, as well as those planted at closer spacing (30 × 30 cm) with STK fertilizer, produced the heaviest fibers (0.32–0.34 g). In contrast, the control treatment consistently resulted in lighter fibers (0.29 g), as shown in Figure 2g. These findings confirm that both organic (vermicompost) and inorganic (STK) fertilizers are effective in enhancing fiber weight, but their effectiveness depends on planting distance [61].

3.9 Length of liniuan fibers

The data in Table 1 showed that planting distance and fertilizer management did not influence the length of *liniuan* fiber strands. The interaction effect was also absent. The mean values ranged from 48.36 cm to 50.60 cm at an 80 x 50 x 30 cm planting distance, 49.18 cm to 50.27 cm at a 60 x 30 cm planting distance, and 46.91 cm to 51.89 cm at a 30 x 30 cm planting distance. Changes in planting distance and the nutrient composition provided by fertilizers might not significantly affect fiber length during this growth phase. These external factors seem to have a limited impact on the genetic mechanisms governing fiber elongation at this stage.

Environmental factors have played a significant role in fiber elongation, such as optimized and stable climate (e.g., temperature, humidity, and lighting) supported fiber elongation [56]. When these environmental variables remain optimal across treatments, they could overshadow the effects of planting distance or fertilizer management on fiber length. It is unlikely that substantial changes in the length of *liniuan* fiber strands occur within the observed growth period. Perhaps the most significant variations due to planting distance or fertilizer management occur at stages of development not captured in this study. In this specific case, the genetic stability or growth characteristics of tissue-cultured Red Spanish Pineapple seem to override any potential impact of planting distance and specific fertilizer management on fiber length. The fiber length of *liniuan* was not affected by planting distance and fertilizer management, and this was probably due to internal (gene) and external (environmental) factors. It has been reported in studies that genetically regulating cellulose and lignin in pineapple fibers is the main determinant of RSP fiber elongation and tensile strength [62].

3.10 Length of bastos fibers

The interaction of planting distance and fertilizer management did not greatly affect the weight of *bastos* fiber strands. The data in Table 1 also showed that these factors did not influence the length of *bastos* fiber strands, where the length ranged from 52.02 cm to 55.93 cm at an 80 x 50 x 30 cm planting distance, 53.80 cm to 54.64 cm at a 60 x 30 cm planting distance, and 52.06 cm to 56.04 cm at a 30 x 30 cm planting distance. Factors suggest that changes in the planting distances or fertilizer management did not have a large effect on the fiber length. Across different planting distances, the mean strand length remained relatively steady, ranging from 52.02 to 56.04 cm. The mean fiber strand length remained relatively consistent across different planting distances. Lengths ranged from 52.02 to 56.04 cm, suggesting that a standard fiber length prevails not only regardless of the fertilizer management strategy adopted but also irrespective of its planting distance. However, the study found no effect of the placement distance nor specific fertilizer management on bastos fiber strand length for tissue-cultured Red Spanish Pineapple. Hence, similar fiber lengths were found in all treatments and distances, both factors had little effect on *bastos* fibers.

The data exhibited similar fiber strands in *bastos* RSP but with minimal influence by a distance of planting and fertilizer management. Studies have shown that external factors (e.g., temperature and planting density) did not significantly influence fiber length in cotton. Similarly, the length of fiber also showed stable results regardless of agricultural practices applied [60]. Therefore, these factors such as planting distance and types of fertilizers did not make a direct contribution to influence *bastos* fiber length in RSP but may attributed to genetic traits such as high cellulose content and crystallinity.

Table 1. Growth and fiber yield performance of tissue-cultured Red Spanish Pineapple (RSP) as influenced by different fertilizer management planted at different planting distance.

Fertilizer Management	Planting Distance	Plant Height (cm) *	No. of Leaves *	Leaf Length (cm) *	Leaf Width (cm) *	No. of *Liniuan* Fiber Strands *	No. of Bastos Fiber Strands *	Weight of *Liniuan* Fiber Strands (g) ns	Weight of *Bastos* Fiber Strands (g) *	Length of *Liniuan* Fiber Strands (cm) ns	Length of *Bastos* Fiber Strands (cm) ns
T1 – Control (No Fertilizer)	80 × 50 × 30	94.78	97	68.24	2.34	29^{ab}	31^{b}	0.24	0.30^{a}	48.36	52.71
	60 × 30	97.94	96	70.52	2.30	28^{b}	31^{b}	0.23	0.30^{a}	49.18	53.80
	30 × 30	96.78	97	69.68	2.69	27^{b}	31^{b}	0.22	0.29^{a}	46.91	52.06
Mean		**96.50^{c}**	**97^{c}**	**69.48^{d}**	**2.44^{b}**	**28.00^{b}**	**31^{c}**	**0.23**	**0.30^{a}**	**48.15**	**52.86**
T2 – STK Rec. (55-40-50)	80 × 50 × 30	101.22	103	72.88	2.99	30^{a}	32^{b}	0.23	0.33^{a}	48.47	52.02
	60 × 30	103.56	104	74.56	2.88	29^{ab}	32^{b}	0.26	0.29^{a}	49.96	54.07
	30 × 30	100.00	103	72.00	2.55	30^{a}	33^{b}	0.26	0.34^{a}	51.89	56.04
Mean		**101.59^{a}**	**103^{ab}**	**73.15^{ab}**	**2.80^{a}**	**29.67^{a}**	**32^{b}**	**0.25**	**0.32^{a}**	**50.10**	**54.04**
T3 – ASU Rec. (56-56-56)	80 × 50 × 30	100.11	103	72.08	2.50	29^{ab}	33^{a}	0.24	0.29^{b}	50.35	53.47
	60 × 30	99.89	102	71.92	3.08	30^{a}	33^{a}	0.23	0.29^{b}	49.98	54.51
	30 × 30	101.56	102	73.12	2.43	28^{b}	33^{a}	0.22	0.24^{b}	49.89	53.71
Mean		**100.52^{ab}**	**102^{b}**	**72.37^{bc}**	**2.67^{ab}**	**29.00^{ab}**	**33^{a}**	**0.23**	**0.28^{b}**	**50.07**	**53.90**
T4 – Vermicompost (20 t/ha)	80 × 50 × 30	100.44	102	73.32	2.56	29^{ab}	32^{b}	0.25	0.31^{a}	49.93	55.93
	60 × 30	102.89	101	75.11	2.45	28^{b}	32^{b}	0.24	0.31^{a}	50.27	54.64
	30 × 30	101.56	103	74.14	2.10	31^{a}	31^{b}	0.26	0.32^{a}	50.89	54.11
Mean		**101.63^{a}**	**102^{b}**	**74.19^{a}**	**2.37^{b}**	**29.33^{a}**	**32^{b}**	**0.25**	**0.31^{a}**	**50.36**	**54.89**

Table 1. Growth and fiber yield performance of tissue-cultured Red Spanish Pineapple (RSP) as influenced by different fertilizer management planted at different planting distance. (Continue)

Fertilizer Management	Planting Distance	Plant Height (cm) *	No. of Leaves *	Leaf Length (cm) *	Leaf Width (cm) *	No. of *Liniuan* Fiber Strands *	No. of Bastos Fiber Strands *	Weight of *Liniuan* Fiber Strands (g) ns	Weight of *Bastos* Fiber Strands (g) *	Length of *Liniuan* Fiber Strands (cm) ns	Length of *Bastos* Fiber Strands (cm) ns
Mean		**101.63^{a}**	**102^{b}**	**74.19^{a}**	**2.37^{b}**	**29.33^{a}**	**32^{b}**	**0.25**	**0.31^{a}**	**50.36**	**54.89**
T5 – Vermicompost (40 t/ha)	80 × 50 × 30	97.00	105	69.84	2.24	31^{a}	32^{b}	0.23	0.32^{a}	50.60	54.51
	60 × 30	99.00	103	71.28	2.45	29^{ab}	32^{b}	0.24	0.29^{a}	49.65	54.31
	30 × 30	100.89	104	72.64	2.28	28^{b}	32^{b}	0.24	0.30^{a}	49.98	53.80
Mean		**98.96^{b}**	**104^{a}**	**71.25^{c}**	**2.38^{b}**	**29.33^{ab}**	**32^{b}**	**0.24**	**0.30^{a}**	**50.08**	**54.21**
Planting Distance	**80 × 50 × 30**	**98.71^{b}**	**102**	**71.67**	**2.53**	**29.6**	**32.0**	**0.24**	**0.31**	**49.95**	**53.73**
Mean	**60 × 30**	**100.85^{a}**	**101**	**72.68**	**2.63**	**28.8**	**32.0**	**0.24**	**0.30**	**49.81**	**54.67**
	30 × 30	**100.16^{a}**	**102**	**72.72**	**2.39**	**28.8**	**32.0**	**0.24**	**0.30**	**49.91**	**53.94**
Grand Mean		99.80	101.2	71.76	2.52	29.07	32.0	0.24	0.30	49.89	54.11
CV (Planting Distance)		*3.72%*	*3.83%*	*3.83%*	*10.84%*	*7.70%*	*5.36%*	*8.41%*	*5.68%*	*2.29%*	*4.75%*
CV (Fertilizer Management)		*2.33%*	*1.85%*	*1.85%*	*14.66%*	*4.27%*	*2.87%*	*7.88%*	*8.82%*	*4.82%*	*4.19%*
Interaction (A × B)		ns	ns	*	ns	ns	*	ns	*	ns	ns

CV (Coefficient of Variation) = values indicate variability across planting distances and fertilizer management; * - significant; ns - not significant; Mean values with different letter superscript indicate significant difference ($p<.05$) using Least Significant Difference (LSD) Test

Figure 1. Significant growth and fiber yield responses of tissue-cultured Red Spanish Pineapple to fertilizer management and planting distance: (a) Plant height, (b) Number of leaves, (c) Leaf length, (d) Leaf width, (e) Number of *liniuan* fiber strands, (f) Number of *bastos* fiber strands, and (g) Weight of *bastos* fiber strands. Differences in planting distances or cultural management had little effect on the length of the *bastos* fiber strands in the tissue-cultured Red Spanish Pineapple. The relative absence of significant effects from these

4. Conclusions

Results revealed that among the fertilizers, vermicompost at 20 t/ha and the STK Recommendation (55-40-50) had consistently exhibited positive effects and promoted optimal plant height, leaf length and leaf width, *liniuan* and *bastos* fiber weight. On the other hand, vermicompost application at 40 t/ha had resulted in higher leaves number and *liniuan* fiber. Additionally, the incorporation of vermicompost at specific rates enhanced leaf growth and fiber strand production. Wider leaves were associated with the broadest STK recommendation (55-40-50) and more *bastos fibers* with the ASU recommendation (56-56-56). Wider planting distance influenced the number of *bastos* fiber strands; however, planting distance did not significantly influence most growth parameters. Interaction between fertilizer management and spacing positively affected the number of *liniuan* fibers in most treatments, suggesting site-specific agronomic practices. The study highlights the importance of site-specific fertilization approaches, including the application of vermicompost, for the improved growth and performance of tissue-cultured Red Spanish Pineapple. The outcome of the study is a very critical contribution to the pina fiber industry, as it is aimed at helping preserve the tradition and the livelihoods associated with the Red Spanish Pineapple, as well as fulfill the domestic and international demand for quality fiber.

5. Acknowledgements

The authors would like to acknowledge Aklan State University (ASU) faculty and staff headed by SUC President III, Dr. Jeffrey A. Clarin, Dr. Eva R. Orlina, Dean of the College of Agriculture, Forestry and Environmental Sciences (CAFES), and the Research and Development Services of ASU headed by Dr. Melba L. Ragaas for their guidance and support.

Author Contributions: Vedasto E. conceptualized, crafted the proposal and analyzed the data. Alegrai N.A. conducted and gathered the data in the field. For research articles with several authors, a short paragraph specifying their individual contributions must be provided. All authors have read and agreed to the published version of the manuscript. All authors have read and agreed to the published version of the manuscript

Funding: This research received no external funding.

Conflicts of Interest: The authors declare no conflict of interest=

References

[1] Fiber Development Authority (FIDA). *Statistical Bulletin for the Fiber Industry 2008 Edition*; DA-FIDA: Quezon City, Philippines, **2010**.

[2] Lim, R. Aklan's Piña weaving joins UNESCO's list of intangible cultural heritage of humanity. GMA News, **2023**. https://www.gmanetwork.com/lifestyle/news/107843/aklans-pina-weaving-joins-unescos-list-of-intangible-cultural-heritage-of-humanity/story (accessed 2025-09-01).

[3] De La Cruz, A. B. Exploring challenges of Piña growers in the Province of Aklan. *Int. J. Entrep. Sustain. Stud.* **2021**, *1*(1), 33–43. https://doi.org/10.31098/ijeass.v1i1.555

[4] Chaudhuri, P. S.; Paul, T. K.; Dey, A.; Datta, M.; Dey, S. K. Effects of rubber leaf litter vermicompost on earthworm population and yield of pinea.pple (*Ananas comosus*) in West Tripura, India. *Int. J. Recycl. Org. Waste Agricult.* **2016**, *5*(2), 93–103.

[5] Coelho, R. I.; Lopes, J. C.; Carvalho, A. J. C. D.; Amaral, J. A. T. D.; Matta, F. D. P. Nutritional status and growth caracteristics of pineapple in dystrophic yellow latosol 'Jupi' cultivated in fucntion of NPK fertilization. *Cienc. Agrotecnol.* **2007**, *31*(6), 1696–1971.

[6] Hui, W. A. N. G. Effect of planting density and fertilizer application on fiber yield of ramie (*Boehmeria nivea*). *J. Integr. Agric.* **2012**, *11*(7), 1199–1206.

[7] Deng, G.; Du, G.; Yang, Y.; Bao, Y.; Liu, F. Planting density and fertilization evidently influence the fiber yield of hemp (*Cannabis sativa* L.). *Agronomy* **2019**, *9*(7), 368.

[8] Gestupa, E. J. The Red Spanish Pineapple. Business Diary Philippines. **2020**. https://outbuilds4.rssing.com/chan-3768917/all_p78.html (accessed 2025-09-01).

[9] Malézieux, E.; Bartholomew, D. P. Plant nutrition. In *The Pineapple: Botany, Production and Uses*; Cabi Publishing: Wallingford, UK, **2003**; pp 143–165.
[10] Souza, L. F. S.; Reinhardt, D. H. Pineapple. In *Fertilizing for High Yield and Quality Tropical Fruits of Brazil*; IPI Bulletin 18; International Potash Institute: Zug, Switzerland, **2007**; pp 179–201.
[11] Omotoso, S. O.; Akinrinde, E. A. Effect of nitrogen fertilizer on some growth, yield and fruit quality parameters in pineapple (*Ananas comosus* L. Merr.) plant at Ado-Ekiti Southwestern, Nigeria. *Int. Res. J. Agric. Sci. Soil Sci.* **2013**, *3*(1), 11–16.
[12] Cunha, J. M.; Freitas, M. S. M.; Carvalho, A. J. C. D.; Caetano, L. C. S.; Pinto, L. P.; Peçanha, D. A.; dos Santos, P. C. Foliar content and visual symptoms of nutritional deficiency in pineapple 'Vitória'. *J. Plant Nutr.* **2021**, *44*(5), 660–672.
[13] Choo, L. N. L. K.; Ahmed, O. H.; Razak, N. A.; Sekot, S. Improving nitrogen availability and *Ananas comosus* L. Merr var. Moris productivity in a tropical peat soil using clinoptilolite zeolite. *Agronomy* **2022**, *12*(11), 2750.
[14] Gestupa, E. J. The Red Spanish Pineapple. Business Diary Philippines. **2020**. https://outbuilds4.rssing.com/chan-3768917/all_p78.html (accessed 2025-09-01).
[15] Arcalas, J. E. China fuels Philippines pineapple exports to record $787 million earnings in 2024. Philstar Global, **2025**, March 18. https://www.philstar.com/business/2025/03/18/2429107/china-fuels-philippines-pineapple-exports-record-787-million-earnings-2024 (accessed 2025-09-01).
[16] Wahid, A. Pineapple fiber: A sustainable option for your future fashion. ecomaniac.org, **2022**. https://ecomaniac.org/pineapple-fiber/ (accessed 2025-09-01).
[17] Señeris, G. T.; Vedasto, E. P.; Ragaas, M. L. Prevalence of insect pests, beneficial organisms and diseases of abaca (*Musa textilis* Nee) in two municipalities of Aklan, Philippines. *Univ. J. Agric. Res.* **2022**, *10*(3), 275–287. https://doi.org/10.13189/ujar.2022.100309
[18] Señeris, G. T.; Vedasto, E. P.; Teodosio, M. M.; Ragaas, M. L.; Teodosio, L. J. Morphological characteristics of abaca (*Musa textilis* Nee') cultivars grown in two municipalities of Aklan, Philippines. *Univ. J. Agric. Res.* **2022**, *10*(2), 175–183. https://doi.org/10.13189/ujar.2022.100209
[19] Muhammad, N.; Maina, B. M.; Aljameel, K. M.; Maigandi, S. A.; Buhari, S. Nutrient intake and digestibility of Uda rams fed graded levels of *Parkia biglobosa* (African locust bean) yellow fruit pulp. *Int. J. Livest. Res.* **2016**, *6*(5), 33–42. https://doi.org/10.5455/ijlr.20160427090936
[20] Rekha, G. S.; Kaleena, P. K.; Elumalai, D.; et al. Effects of vermicompost and plant growth enhancers on the exo-morphological features of *Capsicum annum* (Linn.) Hepper. *Int. J. Recycl. Org. Waste Agricult.* **2018**, *7*(1), 83–88. https://doi.org/10.1007/s40093-017-0191-5
[21] Mahmud, M.; Abdullah, R.; Yaacob, J. S. Effect of vermicompost on growth, plant nutrient uptake and bioactivity of *ex vitro* pineapple (*Ananas comosus* var. MD2). *Agronomy* **2020**, *10*(9), 1333. https://doi.org/10.3390/agronomy10091333
[22] Chamani, E.; Joyce, D. C.; Reihanytabar, A. Vermicompost effects on the growth and flowering of *Petunia hybrida* Dream Neon Rose. *Am.-Eurasian J. Agric. Environ. Sci.* **2008**, *3*(3), 506–512.
[23] Chen, Z. K.; Tao, X. P.; Khan, A.; Tan, D. K. Y.; Luo, H. H. Biomass accumulation, photosynthetic traits, and root development of cotton as affected by irrigation and nitrogen-fertilization. *Front. Plant Sci.* **2018**, *9*, 173. https://doi.org/10.3389/fpls.2018.00173
[24] Chen, Y. H.; Liu, L.; Guo, Q. S.; Zhu, Z. B.; Zhang, L. X. Effects of different water management options and fertilizer supply on photosynthesis, fluorescence parameters and water use efficiency of *Prunella vulgaris* seedlings. *Biol. Res.* **2016**, *49* (1), 12. https://doi.org/10.1186/s40659-016-0069-4
[25] Studer, C.; Hu, Y. C.; Schmidhalter, U. Evaluation of the differential osmotic adjustments between roots and leaves of maize seedlings with single or combined NPK-nutrient supply. *Funct. Plant Biol.* **2007**, *34*(3), 228–236. https://doi.org/10.1071/FP06294
[26] Hochmuth, G.; Hanlon, E.; Overman, A. *Fertilizer Experimentation, Data Analyses, and Interpretation for Developing Fertilization Recommendations — Examples with Vegetable Crop Research: SL345 SS548*; EDIS, **2011**. https://doi.org/10.32473/edis-ss548-2011

[27] Neri, J. C.; Meléndez Mori, J. B.; Vilca Valqui, N. C.; Huaman Huaman, E.; Collazos Silva, R.; Oliva, M. Effect of planting density on the agronomic performance and fruit quality of three pineapple cultivars (*Ananas comosus* L. Merr.). *Int. J. Agron.* **2021**, *2021*, 5559564. https://doi.org/10.1155/2021/5559564

[28] Hung, N.; Thoa, D.; Huong, N. Effect of planting density on growth, development and yield of irrigated pineapple in Nghe An Province. *Acta Hortic.* **2011**, *902*, 307–311. https://doi.org/10.17660/ActaHortic.2011.902.34

[29] Malézieux, E.; Cote, F.; Bartholomew, D. Crop environment, plant growth and physiology. In *The Pineapple: Botany, Production and Uses*; Bartholomew, D. P., Paull, R. E., Rohrbach, K. G., Eds.; CABI Publishing, **2003**; pp 69–107. https://doi.org/10.1079/9780851995038.0069

[30] Lopattananon, N.; Panawarangkul, K.; Sahakaro, K.; Ellis, B. Performance of pineapple leaf fiber–natural rubber composites: The effect of fiber surface treatments. *J. Appl. Polym. Sci.* **2006**, *102*(2), 1974–1984. https://doi.org/10.1002/app.24584

[31] Balan, H. R.; Escol, J. G.; Baranggan, J. L.; Cubao, C. R. D. Growth performance of economically-important plants using vermicompost derived from Kibalisa Eco-waste Center. *Int. J. Sci. Res. Publ.* **2019**, *9*(3), 709–714. https://doi.org/10.29322/IJSRP.9.03.2019.p8799

[32] Joshi, R.; Vig, A. P. Effect of vermicompost on growth, yield, and quality of tomato (*Lycopersicum esculentum* L.). *Afr. J. Basic Appl. Sci.* **2010**, *2*(3–4), 117–123.

[33] Mahmud, M.; Abdullah, R.; Yaacob, J. S. Effect of vermicompost amendment on nutritional status of sandy loam soil, growth performance, and yield of pineapple (*Ananas comosus* var. MD2) under field conditions. *Agronomy* **2018**, *8*(9), 183. https://doi.org/10.3390/agronomy8090183

[34] Pegoraro, R. F.; Souza, B. A. M. D.; Maia, V. M.; Silva, D. F. D.; Medeiros, A. C.; Sampaio, R. A. Macronutrient uptake, accumulation, and export by the irrigated 'Vitória' pineapple plant. *Rev. Bras. Cienc. Solo* **2014**, *38*(3), 896–904. https://doi.org/10.1590/S0100-06832014000300021

[35] Crisóstomo, L. A. *Fertilizing for High Yield and Quality: Tropical Fruits of Brazil*; International Potash Institute, **2007**.

[36] Chaudhuri, P. S.; Paul, T. K.; Dey, A.; et al. Effects of rubber leaf litter vermicompost on earthworm population and yield of pineapple (*Ananas comosus*) in West Tripura, India. *Int. J. Recycl. Org. Waste Agricult.* **2016**, *5*(2), 93–103. https://doi.org/10.1007/s40093-016-0120-z

[37] Ludibeth, S. M.; Marina, I. E.; Vicenta, E. M. Vermicomposting of sewage sludge: Earthworm population and agronomic advantages. *Compost Sci. Util.* **2012**, *20*(1), 11–17. https://doi.org/10.1080/1065657X.2012.10737016

[38] Majlessi, M.; Eslami, A.; Najafi Saleh, H.; et al. Vermicomposting of food waste: Assessing the stability and maturity. *J. Environ. Health Sci. Eng.* **2012**, *9*(1), 25. https://doi.org/10.1186/1735-2746-9-25

[39] Song, X.; Liu, M.; Wu, D.; Griffiths, B. S.; Jiao, J.; Li, H.; Hu, F. Interaction matters: Synergy between vermicompost and PGPR agents improves soil quality, crop quality, and crop yield in the field. *Appl. Soil Ecol.* **2015**, *89*, 25–34. https://doi.org/10.1016/j.apsoil.2015.01.005

[40] Kashem, M. A.; Sarker, A.; Hossain, I.; Islam, M. S. Comparison of the effect of vermicompost and inorganic fertilizers on vegetative growth and fruit production of tomato (*Solanum lycopersicum* L.). *Open J. Soil Sci.* **2015**, *5*(2), 53–58. https://doi.org/10.4236/ojss.2015.52006

[41] Kumar, M.; Raghav, M.; Verma, A.; Bhatt, L.; Singh, R.; Bisht, Y. S.; Rawat, A. S. Influence of nitrogen and plant spacing on edible leaf and seed yield of vegetable amaranth (*Amaranthus* spp. L.). *J. Plant Nutr.* **2025**, *48*(1), 1–12.

[42] Chen, Y.; Hu, S.; Guo, Z.; Cui, T.; Zhang, L.; Lu, C.; et al. Effect of balanced nutrient fertilizer: A case study in Pinggu District, Beijing, China. *Sci. Total Environ.* **2021**, *754*, 142069. https://doi.org/10.1016/j.scitotenv.2020.142069

[43] Manna, M. C.; Swarup, A.; Wanjari, R. H.; Ravankar, H. N.; Mishra, B.; Saha, M. N.; et al. Long-term effect of fertilizer and manure application on soil organic carbon storage, soil quality and yield sustainability under sub-humid and semi-arid tropical India. *Field Crops Res.* **2005**, *93*(2–3), 264–280. https://doi.org/10.1016/j.fcr.2004.10.006

[44] Kaamoga, H. Effect of plant spacing and nutrient source on growth and yield of pineapple (*Ananas comosus*) in Wakiso District. Doctoral dissertation, Makerere University, **2018**.

[45] Anwari, G.; Moussa, A. A.; Wahidi, A. B.; Mandozai, A.; Nasar, J.; Abd El-Rahim, M. G. M. Effects of planting distance on yield and agro-morphological characteristics of local rice (Bara variety) in northeast Afghanistan. *Curr. Agric. Res. J.* **2019**, *7*(3), 350. https://doi.org/10.12944/CARJ.7.3.11

[46] Tadeo, S. B. Growth and yield performance of NSIC Rc. 160 (Tubigan 14) as affected by planting distance under Abra condition. *IAMURE Int. J. Ecol. Conserv.* **2022**, *38*(1), 1–11.

[47] Rahmawati, R. Pengaruh beberapa jarak tanam terhadap pertumbuhan dan hasil tanaman kacang tanam varietas kelinci (*Arachis hypogeae* L.). *Menara Ilmu* **2017**, *1*(1), 9–16.

[48] Indrayanti, A. L. Pengaruh jarak tanam dan jumlah benih terhadap pertumbuhan vegetatif jagung muda. *J. Media Sains* **2010**, *2*(2), 153–196.

[49] Wulandari, R.; Suminarti, N. E.; Sebayang, H. T. Pengaruh jarak tanam dan frekuensi penyiangan gulma pada pertumbuhan dan hasil tanaman bawang merah (*Allium ascalonicum*). *J. Prod. Tanaman* **2016**, *4*(7), 547–553. https://doi.org/10.21176/protan.v4i7.327

[50] Murti, A. C.; Al Machfudz, W. D. P.; Prihatiningrum, A. E.; Arifin, S. Effect of planting distance and bulb size on growth and production of shallots (*Allium ascalonicum* L.). *IOP Conf. Ser. Earth Environ. Sci.* **2022**, *1104*(1), 012002. https://doi.org/10.1088/1755-1315/1104/1/012002

[51] Pahalvi, H. N.; Rafiya, L.; Rashid, S.; Nisar, B.; Kamili, A. N. Chemical fertilizers and their impact on soil health. In *Microbiota and Biofertilizers*; Dar, G. H., Bhat, R. A., Mehmood, M. A., Hakeem, K. R., Eds.; Springer: Cham, Switzerland, **2021**, *2*, 1–20. https://doi.org/10.1007/978-3-030-74566-7_1

[52] Ozlu, E.; Kumar, S. Response of soil organic carbon, pH, electrical conductivity, and water stable aggregates to long-term annual manure and inorganic fertilizer. *Soil Sci. Soc. Am. J.* **2018**, *82*(5), 1243–1251. https://doi.org/10.2136/sssaj2018.02.0074

[53] Omotoso, S. O.; Akinrinde, E. A. Effect of nitrogen fertilizer on some growth, yield, and fruit quality parameters in pineapple (*Ananas comosus* L. Merr.) plant at Ado-Ekiti Southwestern, Nigeria. *Int. Res. J. Agric. Sci. Soil Sci.* **2013**, *3*(1), 11–16. https://doi.org/10.14303/irjas.2013.010

[54] Li, D.; Jing, M.; Dai, X.; Chen, Z.; Ma, C.; Chen, J. Current status of pineapple breeding, industrial development, and genetics in China. *Euphytica* **2022**, *218*(6), 85. https://doi.org/10.1007/s10681-022-03016-3

[55] Valentina, L.; Seephuak, P.; Booncharoen, K.; Chotikamas, T.; Vanichpakorn, P.; Sripaoraya, S. Effects of plant materials and plant densities on pineapple (*Ananas comosus* var. srivijaya) growth under intercropping with young oil palm (*Elaeis guineensis* Jacq.) in lowland área. *Int. J. Agric. Technol.* **2024**, *20*(4), 1639–1654.

[56] Tulin, E. P. B.; Bande, M. M. Agroecological assessment of different cultural practices of pineapple, *Ananas comosus* (Linn) Mer. (Var. Red Spanish) for sustainable fiber production in geo-textile industry in Balete, Aklan. *Int. J. Environ. Rural Dev.* **2018**, *9*(1), 18–24.

[57] Owureku-Asare, M.; Agyei-Amponsah, J.; Agbemavor, S. W. K.; Apatey, J.; Sarfo, A. K.; Okyere, A. A.; Dodobi, M. T. Effect of organic fertilizers on physical and chemical quality of sugar loaf pineapple (*Ananas comosus* L.) grown in two ecological sites in Ghana. *Afr. J. Food Agric. Nutr. Dev.* **2015**, *15*(2), 9982–9995. https://doi.org/10.18697/ajfand.69.15045

[58] Ahlersmeyer, A. J. Methods for improving potassium fertilizer recommendations for corn in South Dakota. Doctoral dissertation, South Dakota State University, **2023**.

[59] Fang, X.; Yang, Y.; Zhao, Z.; Zhou, Y.; Liao, Y.; Guan, Z.; Zhao, S. Optimum nitrogen, phosphorous, and potassium fertilizer application increased chrysanthemum growth and quality by reinforcing the soil microbial community and nutrient cycling function. *Plants* **2023**, *12*(23), 4062. https://doi.org/10.3390/plants12234062

[60] Ibrahim, I. A.; Yehia, W. M.; Saleh, F. H.; Lamlom, S. F.; Ghareeb, R. Y.; El-Banna, A. A.; Abdelsalam, N. R. Impact of plant spacing and nitrogen rates on growth characteristics and yield attributes of Egyptian cotton (*Gossypium barbadense* L.). *Front. Plant Sci.* **2022**, *13*, 916734. https://doi.org/10.3389/fpls.2022.916734

[61] Islam, M. A.; Ferdous, G.; Akter, A.; Hossain, M. M.; Nandwani, D. Effect of organic, inorganic fertilizers and plant spacing on the growth and yield of cabbage. *Agriculture* **2017**, *7*(4), 31.

[62] Chaves, D. M.; Araújo, J. C.; Gomes, C. V.; Gonçalves, S. P.; Fangueiro, R.; Ferreira, D. P. Extraction, characterization and properties evaluation of pineapple leaf fibers from Azores pineapple. *Heliyon* **2024**, *10*(4), e26698. https://doi.org/10.1016/j.heliyon.2024.e26698

[45] Anwari, G.; Moussa, A. A.; Wahidi, A. B.; Mandozai, A.; Nasar, J.; Abd El-Rahim, M. G. M. Effects of planting distance on yield and agro-morphological characteristics of local rice (Bara variety) in northeast Afghanistan. *Curr. Agric. Res. J.* **2019**, *7*(3), 350. https://doi.org/10.12944/CARJ.7.3.11

[46] Tadeo, S. B. Growth and yield performance of NSIC Rc. 160 (Tubigan 14) as affected by planting distance under Abra condition. *IAMURE Int. J. Ecol. Conserv.* **2022**, *38*(1), 1–11.

[47] Rahmawati, R. Pengaruh beberapa jarak tanam terhadap pertumbuhan dan hasil tanaman kacang tanam varietas kelinci (*Arachis hypogeae* L.). *Menara Ilmu* **2017**, *1*(1), 9–16.

[48] Indrayanti, A. L. Pengaruh jarak tanam dan jumlah benih terhadap pertumbuhan vegetatif jagung muda. *J. Media Sains* **2010**, *2*(2), 153–196.

[49] Wulandari, R.; Suminarti, N. E.; Sebayang, H. T. Pengaruh jarak tanam dan frekuensi penyiangan gulma pada pertumbuhan dan hasil tanaman bawang merah (*Allium ascalonicum*). *J. Prod. Tanaman* **2016**, *4*(7), 547–553. https://doi.org/10.21176/protan.v4i7.327

[50] Murti, A. C.; Al Machfudz, W. D. P.; Prihatiningrum, A. E.; Arifin, S. Effect of planting distance and bulb size on growth and production of shallots (*Allium ascalonicum* L.). *IOP Conf. Ser. Earth Environ. Sci.* **2022**, *1104*(1), 012002. https://doi.org/10.1088/1755-1315/1104/1/012002

[51] Pahalvi, H. N.; Rafiya, L.; Rashid, S.; Nisar, B.; Kamili, A. N. Chemical fertilizers and their impact on soil health. In *Microbiota and Biofertilizers*; Dar, G. H., Bhat, R. A., Mehmood, M. A., Hakeem, K. R., Eds.; Springer: Cham, Switzerland, **2021**, *2*, 1–20. https://doi.org/10.1007/978-3-030-74566-7_1

[52] Ozlu, E.; Kumar, S. Response of soil organic carbon, pH, electrical conductivity, and water stable aggregates to long-term annual manure and inorganic fertilizer. *Soil Sci. Soc. Am. J.* **2018**, *82*(5), 1243–1251. https://doi.org/10.2136/sssaj2018.02.0074

[53] Omotoso, S. O.; Akinrinde, E. A. Effect of nitrogen fertilizer on some growth, yield, and fruit quality parameters in pineapple (*Ananas comosus* L. Merr.) plant at Ado-Ekiti Southwestern, Nigeria. *Int. Res. J. Agric. Sci. Soil Sci.* **2013**, *3*(1), 11–16. https://doi.org/10.14303/irjas.2013.010

[54] Li, D.; Jing, M.; Dai, X.; Chen, Z.; Ma, C.; Chen, J. Current status of pineapple breeding, industrial development, and genetics in China. *Euphytica* **2022**, *218*(6), 85. https://doi.org/10.1007/s10681-022-03016-3

[55] Valentina, L.; Seephuak, P.; Booncharoen, K.; Chotikamas, T.; Vanichpakorn, P.; Sripaoraya, S. Effects of plant materials and plant densities on pineapple (*Ananas comosus* var. srivijaya) growth under intercropping with young oil palm (*Elaeis guineensis* Jacq.) in lowland área. *Int. J. Agric. Technol.* **2024**, *20*(4), 1639–1654.

[56] Tulin, E. P. B.; Bande, M. M. Agroecological assessment of different cultural practices of pineapple, *Ananas comosus* (Linn) Mer. (Var. Red Spanish) for sustainable fiber production in geo-textile industry in Balete, Aklan. *Int. J. Environ. Rural Dev.* **2018**, *9*(1), 18–24.

[57] Owureku-Asare, M.; Agyei-Amponsah, J.; Agbemavor, S. W. K.; Apatey, J.; Sarfo, A. K.; Okyere, A. A.; Dodobi, M. T. Effect of organic fertilizers on physical and chemical quality of sugar loaf pineapple (*Ananas comosus* L.) grown in two ecological sites in Ghana. *Afr. J. Food Agric. Nutr. Dev.* **2015**, *15*(2), 9982–9995. https://doi.org/10.18697/ajfand.69.15045

[58] Ahlersmeyer, A. J. Methods for improving potassium fertilizer recommendations for corn in South Dakota. Doctoral dissertation, South Dakota State University, **2023**.

[59] Fang, X.; Yang, Y.; Zhao, Z.; Zhou, Y.; Liao, Y.; Guan, Z.; Zhao, S. Optimum nitrogen, phosphorous, and potassium fertilizer application increased chrysanthemum growth and quality by reinforcing the soil microbial community and nutrient cycling function. *Plants* **2023**, *12*(23), 4062. https://doi.org/10.3390/plants12234062

[60] Ibrahim, I. A.; Yehia, W. M.; Saleh, F. H.; Lamlom, S. F.; Ghareeb, R. Y.; El-Banna, A. A.; Abdelsalam, N. R. Impact of plant spacing and nitrogen rates on growth characteristics and yield attributes of Egyptian cotton (*Gossypium barbadense* L.). *Front. Plant Sci.* **2022**, *13*, 916734. https://doi.org/10.3389/fpls.2022.916734

[61] Islam, M. A.; Ferdous, G.; Akter, A.; Hossain, M. M.; Nandwani, D. Effect of organic, inorganic fertilizers and plant spacing on the growth and yield of cabbage. *Agriculture* **2017**, *7*(4), 31.

[62] Chaves, D. M.; Araújo, J. C.; Gomes, C. V.; Gonçalves, S. P.; Fangueiro, R.; Ferreira, D. P. Extraction, characterization and properties evaluation of pineapple leaf fibers from Azores pineapple. *Heliyon* **2024**, *10*(4), e26698. https://doi.org/10.1016/j.heliyon.2024.e26698

ASEAN
Journal of Scientific and Technological Reports
Online ISSN:2773-8752

Research article

Integration of Innovative Waste Management Systems for Sustainable Development in Khun Thale: The SDG Station Model

Somprat Wuttijan[1], Nara Phongphanich[2], and Pongsak Noparat[3*]

[1] Faculty of Humanities and Social Sciences, Suratthani Rajabhat University, Surat Thani, 84100, Thailand
[2] Faculty of Humanities and Social Sciences, Suratthani Rajabhat University, Surat Thani, 84100, Thailand
[3] Faculty of Science and Technology, Suratthani Rajabhat University, Thailand, Surat Thani, 84100, Thailand
* Correspondence: pongsak@sru.ac.th

Citation:
Wuttijan, S.; Phongphanich, N.; Noparat, P. Integration of innovative waste management systems for sustainable development in Khun Thale: The SDG station model. *ASEAN J. Sci. Tech. Report.* **2025**, *28*(6), e259527. https://doi.org/10.55164/ajstr.v28i6.259527.

Article history:
Received: May 27, 2025
Revised: September 29, 2025
Accepted: October 1, 2025
Available online: October 20, 2025

Abstract: Waste management in Khun Thale Subdistrict faces significant challenges, with inefficient sorting systems leading to missed resource recovery opportunities. This study employed Human-Centered Design methodology to develop and implement innovative waste management solutions through the "SDG Station" project. Waste composition analysis revealed that paper waste (38%), plastic (30%), and organic waste (17%) were the primary components in general areas, whereas flea market waste consisted predominantly of organic matter (73%). The project implemented multiple interconnected systems: a recycling incentive program ("Trash Lucky") that collected 3,434 kg of recyclable materials across three phases; an organic waste processing system that produced 2,052 cubic meters of biogas from 42,634 kg of organic waste; and vermicomposting that generated 485 kg of soil conditioner from 56 kg of waste. Innovative applications included biogas pipeline delivery to food vendors, which reduced cooking costs and created economic benefits for students through mandated food price reductions. Integrating agrivoltaic farming systems enhanced resource utilization through the "Farm to Table" concept. Overall, the project achieved significant greenhouse gas reductions, totaling 23,976.11 kg CO_2eq, and demonstrated alignment with 11 of the Sustainable Development Goals. The implemented waste bank model offers valuable policy frameworks for scaling sustainable waste management practices throughout Thailand.

Keywords: Waste management; recycling; biogas production; vermicomposting; greenhouse gas reduction

1. Introduction

Waste management presents significant challenges across Thailand, with inefficient sorting and disposal systems posing a threat to environmental sustainability and public health. The United Nations Development Programme's Low Carbon Cities project identified that approximately 60% of municipal waste consists of organic materials, while 25-30% comprises potentially recyclable inorganic materials, including plastics, glass, and paper [1]. Despite this recovery potential, recycling rates remain alarmingly low, with most waste being improperly managed [2]. Surat Thani Province was designated as one of fifteen pilot provinces in Thailand pursuing the Sustainable Development Goals (SDGs) outlined by the National Economic and Social Development Council. As an SDG Integrator, the UNDP selected Surat Thani Province to coordinate joint

efforts toward national sustainability targets [3]. Attaining the Sustainable Development Goals (SDGs) by 2030 represents a global challenge that nations worldwide are endeavoring to meet, and effective waste management serves as a crucial component in achieving these goals [4]. Through a comprehensive potential assessment, Khun Thale Subdistrict emerged as an ideal intervention site based on its demonstrated commitment to efficient waste management, clear Key Performance Indicators for sustainable development, and willingness to provide space, financial support, and personnel necessary for establishing a community waste bank, designated as an "SDG Station" [5]. The assessment of the Khun Thale Subdistrict revealed critical challenges in existing waste management practices. Monthly waste generation ranged from 15 to 70 tons [1], fluctuating with academic semester schedules and campus activities. All collected waste was transported to a landfill disposal site managed by SRT Power Green Co., Ltd., located within Tha Rong Chang Subdistrict, representing significant lost opportunities for resource recovery and environmental impact reduction [6]. Key issues identified included inadequate separation infrastructure, insufficient incentives for recycling participation, and untapped potential for organic waste utilization.

The "Innovative Solutions for Waste Bank Development" project was established through a strategic collaboration between UNDP and Khun Thale Subdistrict, with co-financing provided by multiple stakeholders, including Cargill Thailand, Government Savings Bank, and Thailand Policy Lab. Bright Management Consulting Co., Ltd. was a project consultant, bringing technical expertise to implementation efforts [7]. The initiative commenced in late 2023, with data collection and project development activities spanning from January 2024 through September 2025. This comprehensive initiative established three primary objectives: (1) creating a circular economy society within Khun Thale Subdistrict using human-centered design principles integrated with zero waste targets; (2) developing and testing a replicable waste bank model applicable to similar organizations and communities; and (3) formulating evidence-based policy options for provincial-level implementation [8]. Implementation focused on five interconnected activity streams: establishing a sustainable waste bank, monitoring and evaluating waste management systems, developing policy recommendations, creating participatory engagement programs, and proposing strategies for scale-up. The project addressed multiple waste streams through tailored interventions. For recycling, incentivized measures included prize-based competitions, exchange programs, and direct sales channels designed to motivate participation and behavior change. Organic waste management incorporates biogas production systems, vermicomposting operations, and non-turnover composting techniques to generate value-added products [9]. These operations were centralized at the Organic Waste Management Station (SDG Station), the operational hub for collection and processing. Additional innovations included integrating vegetable growing systems with solar cells (Agrivoltaic Farming) to maximize resource utilization and create "Farm to Table" opportunities. This approach exemplified the project's commitment to circular economy principles by transforming waste output into productive inputs for food production [10].

The comprehensive approach aligned with multiple Sustainable Development Goals, particularly SDG 11 (Sustainable Cities and Communities), SDG 12 (Responsible Consumption and Production), and SDG 13 (Climate Action). Additional connections were made to SDG 1 (No Poverty), SDG 3 (Good Health and Well-being), SDG 4 (Quality Education), and SDG 10 (Reduced Inequalities) through various project components addressing economic opportunity, community resilience, and educational engagement [11]. Waste management challenges through an integrated, multi-stakeholder approach. The Khun Thale Subdistrict project represents a significant advancement in sustainable development practices for Thailand. The initiative demonstrates how localized interventions can simultaneously address environmental challenges while creating measurable economic and social benefits within the framework of global sustainability goals.

2. Materials and Methods

2.1 Sustainable Waste Bank Development

Comprehensive waste composition analysis identified two primary sources at Khun Thale Subdistrict: institutional waste (from buildings, dormitories, and cafeterias) and flea market waste (generated twice weekly). Survey methodologies included sorting physical waste by category, weighing it, and analyzing its composition. A total of 100 kg of waste was sampled, with three replicates per sampling event. Samples were collected three times per month, and the results were used to calculate the average waste composition. Results revealed institutional waste consisted of 38% paper, 30% plastic, and 17% organic materials, while flea market

waste comprised 73% organic matter (primarily food scraps), 19% plastic, and 6% paper [12]. The project employed multi-level stakeholder engagement through targeted interviews, participatory workshops, and collaborative planning sessions with administrators, staff, students, and local businesses. This approach established ownership among key participants while identifying barriers to effective waste management, including insufficient infrastructure and limited incentives for separation behaviors [11]. Human-centered design principles guided the development of 50 strategically placed waste collection points with clear visual separation indicators. Two configurations were deployed: 25 three-bin systems (general, recyclable, organic) and 25 four-bin systems (adding hazardous waste separation). Systems incorporated weather-resistant roofing and instructional signage designed based on user feedback and observed behavior patterns [7]. Fifty strategic waste collection points were installed throughout the Khun Thale Subdistrict, with two distinct configurations: 25 three-bin systems (general, recyclable, organic) and 25 four-bin systems (Table 1), including hazardous waste separation [8].

Table 1. Waste separation infrastructure deployment

Location Type	3-Bin Systems	4-Bin Systems	Total Bins
Academic Buildings	10	8	62
Dormitories	6	10	58
Cafeterias	4	2	20
Outdoor Areas	5	5	35
Total	**25**	**25**	**175**

2.2 Recycling Waste Management

This incentive-based program operated across three implementation phases, collecting 3,434 kg of recyclable materials. Participation evolved significantly across phases: Phase 1 (Aug-Oct 2023) collected 116 kg primarily from community members (99.5%); Phase 2 (Nov 2023-Mar 2024) collected 1,085 kg with increased staff participation (21%); Phase 3 (Jun-Aug 2024) collected 2,233 kg with staff contributing 76% of materials, demonstrating successful institutional adoption. The project implemented multiple incentive mechanisms tailored to different participant motivations: high-value prize drawings, competitive waste collection contests, direct exchange for everyday items, and conventional sales to recycling shops. This multi-channel approach accommodated diverse participant preferences while consistently reinforcing separation behaviors [9]. This faculty-focused campaign aimed to promote behavior changes through consistent messaging and progressive goal setting. The 30-day format helped establish habits, while friendly competition between departments increased engagement. The challenge collected 682 kg of recyclable materials, representing 63% of the Phase 2 "Trash Lucky" collection volume. Targeting dormitory housekeeping staff initially, this exchange program allowed participants to accumulate points for sorted recyclables and redeem them for higher-value items than those available through direct sales. Two collection events (July and August 2024) yielded 2,231.2 kg of recyclable materials, demonstrating effective motivational design and operational scalability.

2.3 Organic Waste Management

The project implemented an anaerobic digestion system for processing food waste, collecting inputs from cafeterias in Khun Thale Subdistrict and the Khun Thale Sub-district Municipality. Operations commenced in October 2023, processing 42,634 kg of organic waste and generating 2,052 cubic meters of biogas. The system included a pipeline delivering biogas directly to food vendors, reducing cooking costs and creating economic benefits through mandated food price reductions. This intervention reduced greenhouse gas emissions by 23,715 kg CO_2eq [6]. A two-trough vermicomposting system utilizing African Night Crawler (AF) species processed food scraps and produce waste. Beginning in March 2024, the system converted 56 kg of organic waste into 485 kg of vermicompost, resulting in a reduction of 38.11 kg CO_2eq in greenhouse gas emissions. The resulting soil conditioner served dual purposes: it generated revenue through commercial sales and was used for on-site organic vegetable cultivation [10]. The project implemented non-turnover

composting using pot rests and ground heap methods to process an abundance of leaf and branch waste. Materials underwent mechanical size reduction to accelerate the decomposition process. This passive system required minimal maintenance while producing approximately 480 kg of compost, which was used primarily as a soil amendment for agricultural applications [12]. The project employed systematic data collection through waste logs, production metrics, and emissions calculations. Key performance indicators included waste diversion rates, biogas production volume, compost yields, carbon reduction metrics, and economic benefits. This framework enabled the calculation of the Khun Thale Subdistrict's carbon footprint (Scopes 1-3) and quantified the greenhouse gas reductions resulting from project interventions.

2.4 Innovative Applications

The project integrated solar power generation with agricultural production, mounting photovoltaic panels above vegetable cultivation areas. This dual-use system optimizes space utilization while providing partial shading beneficial for lettuce varieties. The system, scheduled for complete implementation in September 2024, represented a significant advancement in land-use efficiency and sustainable resource integration. Organic waste-derived soil amendments supported the growth of quick-growing salad crops, including Green Oak, Red Oak, and Green Cos lettuce, with 35–45-day maturation cycles. This closed-loop system exemplified circular economy principles by transforming waste outputs into valuable food products, enhancing food security while demonstrating practical applications of waste valorization [9]. A digital monitoring system provided data collection, analysis, and reporting capabilities through the "Zero Waste application." This tool functioned as the central database for waste management metrics, enabling continuous operational assessment and verification. The application facilitated active participation from target groups while serving as an innovative instrument for Monitoring, Reporting, and Verification (MRV) requirements.

3. Results and Discussion

3.1 Waste Composition Analysis

Analysis of waste composition at Khun Thale Subdistrict revealed distinct patterns across different campus areas. General institutional waste consisted primarily of paper waste (38%), plastic waste (30%), and organic waste (17%), with the remaining 15% comprising various other materials (Fig. 1), including glass, metal, and hazardous items [6]. This composition differs significantly from typical municipal waste in Thailand, where organic waste typically constitutes 60% of total waste [1]. The high proportion of paper waste reflects the significant contributions from academic activities, including cardboard, paper towels, and printed materials. Student dormitories emerged as critical points of waste generation, particularly for plastic waste, which lacked efficient sorting and management systems. Housekeeping staff had initiated some informal recycling efforts, but volumes remained relatively low before project implementation [8]. Flea market waste exhibited a markedly different composition, with organic waste—primarily food scraps, vegetables, and fruits—constituting 73% of the total. Plastic waste accounted for 19% of the total, while paper waste accounted for only 6%. This high organic fraction presented challenges and opportunities for value recovery, mainly through biogas production systems [9]. Waste generation fluctuated significantly throughout the academic year, ranging from approximately 15 tons during break periods to 70 tons during peak semester activities, as shown in Table 2. This variation necessitated flexible management systems capable of accommodating substantial volume changes while maintaining operational efficiency [5]. The distinct waste compositions of different campus areas highlighted the need for tailored intervention strategies rather than a uniform approach. The predominance of potentially recyclable materials (paper and plastic comprising 68% of institutional waste) indicated significant opportunities for waste diversion through improved collection systems and incentive programs [3].

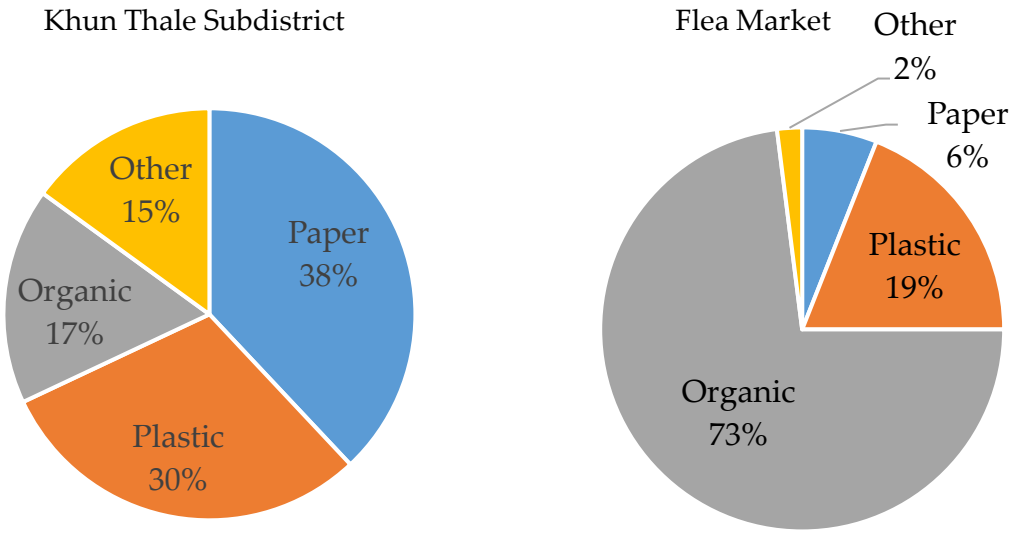

Figure 1. Waste composition comparison between Khun Thale Subdistrict and flea market.

Table 2. Monthly waste generation by source

Month (2023)	Academic Buildings (tons)	Dormitories (tons)	Cafeterias (tons)	Flea Market (tons)
Jan	8.2	4.5	2.8	3.4
Feb	12.5	6.3	3.9	4.1
Mar	15.8	7.2	4.5	4.3
Apr	3.2	1.8	0.9	4.2
May	2.8	1.5	0.7	4.1
Jun	14.3	6.9	4.2	4.4
Jul	17.5	8.5	5.1	4.5
Aug	19.2	9.3	5.8	4.7

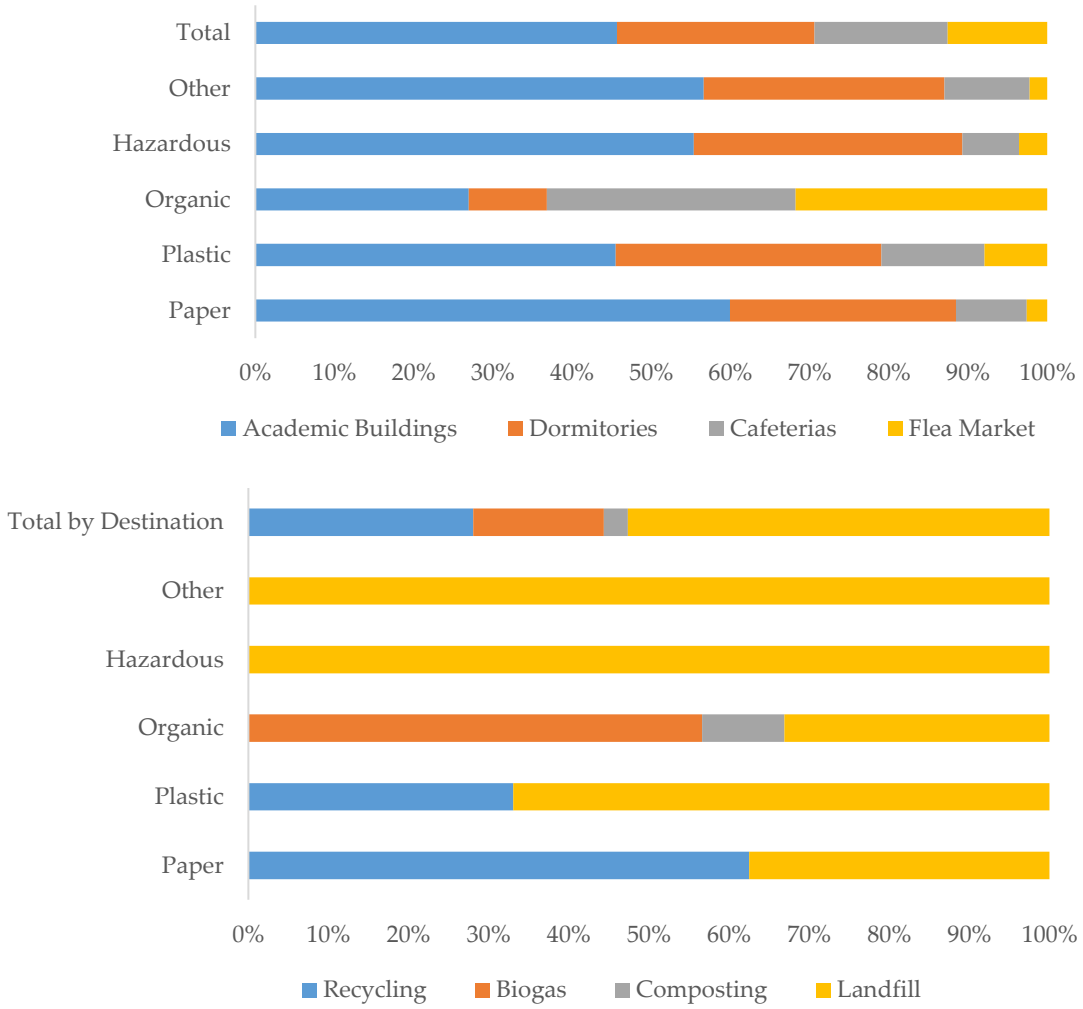

Figure 2. Waste flow diagram in Khun Thale Subdistrict.

3.2 Waste Management Infrastructure

Based on the results of the waste characterization, the project implemented a comprehensive infrastructure upgrade to facilitate waste separation at the source. Each installation featured overhead roofing structures to prevent rainwater contamination and educational signage with visual indicators for proper waste categorization. Placement prioritized high-waste generation areas, including dormitories, cafeterias, and academic buildings [7]. The infrastructure implementation yielded significant improvements in waste separation behaviors. Pre-implementation measurements showed baseline separation rates of 18.3% for recyclables, 12.5% for organic waste, and 8.6% for hazardous materials. Aeparation rates increased to 62.7%, 57.2%, and 43.5%, respectively [10]. While these improvements represent substantial progress toward achieving target separation rates (70% recyclables, 65% organic, and 50% hazardous), as shown in Figure 3, the results indicate room for continued behavioral change interventions. The most significant gains were observed in recyclable separation, likely due to the influence of complementary incentive programs. The lower hazardous waste separation effectiveness suggests the need for additional educational interventions to ensure proper disposal of these materials [9].

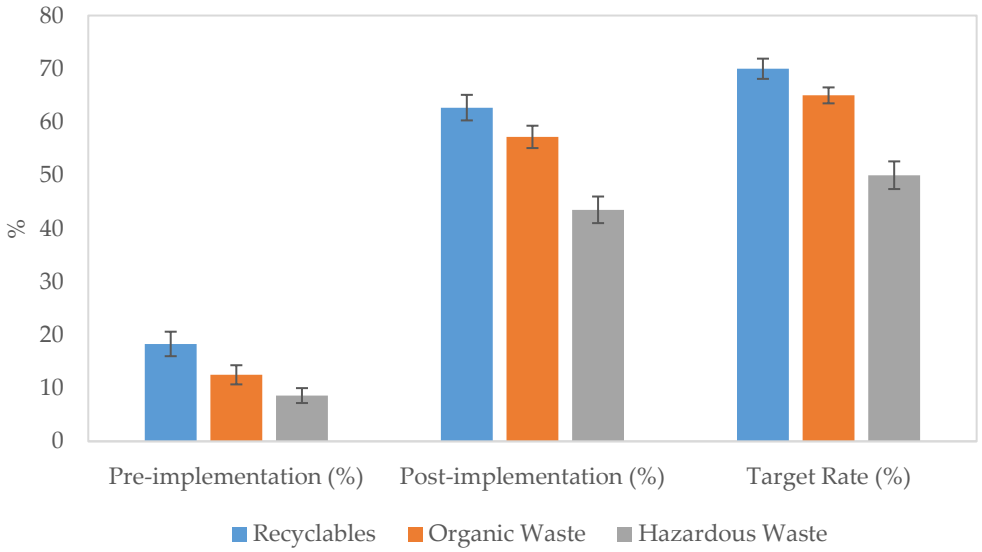

Figure 3. Waste separation effectiveness pre- and post-infrastructure implementation

3.3 Recycling Program Outcomes

The "Recycling Waste to Win Luck with Trash Lucky" program demonstrated significant progression across its three implementation phases, collecting 3,434 kg of recyclable materials. Phase 1 (Aug-Oct 2023) yielded modest results (116 kg), with community members contributing 99.5% of materials. Phase 2 (Nov 2023-Mar 2024) showed substantial growth (1,085 kg) with increased staff participation (21%) (Table 3). Phase 3 (Jun-Aug 2024) achieved the highest collection (2,233 kg), with staff participation rising dramatically to 76%, indicating successful institutional adoption [12]. This evolution reflects the effective diffusion of recycling behaviors throughout the Khun Thale Subdistrict, with initial community champions gradually influencing broader participation. The shift in participant demographics suggests the successful normalization of recycling practices among staff, consistent with findings by Wijayanti and Suryani [10] regarding the social influence on waste separation programs. The "30 Days Zero Waste Challenge" campaign targeting faculty members resulted in the collection of 682 kg of recyclable materials, representing 63% of the Phase 2 "Trash Lucky" collection. This time-bounded initiative employed structured goal-setting and interdepartmental competition to foster habit formation, aligning with behavioral change approaches documented by Rachman et al. [5]. The "Separate and Exchange Things" activity initially targeted dormitory housekeeping staff but expanded to include broader participation, collecting 2,231.2 kg of recyclables across two events (July and August 2024). This point-based exchange system provided tangible incentives beyond traditional recycling markets, creating higher perceived value for separation behaviors [8]. Combined recycling initiatives diverted 6,347.2 kg of materials from landfill disposal, demonstrating the efficacy of multi-channel incentive programs tailored to specific participant motivations [7].

Table 3. Recycling program results by initiative and phase

Program	Time Period	Participants	Total Recyclables (kg)	% of Total Collection
Trash Lucky Phase 1	Aug-Oct 2023	Community: 100%, Staff: 0%	116.0	3.4%
Trash Lucky Phase 2	Nov 2023-Mar 2024	Community: 79%, Staff: 21%	1,085.0	31.6%
Trash Lucky Phase 3	Jun-Aug 2024	Community: 24%, Staff: 76%	2,233.0	65.0%
Total	**Aug 2023-Aug 2024**	**Mixed**	**3,434**	**100%**

3.4 Organic Waste Management Achievements

The project's organic waste management systems demonstrated significant resource recovery and environmental benefits across multiple technologies. Biogas production commenced in October 2023, processing 42,634 kg of organic waste primarily from cafeterias, and generating 2,052 cubic meters of biogas. This output achieved greenhouse gas reductions of 23,715 $kgCO_2eq$ through the displacement of conventional cooking fuels [6]. The May 2024 installation of a biogas pipeline system for food vendors created economic benefits by reducing cooking costs, which in turn led to policy requirements for vendors to lower food prices for students [9]. Vermicomposting operations using African Night Crawler (AF) species in a two-trough system began in March 2024. This system demonstrated remarkable conversion efficiency, transforming 56 kg of organic waste into 485 kg of vermicompost with a conversion ratio of 8.66:1. The process reduced greenhouse gas emissions by 38.11 $kgCO_2eq$ while producing high-value soil amendments for agricultural applications [10]. Non-turnover composting using pot rest and ground heap methods processed leaf and branch waste, producing approximately 480 kg of compost. This passive system required minimal maintenance while achieving effective decomposition through mechanical size reduction of input materials [12]. Combined organic waste management technologies processed 43,690 kg of materials and achieved total GHG reductions of 23,976.11 $kgCO_2eq$ (Table 4). This integrated approach demonstrates the successful implementation of appropriate technologies at an institutional scale, consistent with findings by Rachman et al. [5] regarding effective organic waste valorization strategies.

Table 4. Organic waste management performance metrics

Technology	Input (kg)	Output	Conversion Ratio	GHG Reduction ($kgCO_2eq$)
Biogas Production	42,634	2,052 m^3	0.048 m^3/kg	23,715
Vermicomposting	56	485 kg compost	8.66 kg/kg	38.11
Non-turnover Composting	~1,000	480 kg compost	0.48 kg/kg	223
Total	**43,690**	**-**	**-**	**23,976.11**

3.5 Innovation Integration

The biogas pipeline system, implemented in May 2024, directly connected organic waste processing and cafeteria operations. This infrastructure provided biogas to 12 food vendors, resulting in a monthly reduction of approximately 24,000 Baht in cooking fuel costs (Table 5). The economic benefit translated directly to students through mandated food price reductions of 5-10 Baht per meal, affecting approximately 2,500 daily consumers [9]. This integration exemplifies successful closed-loop resource management, with waste outputs from one system becoming valuable inputs for another. The agrivoltaic farming system, combining solar power generation with agricultural production, became operational in September 2024. This integrated approach maximizes land-use efficiency while creating complementary benefits: partial shading for lettuce varieties and renewable energy for system operations. Monthly production capacity reached 240 kg of organic produce, generating approximately 12,500 Baht in revenue while reducing energy costs by 30% compared to conventional systems [10]. The economic impacts extended beyond direct financial benefits to include significant social value. Organic produce from the agrivoltaic system supported 75 underprivileged students at Seuksasongkroa Surat Thani School, enhancing food security for vulnerable populations. The system served as an educational platform for sustainable agriculture practices, aligned with findings by Khan et al. [6] regarding the educational value of integrated waste management demonstrations. The Zero Waste application provided digital infrastructure connecting multiple system components, enhancing operational efficiency by 15% through improved data collection and analysis capabilities. This technological integration facilitated comprehensive monitoring while engaging 180 active users in waste management participation [12].

Table 5. Economic and social benefits of integrated systems

Innovation	Implementation Date	Direct Beneficiaries	Economic Benefit	Social/Environmental Benefit
Biogas Pipeline	May 2024	12 food vendors, ~2,500 students	24,000 Baht /month vendor savings, 5-10 Baht /meal student savings	23,715 $kgCO_2eq$ reduction
Agrivoltaic Farming	Sep 2024	University community, 75 underprivileged students	12,500 Baht /month revenue, 30% energy cost reduction	240 kg/month organic produce, educational opportunities
Zero Waste App	Apr 2024	Project staff, 180 active users	15% increase in operational efficiency	Improved data collection, enhanced participation

3.6 SDG Alignment and Policy Development

The project aligned with 7 Sustainable Development Goals, demonstrating comprehensive sustainability integration as shown in Table 6. Primary connections include SDG 11 (Sustainable Cities), SDG 12 (Responsible Consumption), and SDG 13 (Climate Action) through waste diversion and GHG reductions. Beyond these direct linkages, the initiative also contributes indirectly to SDG 3 (Good Health and Well-being) by reducing pollution-related health risks and SDG 8 (Decent Work and Economic Growth) through the creation of green jobs in waste valorization. This indicates that the project does not merely address waste management as an isolated issue but embeds it within a broader socio-economic and environmental framework. Moreover, aligning local practices with global sustainability targets highlights the potential scalability and replicability of the approach, offering lessons for both national policy design and international case comparisons. Such integration underscores the importance of community-driven waste solutions as catalysts for systemic change, bridging grassroots action with global sustainability agendas [13]. Additional alignments include SDG 2 (Zero Hunger) via agrivoltaic farming and SDG 7 (Affordable Clean Energy) through biogas production [11]. Policy Journey Map findings, developed through stakeholder workshops, identified critical transition points for scaling operations. Institutional policies that support vendor price reductions through biogas savings demonstrate effective policy mechanisms that link environmental and social benefits. Analysis revealed three essential policy components for replication: mandatory waste separation requirements, financial incentive structures, and formalized public-private partnerships [5]. The scale-up potential analysis identified a phased implementation pathway: short-term expansion to five additional educational institutions (potentially diverting 249 tons/year of waste), medium-term municipal adoption across Surat Thani (2,490 tons/year), and long-term provincial/national integration (24,900 tons/year). Key enablers include knowledge-sharing platforms, municipal waste bank regulations, and carbon credit mechanisms. The economic analysis projects proportional growth in benefits from 1.2 million Baht/year to 600 million Baht/year at the national scale [10]. The multi-stakeholder approach proved essential for sustainable implementation, consistent with findings by Samadikun et al. [12] regarding institutional partnerships in waste management initiatives.

Table 6. SDG alignment of project components

SDG	Project Component	Key Performance Indicator	Current Achievement
SDG 2	Agrivoltaic farming	Organic food production	240 kg/month
SDG 7	Solar integration	Renewable energy generation	3.2 kWh/day
SDG 8	Economic benefits	Cost savings for students	5-10 Baht/meal
SDG 11	Waste separation infrastructure	Waste separation rate	62.7% (recyclables)
SDG 12	Recycling program	Recycling diversion rate	6,347 kg diverted
SDG 13	Biogas production	GHG reduction	23,715 kgCO_2eq
SDG 17	Multi-stakeholder partnership	Organizations engaged	5 institutional partners

4. Conclusions

The "Innovative Solutions for Waste Bank Development in Khun Thale Subdistrict" project demonstrated the effectiveness of integrated waste management systems using human-centered design approaches. Comprehensive waste characterization enabled targeted interventions: improved infrastructure for source separation, incentive-based recycling programs, and appropriate technologies for organic waste valorization. Key achievements include diverting 6,347.2 kg of recyclables through multi-channel incentives, producing 2,052 cubic meters of biogas from 42,634 kg of organic waste, and achieving total greenhouse gas reductions of approximately 33,086 kg CO_2eq. The project's circular economy approach generated significant economic and social benefits, including reduced cooking costs for vendors, lower food prices for students, and access to organic produce for underprivileged children. Integration innovations, particularly the biogas pipeline and agrivoltaic farming, demonstrated successful closed-loop resource management with multiple sustainability benefits. Alignment with the 11 Sustainable Development Goals demonstrated the project's comprehensive impact on sustainability. Analysis of scale-up potential identified pathways from institutional to national implementation, with proportional increases in environmental and economic benefits at each level. Critical success factors included multi-stakeholder engagement, tailored incentive systems, appropriate technology selection, and policy mechanisms linking environmental and social outcomes. Future directions should focus on expanding the waste bank model to additional institutions, developing knowledge-sharing platforms, and creating supportive policy frameworks at the municipal and provincial levels. This project offers a replicable model for waste management in educational institutions that addresses environmental challenges while generating measurable economic and social benefits within Thailand's sustainable development framework.

5. Acknowledgements

The authors would like to thank the members of the community in Khun Thale Subdistrict, Mueang District, Surat Thani Province, Thailand, for their participation and valuable insights throughout the study. Special thanks to the anonymous reviewers for their constructive comments and suggestions, which helped improve the quality of this manuscript.

Author Contributions: SW conceptualization, formal analysis, project administration, resources and writingreviewand editing. NP interpretation of data analysis and writing-review. PN data curation,formal analysis, investigation, methodology, visualization and writing-original draft. All authors have readand agreed to the published version of the manuscript.

Funding: This work is financially supported by the United Nations Development Programme (UNDP), Thailand Science Research and Innovation (TSRI), and the National Science, Research and Innovation Fund (NSRF) (NRIIS number 4794282)

Conflicts of Interest: We declare that we have no conflict of interest.

References

[1] UNDP Thailand - United Nations Development Programme. Innovative Solutions for Waste Bank Development in Surat Thani. **2024**, December 15. https://www.undp.org/thailand/projects/innovative-solutions-waste-bank-development-surat-thani (accessed 2025-04-02).

[2] The Ministry of Natural Resources and Environment Thailand. Report on the Situation of Community Waste Disposal Facilities in Thailand. **2024**, November 20. https://www.pcd.go.th/publication/29509/ (accessed 2025-04-02).
[3] Susilowati, S.; Herdiansyah, H. Application of waste bank use in reducing household waste in sub-urban area?. *J. Phys.: Conf. Ser.* **2019**, *1381*, 012050. https://doi.org/10.1088/1742-6596/1381/1/012050
[4] Obiorah, C. A.; Ndubuisi, O. G.; Ali, S. E.; Ali, U. T.; Nesiama, O.; Agbakhamen, C. O.; Gumi, S. A. Integrating waste management into sustainable development planning: a framework for urban areas. *Int. J. Innov. Soc. Sci. Humanit. Res.* **2025**, *13*(2), 27-42. doi:10.5281/zenodo.15186894
[5] Rachman, I.; Komalasari, N.; Hutagalung, I. R. Community participation on waste bank to facilitate sustainable solid waste management in a village. *J. Environ. Sci. Sustainable Dev.* **2021**, *4*(2), 327–345. https://doi.org/10.7454/jessd.v4i2.1123
[6] Khan, M. A.; Khan, R.; Al-Zghoul, T. M.; Khan, A.; Hussain, A.; Baarimah, A. O.; Arsha, M. A. Optimizing municipal solid waste management in urban Peshawar: A linear mathematical modeling and GIS approach for efficiency and sustainability. *Case Stud. Chem. Environ. Eng.* **2024**, *9*, 100704. https://doi.org/10.1016/j.cscee.2024.100704
[7] Indrianti, N. Community-based solid waste bank model for sustainable education. *Procedia - Soc. Behav. Sci.* **2016**, *224*, 158–166. https://doi.org/10.1016/j.sbspro.2016.05.431
[8] Samadikun, B. P.; Nugraha, W. D.; Rahayu, A. P.; Napitupulu, J. C. W.; Fuad, T. S.; Amartia, N. U.; Rachmayani, A. H.; Rahma, A. S. G. Study on the development of waste banks post-pandemic in semarang city. *IOP Conf. Ser.: Earth Environ. Sci.* **2023**, *1268*(1), 012006. https://doi.org/10.1088/1755-1315/1268/1/012006
[9] Wulandari, D.; Utomo, S. H.; Narmaditya, B. S. Waste bank: waste management model in improving local economy. *Int. J. Energy Econ. Policy* **2017**, *7*(3), 36–41.
[10] Miftahorrozi, M.; Khan, S.; Bhatti, M. I. B. Waste bank-socio-economic empowerment nexus in indonesia: the stance of Maqasid al-Shari'ah. *J. Risk Financial Manag.* **2022**, *15*(7), 294. https://doi.org/10.3390/jrfm15070294.
[11] Wijayanti, D. R.; Suryani, S. Waste bank as community-based environmental governance: a lesson learned from surabaya. *Procedia - Soc. Behav. Sci.* **2015**, *184*, 171–179. https://doi.org/10.1016/j.sbspro.2015.05.077
[12] Samadikun, B. P.; Nugraha, W. D.; Rahayu, A. P.; Napitupulu, J. C. W.; Fuad, T. S.; Amartia, N. U.; Rachmayani, A. H.; Rahma, A. S. G. The impact of waste bank development on society during endemic era in semarang city. *IOP Conf. Ser.: Earth Environ. Sci.* **2023**, *1268*(1), 012011. https://doi.org/10.1088/1755-1315/1268/1/012011
[13] Kaza, S.; Yao, L.; Bhada-Tata, P.; Van Woerden, F. *What a Waste 2.0: A Global Snapshot of Solid Waste Management to 2050*; World Bank, **2018**. https://doi.org/10.1596/978-1-4648-1329-0

ASEAN
Journal of Scientific and Technological Reports
Online ISSN:2773-8752

Research article

Outdoor Walkway Flooring from Natural Rubber and Reclaimed Rubber Blends with Superior Environmental Resistance

Tiptiwa Sampantamit[1], Apinan Aueaungkul[2], Pornsiri Toh-ae[3], Panita Sumanatrakul[4], Suppachai Sattayanurak[5], and Weerawut Naebpetch[6*]

[1] Faculty of Science and Digital Innovation, Thaksin University, Phatthalung, 93210, Thailand
[2] Faculty of Economics and Business Administration, Thaksin University, Songkhla, 90000, Thailand
[3] Center of Rubber Technology for Community, Faculty of Engineering, Thaksin University, Phatthalung, 93210, Thailand
[4] Faculty of Engineering, Thaksin University, Phatthalung, 93210, Thailand
[5] Faculty of Engineering, Thaksin University, Phatthalung, 93210, Thailand
[6] Faculty of Engineering, Thaksin University, Phatthalung, 93210, Thailand
* Correspondence: weerawut.n@tsu.ac.th

Citation:
Sampantamit, T.; Aueaungkul, A.; Toh-ae, P.; Sumanatrakul, P.; Sattayanurak, S.; Naebpetch, W. Outdoor walkway flooring from natural rubber and reclaimed rubber blends with superior environmental resistance. *ASEAN J. Sci. Tech. Report.* **2025**, *28*(6), e258879. https://doi.org/10.55164/ajstr.v28i6.258879.

Article history:
Received: April 20, 2025
Revised: September 28, 2025
Accepted: October 1, 2025
Available online: October 20, 2025

Abstract: This study systematically investigated the effects of reclaimed rubber (RR) content on the mechanical properties and accelerated aging resistance of natural rubber (NR) vulcanizates for outdoor walkway flooring applications. Six formulations were prepared with NR/RR ratios ranging from 100/0 to 50/100 parts per hundred rubber (phr), maintaining a total rubber content of 100 phr after accounting for the 48-50% actual rubber content in reclaimed rubber (confirmed by thermogravimetric analysis showing 55% mass loss at 350-400°C). Results demonstrated that increasing RR content from 0 to 100 phr progressively decreased tensile strength and elongation at break, while hardness and 300% modulus exhibited slight increases due to residual cross-links and higher filler concentrations in reclaimed rubber. Notably, accelerated aging tests (ASTM D573: 100°C for 22 hours; ASTM G154: UV-A 0.89 W/m² at 340 nm, 60°C for 8 hours, followed by condensation at 50°C for 4 hours, total 168 hours) revealed substantial improvements in aging resistance with increasing RR content. The percentage decrease in tensile strength after aging diminished progressively as RR content increased. The optimized formulation containing 100 phr reclaimed rubber was selected for commercial production. Despite having a relatively lower tensile strength compared to virgin NR formulations, this composition provided adequate mechanical performance while demonstrating superior resistance to environmental degradation. Compression molding at 170°C for 8 minutes produced 1 m² × 0.06 m rubber tiles with anti-slip lozenge patterns. Implementation at a commercial café yielded positive user feedback and achieved an approximately 30% cost reduction compared to virgin rubber formulations, supporting the sustainable utilization of rubber waste.

Keywords: Natural rubber; reclaimed rubber; outdoor walkway; glooring

1. Introduction

With the growing number of elderly individuals in society, tourism-related businesses have increasingly adapted their facilities to accommodate better the needs of older customers, whose numbers continue to rise each year. One up-and-coming product designed to support this demographic is the rubber walkway. Rubber's natural flexibility makes it soft and comfortable to walk on,

while also offering excellent slip resistance [1], helping to reduce the risk of falls. Typically, synthetic polymers are used to produce these walkway sheets due to their durability and resistance to wear, which contribute to a long service life. However, since Thailand is a leading global producer of natural rubber—and because it is plant-based and environmentally friendly—natural rubber presents an attractive alternative for walkway development. Despite its excellent flexibility, mechanical strength, and slip resistance, natural rubber has a major drawback: poor resistance to oxidation, which limits its durability in outdoor environments [2]. Therefore, to produce rubber walkway sheets suitable for outdoor use, it is essential to research ways to enhance the oxidation resistance of natural rubber, especially in terms of resistance to accelerated aging.

Previous research has consistently focused on enhancing the deterioration resistance of natural rubber. A widely used approach involves modifying its structure to improve its resistance to degradation [3-5]. Saengdee et al. studied the chemical modification of natural rubber at the latex stage under environmentally friendly conditions, aiming to enhance its thermal, ozone, and mechanical properties. Two sequential chemical modifications—epoxidation followed by hydrogenation—were performed in a one-pot system. Natural rubber latex (NRL) was first treated with in situ performic acid, formed from formic acid and hydrogen peroxide, to produce partially epoxidized natural rubber (ENR) latex. This product was then further modified through a hydrogenation reaction using hydrazine and hydrogen peroxide to target the remaining unsaturated units. After vulcanization, all modified NRs retained the excellent mechanical properties of natural rubber due to their ability to undergo strain-induced crystallization. Additionally, the modified NRs showed improved resistance to oil, solvents, and ozone compared to the unmodified NR. These findings suggest that hydrogenated epoxidized natural rubbers (HENRs) can overcome the limitations of natural rubber, potentially expanding its range of applications [4]. Another commonly used approach to enhance the aging resistance of natural rubber is by blending it with rubbers that possess excellent aging resistance properties [6-8]. Developing high-value reclaimed rubber (RR) plays a crucial role in promoting sustainability within the rubber industry. To achieve eco-friendly recycling of waste rubber and expand the applications of RR, a material with potential reinforcing and plasticizing effects on natural rubber (NR) composites was produced through a thermo-oxidative reclamation process. The degree of reclamation was regulated by varying the amount of soybean oil used. The plasticizing effect of RR was evidenced by a reduction in torque during vulcanization and an increase in elongation at break of NR/RR composites as the reclamation level increased. Additionally, incorporating RR enhanced the tensile strength, thermal stability, and rheological properties of the NR/RR composites. The formation of new bound rubber in the NR/RR system further confirmed the reinforcing effect of RR. Scanning electron microscope images revealed that the average particle size of RR reached the nanoscale, and its dispersion within the composites improved with higher degrees of reclamation, as indicated by the Payne effect. Overall, this study highlights the dual reinforcing and plasticizing functions of RR, contributing to its value-added use and expanded application potential [7].

Accordingly, this study adopted a method to enhance the properties of natural rubber by blending it with reclaimed rubber. The effects of different reclaimed rubber contents on the mechanical and aging resistance properties were investigated. The formulation that demonstrated the most balanced overall performance was used to produce rubber flooring sheets, which were then applied in "Nai Susn Sri" commercial shop settings.

2. Experimental

2.1 Materials

Natural rubber (RSS #3, Thai Hua Rubber Public Co., Ltd., Thailand) and Reclaimed rubber (UCD-105, Union Commercial Development Co., Ltd., Thailand) were used as raw elastomers. Zinc oxide (White seal grade, UTIDS Enterprise, Co., Ltd, Thailand), Stearic acid (Imperial, Co., Ltd, Thailand), Carbon black (N550, Thai Tokai Carbon Product Co., Ltd., Thailand), Calcium carbonate (Caliofil100, Sand and Soil Industry Co., Ltd., Thailand), Paraffinic oil (Tudalen 13-grade, H&R ChemPharm (Thailand) Co., Ltd., Thailand), Paraffin wax (China Petroleum & Chemical Co., Ltd., China), Tetramethylthiuram disulfide: TMTD (Kawaguchi, Co., Ltd, Japan), N-cyclohexyl-2-benzothia zolesulphenamide: CBS (Kawaguchi, Co., Ltd, Japan) and Sulfur (Siam Chemical, Co., Ltd, Thailand) were used as rubber additives in the compound formulations.

2.2 Compound preparation

Rubber compounds were prepared using the formulations listed in Table 1, which were mixed using an open two-roll mill. The formulation does not use 100 phr of virgin natural rubber, as reclaimed rubber contributes approximately 50% rubber content. The compounding operation was initiated by masticating the natural rubber and reclaimed rubber for at least 3 minutes through the controlled distance of the front and back mill rolls (so-called nip width) at the initial mixing temperature. Zinc oxide, stearic acid, and paraffin wax were then added and mixed for approximately 3 minutes. Carbon black, calcium carbonate, and paraffinic oil were continuously incorporated in this step. The nip was changed twice, and finally, TMTD, CBS, and sulfur were added, resulting in a total mixing time of 25 minutes. The compounds were sheeted out at a thickness of 5 mm and stored at room temperature overnight.

Table 1. Rubber compound formulation.

Ingredients	**Quantity (phr)**					
Natural rubber (RSS#3)	100	90	80	70	60	50
Reclaimed rubber (UCD-105)	-	20	40	60	80	100
Zinc oxide	5	5	5	5	5	5
Stearic acid	1	1	1	1	1	1
Carbon black (N550)	40	40	40	40	40	40
Calcium carbonate (Caliofil100)	100	100	100	100	100	100
Paraffinic oil	15	15	15	15	15	15
Paraffin wax	2	2	2	2	2	2
TMTD	0.3	0.3	0.3	0.3	0.3	0.3
CBS	1.5	1.5	1.5	1.5	1.5	1.5
Sulfur	1	1	1	1	1	1
Curing time (t_{c90})	**5:50**	**6:08**	**6:49**	**7:23**	**7:50**	**8:00**

2.3 Sample preparation

Standard sheets were prepared by compression moulding the rubber compounds at 170 °C, each case for its optimal cure time (t_{c90}) determined by a Moving Die Rheometer, MDR (MDR-U6S, U-Can Dynatex Inc., Taichung, Taiwan) at a molding temperature. Test specimens for tensile properties were cut from the standard sheets using the standard dies (Die C dumb-bell, ASTM D412).

2.4 Measurements

2.4.1 Hardness

The test specimens, in the shape of a square, were 6×6 cm in size and 0.9 cm in thickness, as per ASTM D2240. They were measured using a hardness tester, Model GX-02 (Teclock Co., Ltd., Japan). Type A probes were used by measuring the four corners of the test piece and the center of the test piece, and then taking the average of the measured values.

2.4.2 Tensile properties

The tensile test was performed using a universal tensile testing machine (Tech Pro, CG Engineering Ltd., Part., Thailand) at a crosshead speed of 500 mm/min, according to ASTM D412. Tensile strength, 300% modulus, and elongation at break of specimens were measured five times. Finally, the average results were calculated.

2.4.3 Aging resistance

For heat aging resistance, samples prepared for the tensile test were placed in a hot-air oven at 100 °C for 22 h before the tensile measurement according to ASTM D573. The changes to properties, caused by aging in the oven, were assessed.

For weathering resistance, samples were placed inside the QUV machine. The testing cycle used UV-A at 0.89 W/m², 340 nm, at 60 °C for 8 h, followed by condensation at 50 °C for 4 h, with a total testing time of 168 h, as per ASTM G154. The changes to properties, caused by aging in the oven, were assessed.

3. Results and Discussion

As shown in Table 1, the theoretical rubber content should be 100 parts per hundred rubber (phr) in all formulations. However, when reclaimed rubber is incorporated, the total phr exceeds 100. This is because reclaimed rubber, produced through the recycling of end-of-life tires, comprises both rubber and non-rubber additives. According to the supplier of UCD-105 grade reclaimed rubber, the rubber content is approximately 48 % ± 3%.

To validate this, thermogravimetric analysis (TGA) was performed to examine weight changes in the material under thermal conditions. The results indicated that the reclaimed rubber exhibited approximately 55% mass loss at 350–400 °C (Figure 1), a temperature range associated with the decomposition of rubber and other polymers [9,10]. These findings are consistent with the manufacturer's data, confirming that the reclaimed rubber used in this study contains roughly 50% rubber and 50% additives. Therefore, after adjusting for rubber content, each formulation in this study maintained a consistent base of 100 phr rubber.

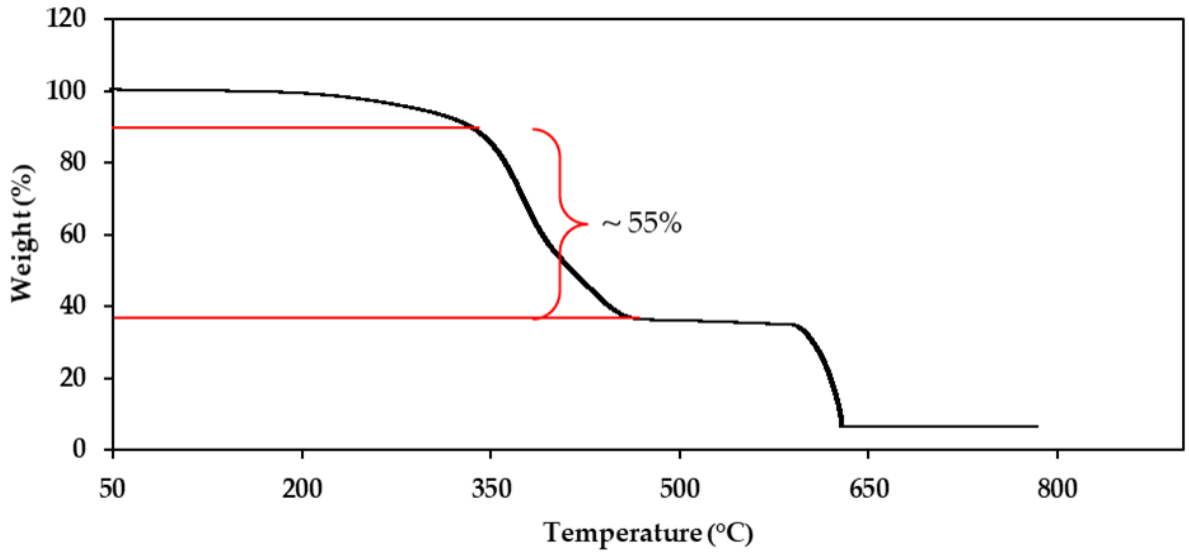

Figure 1. TGA curves of reclaimed rubber (grade UCD-105).

In developing a rubber compound suitable for outdoor walkway flooring, natural rubber was blended with reclaimed rubber. Natural rubber is renowned for its exceptional mechanical properties, but it is highly susceptible to degradation by oxygen, ozone, and UV radiation. Reclaimed rubber, on the other hand, has superior environmental resistance but suffers from significantly reduced mechanical strength due to prior thermal and mechanical degradation. Figure 2(A) illustrates the relationship between tensile strength, elongation at break, and reclaimed rubber content. As the proportion of reclaimed rubber increases, both tensile strength and elongation at break decline, particularly tensile strength. This is primarily due to the shortened molecular chains in reclaimed rubber, resulting from the recycling process, which lowers the average molecular weight and diminishes tensile strength. Rubber strength typically depends on molecular weight, cross-link density, and the presence of filler reinforcement. A higher reclaimed rubber content increases the filler concentration and simultaneously decreases molecular weight, compounding the reduction in strength [11].

Elongation at break also shows a mild decline with increasing reclaimed rubber. While reclaimed rubber has a lower molecular weight, it contributes to a broader molecular weight distribution in the blend, enhancing molecular mobility. As a result, the reduction in elongation is less pronounced, even at 100 phr of reclaimed rubber. Figure 2(B) presents the relationship between hardness, 300% modulus, and reclaimed rubber content. Both hardness and modulus were observed to increase slightly with a higher reclaimed rubber content. This can be attributed to the residual cross-links present in reclaimed rubber, which raise the overall

cross-link density of the compound. Additionally, the reclaimed rubber contains fillers, which further contribute to increased hardness and modulus. Reclaimed rubber generally contains reinforcing fillers, as it is derived from tires. Consequently, increasing the proportion of reclaimed rubber also increases the filler content, enhancing rubber–filler interactions and resulting in higher hardness, in agreement with previous studies [11].

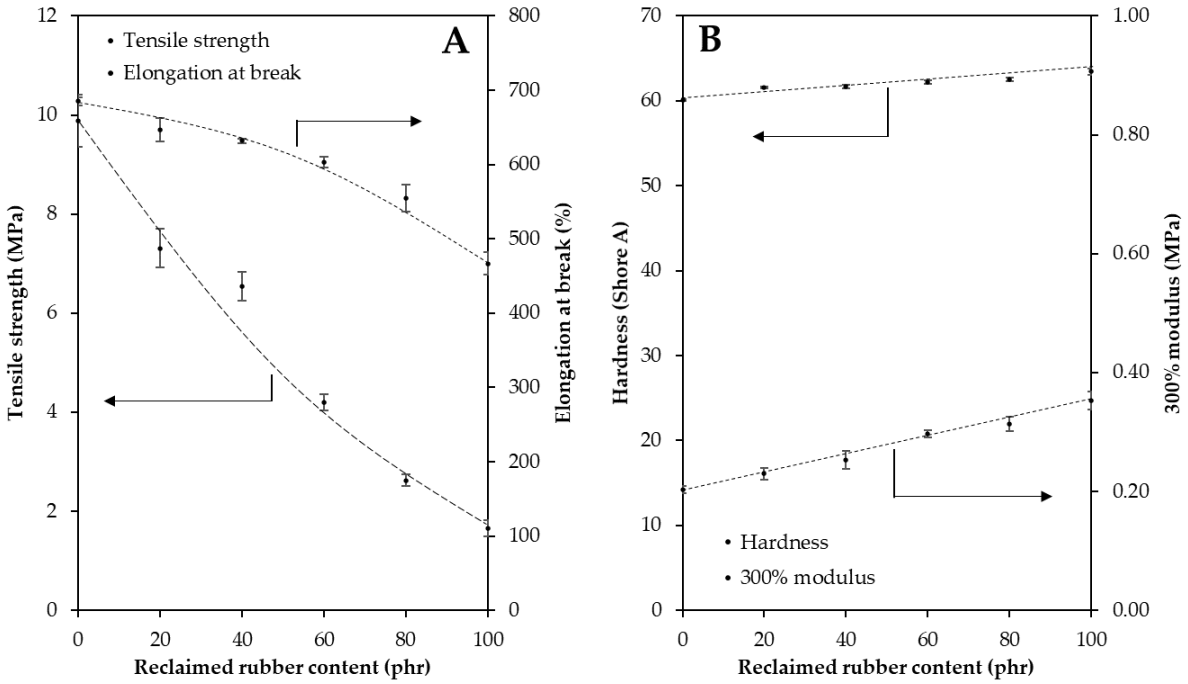

Figure 2. Effect of reclaimed rubber content on tensile strength, elongation at break (A), hardness, and 300% modulus (B).

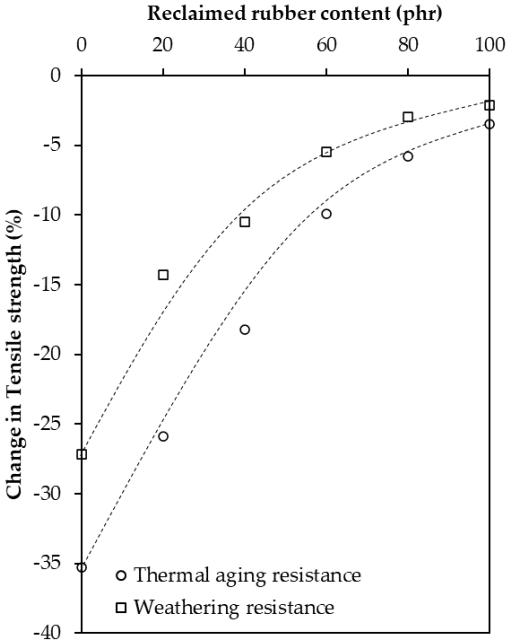

Figure 3. Effect of Reclaimed Rubber Content on the Aging Behavior of Vulcanized Rubber.

The aging behavior of vulcanized rubber blends was evaluated via accelerated thermal and UV aging tests (Figure 3). The percentage decrease in tensile strength due to aging was found to diminish as reclaimed rubber content increased, indicating improved resistance to aging. This can be explained by the degradation mechanism: aging typically involves oxidative cleavage of double bonds, resulting in a reduction of tensile strength. Reclaimed rubber, derived from used tires, contains residual anti-aging agents and a reduced concentration of double bonds. Together, these factors enhance aging resistance and potentially reduce the need for added antioxidants in future product formulations [9].

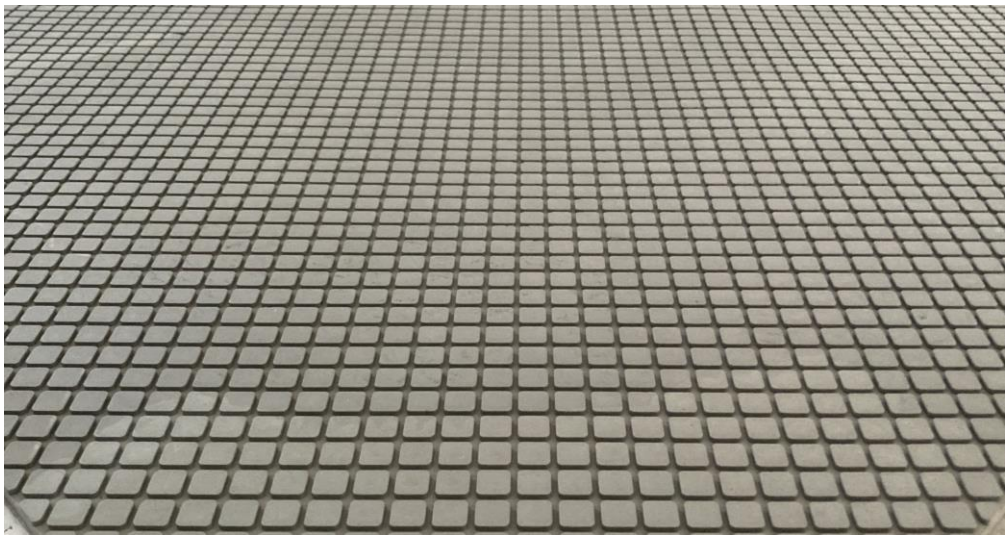

Figure 4. Molding process of outdoor rubber walkway products.

Figure 5. Nai Susn Sri Café has outdoor walkway rubber flooring installed.

Based on the study of the effects of reclaimed rubber content on the mechanical properties and resistance to degradation from both heat and UV radiation, the results were used to develop an outdoor walkway rubber flooring product. The selected rubber formulation contained 100 phr of reclaimed rubber. Although the tensile strength test results were quite low, the material remained sufficiently strong for practical use. At the same time, excellent resistance to degradation is essential for outdoor walkway applications. The molded product was a rubber tile with dimensions of 1 square meter and a thickness of 0.06 meters. Its surface featured a lozenge-shaped pattern to provide slip resistance. The molding process was carried out at a

temperature of 170°C for 8 minutes. The resulting product is shown in Figure 4. The outdoor walkway rubber flooring was then tested in a real-life application at "**Nai Susn Sri**," a cozy, homemade-style café located in Srinakarin District, Phatthalung Province. The café features a spacious area with various engaging activities for customers, as well as beautiful photo spots. After installing the rubber walkway around the café, the atmosphere transformed, as shown in Figure 5. The design of the walkway complements the café's overall aesthetic very well. When gathering feedback from users—primarily the café's customers—most expressed high satisfaction with their first impression of the rubber flooring, noting its soft and comfortable feel underfoot throughout the path. Families, particularly those with elderly mothers or young children, appreciated the walkway even more, as it made them feel safer while walking around the premises. Using reclaimed rubber can lower production costs by approximately 30% because it replaces a portion of expensive virgin rubber with a material that has already been processed, thereby reducing both raw material and energy expenses. At the same time, it supports sustainability by diverting end-of-life tires and other rubber waste from landfills and incineration, conserving natural resources, and cutting greenhouse-gas emissions associated with harvesting latex and manufacturing new rubber. This combination of significant cost savings and reduced environmental impact makes reclaimed rubber an attractive option for manufacturers seeking both economic and ecological benefits.

4. Conclusions

This study successfully developed outdoor walkway flooring from natural rubber/reclaimed rubber blends, demonstrating that reclaimed rubber content significantly influences both mechanical properties and aging resistance. Experimental results showed that increasing the reclaimed rubber content from 0 to 100 phr progressively reduced tensile strength and elongation at break, due to the shortened molecular chains resulting from the recycling process. Conversely, hardness and 300% modulus exhibited slight increases attributed to residual cross-links and elevated filler concentrations inherent in reclaimed rubber. Accelerated aging tests revealed that reclaimed rubber incorporation markedly enhanced environmental resistance. The percentage decrease in tensile strength after thermal aging (100°C, 22 hours) and UV aging (0.89 W/m² at 340 nm, 168 hours) diminished progressively with increasing reclaimed rubber content. This superior aging resistance stems from the presence of residual anti-aging agents and reduced concentrations of double bonds in reclaimed rubber. Based on a comprehensive evaluation, the formulation containing 100 parts per hundred rubber (phr) of reclaimed rubber was selected for commercial production. Although the tensile strength was lower than that of virgin natural rubber formulations, the material maintained adequate mechanical performance for practical applications while demonstrating exceptional degradation resistance, essential for outdoor environments. Commercial implementation at Nai Susn Sri Café in Phatthalung Province validated the product's performance, with users reporting high satisfaction regarding comfort and safety, particularly among elderly customers and families with young children. The technology transfer to community entrepreneurs generated measurable socioeconomic benefits, including approximately 30% production cost reduction, increased customer visits, enhanced local product sales, and improved accessibility for elderly and disabled individuals. These outcomes align with UN Sustainable Development Goals 1 and 3, contributing to poverty alleviation and promoting well-being across all age groups.

5. Acknowledgements

The authors would like to thank the Program Management Unit on Area-Based Development (PMU A) for research funding support in the Phatthalung Model: Research and Social Innovation for Personalized Poverty Alleviation (2024), Project ID 195144. The Center of Rubber Technology for Community (CRTC), Faculty of Engineering, Thaksin University, is also acknowledged for providing the space and machinery necessary for research. Moreover, AI-assisted writing tools were used in preparing the manuscript.

Author Contributions: Conceptualization, T.S., W.N., and A.A.; methodology, W.N., P.T., P.S. and S.S.; validation, W.N., T.S., P.T., P.S. and S.S.; formal analysis, W.N., P.T., P.S. and S.S.; investigation, all authors; resources, T.S., W.N. and A.A.; data curation, all authors; writing—original draft preparation, T.S. and W.N.; writing—review and editing, all authors; visualization, T.S. and W.N.; supervision, W.N.; project administration, T.S. and W.N.; funding acquisition, T.S., W.N., and A.A.

Funding: This research was funded by Program Management Unit on Area-Based Development (PMU A) in the Phatthalung Model: Research and Social Innovation for Personalized Poverty Alleviation (2024), Project ID 195144. The Article Processing Charges (APC) were funded by Sub-project: Establishment of Social Safety Network to Enhance the Inclusive Economy Model Based on Highland-Lowland Ecological System in Phatthalung Province.

Conflicts of Interest: The authors declare that they have no known competing financial interests or personal relationships that could have appeared to influence the work reported in this paper.

References

[1] Mark, J. E. *Physical Properties of Polymers Handbook*; Springer: New York, **2007**.

[2] Puskas, J. E.; Chiang, K.; Barkakaty, B. Natural rubber (NR) biosynthesis: perspectives from polymer chemistry. In *Chemistry, Manufacture and Applications of Natural Rubber*; K. N. G. S. Ooi, Ed.; Woodhead Publishing, **2014**; pp 30–67. https://doi.org/10.1533/9780857096913.1.30

[3] Tessanan, W.; Chanthateyanonth, R.; Yamaguchi, M.; Phinyocheep, P. Improvement of mechanical and impact performance of poly (lactic acid) by renewable modified natural rubber. *J. Clean. Prod.* **2020**, *276*, 123800. https://doi.org/10.1016/j.jclepro.2020.123800

[4] Saengdee, L.; Phinyocheep, P.; Daniel, P. Chemical modification of natural rubber in latex stage for improved thermal, oil, ozone and mechanical properties. *J. Polym. Res.* **2020**, *27*(275), 1–13. https://doi.org/10.1007/s10965-020-02246-7

[5] Tessanan, W.; Ratvijitvech, T.; Thanawan, S.; Amornsakchai, T.; Phinyocheep, P. Development of waterborne epoxy-based resin incorporated with modified natural rubber latex for coating application. *Sci. Rep.* **2024**, *14* (1), 26603. https://doi.org/10.1038/s41598-024-77990-7

[6] Mao, Z.; Wang, W.; Mao, G. Improving the Thermal Aging Resistance of γ-Vulcanized Polybutadiene Rubber (BR)/Nature Rubber (NR) Blends with Sulfur Added. *Adv. Mater. Sci. Eng.* **2021**, *2021*, 5782539. https://doi.org/10.1155/2021/5782539

[7] Ren, T.; Song, P.; Yang, W.; Formela, K.; Wang, S. Reinforcing and plasticizing effects of reclaimed rubber on the vulcanization and properties of natural rubber. *J. Appl. Polym. Sci.* **2023**, *140*(10), e53580. https://doi.org/10.1002/app.53580

[8] Shokoohi, S.; Naderi, G. Natural rubber/natural rubber reclaim nanocomposites: Role of functional nanoparticles, mixing sequences and coupling agents. *Polyolefins J.* **2021**, *8*(2), 115–122. https://doi.org/10.22063/poj.2021.2893.1182

[9] Zhang, Y.; Zhang, Z.; Wemyss, A. M.; Wan, C.; Liu, Y.; Song, P.; Wang, S. Effective thermal-oxidative reclamation of waste tire rubbers for producing high-performance rubber composites. *ACS Sustainable Chem. Eng.* **2020**, *8*(24), 9079–9087. https://doi.org/10.1021/acssuschemeng.0c02292

[10] Singh, P.; Singh, D. N. Polymer composites from waste plastics and reclaimed rubber from tires for sustainable development. *J. Appl. Polym. Sci.* **2024**, *141*(46), e56244. https://doi.org/10.1002/app.56244

[11] Naebpetch, W.; Junhasavasdikul, B.; Saetung, A.; Tulyapitak, T.; Nithi-Uthai, N. Influence of filler type and loading on cure characteristics and vulcanisate properties of SBR compounds with a novel mixed vulcanisation system. *Plast. Rubber Compos.* **2017**, *46*(3), 137–145. https://doi.org/10.1080/14658011.2017.1299419.

ASEAN
Journal of Scientific and Technological Reports
Online ISSN:2773-8752

Academic article

Enhancement of Bioactive Compounds and Nutrient Content in Rosemary (*Salvia rosmarinus*) Using Nano-Magnesium and NPK Fertilization: A GC-MS Analysis

Dhafir Abed Alkhadim Jameel Altaweel[1*]

[1] Department of Biology, College of Education, University of Al-Qadisiyah, Iraq.
[*] Correspondence:dhafir.altaweel@qu.edu.iq; (D.A.J. Altaweel)

Citation:
Altaweel, J.A.A.D. Enhancement of bioactive compounds and nutrient content in rosemary (*Salvia rosmarinus*) using nano-magnesium and NPK fertilization: A GC-MS analysin. *ASEAN J. Sci. Tech. Report.* **2025**, 28(6), e261168. https://doi.org/10.55164/ajstr.v28i6.261168

Article history:
Received: September 6, 2025
Revised: September 24, 2025
Accepted: September 27, 2025
Available online: October 24, 2025

Abstract: This study investigated the effects of nano-magnesium and unbalanced NPK fertilizers on nutrient content and bioactive compounds in rosemary (Salvia rosmarinus) during the 2021-2022 growing season in Al-Qadisiyah, Iraq. Nine treatments were applied: control, nano-magnesium (1 and 2 g/L), NPK (1 and 2 g/L), and their combinations, with three replications each. Foliar applications were administered to six-week-old seedlings, with harvest occurring 30 days post-treatment. Nutrient analysis revealed that the nano-magnesium (1 g/L) + NPK (2 g/L) combination yielded the highest nitrogen content (1.96%), while nano-magnesium alone (2 g/L) produced the lowest (0.98%). Phosphorus peaked at 0.277% with nano-magnesium (2 g/L) versus 0.100% in controls. Potassium reached 1.211% with combined nano-magnesium + NPK (both 1 g/L), while NPK alone (2 g/L) showed the minimum (0.588%). Total lipids increased from 0.852% (control) to 1.038% (nano-magnesium + NPK, both 2 g/L). Carbohydrate content varied dramatically, with the highest value of 13.77% (nano-magnesium 2 g/L + NPK 1 g/L) contrasting sharply with 4.675% (both fertilizers at 2 g/L). GC-MS profiling revealed substantial variation in bioactive compounds: control plants contained 16 compounds, while treatments ranged from 2 compounds (nano-magnesium at 2 g/L alone) to 36 compounds (NPK at 1 g/L + nano-magnesium at 2 g/L). n-hexadecanoic acid emerged as the predominant compound across treatments, ranging from 3.26% to 35.17%. These findings demonstrate that nano-magnesium and NPK fertilization significantly enhance the nutritional and phytochemical profiles of rosemary, with combined applications showing synergistic effects on the diversity of bioactive compounds.

Keywords: *Salvia rosmarinus*; nano-magnesium; NPK fertilizer; GC-MS analysis; n-hexadecanoic acid

1. Introduction

Rosemary (*Salvia rosmarinus*), formerly classified as *Rosmarinus officinalis*, is an evergreen, aromatic shrub belonging to the Lamiaceae family, characterized by needle-like leaves and bilaterally symmetrical flowers ranging from light blue to white [1]. This Mediterranean native species thrives in dry, rocky environments and has adapted to various soil types, though it shows a preference for clay soils [2]. The plant exhibits remarkable morphological diversity, leading botanists to classify it into three distinct species: *Salvia rosmarinus*, *Salvia jordanii*, and *Salvia granatensis* [3]. The therapeutic and commercial value of rosemary stems from its rich phytochemical profile.

Essential oils extracted from rosemary have been shown to possess documented antibacterial, antifungal, antiviral, anti-inflammatory, antitumor, anticoagulant, and antioxidant properties [4,5]. These characteristics have facilitated widespread applications in food preservation, cosmetic formulations, and pharmaceutical preparations [6]. Phytochemical analyses have identified key bioactive molecules, including flavonoids such as eriocitrin, luteolin, hesperidin, diosmin, and various glucosides, distributed throughout the leaves, flowers, and roots during different developmental stages [7].

Agricultural nanotechnology represents a paradigm shift in crop production systems, offering solutions to enhance yield while reducing synthetic chemical inputs [8,9]. Nanofertilizers exhibit superior solubility and distribution characteristics compared to conventional fertilizers, thereby minimizing nutrient mineralization and enhancing bioavailability [10]. These materials, typically ranging from 1 to 100 nanometers in diameter, exhibit enhanced penetration through plant surfaces due to their high surface area-to-volume ratio [11]. Magnesium plays crucial roles in photosynthesis as the central atom in chlorophyll molecules, in the formation of ATP, in enzyme activation, and in protein synthesis [12]. In higher plants, magnesium concentrations typically range from 80 μmol/g dry weight, constituting 0.5-3% of total dry matter [13,14]. A magnesium deficiency disrupts protein synthesis and reduces chlorophyll content, ultimately affecting photosynthetic efficiency [15,16]. Nitrogen, phosphorus, and potassium (NPK) represent essential macronutrients for plant growth and development [17]. Global NPK consumption exceeds 21.6 million tons annually, with China alone accounting for a substantial portion of this usage [18]. Foliar application of NPK fertilizers can effectively address nutrient deficiencies, particularly when soil conditions limit nutrient availability due to pH, moisture, or competition with other ions [19, 20, 21].

Despite extensive research on conventional fertilization strategies for medicinal plants, limited information exists regarding the synergistic effects of nano-magnesium and NPK fertilizers on the bioactive compound profiles of rosemary. This study aimed to evaluate the individual and combined effects of nano-magnesium and unbalanced NPK fertilizers at varying concentrations on the nutrient content and phytochemical composition of rosemary plants, using comprehensive analytical techniques, including GC-MS profiling.

2. Materials and Methods

2.1 Experimental Site and Design

This study was conducted in a private nursery in Al-Jamaa district, Al-Qadisiyah Governorate, Iraq (31°56'N, 44°55'E) during the 2021-2022 agricultural season. The experiment was conducted in a completely randomized design with nine treatments and three replications per treatment, resulting in a total of 27 experimental units. The soil's physical and chemical properties were analyzed prior to planting, according to established methods [22]. The effect of foliar spraying of magnesium nano-fertilizer with its recommended and half-recommended concentrations, and unbalanced NPK fertilizer with its recommended and half-recommended concentrations as well, in addition to the mixture between them, on some characteristics. Botanical and chemical properties of the rosemary plant. Rosemary seedlings, at the age of six weeks, were transferred to poles that had been previously prepared on October 15, 2021. The plants were sprayed with different concentrations of the fertilizers used in this study on January 15, 2022. The date of harvest and taking the necessary measurements for the study was February 15, 2022. These piles were filled with a mixed soil of predetermined physical and chemical characteristics before planting, with the addition of Dutch peat moss at a 1:2 mixing ratio.

2.2 Plant Material and Treatment Application

Six-week-old rosemary (*Salvia rosmarinus*) seedlings were transplanted into prepared pots on October 15, 2021. The growing medium consisted of local soil mixed with Dutch peat moss at a 2:1 ratio. The treatments included: (1) Control (distilled water); (2) Nano-magnesium 1 g/L; (3) Nano-magnesium 2 g/L; (4) NPK 1 g/L; (5) NPK 2 g/L; (6) Nano-magnesium 1 g/L + NPK 1 g/L; (7) Nano-magnesium 1 g/L + NPK 2 g/L; (8) Nano-magnesium 2 g/L + NPK 1 g/L; (9) Nano-magnesium 2 g/L + NPK 2 g/L. Foliar applications were administered on January 15, 2022, using a hand sprayer until complete leaf coverage was achieved. Plants were harvested on February 15, 2022, for analysis.

2.3 Nutrient Analysis

Total nitrogen was quantified using the Kjeldahl method [23]. Digested samples (10 mL) were mixed with 35% NaOH (10 mL) in a Macro Kjeldahl distillation apparatus (Germany). Ammonia was distilled for 30-40 minutes into 4% H_3BO_3 (50 mL) and titrated with 0.05 M H_2SO_4. Nitrogen percentage was calculated using:

N (%) = (Acid volume × Acid normality × 14) / (1000 × Sample weight) × 100

Phosphorus content was determined using the ascorbic acid-ammonium molybdate method [24]. Digested samples (10 mL) were diluted to 50 mL. An aliquot (10 mL) was mixed with ascorbic acid (0.1 g) and ammonium molybdate reagent (4 mL), heated until a blue color developed, and measured spectrophotometrically at 620 nm. A standard curve was prepared using KH_2PO_4 solutions (1-6 mg/L). Potassium was measured using flame photometry (ELICO model CL 361, India) following established protocols [25].

2.4 Biochemical Analysis

Total lipids were extracted and quantified according to the sulfuric acid-phosphovanillin method [26]. Fresh samples (1 g) were homogenized in extraction solvent (10 mL) for 10 minutes, followed by centrifugation at 10,000 rpm for 10 minutes. The supernatant was stored at 2-8°C for 48 hours. A sample extract (10 μL) was mixed with concentrated H_2SO_4 (1 mL), incubated at 100°C for 20 minutes, cooled, and then mixed with phosphovanillin reagent (2 mL). Absorbance was measured at 530 nm after 15 minutes. Total carbohydrates were determined using the phenol-sulfuric acid method [27]. This colorimetric method provides a reliable means of quantifying the total carbohydrate content in plant tissues.

2.5 GC-MS Analysis of Bioactive Compounds

Bioactive compound extraction and analysis were performed using modified protocols [28]. Dried plant material (1 g) was extracted with 99% methanol (10 mL) with continuous stirring for 5 minutes, then kept in darkness for 6 hours at room temperature. The extract was filtered through 0.45 μm syringe filters and concentrated with hexane (1 mL). GC-MS analysis was performed on an HP-5MS capillary column (30 m × 0.25 mm i.d., 0.25 μm film thickness) with helium carrier gas at 1.0 mL/min. Injection volume was 1 μL in splitless mode. Temperature programming: initial 50°C (2 min), ramped at 3°C/min to 200°C, then 10°C/min to 280°C (held 10 min). Injector, interface, and ion source temperatures were 250°C, 280°C, and 230°C, respectively. Mass spectra were recorded at 70 eV, scanning from 40 to 450 m/z. Compounds were identified by comparing them with NIST and Wiley libraries, and retention indices were determined based on n-alkane standards [29].

2.6 Statistical Analysis

The data were subjected to analysis of variance (ANOVA) using appropriate statistical software. Means were compared using the least significant difference (LSD) test at $P \leq 0.05$ significance level.

3. Results and Discussion

3.1 Effects on Macronutrient Content

Nitrogen concentration in rosemary plants exhibited substantial variation across treatments, ranging from 0.98% to 1.96% (Table 1). The combined treatment of nano-magnesium (1 g/L) with NPK (2 g/L) achieved the highest nitrogen accumulation (1.96%), followed by NPK (2 g/L) alone (1.82%) and the combination of nano-magnesium (2 g/L) with NPK (1 g/L) at 1.75%. Control plants maintained intermediate nitrogen levels at 1.42% (Table 1). Notably, nano-magnesium treatments alone showed contrasting effects: the 1 g/L concentration enhanced nitrogen to 1.56% (9.9% increase over control), while 2 g/L significantly reduced it to 0.98% (31% decrease) (Figure 1). This concentration-dependent response aligns with studies demonstrating that excessive nano-particle concentrations can disrupt nitrogen metabolism through interference with nitrate reductase activity [30,31]. Phosphorus accumulation demonstrated a clear dose-response relationship with nano-magnesium application. The 2 g/L nano-magnesium treatment resulted in the maximum phosphorus content (0.277%), representing a 177% increase over the control plants (0.100%). The 1 g/L concentration also enhanced phosphorus uptake to 0.234% (134% increase). NPK fertilization alone yielded moderate improvements, with 1 g/L and 2 g/L treatments resulting in 0.189% and 0.212% phosphorus, respectively. Combined treatments showed intermediate effects, with values ranging from 0.156% to 0.223%. These findings

correspond with reports that nano-formulations enhance phosphorus solubility and reduce fixation in soil-colloid complexes, thereby increasing bioavailability [32,33]. Potassium dynamics revealed complex interactions between treatments. The synergistic combination of nano-magnesium (1 g/L) with NPK (1 g/L) resulted in the highest potassium concentration (1.211%), a 102% increase over the control (0.599%). Individual nano-magnesium treatments at 1 g/L and 2 g/L resulted in 0.812% and 0.945% potassium, representing increases of 35.6% and 57.8%, respectively. Conversely, NPK (2 g/L) alone slightly reduced potassium to 0.588%, suggesting potential antagonistic effects at higher NPK concentrations. This phenomenon has been attributed to competitive inhibition between NH4+ and K+ ions for root uptake sites [34,35].

Table 1. Effects of nano-magnesium and NPK fertilization on macronutrient content and biochemical composition of rosemary (***Salvia rosmarinus***)

Treatment	N (%)	P (%)	K (%)	Total Lipids (%)	Total Carbohydrates (%)
Control	1.42 ± 0.08^{c}	0.100 ± 0.006^{f}	0.599 ± 0.021^{e}	0.852 ± 0.015^{f}	8.213 ± 0.32^{c}
Nano-Mg 1 g/L	1.56 ± 0.09^{b}	0.234 ± 0.011^{b}	0.812 ± 0.028^{c}	0.912 ± 0.018^{d}	6.892 ± 0.28^{d}
Nano-Mg 2 g/L	0.98 ± 0.06^{e}	0.277 ± 0.013^{a}	0.945 ± 0.031^{b}	0.967 ± 0.020^{c}	5.747 ± 0.24^{e}
NPK 1 g/L	1.67 ± 0.10^{b}	0.189 ± 0.009^{c}	0.734 ± 0.025^{d}	0.889 ± 0.017^{e}	5.438 ± 0.22^{ef}
NPK 2 g/L	1.82 ± 0.11^{a}	0.212 ± 0.010^{b}	0.588 ± 0.020^{e}	0.923 ± 0.019^{d}	5.174 ± 0.21^{f}
Nano-Mg 1 + NPK 1 g/L	1.48 ± 0.09^{c}	0.178 ± 0.008^{cd}	1.211 ± 0.038^{a}	0.934 ± 0.019^{d}	7.456 ± 0.30^{d}
Nano-Mg 1 + NPK 2 g/L	1.96 ± 0.12^{a}	0.156 ± 0.007^{de}	0.823 ± 0.029^{c}	0.978 ± 0.021^{bc}	6.234 ± 0.26^{e}
Nano-Mg 2 + NPK 1 g/L	1.75 ± 0.10^{ab}	0.223 ± 0.011^{b}	0.967 ± 0.032^{b}	0.989 ± 0.022^{b}	13.77 ± 0.48^{a}
Nano-Mg 2 + NPK 2 g/L	1.23 ± 0.08^{d}	0.167 ± 0.008^{d}	0.856 ± 0.030^{c}	1.038 ± 0.023^{a}	4.675 ± 0.19^{g}
LSD (0.05)	0.14	0.021	0.067	0.034	0.58

Values are means ± SE (n = 3). Different superscript letters within columns indicate significant differences at $P \leq 0.05$ according to the LSD test.

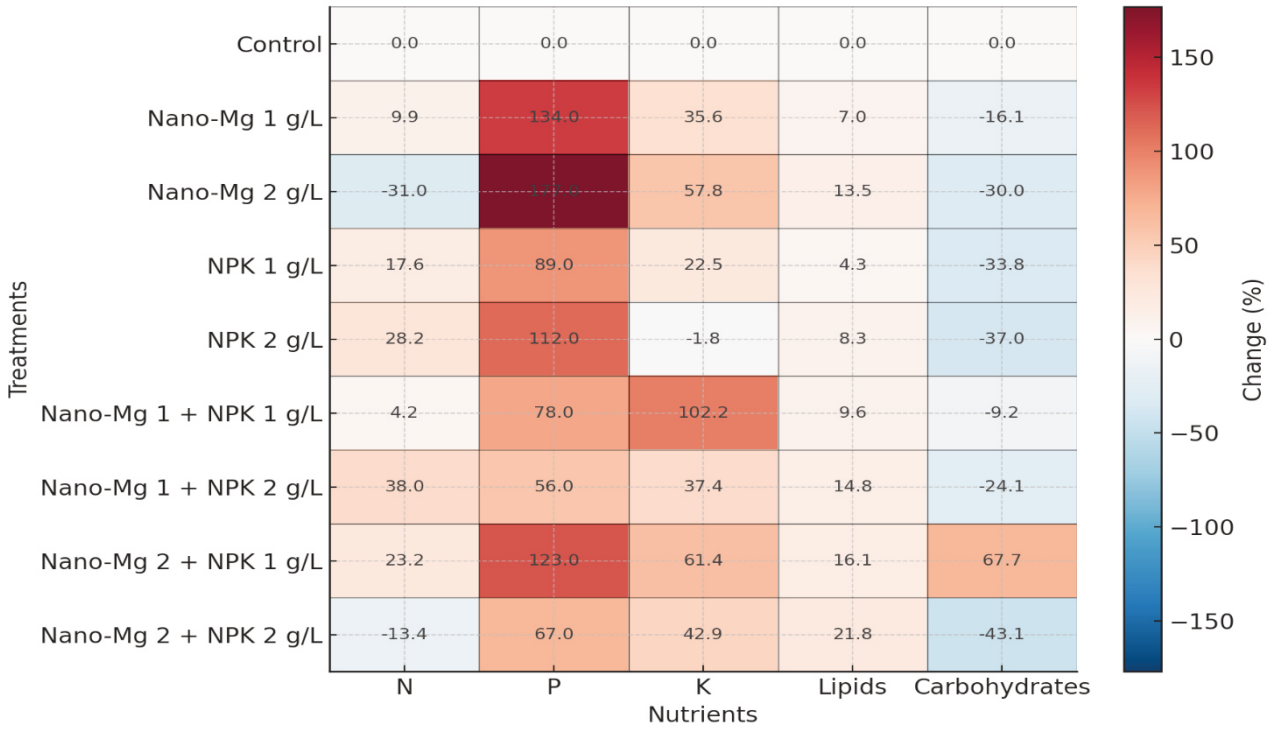

Figure 1. Heatmap visualization of nutrient responses to fertilization treatments

3.2 Biochemical Composition Changes

Lipid biosynthesis responded positively to most fertilization treatments, with content ranging from 0.852% in controls to 1.038% in plants receiving nano-magnesium (2 g/L) + NPK (2 g/L) (Table 2). Individual nano-magnesium treatments increased lipids to 0.912% (1 g/L) and 0.967% (2 g/L), representing 7.0% and 13.5% enhancements, respectively. NPK alone showed moderate effects, with 0.889% at 1 g/L and 0.923% at 2 g/L. The highest lipid accumulation in combined high-concentration treatments (a 21.8% increase) correlates with magnesium's role as a cofactor in acetyl-CoA carboxylase, the rate-limiting enzyme in fatty acid biosynthesis [36, 37]. Carbohydrate accumulation exhibited inverse relationships with fertilizer concentration, contrasting with other parameters. Control plants maintained 8.213% carbohydrates. Individual nano-magnesium treatments reduced carbohydrates to 6.892% (1 g/L) and 5.747% (2 g/L), representing decreases of 16.1% and 30.0% compared to the control. NPK treatments showed similar trends: 5.438% at 1 g/L and 5.174% at 2 g/L. Remarkably, the combination of nano-magnesium (2 g/L) with NPK (1 g/L) produced the highest carbohydrate content (13.77%), a 67.7% increase over the control. However, both fertilizers at 2 g/L resulted in the lowest value (4.675%), a 43.1% reduction (Table 3). This biphasic response suggests that moderate fertilization enhances carbohydrate storage, whereas excessive levels promote utilization for growth processes [38, 39].

Table 2. Biochemical composition changes in rosemary under different fertilization regimes

Treatment	Total Lipids (%)	Change vs Control (%)	Total Carbohydrates (%)	Change vs Control (%)	Lipid: Carbohydrate Ratio
Control	0.852 ± 0.015^{f}	—	8.213 ± 0.32^{c}	—	0.104
Nano-Mg 1 g/L	0.912 ± 0.018^{d}	+7.0	6.892 ± 0.28^{d}	-16.1	0.132
Nano-Mg 2 g/L	0.967 ± 0.020^{c}	+13.5	5.747 ± 0.24^{e}	-30.0	0.168
NPK 1 g/L	0.889 ± 0.017^{e}	+4.3	5.438 ± 0.22^{ef}	-33.8	0.163
NPK 2 g/L	0.923 ± 0.019^{d}	+8.3	5.174 ± 0.21^{f}	-37.0	0.178
Nano-Mg 1 + NPK 1 g/L	0.934 ± 0.019^{d}	+9.6	7.456 ± 0.30^{d}	-9.2	0.125
Nano-Mg 1 + NPK 2 g/L	0.978 ± 0.021^{bc}	+14.8	6.234 ± 0.26^{e}	-24.1	0.157
Nano-Mg 2 + NPK 1 g/L	0.989 ± 0.022^{b}	+16.1	13.77 ± 0.48^{a}	+67.7	0.072
Nano-Mg 2 + NPK 2 g/L	1.038 ± 0.023^{a}	+21.8	4.675 ± 0.19^{g}	-43.1	0.222

Values are means ± SE (n = 3). Different superscript letters indicate significant differences at $P \leq 0.05$.

Table 3. Carbon allocation patterns under different fertilization treatments

Treatment	Primary Metabolites (%)	Secondary Metabolites* (%)	Storage: Structural Ratio	Metabolic Efficiency Index**
Control	9.065	—	9.64	1.00
Nano-Mg 1 g/L	7.804	↓	7.56	0.86
Nano-Mg 2 g/L	6.714	↓↓	5.94	0.74
NPK 1 g/L	6.327	↑	6.12	0.70
NPK 2 g/L	6.097	↑	5.61	0.67
Combined (optimal)***	14.759	↑↑↑	13.93	1.63
Combined (high)****	5.713	↑↑	4.50	0.63

*Based on GC-MS compound diversity; **Normalized to control = 1.00; ***Nano-Mg 2 + NPK 1 g/L; ****Nano-Mg 2 + NPK 2 g/L

3.3 Detailed GC-MS Profile Analysis

Control plants exhibited a baseline metabolite profile of 16 bioactive compounds. n-hexadecanoic acid dominated at 24.30%, followed by 14-β-H-pregna (18.45%), 9-Octadecenoic acid (12.78%), and Oleic acid (8.92%) (Table 4). Minor constituents included Heptacos-1-ene (5.34%), Triacontane (4.67%), 3-Methyldotriacontane (3.89%), and 1-Tetracosene (0.35%). This profile represents the inherent metabolic capacity of unfertilized

rosemary under experimental conditions [40]. Nano-magnesium (1 g/L) drastically simplified the metabolite profile to four compounds: 9-Tricosene emerged as the principal constituent (43.18%), followed by 2-Diazo-1,3-di(2'-naphthyl) propane-1,3-dione (35.41%), Cyclotetracosane (18.16%), and n-Hexadecanoic acid reduced to 3.26%. This 75% reduction in compound diversity suggests metabolic streamlining under mild nano-particle stress [41]. At 2 g/L, nano-magnesium further reduced diversity to only two compounds: Z-12-Pentacosene (64.83%) and n-Hexadecanoic acid (35.17%). The emergence of Z-12-Pentacosene, absent in all other treatments, indicates activation of specific biosynthetic pathways possibly related to stress response mechanisms [42,43]. NPK (1 g/L) substantially enhanced metabolite diversity to 27 compounds. n-hexadecanoic acid remained predominant (17.37%), accompanied by newly synthesized compounds including endo-Borneol (0.88%), various long-chain alkenes (1-Hexacosene: 3.45%, 9-Hexacosene: 2.89%), and complex terpenoids. Eight compounds overlapped with the controls, suggesting an enhancement rather than a disruption of basal metabolism [44]. NPK (2 g/L) maintained high diversity with 24 compounds. Pentacos-1-ene became the principal constituent (24.45%), while n-Hexadecanoic acid decreased to 13.76%. Unique compounds included 2-Methylhentriacontane (1.08%) and various branched-chain hydrocarbons, indicating altered lipid metabolism pathways [45]. The combination of NPK (1 g/L) with nano-magnesium (1 g/L) yielded 29 distinct compounds. n-hexadecanoic acid (9.29%) remained significant, while 14-β-H-pregna appeared twice with different retention times (2.71% and 2.90%), suggesting structural isomers. Hexanedioic acid bis(2-ethylhexyl ester) (4.56%) and Heptacosane (0.89%) represented new biosynthetic products [46]. NPK (2 g/L) + nano-magnesium (1 g/L) produced 27 compounds with n-Hexadecanoic acid at 10.85%, endo-Borneol at 0.86%, and enhanced terpenoid diversity. The presence of both volatile (endo-Borneol) and non-volatile compounds suggests activation of multiple biosynthetic pathways [47]. The NPK (1 g/L) + nano-magnesium (2 g/L) combination maximized compound diversity, resulting in 36 metabolites. Octadec-9-enoic acid (6.88%) and n-Hexadecanoic acid (6.94%) showed similar abundances. Novel compounds included Neophytadiene (0.68%), associated with chlorophyll degradation, and Hexacosane-1-iodo (0.68%), indicating halogenation reactions [48, 49]. NPK (2 g/L) + nano-magnesium (2 g/L) maintained high diversity with 28 compounds. n-Hexadecanoic acid (9.25%) and 14-β-H-pregna (2.11%) remained consistent markers, while Tetracosane appeared at the lowest concentration (0.60%) [50].

3.4 Metabolic Pathway Implications

The observed metabolite profiles suggest differential regulation of biosynthetic pathways. The predominance of fatty acids (C16-C30) across treatments indicates active lipid metabolism (Figure 2), which is essential for maintaining membrane integrity and signaling [51]. The presence of terpenoids, such as endo-Borneol, in NPK treatments suggests enhanced methylerythritol phosphate (MEP) pathway activity, which is responsible for monoterpene biosynthesis [52]. The reduction in metabolite diversity observed with nano-magnesium alone, in contrast to the enhancement in combined treatments, supports the hypothesis of hormetic responses to nanoparticles. Low-level stress may prime defensive pathways, while optimal nutrition enables expression of full metabolic potential [53,54]. These findings demonstrate that targeted fertilization can manipulate both nutritional and phytochemical profiles of rosemary. The 102% increase in potassium with combined nano-magnesium (1 g/L) + NPK (1 g/L) has implications for osmotic regulation and drought tolerance [55]. The variable n-hexadecanoic acid content (3.26-35.17%) across treatments presents opportunities for producing rosemary with specific antimicrobial properties suitable for pharmaceutical applications [56]. The inverse relationship between carbohydrate storage and fertilizer concentration suggests that timing is crucial for optimal harvest. Lower fertilizer rates may be preferable when targeting carbohydrate-derived products, while higher rates optimize lipid and specialized metabolite production [57]. The maximum compound diversity (36 metabolites) achieved with NPK (1 g/L) and nano-magnesium (2 g/L) represents optimal conditions for producing chemically complex essential oils, valued in the aromatherapy and perfumery industries [58].

Table 4. Comprehensive GC-MS profile of bioactive compounds in rosemary under different fertilization treatments

Treatment	Total Compounds	Major Compound (%)	n-Hexadecanoic Acid (%)	Unique Compounds*	Shannon Diversity Index**	Compound Classes***
Control	16	n-Hexadecanoic acid (24.30)	24.30	—	2.48	FA(7), HC(4), ST(3), OT(2)
Nano-Mg 1 g/L	4	9-Tricosene (43.18)	3.26	Z-12-Pentacosene	1.24	FA(1), HC(2), OT(1)
Nano-Mg 2 g/L	2	Z-12-Pentacosene (64.83)	35.17	Z-12-Pentacosene	0.66	FA(1), HC(1)
NPK 1 g/L	27	n-Hexadecanoic acid (17.37)	17.37	endo-Borneol, 15 others	2.94	FA(9), HC(8), TP(5), ST(3), OT(2)
NPK 2 g/L	24	Pentacos-1-ene (24.45)	13.76	2-Methylhentriacontane, 14 others	2.87	FA(8), HC(10), ST(3), OT(3)
Nano-Mg 1 + NPK 1 g/L	29	n-Hexadecanoic acid (9.29)	9.29	Hexanedioic acid ester, 16 others	3.12	FA(10), HC(9), ST(4), ES(3), OT(3)
Nano-Mg 1 + NPK 2 g/L	27	n-Hexadecanoic acid (10.85)	10.85	15 unique	3.01	FA(9), HC(8), TP(4), ST(3), OT(3)
Nano-Mg 2 + NPK 1 g/L	36	Octadec-9-enoic acid (6.88)	6.94	Neophytadiene, Hexacosane-1-iodo, 22 others	3.43	FA(12), HC(11), TP(5), ST(4), ES(2), OT(2)
Nano-Mg 2 + NPK 2 g/L	28	n-Hexadecanoic acid (9.25)	9.25	Tetracosane, 17 others	3.08	FA(10), HC(9), ST(4), TP(3), OT(2)

*Compounds not found in control; **H' = -Σ (pi × ln pi); ***FA: Fatty acids, HC: Hydrocarbons, TP: Terpenoids, ST: Steroids, ES: Esters, OT: Others

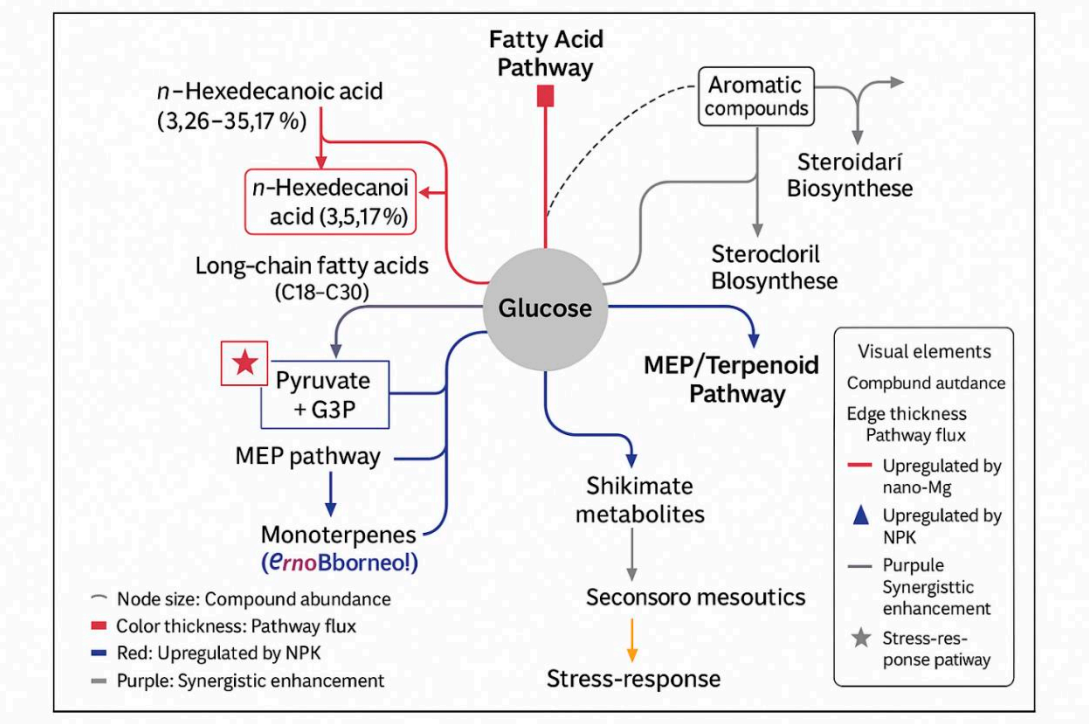

Figure 2. Metabolic pathway network diagram showing fertilization effects on biosynthetic routes

4. Conclusions

This study demonstrated that nano-magnesium and unbalanced NPK fertilizers, both individually and in combination, significantly alter the nutritional and phytochemical profiles of rosemary (*Salvia rosmarinus*). The most striking finding was the concentration-dependent and treatment-specific responses across all measured parameters, highlighting the complex nature of plant responses to nano-fertilization. The combined application of nano-magnesium (1 g/L) with NPK (2 g/L) optimized nitrogen accumulation (1.96%), while nano-magnesium alone at 2 g/L maximized phosphorus content (0.277%). The synergistic combination of both fertilizers at 1 g/L each produced the highest potassium concentration (1.211%), demonstrating that optimal nutrient accumulation requires balanced fertilization rather than maximum application rates. The inverse relationship observed between lipid and carbohydrate accumulation, particularly the 67.7% increase in carbohydrates with nano-magnesium (2 g/L) + NPK (1 g/L) versus the 43.1% decrease with both at 2 g/L, indicates fundamental shifts in carbon allocation patterns under different fertilization regimes. GC-MS profiling revealed that metabolite diversity ranged dramatically from 2 compounds (nano-magnesium 2 g/L alone) to 36 compounds (NPK 1 g/L + nano-magnesium 2 g/L), suggesting that combined treatments activate multiple biosynthetic pathways simultaneously. The consistent presence of n-hexadecanoic acid across treatments, albeit at varying concentrations from 3.26% to 35.17%, establishes this compound as a potential biomarker for assessing the effects of fertilization on rosemary quality. From a practical perspective, these findings suggest that nano-magnesium at 1 g/L, combined with NPK at 1-2 g/L, represents the optimal fertilization strategy for enhancing both nutritional content and bioactive compound diversity in rosemary cultivation. The dramatic reduction in metabolite diversity with nano-magnesium alone at 2 g/L warns against excessive nano-fertilizer application, which may induce stress responses rather than beneficial effects.

5. Acknowledgments

I am grateful to the University of Al-Qadisiyah, College of Education, Department of Biology, for the academic support and facilities essential to conducting this study.

Author Contributions: Conceptualization, D.A.A.J. A.; methodology, D.A.A.J. A.; software, D.A.A.J. A.; validation, D.A.A.J.A.; formal analysis, D.A.A.J.A.; investigation, D.A.A.J. A.; resources, D.A.A.J. A.; data curation, D.A.A.J.A.; writing original draft preparation, D.A.A.J. A.; writing review and editing, D.A.A.J. A.; visualization, D.A.A.; supervision, D.A.A.J. A.; project administration, D.A.A.J. A.; funding acquisition, D.A.A.J. A.; D.A.A.J. A. have read and agreed to the published version of the manuscript.

Funding: Not Applicable.

Conflicts of Interest: The authors declare that they have no conflicts of interest.

References

[1] Arnold, N.; Valentini, G.; Bellomaria, B.; Hocine, L. Comparative study of the essential oils from Rosmarinus eriocalyx Jordan & Fourr. from Algeria and R. officinalis L. from other countries. *J. Essent. Oil Res.* **1997**, *9*, 167–175. https://doi.org/10.1080/10412905.1997.9699454

[2] Ribeiro-Santos, R.; Carvalho-Costa, D.; Cavaleiro, C.; Costa, H.S.; Albuquerque, T.G.; Castilho, M.C.; Sanches-Silva, A. A novel insight on an ancient aromatic plant: The rosemary (*Rosmarinus officinalis* L.). *Trends Food Sci. Technol.* **2015**, *45*, 355–368. https://doi.org/10.1016/j.tifs.2015.07.015

[3] Benaim, G.; Sanders, J.M.; Garcia-Marchán, Y.; Colina, C.; Lira, R.; Caldera, A.R.; Urbina, J.A. Amiodarone has intrinsic anti-trypanosoma cruzi activity and acts synergistically with posaconazole. *J. Med. Chem.* **2006**, *49*, 892–899. https://doi.org/10.1021/jm050691f

[4] Begum, A.; Sandhya, S.; Vinod, K.R.; Reddy, S.; Banji, D. An in-depth review on the medicinal flora Rosmarinus officinalis (Lamiaceae). *Acta Sci. Pol. Technol. Aliment.* **2013**, *12*, 61–74.

[5] Ojeda-Sana, A.M.; van Baren, C.M.; Elechosa, M.A.; Juárez, M.A.; Moreno, S. New insights into antibacterial and antioxidant activities of rosemary essential oils and their main components. *Food Control* **2013**, *31*, 189–195. https://doi.org/10.1016/j.foodcont.2012.09.022

[6] Stefanovits-Bányai, É. Antioxidant effect of various rosemary (*Rosmarinus officinalis* L.) clones. *Acta Biol. Szeged.* **2003**, *47*, 111–113.

[7] Del Baño, M.J.; Lorente, J.; Castillo, J.; Benavente-García, O.; Marín, M.P.; Del Río, J.A.; Ibarra, I. Flavonoid distribution during the development of leaves, flowers, stems, and roots of Rosmarinus officinalis. Postulation of a biosynthetic pathway. *J. Agric. Food Chem.* **2004**, *52*, 4987–4992. https://doi.org/10.1021/jf040078p

[8] Mousavi, S.R.; Rezaei, M. Nanotechnology in agriculture and food production. *J. Appl. Environ. Biol. Sci.* **2011**, *1*, 414–419.

[9] Kumar, K. Nanobiotechnology and its implementation in agriculture. *J. Adv. Bot. Zool.* **2013**, *1*, 1–3.

[10] Naderi, M.R.; Danesh-Shahraki, A. Nanofertilizers and their roles in sustainable agriculture. *Int. J. Agric. Crop Sci.* **2013**, *5*, 2229–2232.

[11] Mohamed, S.; El-Ghait, E.M.A.; El Shayeb, N.S.; SA, G.Y.; Shahin, A.A. Effect of some fertilizers on improving growth and oil productivity of basil (*Ocimum basilicum*, L.) cv. Genovese plant. *Egypt. J. Appl. Sci.* **2015**, *30*, 384–399.

[12] Marschner, H. *Mineral Nutrition of Higher Plants*, 2nd ed.; Academic Press: London, UK, **1995**.

[13] Beale, S.I. Enzymes of chlorophyll biosynthesis. *Photosynth. Res.* **1999**, *60*, 43–73. https://doi.org/10.1023/A:1006297731456

[14] Stern, K.R.; Janseky, S.; Bidlack, J.E. *Introduction to Plant Biology*; McGraw-Hill Higher Education: New York, NY, USA, **2003**.

[15] Delfani, M.; Baradarn Firouzabadi, M.; Farrokhi, N.; Makarian, H. Some physiological responses of black-eyed pea to iron and magnesium nanofertilizers. *Commun. Soil Sci. Plant Anal.* **2014**, *45*, 530–540. https://doi.org/10.1080/00103624.2013.863911

[16] Singh, M.D.; Gautam, C.; Patidar, O.P.; Meena, H.M.; Prakasha, G.; Vishwajith. Nano-fertilizers is a new way to increase nutrients use efficiency in crop production. *Int. J. Agric. Sci.* **2017**, *9*, 3831–3833.

[17] Sadras, V.O. The N:P stoichiometry of cereal, grain legume and oilseed crops. *Field Crops Res.* **2006**, *95*, 13–29. https://doi.org/10.1016/j.fcr.2005.01.020
[18] Liu, Y.; Pan, X.; Li, J. A 1961–2010 record of fertilizer use, pesticide application and cereal yields: A review. *Agron. Sustain. Dev.* **2015**, *35*, 83–93. https://doi.org/10.1007/s13593-014-0259-9
[19] Ling, F.; Silberbush, M. Response of maize to foliar vs. soil application of nitrogen–phosphorus–potassium fertilizers. *J. Plant Nutr.* **2002**, *25*, 2333–2342. https://doi.org/10.1081/PLN-120014698
[20] Singh, J.; Singh, M.; Jain, A.; Bhardwaj, S.; Singh, A.; Singh, D.; Dubey, S. An introduction of plant nutrients and foliar fertilization: A review. In *Precision Farming: A New Approach*; Daya Publishing Co.: New Delhi, India, **2013**.
[21] Girma, K.; Martin, K.; Freeman, K.; Mosali, J.; Teal, R.; Raun, W.R.; Arnall, D. Determination of optimum rate and growth stage for foliar-applied phosphorus in corn. *Commun. Soil Sci. Plant Anal.* **2007**, *38*, 1137–1154. https://doi.org/10.1080/00103620701328016
[22] Page, A.L.; Miller, R.H.; Keeney, D.R. *Methods of Soil Analysis. Part 2: Chemical and Microbiological Properties*, 2nd ed.; American Society of Agronomy: Madison, WI, USA, **1982**.
[23] Cresser, M.; Parsons, J.W. Sulphuric-perchloric acid digestion of plant material for the determination of nitrogen, phosphorus, potassium, calcium and magnesium. *Anal. Chim. Acta* **1979**, *109*, 431–436. https://doi.org/10.1016/S0003-2670(01)84273-2
[24] Olsen, S.R.; Sommers, L.E. Phosphorus. In *Methods of Soil Analysis, Part 2: Chemical and Microbiological Properties*; Page, A.L., Ed.; Agronomy Monographs 9; ASA-SSSA: Madison, WI, USA, **1982**; pp. 403–430.
[25] Horneck, D.A.; Hanson, D. Determination of potassium and sodium by flame emission spectrophotometry. In *Handbook of Reference Methods for Plant Analysis*; Kalra, Y.P., Ed.; CRC Press: Washington, DC, USA, **1998**; pp. 157-164.
[26] Gessner, M.O.; Neumann, P.T. Total lipids. In *Methods to Study Litter Decomposition*; Graça, M.A.S., Bärlocher, F., Gessner, M.O., Eds.; Springer: Dordrecht, The Netherlands, **2005**; pp. 91–95. https://doi.org/10.1007/1-4020-3466-0_13
[27] Masuko, T.; Minami, A.; Iwasaki, N.; Majima, T.; Nishimura, S.I.; Lee, Y.C. Carbohydrate analysis by a phenol-sulfuric acid method in microplate format. *Anal. Biochem.* **2005**, *339*, 69–72. https://doi.org/10.1016/j.ab.2004.12.001
[28] Muhit, M.A.; Tareq, S.M.; Apu, A.S.; Basak, D.; Islam, M.S. Isolation and identification of compounds from the leaf extract of Dillenia indica Linn. *Bangladesh Pharm. J.* **2010**, *13*, 49–53.
[29] Jalali-Heravi, M.; Moazeni, R.S.; Sereshti, H. Analysis of Iranian rosemary essential oil: Application of gas chromatography-mass spectrometry combined with chemometrics. *J. Chromatogr. A* **2011**, *1218*, 2569-2576. https://doi.org/10.1016/j.chroma.2011.02.048
[30] Liu, R.; Lal, R. Potentials of engineered nanoparticles as fertilizers for increasing agronomic productions. *Sci. Total Environ.* **2015**, *514*, 131–139. https://doi.org/10.1016/j.scitotenv.2015.01.104
[31] Raliya, R.; Saharan, V.; Dimkpa, C.; Biswas, P. Nanofertilizer for precision and sustainable agriculture: Current state and future perspectives. *J. Agric. Food Chem.* **2018**, *66*, 6487–6503. https://doi.org/10.1021/acs.jafc.7b02178
[32] Kah, M.; Kookana, R.S.; Gogos, A.; Bucheli, T.D. A critical evaluation of nanopesticides and nanofertilizers against their conventional analogues. *Nat. Nanotechnol.* **2018**, *13*, 677–684. https://doi.org/10.1038/s41565-018-0131-1
[33] Solanki, P.; Bhargava, A.; Chhipa, H.; Jain, N.; Panwar, J. Nano-fertilizers and their smart delivery system. In *Nanotechnologies in Food and Agriculture*; Rai, M., Ribeiro, C., Mattoso, L., Duran, N., Eds.; Springer: Cham, Switzerland, **2015**; pp. 81–101. https://doi.org/10.1007/978-3-319-14024-7_4
[34] Fageria, V.D. Nutrient interactions in crop plants. *J. Plant Nutr.* **2001**, *24*, 1269–1290. https://doi.org/10.1081/PLN-100106981
[35] Rietra, R.P.; Heinen, M.; Dimkpa, C.O.; Bindraban, P.S. Effects of nutrient antagonism and synergism on yield and fertilizer use efficiency. *Commun. Soil Sci. Plant Anal.* **2017**, *48*, 1895–1920. https://doi.org/10.1080/00103624.2017.1407429
[36] Shaul, O. Magnesium transport and function in plants: The tip of the iceberg. *Biometals* **2002**, *15*, 307–321. https://doi.org/10.1023/A:1016091118585
[37] Guo, W.; Nazim, H.; Liang, Z.; Yang, D. Magnesium deficiency in plants: An urgent problem. *Crop J.* **2016**, *4*, 83–91. https://doi.org/10.1016/j.cj.2015.11.003

[38] Hermans, C.; Hammond, J.P.; White, P.J.; Verbruggen, N. How do plants respond to nutrient shortage by biomass allocation? *Trends Plant Sci.* **2006**, *11*, 610–617. https://doi.org/10.1016/j.tplants.2006.10.007
[39] Cakmak, I.; Yazici, A.M. Magnesium: A forgotten element in crop production. *Better Crops* **2010**, *94*, 23–25.
[40] Aparna, V.; Dileep, K.V.; Mandal, P.K.; Karthe, P.; Sadasivan, C.; Haridas, M. Anti-inflammatory property of n-hexadecanoic acid: Structural evidence and kinetic assessment. *Chem. Biol. Drug Des.* **2012**, *80*, 434–439. https://doi.org/10.1111/j.1747-0285.2012.01418.x
[41] Ma, J.F.; Taketa, S.; Yang, Z.M. Aluminum tolerance genes on the short arm of chromosome 3R are linked to organic acid release in triticale. *Plant Physiol.* **2000**, *122*, 687–694. https://doi.org/10.1104/pp.122.3.687
[42] Tripathi, D.K.; Singh, S.; Singh, S.; Mishra, S.; Chauhan, D.K.; Dubey, N.K. Micronutrients and their diverse role in agricultural crops: Advances and future prospective. *Acta Physiol. Plant.* **2015**, *37*, 139. https://doi.org/10.1007/s11738-015-1870-3
[43] Rico, C.M.; Majumdar, S.; Duarte-Gardea, M.; Peralta-Videa, J.R.; Gardea-Torresdey, J.L. Interaction of nanoparticles with edible plants and their possible implications in the food chain. *J. Agric. Food Chem.* **2011**, *59*, 3485–3498. https://doi.org/10.1021/jf104517j
[44] Kunst, L.; Samuels, L. Plant cuticles shine: Advances in wax biosynthesis and export. *Curr. Opin. Plant Biol.* **2009**, *12*, 721–727. https://doi.org/10.1016/j.pbi.2009.09.009
[45] Samuels, L.; Kunst, L.; Jetter, R. Sealing plant surfaces: Cuticular wax formation by epidermal cells. *Annu. Rev. Plant Biol.* **2008**, *59*, 683–707. https://doi.org/10.1146/annurev.arplant.59.103006.093219
[46] Santos, C.C.; Salvadori, M.S.; Mota, V.G.; Costa, L.M.; de Almeida, A.A.; de Oliveira, G.A. Antinociceptive and antioxidant activities of phytol in vivo and in vitro models. *Neurosci. J.* **2013**, *2013*, 949452. https://doi.org/10.1155/2013/949452
[47] Bhardwaj, R.; Yadav, A.; Sharma, P.; Sharma, R.A. Combination of diosgenin with conjugated linoleic acid attenuates inflammation via modulation of PI3K/Akt/NFκB pathway in colon cancer. *Mol. Nutr. Food Res.* **2014**, *58*, 2180–2188.
[48] Taiz, L.; Zeiger, E.; Møller, I.M.; Murphy, A. *Plant Physiology and Development*, 6th ed.; Sinauer Associates: Sunderland, MA, USA, **2015**.
[49] Maathuis, F.J. Physiological functions of mineral macronutrients. *Curr. Opin. Plant Biol.* **2009**, *12*, 250–258. https://doi.org/10.1016/j.pbi.2009.04.003
[50] Ramakrishna, A.; Ravishankar, G.A. Influence of abiotic stress signals on secondary metabolites in plants. *Plant Signal. Behav.* **2011**, *6*, 1720–1731. https://doi.org/10.4161/psb.6.11.17613
[51] Yang, L.; Wen, K.S.; Ruan, X.; Zhao, Y.X.; Wei, F.; Wang, Q. Response of plant secondary metabolites to environmental factors. *Molecules* **2018**, *23*, 762. https://doi.org/10.3390/molecules23040762
[52] Hawkesford, M.; Horst, W.; Kichey, T.; Lambers, H.; Schjoerring, J.; Møller, I.S.; White, P. Functions of macronutrients. In *Marschner's Mineral Nutrition of Higher Plants*, 3rd ed.; Marschner, P., Ed.; Academic Press: San Diego, CA, USA, **2012**; pp. 135–189. https://doi.org/10.1016/B978-0-12-384905-2.00006-6
[53] Rastogi, A.; Zivcak, M.; Sytar, O.; Kalaji, H.M.; He, X.; Mbarki, S.; Brestic, M. Impact of metal and metal oxide nanoparticles on plant: A critical review. *Front. Chem.* **2017**, *5*, 78. https://doi.org/10.3389/fchem.2017.00078
[54] Rizwan, M.; Ali, S.; Qayyum, M.F.; Ok, Y.S.; Adrees, M.; Ibrahim, M.; Zia-ur-Rehman, M.; Farid, M.; Abbas, F. Effect of metal and metal oxide nanoparticles on growth and physiology of globally important food crops: A critical review. *J. Hazard. Mater.* **2017**, *322*, 2–16. https://doi.org/10.1016/j.jhazmat.2016.05.061
[55] Wang, M.; Zheng, Q.; Shen, Q.; Guo, S. The critical role of potassium in plant stress response. *Int. J. Mol. Sci.* **2013**, *14*, 7370–7390. https://doi.org/10.3390/ijms14047370
[56] Fattahi, B.; Nazeri, V.; Kalantari, S.; Bonfill, M.; Fattahi, M. Essential oil variation in wild-growing populations of *Salvia reuterana* Boiss. collected from Iran: Using GC-MS and multivariate analysis. *Ind. Crops Prod.* **2016**, *81*, 180–190. https://doi.org/10.1016/j.indcrop.2015.11.061
[57] Bajpai, V.K.; Agrawal, P. Studies on phytochemicals, antioxidant, free radical scavenging and lipid peroxidation inhibitory effects of *Trachyspermum ammi* seeds. *Indian J. Pharm. Educ. Res.* **2015**, *49*, 58–65. https://doi.org/10.5530/ijper.49.1.8
[58] Bakkali, F.; Averbeck, S.; Averbeck, D.; Idaomar, M. Biological effects of essential oils—A review. *Food Chem. Toxicol.* **2008**, *46*, 446–475. https://doi.org/10.1016/j.fct.2007.09.106

ASEAN
Journal of Scientific and Technological Reports
Online ISSN:2773-8752

Lists of Reviewers Manuscripts of research articles and academic articles

Lists of Reviewers Manuscripts of research articles and academic articles of ASEAN Journal of Scientific and Technological Reports (AJSTR). ISSN 2773-8752 (Online), Volume 28, No. 1-6. (January – December 2025) were reviewed by the reviewers as follows

1.	Prof. Dr.	Alaa Hussein Oleiwi	Department of Electrical Engineering, Al-Iraqia University
2.	Prof. Dr.	Jitladda Sakdapipanich	Faculty of Science, Mahidol University
3.	Prof. Dr.	Mansoor Abed Aboohanah	Faculty of Agriculture, University of Kufa
4.	Prof. Dr.	Piya Kovintavewat	Faculty of Science and Technology, Nakhon Pathom Rajabhat University
5.	Prof. Dr.	Suched Likitlersuang	Faculty of Engineering, Chulalongkorn University
6.	Prof. Dr.	Wasan H. Mazeil Al-Shammeryi	Wasit University
7.	Assoc. Prof. Dr.	Abideng Hawa	Faculty of Engineering, Princess of Naradhiwas University
8.	Assoc. Prof. Dr.	Ampol Karoonsoontawong	Faculty of Engineering, King Mongkut's University of Technology Thonburi
9.	Assoc. Prof. Dr.	Anothai Ngamvicha	Faculty Member of the School of Management Science, Sukhothai Thammathirat Open University
10.	Assoc. Prof. Dr.	Apiwat Muttamara	Faculty of Engineering, Thammasat University
11.	Assoc. Prof. Dr.	Benjaphorn Prapagdee	Faculty of Environment and Resource Studies, Mahidol University
12.	Assoc. Prof. Dr.	Boonyang Plangklang	Faculty of Engineering Rajamangala University of Technology Thanyaburi
13.	Assoc. Prof. Dr.	Chanthima Phungamngoen	Faculty of Technology, Khon Kaen University
14.	Assoc. Prof. Dr.	Chatree Homkhiew	Faculty of Engineering, Rajamangala University of Technology Srivijaya
15..	Assoc. Prof. Dr.	Chayut Ngamkhanong	Faculty of Engineering, Chulalongkorn University
16.	Assoc. Prof. Dr.	Chompoonoot Kasemset	Department of Industrial Engineering, Chiang Mai University
17.	Assoc. Prof. Dr.	Chuleemas Boonthai Iwai	Faculty of Agriculture, Khon Kaen University
18.	Assoc. Prof. Dr.	Ekwipoo Kalkornsurapranee	Faculty of Science and Technology, Prince of Songkla University
19.	Assoc. Prof. Dr.	Isaratat Phung-on	Maintenance Technology Center, ISTRS, King Mongkut's University of Technology Thonburi
20.	Assoc. Prof. Dr.	Jaruwan Wongthanate	Faculty of Environment and Resource Studies, Mahidol University
21.	Assoc. Prof. Dr.	Jompob Waewsak	Faculty of Engineering, Thaksin University

22.	Assoc. Prof. Dr.	Khundej Suriharn	Faculty of Agriculture, Khon Kaen University
23.	Assoc. Prof. Dr.	Khwanyuruan Naksuwankul	Faculty of Science, Mahasarakham University
24.	Assoc. Prof. Dr.	Kiriya Sungthongwises	Faculty of Agriculture, Khon Kaen University
25.	Assoc. Prof. Dr.	Kumnpee Puangthong	Faculty of Environmental Management, Prince of Songkla University.
26.	Assoc. Prof. Dr.	Mallika Boonmee Kongkeitkajorn	Faculty of Technology, Khon Kaen University
27.	Assoc. Prof. Dr.	Manus Mongkolsuk	Faculty of Radiological Technology, Rangsit University
28.	Assoc. Prof. Dr.	Meechai Thepnurat	Faculty of Education, Chiang Rai Rajabhat University
29.	Assoc. Prof. Dr.	Monthon Lertcanawanichakul	School of Allied Health Sciences, Walailak University
30.	Assoc. Prof. Dr.	Nachawit Tikul	Faculty of Architecture and Environmental Design, Maejo University
31.	Assoc. Prof. Dr.	Narit Thaochan	Faculty of Natural Resources, Prince of Songkla University
32.	Assoc. Prof. Dr.	Norrarat Wattanamongkhol	Faculty of Engineering, Burapha University
33.	Assoc. Prof. Dr.	Orawan Oupathumpanont	Faculty of Home Economics Technology, Rajamangala University of Technology Thanyaburi
34.	Assoc. Prof. Dr.	Panjai Tantatsanawong	Faculty of Science, Silpakorn University.
35.	Assoc. Prof. Dr.	Pantip Klomjek	Faculty of Agriculture, Natural Resource and Environment Naresuan University
36.	Assoc. Prof. Dr.	Panumart Rithichai	Faculty of Science and Technology, T hammasat University
37.	Assoc. Prof. Dr.	Panya Sunintaboon	Faculty of Science, Mahidol University
38.	Assoc. Prof. Dr.	Patcharavadee Sriboonruang	Faculty of Agriculture, Kasetsart University
39.	Assoc. Prof. Dr.	Phayung Meesad	School of Information Technology, King Mongkut's University of Technology North Bangkok
40.	Assoc. Prof. Dr.	Phrueksa Lawongsa	Faculty of Agriculture, Khon Kaen University
41.	Assoc. Prof. Dr.	Pornthap Thanonkeo	Faculty of Technology, Khon Kaen University
42.	Assoc. Prof. Dr.	Prasart Kermanee	Faculty of Science, Kasetsart University
43.	Assoc. Prof. Dr.	Prawit Kongjan	Faculty of Science and Technology, Prince of Songkla University
44.	Assoc. Prof. Dr.	Preenithi Aksorn	Faculty of Engineering, Khon Kaen University

45.	Assoc. Prof. Dr.	Preuttiporn Supaphon	Faci;tu pf Education, Thaksin University
46.	Assoc. Prof. Dr.	Pupong Pongcharoen	Faculty of Engineering, Naresuan University
47.	Assoc. Prof. Dr.	Qassim Ammar Ahmood	College of Engineering, Qassim University
48.	Assoc. Prof. Dr.	Rachadaporn Benchawattananon	Faculty of Science, Khon Kaen University
49.	Assoc. Prof. Dr.	Rattana Jariyaboon	Prince of Songkla University, Songkhla
50.	Assoc. Prof. Dr.	Rattiphorn Sumang	Faculty of Science and Technology, Pibulsongkram Rajabhat University
51.	Assoc. Prof. Dr.	Samroeng Rakson	Faculty of Engineering, Rajamangala University of Technology Rattanakosin
52.	Assoc. Prof. Dr.	Sara Bumrungsri	Faculty of Science, Prince of Songkla University
53.	Assoc. Prof. Dr.	Sarunyaporn Maksup	Faculty of Science, Silpakorn University
54.	Assoc. Prof. Dr.	Sasivimon Sukaphat	Faculty of Science, Srinakharinwirot University
55.	Assoc. Prof. Dr.	Sirichai Yodwangjai	College of Industrial Technology, King Mongkut's University of Technology North Bangkok
56.	Assoc. Prof. Dr.	Somjate Patcharaphan	Faculty of Engineering, Kasetsart University
57.	Assoc. Prof. Dr.	Sompong O-thong	Faculty of Graduate Studies, Mahidol University
58.	Assoc. Prof. Dr.	Sorapong Benchasri	Faculty of Technology and Community Development, Thaksin University
59.	Assoc. Prof. Dr.	Sriwiang Rittisak	Faculty of Digital Agro-Industry, King Mongkut's University of Technology North Bangkok
60.	Assoc. Prof. Dr.	Supawadee Thawaro	Faculty of Science and Technology, Nakhon Si Thammarat Rajabhat University
61.	Assoc. Prof. Dr.	Supawadee Theerathammakorn	School of Science and Technology, Sukhothai Thammathirat Open University
62.	Assoc. Prof. Dr.	Suratsavadee Koonlaboon Korkua	School of Engineering and Technology, Walailak University
63.	Assoc. Prof. Dr.	Suthasinee Thapphasaraphong	Faculty of Pharmaceutical Sciences, Khon Kaen University
64.	Assoc. Prof. Dr.	Teerawat Simmachan	Faculty of Science and Technology, Thammasat University
65.	Assoc. Prof. Dr.	Thanatchai Kulworawanichpong	School of Electrical Engineering, Suranaree University of Technology
66.	Assoc. Prof. Dr.	Thitirat Siriborvornratanakul	Graduate School of Applied Statistics, National Institute of Development Administration
67.	Assoc. Prof. Dr.	Tosaphol Ratniyomchai	Institute of Engineering, Suranaree University of Technology

68.	Assoc. Prof. Dr.	Trinet Yingsamphancharoen	College of Industrial Technology, King Mongkut's University of Technology North Bangkok
69.	Assoc. Prof. Dr.	Warangkhana Riansut	Faculty of Science and Digital Innovation, Thaksin University
70.	Assoc. Prof. Dr.	Wararit Panichkitkosolkul	Faculty of Science and Technology, Thammasat University
71.	Assoc. Prof. Dr.	Waressara Weerawat	Industrial Engineering, Mahidol University
72.	Assoc. Prof. Dr.	Chuwong Pongcharoenpanich	School of Engineering, King Mongkut's Institute of Technology Ladkrabang
73.	Assoc. Prof. Dr.	Jiraphon Srisertpol	Institute of Engineering, Suranaree University of Technology
74.	Assoc. Prof. Dr.	Jiraporn Inthasan	Faculty of Agricultural Production, Maejo University
75.	Assoc. Prof. Dr.	Jirawat Damrianant	Faculty of Engineering, Thammasat University
76.	Assoc. Prof. Dr.	Kanchana Usuwanthim	culty of Allied Health Sciences, Naresuan University
77.	Assoc. Prof. Dr.	Kanita Tangkananura	Faculty of Environment, Kasetsart University
78.	Assoc. Prof. Dr.	Phumin Kirawanich	Faculty of Engineering, Mahidol University
79.	Assoc. Prof. Dr.	Sawai Boukaew	Songkhla Rajabhat University
80.	Assoc. Prof. Dr.	Somyot Detpiratmongkol	Faculty of Agricultural Technology, King Mongkut' s Institute of Technology Ladkrabang
81.	Assoc. Prof. Dr.	Teepanis Chachiyo	Faculty of Science, Naresuan University
82.	Assoc. Prof. Dr.	Weerasak Ussawawongaraya	Faculty of Applied Science, King Mongkut's University of Technology North Bangkok
83.	Assoc. Prof.	Boonrucksar Soonthornthum	National Astronomical Research Institute of Thailand
84.	Assoc. Prof.	Pattana Ratchawong	Faculty of Agriculture Natural Resources and Environment, Naresuan University
85.	Asst. Prof. Dr.	Achaporn kwangsawad	**Faculty of Business Administration, Rajamangala University of Technology Rattanakosin**
86.	Asst. Prof. Dr.	Adulsman Sukkaew	Faculty of Science and Technology for Agriculture, Yala Rajabhat University
87.	Asst. Prof. Dr.	Apichai Bourchookarn	Faculty of Science and Technology, Prince of Songkla University
88.	Asst. Prof. Dr.	Athakorn Promwee	School of Agricultural Technology and Food Industry, Walailak University
89.	Asst. Prof. Dr.	Bootsrapa Leelawa	Faculty of Science and Technology, Thammasat Universit
90.	Asst. Prof. Dr.	Chaisit Niyasom	Faculty of Science and Digital Innovation, Thaksin University

91.	Asst. Prof. Dr.	Chaisit Thongjoo	Faculty of Agriculture at Kamphaeng Saen, Kasetsart University
92.	Asst. Prof. Dr.	Chaiwut Bourneow	Faculty of Public Health, Mahasarakham University
93.	Asst. Prof. Dr.	Chaiyapong Ruangsuwan	Faculty of Science, Khon Kaen University
94.	Asst. Prof. Dr.	Chanida Palanuvej	College of Public Health Sciences, Chulalongkorn University
95.	Asst. Prof. Dr.	Chanika Saenge Chooklin	Faculty of Science and Fisheries Technology, Rajamangala University of Technology Srivijay
96.	Asst. Prof. Dr.	Chivalrat Masingboon	Faculty of Science and Engineering, Kasetsart University
97.	Asst. Prof. Dr.	Duenpen Kochakornjarupong	Faculty of Science and Digital Innovation, Thaksin University
98.	Asst. Prof. Dr.	Issariyaporn Damrongrak	Faculty of Science Technology and Agriculture, Yala Rajabhat University
99.	Asst. Prof. Dr.	Jakkrapong Kangsopa	Faculty of Agricultural Production, Maejo University
100.	Asst. Prof. Dr.	Jenjira Chumpookam	Faculty of Agriculture, Kasetsart University
101.	Asst. Prof. Dr.	Jiraroj Tosasukul	Faculty of Science, Naresuan University
102.	Asst. Prof. Dr.	Juthathip Chalermphol	Faculty of Agriculture, Chiang Mai University
103.	Asst. Prof. Dr.	Kairat Jeroenrat	Faculty of Engineering at Kamphaeng Saen, Kasetsart University
104.	Asst. Prof. Dr.	Khakhanang Ratananikom	Faculty of Science and Health Technology, Kalasin University
105.	Asst. Prof. Dr.	Kiadtisak Saenboonruang	Faculty of Engineering, Kasetsart University
106.	Asst. Prof. Dr.	Kiattisak Rattanadilok Na Phuket	College of Innovation and Management, Sonkhla Rajabhat University
107.	Asst. Prof. Dr.	Komkrich Chokprasombat	Faculty of Science and Digital Innovation, Thaksin University
108.	Asst. Prof. Dr.	Krajana Thaincho	Faculty of Natural Resources, Prince of Songkla University
109.	Asst. Prof. Dr.	Krittika Kaewchumnong	Faculty of Science, Prince of Songkla University
110.	Asst. Prof. Dr.	Kun Silprasit	Faculty of Environmental Culture and Ecotourism, Srinakharinwirot University
111.	Asst. Prof. Dr.	Mantaka Werapong	Faculty of Science and Technology, Nakhon Si Thammarat Rajabhat University
112.	Asst. Prof. Dr.	Monthathip Kongmee	Faculty of Agriculture at Kamphaeng Saen Campus, Kasetsart University
113.	Asst. Prof. Dr.	Nadh Ditcharoen	Faculty of Science, Ubonratchathani University

114.	Asst. Prof. Dr.	Nantiya Panomjan	Faculty of Technology and Community Development, Thaksin University
115.	Asst. Prof. Dr.	Narin Charoenphun	Faculty of Science and Arts, Burapha University
116.	Asst. Prof. Dr.	Nipon Tanpaiboonkul	Faculty of Environment and Resource Studies, Mahasarakham University
117.	Asst. Prof. Dr.	Nutchanat Chamchoi	Faculty of Technology, Khon Kaen University
118.	Asst. Prof. Dr.	Ong-arge Insung	Faculty of Agricultural Technology, Rajamangala University of Technology Srivijaya
119.	Asst. Prof. Dr.	Orawan Monthakantirat	Faculty of Pharmaceutical Sciences, Khon Kaen University
120.	Asst. Prof. Dr.	Orawan Srisompun	Faculty of Technology, Mahasarakham University
121.	Asst. Prof. Dr.	Ornprapa Thepsilvisut	Faculty of Science and Technology, Thammasat University
122.	Asst. Prof. Dr.	Pachara Pholnak	Faculty of Science and Digital Innovation, Thaksin University
123.	Asst. Prof. Dr.	Pakorn Leesutthiporncha	Faculty of Science and Technology, Thammasat University
124.	Asst. Prof. Dr.	Panamas Treewannakul	Faculty of Agriculture, Kasetsart University
125.	Asst. Prof. Dr.	Patcharaporn Pimchan	Faculty of Science and Technology, Rajabhat Maha Sarakham University
126.	Asst. Prof. Dr.	Pattraporn Pukklay	Faculty of Basic Science, MaeJo-Phrae University
127.	Asst. Prof. Dr.	Peeranart Kiddee	Faculty of Science and Digital Innovation, Thaksin University
128.	Asst. Prof. Dr.	Pikaned Uppacha	Faculty of Engineering, Rajamangala University of Technology Isan
129.	Asst. Prof. Dr.	Pitchya Tangsombatvichit	Faculty of Science and Technology, Rajamangala University of Technology Suvarnabhumi
130.	Asst. Prof. Dr.	Pollawat Charoeythornkhajhornchai	Faculty of Engineering, Burapha University
131.	Asst. Prof. Dr.	Pongsak Noparat	Faculty of Science and Technology, Suratthani Rajabhat University
132.	Asst. Prof. Dr.	Punnanee Sumpavapol	Faculty of Agro-Industry, Prince of Songkla University
133.	Asst. Prof. Dr.	Punyisa Trakoonyingcharoen	Faculty of Agriculture at Kamphaeng Saen, Kasetsart University
134.	Asst. Prof. Dr.	Rachasak Somyanonthanakul	Faculty of Science, Rangsit University
135.	Asst. Prof. Dr.	Ronnachai Poowanna	Faculty of Natural Resources, Rajamangala University of Technology Isan
136.	Asst. Prof. Dr.	Ronnakrit Rattanamala	Faculty of Science and Technology, Nakhon Ratchasima Rajabhat University

137.	Asst. Prof. Dr.	Rungrawee Thongdon-a	Faculty of Science and Agricultural Technology, Rajamangala University of Technology Lanna
138.	Asst. Prof. Dr.	Sakulrat Hansuek	Faculty of Agriculture, Rajamangala University of Technology Srivijaya
139.	Asst. Prof. Dr.	Saowapa Chotisuwan	Faculty of Science and Technology, Prince of Songkla University
140.	Asst. Prof. Dr.	Sopa Choopeng	Faculty of Agricultural Technology, Rajabhat Maha Sarakham University
141.	Asst. Prof. Dr.	Sukhonthip Ditcharoen	Faculty of Science, Khon Kaen University
142.	Asst. Prof. Dr.	Supachai Amkha	Faculty of Agriculture at Kamphaeng Saen, Kasetsart University
143.	Asst. Prof. Dr.	Supawadee Manatrinon	Faculty of Animal Sciences and Agricultural Technology, Silpakorn University
144.	Asst. Prof. Dr.	Suphada Kiriratnikom	Faculty of Technology and Community Development, Thaksin University
145.	Asst. Prof. Dr.	Supoj Hengpraprohm	Faculty of Science and Technology, Nakhon Pathom Rajabhat University
146.	Asst. Prof. Dr.	Supojjanee Sansook	Faculty of Science and Technology, Princess of Naradhiwas University
147.	Asst. Prof. Dr.	Suttijit Sriwatcharakul	School of Science, King Mongkut's Institute of Technology Ladkrabang
148.	Asst. Prof. Dr.	Tanasai Sucontphunt	Graduate School of Applied Statistics, National Institute of Development Administration
149.	Asst. Prof. Dr.	Tanate Chaichana	School of Renewable Energy, Maejo University
150.	Asst. Prof. Dr.	Tanayut Chaithongrat	Faculty of Engineering Mahasarakham University
151.	Asst. Prof. Dr.	Thaveechai Kalasin	Faculty of Engineering, Rajamangala University of Technology Lanna
152.	Asst. Prof. Dr.	Thawatchai Tepnual	Faculty of Science and Digital Innovation, Thaksin University
153.	Asst. Prof. Dr.	Thaweesak Khongtuk	Faculty of Business Administration, Rajamangala University of Technology Suvarnabhumi
154.	Asst. Prof. Dr.	Theanchai Wiwasuku	School of Science, Walailak University
155.	Asst. Prof. Dr.	Titipong Kaewlek	Faculty of Allied Health Sciences, Naresuan University
156.	Asst. Prof. Dr.	Tomorn Nunkaew	Faculty of Medicine, Princess of Naradhiwas University
157.	Asst. Prof. Dr.	Warisa Wisittipanich	Faculty of Engineering, Chiang Mai University
158.	Asst. Prof. Dr.	Wattananarong Markphan	Faculty of Science and Technology, Nakhon Si Thammarat Rajabhat University
159.	Asst. Prof. Dr.	Weeraya Treewanjutha	Science and Technology, Prince of Songkla University

160.	Asst. Prof. Dr.	Wijitra Liaotrakoon	Faculty of Agricultural Technology and Agro Industry, Rajamangala University of Technology Suvarnabhumi
161.	Asst. Prof. Dr.	Wipop Paengwangthong	Geographic Information Science, University of Phayao
162.	Asst. Prof. Dr.	Wirach Taweepreda	Faculty of Science, Prince of Songkla University
163.	Asst. Prof. Dr.	Wisatre Kongchareonsuntorn	Faculty of Science, Burapha University
164.	Asst. Prof. Dr.	Wishthida Chantrapornchai	Faculty of Agro-Industry, Kasetsart University
165.	Asst. Prof. Dr.	Worapot Sirirak	Faculty of Engineering, Rajamangala University of Technology Lanna Chiangrai
166.	Asst. Prof. Dr.	Worawit Maneepitaksanti	Faculty of Agriculture, Chiang Mai University
167.	Asst. Prof. Dr.	Yaowarat Wongsrisakulkaew	Faculty of Agricultural Technology, Rajamangala University of Technology Thanyaburi
168.	Asst. Prof. Dr.	Apichat Buakla	School of Engineering, University of Phayao
169.	Asst. Prof. Dr.	Aunthicha Phommuangkhuk	Faculty of Agriculture at Kamphaeng Saen, Kasetsart University
170.	Asst. Prof. Dr.	Chidchanok Choksuchat,	Faculty of Science Prince of Songkla University
171.	Asst. Prof. Dr.	Chuthamat Laksanakit	Faculty of Engineering, Rajamangala University of Technology Srivijaya
172.	Asst. Prof. Dr.	Janyawat Tancharoenrat Vuthijumnon	College of Integrated Science and Technology, Rajamangala University Technology of Lanna
173.	Asst. Prof. Dr.	Jutamas Kumchai	Faculty of Agriculture, Chiang Mai University
174.	Asst. Prof. Dr.	Kaewta Limhang	Sciences and Agricultural Technology, Silpakorn University
175.	Asst. Prof. Dr.	Khwunta Khawmee	Faculty of Natural Resources, Prince of Songkla University
176.	Asst. Prof. Dr.	Molruedee Sonthi	Faculty of Marine Technology, Burapha University
177.	Asst. Prof. Dr.	Nareemas Chehlaeh	Faculty of Science and Technology, Prince of Songkla University
178.	Asst. Prof. Dr.	Naruephat Tangmankongworakoon	Faculty of Environmental Culture and Ecotourism, Srinakharinwirot University
179.	Asst. Prof. Dr.	Natkanin Supamethano	Faculty of Sciences and Liberal Arts, Rajamangala University of Technology Isan
180.	Asst. Prof. Dr.	Nattawut Rungjindamai	School of Science, King Mongkut's Institute of Technology Ladkrabang
181.	Asst. Prof. Dr.	Niwat Muangkeow	School of Agricultural Technology and Food Industry, Walailak University
182.	Asst. Prof. Dr.	Noocharin Tippayawannakorn,	Faculty of Applied Science, King Mongkut's University of Technology North Bangkok

183.	Asst. Prof. Dr.	Noppakorn Phuraya	Faculty of Engineering, Mahidol University
184.	Asst. Prof. Dr.	Peeranart Kiddee	Faculty of Science and Digital Innovation, Thaksin University
185.	Asst. Prof. Dr.	Pornanan Boonkorn	Faculty of Science, Lampang Rajabhat University
186.	Asst. Prof. Dr.	Promphak Boonraksa	Faculty of Engineering, Rajamangla University of Technology Suvarnabhumi
187.	Asst. Prof. Dr.	Rattana Wongchupan	Faculty of Science and Technology, Surat Thani Rajabhat University
188.	Asst. Prof. Dr.	Rittipun Rungruang	Faculty of Science and Technology, Suan Dusit University
189.	Asst. Prof. Dr.	Siraprapa Manomat	Faculty of Applied Science, King Mongkut's University of Technology North Bangkok
190.	Asst. Prof. Dr.	Sirinda. Kusump	Faculty of Science and Technology, Thammasat University
191.	Asst. Prof. Dr.	Thanasak Sae-leaw	Faculty of Agro-Industry Prince of Songkla University
192.	Asst. Prof. Dr.	Thanchuda Phannikul	Faculty of Engineering, Ubon Ratchathani University
193.	Asst. Prof. Dr.	Thitipong Jamrus	Faculty of Engineering, Khon Kaen University
194.	Asst. Prof. Dr.	Tinnakorn Theansungnoen	Cosmetic Science, Mae Fah Luang University
195.	Asst. Prof. Dr.	Uraiwan Tongkaemkaew	Faculty of Technology and Community Development, Thaksin University
196.	Asst. Prof. Dr.	Visit Boonchom	Faculty of Science and Digital Innovation, Thaksin University
197.	Asst. Prof. Dr.	Wasinee Noonpakdee	College of Innovation, Thammasat University
198.	Asst. Prof. Dr.	Yupaporn Wiriyananont	Faculty of Science and Technology, Phra Nakhon Si Ayutthaya Rajabhat University
199.	Asst. Prof.	Kanokwan Yantaboot	Faculty of Science and Technology, Surindra Rajabhat University
200.	Asst. Prof.	Kittichat Paopongpaiboon	Faculty of Industrial Technology, Surindra Rajabhat University
201.	Dr.	Khamphe Phoungthong	Faculty of Environmental Management, Prince of Songkla University
202.	Dr.	Mallika Kliangkhlao	School of Engineering and Technology Academic, Walailak University
203.	Dr.	Marisa Raketh	Universitat Rovira i Virgili, Spain
204.	Dr.	Nutt Nuntapong	Faculty of Natural Resources, Prince of Songkla University
205.	Dr.	Peerawat Khongkliang	Thaksin University

206.	Dr.	Ratchanee Puttha	Faculty of Agricultural Production, Maejo University
207.	Dr.	Sakkarin Chingulpitak	King Mongkut's University of Technology Thonburi
208.	Dr.	Siriporn Lunprom	Department of Biotechnology, Faculty of Technology, Khon Kaen
209.	Dr.	Srisuda Chaikitkaew	Faculty of Technology, Khon Kaen University
210.	Dr.	Srurat Chuayboon	Faculty of Engineering, King Mongkut's Institute of Technology Ladkrabang,
211.	Dr.	Sukonlarat Chanthong	Prince of Songkla University
212.	Dr.	Suparada Surapanthanakorn	Science and Technology, Prince of Songkla University
213.	Dr.	Supreena Srisaikham	Faculty of Agricultural Technology, Burapha University
214.	Dr.	Wantanasak Suksong	King Mongkut's University of Technology North Bangkok
215.	Dr.	Wisan Odton	Faculty of Technology and Community Development, Thaksin University
216.	Dr.	Worradorn Phairuang	Faculty of Social Sciences, Chiang Mai University
217.	Dr.	Cholwich Nattee	Sirindhorn International Institute of Technology, hammasat University
218.	Dr.	Chonticha Mamimin	Faculty of Graduate Studies, Mahidol University
219.	Dr.	Naphat Kaewpiban	Faculty of Science and Digital Innovation, Thaksin University
220.	Dr.	Phatsaphan Charnwasununth	Faculty of Architecture, Chulalongkorn University
221.	Dr.	Philaiwan Pornprasit	Faculty of Engineering and Agro-Industry, Maejo University
222.	Dr.	Pinnarat Nuchpho	Faculty of Management Science, Pibulsongkram Rajabhat University
223.	Dr.	Thidapath Anucharn	School of Information and Communication Technology, University of Phayao
224.	Lecturer	Ajaree Naco	Faculty of Science and Digital Innovation, Thaksin University
225.	Lecturer	Santat Sinjaroonsak	Faculty of Agriculture, Princess of Naradhiwas University

ASEAN
Journal of Scientific and Technological Reports
Online ISSN: 2773-8752

Article type

Type of the Paper (Article, Review, Communication, etc.) *about 8,000 words maximum*

Title (Palatino Linotype 18 pt, bold)

Firstname Lastname[1], Firstname Lastname[2] and Firstname Lastname[2*]

[1] Affiliation 1; e-mail@e-mail.com
[2] Affiliation 2; e-mail@e-mail.com
* Correspondence: e-mail@e-mail.com; (one corresponding authors, add author initials)

Citation:
Lastname, F.; Lastname, F.; Lastname, F. Title. *ASEAN J. Sci. Tech. Report.* **2023**, *26*(X), xx-xx. https://doi.org/10.55164/ajstr.vxxix.xxxxxx

Article history:
Received: date
Revised: date
Accepted: date
Available online: date

Abstract: A single paragraph of about 400 words maximum. Self-contained and concisely describe the reason for the work, methodology, results, and conclusions. Uncommon abbreviations should be spelled out at first use. We strongly encourage authors to use the following style of structured abstracts, but without headings: (1) Background: Place the question addressed in a broad context and highlight the purpose of the study; (2) Methods: briefly describe the main methods or treatments applied; (3) Results: summarize the article's main findings; (4) Conclusions: indicate the main conclusions or interpretations.

Keywords: keyword 1; keyword 2; keyword 3 (List three to ten pertinent keywords specific to the article yet reasonably common within the subject discipline.)

1. Introduction

The introduction should briefly place the study in a broad context and highlight why it is crucial. It should define the purpose of the work and its significance. The current state of the research field should be carefully reviewed and critical publications cited. Please highlight controversial and diverging hypotheses when necessary. Finally, briefly mention the main aim of the work. References should be numbered in order of appearance and indicated by a numeral or numerals in square brackets—e.g., [1] or [2, 3], or [4–6]. See the end of the document for further details on references.

2. Materials and Methods

The materials and methods should be described with sufficient details to allow others to replicate and build on the published results. Please note that your manuscript's publication implicates that you must make all materials, data, computer code, and protocols associated with the publication available to readers. Please disclose at the submission stage any restrictions on the availability of materials or information. New methods and protocols should be described in detail, while well-established methods can be briefly described and appropriately cited.

Interventional studies involving animals or humans, and other studies that require ethical approval, must list the authority that provided approval and the corresponding ethical approval code.

2.1 Subsection

2.1.1. Subsubsection

3. Results and Discussion

This section may be divided by subheadings. It should provide a concise and precise description of the experimental results, their interpretation, as well as the experimental conclusions that can be drawn.Authors should discuss the results and how they can be interpreted from previous studies and the working hypotheses. The findings and their implications should be discussed in the broadest context possible. Future research directions may also be highlighted.

3.1. Subsection

3.1.1. Subsubsection

3.2. Figures, Tables, and Schemes

All figures and tables should be cited in the main text as Figure 1, Table 1, etc.

Figure 1. This is a figure. Schemes follow the same formatting.

Table 1. This is a table. Tables should be placed in the main text near the first time they are cited.

Title 1	Title 2	Title 3
entry 1	data	data
entry 2	data	data [1]

[1] Table may have a footer.

3.3. Formatting of Mathematical Components

This is example 1 of an equation:

$$a = 1, \tag{1}$$

The text following an equation need not be a new paragraph. Please punctuate equations as regular text. This is example 2 of an equation:

$$a = b + c + d + e + f + g + h + i + j + k + l + m + n + o + p + q + r + s + t + u \tag{2}$$

The text following an equation need not be a new paragraph. Please punctuate equations as regular text. The text continues here.

4. Conclusions

Concisely restate the hypothesis and most important findings. Summarize the significant findings, contributions to existing knowledge, and limitations. What are the future directions? Conclusions MUST be well stated, linked to original research question & limited to supporting results.

5. Acknowledgements

Should not be used to acknowledge funders – funding will be entered as a separate. As a matter of courtesy, we suggest you inform anyone whom you acknowledge.

Author Contributions: For research articles with several authors, a short paragraph specifying their individual contributions must be provided. The following statements should be used "Conceptualization, X.X. and Y.Y.; methodology, X.X.; software, X.X.; validation, X.X., Y.Y. and Z.Z.; formal analysis, X.X.; investigation, X.X.; resources, X.X.; data curation, X.X.; writing—original draft preparation, X.X.; writing—review and editing, X.X.; visualization, X.X.; supervision, X.X.; project administration, X.X.; funding acquisition, Y.Y. All authors have read and agreed to the published version of the manuscript." Please turn to the CRediT taxonomy for the term explanation. Authorship must be limited to those who have contributed substantially to the work reported.

Funding: Please add: "This research received no external funding" or "This research was funded by NAME OF FUNDER, grant number XXX" and "The APC was funded by XXX". Check carefully that the details given are accurate and use the standard spelling of funding agency names at https://search.crossref.org/funding. Any errors may affect your future funding.

Conflicts of Interest: Declare conflicts of interest or state "The authors declare no conflict of interest." Authors must identify and declare any personal circumstances or interest that may be perceived as inappropriately influencing the representation or interpretation of reported research results. Any role of the funders in the design of the study; in the collection, analyses or interpretation of data; in the writing of the manuscript, or in the decision to publish the results must be declared in this section. If there is no role, please state "The funders had no role in the design of the study; in the collection, analyses, or interpretation of data; in the writing of the manuscript, or in the decision to publish the results".

References

References must be numbered in order of appearance in the text (including citations in tables and legends) and listed individually at the end of the manuscript. We recommend preparing the references with a bibliography software package, such as EndNote, ReferenceManager to avoid typing mistakes and duplicated references. Include the digital object identifier (DOI) for all references where available.

Citations and references in the Supplementary Materials are permitted provided that they also appear in the reference list here.

In the text, reference numbers should be placed in square brackets [ ] and placed before the punctuation; for example [1], [1–3] or [1, 3]. For embedded citations in the text with pagination, use both parentheses and brackets to indicate the reference number and page numbers; for example [5] (p. 100), or [6] (pp. 101–105).

Using the American Chemical Society (ACS) referencing style

[1] Author 1, A.B.; Author 2, C.D. Title of the article. *Abbreviated Journal Name* Year, *Volume*, page range.

[2] Author 1, A.; Author 2, B. Title of the chapter. In *Book Title*, 2nd ed.; Editor 1, A., Editor 2, B., Eds.; Publisher: Publisher Location, Country. **2007**, Volume 3, pp. 154–196.

[3] Author 1, A.; Author 2, B. *Book Title*, 3rd ed.; Publisher: Publisher Location, Country, **2008**, pp. 154–196.
[4] Author 1, A.B.; Author 2, C. Title of Unpublished Work. *Abbreviated Journal Name* stage of publication (under review; accepted; in press).
[5] Author 1, A.B. (University, City, State, Country); Author 2, C. (Institute, City, State, Country). Personal communication, 2012.
[6] Author 1, A.B.; Author 2, C.D.; Author 3, E.F. Title of Presentation. In Title of the Collected Work (if available), Proceedings of the Name of the Conference, Location of Conference, Country, Date of Conference; Editor 1, Editor 2, Eds. (if available); Publisher: City, Country, Year (if available); Abstract Number (optional), Pagination (optional).
[7] Author 1, A.B. Title of Thesis. Level of Thesis, Degree-Granting University, Location of University, Date of Completion.
[8] Title of Site. Available online: URL (accessed on Day Month Year).

Reviewers sugestion

1. Name, Address, e-mail
2. Name, Address, e-mail
3. Name, Address, e-mail
4. Name, Address, e-mail

URL link:

Notes for Authors >>
https://drive.google.com/file/d/1r0zegnIVeQqe4iLQyT1xDEIinNggINPD/view?usp=sharing
https://drive.google.com/file/d/1r0zegnIVeQqe4iLQyT1xDEIinNggINPD/view?usp=sharing

Online Submissions >> https://ph02.tci-thaijo.org/index.php/tsujournal/user/register

Current Issue >> https://ph02.tci-thaijo.org/index.php/tsujournal/issue/view/16516

AJSTR Publication Ethics and Malpractice >> https://ph02.tci-thaijo.org/index.php/tsujournal/ethics

Journal Title Abbreviations >> http://library.caltech.edu/reference/abbreviations

ASEAN
Journal of Scientific and Technological Reports
Online ISSN:2773-8752

ASEAN
Journal of Scientific and Technological Reports
Online ISSN:2773-8752

ASEAN Journal of Scientific and Technological Reports (AJSTR)
Institute of Research and Innovation, Thaksin University, Phatthalung Campus
222 Moo. 2, Baan Prao Sub-District, Papayom District, Phatthalung, 93210, Thailand
Tel. +668 1540 7304